ADHESIVE FORMULATIONS FOR LENS APPLICATIONS

SIMSON MCCREATH

A thesis submitted to the Department of Pure and Applied Chemistry, University of Strathclyde, in part fulfilment of the requirements for the degree of Doctor of Philosophy

October 2015

Declaration

This thesis is the result of the author's original research. It has been composed by the author and has not been previously submitted for examination which has led to the award of a degree.

The copyright of this thesis belongs to the author under the terms of the United Kingdom Copyright Acts as qualified by University of Strathclyde Regulation 3.50. Due acknowledgement must always be made of the use of any material contained in, or derived from, this thesis.

Signed: Date:

Acknowledgments

Firstly I would like to express my sincere gratitude to Polaroid® Eyewear for their support in funding this work. I would especially like to that Dr E. Boinard and Dr P. Boinard for establishing the contact with the University of Strathclyde. Their continued interest and support of the work carried out in the University has been critical in helping the project move forward. I would also like to thank them for their help when I was conducting work at the Vale of Leven industrial estate as they were always ensuring that my visits were enjoyable, which is also the case for the rest of the staff working at the Polaroid® Eyewear.

I would like to thank my academic supervisor Dr J. J. Liggat for his continued help, enthusiasm and expert technical guidance throughout the project of work. I would also like to thank Prof R. Pethrick for his help during my project as his continued enjoyment in helping was a great motivation. I would also like to thank Dr P. L. Tang for his assistance both in using infrared spectrometers along with his knowledge of other possible infrared techniques in experimental design. I would also like to extend my thanks to Prof. I. Watts for allowing me to carry out work at the University of Surrey and making my time down there very enjoyable.

Most of my project would have not been possible if it were not for the excellent work of the technical staff at the University. I would like to take this opportunity to thanks Mr C. Irvine and Dr J. Parkinson for their help using the Nuclear magnetic resonance spectrometers, Mrs P. Keatings for her help using the mass spectrometry suite, Mr L. McCulloch for his technical help in the laboratory and the running of thermal analysis and also all the office staff for the help which I received during my studies.

Next I would like to that my fellow colleges for their support, help, informative discussions and mostly putting up with me.

Finally I would like to thank my parents, my partner and my daughter as without their support throughout all of my studies it would have not been possible to reach where I am in my career.

Abstract

The work presented within this thesis was focused on the development of a novel polyurethane adhesive which could be used in the construction of sunglass lens. This adhesive must satisfy certain objectives: (i) the cured adhesive must be optically clear with the final haze value < 1.5% when laminated between two layers of plastic, (ii) the adhesive must bond cellulose triacetate, bisphenol-A polycarbonate and any other laminate combinations containing these plastics, (iii) each fully cured laminate must have a peel strength of $\geq$ 3 N mm^{-1} as determined by 180° T-peel testing and (iv) the fully cured adhesive must be free of thermal transitions within the window of -20°C to 100°C which would otherwise affect the in-use performance.

To achieve these aims a series of aliphatic and aromatic polyurethane adhesive based on IPDI and MDI were formulated. Within these formulations a range of softsegments were used which included PPG, PCD and PDEGA. Finally, less conventional chain-extenders were used to improve the final haze value of the adhesive. Cellulose triacetate was tested both as received and following saponification of the interface. Polycarbonate was used as received and following pre-treatment of the interface by an ethanolamine in isopropyl alcohol solution.

The results within this thesis have shown that adhesion to multiple interfaces is a complex task. Using MDI-based adhesives it was shown that the compatibility with polycarbonate was high and surface pre-treatment by ethanolamine was not required. In most instances, peel strengths of $\geq$ 3 N mm^{-1} were obtained. Cellulose triacetate however, had a poor compatibility with MDI-based polyurethanes. In all instances the peel strength obtained was < 1 N mm^{-1}. In order to obtain laminates of $\geq$ 3 N mm^{-1} saponification of the interface was required. Deacetylation of the interface leaves a regenerated cellulose surface and these labile hydroxyl groups able to react with the isocyanate groups within the prepolymer adhesive. Obtaining MDI adhesives of low haze was not straight forward. It was shown that using noncrystalline soft-segments such as PPG and PDEGA was the best approach but their application was problematic. Due to the requirement for surface treatment of cellulose triacetate and the difficulty of application, MDI-based polyurethanes were thus shown not to be appropriate.

Following this IPDI-based adhesives were next tested. For these adhesives, noticeable differences in both the adhesion behaviour and the haze values were observed. Moving to an aliphatic isocyanate improved the compatibility with cellulose triacetate, whilst not reducing the performance with polycarbonate. When using either PPG or PCD, low peel strengths values where obtained with cellulose triacetate and like MDI-based adhesives saponification was required for high peel strength. When using the soft-segment PDEGA however, peel strength of ≥ 3 N mm^1 were obtained and this value was obtained regardless of surface treatment. It was shown that this improved adhesion was linked to IPDI-based adhesives having a phase-separated morphology which promotes adhesion by hydrogen bonding. This phase-separated morphology was also advantageous towards the haze, with values well inside the 1.5% obtained. Thus it was shown that in order to obtain an optically clear adhesive with a haze of < 1.5% that is void of thermal transition between -20°C to 100°C and can bond either untreated cellulose triacetate or polycarbonate with a peel strength of ≥ 3 N mm^{-1} was only possible using a polyurethane adhesive based on IPDI and PDEGA.

Contents Chapter 1 Introduction

List of Figures

Figure 1.01: Schematic of a single screw extruder *top* and schematic of a film die *bottom*.

Figure 1.02: Schematic of blow film extrusion process.

Figure 1.03: Schematic of the solution casting process of a polymer film.

Figure 1.04: Knife on roller web coating schematic.

Figure 1.05: Schematic of wire wound Meyer Bar.

Figure 1.06: Structure of cellulose *left* and cellulose triacetate *right*.

Figure 1.07: Structure of bisphenol-A polycarbonate.

Figure 1.08: Dipole – dipole lowest energy configurations (a) two isolated dipoles with head to tail orientation and (b) three dipoles with a more complex structure.

Figure 1.09:   Schematic of covalent bond formation between reactive isocyanate groups of adhesive and hydroxyl groups at the substrate interface.

Figure 1.10:   Hydrogen bonding can occur in small molecule such as (a) carboxylic acids or within polymers like (b) cellulose and (c) nylon 6,6.

Figure 1.11:   Polymer diffusion between two amorphous polymers leading to chain entanglement and adhesion.

List of tables

Table 1.01:   Sources of active hydrogens in polyurethane/urea chemistry, structures and relative reaction rates.

Table 2.01: Thermal and mass data of raw materials.

Table 3.01: Peel, haze and mode of failure data for MDI-TMP-PPG cured PUU adhesive. [The data in bold will be discussed within this section].

Table 3.02: Characteristic peaks of MDI-TMP-PPG cured PU-U adhesive from all five laminate combinations.

Table 3.03: Peel, haze and mode of failure data for MDI-TMP-PPG-DEPD cured PU-U adhesive. [The data in bold will be discussed within this section].

Table 3.04: Characteristic peaks of MDI-TMP-PPG-DEPD cured PU-U adhesive from all five laminate combinations.

Abbreviation list

Ultraviolet	UV
Secondary ion mass spectroscopy	SIMS
X-ray photoelectron spectroscopy	XPS
Hydridosilane	SiH
Alkenyl group	$-CH=CH_2$
Methylene diphenyl diisocyanate	MDI
Toluene diisocyanate	TDI
Hexamethylene diisocyanate	HMDI
Isophorone diisocyanate	IPDI
1,4-diazabicyclo-[2.2.2]-octane	DABCO
Cellulose triacetate	TAc
Polycarbonate	PC
Fourier transform infrared attenuated total reflectance	ATR
Nuclear magnetic resonance spectroscopy	NMR
Matrix assisted laser desorption ionisation time of flight mass spectrometry	MALDI-MS spectroscopy
Differential scanning calorimetry	DSC
Glass transition temperature	T_g
Thermal gravimetric analysis	TGA
Polyurethane	PU
Poly(propylene glycol)	PPG
Trimethylolpropane	TMP
Polyurethane-urea	PU-U
2,2-diethyl-1,3-propane diol	DEPD
1,3-butane diol	BD
1,2-propane diol	PD
Treated cellulose triacetate	TAc(t)

Chapter 1 Introduction

Developing a pair of sunglasses can be mistaken for being a simple and straightforward process, however it is not until the steps required for their manufacture are detailed that the true complexity is exposed. From a customer's point of view sunglasses require such things as a variety of styles, a variety of functionalities while still demanding the primary function of protecting the eyes from harmful ultraviolet and reflected sun light. From a manufacturing point of view, the style of the sunglasses is of lower priority as it comes towards the end of the development timeline. The main focus is on the materials used to form the sunglasses and developing robust methods for their manufacture which consistently deliver high quality products.

The manufacturing process plus the materials used in forming sunglasses can be split into two main areas: the frame and the lens. The frame is generally formed by injection moulding, which requires heating a thermoplastic base material to a predetermined temperature that allows it to flow. When fluid the thermoplastic material can be mixed with dyes and other additives to obtain the specified properties. Once homogeneous the molten material is forced under pressure into a mould which is then cooled to lock the polymer in the shape of the desired fame. A much more complex process is encountered during actual production of the frame, with this explanation of this key component being much simplified.

More challenging and of more interest is the manufacture of the sunglass lens. This component consists of a multi-layer laminate material which gives the final product its main function of eye protection but still allowing for varying lens styles e.g. thickness, colour, coatings etc. Having a layer which contains a polariser or ultraviolet (UV) light blocker will help prevent reflected or harmful rays reaching the eye, while other layers can be added to the laminate to enhance shock resistance, toughness, flexibility and scratch resistance. Also of environmental interest is to try and use materials that can be obtained from renewable sources.

Understanding that no one polymer material will be able to deliver all of these properties highlights the need to form a multi-layer laminate. Forming such laminates results in a final material with properties that are a hybrid of all the materials added. Lamination of a multi-layer material presents its own manufacturing issues as now

different interfaces are required to be bonded together. Adhesion of different interfaces has been a problem for many years because of the difficulty in identifying a suitable adhesive which is compatible with different surface chemistries. Often using different adhesives for each lamination step is a solution; however, this adds unwelcomed complexity to the manufacturing process as now a method is required which can apply different adhesives to different layers simultaneously. This will require expensive equipment or will require multiple laminations which is time consuming and more capital intensive. Another alternative that is commonly used is to identify a potential surface treatment which boosts the compatibility of the interface towards the chosen adhesive. Although an attractive alternative, it introduces the need for treatment lines which presents the opportunity for contamination of the laminate interface and also adds to the manufacturing time. The ideal scenario is to identify or develop an adhesive which is capable of bonding a variety of materials together giving a strong laminate without the need for surface treatment. However, if such an adhesive material is developed it must be optically clear, flexible, have a low glass transition temperature, be water resistant, be solvent resistant and be resistant to ultra-violet degradation.

Within this report details on the synthesis of a variety of optically clear polyurethane adhesive will be described. The characterisation of each material will be discussed along with the molecular level design of each adhesive. Lamination materials and the lamination process will be discussed along with the physical characteristics. Finally the chemical and physical results will be used to determine the optimum formulation based on strength, clarity, haze and easy of manufacture.

1.10 Polymer Film

Polymer films are employed in a number of different applications e.g. sunglass lenses, food packaging, construction, imaging film, barrier films etc. This, coupled with the variety of available polymer materials, contributes to the vast number of applications in which polymer films are used. Common functional groups found in polymer films are styrenic, polyester, polyimide, polyamide (nylons), polyolefin, fluoropolymer, polyvinyl/acrylic, elastomer and rubber. Each polymer type will present the opportunity to bring different properties to the application of choice e.g. polycarbonate

films are used in safety glasses were clarity and toughness are required, whereas cellulose triacetate is used as the transparent base film to support the photosensitive emulsion in photographic film.[1,2] The processing used in production of polymer films will vary from polymer to polymer as each will have different characteristics associated with the materials ability to flow or be put in solution.

1.101 Extrusion

Possibly one of the most versatile manufacturing processes which can be used when forming polymer films is extrusion. Extrusion is a bulk polymer processing technique used to melt then reshape thermoplastic materials however, reactive extrusion is also possible. An extruder consists of two basic components: a single (or twin) screw(s) which can be from three to four meters in length and a barrel in which the screw(s) is enclosed (see figure 1.01). The barrel can be heated or cooled and will often have ports along its length which allow for venting of entrapped gas evolved from the polymer during melting or addition of additives.

To perform extrusion, polymer beads (or powder) are loaded into a feed hopper which feeds the material into the barrel containing the screw. This initial part of the barrel, known as the feed zone is where the polymer melts under frictional and conventional heating.[3] The screw drives the molten polymer along the barrel into the compression zone of the barrel which helps to evolve any gas trapped within the polymer material. As the material progress down the barrel it is accompanied by a gradual increase in temperature; this increases the viscoelastic fluids mobility and this gradual heating reduces the probability of thermal degradation which can occur if the heating gradient is too steep. Once the molten material is at the right temperature and is flowing fluidly, the polymer then enters the final part of the barrel known as the metering zone. Prior to entering the metering zone it is possible to introduce additive such as UV stabilisers or fire retardants into the polymer material.
Within the metering zone the screw homogenises the material before it enters the processing die at the end of the barrel.

The need for a die is to take the material from the cylindrical barrel and reshape it into the profile of the product. A film die (see figure 1.01) will mould the molten plastic into a sheet, which will have thickness given by the profile of the die. This film is then

either placed over cooled rollers or put on top of a cold water bath which cools the polymer locking the film into place. This film once cooled can be further processed e.g. surface treated followed by slitting to the desired width and then wound onto a roll for storage. Applying a film die directly to the end of the extruder is the most conventional way of bulk film formation; however, there are other options available.
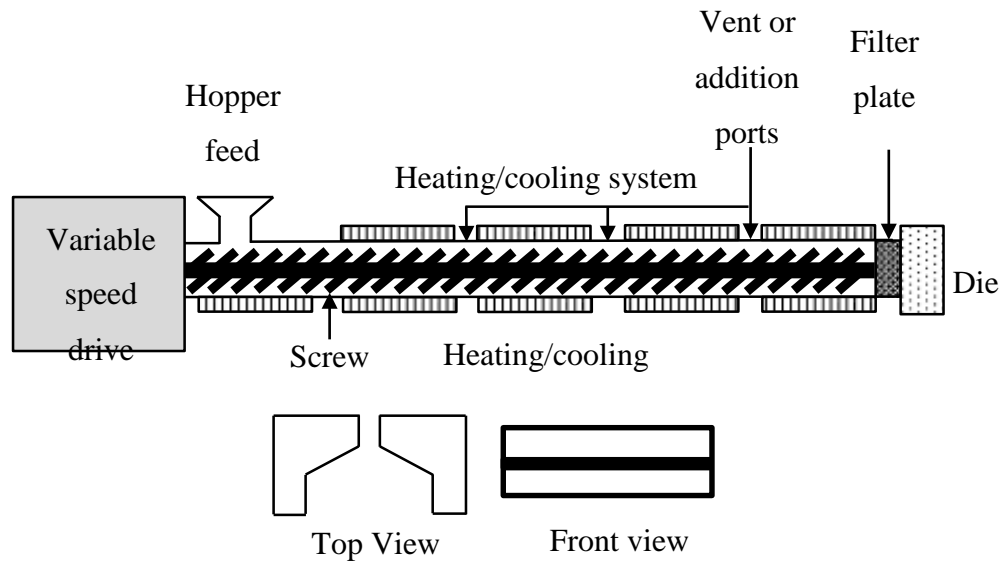
Figure 1.01: Schematic of a single screw extruder *top* and schematic of a film die bottom.[4]

1.102 Blow film

Blow film extrusion follows the same process as previously detailed for extrusion up until the die is reached. The die used is an annular slit die which forms a thin walled tube extrudate as it exits the die in a vertical direction. Positioned at the centre of the die is an inlet for the introduction of compressed air to balloon the polymer tube. The dimensions of expanded polymer film are controlled by both the air pressure and the speed at which the polymer leaves the die. At the top of the die a high-speed air ring is positioned to cool the molten material as it exits the die. The process then continues in a vertical direction with the ballooned film drawn up a cooling column. Positioned at the top of the column are two nip rollers which collapse the ballooned material and this is the beginning of a roller system which takes the film to the final collection point. An advantage of the blow film process over standard extrusion is that both flat and tube films can be produced in a single operation.
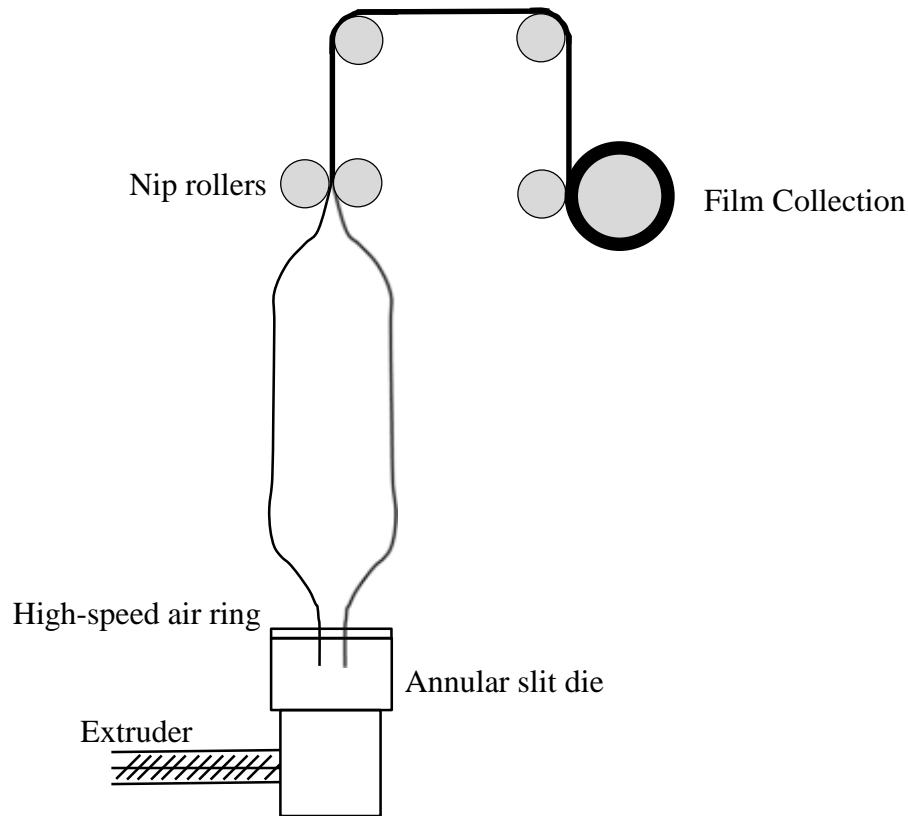
Figure 1.02: Schematic of blow film extrusion process.[3]

1.103 Casting Film Line

Solution casting of polymer films is the oldest method used in polymer film production with the earliest examples dating back to the late 19th century. Presently the technique is carried out industrially as a continuous process for the production of polymer films with high end optical applications.[5]

When making a polymer film using this process there are three variables that should be considered when selecting the raw materials: firstly the polymer of choice must be soluble in an appropriate solvent, the solution obtained should be stable with minimum residual solid content giving a solution of workable viscosity and finally the formation of a homogeneous film which can be easily removed from the casing support.[5] The polymer film is cast from a dope solution which requires the polymer and any additives being dissolved in an appropriate solvent. Each solvent used needs to readily dissolve the polymer but also be highly volatile to ensure casting and drying of the film can occur within a short time frame. The concentration of the solution must be carefully

5

controlled as the viscosity of the solution and the parameters used in the casting process will be influenced by this concentration. Also the temperature at which the solution is prepared and applied must be controlled to ensure that the viscosity of the dope solution does not change.
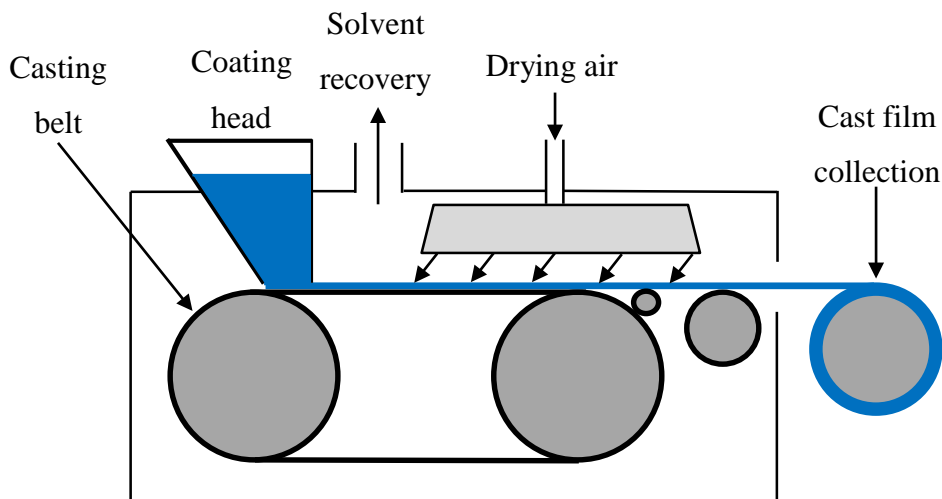
Figure 1.03: Schematic of the solution casting process of a polymer film.[4] The initial step of the casting process requires that the dope solution is applied to a moving casting belt. The coating head used to apply the dope will contain a hopper of the solution and a slot die or a doctor blade die which controls the thickness of application. The belt must be highly polished to ensure a smooth surface is obtained and commonly is made from highly polished stainless steel or chrome plated steel but may also be made from copper or in some specialised processes a fluoropolymer belt is used. Irrespective of the material used in the casting belts construction it is essential that the cast film can be easily removed once formed.

Next, air is introduced to dry the film by aiding the removal of the solvent from the dope solution precipitating out the polymer. Dry air sweeps in the opposite direction from the propagation film collecting the evaporating solvent. Belt speed along with the air flow rate will have an effect on the film thickness, it is common in industrial processes to have a gauging system which monitors and controls this thickness. The solvent rich air then is removed and goes through a solvent collection process. This reduces the production cost as the solvent can be reused and also reduces air pollution. Finally the dry film is removed from the casting support, followed by slitting to the

desired width and collected by windup onto a roll. In some processes before the film reaches wind-up it will undergo a pre-treatment such as corona, flame or solution based, leaving an activated surface.

Common polymer films that are prepared in this way are cellulose triacetate, with the casting solvent being either dichloromethane or an alcohol, polycarbonate with the casting solvent being dichloromethane, and polyvinyl chloride, with the casting solvent of tetrahydrofuran or methyl ethyl ketone. Films of these materials are generally prepared in this way when they are required for optical applications such as monitor displays or sport glass lenses.

1.11 Multilayer Polymer Films

Surface treatments are commonly required when the interfaces of different materials are incompatible e.g. in lamination of multilayer laminates which contain more than a single polymer. Multilayer polymer laminates are used when a single material does not reach the required specifications e.g. a squeezable tomato sauce bottle is a three layer laminate of poly(ethylene terephthalate) – ethylene vinyl alcohol – poly(ethylene terephthalate). The poly(ethylene terephthalate) layers give the bottle strength, flexibility, chemical resistance and acts as a moisture barrier; however, it allows the permeation of oxygen which can spoil the contents.[3] The ethylene vinyl alcohol layer acts as the oxygen barrier.

Sunglasses lenses are such an application in which a variety of properties are required such as transparency, flexibility, strength, chemical resistance and scratch resistance. To obtain such properties a multilayer laminate is required and this introduces added complications into the manufacturing process. Added complications will include such issues as being able to source or make the polymer films needed, finding a suitable method for laminating the films together, having the correct equipment to carry out the lamination, surface treatment lines may be required, forming the lens after lamination etc. Laminate materials will be constructed from cellulose triacetate, polycarbonate or a hybrid of both and will require the use of a suitable adhesive to bond these layers together. The application of this adhesive will determine the success or failure in forming such a laminate and will be applied using a suitable web coating technique.

1.111 Knife Coating

Knife coating is a web coating method used for applying liquids onto the surface of a solid polymer film with great accuracy. The process requires an excess of the coating material being placed at one side of the doctor blade and as the polymer film is drawn past the blade the excess material is removed leaving a pre-set thickness of material on top of the film (see figure 1.04). This technique is a low cost method for the application of high viscosity coatings such as hot melt adhesives and rubber coatings. There are many variations of the simple set-up e.g. when used for hot melt adhesive applications the blade is often heated to keep the material viscosity low enough to allow it to pass under the blade.
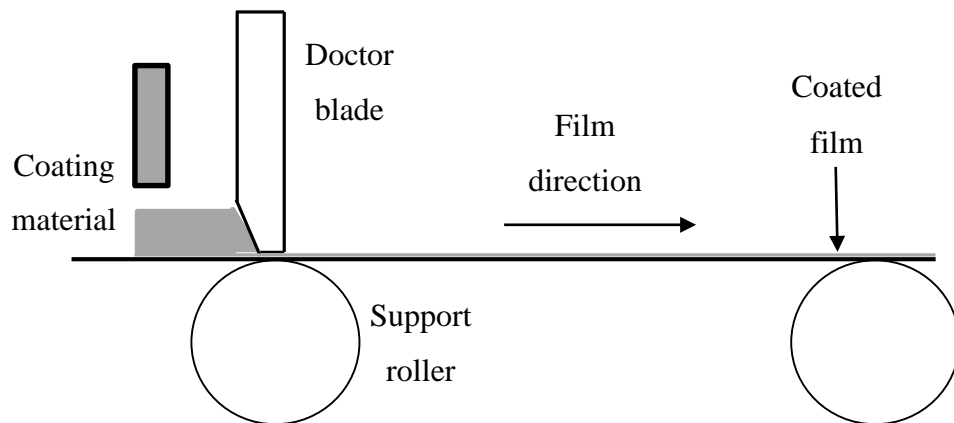
Figure 1.04: Knife on roller web coating schematic.[4]
Advantages of this web coating technique are that it can be easy installed and is of low cost. Such a coating system has very few moving parts making it very robust and reliable. The technique does have some disadvantages: the blade must be well polished to ensure that a smooth coating is obtained as any scratches will be visible in the coating, after coating the blade requires cleaning which depending on the material being used could result in considerable down time and the adjustment of the gap is usually time consuming which again reduce the productivity if multiple thicknesses are required. Away from these disadvantages this coating technique when employed properly will deliver good quality coatings.

1.112 Metering Rod (Meyer Bar) Coating

The metering rod, or as it is more commonly called the Meyer bar, is a very common method used for web coating of flexible polymer films. The rod coating technique was developed in the early 1900's by Charles Meyer of the Meyer Coating Machine

Company. Coating using this technique makes use of a wire wound or machined stainless steel bar which is in contact with the polymer film. The spacing of the wire or the machined grooves precisely determines the thickness of the coating applied to the polymer film as it moves past the Meyer bar. The diameter of the wire spiralled round the bar is directly proportional to the thickness of the wet coating left on the polymer film. At the exiting side of the Meyer bar are stripes of the liquid coating which are separated by the distance between the wire windings.[4] As the surface tension of the liquid is not strong enough to support these stripes they begin to collapse, merging with one another to form a smooth and flat coating. The coating can then be UV or thermally cured and if a laminate is being formed then the other film is brought into contact with the wet surface.
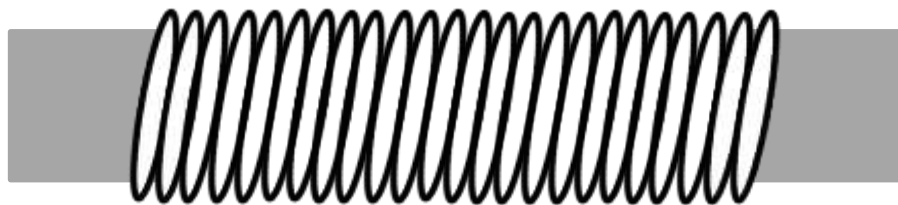
Figure 1.05: Schematic of wire wound Meyer Bar.[6]
Although in theory Meyer bar coating appears as a relatively simple process, practically there are some factors to consider that will have an influence on the thickness of the final coating. Such factors that will influence the final coating thickness are the viscosity versus temperature of the liquid being used, the polymer film tension, the speed at which the polymer film is traveling under the Meyer bar, the ability of the adhesive to wet the polymer surface, the degree to which the coating liquid penetrates the polymer film, etc.[6] Furthermore, high viscosity liquids may coat the wire which reduces the amount of adhesive that passes through each gap. In practice however, these factors are overcome by a simple trial-and-error approach until the desired coating thickness is obtained.

1.12 Lamination

Lamination is the process where two or more polymer films are jointed together forming a laminated material. The process used to join the two materials together will include either heat or pressure and commonly both. Industrially lamination is used

when a single polymer film does not satisfy the properties specified, meaning that several and differing materials are used to obtain a hybrid of all their properties. Fortunately there are a variety of available ways to perform lamination which depends greatly on the materials and application. In bulk polymer laminate formation, co-extrusion is generally used by which two or more extruders are fed into a stacked die which is able to lay one film on top of the other. This is also possible with blow film, which will have a multi-inlet die allowing for multiple layers to be blown and formed into a single process.

More commonly however, lamination is better connected with the adhesive and coating industry. Lamination of this type makes uses of well-known techniques as Gravure, reverse roll, knife on roll and metering rod coating. All these techniques add a liquid coating onto a moving solid polymer film at a controlled thickness. In coating applications the applied material then goes through a curing process such as heat, UV radiation or atmospheric moisture. Alternatively when adhesion is being carried out a second surface is brought into contact with the coated film using nip rollers to press the laminate together. Following this process will be the appropriate curing process such as heat, UV radiation or moisture, however, the final curing mode is only possible when one (or both) of the films allow water permeation.

A simple lamination line set-up will consist of multiple stations such as: unwind, surface pre-treatment, adhesive or coating application, laminating nip rollers, curing and rewind. The unwind station introduces the base film into the line at a controlled speed while keeping the film under tension. The whole process is performed under tension to ensure contact with rollers and also to move the film along the line. The speed at which the process is performed and the tension the line is under will have an effect on the thickness of an adhesive or coating layers. When multi-layered laminates are being formed extra unwind stations will be positioned along the line to introduce the next component of the laminate.

Pre-treatment stations are used to activate or clean the surface before any adhesive or coating is applied to the base film. Commonly this can be simply an air blade to clean the interface or corona treatment if surface treatment is required due to the film being used having a low surface tension with poor wetting towards the adhesive. The coating

or adhesive application station introduces a liquid material onto one surface of the laminate by any of the previously mentioned techniques. Next the second film of the laminate will be placed onto the coated base roll, with the laminate material passing through a set of nip rollers to press the laminate together. Curing of the laminate is an essential process due to the need to develop an initial tack or green strength to ensure that slippage between the layers does not occur during rewind. The definition of green strength in this case is the ability of an adhesive to hold two surfaces together when brought into contact before developing its ultimate bond properties when fully cured. The rewind station drives the full process while helping keep it under tension and importantly collects the final laminate material.

1.13 Cellulose Triacetate

Of all the commercially available organic polyesters of cellulose, cellulose acetate is recognised as being the most important.[7] Cellulose acetate was discovered by T. Schützenberger in 1869 were it was discovered that reacting cellulose with acetic anhydride resulted in cellulose acetate formation. This was followed by its commercialisation in 1903 by Cross and Bevan. By 1924, Celanese, a United States based company commercially produced fibre, sheet, rod and tube forms of cellulose acetate. Finally cellulose triacetate was made commercially available by Tricel in 1954.[8] Cellulose triacetate can be used in applications such as semipermeable membrane in reverse osmosis or textiles, but in this report the application of this polymer in optical films is of more interest.[9,10] Interestingly it is a commonly known polymer used in film manufacture as it replaced cellulose nitrate (which has flammability issues) as the base material in photographic films. Photographic films require that the polymer used must possess the appropriate mechanical and optical properties such as transparency, curl recovery and low optical anisotropy.

To ensure that the polymer film has all these properties great care must be taken during its manufacture. Cellulose triacetate manufacture can be split into two common types: heterogeneous acetylation of which the fibrous process is the best known and homogeneous acetylation of which the solution process is the most common. During heterogeneous acetylation a diluent (commonly benzene or toluene) is added to the reaction medium of dry acetic anhydride in acetic acid with a small catalytic amount

of sulphuric or perchloric acid catayst.[11] For heterogeneous acetylation, the cellulose material retains most of its structure as it stays in a different state from the reaction medium. This method is commonly implemented when acetylating fibres or membranes as the strength and structure of the native cellulose is retained. During homogeneous acetylation, the reaction is carried out minus the diluent component and this allows the triacetate to solubilise in the reaction medium as it is produced during the reaction.[12] As the cellulose triacetate molecules are now becoming part of the reaction medium the overall structure undergoes major change.
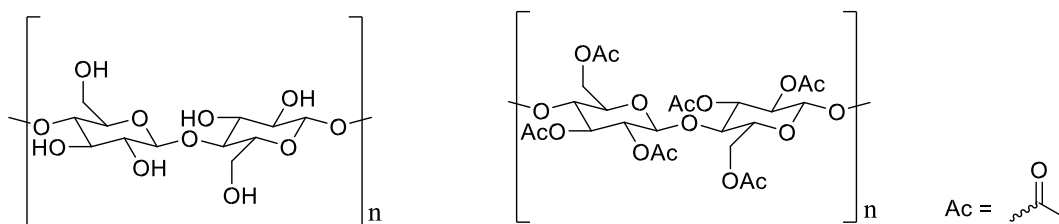
Figure 1.06: Structure of cellulose *left* and cellulose triacetate *right*.
Within both these reactions the mechanism by acetylation occurs is considered to be the same and follows erosion theory. Erosion theory is based on the biphasic morphology of cellulose (amorphous and crystalline phases). The proportion of these phases is inherent of the cellulose source and its manufacturing history. Erosion theory states that the more accessible amorphous phase of the cellulose are acetylated first, this allows the reaction medium access to the exterior face of the more organised and less penetrable crystalline phase. During heterogeneous acetylation these crystalline regions remain inaccessible and it is mainly the exterior surface of the crystalline phase that becomes acetylated. In homogeneous acetylation as the exterior face is functionalised it becomes part of the solution exposing a new crystalline surface for the reaction to take place.[12] It is this layer by layer erosion process that is believed to be the mechanism for the acetylation reaction. This mechanism makes it is possible to imagine that the isolated cores of unreacted cellulose can still be present in the material even when approaching the reactions completion. Currently erosion theory is still the most widely accepted tool for understanding bulk acetylation of cellulose. However, it is still short of explaining why factors such as accessibility and reactivity influence the overall acetylation process.

Cellulose triacetate is used in sunglasses manufacture due to it possessing a host of key properties required of an optical base film:

- High optical transparency in the visible region of the electromagnetic spectrum (400-700 nm),
- Solvent casting process for cellulose triacetate are well understood and the obtained films have the same refractive index in all direction (optically isotropic),
- The films obtained are strong, tough and hard while still being flexible which is advantageous when used in a sunglass lens,
- The physical properties and appearance of the film can be tuned using plasticisers and other additives,
- Cellulose triacetate films can be easily cut and reshaped into the desired lens shape. [13]

As previously mentioned, manufacturing a film from cellulose triacetate is a wellknown process. Solvent casting is the technique of choice, whereby a homogeneous polymer solution of cellulose triacetate and a plasticiser (plus any other additives) in dichloromethane is prepared. This solution is then filtered to ensure that any undissolved material is removed to reduce the opportunity of introducing optical defects into the film. Degassing of the solution then follows to remove any entrapped air bubbles which would be evolved into the film during casting. Casting is next performed by applying the homogeneous polymer solution onto a moving clean polished surface by means of a casting die (see section 1.103 for more information). As solvent begins to evaporate a polymer gel forms which requires further drying due to it containing entrapped solvent. This is possible by putting the film through a drying process to remove residual solvent. Once dry the film is collected by winding onto a roll. The collected film can then be trimmed or slit to the desired dimensions and is ready for use as a base film. It is possible at this point to further process the film e.g. lamination with another film or surface treatment to leave a functionalised active surface. Cellulose triacetate films cannot be obtained by melting processes as it degrades before ever reaching its melt temperature.[9]

1.14 Polycarbonate

Polycarbonates are a family of thermoplastics that have interesting properties such as high optical transparency, good heat resistance, high-impact strength, good rigidity and low moisture absorption. This class of polymer can be identified by the characteristic carbonate bond which is formed during polymerisation. Currently the polycarbonate of bisphenol-A is the most commonly used (see figure 1.07). Bisphenol-A polycarbonate was first commercially produced by Bayer over 50 years ago under the trade name "Makrolon".[14] As polycarbonates are thermoplastic materials they can be processed using conventional manufacturing techniques such as extrusion. The ease of processing means that they have found a number of varying applications such as; substituting glass in windows, safety glasses and various automotive parts. Synthesis of linear polycarbonates involves reacting a diol (normally aromatic) with a carbonic acid derivative e.g. bisphenol A and phosgene.[14]

The interfacial polycondensation between bisphenol-A (2,2-di(4-hydroxyphenyl)propane) and phosgene (carbonyl dichloride) is mostly carried out in a dichloromethane – water mixture. The reaction also contains sodium hydroxide to ensure the removal of the hydrogen chloride by-product. Alternatively the polycarbonates can be accessed by ester exchange between bisphenol-A and diphenyl carbonate.[15]
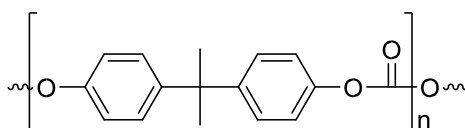
Figure 1.07: Structure of bisphenol-A polycarbonate.

From either method the polycarbonate obtained is an amorphous polymer that possesses the unique properties mention previously. Although polycarbonate has high impact strength, it has a relatively soft surface which limits its scratch resistance. In lens application where polycarbonate is positioned at the peripheral face a hard coat will be applied to protect this soft interface. Polycarbonate hard coatings are generally an inorganic/organic hybrid system (based on a metal hydroxide and an organosiloxane) which is processed using the sol-gel method.[16] Also during long term exposure to ultra-violet light, polycarbonate has a tendency to yellow and become brittle. Stabilisation of the polymer from photolysis by ultraviolet light can be

achieved using benzophenone derivatives such as 2hydroxybenzophenone or 2-hydroxybenzotriazoles.[15] As these molecules are highly conjugated they are able to retard degradation. This is possible as the benzophenone forms a quinoid structure upon exposure to ultra-violet radiation which is converted to heat as it returns to the original conjugated structure. Other common ultra-violet stabilisers used with polycarbonate also include acrylic and aryl esters, hindered amine, and metal salts.[14] Both ultra-violet stabilisation and hard coating are required whenever polycarbonate is a component within a lens structure.

1.15 Adhesion Promoters

A problem that is encountered in many manufacturing processes is incompatibility of materials and is often attributed to the difference in surface chemistries. The variety of available adhesives reflects that no one adhesive can cater for all possible applications. During lamination of novel multilayer polymer laminates, the initial problem that is encountered is selecting the correct kind of structural adhesive that best serves the application. Common types of structural adhesives used are epoxy, polyurethane, reactive acrylic, toughened acrylic, anaerobic acrylic and silicone based materials.[17] Knowledge of the underlying chemistry of each is essential as the properties obtained will be related to the functionality present. Adhesive interactions at the substrate-adhesive interface will also be governed by this chemistry.

Further explanation of the functionality of various adhesive types will be discussed in more detail in a later section (see section 1.30) and the properties that each brings. Discussed now will be the best methods for increasing the compatibility of surfaces towards adhesion by means of an adhesion promoter for polymers. The need for an adhesion promoter is to alter or change the surface to promote adhesion between the substrate and the adhesive. Common adhesion promoter processes for polymer films are either chemical or plasma treatments but other processes do exist.[18] Chemical treatments are aimed at changing the functional groups and morphology at the surface by performing a chemical reaction whereas; plasma treatments are aimed at introducing oxygen containing functionality to the surface.

1.151 Chemical Treatment

Chemical treatments are applied when the only option available is to create new functional groups on one or both surfaces to promote adhesion. This form of adhesion promoter induces a physical and chemical change to the surface of the polymer material which is permanent. Generally the reason such chemical treatments are performed is to improve the inherent poor polarity at the polymers interface which is a known shortfall of using polymer materials.[18] When the polarity is increased at the surface, the opportunity for intermolecular polar forces between the substrate and adhesive are increased which helps promote adhesion. If the correct functional groups are introduced covalent bonds between the substrate and adhesive or coating can be formed. Increased interface polarity will also help promote wetting of the surface towards any adhesive or coating.

Silanes are often used as adhesion promoters due to their diversity, compatibility and the excellent enhancement of adhesion they bring. Silanes of this type that are used to promote adhesion have the general formula R-Si(OR')$_3$.[19] An application where silanes are successfully used in promoting adhesion is with epoxy and polyurethane adhesives in bonding aluminium or mild steel substrates.[20] Another chemical surface treatment is chlorination of the surface which also serves to increase the surface polarity and adhesion. Beholz et al displayed successful chlorination of high density polyethylene using a solution containing sodium hypochlorite and acetic acid.[21] The chlorination treatment of the surface resulted in chlorine atoms being added to the surface (confirmed by x-ray photoelectron spectroscopy) which resulted in enhancement of the adhesion between the polymer and paint used in this application. Although such chemical treatments are effective they are often used as last option due to the generally environmentally unfriendly chemicals that are used. Nevertheless, they are effective adhesive promoters and are still used today.

1.152 Plasma Treatment

Plasma treatments are also a viable way to activate the interface to gain greater adhesion of materials. Treatments of this type are similar to chemical treatments as they promote polymer adhesion through surface functionalisation but with minimal morphological change. Plasma treatments serve as adhesion promoters as they increase the surface polarity by introducing oxygen containing functional groups

which increases both surface wetting and adhesion.[22] Alternatively they can simply remove surface contaminants to improve adhesion or allow for reorientation of existing functional groups making them available for bonding.

Plasma treatments are performed at low temperature and low gas pressure, where ionisation by glow discharge of a gaseous species is used to form ions, electrons, radicals and other excited molecular fragments. This process is performed in close proximity to the polymer surface which results in it becoming activated. When plasma modification is performed on polymers the most common gases used are air, argon, hydrogen, helium, oxygen, carbon dioxide, ammonia, fluorine and sulphur dioxide.[23] In some instances the previously mentioned gases are replaced by a gaseous organic monomer such as CH_4, C_2H_4, C_2H_6, C_2F_4 or C_2H_6 which is ionised using glow discharge. These ionised monomers can then be deposited onto the surface of the polymer substrate using plasma polymerisation leaving and activated surface. Materials that commonly receive plasma treatment to improve their adhesion characteristics are polyethylene and polypropylene.[24]

Petasch et al performed a plasma treatment initiated from microwaves on polyethylene, polypropylene and poly(ethylene terephthalate) polymer films using different plasma gas environments. The adhesion strength in an oxygen plasma treatment for polyethylene increased 20 fold in 6 seconds, for polypropylene 7 fold in 15 minutes and for poly(ethylene terephthalate) it increased 20% in 15 minutes. The bond strength increase for polyethylene and polypropylene was attributed to the introduction of hydroxyl, carboxyl, carbonyl and ester groups whereas in poly(ethylene terephthalate) was attributed to the ester groups already in the polymer becoming more available.[24] The main advantages of such plasma treatments are; the short time of treatment, the modified layer is limited to the very surface leaving the bulk unchanged and unlike most chemical process plasma treatment is environmentally friendly. The main drawbacks are the requirement for the process to be carried out at reduced pressure, developing reliable process parameters for the novel application can take many iterations and it is very difficult to control the proportion of functional species formed across the interface.[25]

1.153 Flame Treatment

Flame treatments are a useful technique for improving the surface polarity of polymers as they introduce new oxygen containing functional groups.[26,27] This makes it an essential technique for the surface treatment of polyolefin based materials that are inherently hydrophobic, thus problematic in polymer applications that require good surface wetting e.g. adhesion with inks, paints, adhesives or coatings.[23] Polymers that fall into this category are polyethylene, polypropylene and poly(ethylene terephthalate) with each of these materials being commonly used in the previously mentioned applications.

A real strength of flame treatments as an adhesion promotion technique is its ease of construction and operation as it essentially only requires a burner connected to a fuel source. The size or number of the burners required and their geometry is application dependent e.g. a plastic bottle formed through blow moulding will typically be treated using three burners. Three burners allow for uniform modification across the entire surface of the bottle, this is ensured by continuously rotating the bottle as it passes over the burners. The extent to which the bottle is flame treated depends on factors such as; the air to fuel mixture of the burners, flame temperature, flame contact time, the air-fuel gas flow time and the distance between the flame and polymer surface for treatment. Following treatment the now activated surface contains new oxygen containing polar groups such as hydroxyl, carboxyl and carbonyl. The mechanism by which the surface is oxidised follows a free radical degradation mechanism, with the radicals being produced in the flame and reacting with the polymer surface.[23,26] In polypropylene this occurs at the tertiary carbon on the chain and for polyethylene it occurs at random points along the polymer chain.[26] For polypropylene there are two main steps that contribute to the degradation mechanism; firstly the C-H bonds break along the polymer due to the high flame temperatures and secondly the insertion of oxygen based groups at these broken bond positions. The improved wettability and adhesion observed in polypropylene is attributed to the conversion of the pendent methyl group CH_3 into CH_2-OH.[28]

1.154 Corona Treatment
Corona treatment is one of the most commonly used methods for the surface treatment of polymers, especially in the packaging industry.[29] The name corona is used to

describe the phenomenon which occurs when a gas passes between two low energy electrodes which are operating at high frequency. Generally the treatment is carried out in air which normally acts as a good electrical insulator, however, when a strong enough field is applied the air begins to ionise (giving molecules in an excited state, ions and radicals) and conducts electricity.[29] When the gap between the two electrodes is clear a sudden electric discharge occurs which will develop into an arc or sparks between the electrodes. If however, a polymer film is placed between the electrodes the conductive path becomes interrupted and an arc is no longer observed and is now replaced with a diffuse glow. When performed at atmospheric pressure which is most common, the process is known as corona discharge treatment.

During corona discharge treatment, the surface of the polymer undergoes both physical and chemical changes which are treatment parameter and polymer dependent. Oxidation is the main mechanism of the chemical change observed during corona discharge treatment. Oxidation introduces new functional groups such as carboxyl, carbonyl and hydroxyl to the surface, with each helping to promote adhesion. The mechanism by which oxidation occurs is similar to flame treatment, being an oxygen radical can perform either hydrogen abstraction or chain scission followed by oxygen insertion as shown by Zhang et al and Kushner et al.[29,30] Both processes will generate two highly reactive species which rapidly react to yield a polymer with a functionalised oxidised surface layer.

Corona discharge treatment can also result in a molecular weight increase due to radical crosslinking reactions occurring. Whenever the cross-linking reaction is observed then the materials obtained displayed added strength and an increased melting point.[29] The possibility of cross-linking occurring becomes clear when the oxidation mechanism is again considered. During the corona process a peroxy radical can carry out two different processes: (1) polymer chain scission which results in the molecular weight falling or (2) chain addition which gives a molecular weight rise. It was reported that (1) is favoured during normal treatments (short treatment) times whereas (2) is favoured under more extreme conditions (e.g. >30 minutes at a high power).[31]

Physical surface changes can also be observed following corona discharge treatment of polymer films. During the corona process high energy excited species strike the films surface during treatment, which can form small micropits. These micropits are small indentations dug into the films surface following the collision with the excited species. Depending on the extent to which micropitting has occurred it can lead to either increased or decreased adhesion. Increased adhesion would be obtained when a lock and key type mechanism occurs or due to the increased surface area. Alternatively it can lead to a reduced contact area giving a reduced adhesion or the adhesion can be affected due to the number of pits resulting in stress concentration. To what extent the micropits or surface roughening affect the overall adhesion of the film can only be determined when the following factors are considered; the polymer being treated, the surface energy, the viscosity of the adhesive or coating being applied and the size/shape of the micropits. The roughing of the surface was also found to only occur when in conjunction with oxidation, making oxygen essential to the surface roughening effect.

Successful surface treatment of the material using corona discharge can only be ensured when the humidity is controlled.[30] When the humidity is high it generally means the surface moisture of the film will be high which results in a less effective treatment. To combat the rise in humidity a stronger treatment or longer treatment will be required to obtain the same adhesion enhancement results. This could possibly suggest that the presence of surface moisture could retard the initial hydrogen abstracting or that this initial abstraction process is an equilibrium process and reversible.[29] Overall corona discharge treatment is a robust and cheap process to use on polymer films (especially polyolefins) which makes it a widely used technique for adhesion promotion.

1.20 Adhesion

The word adhesion can be interpreted in a variety of ways; however, when describing a structural adhesive, it is used to describe the joining of two materials together that can oppose separation. Adhesion in this sense could also be used to describe such applications as; adding a protective polymer coating to protect a metal component, metal plating of a polymer film (metallisation) or the bonding of two films together to form a laminate.[32] In order to understand adhesion forces various mechanisms of

adhesion have been proposed and these will be discussed in the following section (see section 1.21). The modes by which an adhesion bond fails have also been investigated, also the force required to cause this failure is often called the magnitude (or strength) of adhesion (see section 1.22) and is measured using tensile testing methods.

Adhesion gets split into two different sub-sections: fundamental adhesion which accounts for the mechanism occurring at a molecular level and practical adhesion which is the measuring of actual test pieces to determine the joint/laminate strength.

Fundamental adhesion - refers to the combined forces (or energy) that each molecular interaction contributes to the overall adhesion. Mechanisms have been developed to interpret response of atomic and molecular forces at the bonding interface e.g. hydrogen bonding, chemical bonding, Van der Waals forces etc. To fully understand what possible modes of fundamental adhesion are occurring requires characterisation of the surface, this has led to the development of surface sensitive techniques such as secondary ion mass spectroscopy (SIMS) and X-ray photoelectron spectroscopy (XPS). Understanding the surface of each interface allows the chemist to determine which materials will be compatible and also which are incompatible (requires adhesion promotion see section 1.15).

Practical adhesion - once the laminate or coating has been formed the performance/strength requires testing. Information on the bond strength can be accessed through a variety of tests methods which allows access to a variety of parameters (e.g. from a peel test can obtain peel strength, modulus, mode of failure, trace of test piece performance etc). Essentially the need for practical adhesion testing is to characterise how strong the joint/laminate actually is. The value obtained from such testing will be depended on the testing parameters – dimension e.g. angle, peel speed, sample width/length etc. The value obtained will not only be a result of the interface adhesion but will also display the mechanical response of the adhesive and substrate materials. The performance can be evaluated by both the strength and mode of failure. The mode of failure will also give information on the compatibility of the materials in the joint/laminate (see section 1.22).

1.21 Adhesion Theories

Fundamental adhesion describes the processes occurring at the interface between two materials and must be considered whenever using an adhesive during lamination or joint formation. Maximising the number of interactions becomes possible when the mechanisms of atomic, molecular and mechanical adhesion are considered. These mechanisms have been developed to explain why some materials display high tensile strength during mechanical testing when other materials display low strengths. They also help to explain the need for surface promotion techniques and why selecting the correct adhesive type requires much investigation.

In the adhesion industry it is now accepted that when bonding materials together there are a variety of mechanisms occurring simultaneously. This does not imply that all the adhesion mechanisms occurring contribute equally to the strength and this makes understanding each mechanism important. Currently there are four principal theories used to explain adhesion of polymers: (1) mechanical (2) chemical (3) absorption and (4) diffusion.[33] Each of these principal mechanisms will be considered in turn and the main factors that explain their contribution to fundamental adhesion discussed.

1.211 Mechanical Theory

Of all the theories used to explain adhesion, mechanical theories are the oldest and most intuitive. Mechanical adhesion is explained as the physical interaction of the adhesive with surface roughness or pores. More commonly this type of adhesion is referred to as the "hook and eye" approach to bonding. The ability for a liquid adhesive to wet the surface or penetrate pores allows for a high surface area of contact between the substrate and adhesive. As the adhesive hardens during cure it hooks onto the surface and will resist separation through mechanical adhesion. This theory of adhesion can be used to explain the adhesion of roughened surfaces e.g. wood, textiles but did not explain adhesion to smooth surfaces. Following this observation is was agreed that adhesion does not occur via one mechanism but in fact by a combination of mechanisms.[34] Nevertheless the phenomenon of mechanical adhesion does contribute to the overall adhesion in a number of systems and is still a valid mechanism.

Presently mechanical interlocking is considered significant on both the macro and micro scale. Early work on the mechanical theory was on the macro scale using composite materials such as textile cords that were embedded in a rubber composite in car tyres. The macro scale interaction of the natural fibres with the rubber is small unless the fibre end was embedded within the rubber matrix.[34] The strength obtained from the composite material is solely based on the number and depth of natural fibres that penetrated into the rubber matrix.[35] Also macro scale interlocking is found in the adhesion of leather which is important to the foot industry. To successfully form the leather-to-adhesive bond it is essential that fibres penetrate the adhesive layer. A strong bond will result via mechanically interlocking between both materials once the adhesive has cured.

More recently due to the advancements in microscopy, smaller scale examples of mechanical adhesion have been observed. Work by Packham on the bonding of molten polyethylene to aluminium is a well know example of micro scale mechanical interlocking adhesion.[36] This work explored the effects that different treatment of aluminium had on the adhesion to polyethylene. The major finding by Packham was the size and shape of pores formed during the anodizing of aluminium within an acidic electrolyte had a direct effect on the adhesion. These pores are introduced during the build-up of an oxide layer on the aluminium surface during the anodizing treatment. Electron microscopy of a polyethylene surface that had been in contact with the treated aluminium displayed clusters of whiskers that had been embedded within the oxide pores. He explained the improved adhesion was the result of the micro scale mechanical interlocking. It is clear mechanical interlocking can have a significant effect on the overall adhesion process but it will not be the only mechanism of adhesion occurring.

1.212 Adsorption Theory

Interactions that occur between the adhesive and substrate such as Van der Waals are the basis to which adsorption theory is constructed. This theory does not account for primary bonds such as covalent, ionic and metallic (see section 1.213 chemical theories) which are much stronger than the secondary bonding of dispersion (London), induction (Debye) and orientation (Keesom) forces used in this theory. Van der Waals

forces play a key part in explaining phenomena related to interaction between the substrate and adhesion in processes such as wetting or spreading of the surface. A better understanding of secondary forces can be obtained from materials in the solid or liquid phase as the molecules have intimate contact with one another. Methane at room temperature is a gas however, at -182°C it is a solid held together by dipole interactions.[37] Orientation of the molecules to maximise attractive forces through dipole interactions is an essential process of absorption theory. Van der Waals bonding interactions are a collection of dispersion, orientation and induction forces which will now be covered in turn.

Dispersion or London dispersion forces (more appropriate when discussing adhesion) is the theory used to describe that neutral symmetrical molecules such as hydrogen or argon also display attractive adhesion forces. Inherently neutral molecules such as argon will not possess dipole – dipole interactions or dipole – molecule interactions however, as these molecules can be collected as a liquid or a solid there must be some form of attractive force present. This situation was initially developed in the 1930s by F. London when working on molecular interactions.[38] A molecule that is neutral will have on average a symmetrical electron distribution. If the electron distribution was considered at a single instance however, the likelihood of having a symmetrical distribution of electron density is unlikely as the electrons will have a definite distribution and a dipole moment.[38] This short lived dipole moment can then induce a dipole moment onto an adjacent molecule. As there will be a difference in charge between these two molecules there will be a net force of attraction. The dispersion force is the force of attraction that results from averaging all the possible instantaneous configurations that the electrons within the first molecule can occupy. London dispersion forces are universal and exist in all situations where molecules come into intimate contact on a molecular level. Secondary interactions of this sort are weak compared to covalent bonds e.g. $5 - 50$ kJ mol^{-1} for dispersion forces compared to $60 - 700$ kJ mol^{-1} for covalent bonds but it is the high number of possible interaction that make dispersion forces a key part of Van der Waal forces and adsorption theory.[39] In polyurethane chemistry hydrogen bond strengths can vary from 24 kJ mol^{-1} for phase mixing interactions (urethane N-H with ether oxygen) to 47 kJ mol^{-1} in phase separation interactions (urethane N-H with urethane carbonyl).

Dipole – dipole interactions or Keesom orientation forces also play a part in explaining adsorption theory.[40] Firstly a molecule will possess a permanent dipole when there is a noticeable difference in electronegativity of the bond and the electron density distribution is not symmetrical. As a consequence in a simple covalently bonded molecule one end will possess a net positive charge, with the other a net negative charge, even though the overall molecule will be electrically neutral. Molecules that have dipole moments will therefore be able to interact with one another when sufficiently close. If ample movement is available then alignment or orientation of molecules to maximise attractive forces will occur. This process is known as the Keesom orientation force after W. H. Keesom who investigated dipole – dipole interactions.[40] Permanent dipole – dipole interactions of this type will have bond energies in the range of $4 - 20$ kJ mol^{-1}.[39]

Like in dispersion interactions whereby a neutral molecule can interact with another neutral molecule through a small difference in electron density, molecules that possess a dipole can also interact with neutral molecules through a similar process.[40] The molecule that possesses a dipole moment will be able to induce a dipole moment to the neutral molecule by polarisation of its electric field. This process is known as the inductive effect or Debye induction after P. Debye who worked extensively within this field. Bond energies of such dipole – induce dipole interaction are considered weak with values usually less than 2 kJ mol^{-1}.[39]

London, Debye and Keesom interactions are grouped together under Van der Waals interactions when discussing adsorption theory as they all occur together. The total contribution of the adsorption component is often assumed to be the summation of all the individual dispersion, induction and orientation interaction energies. Ideally charges would like to align head to tail as this maximises attractive forces and minimises repulsive forces (see figure 1.08).
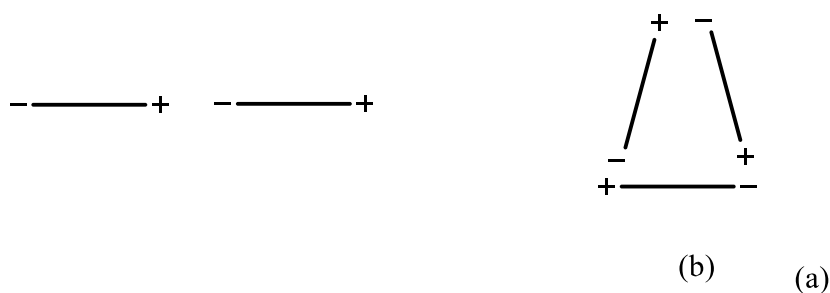
(b)   (a)

Figure 1.08: Dipole – dipole lowest energy configurations (a) two isolated dipoles with head to tail orientation and (b) three dipoles with a more complex structure.

It is unlikely that such pairwise alignment would occur in the condensed phase for a liquid or solid and consequently more complex structures will result. This makes full interpretation of the adsorption mechanism between an adhesive and substrate complex as the attractive forces that result will be influenced by environment, chemical functionality, morphology etc. however, adsorption theory is still extensively used to help explain overall adhesion.

1.213 Chemical Theory

Chemical theories are based upon the formation of chemical bonds between the adhesive and substrate which can be covalent, ionic or metallic bonds along with hydrogen bonding and acid-base interactions. As polymer adhesion is of interest the only possible bonds will be covalent in nature and form after the reaction of the adhesive with active groups at the interface. In polymer adhesion forming primary interactions such as covalent bonds between the adhesive and the substrate presents an attractive route of adhesion as chemical bonds form joining both materials as shown in figure 1.09. Covalent bonds have bond energies in the range $60 - 700$ kJ mol^{-1} which is around $10 - 20$ times stronger than Van der Waals interactions.[39] The ability to exploit this mode of bonding will depend on the molecular weight of the adhesive as the number of reactive end groups will depend on the weight and functionality, adhesives ability to wet the substrate surface, substrates interface having compatible functionality and correct curing conditions.

Covalent bond formation as the adhesive cures will create chemical links between the adhesive and the interface. Adhesion of this type is strong as covalent bonds will need to be cleaved before the bond will fail at the interface. If a higher molecular weight polymer is used, the number of free reactive end groups is reduced which limits the potential for covalent bonding. This occurs as most reactive groups are consumed in matrix formation which reduces the number available for reaction with the interface. When such a situation is presented another mode of physical bonding can be exploited which is to maximise hydrogen bonding.
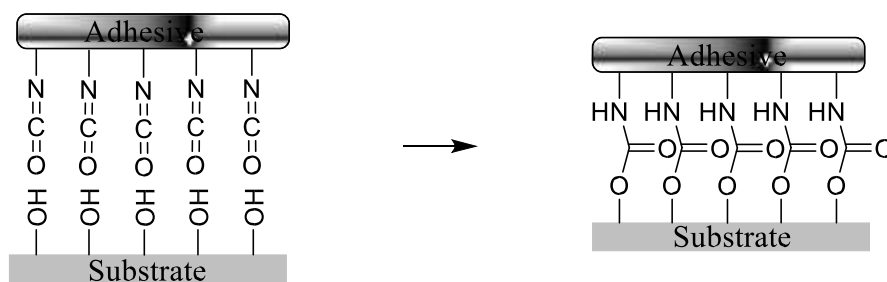
Figure 1.09: Schematic of covalent bond formation between reactive isocyanate groups of adhesive and hydroxyl groups at the substrate interface.

Hydrogen bonding is a strong interaction that occurs between a hydrogen donor atom that possesses a net positive charge due to being bonded to a more electronegative atoms e.g. oxygen or nitrogen that is stabilised by an electronegative atom that is in close proximity. Hydrogen bonding can be found in the dimerization of organic carboxylic acids, however, it is also found in polymers and gives cellulose its crystalline domains as well as giving nylon its high strength (see figure 1.10). Typical hydrogen bonds have energies of around $40 - 50$ kJ mol^{-1}, which positions them between Van der Waals and covalent bonds.[41] Engineering the adhesive formulation to maximise hydrogen bonding can help obtain high bond strength with certain polymer substrates.

In an adhesion situation where a liquid comes into intimate contact with a solid there are three possible types of hydrogen bonding;

- Functional groups such as ester, ketones, ethers or aromatic ring can act as proton acceptor in polymers such as poly(methyl methacrylate), polystyrene, polycarbonate,
- Partially hydrogenated polymer such as poly(vinyl chloride) or chlorinated polyolefins can act as proton donors
- Functional groups can be both a proton donor and acceptor, this is observed in polymers such as polyamides (nylons), poly(vinyl alcohols) and polyurethanes.
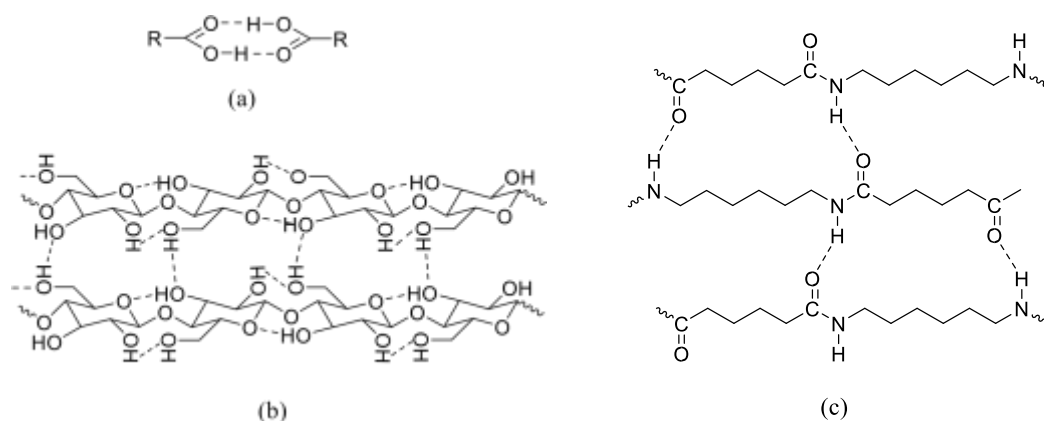
Figure 1.10: Hydrogen bonding can occur in small molecule such as (a) carboxylic acids or within polymers like (b) cellulose and (c) nylon 6,6.[42] Hydrogen bonding can increase the bond strength in some adhesive application however; it will not be the sole mechanism relied on for adhesion due to its susceptibility to water ingress which can plasticise the interface of the substrate resulting in a weak boundary layer and subsequent bond failure.[43] Acid – base interactions are another key theory that falls into the chemical category of adhesion. Interactions of this type are based upon the Lewis and Brønsted theories of acids and bases.[33]

An acid will classically be defined as a molecule or compound containing a hydrogen atom that may be replaced by a metal resulting in a salt compound being formed. This simple explanation of an acid material specifies that an acid will donate a hydrogen atom or proton and this will define a base as a compound that accepts a proton (historically this associated a base with hydroxyl groups). When discussing adhesion, this simple acid – base chemistry is not very useful for understanding what processes are occurring as these reaction are of small molecules in solution.[44]

Extending acid – base chemistry to Brønsted's interpretation a greater understanding of how such interactions can occur in adhesion becomes clearer. Brønsted defined an acid as a compound that was able to donate a proton and a base as a compound that could accept a proton.[44]   Applying Brønsted's theory to the reaction of acetic acid (acid) and water (conjugate base) the products are hydronium and an acetate ion which are the conjugate acid and base respectively. As the CH^3COO^- ion would not be commonly regarded to as a base, Brønsted was able to through his theory free the hydroxyl ion as being associated with the only type of base compound (see scheme

1.1).[44] This reclassification of the theory still gets used today as it allows adhesion phenomena to be better explained using acid – base interactions.

$$CH_3COOH \quad + \quad H_2O \quad \rightleftharpoons \quad H_3O^+ \quad + \quad CH_3COO^- \qquad [\text{Scheme 1.1}]$$

Acid		Conjugate Base		Conjugate Acid	Base
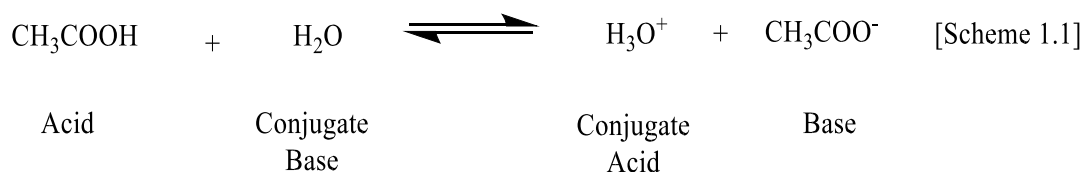
Lewis expanded acid – base theory and his addition is commonly used in the explanation of interactions occurring in adhesion based applications. Lewis changed the definition of an acid to a compound that can accept an electron pair, making a base a compound that can donate an electron pair. This expansion of acid – base theory by Lewis redefined an acid by freeing the concept of acidity beyond a species that contains hydrogen.[44] Considering a common acid – base reaction e.g. the reaction of H^+ with OH^- to give H_2O, Lewis theory can still be applied (see scheme 1.2). The basic OH^- or nucleophile donates a non-bonding pair of electrons to the acidic or electrophilic H^+. Lewis theory commonly is used to explain the adhesion seen between metal surfaces and polymer adhesives through electron donation (see scheme 1.3).

$$H^+ \quad + \quad OH^- \quad \rightleftharpoons \quad H_2O \qquad\qquad [\text{Scheme 1.2}]$$

[Scheme 1.3]

Acceptor   Donor
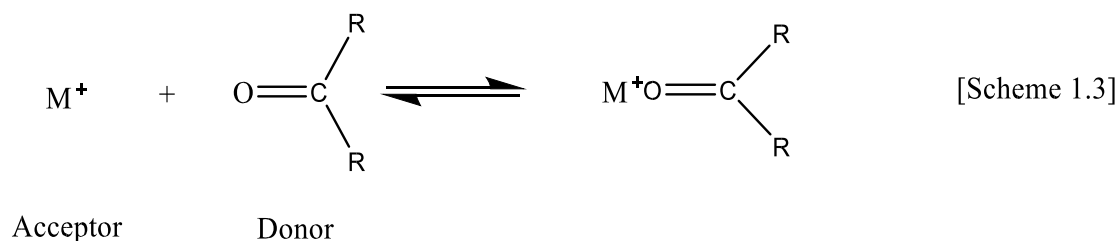
M^+ = Metal Cation

Considering all the kinds of possible chemical bonding theories it is possible to see that a number of mechanisms can be occurring simultaneously. This makes it difficult to deconvolute the exact contribution that each kind of chemical bonding is responsible for within the overall strength. Nevertheless, a good understanding of chemical

theories will help with the prediction of substrate – adhesive compatibility, possible mechanisms of bonding and the wetting behaviour that will be encountered.

1.214 Diffusion Theory

The final theory of adhesion that is commonly encountered comes under the label diffusion theory. This theory is based on when two polymer films come into intimate contact with one another it is possible for the migration of chain ends across the interface resulting in the polymers adhering.

Early work developing this theory of adhesion was carried out by Russian workers including Voyutski and they were able to demonstrate good agreement between theoretical predictions and experimental work.[45]   Within this study they analysed unvulcanised rubber and investigated its auto-adhesion properties (auto-adhesion = adhesion between two films of the same material). From this work they suggested that long parts of the polymer chain were able to interpenetrate across the interface and after sufficient time the two parts appear to hold together as one. For such molecular motion to be feasible there must be a considerable amount of motion, little to no cross-linking and for the materials to be well above their glass transition temperatures. The glass transition temperature is a primary thermal event which displays where a polymeric material goes from hard and glassy to soft and rubbery. Figure 1.11 displays a schematic representation of the diffusion of polymer chain across the interface which results in disappearance of the interface as the polymer chains become more entangled.
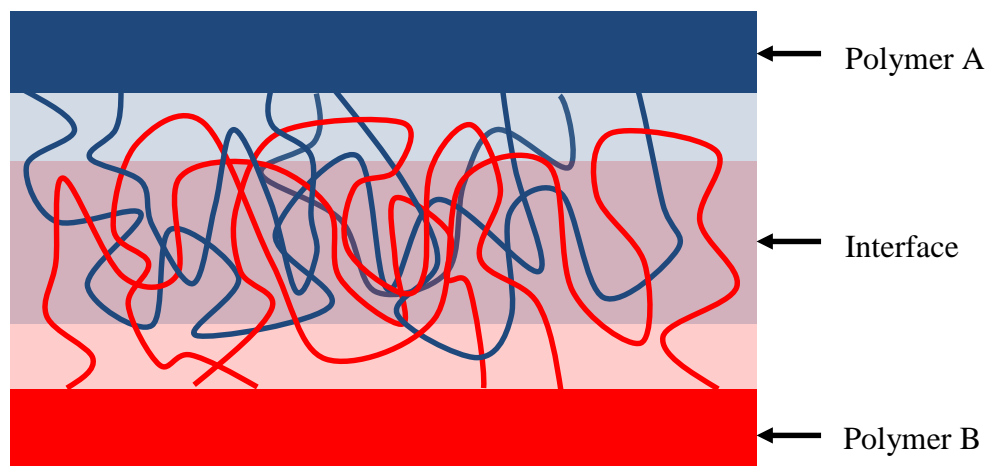
Figure 1.11:   Polymer diffusion between two amorphous polymers leading to chain entanglement and adhesion.

Since this early work, this theory has been expanded through the use of modelling which aids with understanding and interpreting the polymer diffusion processes occurring. Vaesin et al extended diffusion theory by mathematically modelling the force required to separate two different polymer surfaces.[45] The mathematics involved in developing this model are out with the scope of this thesis but it was identified that the force was dependent on factors such as: rate of separation, contact time of the polymers and molecular weight of the polymers. This early model was clarified by experimental work which involved developing a relationship between contact time and adhesive strength of nitrile rubber with natural rubber. A further study which involved peel testing of different molecular weight polyisobutylenes from cellophane was further clarification of the model.[25]

More recently diffusion of polymers has been the subject of further modelling. These models are based on the time taken for diffusion to occur between two amorphous polymers above their glass transition temperature. Modelling of polymer diffusion theory is built around Brownian motion of molecules and this splits the rate of diffusion into five different time regions. These regions are sorted by order of increasing relaxation time starting with individual chain segment short-range Fickian diffusion, Rouse relaxation of chain entanglements, full chain undergoing Rouse relaxation, reptation diffusion or chain creep and finally long-range Fickian diffusion.[46] The detailed discussion of the time scales for each process is out with the scope this report however, from this short discussion it is possible to deduce that modelling of diffusion processes is rather complex.

To better understand results obtained experimentally which can either have low or high interface strengths two models have been developed. The nail solution model is used for weak interface diffusion where interpenetration is low and failure is mostly due to the removal of chain ends across the interface.[47] This model is constructed around two polymers being held together by interpenetration molecular chain ends. By summing both the number and depth of chain ends that cross the interface it is possible to calculate what is force required to overcome the adhesion per unit length of chain end. When interpenetration become greater and the interface cannot easily be distinguished, the vector percolation theory model is applied. Due to high levels of chain diffusion,

the interface will populate a larger volume compared to the nail model, making its capacity towards energy dissipation greater and therefore more resistant to rupture. Accordingly the model must calculate the depth of interpenetration from one substrate to the other but must also account for polymer chains that have passed across the interface multiple times. Consequently to separate the substrate materials both bond rupture and disentanglement are required.

Furthermore, vector percolation theory also needs to account for the breakdown process that can occur in three-dimensions. This model factors in the possible modes of chain entanglement and accounts for the increasing matrix like characteristics that the interface contains.

In applications where diffusion is present it will be a contributing factor to the overall adhesion along with other adhesion mechanisms e.g. mechanical, chemical, adsorption etc. Recently due to advancements in computing technology, experimental and computational results for processes like diffusion and interpenetration are now becoming more consistent. Surface sensitive techniques such as secondary ion mass spectroscopy and X-ray photoelectron spectroscopy have made it now possible to directly observe polymer diffusion.[48]

1.22 Adhesion Failure Modes

Understanding the possible ways in which an adhesive can fail will assist in the determination of a product's lifetime. The application, in which the adhesive is used, coupled with the substrate type and their orientation, will strongly influence the mode of failure. These parameters will also influence the methods that can be used to determine the mode of failure. During tensile testing for example the minimum strength required to cause a failure can be obtained.

It is well known adhesive failures within a product commonly results from long term exposure to sources of humidity such as water submersions of joints and this makes understanding both the failure along with the joints lifetime essential.[49] As mentioned, the application in which the adhesive is required to serve will dictate the type of adhesive used. This will be combined with the type of substrate, adhesion promotion and possible joint protection method. The modes of failure that can occur in such a joint can be in a number of places as a result:

- cohesive failure of the substrate
- adhesive failure at the substrate – adhesive interface
- cohesively within the adhesive
- adhesive failure at the substrate – adhesion promoter interface
- cohesive failure within the substrate – adhesion promoter layer
- adhesive failure between the adhesion promoter and primer
- cohesive failure within the primer
- Commonly the mode of failure obtained can be a mixture of one or more of the above modes.[50] By successfully identifying the origin of the failure it is possible to determine the weakest component of the system which assists in the prediction of where subsequent failures are most likely to occur. Gaining this information can assist with the diagnosis of future failures along with solutions to help perturb or remove the failure altogether.
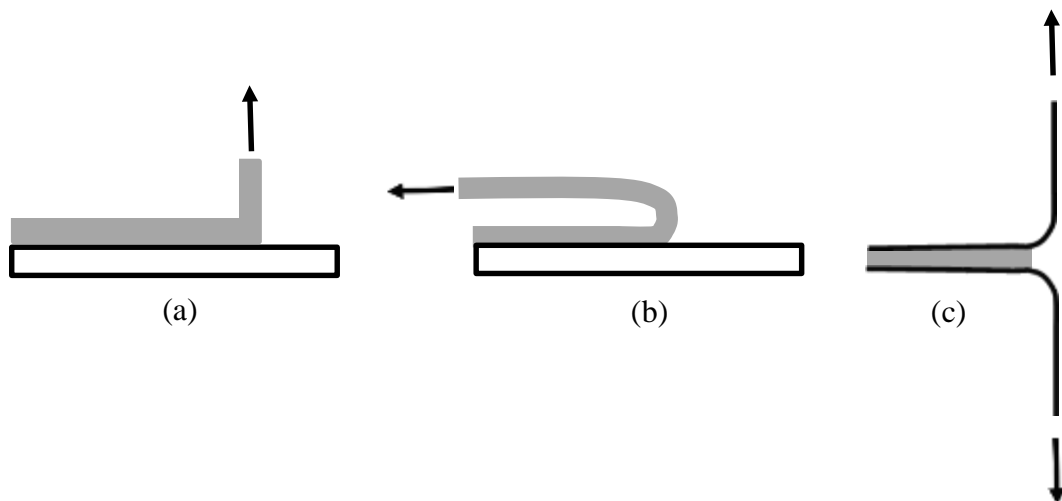
Figure 1.12: Peel testing arrangements commonly used. (a) 90° peel, (b) 180° peel and (c) 180° T-peel.[51]

Gaining such information is possible by either waiting on a failure occurring or more commonly by testing of the system using mechanical techniques. For adhesive applications, the most common method of testing are peel based. A peel test determines the energy/force required in removing or peeling a flexible material from a substrate with the de-bonding force recorded giving a measure of the adhesion

strength.[51] Commonly peel testing is performed in adhesive applications where the substrate is ridged and the adhesive is peeled off at a defined angle (see figure 1.12 (a) and (b)). Unfortunately not all applications have a ridged substrate meaning that another test is required namely a 180° T-peel test to measure the adhesion strength (see figure 1.12 (c)). Within both these tests, the strength is calculated based on the force per unit width making it essential to have the test piece standardised to ensure repeatability. The test procedure also has to be standardised as changes in the peel rate will also affect the results obtained.

In peel testing a profile or trace of the full test is obtained that is commonly plotted as peel force (N) versus extension (mm). Following the production of a stable crack (crack initiation data from start of the test often discarded), the average peel strength can be calculated along with the deviation, mean and any systematic variations can be easily observed.[51] The peel strength as a result can be calculated using the following formula:

$$P = \frac{F}{w}(\lambda - \cos \omega) - W_\lambda t \qquad \text{Equation 1.1}$$

P = peel strength in N mm^{-1}, F = force in N, w = sample width in mm, λ = extension ratio (extended length/original length), ω = peel angle, W_λ = strain-energy for extension λ and t is sample thickness.[51]

(a)

(b)

(c)

(d)
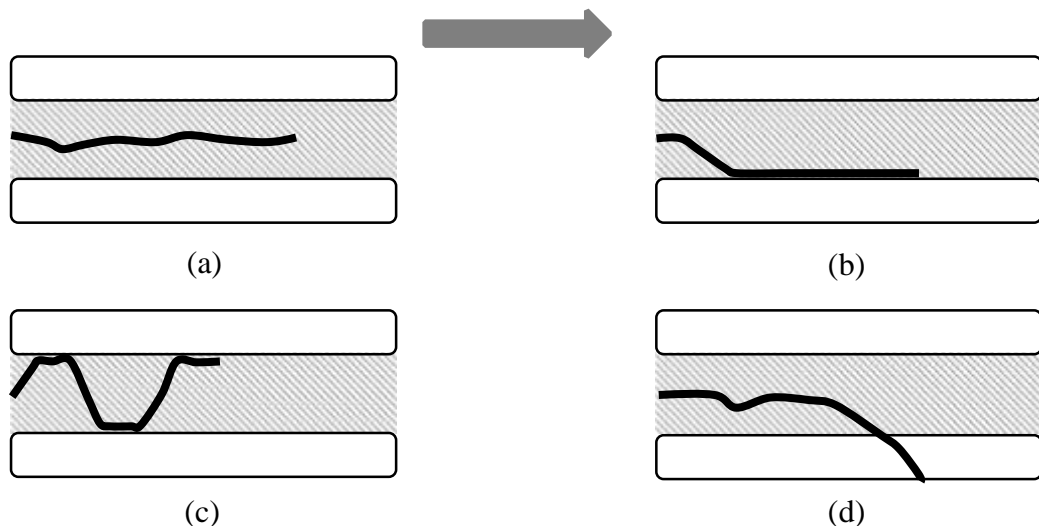
Figure 1.13: Common modes of failure encountered during 180° T-peel testing of plastics. (a) Cohesive within adhesive, (b) adhesive at the interface, (c) jumping

adhesive failure and (d) cohesive substrate failure (grey arrow indicates direction that crack is traveling).[53]

Depending on the experimental conditions selected equation 1.1 can be further simplified. If the peel extension is considered negligible (very common) it results in λ being equal to 1 and W_λ bring equal to 0. For peel angles of 90° and 180° equation 1.1 is simplified to:

$$P_{\pi 2} = \frac{F}{w}$$ Equation 1.2

$$P_{\pi} = \frac{2E}{w}$$ Equation 1.3

Where $\pi/2$ is a peel angle of 90° and π is a peel angle of 180°.[52]

Calculation of the peel strength using the above formula can then be reported combined with the mode of failure which is obtained from inspection of the test piece. Four common modes of failure encountered when peel testing plastic substrates are: cohesive within the adhesive, adhesive at the interface, jumping adhesive failure and cohesive failure of the substrate as shown in figure 1.13. In an ideal material which is homogeneous, the crack formed during the peel test will propagate perpendicular to the direction of the largest stress. When the weakest component within the joint/laminate is the adhesive layer itself, the crack will remain in this layer throughout the test resulting in a cohesive failure of the adhesive (figure 1.13 (a)). Adhesive failures identify that the adhesive-substrate interface is the weakest component within the joint. In adhesive failures of this type, the crack will start cohesively within the adhesive but will migrate to one interface and follow that interface for the remainder of the test as shown in figure 1.13 (b).

If an oscillating shear is used the adhesive failure can jump from one interface to interface the other however, this is also possible when two different substrates or two different thicknesses of substrate are used. Finally if the adhesion strength is high, a cohesive failure of the substrate can occur. Failures of this type display that the adhesive matrix does not compromise the joint strength as the adhesive has a greater matrix strength than the substrate.

From the mode of failure and the strength obtained, the practically of the adhesive joint can be evaluated for the proposed application. The mode of failure obtained is the result of complex interactions between the adhesive with the interface which are inherent of the stresses and energy within the adhesive layer. It is the balance between these parameters which dictates where the joint will de-bond or fail. In some cases the failure will simply initiate and propagate within the weakest region of the joint e.g. at the interface. However, in many cases residual stresses within the adhesive layer will drive de-bonding along a certain path which does not correspond to the weakest component. Caution must be advised when interpreting data collected as when the experimental set-up is not optimised for the application invalid data will be obtained. Nevertheless adhesion failure modes are still very informative and must be considered in any application in which an adhesive is present.

1.30 Adhesives

An adhesive is defined as a material that can bond two substrates together and then be able to resist separation. When selecting an adhesive for any application it is essential to consider some vital parameters to ensure it is fit for purpose such as the adhesive chemistry, the curing chemistry, the compatibility with the interface(s), if incompatible then available surface treatments, the delivery method for the adhesive, the manufacturing demands of using such a material, the testing parameters for the purpose and the aesthetics.[17] The level of priority that each of these parameters is given will differ from application to application but are useful for narrowing down the choice of adhesive. In order to understand what possible adhesives are applicable for the proposed application the chemistry of the system must first be considered.

Generally the adhesive is named after the kind of chemical functional group present or formed e.g. epoxy, acrylic, polyurethane, silicone. An epoxy adhesive gets its name from the epoxy ring present in one of the starting materials whereas polyurethane adhesives are named after the group formed during cure. Within this report the material of choice must be readily used in lamination, the adhesive of selected must be structural in nature to ensure that the adhesive will contribute to the laminate strength. Some typical structural adhesives will be discussed and their suitability for use within a lens laminate considered.

1.31 Epoxy Adhesives

Within the adhesive industry and more specifically the structural adhesive industry, epoxy based adhesives are the most widely used.[54] Epoxy adhesives are classified by the presence of free three-membered epoxy or oxirane ring(s) (two carbon atoms with a single bridging oxygen atom) within the formulation, these groups are commonly positioned at the terminus of the molecule. They are extremely versatile materials from a formulation view point and this has contributed to the large availability of varying types of epoxy based adhesives. The large variety of epoxy resin molecules, combined with the a large number of available curing chemistries means that an epoxy adhesive can be formulated to meet specific demands e.g. shelf life, cure time, cure temperature, shrinkage, resistance, toughness etc.[54] The variety of available starting materials means epoxy adhesives can service an extensive range of components. Often epoxy adhesives are used when bonding two materials of varying composition together; this can often be difficult as each adherent will present a different kind of surface chemistry.

1.311 Unmodified Epoxy Adhesives

Substrates that are often bonded with epoxy adhesives include; aluminium (plus alloys of aluminium), titanium alloys, carbon steels, nickel, copper, fibre reinforced plastics (both thermoplastic and thermoset), glass and wood.[54]

(a)

(b)

(c)

(d)

(e)
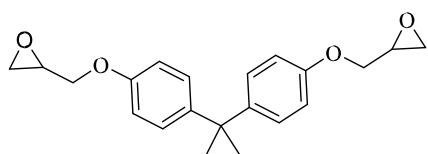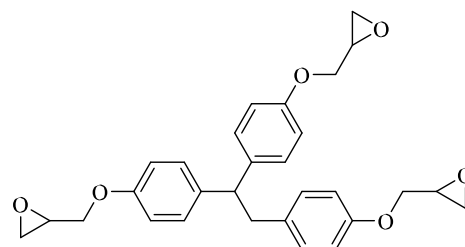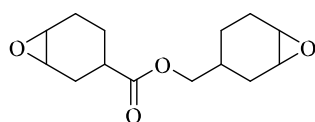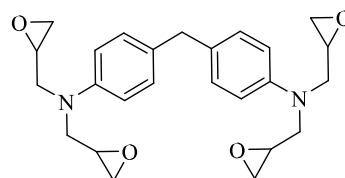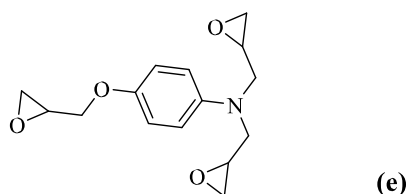
Figure 1.14: Common commercially available epoxy resins (a) diglycidylether of bisphenol A, (b) Huntsman's Tactix 742, (c) Huntsman's Araldite CY 179, (d) Huntsman's Araldite MY 721 and (e) Huntsman's Araldite MY0515.[54]

Industries that exploit this flexibility are automotive, aerospace, construction, electrical, abrasives, furniture and consumer. Common epoxy adhesive resin materials (see figure 1.14) are liquids or semi-solid and they require reaction with a hardener or curing agent before they can set into a solid adhesive. When the correct curing chemistry and conditions are applied then a cross-linked solid material will be produced. Early epoxy adhesives which are now referred to as unmodified epoxies were simple formulations containing only epoxy resin and hardener, this mixture when cured was of high tensile strength but was also inherently brittle and possessed poor peel behaviour.
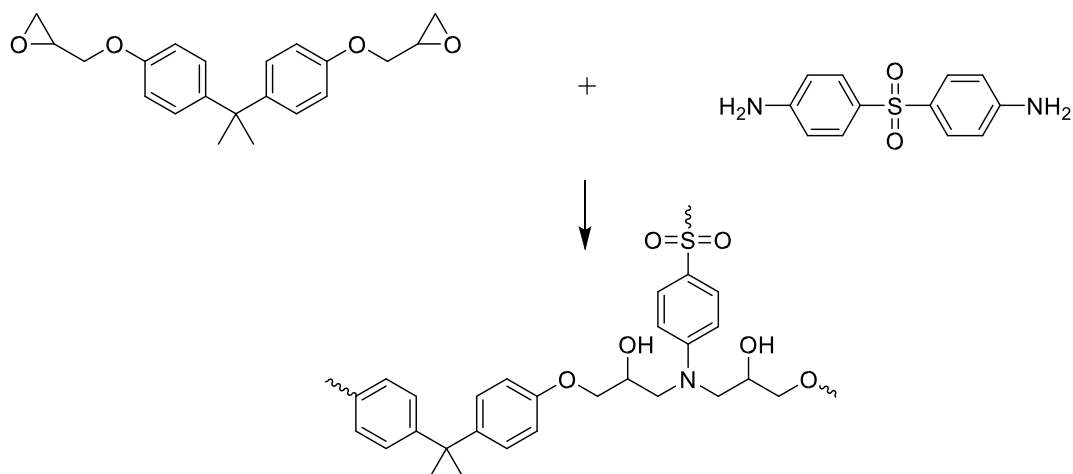
Figure 1.15: Epoxy curing reaction between bisphenol-A epoxy resin and 4,4'sulfonyldianiline.[54]

The ring opening process of the oxirane structure which leads to the cure of an epoxy adhesive is achieved in the presence of a hardening agent that has active hydrogen. The active hydrogen can be aliphatic or aromatic in nature and most commonly will be within an amine or hydroxyl functional group, but it may also be within tertiary amines, imidazoles, BF_3 complexes and antimony fluoride complexes.[54] When an

amine with more than two active hydrogens and a di-terminated epoxy resin are used the addition reaction will lead to a cross linked structure. Figure 1.15 displays the addition reaction between the epoxy resin of bisphenol-A and 4,4'-sulfonyldianiline. Active hydrogens of the amine will ring open the epoxy leaving a free secondary NH. Once all primary N-H hydrogens have been consumed, secondary N-H groups will start to react which leads to cross-linking within the matrix. When two epoxy groups have consumed both the primary and secondary N-H (figure 1.15), further cross-linking via the active hydrogen of the hydroxyl group can occur. Further methods for curing of an epoxy adhesive are available but they will not be detailed within this report.

1.312 Toughened Epoxy Adhesives

Today's epoxy formulations are normally termed as toughened adhesives and this refers to the enhanced impact resistance that they possess when compared to unmodified epoxies. Toughened epoxies where first developed in the 1960's when it was discovered that the addition of a reactive liquid polymer resulted in a distinct improvement in the cured epoxies toughness. This discovery led to the formulation of adhesives that had both better physical and mechanical properties in both the uncured or cured state. Initially the introduction of high molecular weight polymers such as phenoxy resins, polyvinyl acetal resins and polyamides were used as the secondary phase as they introduce greater flexibility into the final cured material. A secondary phase is an immiscible material that phase separates from resin upon cure. The net result was an observed improvement in peel character and tensile strength but this was offset by a poorer high temperature performance.

Most recent attempts at improving the epoxy adhesive strength stems from work carried out on high impact polystyrene chemistry. It was observed that when a discrete amount of a solid secondary phase was dispersed through a polystyrene matrix, the result was a high impact material. This was applied to epoxy adhesives using three main strategies: reactive liquid polymers, reactive elastomers and thermoplastic modifiers.[55]

Reactive liquid polymers: Liquid rubbers such as acrylonitrile-butadiene copolymers or long chained polyether's are effective additives for improving the cured materials

toughness of epoxy adhesives.[56] In order to gain the increased toughness a prereaction step is required by which the epoxy resin or hardener material is reacted with the active end groups of the reactive liquid polymer.[55]
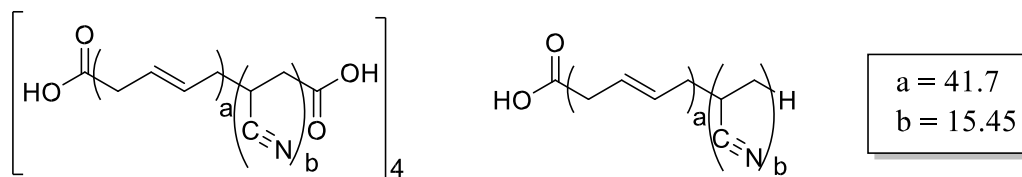
Hycar CTBN 1300X13
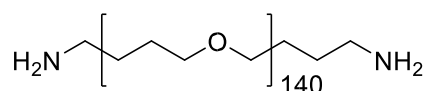
Dynamar HC-1101

Figure 1.16: Pre-reacted acrylonitrile-butadiene rubber commercially available from Noveon *top* and pre-reacted amine hardener commercially available from Dyneon LLC *bottom*.[55]

Polymers used for this process will have molecular weights that range from 3000 – 10,000 and are often either carboxylic acid or hydroxyl terminated for the acrylonitrile-butadiene rubbers with the hardeners being amine terminated.

Reactive elastomers: Unlike the reactive liquid polymers the reactive elastomer polymers are solids and have higher molecular weights of 200,000 to 300,000.[55] Like the reactive liquid polymers they require pre-reaction with the epoxy resin to ensure that the final cured material has an increased toughness. Most available hardeners of this type can be dissolved into the epoxy before pre-reaction or added in an appropriate solvent which can be recovered later. The solvent free approach however, is generally the preferred option as it removes the need for solvent recovery.

Thermoplastic modifiers: The previous examples of secondary phase toughening agents (reactive liquid polymers and reactive elastomers) required pre-reacting with the epoxy resin to observe any property enhancement, for thermoplastic modifiers this is not the case. The thermoplastic modifier is generally dissolved into the epoxy resin using either a solvent or simply by taking the thermoplastic above its melt temperature.

Some thermoplastics that are readily used for such modification are shown in figure 1.18.
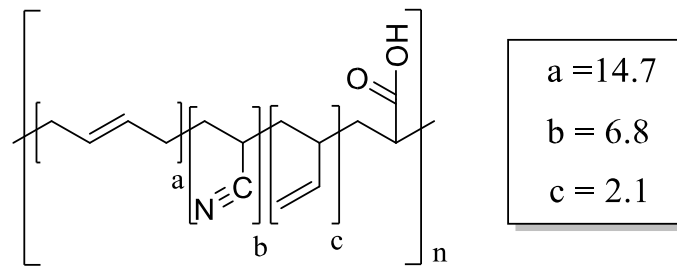
Figure 1.17: A typical carboxylated acrylonitrile-butadiene elastomer used for secondary phase toughening of an epoxy resin.

To ensure that thermoplastic modifiers indeed act as a toughening agent and not only induce flexibility, then the material must achieve the required secondary phase character during cure and react with some of the epoxy resin. This is general achieved by ensuring that the thermoplastic used is of a high molecular to ensure that there is a difference in the solubility parameters to encourage secondary phase formation and having available active groups.

(a)

(b)

(c)
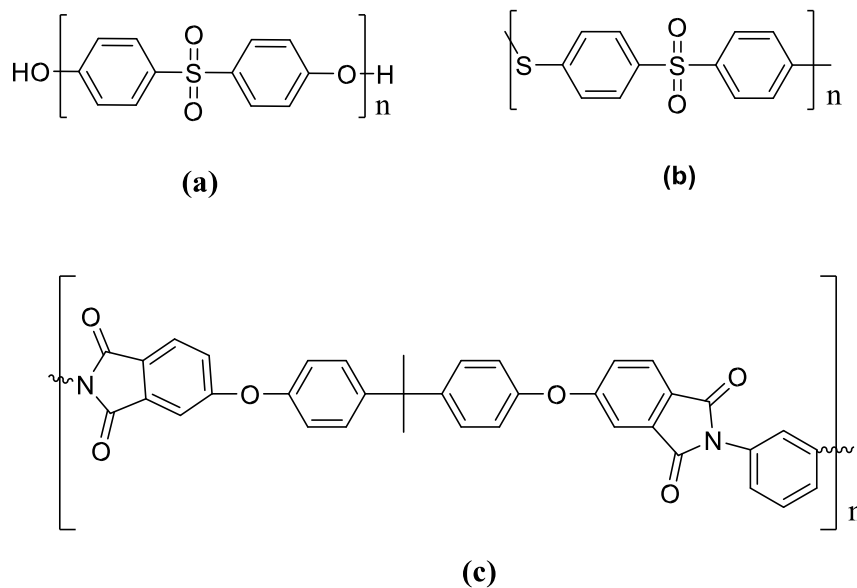
Figure 1.18: Thermoplastic modifiers (a) poly(ethersulphone), (b) poly(phenylenesulphidesulphone) and (c) poly(etherimde) which are used to introduce secondary phase reinforcement to epoxy adhesives.[55]

Even after viewing all the recent developments in epoxy adhesive e.g. toughened epoxy materials showing greater impact resistance and reduced brittleness, an epoxy resin based adhesive will not be suitable for the intended application as an adhesive in a lens. Reasons behind this conclusion are the brittle characteristics of the parent material, UV degradation susceptibility and finally the poor flexibility at low temperatures (above room temperature glass transition).[57] The need to formulate an epoxy with additives to gain the desired properties will almost certainly have an impact on the optical clarity of the cured adhesive which will make it un-suitable for the lens application.

1.32 Acrylic Based Adhesives

Acrylic based adhesives cover three main groups of polymer adhesive namely, the acrylic, cyanoacrylate and toughened acrylic adhesives. This class of polymer adhesive is an extremely versatile type of reactive adhesive that are continually being integrated into many industrial processes. They are also commonly encountered in the consumer market as they have short cure times and high bond strength combined with their ease of application. Adhesives of this type have been used for well over 50 years and a recent resurgence in their application is apparent due to new monomers, curing systems and applications being found.[58,59]

1.321 Acrylic Adhesives

The family of adhesives known as acrylics are constructed from the esters of acrylic or substituted acrylic acids and are generally split into two types the acrylates(I)/methacrylates(II) or the cyanoacrylates (III) (see section 1.322 for cyanoacrylates). Within this section the acrylates and methacrylates will be discussed and the free-radical polymerisation chemistry that leads to their cure.

Acrylic adhesives are formulated using unreacted methacrylate (or acrylate) monomer, a toughening or thickening polymer to regulate viscosity, adhesion promoters, and a polymerisation agent.[59] These structural adhesives show great versatility to the formulator as there are a large number of different monomers and resins at their disposal. Cured materials can be formulated to be flexible but tough or hard yet ridged, which is all dependent on the glass transition temperature of the material coupled with the functionality of the monomer.
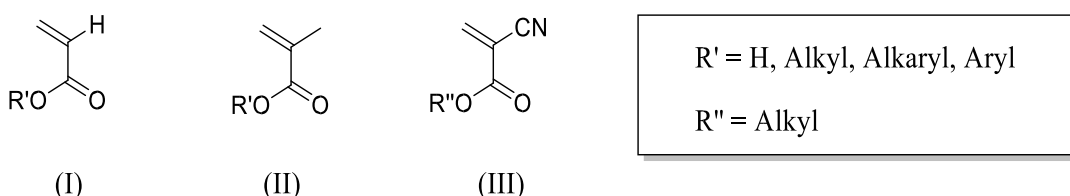
Figure 1.19: Acrylic acid monomer units used in acrylic adhesives (I) acrylate, (II) methacrylate and (III) cyanoacrylate.[60]

The viscosity of acrylic adhesives is commonly low enough to promote wetting of various substrates and to allow for rapid application to the part(s) being bonded. Following application free radical polymerisation then proceeds by sequential addition rapidly, curing the liquid into the final solid material.[60] Inducing free radical cure of the adhesive can be carried out in a variety of ways such as ultraviolet light, applying an activator to a substrate interface, reaction with an impurity/contamination on the substrate interface, by having a two component adhesive that reacts upon mixing or most commonly introduction of air or heat.

In the 1950s some of the earliest acrylic adhesives based on methacrylate monomer were mixed with an organic peroxide and upon introduction of an amine or metal salt would initiate the free radical cure and they were used to bond poly(methyl methacrylate) sheets in aircraft canopies. These two components systems contain an organic initiator e.g. benzoyl peroxide and are catalysed by tertiary amine catalyst e.g. dimethylbenzylamine.[59] The organic peroxide component of these two part systems activates the polymerisation and will be kept separate from the monomer (and other formulation additives) containing the amine. Peroxides will often be supplied as solutions or pastes containing a plasticiser which will allow for sufficient mixing of the two components. Typically, commercially available acrylic adhesives of this type will have a working time of between 1-2 minutes and will have cure times of around one hour. Conversely, the activating peroxide can be applied to one or both substrates prior to the acrylic formulation applied to the joint. This method is only appropriate when the gap between substrates is small enough that effective mixing occurs during joint compression. For large gaps the previous two component system applies to ensure that full cure will be obtained.

1.322 Cyanoacrylate Adhesives

Next in the acrylic family, namely the cyanoacrylates, is another version of these rapid cure structural adhesives. The key difference between the cyanoacrylates and the acrylate is the introduction of the C≡N group where previously a proton was found for the acrylates or a methylene for the methacrylates. Cyanoacrylate systems are normally one-component adhesives based on alkyl-2-cyanoacrylate monomers.[61] The rapid polymerisation occurs when the system becomes exposed to source of nucleophiles which results in the formation of high molecular weight linear polymers.[62] A major difference observed for these types of structural adhesives are that they contain high monomer content with only a small proportion of additives.
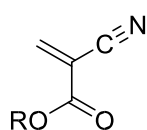
R = Methyl	CH_3-
Ethyl	CH_3CH_2-
n-Butyl	$CH_3(CH_2)_3-$
Allyl	$CH_2=CHCH_2-$
β-Methoxyethyl	$CH_3OCH_2CH_2-$
β-Ethoxyethyl	$CH_3CH_2OCH_2CH_2-$

Figure 1.20: The most commercially important alkyl -2- cyanoacrylate esters.[62]
The production of alkyl-2-cyanoacrylate esters can be achieved by a variety of synthetic routes; however, the most important and commonly used is the Knoevenagel condensation of formaldehyde and an alkyl cyanoacrylate.[63] Low molecular weight poly(alkyl-2-cyanoacrylate) polymers are formed during the base catalysed reaction. The monomer can be obtained by subsequent depolymerisation under vacuum in the presence of an acid (such as sulphur dioxide), with the monomer being collected by distillation. To ensure that the monomers do not react within the collection vessel radical and anionic polymerisation inhibitors must be present.

Alkyl-2-cyanoacrylate monomers are polymerizable via radical or anionic methods but for adhesive applications the anionic method of chain growth dominates. Cyanoacrylates possess two electron withdrawing groups which pull electron density away from the π-electron system making the β-carbon more susceptible to nucleophilic or anionic attack.[62] This forms a tertiary carbanion at the α-carbon which can be further stabilised by delocalisation via structure 1 and 2 (see figure 1.21).
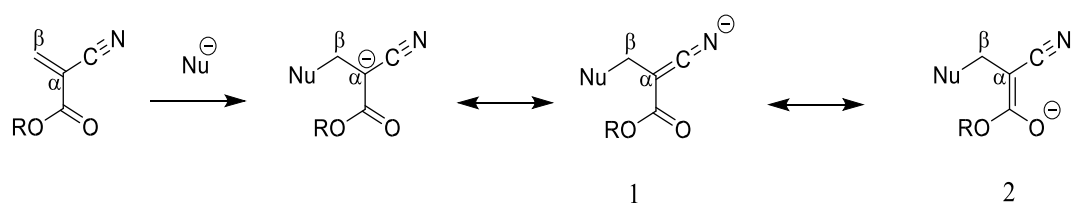
Figure 1.21: Nucleophilic addition reaction scheme of an alkyl-2-cyanoacrylate and resonance stabilised forms 1 and 2.[62]

The rapid curing of these systems can be explained by the unhindered electrophilic βcarbon coupled with the stabilised carbanion. During adhesion, the curing process will be initiated by a nucleophilic activator that is applied to the substrate. If the species that initiates the polymerisation is an ion then the curing processes will proceed by an anionic mechanism. However, if the activating species were a neutral molecule (an amine for example) then the subsequent polymerisation will proceed using a zwitterionic mechanism (see figure 1.22). Irrespective of the mechanism of cure, the process will be rapid and will occur at a much faster rate than that of radical polymerisation.[61] Commonly ionic polymerisations are highlighted for their sensitivity towards termination reactions; however, for cyanoacrylate termination is only observed when a strong acid is present.

As previously mentioned cyanoacrylate adhesives are one-component materials which contain a low amount of additives. These additives are added in small amounts to help improve the performance profile of the adhesive and can be split into two sets: additives that interfere with the polymerisation process itself or additives that alter the final properties of the polymer. Stabilisers are often added as an additive as they allow for a balance to be struck between cure speed and formulation stability which are known problems associated with cyanoacrylates. This can be controlled by careful selecting an appropriate anionic polymerisation inhibitor e.g. sulphonic acid, sulphur dioxide, sulphamides or boric acid chelates.[61] Phenolic free radical inhibitors such as hydroquinone or hindered phenols are also added to improve the curing characteristics of cyanoacrylate systems.

Zwitterionic   Anionic
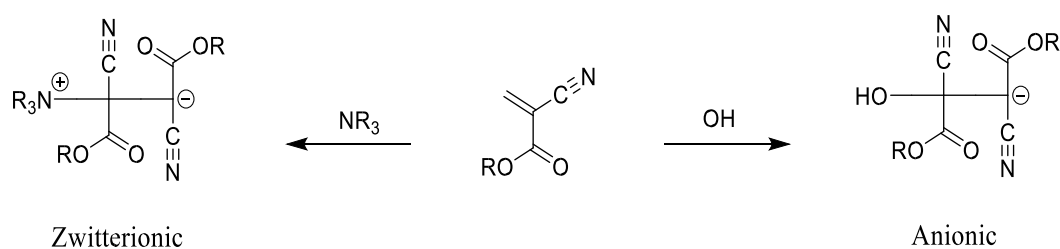
Figure 1.22: Schematic of the possible curing modes of alkyl-2-cyanoacylates adhesives following an anionic or zwitterionic mechanism.[62]

Accelerators can often be added to cyanoacrylate adhesives to increase the rate of cure. These compounds only increase the rate of polymerisation as they are nucleophilic enough to serve as an initiator. The mechanism by which accelerators work is still unclear , it has been suggested that they can isolate metal anions which increases ion separation at growing chain ends or by activation of anions on the substrate. Examples of compounds that are commonly used as accelerators are crown ethers, polyalkene oxides, podands and calixarenes.[61] Plasticisers are also commonly added to cyanoacrylate adhesives to improve the brittleness that these materials display. This can be achieved by adding materials that do not copolymerise with the adhesive which are often ester based or high molecular weight alkyl cyanoacrylates. These additives alter the final properties of the adhesives by slowing down the curing rate.

1.323 Toughened Acrylic Adhesives

Like in epoxy adhesives rubber based toughening agents such as acrylonitrilebutadiene-styrene and methacrylate-butadiene-styrene copolymers are often added to improve the adhesives performance. It is believed that the increased toughness can only be obtained when a secondary phase of small rubber particles is formed. The ability of the cured material to absorb and dissipate energy during impact is attributed to these rubber particles. Formulations also will commonly include free radical stabilisers, curing accelerators, adhesion promoters (can be applied to substrate or mixed with adhesive before application) cross-linking agents and fillers.[59] Non-toughened acrylic adhesives are rigid, brittle polymer which makes them able to carry high loads and have high tensile strength but this is coupled with poor impact resistance and poor peel strength.[64] Thus highlighting the need to find and implement a method that improves the overall toughness of the adhesive.

The monomer used within the toughened acrylic adhesive will be determined by a variety of factors such as: the solubility of the rubber toughening agent in the monomer, the volatility and the cure speed. Alkyl acrylate polymerise to give adhesives properties of high-modulus, high glass transition (commonly around 100°C) and glassy morphology. Volatility of methacrylate polymers are normally linked to the odour associated with the final cured adhesive. Volatile methyl methacrylate based adhesives are usually termed high odour tack free adhesives, while formulations based on the less volatile hydroxyethyl, hydroxypropyl, ethylhexyl or tetrahydrafurfuryl methacrylates are termed as low odour adhesives. The curing reaction occurs at room temperature by free radical polymerisation usually initiated by a peroxide or hydroperoxide. Cure accelerators are applied to the interface when using a one-part adhesive or mixed with the adhesive prior (within a solvent or a paste) to application. An industrially common accelerator which is a reducing agent, is the aromatic amine N,N-dimethylaniline. Also substituted thioureas such as ethylene thiourea or benzoyl thiourea can be also be used as the reducing agent but are not as commonly used due to their toxicity.[64] Transition metal catalysts can also be used to improve the cure speed of toughened acrylic adhesives.

A common application where toughened acrylic adhesives excel is in the bonding of steel joints that have an adhesive thickness less than 1 mm. One-part toughened adhesives are used for this task with the adhesive applied to one face and the activator to the other face. As the joint is closed the cure is initiated, with handling strength normally developed in a few minutes and full strength in a period of hours. The limitation with this particular method is that as the adhesive width goes beyond 1 mm incomplete cure will occur as the activator will not be able to diffuse through the material as it hardens.

To ensure this does not occur when thicker adhesive layers are required a two part adhesive is applied. The two parts will commonly be the monomer mixture with stabilisers, inhibitors, fillers etc. and the activator which will be a solution or paste. The mixing can be performed by dynamically mixing the two materials together followed by subsequent application as a continuous bead. More commonly a static mixing nozzle is used as both parts are homogeneously mixed as they are pushed down

the nozzle. At the tip of the nozzle the homogeneously mixed material can be applied as a continuous bead on to one substrate before the joint is closed. The previous methods of mixing are also used for other adhesive types. A method which is unique to acrylics is the "non-mix" method where two beads are applied simultaneously one on top of the other of each component.[64] Mixing is achieved when the joint is closed which initiates the curing of the acrylic.

Acrylic adhesives appear as an attractive option for lens manufacture. Their clear appearance and fast curing nature coupled with their ease of supply make them a possible option. However, as they are inherently brittle they cannot be used in their native state and a toughened acrylic adhesive will be required. This requires as previously mentioned adding in a toughening agent which will have an effect on the optical properties of the adhesive as the size of the second phase could result in light scattering. They are also high glass transition materials limiting their performance in low temperatures which may be encountered in the proposed application. Finally a large proportion of the research that has been carried out on these systems is for metals and only recently has it been applied to plastics. This could make it a lengthy and difficult project as little literature on the adhesion of cellulosic or polycarbonate based plastic had been carried out with the main focus thus far on polyolefin based plastics.[65]

1.33 Silicone Adhesives

The success of silicone materials is inherent of the variety of forms in which they can be applied e.g. pure fluids, emulsions, solvent based formulation, resins, elastomers etc.[66] The adhesion properties of these materials are also very flexible with silicone based material applied as adhesives, coatings, pressure-sensitive adhesives, mould release agents and sealants.[67] An adhesive is defined as a material which once applied to two other materials will bond them together.

Using silicone chemistry, the ability is presented to formulate a material with different adhesion properties at different interfaces. This is best demonstrated by mould release agents where the adhesive strength between the silicone and the substrate is high but the adhesion between the silicone and the mould is low. Having these different adhesion properties allows for the substrate to be easily removed from the mould. Furthermore, silicone adhesives can be formulated to cure in a matter of seconds or

hours and can be used in applications that are out with the capabilities of most organic adhesive.[68,69] This is reflected by the number of varying industries in which silicone adhesives are used such as the aerospace, textile, construction, electronic, medical and healthcare.

Silicone adhesives are classified as primed, unprimed or self-primed.[66] Primed formulations contain an adhesion promoter within the formulation. Unprimed formulations are systems that are free of any form of adhesion promoter. This is only true for the adhesive itself as the substrate can be surface treated using some form of adhesive promoter. Primed formulations contain a molecule which chemically bonds to the substrate. Forming covalent bonds between the adhesive and the substrate increases the durability of the bond. Most commonly this process is carried out by using an alkoxy silane molecule however, surface activation by corona discharge, flame, or plasma treatments are also used.

Of the three classifications self-primed formulations are the most useful. Within these formulations the adhesion promoter is part of the formulation and is part of the curing chemistry which removes the requirement to perform pre-treatment. With self-primed formulations as with unprimed and primed good adhesive strength with the substrate can be achieved however, the cohesive strength within the matrix is poor. Improving this inherently low cohesive strength can be achieved by the addition of inorganic fillers such as silica or calcium carbonate. When these fillers are incorporated correctly, the network is transformed into a highly elastic material with greater cohesive strength.

1.331 Silicone Addition Cure via Hydrosilyation

Selection of the correct silicone adhesive formulation for the desired application is only achievable after consulting the available method of cure. Silicone based materials have the ability to cure by two methods via addition or condensation reactions. Development of the addition cure method is for processes which require rapid processes and fast cure of deep adhesive sections. This method of cure in which the silicone material becomes cross-linked is faster than condensation cure. This rapid method of cross-linking cure occurs without the liberation of any byproduct.

The hydrosilyation reaction involves the reaction of a hydridosilane (SiH) with an organic alkenyl group (-CH=CH$_2$) as shown in figure 1.23 resulting in the formation of an ethylene bridge.[68] The position of these groups can be at the chain ends to increase the linear length or along the backbone structure to introduce cross-links into the material. Currently platinum catalysed addition curing is the system of choice in silicone based adhesives. Alkenyl groups are positioned at the end of each chain whereas the SiH groups can be found at the chain end or along the backbone structure.
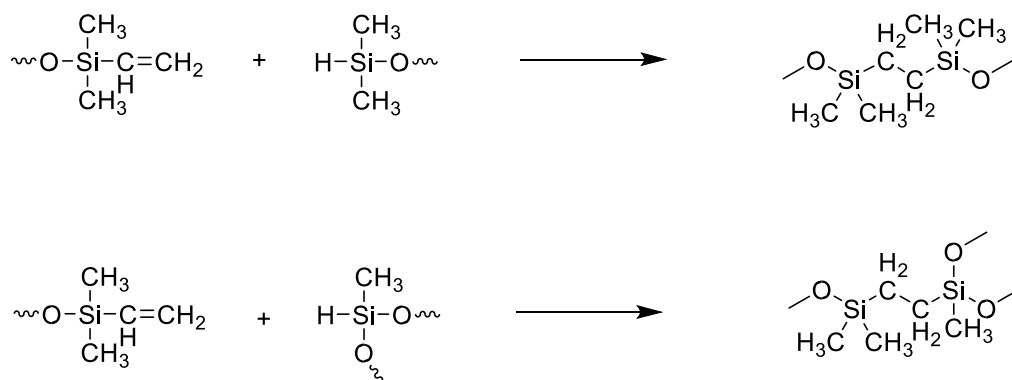
Figure 1.23: Hydrosilyation method of addition cure between an alkenyl group and a hydridosilane. *Top* **reaction hydrosilyation of chain ends** *bottom* **hydrosilyation at sites along the silicone backbone.[68]**

Formulations that are based on the hydrosilyation cure system can be packaged in one or two components. In one component formulations all chemicals are within the same pack making it necessary for an inhibitor to be included which reduces the room temperature reaction rate thus preventing cure in the storage vessel. In two component formulations the base polymer and the cross-linker are stored in separate compartments. Using one of these two delivery methods it is possible to formulate silicone adhesives, sealants and coatings based on addition cure. When formulating such materials it is essential to consider the properties of the uncured formulations such as: pot life, application technique, rheology, application rate and cure performance.

1.332 Silicone Condensation Cure

The condensation cure of silicone materials can be divided into two categories. The first class are silicones that reacted by moisture condensation cure, whereby atmospheric moisture uptake results in hydrolysis and subsequent cross-linking of the polymer matrix. This cross-linking cure method originates at the surface then propagates into the bulk and takes place at room temperature. The second method as

shown in figure 1.24 is the direct condensation of polymer chains with differing functional groups. These adhesives systems are used when fast cure of deep sections of adhesive is required. These systems can be cured at room temperature or at elevated temperature depending on the application and cured time allowed.
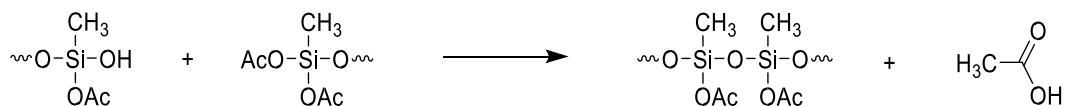
Figure 1.24: Silicone condensation cure with the liberation of acetic acid. (Ac represents an acetate group).[69]

This type of cure is commonly encountered in silicone sealants however; the building industry also exploits this type of curing chemistry in adhesives or coating due to their exceptional durability and weathering properties. This has seen condensation curable silicone materials used in situations where barrier properties against environmental influences such as humidity, rain, pressurised water, gases, sand and dust is essential. Another outstanding property of condensation cured silicone materials is that they can be used in the presence of many other chemical. Silicone based adhesives can also be exposed to ultraviolet radiation without showing any signs of degradation which is a shortfall of common organic adhesives.

1.34 Polyurethane Adhesives

Synthesis of a urethane linkage of an isocyanate and a hydroxyl group was first identified in the 19th century. It was not until the early 1930s that the polyaddition reaction of a diisocyanate and a diol to form a polyurethane was first synthesised by Otto Bayer.[70] These polyurethane materials were initially employed as elastomers, adhesives and coatings in the short period between 1945 and 1947. [71-73] Probably the most famous application of the polyurethane came next with the development of both flexible and rigid foams in 1953 and 1957 respectively.[74] Since their introduction into the field of polymer science less than 100 years ago, the magnitude of available polyurethanes and applications has strongly risen with time. Their application areas are the biomedical industry, sports equipment, automotive parts, furniture and fabrics to name but a few.

Polyurethanes are the product of an exothermic reaction between two molecules; one contains two or more isocyanate groups with another molecule that contains two or more hydroxyl groups. As there are a variety of different starting materials available, the polyurethane field is ever expanding. Different aspects of these molecules can be changed such as using polymeric versions of the isocyanates or polyols of different molecular weight with the combination of both allowing for the fine tuning of the final properties of the polyurethane. Polyurethanes are generally split into six main areas based on their final applications. The percentage consumption of these six main areas as of the year 2000 was 18% automotive, 15% coating, 18% construction, 4% footwear, 29% furniture, 11% thermal insulation and 5% in more specific applications.[75] Within this report the main area of interest in which polyurethane chemistry is used is that of coatings and adhesives.

1.341 Types of Polyurethane Adhesive

Depending on the application of choice the polyurethane formulation can be tailored to deliver the properties required e.g. tough, flexible, high modulus, high tensile strength etc. Fine tuning of the formulation is carried out by correctly selecting the isocyanate, polyol, chain-extender and method of synthesis. The delivery method of the formulation can also be varied to suit the application of choice using solvent free, solvent based, waterborne or hot-melt systems. Depending on the delivery method selected it will change the available application methods e.g. solvent based systems can be applied by spraying whereas hot melt adhesive are applied by a heated doctor blade. Both the formulation of choice and the method of application will impact on the morphology of the final material. Within the remainder of this chapter a brief overview of polyurethanes adhesives will be presented.

1.3411 One-Component Systems

One-component polyurethane adhesives in their earliest sense were formulated entirely of isocyanate. These bulk systems contained either a diisocyanate or polyisocyanate which cured by reaction with active hydrogen present at the substrate interface or by reaction with moisture. The moisture reaction produces a urea group via the mechanism by which a carbamic acid group is formed by the reaction of an isocyanate group with water. This unstable group will decompose to liberate CO_2 leaving an amine which can react with a further isocyanate group to form a urea linkage.[75] Also

possible during the moisture curing process is the formation of biuret groups with both reactions facilitating the increase in molecular weight and adhesive properties.[76]

Isocyanate   Water   Carbamic acid   Amine   Carbon dioxide   Urea
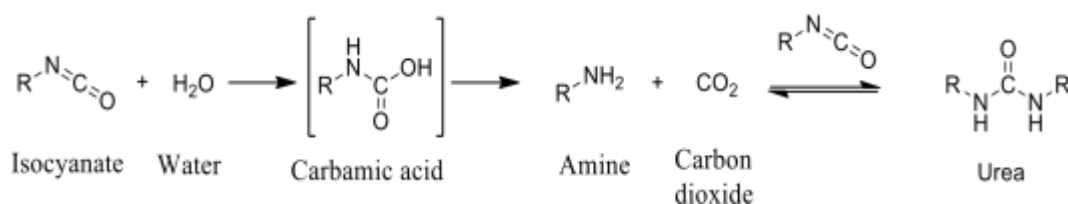
Figure 1.25: Moisture curing reaction of water and isocyanate to form a urea linkage.[75]

Another type of one-component system commonly used are prepolymer based which are formed when a 2:1 excess of isocyanate to polyols is used. Prepolymer systems are commonly used as they have a greater longer pot life due to the free isocyanate content being low. This both increases the workability as the exotherm during cure is smaller but also helps to introduce structure into the adhesive prior to application. Another advantage of prepolymer systems is that the introduced structure helps to reduce shrinkage of the adhesive following cure.

Systems of this type can be used either in solvent or solvent free. Solvent free systems are becoming the systems of choice as they forfeit the need for solvent recover which is often an expensive process. Systems of this type can be very high in viscosity which can limit their application as high temperatures are commonly required for application which can damage sensitive parts during application. Solvent based systems increase the number of potential application methods as the viscosity of the adhesive mixture can be controlled to facilitate application.

Commonly, waterborne systems are now used as they are easy to apply due to the low viscosity of the adhesive while at the same time having an environmentally friendly solvent in water.[76] Waterborne adhesives are used in applications such as shoe sole adhesives, packing adhesives and textile adhesives. Another advantage of these systems is that they can come fully reacted making the adhesive properties obtainable following the removal of water. These systems show good mechanical strength and can be applied as either an emulsion or dispersion. Waterborne polyurethane adhesives are commonly made of aliphatic diisocyanates such as isophorone diisocyanate or hexamethylene diisocyanate with either a polyether or polyester polyol however, aromatic isocyanates such as methylene diphenyl diisocyanate are also encountered.[52]

The consequence of using an aliphatic isocyanate is that the resistance to ultraviolet radiation is increased which is shown by the common application of these systems in coatings.[77,78]

Another common type of one-component system used extensively is a hot-melt adhesive. These adhesive are encountered in two common types: (a) reactive with labile end groups e.g. isocyanate terminated prepolymer which reacts with moisture (see figure 1.25) or (b) are fully cured e.g. highly crystalline material which flows above its melting temperature and sets upon cooling. The first of these two possible systems is a thermoplastic which once fully cured following reaction with moisture becomes a thermoset material. These materials display better high temperature performance compared to fully cured hot-melt adhesives due to the formation of chemical cross-links. The fully cured hot-melt adhesive is a thermoplastic system which is physically cross-linked by hydrogen bonds. Their limited use in high temperature applications is because these physical cross-links are removed during melting however; they are still commonly used due to the ease of application and low toxicity. Both systems display high green strength which is quickly achieved upon cooling as the soft-segment crystallises. Therefore obtaining a high green strength in a short time interval allows for hot-melt adhesives to be used in applications were further manufacturing is required shortly after application. This advantage is exploited for car windscreen installation where a reactive polyurethane hot-melt is used as the window is fixed in place shortly after application and becomes solid following subsequent moisture cure.[79]

1.3412 Two-Component Systems

Two-component polyurethane adhesives are the second major class frequently encountered. As was observed for one-component systems these adhesives can be either solvated or solvent free. Two-component systems are known for their high rates of cure and this makes them the system of choice in many industrial processes. During manufacture curing time slows production making two-component systems a very attractive choice. This coupled with the ability to cure quickly at ambient temperatures is a further advantage of this adhesive system. These adhesives make it possible to perform laminations where moisture penetration is not possible or is limited. As

moisture is not required in the curing process, the possibility of bubble formation in the bond line from CO_2 production is removed or at least limited.

Figure 1.26: (a) Araldite 2026, (b) Lord 7550 and (c) static mixers used for application of solvent free two-component polyurethane adhesives.

The most commonly used solvent based two-component adhesives used are waterborne systems as they use a non-flammable water solvent which is also environmentally friendly. An example of such a system is produced by Ashland under the tradename ISOSET. Within this formulation a base emulsified polymer is reacted with a cross-linking emulsion upon the removal of water.[76] This structural adhesive is used in the bonding of wood to wood in the construction of furniture components. Other common applications of two-component waterborne polyurethane adhesives are bonding metal to plastic in automobiles, wood to foam lamination in construction, and plastic to wood in furniture applications.[16]

Due to the high reactivity of the two polyurethane components they require to be stored in separate compartments prior to application. These systems are formulated using

low molecular weight di- or polyisocyanates which are cured using low molecular weight polyols or polyamines. As one component is stored independent of the other, efficient mixing is essential for successful application. There are many sophisticated industrial meter mixing machines available however, one of the simplest and common applications of these adhesives uses a simple static mixer as shown in figure 1.26.

1.342 Isocyanates used in Polyurethane Adhesives

Of the available isocyanates, the aromatic molecules are the most widely used e.g. in the year 2000 61.3% of the total isocyanate market was attributed to methylene diphenyl diisocyanate (MDI) and 34.1% was attributed to toluene diisocyanate (TDI).[70] With the remaining 4.6% of the market occupied with the aliphatic isocyanate and other more specialised isocyanates split 3.4% and 1.2% respectively.[70] When synthesising an isocyanate molecule, firstly an amine is required, phosgenation of this amine group is then performed to obtain the isocyanate group. Aliphatic isocyanates are obtained by the same process.

1.3421 Aromatic Isocyanates

Aromatic isocyanates are by far the most dominant class with two particular isocyanate molecules being MDI and TDI the most prominent. MDI is synthesised from benzene which in the initial step goes through a nitration process to produce nitrobenzene which is then hydrogenated to form aniline. After purification the aniline is reacted with formaldehyde which forms a complex polyamine mixture generally referred to as methylene dianiline. After further purification to remove unreacted aniline the methylene dianiline is taken through the phogenation reaction which converts the amine into an isocyanate group. The mixture is then purified again to remove unreacted phosgene reagents and the oligomeric mixture of isocyanates is separated using distillation (see figure 1.27).[70] Aromatic isocyanates are often used in adhesive applications where high strength is required. As the MDI molecule is aromatic, ridged hard segments will be formed within the polyurethanes microphase structure which brings stiffness to the adhesive. The influence of MDI on the hard segments structure within polyurethanes adhesives will be discussed further in section 1.38.

The synthetic route used to produce MDI results in two isomers being formed 4,4MDI and 2,4-MDI. In the 4,4'-substitution pattern a symmetrical molecule is obtained with

isocyanates groups of equal reactivity. In 2,4-MDI however, the molecule is asymmetric and this gives rise to a 4-position isocyanate group that is approximately four times more reactive that the 2-position. Commercially available materials of MDI are commonly a mixture of both the 4,4-MDI and 2,4-MDI isomer. MDI based isocyanates also have the ability to form trimer structures which introduce cross-links into the adhesives enhancing the chemical resistance of the final material. One of the major drawbacks encountered using MDI it that it is susceptible to UV degradation.[80] The yellow colouration occurs as conjugation is introduced into the molecule as the methylene bridge is attacked as shown in figure 1.28.[81,82]

$1 = HNO_3 + H_2SO_4$
$2 = H_2 + catalyst$
$3 = (i)CH_2O + HCL$
    $(ii) COCl_2$
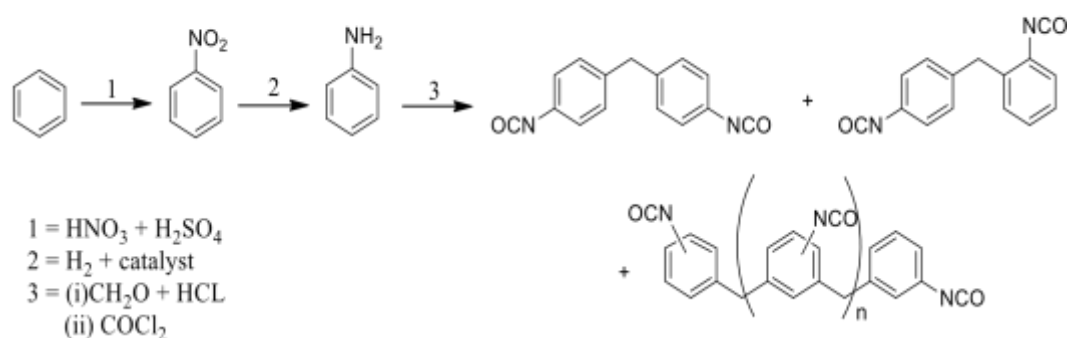
Figure 1.27: Synthetic route used in the production of MDI from benzene.[70]
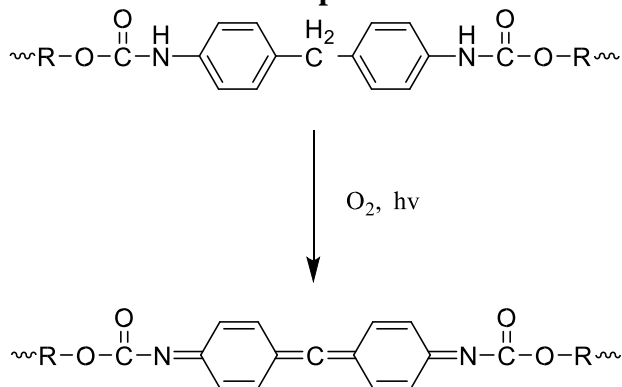
Figure 1.28: Formation of quinoid type structure during UV degradation in MDI.[81,82]

TDI is produced in a very similar process starting with toluene. The nitration process gives a product of dinitrotoluene in a mixture of isomers 2,4 / 2,6 / 2,3 / 3,4 which are then hydrogenated to the diamine compound. At this stage the 2,4 and 2,6 isomers are isolated from 2,3 plus 3,4 isomers as these are not wanted. The purified diamine is

then phosgenated to give the diisocyanate which is taken through a final purification step to remove excess solvent and unreacted phosgene materials. The final distilled product is a liquid mixture of the two isomers (80:20 2,4:2,6 ratio) which is the product used for polymerisations.

The asymmetry within the TDI molecule gives the isocyanate groups varying reactivity. The isocyanate group occupying the 4-position of TDI is approximately four times more reactive that an isocyanate group at the 2-position. On TDI the 4position when compared to the 4-position on MDI is approximately two times more reactive.[70] In 2,6-TDI, the reactivity of the isocyanate groups will be equal as they are both ortho to the methyl group. As both isocyanate groups are connected with the same electronic aromatic ring system, reaction of one isocyanate will reduce the reactivity of the other. As for MDI this aromatic isocyanate aids rigidity in polyurethane adhesives due to the stiff aromatic ring. A major disadvantage of TDI is the high volatility makes it a health hazard.
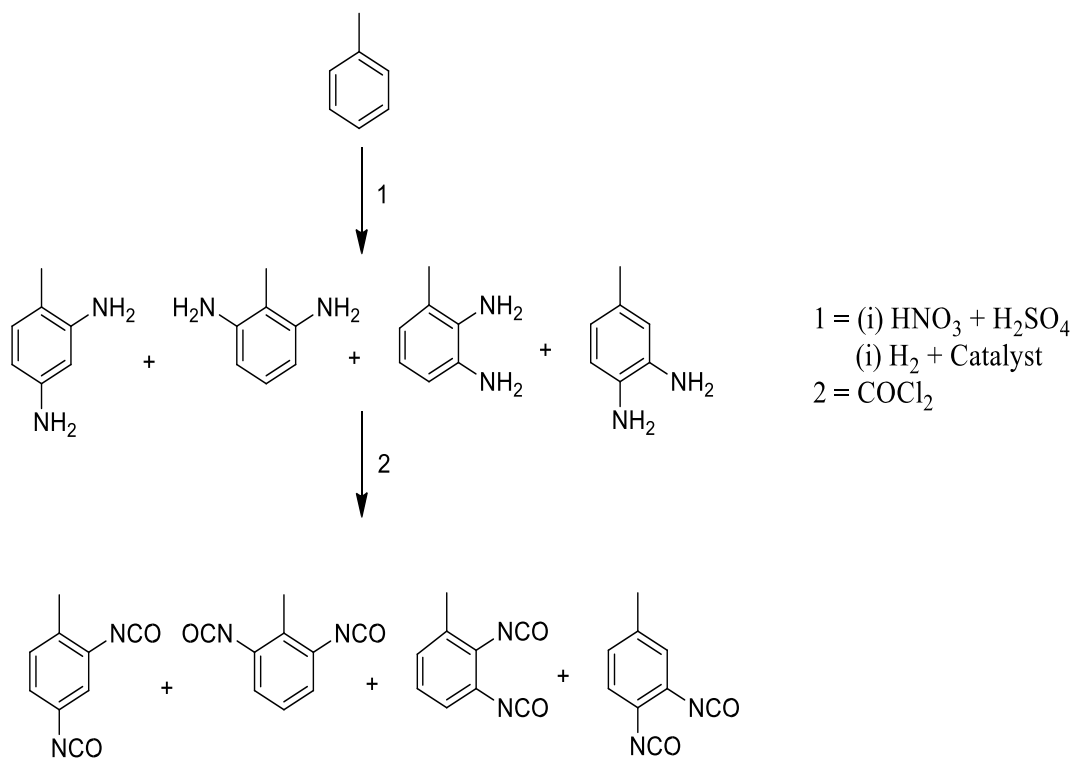
Figure 1.29: Synthetic route used in the production of TDI from toluene.[70]

1.3422 Aliphatic Isocyanates

Aliphatic isocyanates are employed in polyurethane chemistry normally for more specialised application compared to their aromatic neighbours. Hexamethylene

diisocyanate (HMDI) is one of the most commonly used aliphatic isocyanates. It is synthesised from hexamethylene diamine which is produced in vast amounts as it is the monomer used in the production of nylon 6,6.

Next the diamine goes through the phosgene reaction to get the desired isocyanate product of HMDI. This product is highly volatile which makes it a health hazard and is often sold as polymeric HMDI as a result. Forming polymeric materials helps to increase the viscosity and decrease the volatility of HMDI reducing its health risk.

Polymeric versions of HMDI are no longer diisocyanate following the introduction of biuret groups and isocyanurate rings which are trimers (these groups also promote cross-linking). Aliphatic isocyanates of this type do not possess the same rigid molecular structure that is common for the aromatic analogues. As the molecule is symmetric both isocyanate groups will have the same reactivity but compared to the 4-position of MDI these isocyanate groups are two orders of magnitude less reactive. Aliphatic isocyanates are mainly applied where clear coatings are required for they are less susceptible to UV light degradation and more light stable polyurethanes are obtained compared to aromatic versions. A disadvantage of most aliphatic isocyanates is that they do not possess the same internetwork cohesive strength of their aromatic neighbours which gives poorer matrix strength within the microphase structure.[83]
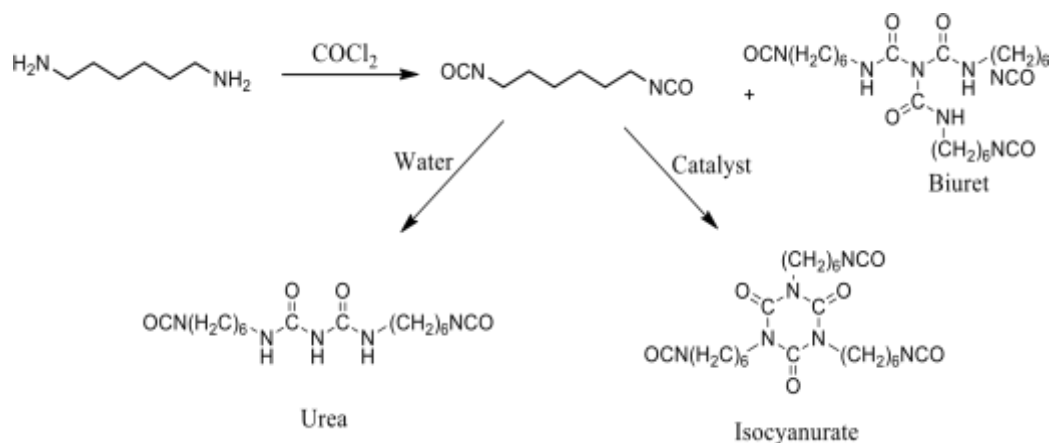
Figure 1.30: Structure of HMDI as synthesised from hexamethylene diamine.[70]
Isophorone diisocyanate (IPDI) is a cyclic aliphatic isocyanate that is produced from acetone. Three molecules of acetone in the presence of a catalyst react to form isophorone, which is then reacted with hydrogen cyanide to give a product of isophorone nitrile. The nitrile product is then taken through a reductive animation step

resulting in isophorone diamine. This diamine is then converted to the diisocyanate by the phosgene process. As was the case for HMDI, IPDI is very volatile so it is often taken through a further reaction step to produce the isocyanurate and biuret adducts.

Compared to HMDI, the aliphatic isocyanate IPDI is much bulkier and is asymmetric with no degree of symmetry. As it is aliphatic it will again when reacted with a polyol give rise to light stable polyurethanes. The secondary isocyanate group has a reactivity on par with HMDI, but the other primary isocyanate group is sterically hindered which reduces the reactivity by a factor of five when compared with the 4position of MDI. It is worth mentioning that the primary isocyanate group has the slowest reactivity of any of the commercial isocyanates.
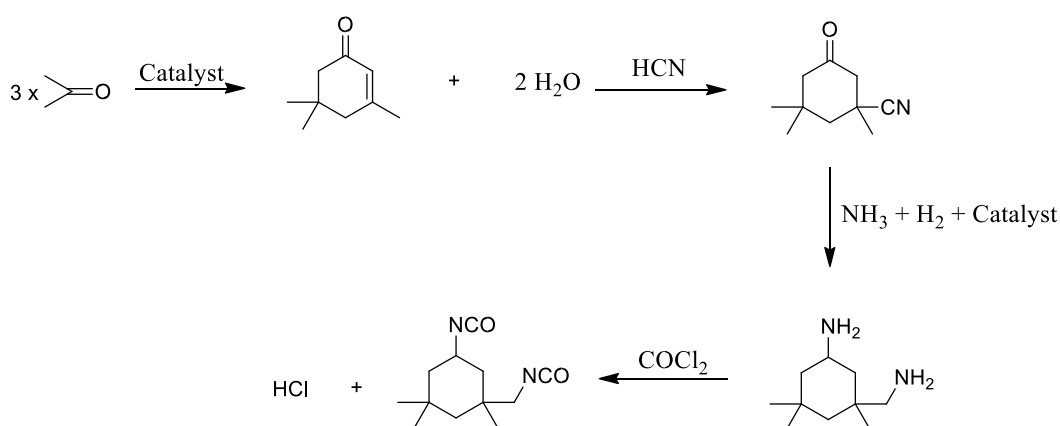
Figure 1.31: The conversion of acetone to IPDI.[70]

1.3423 Isocyanate reactions

The main reaction that an isocyanate will undertake in polyurethane chemistry is with a hydroxyl group to produce a urethane linkage. When diisocyanates and diols are used multiple urethane linkages are formed resulting in the formation of a polyurethane polymer. The success of polyurethane chemistry is mainly attributed to the high reactivity of the isocyanate group. This high reactivity becomes clearer when the four resonance structures of the isocyanate group are observed and how they influences the reactivity (see figure 1.32).
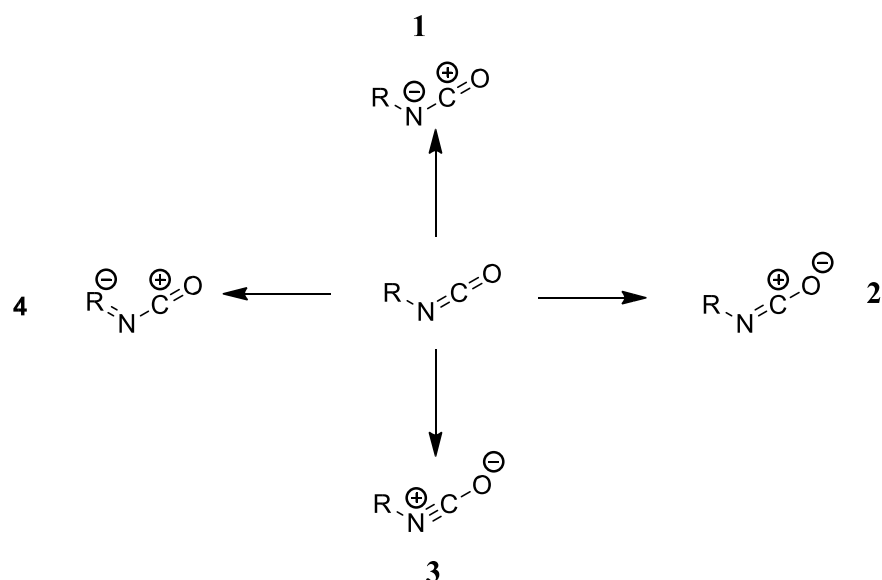
Figure 1.32: Resonance structures of the isocyanate group.[70]

In structure **1** there is an electron-deficient carbon which explains why isocyanates are very reactive towards nucleophilic attack. In polyurethane chemistry structure **1** is more significant than structure **2** and explains why most reactions take place across the C=N bond. Structure **3** only has a very slight contribution to polyurethane chemistry. The final resonance structure, **4,** becomes significant when an aromatic group is present for R.

In aromatic systems the negative charge on R will be spread across the benzene ring which will result in a reduction of the electron density on the carbonyl carbon. Structure **4** displays why aromatic isocyanates (MDI and TDI) are more reactive than aliphatic isocyanates (HMDI and IPDI). As aromatic groups are more electronwithdrawing they have a greater ability to stabilise the negative charge, which reduces the electron density on the carbon making it a better electron acceptor. Hence any R group that is aromatic will possess a greater electron-withdrawing effect which will increase the susceptibility of the carbon within the isocyanate group toward nucleophilic attack.

Isocyanate   Alcohol   Urethane
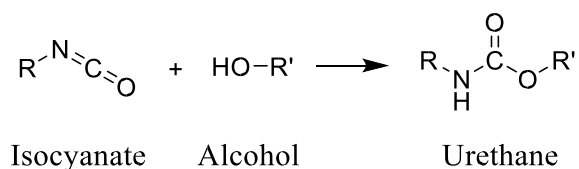
Figure 1.33: Urethane linkage formation in the reaction of an isocyanate with an alcohol.[70]

The production of a urethane link is an exothermic reaction which means that the main driving force is enthalpy through the formation of a more stable product. Aliphatic alcohols react in the order of decreasing reactivity $1^{ry} > 2^{ry} > 3^{ry}$ as the primary alcohol is the most accessible with the least amount of steric hindrance. Aromatic alcohols such as phenols react much slower than aliphatic alcohols and the urethane link is more readily broken. The polyaddition reaction is often accelerated by the addition of catalysts such as acids, bases which the most commonly used are tertiary amines such as triethylamine, and organotin complexes.

Another important reaction is that which occurs between two isocyanate groups and water to form a urea linkage (see figure 1.25). The initial step of the reaction is when an isocyanate group reacts with water to give an amine and carbon dioxide via a carbamic acid intermediate. The amine is then attacked by a free isocyanate group which forms a symmetric urea group. When the reactivity of the isocyanate groups within the diisocyanate molecule are similar such as in 4,4'-MDI, the tendency is to chain extend forming a crystalline polymeric urea. In 2,4-MDI, the difference in reactivity can be exploited by reacting the 4-position as it has an increased reactivity and leave the 2-position which suffers from steric effects free for further reaction.

Urea   Biuret   Urea

Urethane   Isocyanate   Allophonate
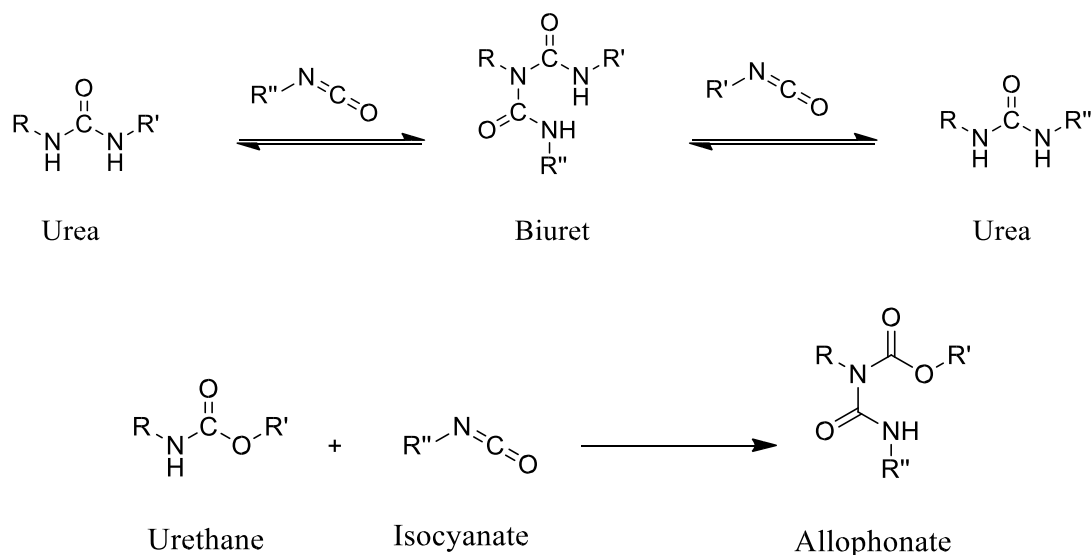
Figure 1.34: Biuret and allophonate by-product formation.[70]

As water is not very soluble within isocyanates it makes the un-catalysed reaction rather slow. Amines can be exploited to produce urea linkages when water diffusion is a problem as they also react at a much greater rate. Introducing primary diamines is also a common tactic to add cross-linking to the polyurethane system. Introducing these cross-links will also boost the resistance to solvents and other chemical process. Primary amines react faster than secondary amines as they are more accessible and it is also worth noting that the un-catalysed reaction of a primary amine can be 100-1000 times faster than a primary alcohol. The more basic the amine is the faster it will react thus making aliphatic amines more reactive than the electron withdrawing aromatic amines. The urea linkage when formed has activated hydrogens present which are susceptible to further reactions with isocyanate groups. This reaction is encouraged when the temperature exceeds 100°C. The rate at which biuret formation occurs is faster than the rate of allophonate formation. This is a reversible reaction but it is commonly used to add cross-linking into the polyurethane. The allophonate reaction requires a higher temperature of around 120140°C before it will start forming. As it is with the biuret the reaction is reversible but is often introduced to gain cross-linking in the system.

Isocyanate groups can also undergo dimerisation and trimerisation in a cycloaddition process. Dimers are formed via a [2+2] cyclo-addition which results in the formation of a four membered ring across the C=N bonds. These dimer sections are more commonly referred to as an uretidinedione. Dimer formation is much more common for the aromatic isocyanates and in MDI for example it is much more common for the 4,4' molecule than the 2,4. The dimerisation of 4,4'-MDI slowly occurs at room temperature but can be accelerated by increasing the temperature to 45°C and the product formed is thermodynamically stable. Aliphatic diisocyanate do not readily form dimer structures although there are examples for catalysed system that utilised trialkylphosphines to obtain polymeric forms.[70]
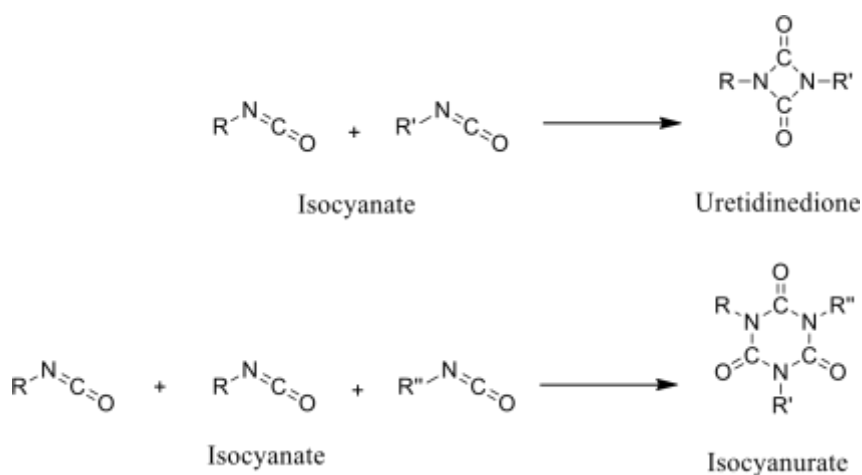
Figure 1.35: Dimer uretidinedione and trimer isocyanurate.[70]

Trimer formation occurs via a [2+2+2] cyclo-addition of three isocyanate groups to form a six-membered ring called an isocyanurate. Once the trimerisation reaction has begun to occur it will continue until all the isocyanate groups have been consumed. Unlike dimer formation trimer structures are readily formed for both aliphatic and aromatic isocyanates. Trimerisation is encouraged by the addition of a catalyst which can be an alkali metal alkoxide or a carboxylic acid salt. Trimerisation again can be purposely introduced as a means of adding branching or it can be an un-wanted side reaction. Isocyanate trimers are thermally stable and not reversible like the dimer moieties. The non-reversible nature of the isocyanurate is possible due to the stable six membered ring compared to the more strained four membered ring of the reversible uretidinedione.

1.343 Polyols used in Polyurethane Adhesives

The polyol component of polyurethanes also has a very significant influence on the properties of the material. Polyol (or soft-segment) polymers are very vast with each having different physical and chemical properties which allow for polyurethanes to be used in many applications. As a result of this diversity the polyurethane industry has thrived from the ever increasing number of available polyols. Having such a variety of soft-segments allow for tailoring of the formulation to obtain specific characteristics e.g. to obtain a rigid foam short chained polyols such a diethylene glycol is used whereas when a flexible foam is required a long linear polyols such as poly(propylene

glycol) with a molecular weight of 2000 is used. Now the most common types of soft-segment used in adhesive formulation will be discussed.

1.3431 Polyether Polyols

Poly(propylene glycol) and poly(ethylene glycol) are the two most widely used polyether polyols globally.[75] Propylene oxide is synthesised from propylene by two basic routes namely chlorohydrin and hydroperoxidation. In the chlorohydrin process propylene is reacted with chlorine in water which gives the chlorohydrin molecule (see figure 1.37). The next step is a dehydrochloronation step which gives the ring closed product poly(propylene oxide). This is the simpler method for the production of propylene oxide but its downfall is that it is difficult to scale up.
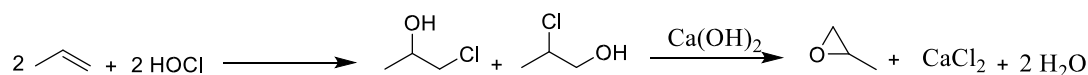
Figure 1.36: Chlorohydrin route to propylene oxide from propylene.[70] The next method namely the hydroperoxidation process is a reaction between propylene with an organic acid which generates propylene oxide and an alcohol byproduct (see figure 1.38). There are two routes to perform this operation using either tertiary-butyl hydroperoxide or ethyl benzene hydroperoxide. This method of propylene oxide production is regularly on scales of 200 to 250 thousand tonnes of propylene oxide per year. Either route can be used to obtain propylene glycol which can be used to form poly(propylene oxide) using either anionic or cationic polymerisation. Both butylene oxide and ethylene oxide are also polymerised in the same way as propylene oxide.

The reaction is initiated by the presence of a branching agent which is commonly the glycol of the alkoxide. This reaction is catalysed in anionic polymerisation by bases such as NaOH or KOH and for cationic polymerisations Lewis acids or Brönstedt super-acids such as BF_3 or PF_5. The branching agent can be a diol or if cross-linking within the matrix is needed triols such as glycerol or trimethylol propane are used. When such polyols are used to initiate the reaction the resultant end groups are hydroxyl terminated.
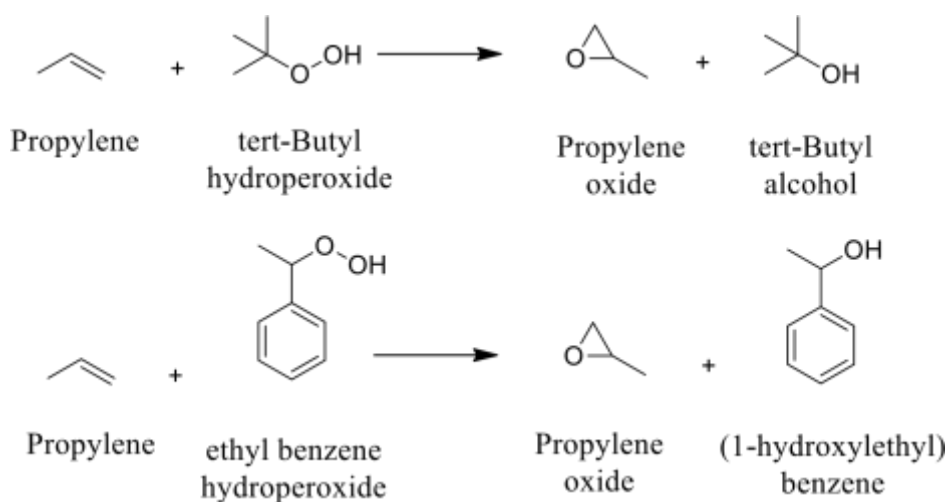
Figure 1.37: **Hydroperoxide route to propylene oxide from propylene.**[70] Introducing higher hydroxyl functionality is often utilised when more flexible materials are required such as in flexible foam applications. Soft-segments produced in the above polymerisation process are known as homopolymers as they only contain the same monomer type. Polymer synthesis is a flexible process and as a consequence the formation of polymers is not limited to just a single monomer type. In some applications, the properties of more than one monomer are required e.g. both propylene oxide and ethylene oxide are often polymerised together for foam applications. Polymers of this type are known as copolymers and they are most commonly synthesised in two ways either block copolymers or random copolymers.
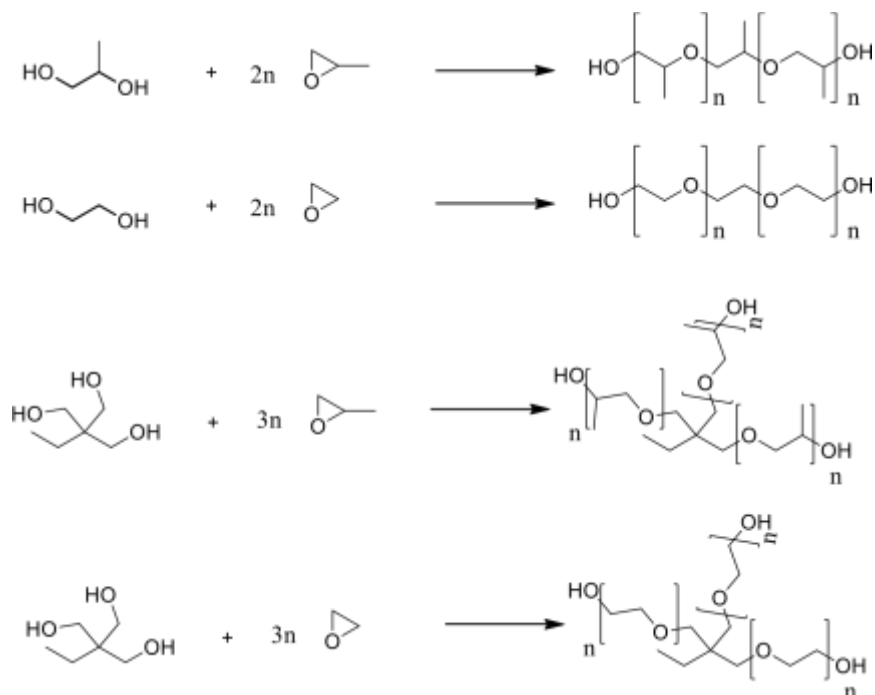
Figure 1.38: Poly(propylene oxide) and poly(ethylene oxide) synthesis using both diol and triol branching agents.[84]

As the molecular weight of the side arms increases the polyurethanes will become more flexible as the isocyanate groups become diluted and spatially more separated. Alternatively lower molecular weight side arms will decrease the flexibility, as the isocyanate hard-segments will be closer together and more concentrated. Random copolymers containing the same monomer units will give different properties when compared to block copolymers.
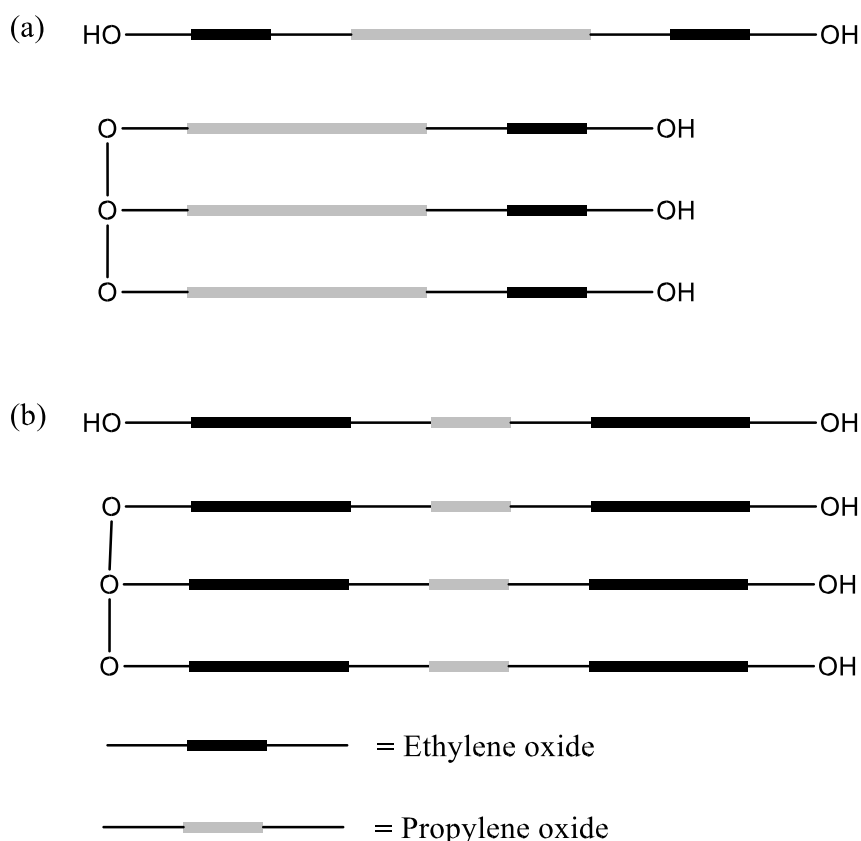
Figure 1.39: Copolymer of poly(ethylene oxide) and poly(propylene oxide). Copolymer type (a) poly(ethylene oxide) terminated diol and triol. Type (b) Block copolymer with internal poly(propylene oxide) block diol and triol.[84]

1.3432 Polyester Polyols

Polyester polyols are the second most commonly encountered kind of soft segment. One of the main advantages that polyester based polyols is that they can be crystalline. Hydrogen bonding between adjacent ester groups within the microstructure of the soft-

segment delivers this crystallinity. Crystallisation of softsegment occurs rapidly allowing for high green strength to be reached in hot melt based adhesive systems. This makes hot melt adhesives appropriate for assembly based applications as the time between adhesive application and handling is low. Having crystallisation within the soft-segment also improves the thermal, fire and solvent resistance of the adhesive when compared to polyether based systems. The main applications of this category of polyester polyols are within elastomers,[85] foams[86] and adhesives.[87] Polyester polyol materials are not without their drawbacks as they are susceptible to hydrolyse at high temperature and high humidity which has been investigated at length to try and resolve.[88]
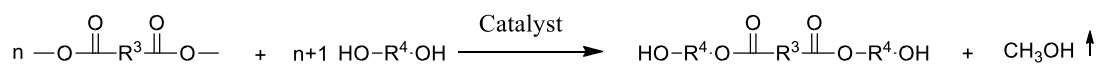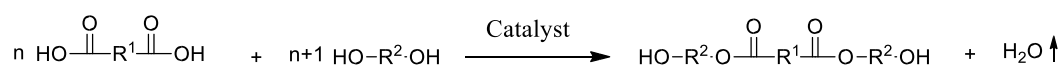
Figure 1.40: Polycondensation reaction between dicarboxylic acids and glycols *top* **and transesterification reaction between dimethyl esters and glycols** *bottom.[84]*

Polycondensation is the most common way to obtain polyester polyols by reaction of a dicarboxylic acid and a diol e.g. adipates are synthesised by using adipic acid and a diol. The alternative route is ring opening polymerisation which is used in the polymerisation of poly(caprolactone).[89,90] When synthesising polyesters via polycondensation of a dicarboxylic acid with a diol, high yields are only possible by the removal of water due to the equilibrium it creates toward the product side. Generation of hydroxyl terminated products is possible by ensuring that there is a stoichiometric excess of the diol. The reaction is a self-catalysed process and will go to completion however, it is rather slow and is often catalysed using p-toluene sulfonic acid, tin compounds or, more recently, enzymes.[91]

Another synthetic route available for the generation of polyesters is via transesterification of dimethyl esters with glycols. The most commonly formed polyester polyols via this route are the adipates, terephthalates and carbonates. The adipates get there name from adipic acid which is the precursor used to form the

polyester with common glycols such as ethylene glycol, 1,4-butane diol and 1,6hexane diol.

Ring opened polyesters are most commonly associated with the lactones. These are cyclic esters which in the presence of glycols and a catalyst form the polyester via ring opening polymerisation. When this process is initiated by a glycol which is a diol the resulting polymer is hydroxyl terminated. The backbone structure of poly(caprolactone) polyesters has five CH_2 groups in a linear chain which increases the hydrophobicity of the molecule, generating polyurethanes with good resistance to hydrolysis which is one of the main issues with implementing some polyester polyurethanes. Other ways in which the hydrolysis resistance of polyester based polyurethanes can be improved is to have a low concentration of ester groups, low overall polyester acidity and by introducing steric hindrance to the polymer.
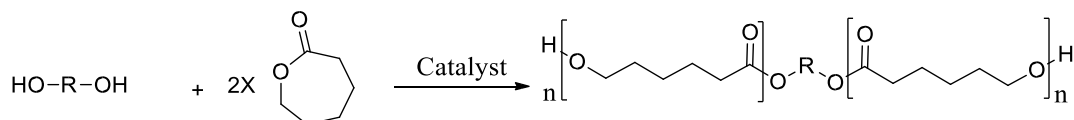
Figure 1.41: Caprolactone ring opening polymerisation for generation of polyester polyols initiated by glycols.[84]

Caprolactone can be polymerised using anionic catalysts, cationic catalysts and organometallic catalysts with the four, seven or eight member rings being readily polymerised however; the five member ring lactone does not undergo polymerisation. Anionic conditions generate polymers with greater molecular weight distributions than under cationic conditions. Common anionic catalysts are bimetallic oxo-alkoxides of aluminium or zinc and for cationic conditions it will normally be a Lewis acid or Brønsted superacid.

1.3433 Other Polyols

Polyurethane synthesis is not limited to aliphatic polyethers or polyesters as a variety of other polyols available. Aromatic polyesters or polysulphones are often used when more rigidity is required within the soft-segment of the polyurethane (see figure 1.43).[92] Aromatic rings within the backbone structure promote π-π stacking giving addition structure to the soft-segment. These stacked moieties reinforce the material leading to more thermally and chemically resistant materials. However, as is common

in polyurethane materials the thermal resistance has a limit and the reinforcement is reduced following decomposition of these stacking interactions. Sulfones also increase the polarity of the soft-segment allowing for addition hydrogen bonding interactions to take place.

(a)   (b)
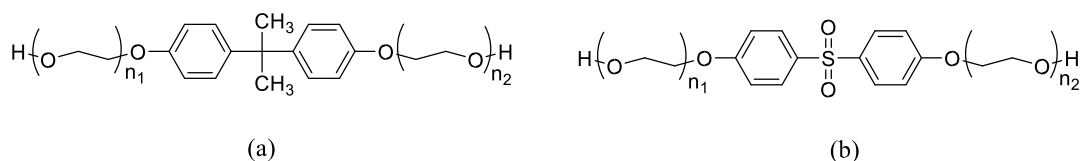
Figure 1.42: Structure of (a) aromatic polyester polyol based on bisphenol-A and (b) aromatic polysulphone polyol based on bisphenol-S.[92,93]

Commonly siloxane based polyol materials are used when the either the hydrophobicity or hydrophilicity requires adjustment. Polysiloxane based soft segments also yield polyurethanes of low surface energy, high gas permeability, combined with the high thermal, UV and oxidative stability of the siloxane.[94] As the hard-segments which consist of diisocyanate and chain-extender are inherently much more polar than siloxane based soft-segments, the microphase morphology is often phase separated. Siloxane based soft-segments have few possible chain to chain reactions, making the architecture of the hard-segment important in high strength materials.[94]

(a)   (b)
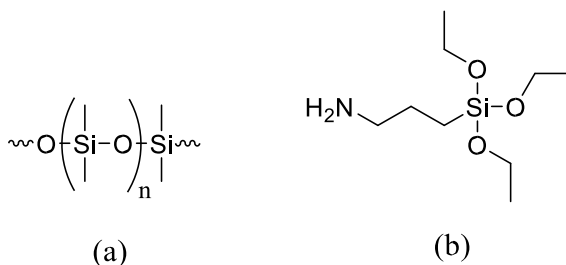
Figure 1.43: (a) Poly(dimethyl siloxane) polymer repeat unit and (b) 3aminopropyltriethoxysilane curing agent.

To improve the low inter chain cohesion within the soft-segment polysiloxanes are commonly used in conjunction with a polyether or polyester.[95-97] Polyurethanes prepared in this way are commonly used in coatings, adhesives, membranes and elastomers.[98-100] In some cases end capping using a silane curing agent is also performed as another method for moisture cure.[99]

It is common for soft-segments to be available in both the hydroxyl and amine terminated forms. With the amine end group comes a change in classification as the material is now a polyurea. Polyureas are known for having high resistance to abrasion, excellent mechanical properties, high chemical and hydrolytic stability. As a consequence their materials are commonly encountered as adhesives, sealants and coatings.[101] The higher reactivity that amines end groups possess compared to hydroxyl groups has resulted in their steady increase in application (see table 1.01). Using a urea group over a urethane group adds an addition hydrogen donating NH group to the hard-segment architecture. This addition hydrogen donating site in certain cases results in more structured hard-segments through formation of ordered bidentate hydrogen bonded urea groups. These highly ordered hard-segments contribute towards the high performance observed in polyurea materials.[101]

Siloxanes, polyethers and polyesters are all commonly available amine terminated making it possible to formulate polyurea materials for various applications. Huntsman is an example provider of amine terminated polyethers under the trade name JEFFAMINE®. Adhesives formulated with polyether amine soft-segments are commonly used in wood glues as they offer high bond strength along with high hydrolytic stability.[102]

Table 1.01: Sources of active hydrogens in polyurethane/urea chemistry, structures and relative reaction rates.[101]

Source of active hydrogen	Structure	Relative reaction rates
Primary aliphatic amine	$R\text{-}NH_2$	100,000
Secondary aliphatic amine	R-NH-R'	20,000-50,000
Primary aromatic amine	Ar-NH	200-300
Primary Hydroxyl	R-OH	100
Water	H_2O	100
Urea	R-NH-CO-NH-R	15
Urethane	R-NH-CO-O-R	0.3

R(') = aliphatic group, Ar = aromatic group

1.35 Chain-Extenders used in Polyurethane Adhesive

Chain-extenders are frequently used in polyurethane synthesis as they facilitate the production of hard blocks. Hard blocks are formed by reacting a low molecular weight diol or diamine with two isocyanate molecules forming a small chain referred to as a block. Diols give polyurethane-based hard blocks and diamines give ureabased hard blocks. It has been reported within the literature by Ryan et al. that the precipitation of the chain-extender in the hard segment will have an effect on the packing arrangement (for definition of precipitation see section 8.11).[103] The effect that the chain-extender has on the packing arrangement was further discussed by Gisselfält et al. who stated that the structure of the hard-segment is influenced by both the chain-extender structure and length.[104] In a paper by Sanchez-Adsuar it was shown that short chain-extenders enhance phase separation and crystalline packing through the formation of smaller blocks which pack more intimately within the hardsegment.[105] Due to the number of differing applications of polyurethanes many linear chain-extenders are available as either aliphatic or aromatic and diol or diamine terminated (see figure 1.45). Selection of a chain-extender will be application based as no one chain-extender can serve every purpose.
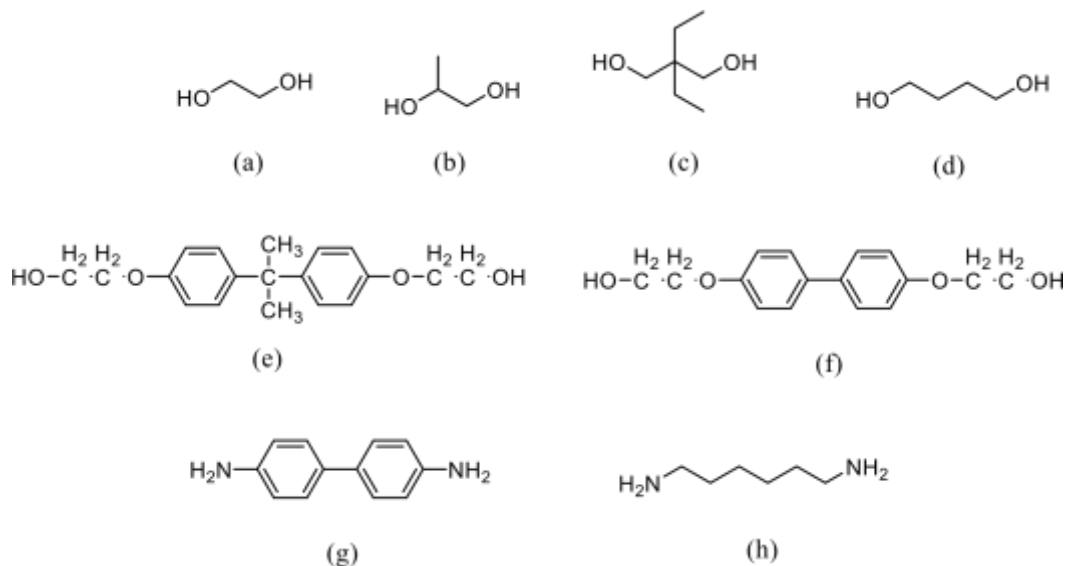
Figure 1.44: Commonly used linear chain-extenders in polyurethane synthesis. (a) ethylene glycol, (b) 1,2-propane diol, (c) 2,2diethyl-1,3-propane diol, (d)

1,4butane diol, (e) bis[4-(β-hydroxyethyl)] bisphenol-A, (f) 4,4'-bis(2hydroxyethoxy)biphenyl, (g) 4,4'-diaminobiphenyl and (h) 1,6-hexane diol.[92] Diol chain-extenders such as ethylene glycol and 1,2-propane diol are commonly encountered however, 1,4-butane diol is the most commonly used in polyurethane synthesis ((a), (b) and (c) in figure 1.45 respectively).[106] The symmetric linear structure of 1,4-butane diol promotes aggregation of hard blocks, as the short block length allows for well-ordered packing. In aromatic based hard blocks e.g. in MDI based systems, the hard-segments are further bonded together through π-π stacking interactions between neighbouring hard blocks which boosts the cohesive strength of the hard-segment. As chain-extension helps promote hard-segment formation it also promotes reinforcement and toughening of the polymer system.

Chain-extension is not limited to linear molecules and when disruption of hardsegment crystallisation is required molecules like glycerol and trimethylolpropane are often used.[103,107] Triol chain-extenders introduce branching into the hardsegment which has been shown by Petrović et al to have a noticeable effect on hardsegment crystallisation when in concentrations of > 15% of the total chain-extender composition. Higher degrees of cross-linking can be introduced by using chainextenders which have OH functionality > 3 as in pentaerythritol (2,2bis(hydroxymethyl)-1,3-propane diol) which has an OH functionality of 4.

(a)   (b)   (c)
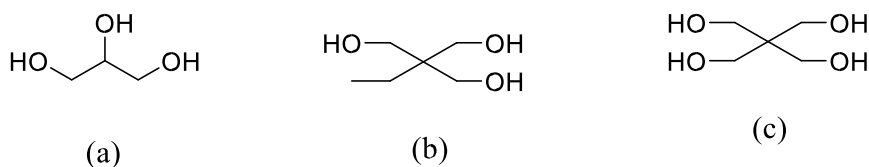
Figure 1.45: Triol chain-extenders used in polyurethane synthesis. (a) Glycerol (propane-1,2,3-triol), (b) trimethylolpropane (2-(hydroxyethyl)-1,3-propane diol) and (c) pentaerythritol (2,2-bis(hydroxymethyl)-1,3-propane diol.

1.36 Catalysts used in Polyurethane Adhesives

Catalysts play an important role in the formation of polyurethane materials. Not only do they increase the rate of reaction but they ensure the chemistry occurring is controlled and that the correct functionality is introduced to the polyurethane network. The two most common catalyst types encountered in polyurethane synthesis are

tertiary amines and organometallic compounds. These catalysts along with some other frequently used catalysts in polyurethane adhesives will now be discussed.

Amine catalysts are known to catalyse the isocyanate-hydroxyl reaction through Lewis base catalysis whereby the amine coordinates with the alcohol polarising the O-H bond.[108] This polarisation activates the hydroxyl group and increases its reactivity towards the isocyanate group.[109] How effective the amine is as a polyurethane catalyst is determined by both the basicity and steric hindrance. Tertiary amine catalysts encountered most frequently are triethylamine and DABCO or 1,4-diazabicyclo-[2.2.2]-octane with the former commonly used in adhesive applications and the later in foam applications.[110]

(a)   (b)
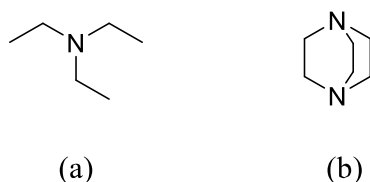
Figure 1.46: Two of the most commonly used tertiary amine catalysts (a) triethylamine and (b) DABCO (1,4-diazabicyclo-[2.2.2]-octane).

The organometallic catalysts function as Lewis acid catalysts by complexing with the isocyanate.[108] Tin complexes of the general formula Bu_2SnX_2 form a complex with the isocyanate group polarising the N=C bond making the already $\delta+$ carbon more susceptible to nucleophilic attack.[111] The mechanism by which the urethane linkage is formed is rather complex and is highly depended upon the organotin complex selected. For adhesive applications the two most commonly used tin catalysts encountered are dibutyltin dilaurate and tin(II) 2-ethylhexanoate however, these catalysts are also encountered in foam applications.

Generally catalyst systems in adhesives contain both a tertiary amine and organometallic complex within the formulation. A synergistic effect is observed by which the co-catalysts system increase the rate of reaction by fivefold compared to dibutyltin dilaurate.[110] This greater reaction rate reduces the time required between application and cure which in industrial process increases productivity.

(a)   (b)
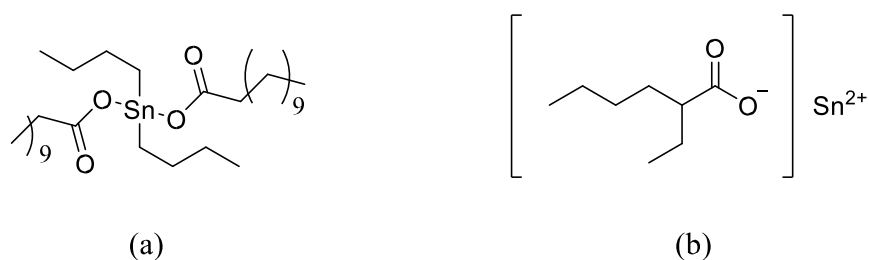
Figure 1.47: The two most commonly used organometallic tin complexes (a) dibutyltin dilaurate and (b) tin(II) 2-ethylhexanoate.

Another common catalyst class encountered is the metal-β-diketones with zirconium acetylacetonate the most commercially used. The successful implementation of zirconium acetylacetonate originates from the greater selectivity toward urethane over urea formation.[108,112] As a result the use of zirconium acetylacetonate in two component urethane coatings has increased because of the comparable reaction rate to dibutyltin dilaurate but with reduced bubbling within coatings.[78] Reduced bubbling is observed using zirconium acetylacetonate over dibutyltin dilaurate as the catalyst has greater selectivity for the urethane reaction compared to the urea reaction. This greater selectivity of zirconium acetylacetonate reduces the amount of CO_2 gas produced during cure as urethane linkages are formed preferentially.

In prepolymer adhesives it is known that different catalysts are often required. This originates from the mode of cure being different as only isocyanates groups are present and moisture is required during cure. Catalysts such as sodium phenoxide, lead naphthenate and ferric 2-ethylhexonate have much greater reaction rates compared to the previously discussed urethane catalysts.[113] Catalysts such as these encourage the reaction of isocyanate groups with the active hydrogens of urethane or urea groups forming a cross-linked network. From this brief discussion it is clear that the selection of the appropriate catalyst is much dependent on the application.

1.37 Strategies for Polyurethane Adhesive Synthesis

There are two strategies available for polyurethanes adhesive synthesis: 1) the polyurethane reaction is carried out during application in a two component process or 2) a proportion of the chemistry is performed prior to application through the formation of polyurethane prepolymers. The application in which the polyurethane is being used

will strongly influence what strategy is selected. A brief overview of each strategy will now be presented along with the advantages and disadvantages.

In two component systems the main advantage is that both components remain separate until application. This ensures that the polyurethane reaction only occurs once both components are mixed. When an appropriate catalyst or hybrid catalyst system is used rapid cure of the formulation occurs, which is partly assisted by the increase in temperature from the exothermic polymerisation reaction. Fast curing reduces the manufacturing time which makes two component polyurethanes useful for line manufacturing process.

Mixing of the polyol with the diisocyanate can be performed in bulk or in solvent. Commonly bulk mixing is performed because the viscosity of the starting materials is low as both components are of low molecular weight (mixing by static mixer sufficient). Having low viscosity also assisted with the available methods of application e.g. Meyer bar can be used due to low viscosity. It also opens up the opportunity to use polyol groups with > 2 functionality (not easily synthesised by prepolymer method) forming a covalently cross-linked materials which is thermally and chemically more resistant. The main disadvantage is that as all polymerisation chemistry is carried out during application it reduces the ability to control the final microphase structure. This reduction in control is often coupled with the mechanical properties being poorer when compared to adhesives prepared by the prepolymer method. The rates at which the components are fed to the point of application are also important if sufficient cure and structure are to be obtained.

Prepolymers are polyurethane molecules which are formed by reacting an excess of one component with the deficit of the other. Most commonly this is performed by reacting a 2:1 stoichiometric excess of isocyanate to polyol forming an isocyanate end-capped prepolymer although this can be performed inverted to yield hydroxyl terminated prepolymers. Using an excess of one versus the other ensures the polymers formed are of low molecular weight as predicted by the Carothers equation.[92,114]

$$1 + r \hspace{5cm} \text{Equation 1.4}$$

$$P_n = \overline{1 + r - 2r\alpha}$$

P_n = Number-average degree of polymerisation

r = stoichiometric ratio α = conversion of

functional groups

If a stoichiometric ratio of 2:1 is used and the conversion of functional groups is 0.99 then the predicted polymer length is 2.99 units. Thus a 2:1 excess of isocyanate will form prepolymers with reactive NCO end groups. Conversely if the ratio is stoichiometric at 1:1 with a degree of conversion of 0.99 the predicted polymer length greatly increases to 1000 units.

The prepolymer method for synthesis of polyurethanes can be performed in two ways: (a) the deficient monomer is added to the reaction flask containing the monomer of excess or (b) the inversion of the first method where the monomer of excess is added to the deficient monomer. Both these methods are used in the production of linear polyurethanes however; these methods are not as successful for functionalities > 2. When the functionality is > 2 cross-links between polymer chains will occur producing a matrix of more complex structure which can no longer be easily processed.

Synthesis can be carried out either in bulk or in solvent. Solvent-based synthesis allows for better control of reaction temperature as the heated produced from exothermic urethane reaction is dissipated into the solvent. As the polymerisation is carried out in solvent it also allows for better control and yields polymers with lower polydispersity. Solvent-based systems are commonly used in coatings and paints as the solvent can evaporate from the open face. A disadvantage of solvent-based systems is they are not useful for lamination applications as the solvent cannot escape and becomes trapped within the joint which often affects the bond strength obtained. Recently solvent-based systems are no longer formulated with organic based solvent as they are expensive to recover and a shift towards water based materials is occurring as it is more environmentally friendly e.g. water-borne polyurethane adhesives.
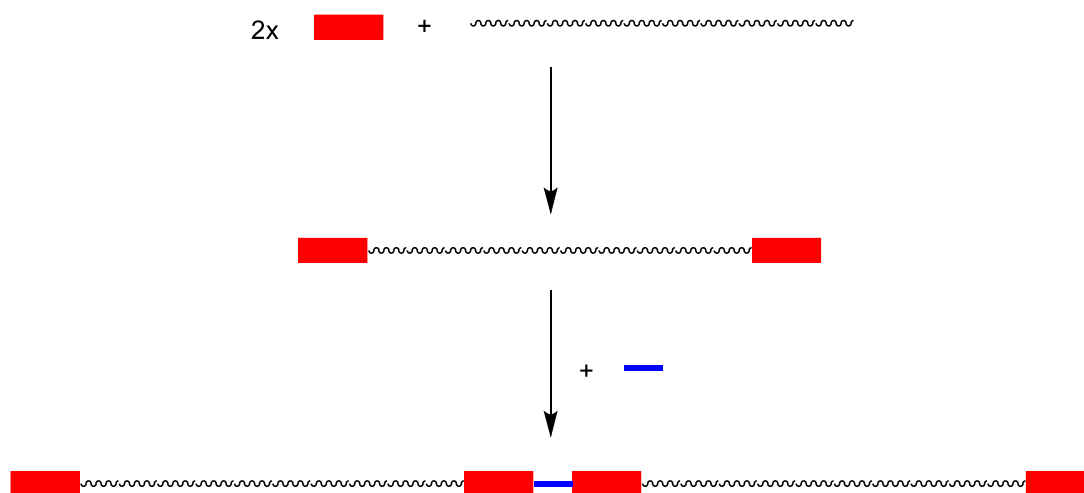
Figure 1.48: **Isocyanate end capped prepolymer production using a 2:1 stoichiometric excess of isocyanate to polyol. [Red square = diisocyanate, black wavy line = polyol and straight blue line = diol chain-extender].**

Polymerisation in the bulk is the more popular process as it does not require solvent recovery. Bulk polymerisation in the formation of polyurethane prepolymers is commonly used in the production of foams, elastomers, coatings and adhesives.[92]

Prepolymers can be produced by two synthetic routes: (a) single stage addition and (b) multistage addition. As the name suggests in single stage prepolymer synthesis all reactants are charged into the reaction vessel at the same time. Differing reaction rates between reactants is commonly accounted for by using suitable catalysts. Synthesis by this route results in a high heat of reaction which, especially in aromatic systems, can lead to unwanted side-products. Although this is the simpler synthetic route the properties of the material formed are often inferior to multistage synthesis as the build-up of the molecular structure is less controlled. In a multistage synthesis firstly an isocyanate end capped prepolymer is produced. This is followed by a chain-extension step which involves the addition of a small molecular weight diol or diamine to couple two prepolymer chains together. At this step, the stoichiometry can be changed to build larger hard blocks and this will require the addition of more isocyanate monomer. Chain-extension is not limited to diol/diamine as it possible to add triols which will introduce chemical cross-linking into the hard segments of the polyurethane microstructure and this increases the thermal resistance. Prepolymer synthesis in the

bulk can be carried out either catalysed or catalyst free using the catalysts detailed previously (see section 1.36).

1.38 Polyurethane Morphology

Having the ability to control and change the morphology of polyurethanes has contributed towards the vast number of applications in which they can be found e.g. foams, adhesives, coatings etc. Careful control of the microphase morphology will help to dictate the final properties of the polyurethane adhesive. Microphase morphology itself is influenced by both the composition and compatibility of the hard towards the soft-segment used in the formation of the polyurethane adhesive. This is further influenced by the type of hard-segment, the hard-segment content and the conditions of cure. Along with the hard-segment, the final morphology of the polyurethane can be altered by the type and length of soft-segment. Finally the method of application will also contribute towards the final microphase morphology with two component adhesives having a different microphase structure to one component prepolymer adhesives.[113]

Hard-segments are formed within polyurethanes by the aggregation of isocyanate hard blocks. These hard-segments are formed primarily via hydrogen bonding between hydrogen accepting carbonyl groups with hydrogen donating N-H groups from urethane or urea groups between neighbouring hard blocks. When an aromatic diisocyanate is used π-π stacking of neighbouring aromatic rings can occur increasing the cohesion of the hard blocks with one another. Hard blocks are formed by reaction of free isocyanate groups with small molecular weight diols e.g. 1,4butane diol or if urea linkages are required a small molecular weight diamine or water can be used.[92] The length of the hard block can be influenced by carefully selecting the correct stoichiometry during synthesis and the structure of the hard block can be controlled via the chain-extender structure e.g. 1,4-butane diol based hard blocks are linear whereas trimethylolpropane based hard blocks are branched.[106,107] In polyurethane prepolymer based adhesives hard blocks of urea are formed during moisture cure. In this situation two isocyanate groups are required and the hard block is formed by a carbamic acid intermediate. As these acid groups are unstable they decompose liberating CO_2 and leave an amine group which reacts with a second isocyanate group

forming the urea. When only prepolymers are present the hard block length is normally short but excess isocyanate can be added to encourage the growth of larger urea based hard blocks.[115]

Another area which can be used to control the morphology of the polyurethane adhesive is the soft-segment.[116] The two greatest factors which influence the morphology of the final polyurethane with respect to the soft-segment are the type and the molecular weight. Within the soft-segment of polyurethane adhesives the two most common types are ether or ester based.[79] In general polyether based polyurethane adhesives have phase mixed morphology whereas in polyesters the morphology is more phase separated. The reasons behind this statement will be discussed further later within this section.

Molecular weight of the soft-segment has a key influence on the morphology of the polyurethane adhesive. If the same stoichiometry ratio of 2.2:1 of diisocyanate to polyol is used for two different molecular weights of polypropylene glycol the hardsegment content will be different e.g. 1000 Mw polypropylene glycol will have a percentage hard-segment of 40 wt% whereas, 2000 Mw the percentage hard-segment drops to 25 wt% (using equation 1.6). Calculation of the hard-segment content is possible by using the formula derived by Flory and it is possible to calculate the chain-extended urethane content using equation 1.5 or the combined urethane plus chain-extended urethane content using equation 1.6.

Using these formulae it can be shown that using a shorter soft-segment will result in an increase in the hard-segment content whereas increasing the soft-segment molecular weight will decrease the hard-segment content. Generally shorter hardsegments lead to polyurethane materials which are ridged and longer soft-segments give more flexible polyurethanes.[79]

It is clear that both the hard and soft-segments will have their own unique influence on the polyurethanes morphology. This is based on the type of each, the compatibility, the percentage content of each and the application. This aside, the most important factor that will influence the morphology of the polyurethane is the application as the material will be tailored to meet those unique demands.

$$\%HS = \frac{100(R-1)(M_{di} + M_{ce})}{(M_{ss} + R(M_{di}) + (R-1)(M_{ce})}$$

<div align="right">Equation 1.5</div>

$$\%HS = \frac{100((R)(M_{di}) + (M_{di} + M_{ce})}{(M_{ss} + R(M_{di}) + (R-1)(M_{ce})}$$

<div align="right">Equation 1.6</div>

M = number average molecular weight, R = stoichiometric ratio of diisocyanate to polyol, subscript "ss" = soft segment, subscript "di" = diisocyanate and subscript "ce" = mole average molecular weight of chain-extender.

In structural polyurethane adhesives used in wood glues the adhesive required needs to be hard and tough while bonding to the wood substrate. In such formulations a stoichiometry of > 2:1 is used to promote the growth of large hard-segments.[117] This combined with the use of short molecular weight soft-segments give very tough structural glues which cure via moisture uptake from the substrate and atmosphere. It is possible to toughen the glue via the soft-segment as is the bases for reactive hot melt polyurethane adhesives.[118] The highly crystalline soft-segment solidifies upon cooling give high green strength and the adhesive cures upon moisture uptake. Both these adhesive will have very different morphologies.

Polyurethane wood glues normally contain a polyether soft-segment such as polypropylene glycol.[117] Polyether soft-segments are known to have a high compatibility with isocyanate based hard-segments which leads to the morphology having a greater degree of phase mixing than a polyester based soft-segment.[83,119] Mixing of the hard-segment with the soft-segment occurs as a result of the favourable hydrogen bonding interactions which occur between the hydrogen accepting ether oxygen with the urethane N-H group.[120,121] These interactions toughen the material as the soft-segment becomes more constrained resulting in an elevation of the soft-segment glass transition temperature. Accompanying this elevated glass transition is a reduction in the low temperature performance of the adhesive. Phase mixing within polyurethanes also becomes more prominent as the hard-segment content is increased.
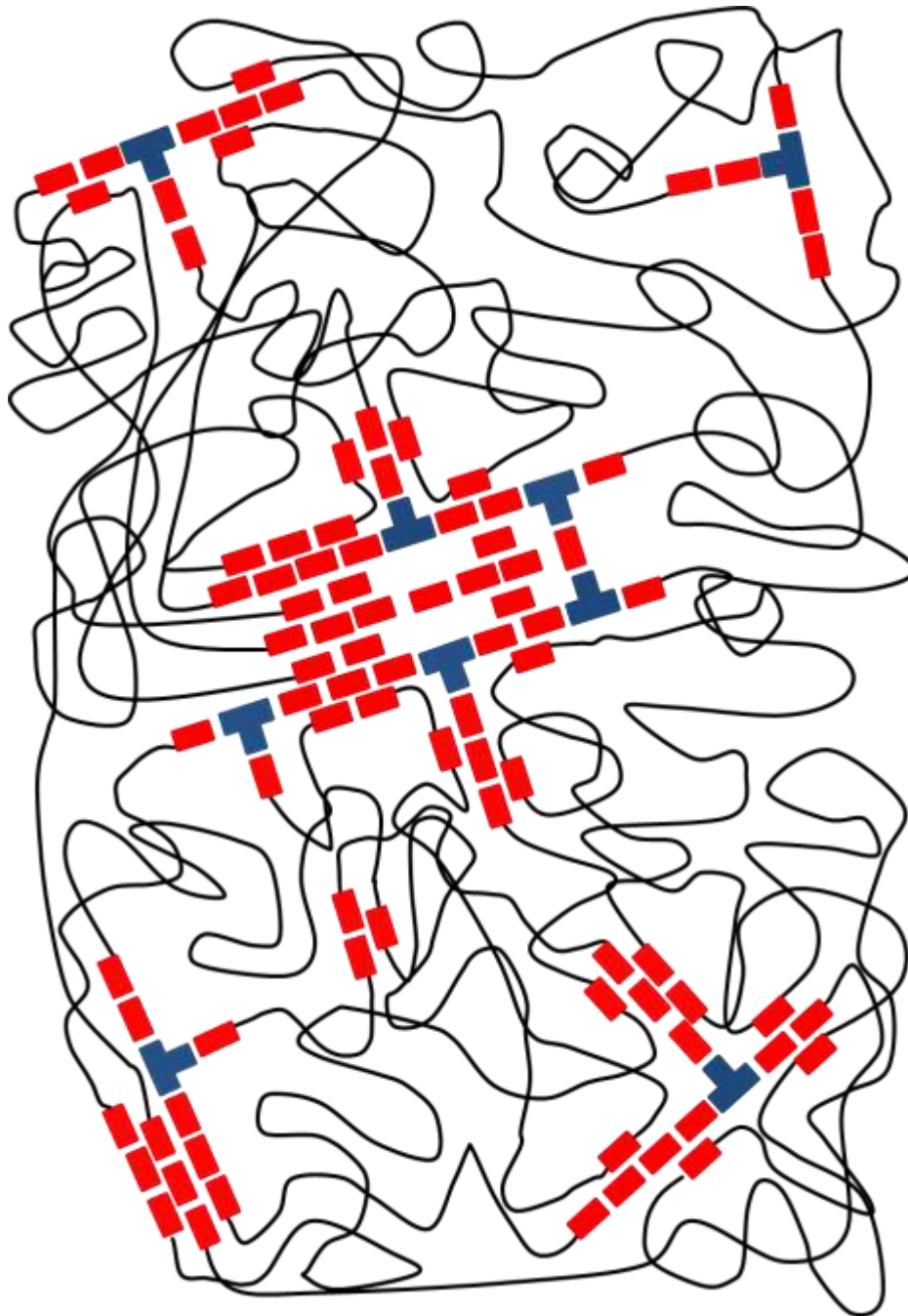
Figure 1.49: General model of polyurethane microphase morphology composed of isocyanate hard blocks with diol chain-extender (red square), isocyanate hard blocks with trifunctional chain-extender (blue T-shape) and polyol soft-segment (black lines).

In polyurethane adhesives which are reactive hot melts the microphase morphology is normally more phase separated. Having phase separation within the adhesive helps to reinforce the adhesive while still maintaining a flexible material.[122] Having minimal

mixing of both the segments is very advantageous for two reasons: firstly as minimal mixing of each phase occurs crystallisation of the polyester soft-segment chains is not inhibited and secondly the small highly cross-linked hard-segment domains reinforce the adhesive. A less constrained soft-segment will suffer a smaller elevation of the soft-segment glass transition and will therefore have better low temperature performance. In epoxy based adhesives an additive such as rubber is required to obtain a similar effect however, in such systems only the impact resistance is improved and not the materials low temperature performance.[55]

Finally, the interface presented by the application of choice may also have an influence on the morphology of the polyurethane adhesive used. When labile functional groups are present at the interface, chemical bonds with the surface can be formed. This is also true when the substrate is permeable to the adhesive as this will result in mechanical hook and eye type adhesion when cured. The morphology becomes more significant when there are no labile groups and the only possible means of bonding is via hydrogen bonds. In this scenario, the adhesive requires a phase separated morphology over phase mixed. As there will be a greater number of donor groups available in the phase separated morphology compared to the phase mixed it would be expected that greater adhesion to the interface will result. The intimate contact of the adhesive with the substrate will also be greater as the softsegment is subjected to less conformational constraints. It is noted however, that the soft-segment and the substrate will require having compatible functionality. There is also the potential to develop surface promotion techniques to either add labile groups to the interface or introduce more hydrogen bonding groups.

1.39 Aim of Research

As presented in the above discussion it is possible to design a polyurethane adhesive for almost any application. Considering this point, polyurethanes are selected by the

author as the adhesive system of choice for the intended application which is production of multilayer laminates containing one or more plastics. Based on a polyurethane adhesive system the four main aims of research are:

- Development of an optically clear adhesive which must have a haze of < 1.5% when laminated between two layers of plastic (cellulose triacetate or bisphenol-A polycarbonate or hybrid containing one of each layer)
- Development of an adhesive which is capable of bonding cellulose triacetate, bisphenol-A polycarbonate and any other laminates combinations containing these plastics
- Production of a fully cured laminate with a peel strength of $\geq$ 3N mm^{-1} as determined by 180° T-peel testing
- Production of a fully cured adhesive free of thermal transitions within the window of -20°C to 100°C which would otherwise affect the in-use performance.

The selection criteria for identification of the materials that are to be used in the production of optically clear adhesives will now be briefly discussed. MDI was selected due to the large volume of literature on MDI based polyurethane materials.[52,76,106,117] This will allow for comparison of physical, chemical and mechanical properties with each MDI formulation within this report. IPDI was selected as its asymmetry structure will lead to clearer final materials. Another key parameter for the selection of IPDI within an optically clear adhesive is it possesses better UV stability than MDI.[82]

To assist with obtaining a clear adhesive each chain-extender has a branched structure. These branching moieties are either due to having > 2 reactive groups as in trimethylolpropane (see figure 1.45 (b)) or due to having steric groups such as methyl/ethyl groups within the chain extenders structure as in 2,2-diethyl-1,3propane diol (figure 1.44 (c)), 1,3-butane diol and 1,2-propane diol (figure 1.44 (b)).
Finally, three different soft-segments were selected; a polyether, a semi-crystalline polyester and an amorphous polyester to screen the adhesion potential of each.

References

(1)   Wydeven, T. *Applied Optics* **1977**, *16*, 717.

(2)   Marsh, K.; Bugusu, B. *Journal of Food Science* **2007**, *72*, R39.

(3)   Dixon, J. *International Life Sciences Institute* **2011**.

(4)   McKeen, L. W. In *Film Properties of Plastics and Elastomers (Third Edition)*;
McKeen, L. W., Ed.; William Andrew Publishing: Boston, 2012, p 57.

(5)   Siemann, U. In *Scattering Methods and the Properties of Polymer
Materials*; Springer Berlin Heidelberg: 2005; Vol. 130, p 1.

(6)   Arthur, A. T. In *Coatings Technology*; CRC Press: 2006, p 19.

(7)   Heinze, T.; Liebert, T. *Progress in Polymer Science* **2001**, *26*, 1689.

(8)   Nevell, T. P. *British Polymer Journal* **1985**, *17*, 378.

(9)   Sata, H.; Murayama, M.; Shimamoto, S. *Macromolecular Symposia* **2004**, *208*, 323.

(10)   Kimura, S.; Sourirajan, S. *AIChE Journal* **1967**, *13*, 497.

(11)   Segal, L.; Bikales, N. M.; Grafflin, M. W.; Spurlin, H. M.; Ott, E. *Cellulose and cellulose derivatives*; Interscience Publishers: New York, 1954.

(12)   Sassi, J.-F.; Chanzy, H. *Cellulose* **1995**, *2*, 111.

(13)   Edgar, K. J.; Buchanan, C. M.; Debenham, J. S.; Rundquist, P. A.; Seiler, B. D.; Shelton, M. C.; Tindall, D. *Progress in Polymer Science* **2001**, *26*, 1605.

(14)   McIntyre, J. E. In *Modern Polyesters: Chemistry and Technology of Polyesters and Copolyesters*; John Wiley & Sons, Ltd: 2004, p 3

(15)   Ebewele, R. O. In *Polymer Science and Technology*; CRC Press: 2000.

(16)   Gilberts, J.; Tinnemans, A. H. A.; Hogerheide, M. P.; Koster, T. P. M. *Journal of Sol-Gel Science and Technology* **1998**, *11*, 153.

(17)   Ewen J.C, K. In *Advances in Structural Adhesive Bonding*; Dillard, D. A., Ed.; Woodhead Publishing: 2010, p 3.

(18)   Awaja, F.; Gilbert, M.; Kelly, G.; Fox, B.; Pigram, P. J. *Progress in Polymer Science* **2009**, *34*, 948.

(19)   Sathyanarayana, M. N.; Yaseen, M. *Progress in Organic Coatings* **1995**, *26*, 275.

(20)   Walker, P. *Journal of Adhesion Science and Technology* **1991**, *5*, 279.

(21)   Beholz, L. G.; Aronson, C. L.; Zand, A. *Polymer* **2005**, *46*, 4604.

(22)   Grace, J. M.; Gerenser, L. J. *Journal of Dispersion Science and Technology* **2003**, *24*, 305.

(23)   Ozdemir, M.; Yurteri, C. U.; Sadikoglu, H. *Critical Reviews in Food Science and Nutrition* **1999**, *39*, 457.

(24)   Petasch, W.; Räuchle, E.; Walker, M.; Elsner, P. *Surface and Coatings Technology* **1995**, *74–75, Part 2*, 682.

(25)   Kwon, O.-J.; Tang, S.; Myung, S.-W.; Lu, N.; Choi, H.-S. *Surface and Coatings Technology* **2005**, *192*, 1.

(26)   Farris, S.; Pozzoli, S.; Biagioni, P.; Duó, L.; Mancinelli, S.; Piergiovanni, L. *Polymer* **2010**, *51*, 3591.

(27)   Pijpers, A. P.; Meier, R. J. *Journal of Electron Spectroscopy and Related Phenomena* **2001**, *121*, 299.

(28)   Briggs, D.; Brewis, D. M.; Konieczko, M. B. *Journal of Materials Science* **1979**, *14*, 1344.

(29)   Zhang, D.; Sun, Q.; Wadsworth, L. C. *Polymer Engineering & Science* **1998**, *38*, 965.

(30)   Rajesh, D.; Mark, J. K. *Journal of Physics D: Applied Physics* **2003**, *36*, 666.

(31)   Kim, C. Y.; Goring, D. A. I. *Journal of Applied Polymer Science* **1971**, *15*, 1357.

(32)   Packham, D. E. In *Handbook of Adhesion*; John Wiley & Sons, Ltd: 2005, p 14.

(33)   Allen, K. W. In *Handbook of Adhesion*; John Wiley & Sons, Ltd: 2005, p 535.

(34)   Allen, K. W. In *Handbook of Adhesion*; John Wiley & Sons, Ltd: 2005, p 275.

(35)   Wake, W. C. *Polymer* **1978**, *19*, 291.

(36)   Bright, K.; Malpass, B. W.; Packham, D. E. *Nature* **1969**, *223*, 1360.

(37)   Packham, D. E. In *Handbook of Adhesion*; John Wiley & Sons, Ltd: 2005, p 60.

(38)   Allen, K. W. In *Handbook of Adhesion*; John Wiley & Sons, Ltd: 2005, p 111.

(39)   Pizzi, A. In *Advanced Wood Adhesives Technology* 1994, p 8.

(40)   Allen, K. W. In *Handbook of Adhesion*; John Wiley & Sons, Ltd: 2005, p 326.

(41)   Allen, K. W. In *Handbook of Adhesion*; John Wiley & Sons, Ltd: 2005, p 38.

(42)   Briggs, D. In *Handbook of Adhesion*; John Wiley & Sons, Ltd: 2005, p 230.

(43)   Prolongo, S. G.; del Rosario, G.; Ureña, A. *International Journal of Adhesion and Adhesives* **2006**, *26*, 125.

(44)   Packham, D. E. In *Handbook of Adhesion*; John Wiley & Sons, Ltd: 2005, p 10.

(45)   Allen, K. W. In *Handbook of Adhesion*; John Wiley & Sons, Ltd: 2005, p 103.

(46)   Wool, R. P. In *Handbook of Adhesion*; John Wiley & Sons, Ltd: 2005, p 341.

(47)   Wool, R. P. In *Handbook of Adhesion*; John Wiley & Sons, Ltd: 2005, p 347.

(48)   Gilbert, J. B.; Rubner, M. F.; Cohen, R. E. *Proceedings of the National Academy of Sciences* **2013**, *110*, 6651.

(49)   Jeong, M.-G.; Kweon, J.-H.; Choi, J.-H. *Journal of Composite Materials* **2013**, *47*, 2061.

(50)   Critchlow, G. W. In *Handbook of Adhesion*; John Wiley & Sons, Ltd: 2005, p 119.

(51)   Packham, D. E. In *Handbook of Adhesion*; John Wiley & Sons, Ltd: 2005, p 311.

(52)   Du, H.; Zhao, Y.; Li, Q.; Wang, J.; Kang, M.; Wang, X.; Xiang, H. *Journal of Applied Polymer Science* **2008**, *110*, 1396.

(53)   Dillard, D. A. In *Handbook of Adhesion*; John Wiley & Sons, Ltd: 2005, p 496.

(54)   Bishopp, J. In *Handbook of Adhesion*; John Wiley & Sons, Ltd: 2005, p 147.

(55)   Aubrey, D. W. In *Handbook of Adhesion*; John Wiley & Sons, Ltd: 2005, p 527.

(56)   Abbey, K. J. In *Advances in Structural Adhesive Bonding*; Dillard, D. A., Ed.; Woodhead Publishing: 2010, p 20.

(57)   Mailhot, B.; Morlat-Thérias, S.; Ouahioune, M.; Gardette, J.-L. *Macromolecular Chemistry and Physics* **2005**, *206*, 575.

(58)   Klemarczyk, P.; Guthrie, J. In *Advances in Structural Adhesive Bonding*; Dillard, D. A., Ed.; Woodhead Publishing: 2010, p 96.

(59)   Briggs, P. C.; Jialanella, G. L. In *Advances in Structural Adhesive Bonding*; Dillard, D. A., Ed.; Woodhead Publishing: 2010, p 132.

(60)   Kneafsey, B. In *Handbook of Adhesion*; John Wiley & Sons, Ltd: 2005, p 12.

(61)   Guthrie, J. In *Handbook of Adhesion*; John Wiley & Sons, Ltd: 2005, p 96.

(62)   Guthrie, J. In *Handbook of Adhesion*; John Wiley & Sons, Ltd: 2005, p 42.

(63)   Jones, G. In *Organic Reactions*; John Wiley & Sons, Inc.: 2004.

(64)   Kneafsey, B. In *Handbook of Adhesion*; John Wiley & Sons, Ltd: 2005, p 546.

(65)   Pang, B.; Ryu, C.-M.; Kim, H.-I. *Journal of Industrial and Engineering Chemistry* **2014**, *20*, 3195.

(66)   Parbhoo, B. In *Handbook of Adhesion*; John Wiley & Sons, Ltd: 2005, p 467.

(67)   Aubrey, D. W. In *Handbook of Adhesion*; John Wiley & Sons, Ltd: 2005, p 363.

(68)   Parbhoo, B. In *Handbook of Adhesion*; John Wiley & Sons, Ltd: 2005, p 469.

(69)   Parbhoo, B. In *Handbook of Adhesion*; John Wiley & Sons, Ltd: 2005, p 471.

(70)   Randall, D. *The Polyurethanes Book*; J. Wiley & sons, LTD, 2002.

(71)   Gruber, E. E.; Keplinger, O. C. *Industrial & Engineering Chemistry* **1959**, *51*, 151.

(72)   Sandler, S. R.; Berg, F. R. *Journal of Applied Polymer Science* **1965**, *9*, 3909.

(73)   Reilly, C. B.; Orchin, M. *Industrial & Engineering Chemistry* **1956**, *48*, 59.

(74)   Farkas, A.; Mills, G. A.; Erner, W. E.; Maerker, J. B. *Industrial & Engineering Chemistry* **1959**, *51*, 1299.

(75)   Randall. D , L. S. *The Polyurethanes Book* Polymer Science & Technology, 2003.

(76)   Dennis, G. L.; Paul, C. In *Handbook of Adhesive Technology, Revised and Expanded*; CRC Press: 2003.

(77)   Lei, L.; Xia, Z.; Cao, G.; Zhong, L. *Colloid Polym Sci* **2014**, *292*, 527.

(78)   Sardon, H.; Irusta, L.; Fernández-Berridi, M. J. *Progress in Organic Coatings* **2009**, *66*, 291.

(79)   Engels, H.-W.; Pirkl, H.-G.; Albers, R.; Albach, R. W.; Krause, J.; Hoffmann, A.; Casselmann, H.; Dormish, J. *Angewandte Chemie International Edition* **2013**, *52*, 9422.

(80)   Umemura, K.; Yamauchi, H.; Ito, T.; Shibata, M.; Kawai, S. *J Wood Sci* **2008**, *54*, 289.

(81)   Servay, T.; Voelkel, R.; Schmiedberger, H.; Lehmann, S. *Polymer* **2000**, *41*, 5247.

(82)   Wang, L.-Q.; Liang, G.-Z.; Dang, G.-C.; Wang, F.; Fan, X.-P.; Fu, W.-B. *Chinese Journal of Chemistry* **2005**, *23*, 1257.

(83)   Chattopadhyay, D. K.; Sreedhar, B.; Raju, K. V. S. N. *Polymer* **2006**, *47*, 3814.

(84)   Tersac, G. *Chemistry and technology of polyols for polyurethanes. Milhail Ionescu. Rapra Technology, Shrewsbury, UK*; John Wiley & Sons, Ltd., 2007; Vol. 56.

(85)   Tang, D.; Noordover, B. A. J.; Sablong, R. J.; Koning, C. E. *Macromolecular Chemistry and Physics* **2012**, *213*, 2541.

(86)   Smith, C. H. *I&EC Product Research and Development* **1963**, *2*, 27.

(87)   Ulkem, I.; Schreiber, H. P. *Journal of Applied Polymer Science* **1994**, *52*, 1857.

(88)   Murata, S.; Nakajima, T.; Tsuzaki, N.; Yasuda, M.; Kato, T. *Polymer Degradation and Stability* **1998**, *61*, 527.

(89)   Soulis, S.; Triantou, D.; Weidner, S.; Falkenhagen, J.; Simitzis, J. *Polymer Degradation and Stability* **2012**, *97*, 2091.

(90)   Cao, W. X.; Lin, G. F.; Li, X. Y.; Feng, X. D. *Polymer Bulletin* **1988**, *20*, 117.

(91)   Rodney, R. L.; Allinson, B. T.; Beckman, E. J.; Russell, A. J.
Biotechnology and Bioengineering **1999**, *65*, 485.

(92)   Król, P. *Progress in Materials Science* **2007**, *52*, 915.

(93)   Liaw, D.-J.; Huang, C.-C.; Liaw, B.-Y. *Polymer* **1998**, *39*, 3529.

(94)   Buckwalter, D. J.; Zhang, M.; Inglefield Jr, D. L.; Moore, R. B.; Long, T. E.
Polymer **2013**, *54*, 4849.

(95)   Kinning, D. J. *The Journal of Adhesion* **2001**, *75*, 1.

(96)   Shi, Z. *J Coat Technol Res* **2013**, *10*, 571.

(97)   Rahman, M. M.; Hasneen, A.; Chung, I.; Kim, H.; Lee, W.-K.; Chun,
J. H. *Composite Interfaces* **2013**, *20*, 15.

(98)   Ni, H.; Skaja, A. D.; Soucek, M. D. *Progress in Organic Coatings* **2000**, *40*,
175.

(99)   Jiang, H.; Zheng, Z.; Song, W.; Wang, X. *Journal of Applied Polymer Science*
2008, *108*, 3644.

(100)   Gharibi, R.; Yeganeh, H.; Gholami, H.; Hassan, Z. M. *RSC Advances* **2014**, *4*,
62046.

(101)   Romanov, S. V.; Panov, Y. T.; Timakova, K. A. *Polym. Sci. Ser. D* **2013**, *6*,
175.

(102)   Clauß, S.; Dijkstra, D. J.; Gabriel, J.; Karbach, A.; Matner, M.; Meckel, W.;
Niemz, P. *Journal of Applied Polymer Science* **2012**, *124*, 3641.

(103)   Li, W.; Ryan, A. J.; Meier, I. K. *Macromolecules* **2002**, *35*, 6306. (104)
Gisselfält, K.; Helgee, B. *Macromolecular Materials and Engineering* **2003**, *288*, 265.

(105)   Sanchez-Adsuar, M. S.; Martín-Martínez, J. M. *Journal of Adhesion Science
and Technology* **1997**, *11*, 1077.

(106)   Chen, T. K.; Chui, J. Y.; Shieh, T. S. *Macromolecules* **1997**, *30*, 5068.

(107)   Petrović, Z. S.; Javni, I.; Divjaković, V. *Journal of Polymer Science Part B:
Polymer Physics* **1998**, *36*, 221.

(108)   Blank, W. J.; He, Z. A.; Hessell, E. T. *Progress in Organic Coatings* **1999**, *35*,
19.

(109)   Schwetlick, K.; Noack, R.; Stebner, F. *Journal of the Chemical Society, Perkin
Transactions 2* **1994**, 599.

(110)   Wegener, G.; Brandt, M.; Duda, L.; Hofmann, J.; Kleszewski, B.; Koch, D.;
Kumpf, R.-J.; Orzesek, H.; Pirkl, H.-G.; Six, C.; Steinlein, C.; Weisbeck, M.
Applied Catalysis A: General **2001**, *221*, 303.

(111)   Houghton, R. P.; Mulvaney, A. W. *Journal of Organometallic
Chemistry* **1996**, *518*, 21.

(112)   Yang, P. F.; Li, T. D. *Journal of Applied Polymer Science* **2013**, *129*, 2399.

(113)   Britain, J. W. *I&EC Product Research and Development* **1962**, *1*, 261. (114)
Cowie J. M. G, A. V. *Polymers: chemistry & physics of modern materials*;
John Wiley & Sons, Ltd, 1992.

(115)   Neff, R.; Adedeji, A.; Macosko, C. W.; Ryan, A. J. *Journal of Polymer Science
Part B: Polymer Physics* **1998**, *36*, 573.

(116)   Martin, D. J.; Meijs, G. F.; Gunatillake, P. A.; McCarthy, S. J.; Renwick, G.
M. *Journal of Applied Polymer Science* **1997**, *64*, 803.

(117)   Ren, D.; Frazier, C. E. *International Journal of Adhesion and Adhesives* **2013**,
45, 118.

(118)   Petrie, E. M. *Metal Finishing* **2008**, *106*, 39.

(119) Chattopadhyay, D. K.; Prasad, P. S. R.; Sreedhar, B.; Raju, K. V. S. N. *Progress in Organic Coatings* **2005**, *54*, 296.

(120) Yılgör, E.; Yılgör, İ.; Yurtsever, E. *Polymer* **2002**, *43*, 6551.

(121) Yilgör, E.; Yurtsever, E.; Yilgör, I. *Polymer* **2002**, *43*, 6561.

(122) Li, F.; Hou, J.; Zhu, W.; Zhang, X.; Xu, M.; Luo, X.; Ma, D.; Kim, B. K. *Journal of Applied Polymer Science* **1996**, *62*, 631.

Chapter 2 – Experimental and Instrumentation

2.00 Experimental

Within this chapter the key experimental techniques and instrumentation used within this research project are presented.

2.01 Cellulose Triacetate Surface Treatment

2.011 Background

Cellulose triacetate films of 125 μm thickness were obtained from Polarway® Polymer Films and the film was used as received. As the film is not hard coated it is possible to perform the saponification surface treatment on both faces. Saponification is the deacetylation reaction of the acetate side groups of cellulose triacetate which leaves regenerated cellulose. The surface treatment was performed to leave hydroxyl groups at the substrate interface which will present the opportunity to form covalent bonds between the reactive prepolymer adhesive and the substrate.
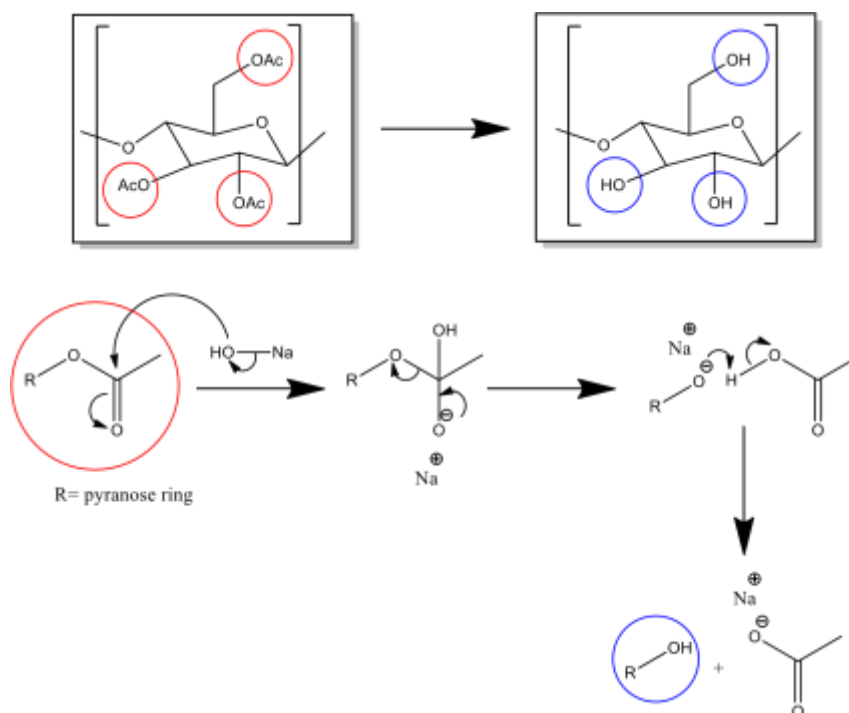
Figure 2.01: Reaction mechanism for the saponification of cellulose triacetate by sodium hydroxide leaving regenerated cellulose.

Saponification is carried out using bases such as sodium hydroxide or sodium methoxide. In sodium hydroxide the deacetylation occurs via nucleophilic attack of

the acetate carbonyl. This in turn results in the liberation of sodium acetate leaving a hydroxyl group on the glucopyranose ring. Saponification of the more accessible primary acetate groups occurs first followed by the secondary acetate groups as they are more sterically hindered. This heterogeneous process occurs initially at the interface face. However, due to the hydrophilic nature of cellulose triacetate reactants will in time diffuse into the bulk making it possible for deacetylation of the full film if enough time is allowed.

2.012 Method for Sample Preparation

Prior to surface treatment test pieces where cut into 25 x 100 cm samples. These samples were saponified using 2.5 M sodium hydroxide at 65°C for four minutes with the samples submerged and continually agitated. Following removal of excess treatment solution film samples are washed at 65°C for four minutes in deionised water with continual agitation. A second cold washing step is next performed using room temperature deionised water for two minutes. Finally the treated sample is dried at room temperature prior to use in lamination without any further processing.

The short treatment time obtained is to serve two purposes; firstly to ensure that the surface treatment could be used in-line during a commercial lamination process and secondly to allow conversion of the surface functionality but limit changes to the surface roughness. A chemical treatment was adopted to ensure that the treatment was permanent and therefore did not change with time. This was essential as previous work with other treatments gave variable result with time e.g. enhancement of corona treatment reduced with time and was affected by changes in humidity.

2.02 Bisphenol-A Polycarbonate Surface Treatment

2.021 Background

Polymer films of bisphenol-A polycarbonate of 175 μm thickness were obtained from Sabic. Surface treatment was performed on one face which requires the removal of a protective anti scratch film which was simply peeled off. The intended surface treatment is the nucleophilic attack of the carbonate linkage by the primary amine of ethanolamine (see figure 2.02). Two potential sites for covalent bonding are introduced by cleavage of this carbonate group. As cleavage of the carbonate bond

occurs between the oxygen and the carbonyl via nucleophilic attack, a primary alcohol is introduced from ethanolamine and a phenol from the carbonate.
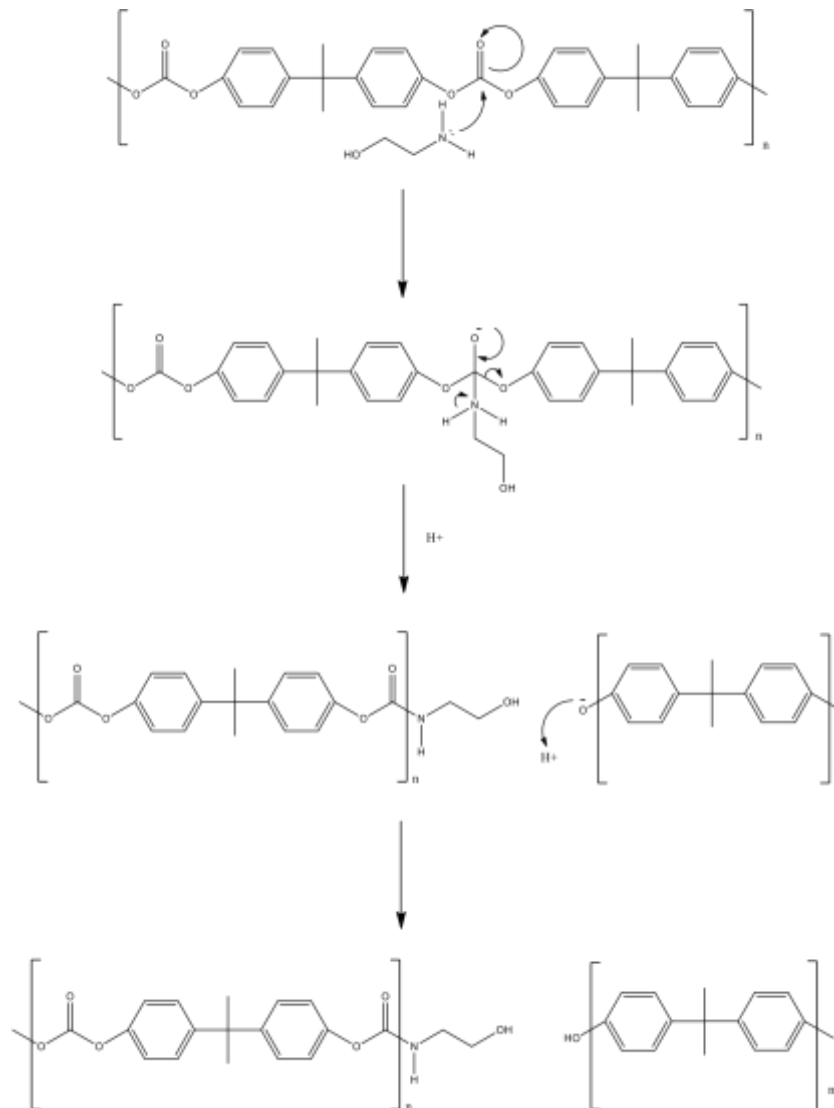
Figure 2.02: Proposed reaction mechanism of the nucleophilic attack of poly (bisphenol A carbonate) by ethanolamine.[1]

2.022 Method for Sample Preparation

Surface treatment of the 175 μm thick polycarbonate film was performed on test pieces 30 cm in width and 50 cm in length. Prior to the treatment, the anti-scratch protective film is removed. This naked face is then wiped with a fine cloth saturated with the treatment solution of 30% ethanolamine in 70% isopropyl alcohol. This wiping process is performed for 60 seconds to ensure that the full surface is treated and this is followed by a 60 second standing period. Next the film is transferred to a 120°C oven

for 120 seconds to promote the carbonate bond cleavage of the carbonate groups at the interface (solution concentration, oven temperature and oven time were determined in previously at Polaroid Eyewear). Surface treated films are now ready for lamination and used without any further processing.

The short treatment time obtained is to serve two purposes; firstly to ensure that the surface treatment could be used in-line during a commercial lamination process and secondly to allow conversion of the surface functionality but limit changes to the surface roughness. A chemical treatment was adopted to ensure that the treatment was permanent and therefore did not change with time. This was essential as previous work with other treatments gave variable result with time e.g. enhancement of corona treatment reduced with time and was affected by changes in humidity.

2.03 Polyurethane Synthesis and Reaction Set-up

Synthesis of isocyanate terminated prepolymers was performed to allow moisture cure of the adhesive following application to the laminate. Prepolymers were chosen over two part polyurethane adhesives as greater control over the final polyurethane morphology is possible via this method.

2.031 Material

Materials used in the synthesis of polyurethane adhesives were all purchased from Sigma-Aldrich unless specified. Isocyanates methylene diphenyl diisocyanate (MDI) and isophorone diisocyanate (IPDI) were both used as received (MDI was stored within the freezer to limit uretidinedione formation). Chain-extenders 1,3-butane diol, 1,2-propane diol, 2,2-diethyl-1,3-propane diol and trimethylolpropane were all dried within a vacuum oven for 48 hours at 80°C prior to use. Polyols 1000 Mw propylene gycol, 2000 Mw poly(caprolactone diol) (Perstorp) and 2500 Mw poly((diethyleneglycol) adipate) were all dried within a vacuum oven for 48 hours at 80°C prior to use.

Table 2.01: Thermal and mass data of raw materials.

Material	Thermal Characteristics[1]	Mass Data[2]

	T_g (°C)	T_g Range (°C)	T_m (°C)	T_m Onset (°C)	T_m Enthalpy (J g^{-1})	Mn	Mw	PDI
PPG	-70	-71 to -69	-	-	-	1008	1033	1.02
PCD	-64	-67 to -58	50	45	57	1695	1824	1.08
PDEGA	-49	-51 to -48	-	-	-	1443	1923	1.33

1 = Determined by DSC, 2 = Determined by MALDI-MS, T_g = Glass transition temperature, T_m = Melting temperature, Mn = number average molecular weight, Mw = weight average molecular weight and PDI = polydispersity index (see section 2.132 for formulae).

2.032 Synthetic procedure

The synthetic procedure used is the same in both cases with the only difference being in reaction time. This difference in reaction time is to account for the differences in the reactivity of the isocyanates groups. All adhesive were synthesised in the bulk using the prepolymer method as detailed below.[2,3]

In all cases an isocyanate end-capped prepolymer is formed using a 2.2:1.0 stoichiometric excess of isocyanate (see equation 1.4 within chapter 1). To the reaction kettle (700 ml capacity), the dried polyol of predetermined weight is added along with 10 mole% of trimethylolpropane chain-extender (10 mole% of hydroxyl content), this mixture is allowed to equilibrate at 75°C for 30 minutes (see figure 2.03 for reaction kettle set up). The reaction kettle is equipped with a nitrogen inlet/outlet, overhead mechanical stirrer, thermocouple and an addition port. The reaction kettle was heated using an oil bath and hot plate.

Figure 2.03: Apparatus used in synthesis of polyurethane adhesives. (a) Reaction kettle complete with nitrogen inlet/outlet, overhead mechanical stirrer, thermocouple, addition port and (b) three necked round bottom flask for preparation of isocyanate.

In a separate 100 ml three necked round bottom flask the isocyanate component is prepared. The round bottom flask is heated using a 100 ml drysil block and hot plate. A stirrer bar is added to the three necked flask which is degassed under vacuum for 1 hour, following this period the flask is filled with dried nitrogen and charged with the isocyanate of predetermined weight. The isocyanate is then equilibrated at 50°C under nitrogen before being added to the reaction kettle. 1 ml portions of the isocyanate are added to the polyol containing reaction kettle with care taken to ensure the reaction temperature does not exceed 85°C.

Once all the isocyanate is added the reaction is left to stir for 3 hours if MDI is used or 5 hours if IPDI is used.[2-5] Following the appropriate elapsed time samples of the adhesive are collected for nuclear magnetic resonance spectroscopy, matrix-assisted laser desorption ionisation mass spectrometry and differential scanning calorimetry. Next curing catalysts were added with 0.05 wt% of dibutyltin dilaurate and 0.05 wt% of triethylamine added (calculated form total formulation weight). Base formulations which are not being chain-extended at this point are degassed at 50°C. Once fully degassed (no visible bubbles or reduction in pressure observed) the adhesive is

transferred to an aluminium tube which is then capped. Next the adhesive is transferred to a vacuum desiccator and stored within the fridge prior to application.

In most adhesive formulations a second synthetic chain-extension step is performed. To the reaction kettle, the dried diol chain-extender of predetermined weight is added in a 2.2:1.0 stoichiometric ratio based on the calculated free isocyanate content. If MDI is the isocyanate, the chain-extension step is carried out for 5 hours and if IPDI is used 19 hours is allowed for the chain-extension step.[2-5] Once the reaction is complete samples are collected for nuclear magnetic resonance spectroscopy, matrixassisted laser desorption ionisation mass spectrometry and differential scanning calorimetry. Next, curing catalysts were added with 0.05 wt% of dibutyltin dilaurate and 0.05 wt% of triethylamine added (calculated form total formulation weight). The formulation is then degassed at 50°C (until no bubbles are visible or any further drop in pressure) and then transferred to the aluminium application tube. Finally, the adhesive is transferred to a vacuum desiccator and stored within the fridge prior to application. All adhesive formulations were applied within 7 days of synthesis.

2.04 Polyurethane Adhesive Lamination

Lamination of both cellulose triacetate (TAc) and polycarbonate (PC) was performed. Six different laminate combinations were tested namely TAc/TAc, TAc(t)/TAc(t), TAc(t)/PC, TAc(t)/PC(t), PC(t)/PC(t) and PC/PC where (t) denotes surface treated (see section 2.01 for TAc and 2.02 for PC). Test laminate were prepared by aligning the two films of choice using one top edge and one side edge to ensure the final laminate was aligned. Once successfully aligned the flush end of the two films are taped together fixing them in place.

A simple lamination process was performed using a set of steel nip rollers and a ChemInstruments laboratory laminator LL-100. Prior to adhesive application the taped end of the laminate is fed through nip rollers and then clamped between the two foam rollers of the laboratory laminator at a pressure of 25 bar. Next the gap between the nip rollers is set using two 40 μm shim pieces which are placed within the laminate. The gap is set by adjusting the nip rollers until the laminate and shims just to pass through the gap (once complete shims are removed). An adhesive bead is applied to the bottom layer with both layers becoming laminated at the nip roller.

This lamination process is performed at 2 m min^{-1}. For MDI based adhesives application temperatures varied from 70°C – 180°C and for IPDI based adhesives application temperatures varied from 50°C – 105°C. Adhesive layers following lamination typically varied between 40-60 μm. Following lamination test pieces were cured at room temperature with the adhesive strength tested at 7 and 30 days (see section 2.16 for peel testing procedure).

Figure 2.04: **Lamination set-up used for the application of polyurethane adhesives.**

2.10 Instrumentation

This section will present the basic theory and methods of the key instrumental technique used within this research project.

2.11 Attenuated Total Reflectance Fourier Transform Infrared Spectroscopy

2.3.1.1 Background

Infrared spectroscopy is used extensively when monitoring chemical reactions and investigating chemical structures. Its success is in part due to the variety of analysis techniques that are available to chemist such as specular reflectance, diffuse reflectance, and internal reflectance. Within this project internal reflectance or as it is better known Fourier transform infrared attenuated total reflectance (ATR) spectroscopy will be discussed.[6,7]

ATR is possible when total internal reflection of infrared radiation occurs within an optically dense medium (e.g. diamond, zinc selenide, germanium, zinc sulphide etc.) with a refractive index of n_1.[8] When this sampling layer come into intimate contact with another material of lower refractive index n_2 (or lower optical density) then total internal reflectance will occur as $n_1 > n_2$.[8] This wave created is known as an evanescent wave and occurs when the angle of incidence from the radiation source exceeds a critical angle θ_{crit} (38.7° for diamond with n = 2.4 for λ = 1000 cm^{-1}) which can be calculated by:

$$\theta_{crit} = \sin^{-1}\frac{n_2}{n_1}$$

Equation 2.1

n_1 = ATR crystal refractive index, n_2 = sample refractive index

Figure 2.05: Schematic of single reflection/bounce ATR instrumental set-up. An evanescent wave occurs at the interface of the sampling material and is positioned at the crest of the incident beam. This evanescent wave penetrates the adjacent material and due to the difference in refractive index returns as the reflected wave (see figure 2.05). This evanescent wave that leaves the ATR crystal is nontransverse, meaning that it has vector components in all spatial directions.[9] These vector components of the evanescent wave will therefore be able to interact with molecules which possess a dipole within the adjacent material being sampled. These interactions will occur in all orientations resulting in an informative probe of the adjacent material. Commonly instruments used in ATR analysis are single reflection/bounce as shown in figure 2.05 however; multi-reflection/bounce instruments are available.

Another analysis parameter that can be varied is the evanescent wave depth of penetration (d_p). This is done by changing the crystal used for analysis or by adjusting

the angle of incidence (θ) in which the infrared beam enters the crystal and thus sample (must be above θ_{crit} for total internal reflection to occur).[8] The relationship between the d_p and how it is affected by wavelength, the refractive index and angle of incidence is given below:

$$d_p = \frac{\lambda}{2\pi\sqrt{(n^2_1\sin^2\theta - n^2_2)}}$$

Equation 2.2

λ is the wavelength of light for source, n_1 is refractive index of diamond, n_2 is refractive index of sample, θ is the entry angle of infrared radiation

This formula displays that the degree of penetration is both wavelength and refractive index dependent. As the wavelength of the infrared radiation is increased, the d_p increases. Infrared spectra however, are not plotted in terms of wavelength but instead are shown in wavenumbers. This changes the relationship, which now displays a decrease in the d_p as the wavenumber is increased. This relationship is commonly observed visually in the relative decrease in band energies of the higher wavenumber vibrations in the ATR spectrum which appear weaker than those obtained by conventional transmission mode. If a comparison with transmission data is required an ATR correction can be applied (available in most software packages). This ATR correction uses mathematics to address the issues of:

- the distortion of the relative band intensities caused by the dependence of the d_p with wavelength
- the dispersion of the refractive index which results in the shift of bands to lower wavenumbers
- deviation from the Beer-Lambert law (there is a logarithmic dependence between the transmission of light as it passes through a substance with an associated absorption coefficient and its path length through the material) which is due to non-polarisation effects[8]

For the above criteria to be fulfilled it is essential to ensure that sufficient contact between the diamond crystal and the sample is obtained. This is possible either by casting a film of the sample onto the crystal or physically clamping the film on top of

the crystal. It is important to note that the pressure of clamp will influence the peak intensity of the IR spectrum obtained.

2.3.1.2 Method

Analysis was carried out on Agilent Technologies 4500 Series Portable FTIR Spherical Diamond ATR. Each spectrum consisted of 128 scans with 8 wavenumbers resolution with the sample depth ~ 2 μm at 1000 wavenumbers. Prior to collecting the background and in between sample replicates the diamond crystal was cleaned using an ethanol soaked soft tissue (anhydrous, $\geq$ 99.5%). Characterisation of each adhesive using ATR was obtained on 30 day 180° T-peel samples. Analysis of each laminate (see section 2.04) was carried out at 9 random positions along the sample length. These 9 spectra were first normalised to account for any differences in clamp pressure and then averaged to determine the variation within the adhesive layer of each different laminate. A final average of all 6 laminates is then plotted to represent the bulk characteristics of that adhesive. All ATR spectral averaging was carried out using LabCognition Panorama with all spectra plotted using OriginPro 9.0.

Next deconvolution analysis of the N-H and C=O regions was carried out on the final average spectra (see appendix B). Each deconvolution was performed using OriginPro version 9.0 software using Gaussian, Lorentzian and Gaussian-Lorentzian cross fitting functions. The function of best fit was determined by the confidence of fit and R^2 values. Within the N-H region peak fitting was used to determine the presence of free N-H, a carbonyl overtone or hydrogen bonded N-H groups within the adhesive. Within the carbonyl region peak fitting was used to determine if free ester, free urethane, hydrogen bonded urethane, free urea, monodentate urea or bidentate urea were present within the adhesive.

2.12 Nuclear Magnetic Resonance Spectroscopy

2.121 Background

In the past 30 years nuclear magnetic resonance spectroscopy (NMR) has established itself as one of the best techniques for the characterisation of polymer materials.
This success in part is due to the flexibility of NMR which can be performed both in solution or in the bulk however, NMR ability to differentiate between chemically

different nuclei within polymers is the main strength of this technique. Using protons that are chemically non-equivalent as an example it is known that when within the same magnetic field they will possess different resonance frequencies. As each of these resonance frequencies will supply different information about the molecular structure it is possible to see why NMR can provide relevant information on both organic small molecules and polymers. Within this section rather than discuss the instrumental theory of the NMR instrument the author will direct the reader's attention to some relevant texts which cover this subject comprehensively. Within these texts nuclear spin, the spectrometer, chemical shifts, spin – spin coupling, splitting patterns, pulse and Fourier transform NMR are all addressed.[9,10] Also within these texts the basic principles of NMR spectroscopy as well a more advanced experiments such as two dimension NMR are discussed in detail.

Polymer NMR studies are most extensively carried out on copolymers as it allows for excellent structural characterisation. NMR studies of this type are extremely useful for polymers such as polyurethanes and the analysis of prepolymer materials. Isocyanate terminated prepolymers are extensively used in many polyurethane technologies such as foams, adhesives and elastomers. Prepolymers of this type can have very different compositions which are dependent on the application of choice.

In adhesive applications the isocyanate terminated prepolymer will contain either an aromatic or aliphatic isocyanate along with a polyether or polyester polyol which can have a variety of molecular weights. Prepolymer materials can also then be further reacted using a chain-extender to introduce hard urethane blocks e.g. diol or triol. Following such reactions using solution state NMR is now a common place analytical technique for determination of the prepolymers structure.

It is possible through the use of both proton (^{1}H) and carbon (^{13}C) NMR to monitor the structure of the prepolymer molecule. In aromatic isocyanate systems it is possible to differentiate between free isocyanate groups and urethane groups. In an MDI based adhesives for example it is possible using ^{1}H NMR to observe the downfield shift of the methine ring protons following the reaction of the isocyanate group with a hydroxyl group. This is possible as the originally symmetric molecule becomes asymmetric

following the formation of the urethane group and as a consequence the methine protons are no longer chemically equivalent (see figure 2.06).
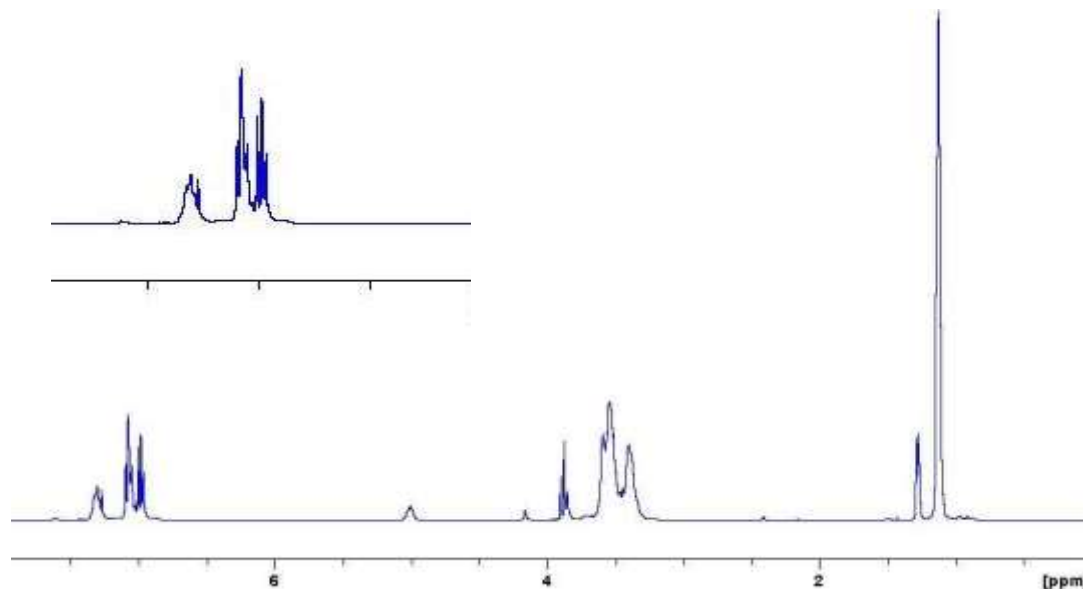
Figure 2.06: ^{1}H NMR spectrum of an MDI based prepolymer adhesive. Inset expanded region displays splitting of the aromatic protons.

^{13}C NMR analysis will also contribute toward characterisation of the prepolymer structure. In an asymmetric diisocyanate system such as IPDI ^{13}C is especially useful as it allows for differentiation of the primary and secondary urethane linkages. Within figure 2.07, the ^{13}C spectrum of an IPDI based prepolymer is shown. Within this ^{13}C spectrum the isocyanate carbonyl shifts downfield once it is part of a urethane linkage. Visible are the different types of urethane groups within the prepolymer, with both primary and secondary urethane linkages visible at 156.6 ppm and 154.4 ppm respectively. Also primary and secondary free isocyanate groups are visible within the spectrum at 123 ppm and 121.8 ppm respectively. In this example ^{13}C NMR indicates that the synthetic conditions used are not selective toward one diisocyanate group, which is shown by the mixture of urethane linkages.
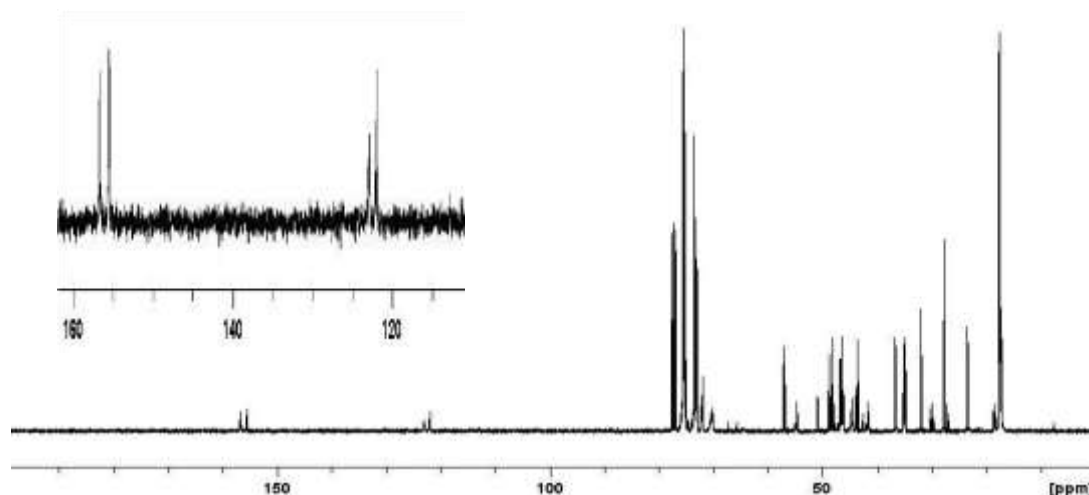
Figure 2.07: Differentiation of primary and secondary urethane groups using ^{13}C NMR in a prepolymer adhesive based on the asymmetric isocyanate IPDI. Inset expanded region displays the isocyanate and urethane section of ^{13}C spectrum.

2.122 Method

Both ^{1}H and ^{13}C NMR experiments were performed by dissolving around 100 mg of sample in 1 ml of d-chloroform. If any solid material was still present the solution was filtered through a Pasteur pipette containing a glass wool filter. The solution was then transferred to a clean NMR tube with the sample depth being between 4.5 cm and 5.5 cm. The instrument used for analysis was a Bruker Avance DPX 400 with the spectral analysis carried out using Bruker's topspin software version 1.3. All spectra were calibrated using the deuterated solvent peak at 6.27 ppm for proton spectra and 66.23 ppm for carbon spectra. Step one prepolymers (contain TMP chain-extender only) were analysed using 16 scans in ^{1}H and 1024 in ^{13}C experiment.

Step two prepolymers (contain TMP plus diol chain-extender) were analysed using 32 scans in ^{1}H and 2048 scans in ^{13}C.

2.13 Matrix assisted laser desorption ionisation Time-of-flight Mass Spectroscopy

2.131 Background

Mass analysis of high molecular weight compounds that are non-volatile is commonly carried out using matrix assisted laser desorption ionisation time of flight mass spectroscopy (MALDI-MS).[11] Implementation of this technique is most common

when analysing large biomolecules such as peptides, proteins, oligonucleotides and oligosaccharides.[12] Another area that it is commonly implemented is in synthetic polymer analysis as it gives information such as the oligomer spacing and molecular weight distribution.[13] These are two areas in which MALDI-MS is used but the scope of this technique is much greater. Within this project the focus was on using MALDI-MS in analysing polyurethane prepolymers.[14]

MALDI-MS is a soft ionisation technique, therefore fragmentation is commonly minimal and the mass spectrum recorded is mostly populated with sample molecular ions. Degradation of the samples is unlikely to occur using the MALDI-MS technique due to the soft nature in which the sample is desorbed and ionised.[15] The key component of this technique is laser desorption ionisation of a sample molecule, which is performed by irradiation of a sample with a high energy laser. When a sample is irradiated at a low rate over an extended period of time, the energy will be able to dissipate throughout the system and into its surroundings resulting in no change to the molecular structure or phase. When a solid sample is carefully irradiated with a large amount of energy over a small time period, the sample will be ionised taking the sample into the analysable phase through desorption. This laser irradiation process can be a continuous or pulsed beam, with pulsed being the most common for MALDI-MS analysis as it is softer in nature than a continuous beam. Possible physical processes which can occur using this technique on a solid are melting, vaporisation, ionisation and if not properly controlled decomposition.[15]

Sample ionisation only occurs if the correct energy source is used e.g. ultraviolet, visible or infrared radiation of the correct wavelength that matches the sample absorption spectrum. This gives two possibilities a) the sample absorbs energy from the radiation source taking molecules into an excited state b) the sample absorbs no energy, therefore is not excited. The laser then must meet certain criteria in order to cause this excitation and ionisation of the sample to occur. The main factors that influence the laser's ability to directly interact with the sample are a) the actual wavelength that the laser generates (UV, visible or IR), b) the power that the laser generates (energy of laser and its area of delivery) and c) the wavelength(s) at which

the sample absorbs. If the laser source matches the sample then ionisation is possible but unfortunately this is not possible with all molecules.

Using MALDI-MS it is possible to get past this shortfall through using a matrix material. Using this approach it is the matrix that is matched with the laser adsorption and not the sample. Analysis is possible by mixing an excess of a matrix material with the sample and forming co-crystals. As the matrix is irradiated by the laser, it will begin ionising with the excess energy being given out to the surroundings which contains the sample, this in turn ionises the sample which is subsequently desorbed. The matrix material, must therefore readily vaporise and thus possess the appropriate molecular mass to promote this process. The matrix must however, not be of too low a molecular mass that it will evaporate during sample preparation or be high in molecular mass that it masks the sample. Matrix materials will often be aromatics which contain polar functional groups (hydroxyl, carboxylic acid groups). These characteristics ensure that the material will provide protons which assist ionisation while being a stable molecule which can readily be prepared in an aqueous solution.

2,5-dihydroxylbenzoic acid   2-(4-Hydroxyphenylazo)benzoic acid

1,8-dihydroxy-9,10-dihydroanthracen-9-one
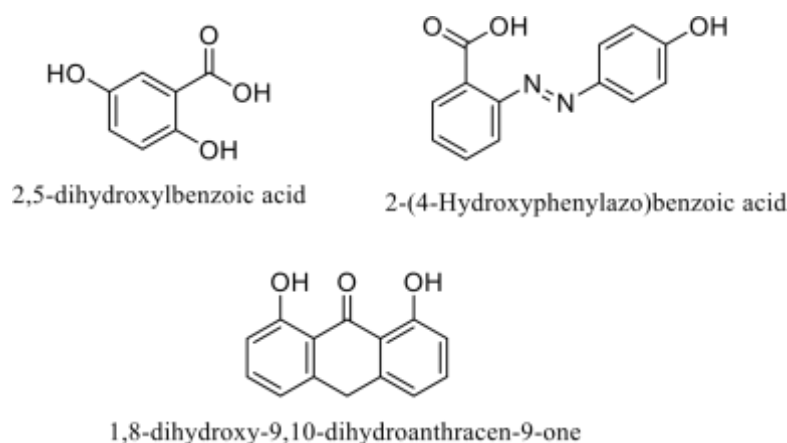
Figure 2.08: Structures of common matrix compounds used in the MALDI-MS analysis of polyurethanes.

Common matrix materials that fit this description are 2,5-dihydroxylbenzoic acid, 2(4-hydroxyphenylazo)benzoic acid and dithranol (1,8-dihydroxy-9,10-dihydroanthracen-9-one) as shown in figure 2.08.[16,17] As the matrix is usually acidic they act as proton donors, resulting in protonated $[M + H]^+$ ions of the sample molecules being obtained. The MALDI-MS method gives good yields of ablated acidic matrix ions, which in turn yields a high proportion of co-ablated molecules of

the sample which are protonated. The previous process can only occur when the matrix-sample complex is co-crystallised to a high quality.[15]

Commonly, polar synthetic polymers produce poor MALDI-MS spectra even when co-crystallised with the matrix. Addition of an alkali metal salt into the matrix recipe has been shown to improve the quality of the spectra observed in many cases. This is achieved by deliberately introducing the alkali metal into the system in the form of an alkali metal salt. The alkali metal being electro-positive will promote gas phase alkali metal cationisation through the stabilisation of the negatively charged polymer in the gas phase. In the analysis of polyurethanes containing a polyester softsegment using a matrix such as dithranol with an alkali metal salt such as sodium trifluoroacetic acid is essential to obtain reasonable spectra. For this system each mass peaks within the MALDI-MS spectra will be 23 mass units higher as each is the sodiated adduct.
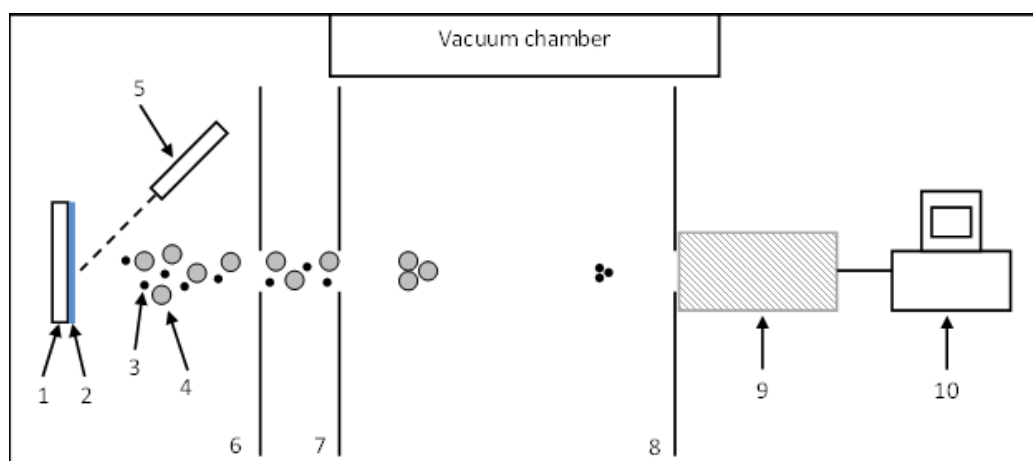
Figure 2.09: MADLDI-MS instrument. 1 = Sample target plate, 2 = Sample, 3 = light ions, 4 = heavy ions, 5 = laser with pulsed beam, 6 = ionisation area, 7 = acceleration field area, 8 = field free time measurement area, 9 = detector and 10 = computer.[18]

Analysis of the ions produced from the MALDI-MS process is possible by using a mass spectrometer. Before entering the time-of-flight tube gas phase ions are subjected to an accelerating potential which can be either positive or negative. As ions enter the time-of-flight tube they will no longer be under the influence of the accelerating potential and enter the field free drift part of the tube where they propagate towards the detector which is situated at the other end of the tube. The time-of-flight

mass spectrometer separates the ions through the known fact that lighter masses will feel the influence of the accelerating potential more than heavier ions, therefore will accelerate faster and reach the detector in a shorter time. Assignment of the mass is then possible by calibrating the instrument using molecules of known mass such as proteins. Next the detector relays this information to a computer where the data can be analysed. Spectra are plotted as % intensity versus mass/charge ratio. The full MALDI-MS process is carried out under vacuum (see figure 2.09).

2.132 Method

Prepolymer adhesives were end capped with ethanol directly after synthesis to prevent an increase of the molecular weight by moisture cure of the free isocyanate. Samples were prepared as a 40 mg ml^{-1} solution in tetrahydrofuran. The matrix used was dithranol or 2-(4-hydroxyphenylazo) benzoic acid in tetrahydrofuran and was prepared as a 20 mg ml^{-1} solution. To promote ionisation of the polyurethane prepolymers sodiated trifluoroacetic acid was also added to the matrix and was prepared in a 1 mg ml^{-1} solution in water. The recipe used for MALDI-MS analysis was 350 μl of matrix and 50 μl of sodiated trifluoroacetic acid. Next matrix and sample were mixed in a 7:1 ratio prior to being placed on the silver analysis tray. Sample solutions were spotted and the solvent was allowed to completely evaporate before being loaded in the analysis chamber. MALDI-MS analysis was carried out on a Kratos Axima-CFR in linear mode using a time-of-flight mass spectrometer with a mass range of 1-150 KDa.

From the data collected it is then possible to calculate the number average molecular weight using:

$$Mn = \frac{\Sigma(NiMi)}{\Sigma(Ni)}$$

Equation 2.3

Where Mn = number average molecular weight, Ni = ion intensity and Mi = ion mass

Then weight average molecular weight is calculated by:

$$Mw = \frac{\Sigma(NiMi^2)}{\Sigma(NiMi)}$$

Equation 2.4

Where Mw = weight average molecular weight

111

Finally, the polydispersity index can then be calculated:

$$PDI = \frac{Mw}{Mn}$$

Where PDI = polydispersity index

2.14 Differential Scanning Calorimetry

2.141 Background

Differential scanning calorimetry (DSC) is a thermal analysis technique that is commonly used in the characterisation of polymer materials due to it being a quantitative means of measuring phase transitions. Using DSC it is possible to determination the temperature and enthalpy changes of phase transitions within a polymer.[19,20] If the polymer possesses regions of crystallinity a primary transition in the form of melting would be observed upon heating whereas if amorphous regions are present it may be possible to observe a secondary phase transitions such as the glass transition temperature (T_g).[20] Measuring phase transition within polymers is possible by monitoring the change to the heat flux through the material as it is going through the phase change. Instruments such as the TA Instruments Q1000 perform analysis such as this routinely (see figure 2.10).

Instruments such as the one mentioned above measure phase transitions in polymers using the analysis cell as shown in figure 2.10 (b). Within this cell a reference pan (empty) and a sample pan are placed with each pan taken through the same heating profile. Both positions are heated independently to ensure that they both maintain the same temperature throughout the heating program.[10] When the sample undergoes a phase transition a variation in the temperature will occur with respect to the reference pan and it is this change in heat flux that can be monitored.

During for example a melting phase transition, the sample pan will lag behind the reference pan as extra energy is required to melt the sample. By plotting temperature versus heat flux a melting peak will be visible as an endotherm. Through normalisation of the sample mass it is possible to obtain enthalpic information on the polymer, such

as the heat of fusion from a melting endotherm. Also the heat capacity change of the glass transition can also be obtained from this normalised data.

(a)   (b)
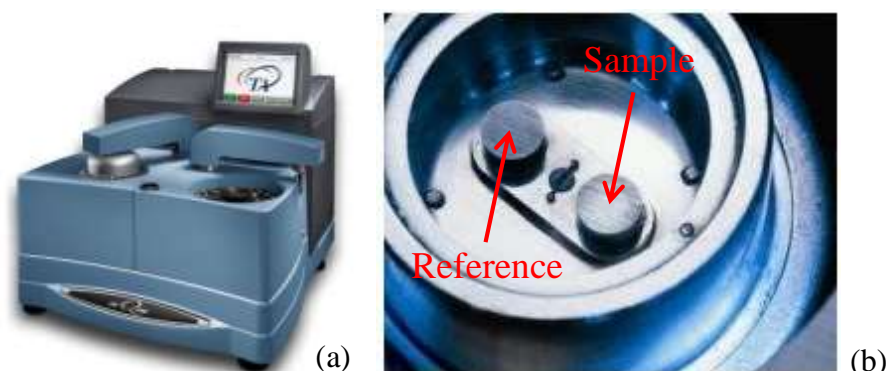
Figure 2.10: Design of a current differential scanning calorimetry instrument (a) and overview of inside the scanning analysis chamber (b).

Figure 2.11 displays a DSC thermogram for a polyurethane prepolymer containing a polyester soft-segment. The soft-segment glass transition occurs at -55°C (1), this is followed by a crystallisation exotherm of the soft-segment at 10°C (2). Within this particular prepolymer both amorphous and crystalline domains are present. Subsequent melting of the ester soft-segment is next observed at 28°C shown by endotherm (3). Curing of the free isocyanate groups of the prepolymer are shown by the large exothermic peak (4) at 230°C. DSC is a very informative technique for the thermal analysis of polyurethanes and when used on fully cured materials it can assist with interpretation of the polymers microphase morphology.

Important thermal transition such as the T_g and T_m will now be discussed in more detail. All polymer materials will be a ridged solid when at a suitably low temperature. As the temperature is increased the amount of energy and ability of the polymer chains to move is increased. This solid to liquid phase transition occurs in two ways and is determined by the organisation of the chains within the material.

A polymer can be either amorphous, semi-crystalline or perfectly crystalline in the solid state. When fully amorphous, the polymers chains within the material are arranged totally random. Polymer of this type follow the specific volume change with temperature path A-B-C (see figure 2.12). At the low temperature end of this path between C-B, the material will be a solid glass. As the temperature is increased, the

113

material passes through the T_g or the glass transition temperature. Once beyond this temperature (B-A) the material will begin to soften and become more rubber like. The T_g is a significant temperature as the properties of the material will change as the system moves above it. With increasing temperature (B-A), the material will move away from being rubbery towards becoming a viscous liquid.
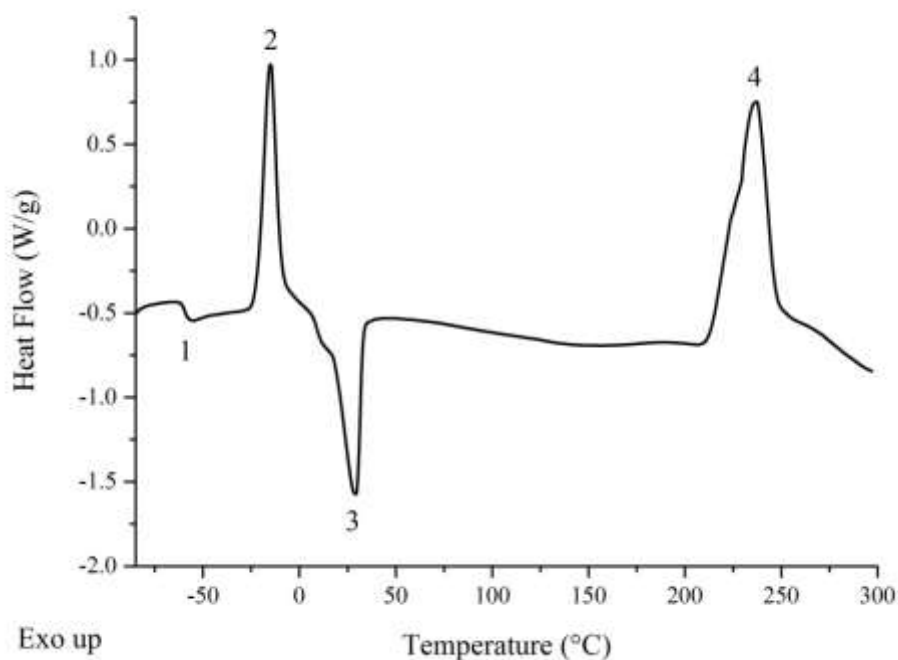
Figure 2.11: **DSC thermogram of a typical semi-crystalline polyurethane prepolymer. Thermogram displays the soft-segment glass transition (1) at 55°C, soft-segment crystallisation exotherm (2) at 10°C, soft-segment melting endotherm (3) at 28°C and exothermic cure at 230°C.**

Perfectly crystalline materials contain polymer chains that are located within regions of three-dimension order known as crystallites. This material will not contain any disordered chains and as a consequence no glass transition will be observed. Upon heating, the perfectly crystalline material will follow path A-G-H. Along this path the material will pass through its melting temperature, $T_m°$ and become a viscous liquid.
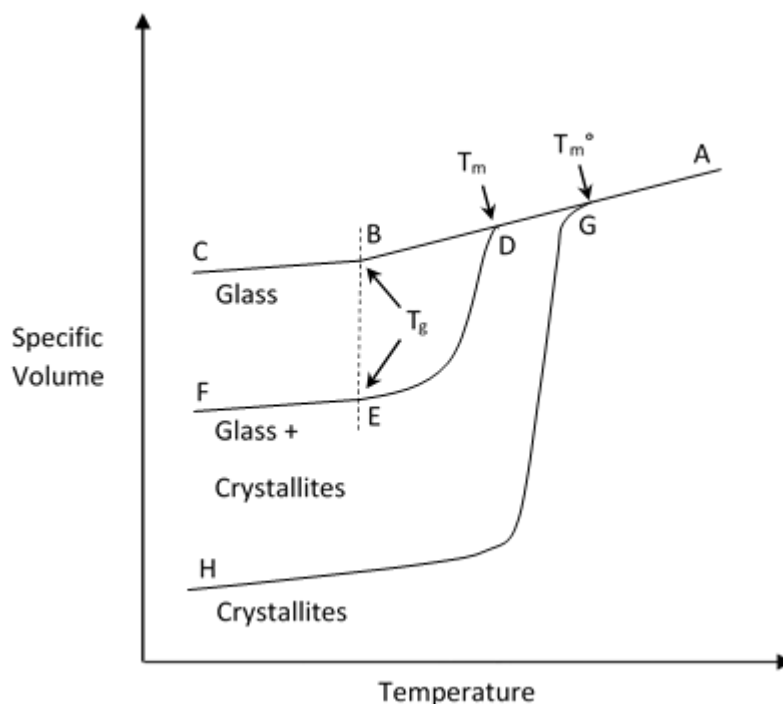
Figure 2.12: Schematic of the solid to liquid transition as represented by the change in specific volume with increasing temperature. A-B-C is a completely amorphous material, A-D-E-F is a semi-crystalline material and A-G-H is a perfectly crystalline material.[21]

More commonly semi-crystalline materials are encountered within practice and follow path A-D-E-F. These materials contain regions of both order and disorder. As a consequence observed for these semi-crystalline material will be both a T_g and T_m, corresponding to the disordered and ordered regions. T_m will occur over a broader range and at a lower temperature compared to $T_m°$. The depression of T_m compared with $T_m°$ arises from semi-crystalline materials containing polymers of various chain lengths and crystallites of various size. Both these factor contribute towards lowering the T_m which can be further influenced by the samples thermal history.

2.142 Method

Both the position and the behaviour of thermal transitions are sensitive to the experimental heating rate, the materials thermal history and the processing history of the material. As samples within this report will be compared with one another, a single heating rate of 10°C min^{-1} was selected. Prepolymer samples were analysed within a nitrogen atmosphere by initially cooling to -90°C and then heating at 10°C min^{-1} to

350°C. For cured samples a cool-heat-cool-reheat experimental procedure was adopted within a nitrogen atmosphere. For the first cooling cycle, the sample is cooled at 10°C min^{-1} to -90°C and held isothermally for 5 minutes. The first heating cycle was used to remove any thermal history from the sample with a ramped heat to 150°C at 10°C min^{-1} used. Next the sample is re-cooled to -90°C at 10°C min^{-1} which again is followed by a 5 minute isothermal hold. On the reheat cycle the sample was again heated at 10°C min^{-1} but this time to the elevated temperature of 300°C.

DSC data is analysed using TA's universal analysis and plotted using OriginPro version 9.0. The glass transition data is quoted as both the position of the glass transition and the range in which the transition occupies. Glass transition temperatures are calculated from the point of inflection which occurs between two linear regions within the base line (calculated by extending the linear regions before and after the transition). Onset and end points of the transition are calculated by identifying where the DSC signal leaves these linear lines. Crystallisation/melting peaks are characterised using both the onset temperature and the peak temperature of the transition. Heat of crystallisation/fusion values are calculated by integrating the area under the peak, with enthalpy values given in J g^{-1}.

To identification of weak thermal transitions, the first derivative of the heat flow is calculated and plotted against temperature (results in appendix A). Calculating and analysis of the first derivative plot is carried out using OriginPro version 9.0. If the feature is ± 10% greater than the baseline it is investigated. Any signals that are clear instrumental noise are excluded from analysis (e.g. signal at 130°C figure A02).

2.15 Thermal Gravimetric Analysis

2.151 Background

As mentioned in the previous section, DSC is a useful tool for monitoring the thermal transitions of polymer materials. The DSC run is plotted as heat flow versus temperature making it simple to identify physical processes such as melting or crystallisation.[10] However, when these transitions are accompanied by a change in the mass of the samples e.g. in degradation where volatile products are liberated and lost to the atmosphere, then analysis of the sample becomes more complex. Following a

thermal transition such as degradation where the sample incurs a mass loss, analysis is much better suited to thermal gravimetric analysis (TGA).[22,23]

TGA experiments are carried out by continuously recording the mass of the sample as it is heated at a constant rate or held isothermally at a constant temperature.[10] Any mass loss that occurs from surface water or trapped solvent which may be absorbed within the sample or products of degradation can be recorded. Analysis is carried out by loading the sample into the furnace which contains a highly accurate electromagnetic balance. The furnace is then sealed and exposed to a flow gas, which is commonly argon for non-oxidative studies or air for oxidative studies. Next the instrument performs the desired heating profile which as previously mentioned will be either isothermal or ramped. Following analysis, percentage mass loss versus temperature is plotted to display the degradation profile of the polymer. Commonly the first derivative of the degradation profile is calculated giving the derivative thermal analysis curve which display the peak rates of degradation from each process occurring.[3] An example TGA curve containing both the degradation and the first derivative are plotted in figure 2.13.
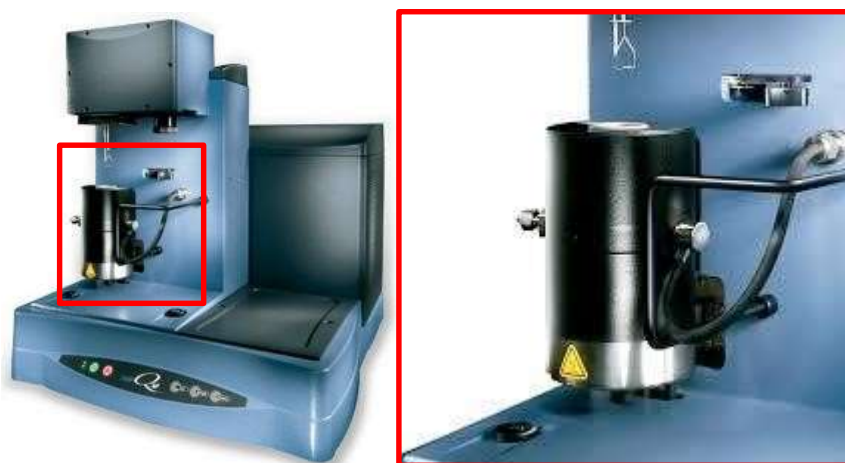
Figure 2.13: TA Q50 TGA instrument displaying highlighted platinum sampling pan and furnace.

Considering together the degradation and derivative curves, a number of features that are characteristic of the polymers decomposition can be observed (figure 2.14). Represented by feature (1) is the onset of polymer degradation which is defined as 5% of the total mass loss. This feature displays the initial temperature at which the

polymer begins to release low molecular mass volatile degradation products (in polyurethanes is normally hard segment fragments). This is followed by primary degradation process (2) which occurs at 329°C in the derivative curve. As the sample begins to further decompose both the second and third decomposition process are observed. The third degradation process is the main decomposition process as shown by the large derivative peak (3) at 401°C whereas, the fourth process can be considered minor and can be seen as a shoulder peak (4) at 426°C. Finally during degradation more stable cross-linked fragments have formed shown by the fifth degradation process which is also visible within the derivative (5) occurring at 543°C.
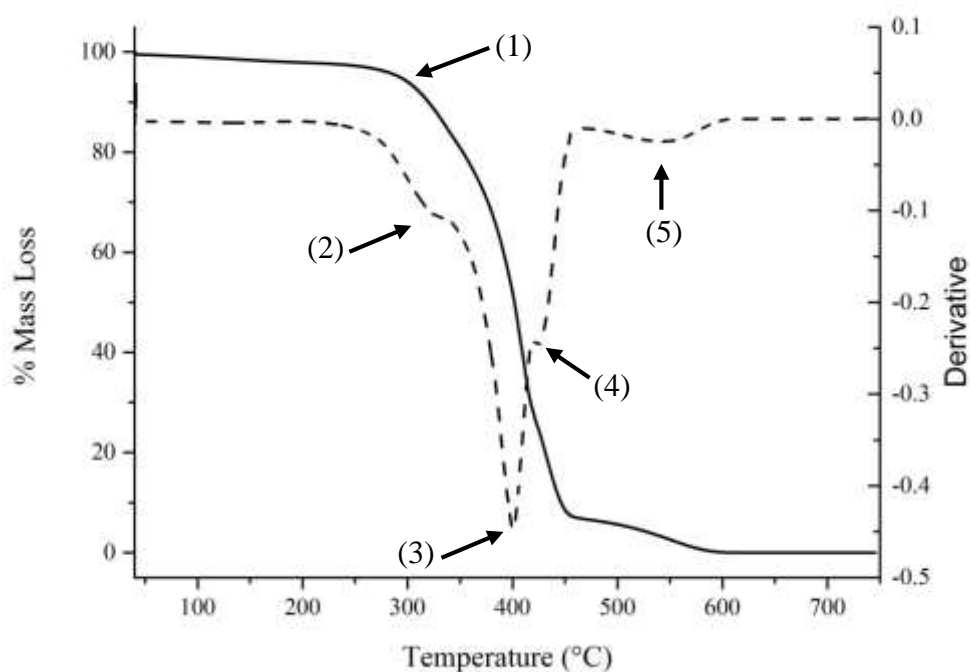
Figure 2.14: TGA degradation curve of a cured polyurethane adhesive (solid black) obtained under argon, complete with first derivative of the degradation curve (dashed black).

Due to recent developments in TGA instrumentation it is now possible to analyse the volatile fragments produced during degradation. Coupling chemical analysis instruments such as FT-IR and mass spectrometry with the TGA allows for detailed analysis of the gases products produced during degradation. With modern instruments it is possible to perform differential thermal analysis measurements to obtain

information on the thermal transitions occurring within the sample. It is therefore possible to characterise the thermal transitions and degradation profile of a given sample using the same instrument.

2.152 Method

Thermal gravimetric analysis was carried out using a TA Q50 TGA using a platinum analysis pan. Cured polyurethanes adhesive samples between 30 – 40 mg were used in TGA analysis. Samples are placed into a clean platinum analysis pan which is then loaded into the instrument furnace. Samples were then taken through a ramped heat from 40°C to 750°C at 10°C min^{-1} under an atmosphere of nitrogen. For each sample the onset of degradation was determined by the temperature at which the sample lost 5% of its initial mass. All TGA curve are plotted using OriginPro 9.0 with the same software package used to calculate the first derivatives.

2.16 180° T-Peel Tensile Test

Tensile testing was used to determine the peel strength in N mm^{-1} of each laminate. Also available from tensile testing was the mode of failure, the effectiveness of each surface treatment and the compatibility of the adhesive with each substrate. Samples were tested at two intervals following lamination namely 7 and 30 days. 7 days was selected as the first test time to determine if the laminated material was cured enough to be further processed. The 30 day test was used to determine two parameters; (a) if the peel strength remained stable when a high strength was obtained following 7 days of cure and (b) when the peel strength was low after 7 could it now be further processed. Following both 7 and 30 days of cure, the target peel strength is set at 3 N mm^{-1} with the target mode of failure being cohesive within the adhesive. 180° Tpeel test experiments were carried out using an Instron 4301 equipped with a 1 kN load cell. As the results obtained are used on a comparison bases the test procedure was standardised as follows. Sample width was fixed at 25 mm, extension length was fixed at 150 mm and extension rate was fixed at 100 mm min^{-1}.

Figure 2.15: 180° T-peel roller system used to ensure correct angle obtained during testing on laminates containing different ply materials.

Laminates constructed using two different substrates are subject to variability in the peel angle as both materials will react differently under the load. To insure that the angle obtained was 180° a roller system was used for all testing as shown in figure 2.15. These rollers were separated by a gap which is greater than the laminate thickness and were highly polished to reduce frictional forces. Within the example roller system within figure 2.15, the gap was set at 500 microns which allowed for testing of adhesive layer up to 150 microns.

Samples traces are plotted as force in kN versus displacement in mm. The first 50 mm of each sample was not considered during strength calculations as in this region the formation of a stable crack is obtained (zone 1 figure 2.16). Peel strength values are then calculated using formula 2.6.

$$P = \frac{L}{w}(1 - \cos\theta)$$
<div align="right">Equation 2.6</div>

P = peel strength in N/mm, L = load in N, w = sample width in mm, θ = peel angle.[24]

As the peel angle used within this study was 180° the equation reduces to:

$$P = \frac{2L}{w}$$
<div align="right">Equation 2.7</div>

Calculation of the peel strength is performed using the average load value obtained between 50 and 150 mm of extension (zone 2 figure 2.16). Values exceeding 3 N mm⁻

[1] obtained during peel testing are classed as a pass whereas, strengths below this value are considered a fail. The target mode of failure is cohesive within the adhesive as this displays good compatibility with the interface. An adhesive mode of failure above 3 N mm^{-1} is still considered a pass but is not considered ideal as the bond may be susceptible to failing from moisture ingress. Cohesive modes of failures within the adhesive also display that the compatibility of the interface and the adhesive is high, making the long term stability of the bond less of an issue. This is in comparison to bonds that are failing adhesively at the interface.
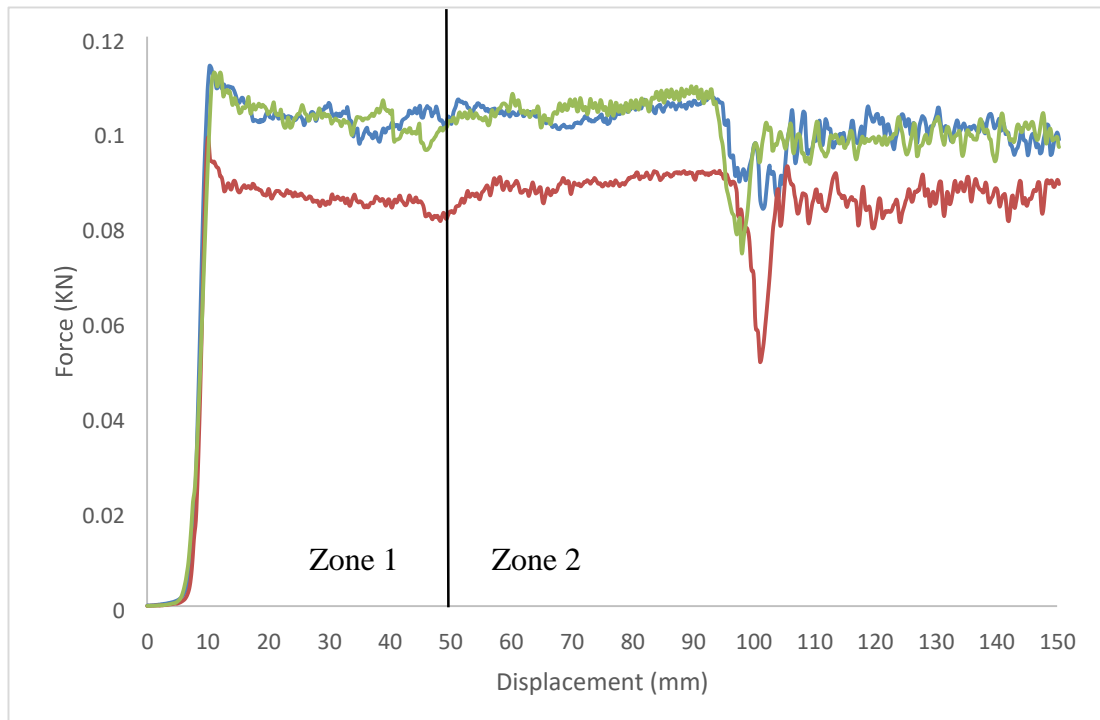
Figure 2.16: **Example of the traces obtained during 180° T-peel testing for calculation of peel strength. Zone 1 is discarded and zone 2 is used in calculation.** 180° peel test measurements are given for 7 and 30 days and are accompanied by the mode of failure observed. The mode of failure is monitored by visual inspection however, when not clear the mode of failure is determined by ATR. This is carried out by placing the peeled interface onto the ATR crystal to investigate if the adhesive is visible or just the substrate. The accepted error in the peel strength measurement is ± 0.5 N mm^{-1}.

Due to the size of the samples it was not possible to store them within a controlled temperature and humidity environment meaning samples were subjected to variations

in these parameters. Unless stated when no data (ND) is presented within the peel strength table it occurs due to the adhesive layer foaming. Foaming of this layer affects the adhesive to substrate interface and makes the data obtained nonrepresentative of the sample.

2.17 Haze Measurements

2.171 Background

Plastics used in optical applications such as sunglass lenses should be both clear and transparent. Any adhesive used in the lamination of such materials must also therefore be clear and transparent. Within this project, the haze of the laminate formed was of interest as any laminate with a haze measurement of > 1.5% will be rejected. This makes measuring the haze of each cured laminate essential for success within this research project. To understand how haze measurements are recorded and the effect that haze has on viewed image, the total transmittance of light through a material must first be considered.

Total transmittance of a translucent material is defined as the ratio of incident light intensity versus transmitted light intensity. The magnitude of this ratio is influenced by the materials properties and this will dictate the proportion of incident light which is absorbed or reflected. Therefore the amount of light transmitted will be the sum of both directly transmitted and diffuse transmitted light. The appearance of the transparent plastic will consequently be influenced by the angular nature of this diffuse scattered light which can occur over either a wide or narrow angle (see figure 2.17).

Diffuse light will alter the image as a result of the scattering effect which occurs as light passes through the translucent material. When scattering occurs over a wide angle, the visual effect that is observed for the image is termed as haze. Within ASTM D 1003 haze is defined as the percentage of light which following transmission through a material has deviated from the incident beam by greater than 2.5°. Visually, haze will make the image appear milky or foggy.
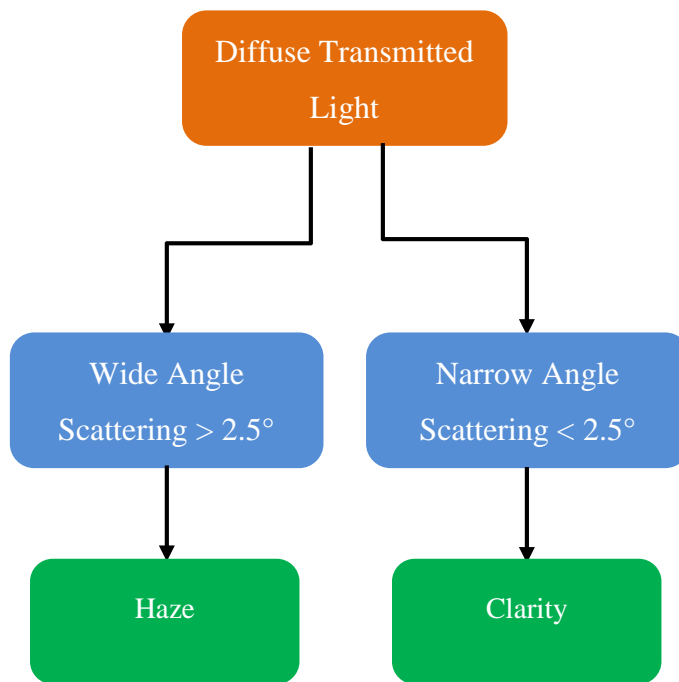
Figure 2.17:   Flow diagram showing the two different kinds of diffuse light and the effect they have on the appearance of an image.[25]

When light is diffusely scattered by a narrow angle of less than 2.5°, the effect to the image quality is different. Diffuse transmitted light of this type will have an effect on the sharpness of the image and will often obscure any fine details. Both these scattering events can be introduced if the material is not processed properly e.g. in manufacturing processes such as lamination and injection moulding. In lamination for example haze can often be encountered due to defects within the adhesive layer. Haze within this layer can be caused by: molecular structure, degree of crystallisation and impurities at the interface or within the adhesive. Therefor during manufacture it is important to consider the final properties of the adhesive, the methods employed to ensure cleanliness, the application method and the final curing mode.

2.172: Method

The haze of each polyurethane adhesive was tested using a BYK Gardner Haze-gard Dual. The haze value quoted for each adhesive is the average of the six laminates tested (see 2.04).

$$Haze = 100\% \cdot \frac{T_{dif}}{T_T}$$
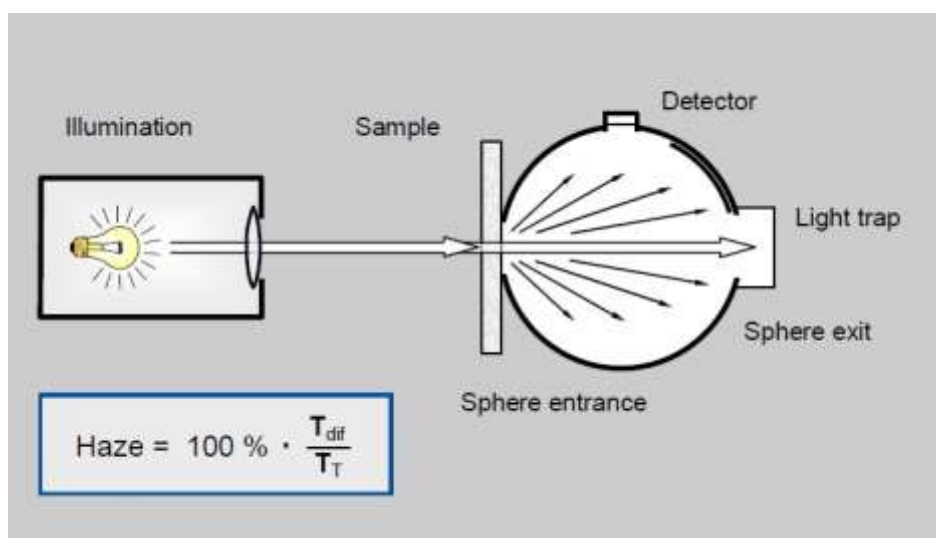
Figure 2.18: Typical instrumental set-up for measurement of sample Haze. T_{dif} = total diffuse light and T_T = total transmitted light.[25]

The haze test employed measures adsorption, transmittance and deviation angle of the incident beam by the laminate material. Testing is performed by placing the sample in the path of a narrow beam of incident light (see figure 2.18). As the incident beam passes through the material it will either pass through unimpeded or be diffusely scattered by the laminate. Both these parts of the beam enter into the sphere which is equipped with a photodetector. From this collected light two quantities can be determined: the total strength of the light beam and the portion of the original beam that has been deviated by an angle of $> 2.5°$. Obtaining these two quantities allow for calculation of both the haze which is calculated from the wide angle diffuse component and the luminous transmittance which is the percentage of the incident beam that has been transmitted through the sample unimpeded. As previously mentioned, the haze values obtained for each laminate must not exceed

1.5%.

References

(1)   Li, C.; Wilkes, G. *Journal of Inorganic and Organometallic Polymers* **1998**, *8*, 33.
(2)   Chattopadhyay, D. K.; Prasad, P. S. R.; Sreedhar, B.; Raju, K. V. S.
N. *Progress in Organic Coatings* **2005**, *54*, 296.
(3)   Korley, L. T. J.; Pate, B. D.; Thomas, E. L.; Hammond, P. T. *Polymer* **2006**, *47*, 3073.

(4)   Sánchez–Adsuar, M. S.; Papon, E.; Villenave, J. J. *Journal of Applied Polymer Science* **2000**, *76*, 1596.

(5)   da Silva, A. L. D.; Martín-Martínez, J. M.; Carlos Moura Bordado, J. *International Journal of Adhesion and Adhesives* **2008**, *28*, 29.

(6)   Chen, G.; Shen, D.; Feng, M.; Yang, M. *Macromolecular Rapid Communications* **2004**, *25*, 1121.

(7)   Masale, M. *Physica B: Condensed Matter* **2002**, *311*, 263.

(8)   Garbassi, F.; Morra , M.; Occhiello, E. *Polymer surfaces, from physics to technology*; Wiley, 1994.

(9)   Williems, D. H.; Fleming, I. *Spectroscopic methods in organic chemistry*; McGraw-Hill book company, 1980.

(10)   Campbell, D.; white, J. R. *Polymer Characterisation Physical Techniques*; Chapman and Hall, 1991.

(11)   Weston, D. J. *Analyst* **2010**, *135*, 661.

(12)   Berkenkamp, S.; van den Boom, D.; Fabris, D. In *MALDI MS*; WileyVCH Verlag GmbH & Co. KGaA: 2013, p 169.

(13)   Li, L. In *MALDI MS*; Wiley-VCH Verlag GmbH & Co. KGaA: 2013, p 313.

(14)   Chattopadhyay, D. K.; Raju, N. P.; Vairamani, M.; Raju, K. V. S. N. *Progress in Organic Coatings* **2008**, *62*, 117.

(15)   Hillenkamp, F.; Jaskolla, T. W.; Karas, M. In *MALDI MS*; WileyVCH Verlag GmbH & Co. KGaA: 2013, p 1.

(16)   Jespersen, S.; Niessen, W. M. A.; Tjaden, U. R.; van der Greef, J. *Journal of Mass Spectrometry* **1998**, *33*, 1088.

(17)   Jaskolla, T. W.; Karas, M.; Roth, U.; Steinert, K.; Menzel, C.; Reihs, K. *Journal of the American Society for Mass Spectrometry* **2009**, *20*, 1104.

(18)   O'Connor, P. B.; Dreisewerd, K.; Strupat, K.; Hillenkamp, F. In *MALDI MS*; Wiley-VCH Verlag GmbH & Co. KGaA: 2013, p 41.

(19)   Wang, C. B.; Cooper, S. L. *Macromolecules* **1983**, *16*, 775.

(20)   Chen, T. K.; Chui, J. Y.; Shieh, T. S. *Macromolecules* **1997**, *30*, 5068.

(21)   Cowie J. M. G, A. V. *Polymers: chemistry & physics of modern materials*; John Wiley & Sons, Ltd, 1992.

(22)   Wang, X.; Fu, Y.; Guo, P.; Ren, L.; Wang, H.; Qiang, T. *Journal of Applied Polymer Science* **2013**, *130*, 2671.

(23)   Cakic, S. M.; Stamenkovic, J. V.; Djordjevic, D. M.; Ristic, I. S. *Polymer Degradation and Stability* **2009**, *94*, 2015.

(24)   Packham, D. E. In *Handbook of Adhesion*; John Wiley & Sons, Ltd: 2005, p 311.

(25)   BYK-Gardner GmbH; Altana, Ed. 2010.

Chapter 3 Aromatic Polyurethane Adhesives based on Poly(propylene glycol)

3.10 Polymers Synthesis Introduction

When attempting to synthesise an optically clear high strength polyurethane (PU) adhesive, a natural starting formulation would be based on hard-segment of methylene diphenyl diisocyanate (MDI) and soft-segment of poly(propylene glycol) (PPG). MDI based adhesives are known for giving high peel strength materials due to the organisation of hard-segments in the polyurethane microstructure.[1] These hard-segments form rigid domains due to π-π stacking of the aromatic rings and hydrogen bonding of the urethane linkages. When sufficient in concentration this organisation of microstructure within the bulk PU material can bring great strength, however, when very high the strength can be coupled with microstructure phase mixing. For the intended application it is essential that the concentration of hardsegments is not too great as this will have an adverse effect on the optical clarity of the final adhesive. During design of the adhesive a degree of phase mixing should be aimed for to promote the potential for an optically clear cured adhesive. Finally, MDI is readily available in its monomeric form since it is globally used in PU foam production and within PU structural adhesives in the footwear assembly industry.[2]

PPG is also an easily obtained starting material as its used in the flexible foams industry making it available in a variety of grades and molecular weights.[1] The low viscosity liquid will aid in synthesis and application of the final adhesive. PPG softsegment materials have high clarity which in theory should aid the intended optical application of the adhesive making it the natural first choice. The high clarity is inherent of the high concentration of pendent methyl groups along the polyol backbone structure which inhibit crystallisation. It may be possible to use the steric hindrance of the methyl groups to disrupt the concentration or domain size of the hard-segments and encourage phase mixing of the bulk microstructure. The use of small molecular weight alcohols as chain-extending agents will aid two processes: increasing the molecular weight of the prepolymer which should increase the green strength after application and also if the chain-extender contains steric pendent groups, this will further disrupt the hard-segment microstructure leading to higher clarity adhesives.
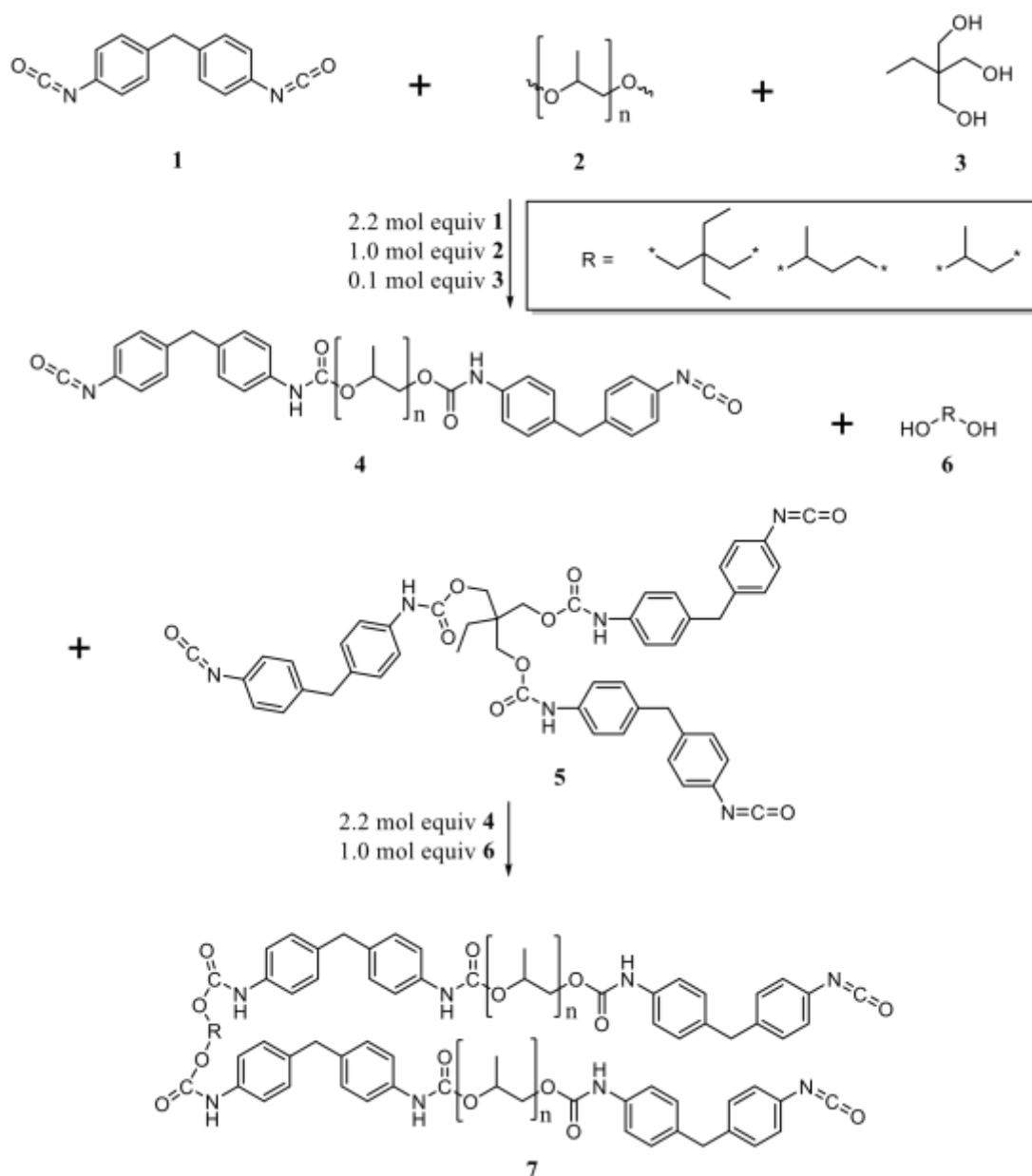
Figure 3.01: General reaction scheme for the synthesis MDI-TMP-PPG based chain-extended polyurethanes adhesives. 1 = MDI, 2 = PPG, 3 = TMP, 4 = MDIPPG prepolymer, 5 = end capped MDI-TMP, 6 = chain-extender and 7 = chainextended prepolymer.

Conversely too much disruption of the hard-segments microstructure will reduce the overall strength of the cured adhesive. To help combat the possibility of the cured matrix being of low strength a tri-functional chain-extender was added to increase the overall matrix strength in the form of trimethylolpropane (TMP). The formation of

physical cross-links will help to boost the overall matrix strength of the cured adhesive as it will encourage the network to form in three dimensions.

The adhesive applied during lamination will be a reactive prepolymer PU. The intended mode of cure will be between an initial catalyst cure (dibutyltin dilaurate and triethylamine as catalysts) followed by a final moisture cure at room temperature, thus making the final fully cured adhesive a polyurethane-urea (PU-U), with the urea component again encouraging hard-segment formation, these groups should help with obtaining a high peel strength adhesives.

The four polymer materials to be synthesised for application and discussed during this section will be:

- MDI-TMP-PPG (base material)
- MDI-TMP-PPG-DEPD
- MDI-TMP-PPG-BD
- MDI-TMP-PPG-PD

Where DEPD (2,2-diethyl-1,3-propane diol) is **6**, BD (1,3-butane diol) is **7** and PD (1,2-propane diol) is **8**.

6   **7**   **8**
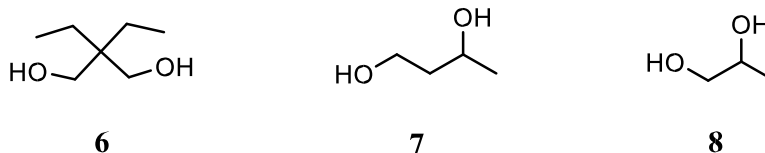
Figure 3.02: Structure of chain-extenders used to disrupt hard-segment formation.

The base formulation MDI-TMP-PPG (formula shows that formulation contains a MDI and PPG prepolymer which contains TMP chain-extender) will be representative of the prepolymer synthesised for the subsequent polymers prior to diol chain-extension. Each chain-extender used has a hindered structure (see figure

3.02) to disrupted hard-segment organisation and if they operate as proposed should lead to optically clear low haze PU-U adhesives. Characterisation of the synthesised prepolymers will be performed by techniques NMR, MALDI-MS and DSC.

Determination of the laminate strength will be determined using 180° T-peel testing of the laminates in triplicate with the average value being present from the three test samples in N mm^{-1}. The thermal behaviour of each cured adhesive will be investigate by DSC and TGA to ensure that there are no thermal transitions operating within the window of practical use that will have an adverse effect on the adhesive performance. For TGA and DSC, a separate sample was prepared using two plies of cellulose triacetate (TAc) to form the laminate which once cured could be removed for testing. Finally, the cured material obtained from each laminate will be investigated by ATR to determine if the mode of cure and bulk adhesive are the same for each of the laminates formed.

3.20 Analysis of MDI-TMP-PPG

3.21 Synthesis Information

Prior to synthesis, PPG (molecular weight 1000) was dried to remove water by placing within a vacuum oven at 80°C for at least 48 hours. The synthesis was performed using reaction set-up as detailed in section 2.03 with the reaction being performed in the temperature window of 85°C – 95°C for three hours. The reaction time was started after the last addition of MDI to the polyol containing reaction vessel. MDI was melted (50 – 60°C within a three necked round bottom flask as in section 2.03) and degassed before being put under a nitrogen atmosphere. To ensure that the exothermic reaction did not exceeded 95°C, MDI was added drop wise in 1 ml portions. The final prepolymer obtained was clear but visually thicker than the starting mixture as a consequence of the molecular weight increase. Prior to catalyst addition samples of the reaction were taken for NMR, MALDI-MS and DSC analysis. After the elapsed reaction times of three hours 0.05 wt% of dibutyltin dilaurate and 0.05 wt% of triethylamine were added as curing catalysts (calculated from batch weight). Following catalyst addition, the formulation was transferred to an aluminium holding tube which was placed within a vacuum desiccator and kept at 0°C with a fridge until being used during lamination (typically not exceeding 7 days). Degassing was performed for six hours once a vacuum of one atmosphere was obtained.

The prepolymer adhesive was applied to six different laminates that were of interest:

- TAc/TAc
- TAc(t)/TAc(t)
- TAc(t)/PC
- TAc(t)/PC(t)
- PC(t)/PC(t)
- PC/PC

Where TAc is cellulose triacetate, PC is bisphenol-A polycarbonate and (t) denotes that the surface of the polymer film has been treated (see section 2.01 and 2.02). As MDI-TMP-PPG was of low viscosity even after synthesis only a low application temperature of 50°C was required to ensure good surface coverage. The lamination process was carried out as detailed in section 2.04 and each laminated materials was cured at room temperature. 180° T-peel testing was carried out initially within 7 days and then after 30 days to determine the peel strength of each laminate with the mode of failure monitored by visual inspection. The cured laminates from the 30 day peel testing were used in the ATR analysis of the fully cured adhesive.

3.22 NMR Analysis

To ensure that reaction between the hydroxyl end groups of the PPG polyol and the isocyanate of MDI had occurred NMR spectroscopy was used. The two nuclei investigated were ^{1}H and ^{13}C as both would be able to display if the polyurethane reaction had occurred. From previous analysis it had been determined that the PPG polyol has both primary and secondary hydroxyl end groups. Both these groups will react but the primary hydroxyl groups will be consumed quicker than the secondary groups.

In figure 3.03 the ^{1}H spectrum for MDI-TMP-PPG is of the isocyanate end-capped prepolymer material used as the first formulation for lamination. At 1.1 ppm the singlet represents the C**H$_3$** groups on the PPG backbone **1'**, while the peak at 0.9 ppm is the C**H$_3$** group of the TMP chain-extender. The C**H$_2$** groups adjacent to the methyl of TMP are visible at 1.6 ppm. Observation of the C**H$_2$**-O protons of TMP is not possible as they are convoluted with the signal from the MDI methylene bridge **10'** at 3.9 ppm. Next encountered are two broad peaks, the first at 3.4 ppm represents the C**H$_2$** of the PPG backbone **3'** and the second at 3.6 ppm represents the C**H** of the PPG

backbone **2'**. Broad peaks such as these are inherent of the atactic nature of the PPG used, meaning there are a variety of possible environments in which these protons can be found. Positioned at 4.1 ppm is the peak which represents the **CH₂**-O groups next to a urethane linkage that have come from the reaction of a primary hydroxyl group **6'**. Methylene **CH₂** bridging groups of the MDI moiety **11'** are next observed at 3.9 ppm. Reaction of the secondary hydroxyl groups to form urethane linkages are next present and their occurrence is confirmed by the **CH** signal at 4.9 ppm.
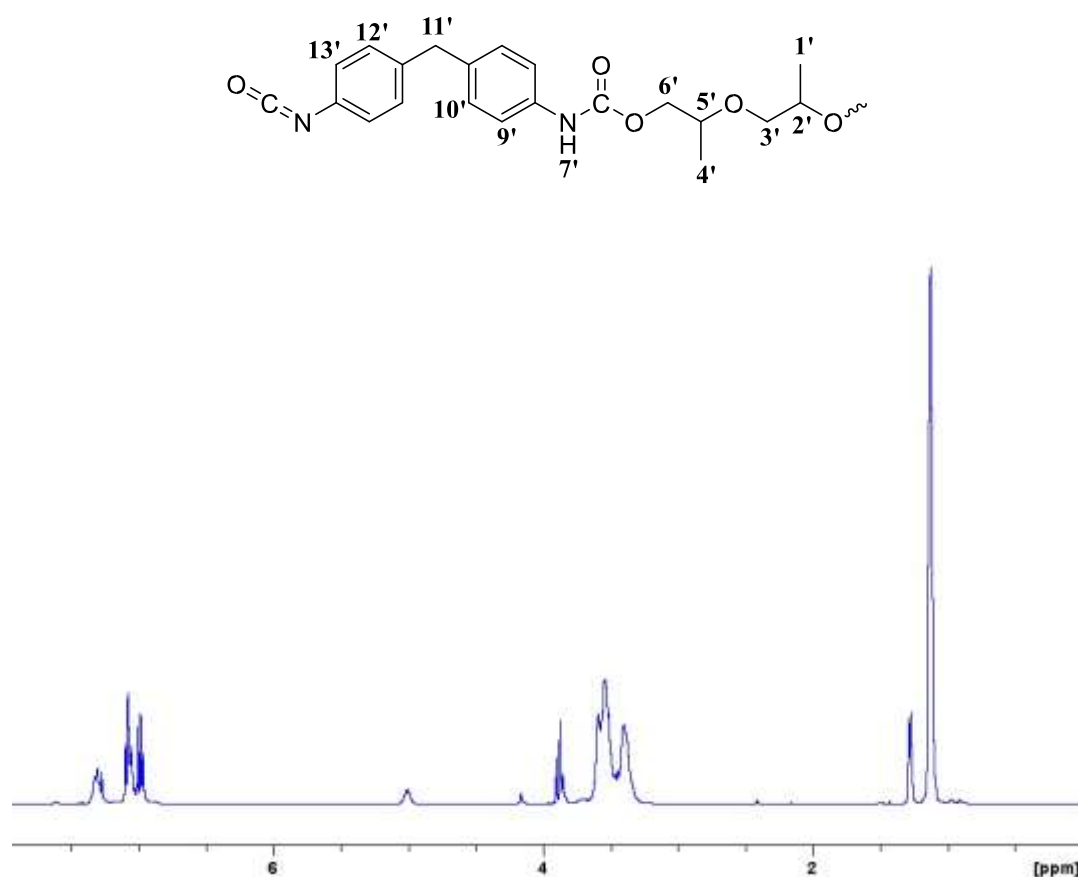
Figure 3.03: ¹H NMR spectrum of MDI-TMP-PPG polyurethane prepolymer in deuterated chloroform.

Next at 7.0 ppm **12'** and 7.1 ppm **13'**, the **CH** of the aromatic protons present on the unreacted ring are observed. As these signal are still visible it infers that there is still the presence of free isocyanates, which are essential for a reactive adhesive. These peaks have become broadened when compared to unreacted MDI (two sharp peaks at 7.0 and 7.1 ppm) and this comes from there being a convoluted contribution of the

meta **CH** protons due to the urethane linkages influence on the ring. At 7.3 ppm the broad peak represents a **NH** proton **7'** which is further evidence of the urethane linkage being formed.[3] Its formation is direct evidence that urethane linkages are present, confirming that a PU prepolymer has been synthesised.

Integration is a useful tool for analysis of ^{1}H NMR as the signal intensity is directly proportional to the number of nuclei at that shift. This makes integration a convenient method for monitoring protons pre- and post-synthesis. Integration of the **NH** versus aromatic ring protons presents a ratio of 1:3.7. This value indicates that the prepolymers within solution must not all MDI-PPG-MDI type as this would give an integration ratio of 1:4. It would be expected based on the ratio obtained that there must be a contribution from higher molecular weight prepolymers. The presence or absence of higher molecular weight prepolymers will be investigated using MALDI-MS (see section 3.23).

Next ^{13}C analysis was performed on the same sample to determine what other information could be collected from the prepolymer. At 17 ppm the methyl carbons of the PPG backbone **1 + 4** are observed followed by the methylene carbon of the MDI molecule **12** at 41 ppm. Next the small peak at 71 ppm represents the secondary carbon atom bound to an oxygen atom within a urethane linkage **6** (prior to the reaction would have been a primary hydroxyl group). At 72 ppm the tertiary carbon from the other PPG end group is observed **5** (prior to reaction would have been secondary hydroxyl). Next encountered are the PPG backbone peaks with the secondary carbon **3** at 73 ppm and the tertiary carbon **2** at 75 ppm. The large triplet at 77.23 ppm can be ignored as this signal is from the deuterated chloroform solvent. The next set of peaks all correspond to carbons that are part of the MDI aromatic ring or the urethane linkage. For MDI in its unreacted state only five different carbons would be expected (ipso, ortho, meta, para and carbonyl in N=C=O) but as a urethane bond is now present the molecule is now asymmetric and additional peaks are observed.
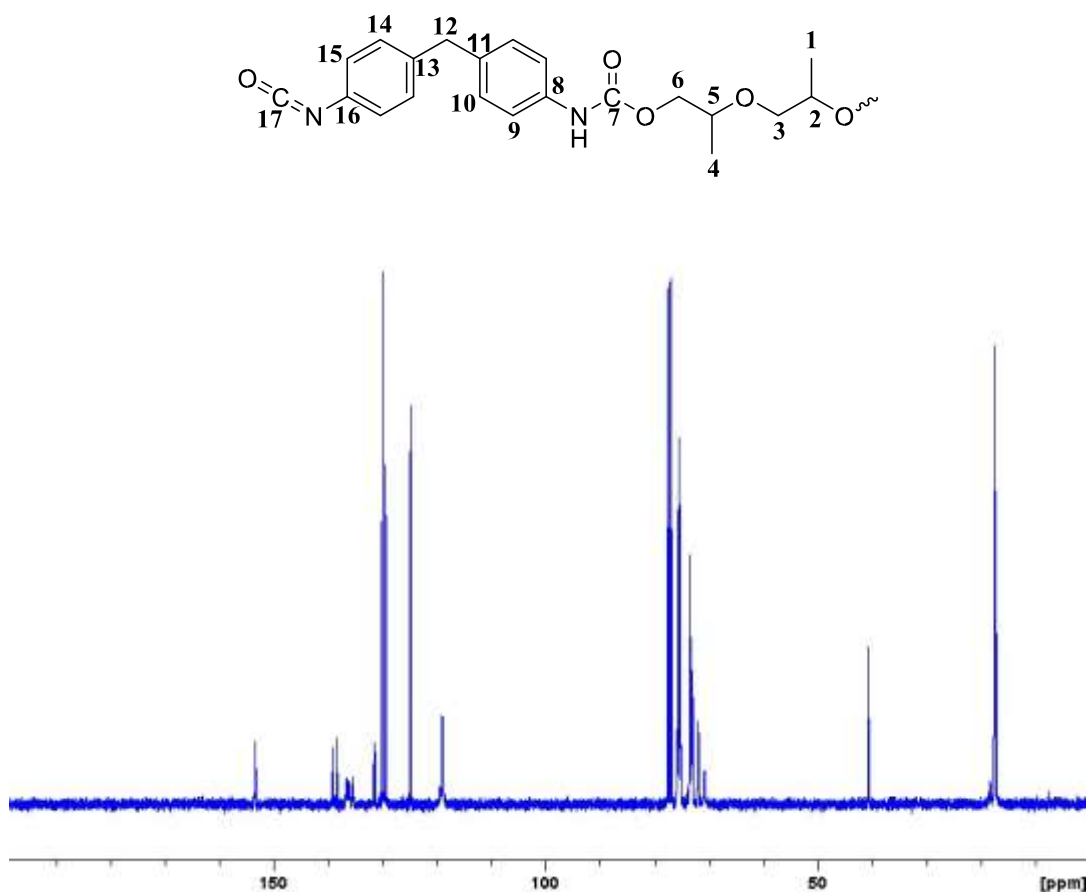
Figure 3.04: ^{13}C NMR spectrum of MDI-TMP-PPG prepolymer in deuterated chloroform.

Carbon atoms positioned ortho to the reacted urethane linkage **9** have a signal at 119 ppm which is an up field shift from 124 ppm for the carbons ortho to the unreacted isocyanate group **15**. At 129 ppm the signal represents the carbon connected to the methylene bridge on the ring that has the urethane linkage **11**. Observed at 130 ppm are two peaks that account for the meta carbons for the reacted ring **10** and **14** of the unreacted ring. The two peaks at 131 ppm are representing the carbonyl carbon **17** of free isocyanate groups and the ring carbon **16** where the isocyanate groups are attached. Following on at 135 ppm, the ring carbon that is connected to the NH of the urethane link **8** is observed. The presence of both peaks **8** and **17** display that not all isocyanate groups have been consumed which must be true if a prepolymer were formed. Further evidence of urethane formation is given by the peak at 136 ppm which represents the ring carbon connected to the NH of the urethane linkage **8**. The peak at 139 ppm represents the ring carbon attached to the methylene bridge **13** on the

unreacted ring. A final piece of evidence of the urethane reaction is shown at 153 ppm and represents the carbonyl within the urethane bond **7**.

3.23 MALDI-MS Analysis

The previous section was able to show that there was both reacted and unreacted isocyanate groups and the presence of urethane linkages. However, to try and fully understand the structure of the prepolymer mass spectrometry data is required. To serve this purpose matrix assisted laser desorption ionisation time-of-flight mass spectrometry (MALDI-MS) analysis was employed to determine the molecular mass of the starting polyol and then the prepolymer adhesive. The matrix used was dithranol which was prepared as a 20 mg ml^{-1} solution in tetrahydrofuran (THF), this was then mixed with a 1 mg ml^{-1} solution of sodiated trifluoroacetic acid (NaTFA) in a 7:1 ratio respectively. MDI-TMP-PPG sample was prepared as a 40 mg ml^{-1} solution in THF which was then mixed with the matrix in a 1:8 ratio of sample to matrix. 1 μl aliquots of the solution were then spotted and dried before analysis.

The mass spectrum of PPG in figure 3.05 displays the di-sodiated adduct of the polyol material with the sodium coming from the small amount of a cationising agent (NaTFA) added to obtain quality spectra. Present at 1045 m/z is the chain-extender TMP that has reacted with three MDI units which are ethanol end-capped (plus one sodium cation). These molecules will contribute to the hard-segments microstructure within the adhesive and their observation was possible as all the starting material was consumed.

For the prepolymer material a shift of the distribution by 592 m/z was observed which correspond to the addition of two MDI units that have had their free isocyanate groups end capped with ethanol to maintain the molecular weight. From this spectrum we can observe that using a 2.2:1.0 excess of isocyanate to polyol makes it possible to obtain an MDI-PPG-MDI end capped prepolymer PUs. A higher molecular mass distribution is also present in the sample spectrum and these correspond to another polymerisation product which is MDI-PPG-MDI-PPG-MDI which is centred around 2700 m/z.
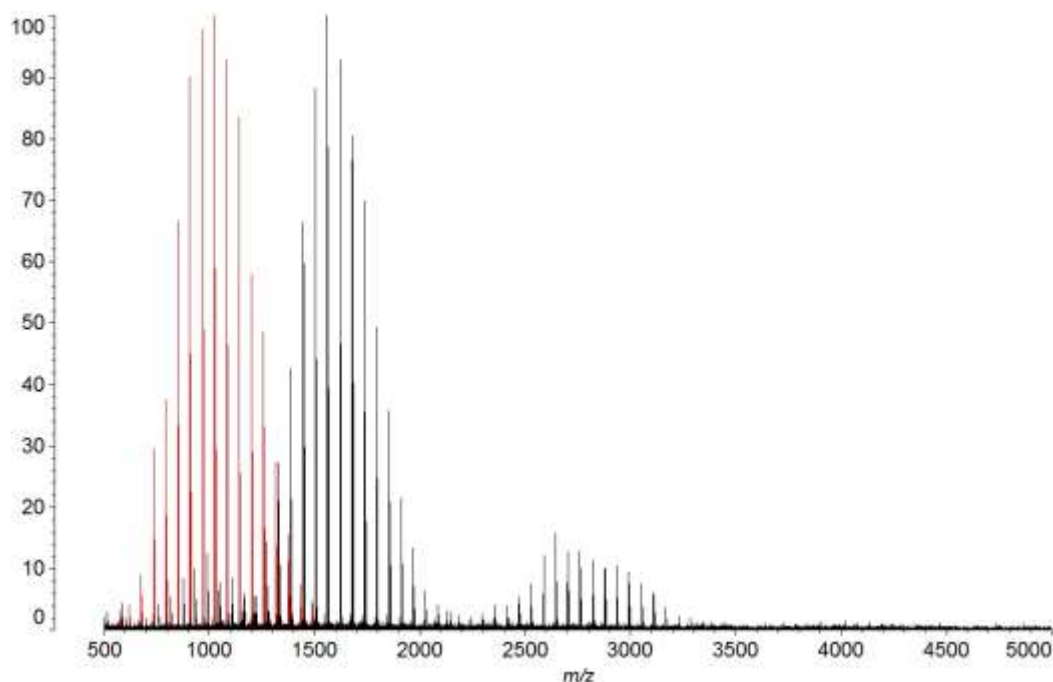
Figure 3.05: MALDI-MS spectra of PPG starting materials in red and the prepolymer MDI-TMP-PPG in black. Both were mixed with the matrix material of dithranol and sodiated trifluoroacetic acid in a 1:8 sample:matrix mixture.

From the MALDI-MS spectrum it is possible to calculate number average molecular weight (Mn), weight average molecular weight (Mw) and polydispersity index (PDI) of PPG. The calculated value of Mn is 1008 m/z and the value for Mw is 1033 m/z. The PDI of the sample is 1.02 and displays that the PPG soft-segment has a narrow distribution (see section 2.132 for formulae). Following synthesis an increase to the value of Mn which is now 1992 m/z and Mw which is now 2463 m/z in formulation MDI-TMP-PPG. A visible broadening of the polymer distribution compared to PPG is supported by the increased PDI value of 1.24. MALDI-MS has allowed for characterisation of the structure of the molecules present in conjunction with the previous NMR analysis.

3.24 DSC and TGA Analysis

Understanding the thermal behaviour of the prepolymer and cured adhesive is important to determine if the current formulation will be appropriate for the likely temperatures that a laminate will be exposed to during manufacture. Two techniques that were selected to investigate if the materials were capable of being stable either

side of a set functional working window of -20°C – 100°C were differential scanning calorimetry (DSC) and thermal gravimetric analysis (TGA). The thermal behaviour of the prepolymer directly after synthesis will be discussed first and fully cured adhesive (adhesive removed from a TAc/TAc laminate) will be discussed second.

Understanding the position of the soft-segment glass transition ($T_g$ss) for each formulation was outlined as an important piece of information to collect. For the prepolymer material, the initial aim was to keep the $T_g$ss as low as possible in an attempt to keep the final cured $T_g$ss out with the identified window. Any increase in $T_g$ss would come from the increase in molecular weight as expected during cure and also any increase in cross-linking. In the current formulation the main mode of cross-linking is via the TMP molecule which is present with the hard-segments of the microstructure. Additional hard-segment cross-linking may occur following moisture cure, as urea is formed it will provide two available NH protons for Hbonding (only one in the urethane linkage). When the hard-segments are well organised they may be further cross-linked through π-π ring stacking of the MDI molecules. Finally when the adhesive is operating above its $T_g$ss it will ensure that the matrix remains flexible and will not compromise the impact resistance of the laminate.

Figure 3.06 contains the DSC thermogram for MDI-TMP-PPG prepolymer. From the thermogram, the recorded $T_g$ss occurs at -29°C (range from -32°C to -35°C) which at this point is outside the specified processing window. Ideally the prepolymer $T_g$ss temperature would be lower as there is a chance it may enter the functional window following cure. Such elevation of the $T_g$ss would make the adhesive out with specification outlined and jeopardise its likelihood of being a valid formulation. Also present in the thermogram of MDI-TMP-PPG are two exothermic peaks at 68°C and 223°C which would indicate some form of curing chemistry occurring. At this point, the lower temperature curing event is not truly understood and the higher temperature cure will be isocyanate based reactions, leading to functional groups such as an isocyanurate. DSC of MDI-TMP-PPG has confirmed that the $T_g$ss is out with the working window at this point meaning the formulation can be used for lamination.
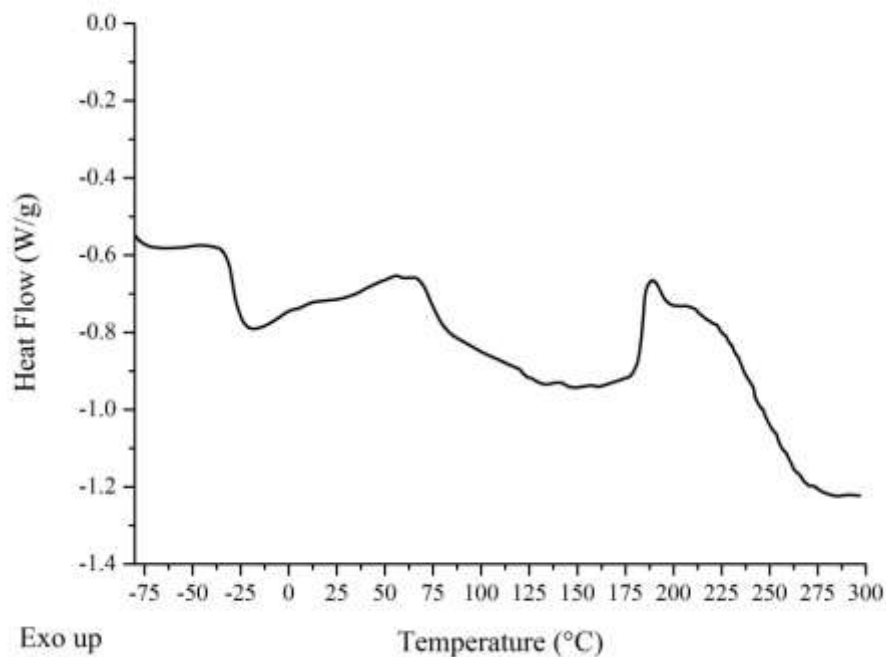
Figure 3.06:   DSC thermogram of catalyst free MDI-TMP-PPG prepolymer sampled directly after synthesis.

After 30 days of room temperature cure between two plies of TAc a portion of the adhesive was removed for DSC analysis. The function of this measurement was to obtain the $T_g$ss of the final PU-U to ensure that it had not entered the functional working window. The experiment performed was a ramped heat from -80°C to 140°C followed by a cooling cycle back to -80°C and then a second ramped heat to 300°C. Figure 3.07 displays the thermogram obtained during DSC analysis of both the first and second heating cycles only. The broadened $T_g$ss acquired on the first heating cycle occurs at -13°C (range from -23°C to -2°C) which has shift +16°C compared to the prepolymer material. After the first heating cycle the obtained $T_g$ss has entered the intended functional working window. Following on from the cooling cycle is the second heating cycle which displayed a $T_g$ss at -8°C which ranged from 18°C to 4°C. This has further shifted the $T_g$ss into the intended processing window which confirms that this formulation will most likely not be a fit for use as the final lens adhesive.
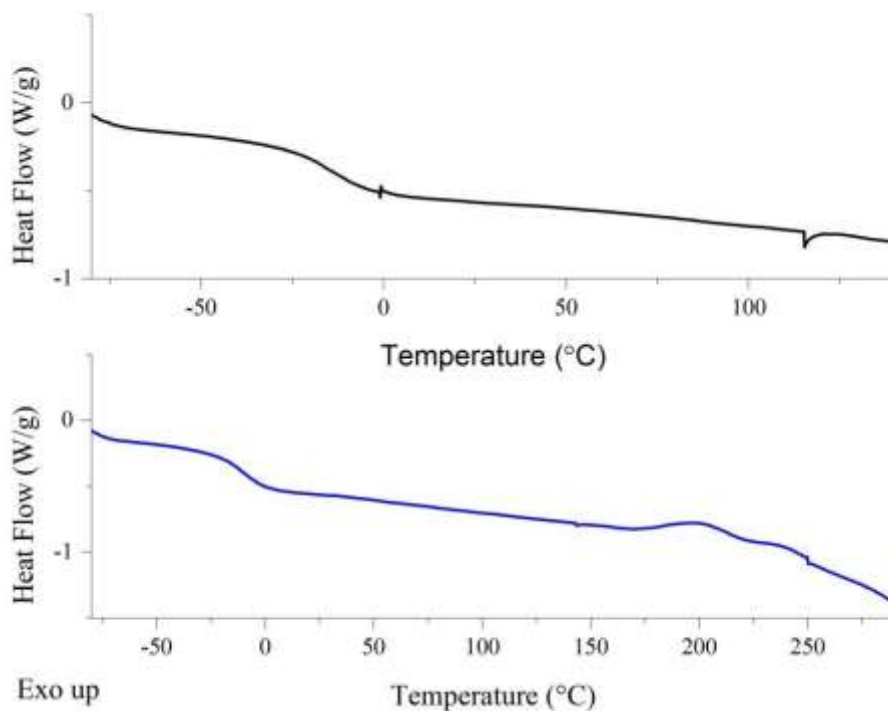
Figure 3.07: DSC thermogram of fully cured MDI-TMP-PPG adhesive, following removal from TAc/TAc laminate. [First heating cycle *top* in black and second heating cycle *bottom* in blue].

The observed shift in the $T_g$ss will most likely be due to better organised hardsegments which result from the reactions that have occurred between the isocyanate end groups upon curing. Hard-segment cross-linking will also occur due to the urea formed by moisture cure. Even though the adhesive will not be used further this data would suggest that PU-U's will be stable within the specified working window.

To determine the thermal stability and that it is out with the processing window TGA was used. The experiment performed was a ramped heat from 40°C – 750°C at 10°Cmin[-1] under nitrogen. Figure 3.08 displays the collected degradation curve and the derivative thermal gravimetric (DTG) curve of the mass loss. The degradation onset (calculated as the temperature where 5% of the total mass is lost) for MDITMP-PPG formulation occurs at 312°C which is well outside the working window (set at 100°C). Three degradation processes are visible from inspection of the DTG curve, with the peak rates at 372°C, 458°C and 561°C respectively. Firstly degradation by de-polymerisation within the hard-segments will dominate and this is present as the peak centred at 372°C.[4,5]

138
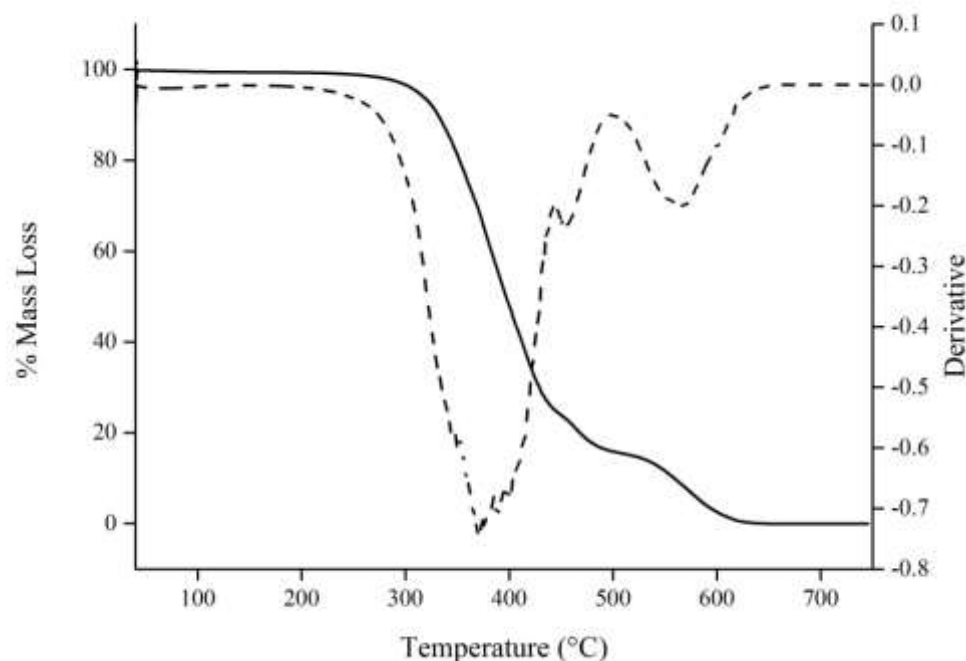
Figure 3.08: TGA and DTG curves of fully cured MDI-TMP-PPG adhesive. [TGA solid line and DTG dashed line].

The second and third degradation processes occurring at higher temperatures may be explained by the known occurrence of MDI based adhesives undergoing aromatic ring fusion which forms a thermally more stable char material and these would degrade at a higher temperature. This will also be accompanied with the degradation of the PPG soft-segments and other fragment of degradation produced.[6,7] Such behaviour was also observed in a similar study by Poljanšek when he was investigating the effect that the free NCO content had on the adhesive properties in one-component polyurethane adhesives.[8]

Thermal analysis has been able to confirm that MDI-TMP-PPG will not be suitable for use within the intended laminate application as the $T_g$ss when cured is within the functional processing window. The most probable source of this problem is due to the 1000 molecular weight soft-segment (PPG) concentrating the number of hardsegments (a high concentration of hard-segments will elevate and broaden the $T_g$ss). The fully cured PU-U adhesive displayed degradation out with the processing window making PU-U adhesives acceptable for use within the intended laminate application. Understanding the material before and after cure has yielded vital information about

PU-U adhesives and leads towards trying hindered chainextenders to try and disrupt hard-segment aggregation.

3.25 180° T-peel Test and Haze

Another key parameter that the PU-U adhesive must fulfil is that once cured it must form a high peel strength laminate with TAc and PC (greater than 3 N mm^{-1} is considered high for the intended application). In order to screen the adhesion potential of MDI-TMP-PPG five different laminates were tested (as detailed in section 2.04) namely TAc/TAc, TAc(t)/TAc(t), TAc(t)/PC(t), PC(t)/PC(t) and PC/PC. TAc(t)/PC was untestable due to the adhesive layer foaming. Each laminate was peeled at 100 mm min^{-1} for an extension of at least 150 mm, with the first 50 mm discarded from the strength value as this is where a stable crack was formed. The haze of the full laminate was also characterised at this point along with the mode of failure for each laminate.

The purpose of performing the 180° T-peel test was to determine the compatibility of MDI-TMP-PPG with different surface chemistries. Three different interface scenarios were present within the test set: untreated (e.g. TAc/TAc or PC/PC), treated (TAc(t)/TAc(t) or PC(t)/PC(t)), and a fully treated hybrid (TAc(t)/PC(t)). These sets of laminates will allow for characterisation of the affinity of MDI-TMPPPG toward TAc and PC, but will also confirm if surface treatment is required. Visual inspection was used to determine the mode of failure as this would identify which part of each laminate was weakest.

For an adhesive to perform well it would be required to form a strong laminate with TAc untreated. From the data in table 3.01 it was identified that this formulation has a poor affinity for the TAc interface. This was identified by the adhesive failures at the TAc interface and also by the low peel strengths obtain (0.2 N mm^{-1} for peel 1 and 0.6 N mm^{-1} for peel 2). The adhesive failure confirms that the surface chemistries at the TAc – adhesive interface have low compatibility. Possible modes of adhesion that may be occurring are interaction of the aromatic rings with the surface or possible H-bonding by the urethane linkage and H-bonding of the PPG ether backbone. As the values are low this would suggest that most of the aromatic rings and urethane hydrogens are involved in forming hard-segments within the polyurethane microstructure (it may also be possible that the ridge structure of the hard-segment

inhibits interaction with the interface as the triacetate does not form a flat surface as TAc has a helical structure). The low peel strength displays that adhesion between MDI-TMP-PPG with untreated TAc is very poor and that adhesion does not show a significant improvement with time.

Saponification of the TAc surface was performed (see section 2.01) to leave a regenerated cellulose surface to increase the compatibility between the reactivity prepolymer adhesive and the substrate. Deacetylation will leave hydroxyl groups at the surface which can react with the free isocyanate of the adhesive forming covalent bonds. Thus covalent bonds should form anchor points between the adhesive and substrate forming a strong interface. Inspection of the collected data confirms that regeneration of cellulose at the surface does boost the interface as after 7 days the recorded peel strength was 3.3 N mm^{-1}. The mode of failure has also changed to being cohesive through the MDI-TM-PPG adhesive, confirming the presence of a strong interface (one test sample displayed a cohesive failure of the TAc ply) and also takes it above the 3 N mm^{-1} set value. The haze data for the collected laminates was < 1.1% which is within the 1.5% threshold value.

Next untreated PC was tested to determine the affinity of the interface with the MDITMP-PPG adhesive. After 7 days of curing, the recorded strength was 4.5 N mm^{-1} and this value fell only slightly to 4.1 N mm^{-1} after 30 days cure. A cohesive failure within the adhesive was observed which displays strong adhesion at the interface to both PC plies. The greater adhesion observed for untreated PC compared to untreated TAc results from a greater surface compatibility at the substrate – adhesive interface. The high density of carbonate linkages along the PC backbone presents many opportunities for H-bonding with the adhesive. This coupled with the high number of possible π-π stacking ring interactions will explain the strong adhesion.[9] **Table 3.01: Peel, haze and mode of failure data for MDI-TMP-PPG cured PUU adhesive. [The data in bold will be discussed within this section].**

Cured Adhesive	Laminate	Peel 1* (N mm^{-1})	Peel 2^x (N mm^{-1})	Failure mode	Haze (%)
MDI-TMP-PPG	**TAc/TAc**	**0.2**	**0.6**	**Adhesive TAc**	**<1.1**
	TAc(t)/TAc(t)	**3.3**	**3.3**	**Cohesive**	

		*	x		
	TAc(t)/PC	ND	ND	ND	
	TAc(t)/PC(t)	3. 6	2.7	Cohesive	
	PC(t)/ PC(t)	3.8	2.7	Cohesive	
	PC/PC	4.5	4.1	Cohesive	
MDI-TMP-PPG-DEPD	TAc/TAc	0.3	0.0	Adhesive TAc	<0.4
	TAc(t)/TAc(t)	2.0	3.0	Adhesive TAc (t)	
	TAc(t)/PC	3.1	3.8	Adhesive TAc(t)	
	TAc(t)/PC(t)	2.3	2.7	Adhesive TAc(t)	
	PC(t)/ PC(t)	2.6	3.3	Adhesive PC(t)	
	PC/PC	4.1	5.4	Adhesive/Cohesive PC Side	
MDI-TMP-PPG-BD	TAc/TAc	0.6	ND	Adhesive TAc	>1.5
	TAc(t)/TAc(t)	2.6	4.2	Adhesive TAc(t)	
	TAc(t)/PC	ND	ND	ND	
	TAc(t)/PC(t)	2.5	2.5	Adhesive TAc(t)	
	PC(t)/ PC(t)	4.7	5.3	Adhesive PC	
	PC/PC	ND	ND	ND	
MDI-TMP-PPG-PD	TAc/TAc	ND	0.6	Adhesive TAc	>1.5
	TAc(t)/TAc(t)	ND	3.0	Adhesive TAc(t)	
	TAc(t)/PC	ND	0.5	Adhesive TAc(t)	
	TAc(t)/PC(t)	ND	0.6	Adhesive TAc(t)	
	PC(t)/ PC(t)	ND	1.1	Adhesive PC	
	PC/PC	ND	1.0	Adhesive PC	

peel 1 collected within 7 days of room temperature cure, x peel 2 collected after 30 days of room temperature cure, ND = No Data

Treatment of PC using an ethanolamine in isopropyl alcohol solution was next performed (see section 2.02 for procedure) to determine its effect on the measured adhesion. The proposed mechanism for the surface treatment of PC is nucleophilic attack of the carbonate linkage by the amine of ethanolamine to leave a phenol and a hydroxyl terminated urethane although the precise mechanism is not known at this

time.[10] In theory this should leave OH functional groups at the surface which should boost adhesion through the formation of covalent bonds with the free isocyanate groups. Peel strength data collected after 7 days displayed a cohesive failure 3.8 N mm^{-1} in strength which decreased to 2.7 N mm^{-1} after 30 days. Compared to untreated PC, the affinity for the surface has been lowered by the surface treatment however, the bond strength obtained would be acceptable based on the 7 day peel data. The lower affinity with the surface of treated PC is based on initial peel data and observed failure. The reduction in strength could possibly be down to the chain cleavage disrupting the number of possible H-bonding and π ring interactions but this would require further investigation to confirm.

Data collected from the hybrid followed what was observed for the previous four laminates, surface treatment is essential for good adhesion between MDI-TMP-PPG with TAc. After 7 days a cohesive failure with a peel strength of 3.6 N mm^{-1} was recorded. After 30 days of cure the value dropped slightly to 2.7 N mm^{-1} and considering the error associated with the measurement of plastic substrates these values would be considered as being very close to one another. The cohesive failure within the adhesive layer displays that the matrix is the weakest part of the laminate. This could be increased by adding more of the TMP chain-extender to the formulation or by increasing the hard-segment concentration. It must be noted that these would affect other properties such as the thermal characteristics and haze of the formulation.

180° T-peel testing has determined that for formulation MDI-TMP-PPG surface treatment of TAc is essential, whereas PC can be used untreated to reach the threshold measurement of 3 N mm^{-1}. When the laminate is formed using these plies the mode of failure is cohesive within the adhesive matrix. This mode of failure has changed from adhesive at the TAc interface to cohesive within the adhesive layer.

The low strength value obtained from this laminate shows the incompatibility of the triacetate surface functionality with the PU-U based on PPG and MDI. Increasing the number of hard blocks before application through chain-extension may help to improve tensile strength; however, chain-extended prepolymer adhesives based on MDI-TMP-PPG will be discussed in the following sections 3.30, 3.40 and 3.50.

3.26 ATR of Peeled Samples

Due to the varying peel strengths obtained it was essential to characterise if (a) the adhesive after 30 days was cured and (b) if once cured was the bulk adhesive the same final material. To investigate the bulk material, ATR was used as it is a nondestructive way to sample the adhesive. ATR was carried out on the five different laminates once they had been peeled after 30 days of curing.
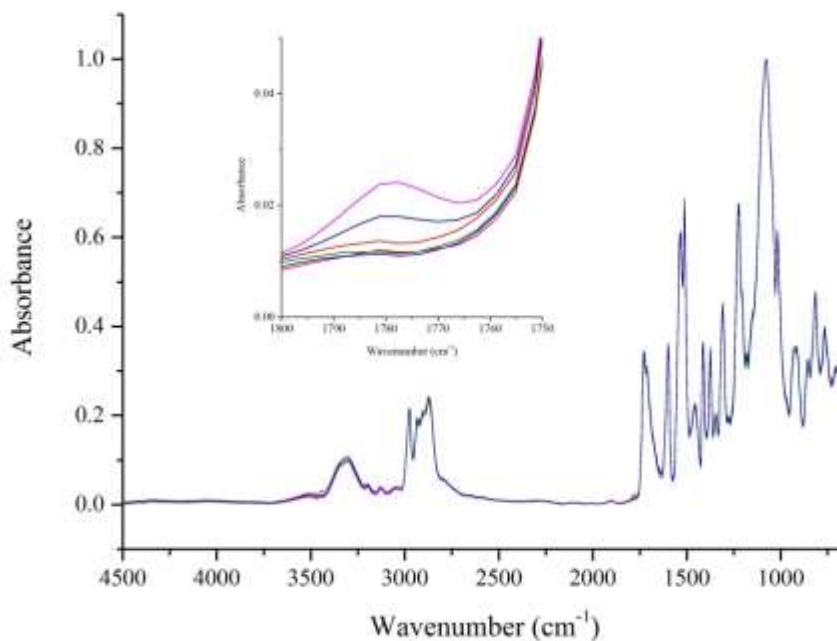
Figure 3.09: ATR spectra of cured MDI-TMP-PPG sampled in-situ after peel testing and includes inset zoomed region of uretidinedione peak. [TAc/TAc in red, TAc(t)/TAc(t) in green, TAc(t)/PC(t) in black, PC(t)/PC(t) in pink and PC/PC in blue. Data collected for each laminate at nine random positions with each spectrum consisting of 128 scans at 8 cm^{-1} resolution. These were then averaged and plotted as the above spectra].

Characterisation of the in-situ cured MDI-TMP-PPG by ATR after 30 days for each laminated material is shown in figure 3.09. **N-H** stretching vibrations are positioned at 3520 cm^{-1} and 3307 cm^{-1}. The position of the later vibration displays that a portion of the N-H groups are within an H-bonded network.[3] **C-H** aromatic stretching vibrations inherent from the MDI segments are next observed at 3035 cm^{-1}. Following

are the aliphatic **C-H** stretching vibrations from PPG with both the asymmetric and symmetric bands present at 2960 cm^{-1} and 2865 cm^{-1} respectively. As there is an absence of any peak between 2260 cm^{-1} – 2280 cm^{-1}, the isocyanate has fallen below the detection limit and it can be assumed that the adhesive is fully cured.

At 1781 cm^{-1} a small peak corresponding to the uretidinedione dimer was observed for PC(t)/PC(t) and PC/PC only.[3] This could be due to the limited moisture ingress through PC allowing isocyanate groups to come together via a [2+2] addition to form the dimer. Interestingly uretdione formation was not observed for any laminates that had a TAc ply. Further evidence of H-bonding can be observed in the position of the **C=O** stretch of the urethane at 1729 cm^{-1}.[11] The broad nature of the carbonyl signal has masked the urea peak (expected around 1700 cm^{-1} – 1640 cm^{-1}) which would be expected as these materials are moisture cured. Evidence of urethane bonds are shown by the **N-H** bending vibration at 1606 cm^{-1}.[11] Further evidence of cure (either urea or urethane functionality) appears at 1535 cm^{-1} which corresponds to **CN** stretching and **N-H** bending vibrations. There would also be a weak aromatic **C-H** signal; however, it is convoluted in with these previous vibrations. Next a first clear sign of urea formation during moisture cure is observed by the **N-H** bending signal at 1508 cm^{-1}.[11]

Aliphatic **C-H** stretching from the PPG and aromatic **C-C** stretching vibrations of MDI are also present at 1450 cm^{-1} and 1421 cm^{-1} respectively. The methyl **C-H** deformation is visible at 1377 cm^{-1} and originates from the PPG backbone structure. Confirmation that the cured adhesive is a PU-U can be seen by the urethane and urea **C-N** bands at 1339 cm^{-1} and 1295 cm^{-1} respectively. PPG vibrations for the **C-H** skeleton vibration and the **C-O-C** ether groups are next observed at 1224 cm^{-1} and 1083 cm^{-1}. The position of the **C-H** aromatic ring vibrations are at 1017 cm^{-1}, 930 cm^{-1}, 859 cm^{-1} and 821 cm^{-1} are characteristic of the 1,4 + 1,2 di-substitution mixture of the monomeric MDI. The final peak at 772 cm^{-1} shows the **C-C** skeleton vibrations of the aliphatic backbone and a contribution of an aromatic **C-H**.

Table 3.02: Characteristic peaks of MDI-TMP-PPG cured PU-U adhesive from all five laminate combinations.

Wavenumber (cm⁻¹)	Vibration	Wavenumber (cm⁻¹)	Vibration
3520	N-H stretching	1421	C-C stretching aromatic
3307	N-H stretching Hbonded	1377	C-H methyl deformation
2989	C-H stretching	1339	C-N urea
2960	C-H asymmetric stretch	1295	C-N urethane
2865	C-H symmetric stretch	1224	C-H aliphatic skeleton
1781[A]	C=O stretching uretidinedione	1083	C-O-C aliphatic ether
1729	C=O stretching urethane Hbonded	1017	C-H aromatic ring
1606	N-H bending urethane	930	C-H aromatic ring
1535	C-N stretch, N-H bending, C-H aromatic ring	859	C-H aromatic ring
1508	N-H bending urea	821	C-H aromatic ring
1459	C-H bend aliphatic	772	C-C aliphatic skeleton

[A] *was only observed in PC(t)/PC(t) and PC/PC*

ATR was able to prove that the final cured material for MDI-TMP-PPG is a PU-U, with both urethane and urea groups present. It has also shown (apart from the uretdione peaks in the PC/PC and PC(t)/PC(t) laminates) that the bulk material is the same, meaning that any differences in peel strength can be attributed to differences in

adhesion at the interface. Finally the adhesive was fully cured as there was no sign of any unreacted isocyanate in any of the final spectra.

3.27 Summary of MDI-TMP-PPG Formulation

In summary MDI-TMP-PPG prepolymer was successfully synthesised as was confirmed by ^{1}H and ^{13}C NMR. The expected molecular weight distribution of the prepolymer MDI-PPG-MDI was confirmed using (2.2:1.0 NCO:OH ratio) MALDIMS, which also identified a higher molecular weight distribution. An increase to Mn, Mw and PDI was observed compared to soft-segment PPG. DSC was able to highlight that the prepolymer $T_g$ss was out with the processing window; however, following cure the $T_g$ss entered the processing window making it unsuitable. TGA analysis displayed that the adhesive when fully cured was stable well outside the processing window, with the onset of degradation not until 312°C. 180° T-peel testing identified two things about the MDI-TMP-PPG adhesive; (a) TAc laminates gave very poor strength values unless the saponification surface treatment was used and (b) PC gave almost the same result with or without surface treatment. Finally ATR was able to confirm that the final cured material was indeed a PU-U.

3.30 Analysis of MDI-TMP-PPG-DEPD

3.31 Synthesis Information

MDI-TMP-PPG-DEPD was next synthesised with the intention of adding defects to the hard-segment domains. Using a sterically hindered diol chain-extender was the route employed to add these defects and also to promote good phase mixing (hardsegment content will also influence morphology). This was achieved by firstly synthesising the MDI-TMP-PPG prepolymer using the same reaction conditions as detailed with section 3.21 and then performing an addition reaction set. The additional step was performed by adding a hydroxyl terminated diol chain-extender using a 2.2:1.0 isocyanate:hydroxyl ratio based on the calculated amount of free NCO remaining after step one. The chain-extension step was also used to lower the free isocyanate content of the adhesive, which would reduce the opportunity for excessive bubbling by CO_2 liberation from urea formation during moisture cure.

Step one was performed as previously detailed in section 3.21 and was a clear liquid which had an observed increase in viscosity from the starting mixture. After addition of 2,2-diethyl-1,3-propane diol (DEPD) the reaction was allowed to stir at 85°C – 95°C for 5 hours before the dual catalyst system of DBTDL and TEA was added. Following diol chain-extension a visual increase in viscosity was observed and was associated with the molecular weight increase caused by the coupling step. To compensate for the molecular weight increase the reaction mixture was slowly heated to 130°C to sufficiently lower the viscosity as this would facilitate flow and allow for the formulation to be poured. Once at temperature, the formulation was poured into an aluminium tube, which was then capped and degassed as previously outlined in section 2.03. The desiccator containing the adhesive filled tube was then placed within a 0°C fridge for storage. Degassing was performed for six hours once a vacuum of one atmosphere was obtained. Samples of the reaction were again taken before catalysed addition, these were analysed by DSC, NMR and MALDI-MS analysis.

MDI-TMP-PPG-DEPD was heated to 130°C before being applied to six laminates which was followed by room temperature cure. These samples were 180° T-peel tested at 7 days and 30 days to determine the peel strength. A further lamination was performed using two plies of TAc which would allow for the fully cured adhesive to be removed for analysis by DSC and TGA. The 30 day peel test samples were also analysed by ATR to characterise the final adhesive and determine its extent of cure.

Analysis of the diol chain-extended materials only will be presented within the remaining sections of this chapter. MDI-TMP-PPG is considered as representative of the reactive intermediate obtained after step one of each chain-extended reaction.

3.32 NMR Analysis
For full spectral characterisation of peaks from MDI and PPG see section 3.22 as this section will only detail peaks that are important to show prepolymer formation or peaks from the chain-extender.
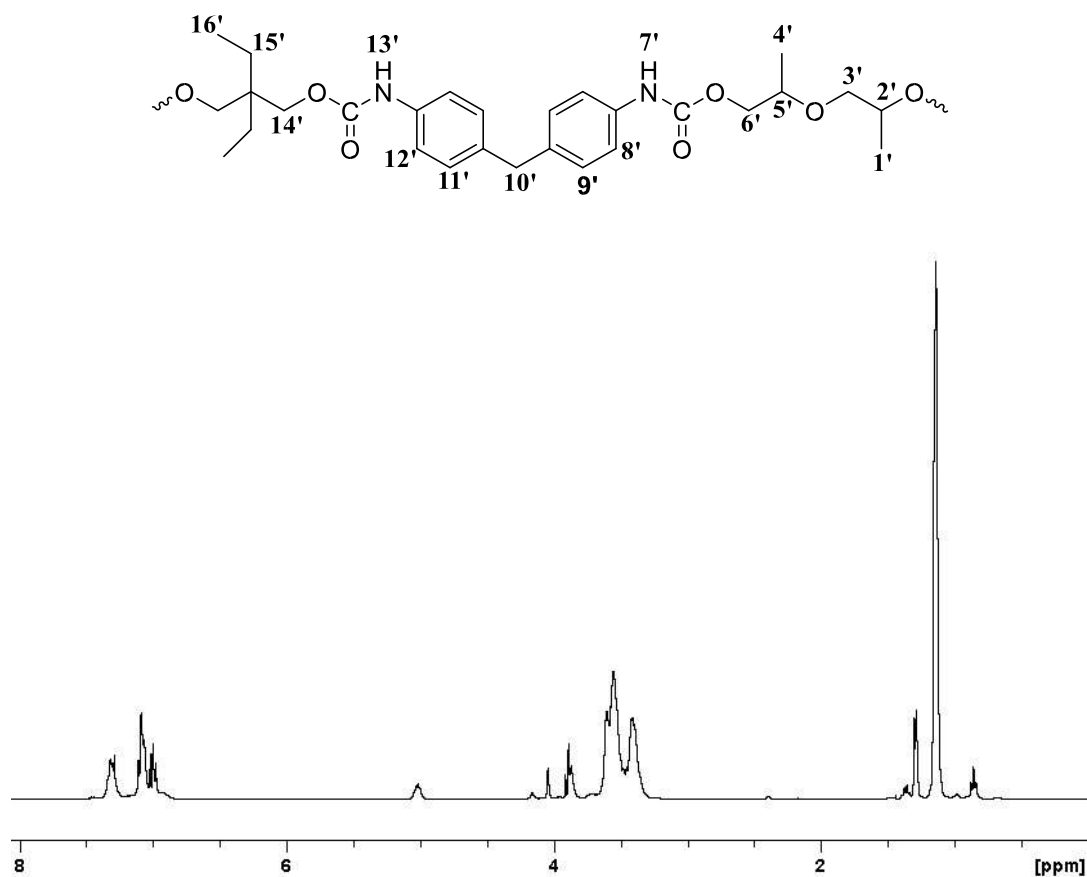
Figure 3.10: ^{1}H NMR spectrum obtained following reaction of MDI-TMP-PPG with DEPD.

DEPD chain-extender contains two steric ethyl groups at the 2 position, evidence of these groups can be observed by the **CH$_3$** signal **16'** at 0.83 ppm and the **CH$_2$** signal **15'** at 1.34 ppm. Evidence that the primary hydroxyl groups from DEPD have reacted is confirmed by the position of **CH$_2$-O-** group **14'** at 4.03 ppm (**CH$_2$-OH** group appears more upfield at 3.40 ppm). Also contained within the spectrum is evidence from the first step of the synthesis. The primary hydroxyl groups of PPG which have been coupled to form urethane linkages can be observed by the position of the **CH$_2$** group **6'** at 3.80 ppm. Evidence that the secondary hydroxyl groups have also reacted is presented by the position of the **CH** groups at 5.00 ppm.

Broader aromatic signals are encountered at 7.1 (**9'** and **11'**) and 7.2 ppm (**8'** and **12'**) when compared to MDI or the previous step one prepolymer MDI-TMP-PPG. This would suggest that reaction of the isocyanate groups with hydroxyl groups of

PPG and DEPD. Retention of peaks that correspond to unreacted rings are also still present at 7.0 ppm, showing that the material is still a prepolymer as there are still reactive chain ends. At 7.3 ppm N**H** protons are observed, this shift is further evidence of urethane and prepolymer formation.
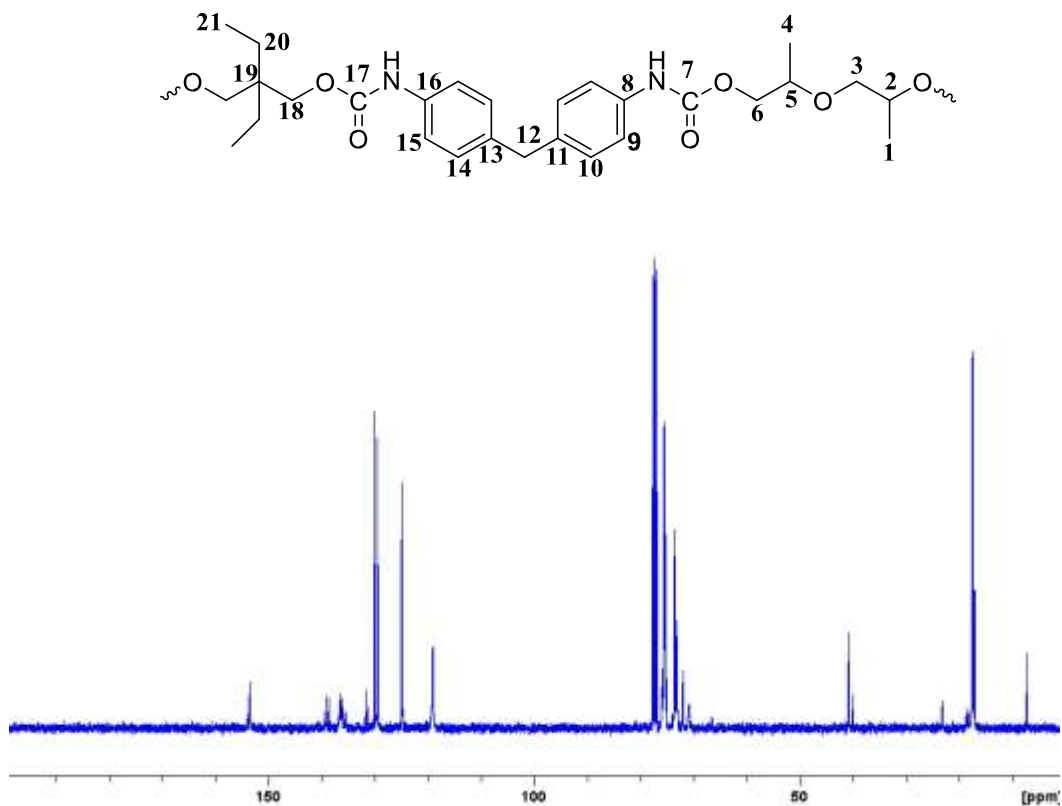
Figure 3.11: ^{13}C NMR spectrum obtained following reaction of MDI-TMP-PPG with DEPD.

^{13}C NMR will give a better indication of free N=C=O groups and is shown in figure 3.11. Also the distribution of aromatic protons indicate that there are fewer unreacted N=C=O groups than reacted urethane groups. Finally the N**H** protons visible at 7.3 ppm **7** and **13** are direct evidence of the formation of urethane bonds. Evidence of the ethyl groups of DEPD are shown by the methyl carbon **21** signal at 7.2 ppm and the methylene carbons signal **20** at 23.1 ppm. The tertiary carbon **19** of the chain-extender is also present with the carbon spectrum at 39 ppm. Evidence of the carbonyl of both urethane (**7** + **17**) and free N=C=O are visible within the ^{13}C spectrum at 153 ppm and 131 ppm respectively (all other peaks within the aromatic region are described within section 3.22).

3.33 MALDI-MS Analysis

To determine the molecular weight increase to the prepolymer following chainextension MALDI-MS was used. The matrix used for the MALDI-MS analysis was dithranol which contained a cationising agent NaTFA (see section 3.23 for more matrix information). A 40 mg ml^{-1} solution of MDI-TMP-PPG-DEPD was prepared in THF and mixed with the matrix (1:8 sample:matrix). 1 μl portions of this sample were then spotted and dried for analysis.

MALDI-MS analysis of the prepolymer adhesive displayed that there were four molecular weight distributions present. Firstly the distribution centred around 1000 m/z was due to unreacted PPG starting material. The occurrence of this peak that was not present in previous analysis suggests that the reaction time of the first step requires a review. Present at 1045 m/z is the chain-extender TMP that has reacted with three MDI units which are ethanol end-capped (plus one sodium cation). These molecules will contribute to the hard segment microstructure within the adhesive and there observation was possible as all the starting material was consumed.
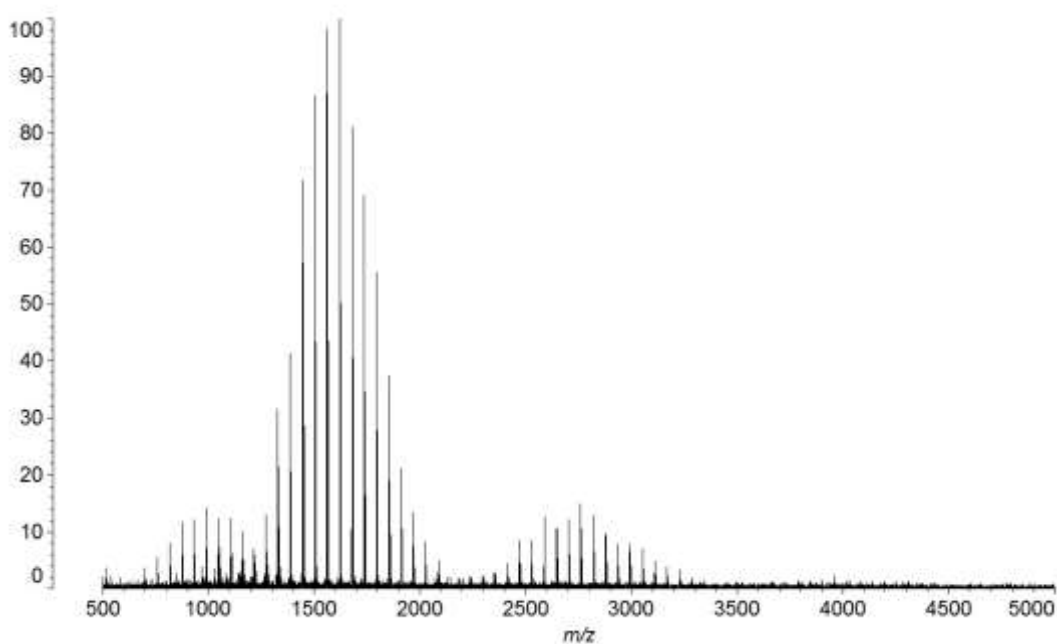
Figure 3.12: MALDI-MS spectrum of MDI-TMP-PPG-DEPD chain-extended prepolymer collected in dithranol/NaTFA.

Following was the peak from the first synthesised MDI-TMP-PPG prepolymer which was the intermediate produced in-situ prior to chain-extension. The appearance of this

distribution suggests that the reaction time from the second step of synthesis also requires a review. The peak of this distribution is centred around 1605 m/z and has a structure of two ethanol end capped MDI units, one Na^+ cation and 18 PPG repeat units. Evidence of this prepolymer would be expected due to the high viscosity of the bulk polymerisation process reducing the effectiveness of the mixing. Also to limit the possibility of isocyanate based side reactions the temperature of synthesis could not exceed 95°C. At temperatures of 120°C – 140°C where the viscosity of the prepolymer mixture is lower, cross-linking by reaction of the active NH of the urethane with free N=C=O is encouraged forming allophonate groups (other isocyanate based reactions will also occur).[12]

The highest end of the molecular weight distribution displays two different polymer lengths, MDI-PPG-MDI-PPG-MDI (2200 to 3200) and MDI-PPG-MDI-DEPD-MDI-PPG-MDI (3200 to 5000). Both will serve to increase the viscosity due to their higher molecular weight; however the second is preferred as it will introduce steric hindrance to the hard-segments and have a disruptive effect on their packing. Prepolymers of structure MDI-PPG-MDI-PPG-MDI are produced during the first step of synthesis. Peak analysis within this upper region of the spectrum displays that some prepolymer molecules have reacted with DEPD, but have not yet become fully chain-extended. Differentiation at the higher end of the spectrum between signal and noise was also difficult. However, prepolymers of structure MDI-PPGMDI-DEPD-MDI-PPG-MDI are visible and form by coupling of two MDI-PPGMDI units by DEPD. Such structures are of interest as they will retard the close packing of hard-segments which should lead to clear adhesives following moisture cure.

Following chain-extension with DEPD there has been further change to Mn, Mw and PDI due to the additional reaction step. Mn has increased to 2069 m/z which is only a slight shift compared to MDI-TMP-PPG but is a large shift compared to PPG. A noticeable increase to Mw is observed and is now 2638 m/z. The calculated PDI is 1.27 which displays that the chain-extension step has increase the polydispersity of the sample.

3.34 DSC and TGA Analysis

Following synthesis of the diol chain-extended prepolymer material, the thermal characteristics of the adhesive formulation were investigated to determine the $T_g$ss (and any other physical processes occurring). As previously mentioned, the $T_g$ss of the material was considered important as it had to be lower than -20°C to be suitable for the intended laminate application. Analysis of the DSC thermogram of MDITMP-PPG-DEPD gives a $T_g$ss of -16°C (range of -21°C to -10°C) which is already above -20°C. Following full cure it would be expected that the $T_g$ss will further increase making this formulation based on its initial data unsuitable as the final adhesive. Also present within the DSC thermogram where two exothermic processes which correspond to adhesive cure. The first of these processes has an onset of 51°C with the peak at 92°C and the second appears at a more elevated onset 183°C with peak temperature 220°C. For the first peak this could be possible consumption of any remaining hydroxyl groups (evidence of PPG starting material in MALDI-MS) and the second could occur from reactions of isocyanates with themselves and urethane groups. These observations are purely based on the temperature ranges that these exothermic peaks are observed and confirm will require further analysis.
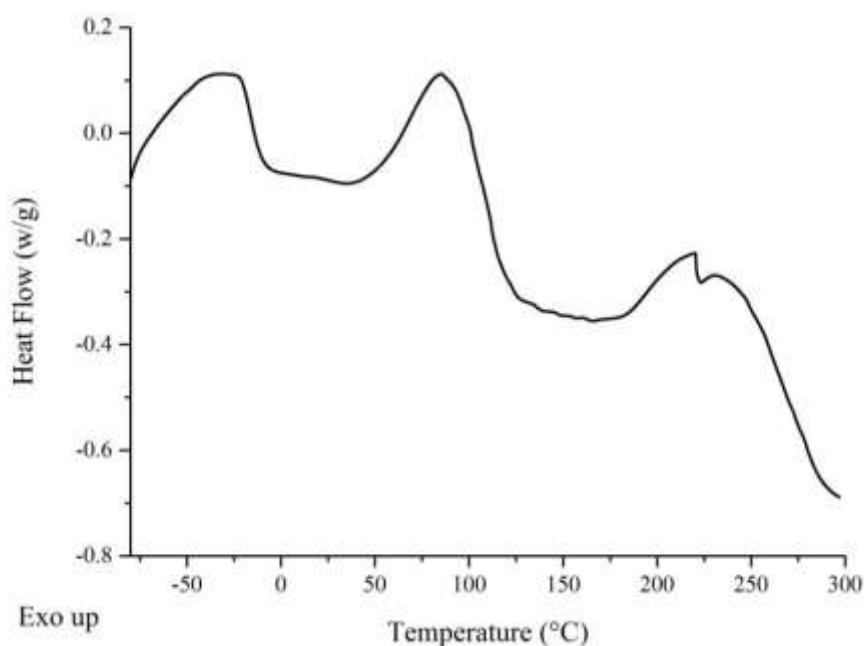
Figure 3.13: **DSC thermogram of MDI-TMP-PPG-DEPD chain-extended prepolymer formulation.**

Following 30 day of curing a portion of the cured material was removed from the TAc/TAc laminate for DSC analysis. The sample was analysed using a heat-coolreheat experiment to determine the final $T_g$ss of the chain-extended adhesive within each heating cycle as shown in figure 3.14. Following the first heating cycle a $T_g$ss of 2°C was recorded which spanned a range of -9°C to 8°C. Following a second heating cycle a $T_g$ss of 8°C was recorded which occurred over a similar range of 2°C to 15°C. The observed increase in $T_g$ss between first and second heating cycles could be due to the experimental temperature range acting as an annealing process.[13] Also the observation of only one glass transition would suggest that there is a high degree of phase mixing between the hard and soft-segments.[8,14]
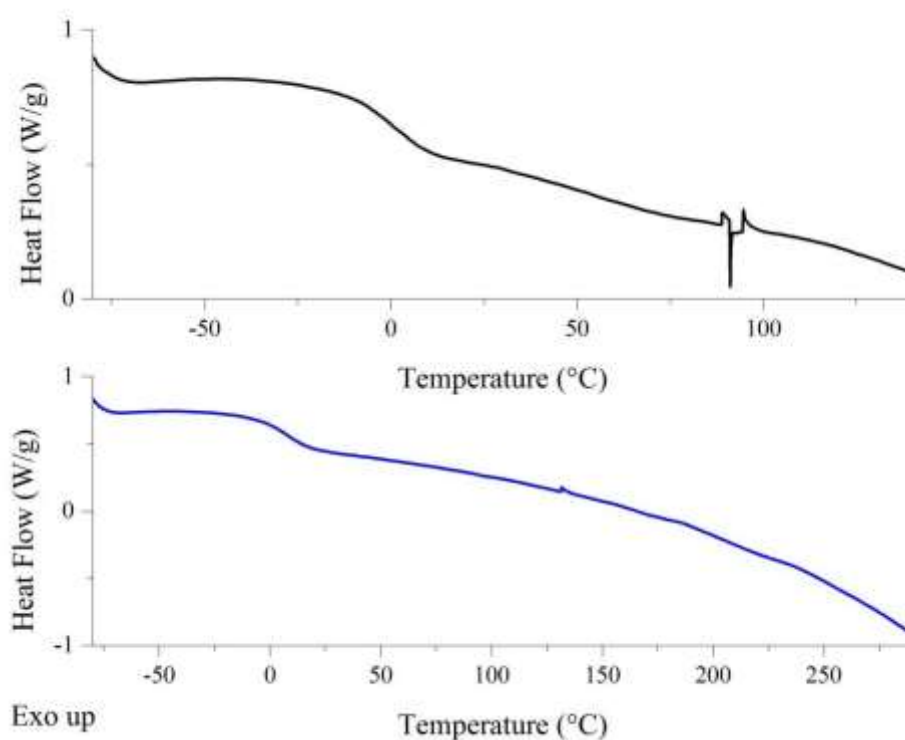
Figure 3.14: DSC thermogram of fully cured MDI-TMP-PPG-DEPD adhesive, following removal from TAc/TAc laminate. [First heating cycle *top* in black and second heating cycle *bottom* in blue].

Recording an above zero glass transition makes this formulation unsuitable (also the case for the previous MDI-TMP-PPG adhesive) for the intended application, as the adhesive will not be flexible below zero. This will influence the impact resistance of the laminate and was set out as a one of the key criteria at the beginning of the project.

Finally the high T_{g}ss encountered could also be the result of a high crosslinking density (through covalent bonds, hydrogen bonding etc.) due to hard-to-soft phase mixing interactions.

TGA was then performed to determine what the onset of degradation was for the PUU cured adhesive. The experiment was carried out over the same range as outlined in section 2.10 and the data is presented in figure 3.15. From the TGA curve, the onset of degradation (temperature at which 5% of the total mass is lost) was 297°C which is 15°C lower than previous formulation where chain-extension was not performed. This would suggest that chain-extension does not have any significant effect on the onset temperature; however, it does reduce it. Inspection of the DTG curve however, does show some differences in the degradation behaviour of this PUU.
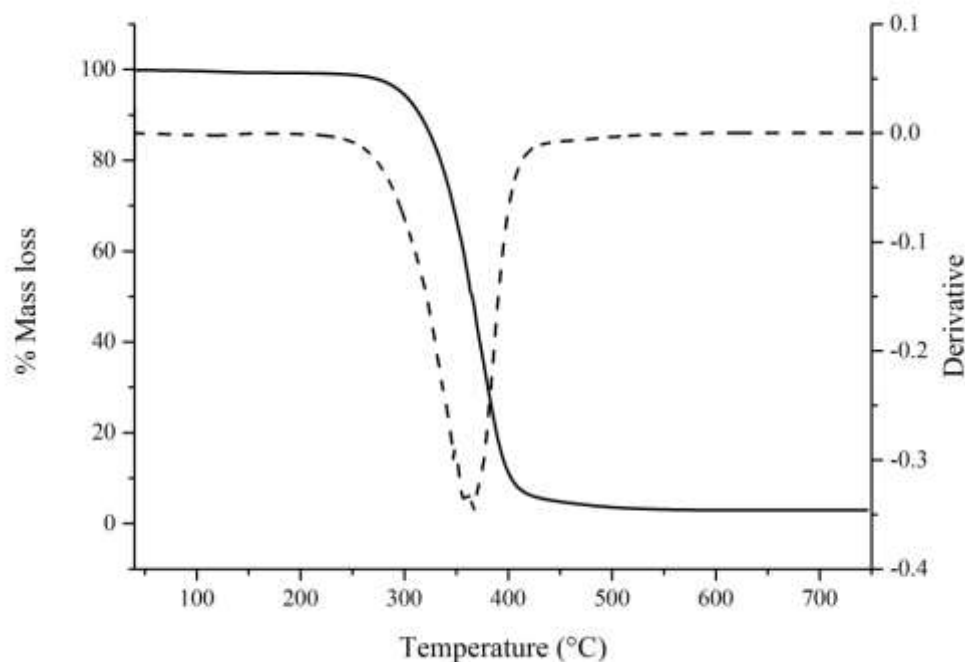
Figure 3.15: TGA and DTG curves of fully cured MDI-TMP-PPG-DEPD adhesive. [TGA solid line and DTG dashed line].

Degradation occurs within one step which is in contrast to the previous cured material which displayed three processes. This single step degradation process could suggest that there is a greater degree of phase mixing within this adhesive, which yields a more uniform degradation profile. The position of DTG peak corresponds to the breaking

of the urethane or urea bonds and was used to calculate the peak degradation rate which occurred at 363°C.[4,5]

Thermal analysis of this PU-U formulation have identified that the material has a $T_g$ss too high for the intended application. The overall thermal stability of the adhesive when fully cured is well outside the temperature that the laminate will be processed at making PU-U based adhesive suitable for the application but not this specific formulation.

3.35 180° T-peel Test and Haze

To quantify the interactions with the ply materials TAc and PC peel testing was again performed. 180° T-peel testing was performed on the six laminates, which were measured after both 7 and 30 days of cure. The laminates used for this study were TAc/TAc, TAc(t)/TAc(t), TAc(t)/PC, TAc(t)/PC(t), PC(t)/PC(t) and PC/PC. These six combinations would evaluate the compatibility with the untreated materials, with the treated materials and what interface had the greatest compatibility.

Testing of the first laminate TAc/TAc displayed poor compatibility between MDITMP-PPG-DEPD and the interface. Poor results of 0.3 N mm^{-1} and 0.0 N mm^{-1} were recorded for the 7 and 30 day tests respectively. An adhesive failure at the TAc interface was the only mode of failure encountered in both tests. Such poor performance with this untreated material was an indication of the lack of active groups at the surface for covalent bonding and due to the lack of available H-bonding opportunities presented by the ether backbone. Following treatment of the TAc interface by saponification, the peel strength of the interface was improved. After 7 days, the recorded peel strength was 2.0 N mm^{-1} which is an improvement compared to the untreated surface, this further increased to 3.0 N mm^{-1} after 30 days. The 30 day measurement is at an acceptable level and meets the set minimum strength measurement however, the adhesive failure still reflects on the apparent incompatibility with the interface.

Table 3.03: Peel, haze and mode of failure data for MDI-TMP-PPG-DEPD cured PU-U adhesive. [The data in bold will be discussed within this section].

Cured Adhesive	Laminate	Peel 1* (N mm^{-1})	Peel 2^x (N mm^{-1})	Failure mode	Haze (%)
MDI-TMP-PPG	TAc/TAc	0.2	0.6	Adhesive TAc	<1.1
	TAc(t)/TAc(t)	3.3	3.3	Cohesive	
	TAc(t)/PC	ND	ND	ND	
	TAc(t)/PC(t)	3.6	2.7	Cohesive	
	PC(t)/ PC(t)	3.8	2.7	Cohesive	
	PC/PC	4.5	4.1	Cohesive	
MDI-TMP-PPG-DEPD	**TAc/TAc**	**0.3**	**0.0**	**Adhesive TAc**	**<0.4**
	TAc(t)/TAc(t)	**2.0**	**3.0**	**Adhesive TAc(t)**	
	TAc(t)/PC	**3.1**	**3.8**	**Adhesive TAc(t)**	
	TAc(t)/PC(t)	**2.3**	**2.7**	**Adhesive TAc(t)**	
	PC(t)/ PC(t)	**2.6**	**3.3**	**Adhesive PC(t)**	
	PC/PC	**4.1**	**5.4**	**Adhesive/Cohesive PC Side**	
MDI-TMP-PPG-BD	**TAc/TAc**	0.5	ND	Adhesive TAc	>1.5
	TAc(t)/TAc(t)	2.6	4.2	Adhesive TAc(t)	
	TAc(t)/PC	ND	ND	ND	
	TAc(t)/PC(t)	2.5	2.5	Adhesive TAc(t)	
	PC(t)/ PC(t)	4.7	5.3	Adhesive PC	
	PC/PC	ND	ND	ND	
MDI-TMP-PPG-PD	**TAc/TAc**	ND	0.6	Adhesive TAc	>1.5
	TAc(t)/TAc(t)	ND	3.0	Adhesive TAc(t)	
	TAc(t)/PC	ND	0.5	Adhesive TAc(t)	
	TAc(t)/PC(t)	ND	0.6	Adhesive TAc(t)	
	PC(t)/ PC(t)	ND	1.1	Adhesive PC	
	PC/PC	ND	1.0	Adhesive PC	

Untreated PC was next tested and the performance was the best of any laminate within this test set. Following 7 days of cure, the peel strength was 4.1 N mm^{-1} which further increased to 5.4 N mm^{-1} after 30 days. The high strength obtained can be explained by the high compatibility of the adhesive with the PC by two main processes: firstly both contain aromatic rings which will encourage π-π stacking at the interface and secondly the large number of carbonate bonds presents many opportunities for H-bonding. Adhesive failures were still observed but these were accompanied by deformation of the PC ply. When the surface treatment was performed it had a reducing effect on the overall strength obtained. After 7 days the strength was 2.6 N mm^{-1} which increased to 3.3 N mm^{-1} after 30 days. This depreciation in the strength could be the result of the chain scission performed during surface treatment affecting the surface adsorption chemistry (e.g. through surface roughening).

Finally to fully understand the possible adsorption chemistry occurring hybrid laminates were tested to determine which interface had the greatest compatibility. After 7 days a peel strength of 3.1 N mm^{-1} was observed for the TAc(t)/PC laminate and this increased to 3.8 N mm^{-1} after 30 days. For the fully treated hybrid laminate (TAc(t)/PC(t)) the numbers were similar with 2.3 N mm^{-1} recorded after 7 days and this increased to 2.7 N mm^{-1} after 30 days. Both laminates failed adhesively at the TAc face but with deformation to the PC substrate. The lower strength when PC(t) was used again supports the theory that surface treatment disrupts the adsorption of the adhesive at the interface. The adhesive failure at the TAc(t) face also further supports that even after treatment, the interface compatibility is still poorer than with PC.

Following 180° T-peel measurements it was observed that TAc could only be used following surface treatment. The chain-extension had little overall effect on the results obtained, with untreated PC performing the best. Finally the improved peel strength observed after 30 days for all laminates (excluding untreated TAc) could suggest that the adhesive is reorganising itself to maximise attractive forces. As the adhesive is curing at room temperature it is above the recorded $T_g$ss making mobility of the polymer groups possible and it has been suggested elsewhere in the literature to occur.[15]

Finally and most significantly the haze measurement recorded for this PU-U adhesive was only 0.4%. When compared to MDI-TMP-PPG, this is a greater than 50% reduction in overall haze and is a significant result. The marked improvement in haze is believed to be due to disruption of the hard-segments within the microstructure of the adhesive as a result of the steric ethyl groups present in the diol chain-extender. Such a significant reduction in the haze recorded, displays that using sterically hindered chain-extenders can lead to clearer PU-U adhesives.

3.36 ATR of Peeled Samples

Characterisation of the bulk cured adhesive was performed using ATR analysis. Analysis of the bulk materials was performed on all six of the laminates after the 30 day tensile test. ATR analysis will determine the chemical functionality of the final cured material and allow for any distinct differences in curing chemistry to be observed. Also ATR will give comparative spectra than can be compared to the base MDI-TMP-PPG formulation characterised previously. Discussed within this section will be peaks that indicate either the PU of the prepolymer or PU-U peaks obtained after 30 days of cure. For discussion of the peaks inherent of the starting materials see section 3.26 and for all characteristic peaks see table 3.04.

As there is an **N-H** stretching band at 3318 cm^{-1} this displays that the cured adhesive can have urethane and urea groups present. The positon of the **N-H** band is characteristic for a hydrogen bonded stretch and this would seem consistent with previous analysis.[3] Furthermore, the observed adhesive failure during tensile testing would support that cross-linking has occurred through both covalent and hydrogen bonding. Carbonyl peaks are also present within the spectrum, with their presence only possible if either urethane or urea linkages have been introduced as the parent soft-segment material is a polyether. Inspection of the expanded carbonyl region displays that the main peak at 1726 cm^{-1} corresponds to the urethane stretch and a noticeable shoulder at ~1710 cm^{-1} for stretching within urea is also visible. The position indicates again H-bonding, this is consistent with hard-segment formation within urethane or urea groups between the carbonyl and **N-H** groups.
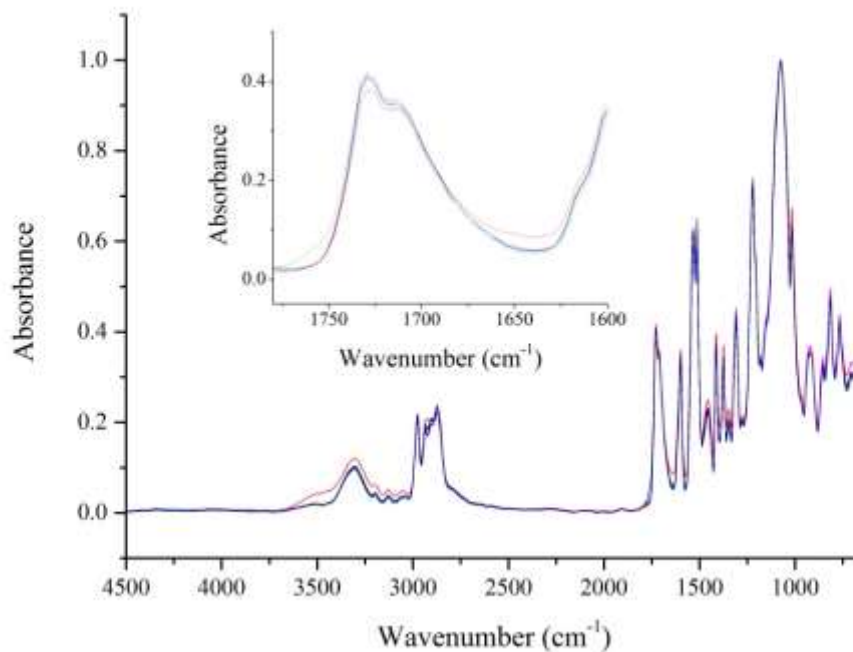
Figure 3.16: ATR spectra of cured MDI-TMP-PPG-DEPD sampled in-situ after tensile testing with inset expanded carbonyl region. [TAc/TAc in black, TAc(t)/TAc(t) in red, TAc(t)/PC in light blue, TAc(t)/PC(t) in pink, PC(t)/PC(t) in green and PC/PC in orange. Data collected for each laminate at nine random positions with each spectrum consisting of 128 scans at 8 cm^{-1} resolution. These were then averaged and plotted as the above spectra].

Confirmation of urethane linkages formed during prepolymer synthesis is shown by the **N-H** bending at 1601 cm^{-1}. Urea formed during moisture cure of the adhesive is shown by the **N-H** bending band at 1508 cm^{-1}. The **C-N** stretching band for both these groups can also be observed at 1535 cm^{-1}. Further **C-N** bands are again visible further into the finger print region with both urethane at 1301 cm^{-1} and urea at 1339 cm^{-1} present.

ATR analysis has allowed for the characterisation of the fully cured PU-U adhesive. The presence of both urethane and urea bands display that the prepolymer urethane has cured through moisture uptake to consume the free isocyanate groups. As there was no band for free isocyanate the adhesive was fully cured after 30 days. Also indicated was that H-bonding was present within the bulk adhesive as could be observed through

the position of the **N-H** and carbonyl bands. Finally chainextension appears to have little effect on the final cure except for the disappearance of the uretdione band previously observed in PC laminates.   Its disappearance is most likely to be due to the reduced free N=C=O content.

Table 3.04: Characteristic peaks of MDI-TMP-PPG-DEPD cured PU-U adhesive from all five laminate combinations.

Wavenumber (cm^{-1})	Vibration	Wavenumber (cm^{-1})	Vibration
3557	N-H stretching	1377	C-H methyl deformation
3318	N-H stretching Hbonded	1339	C-N urea
2980	C-H stretching	1301	C-N urethane
2931	C-H asymmetric stretch	1219	C-H aliphatic skeleton
2876	C-H symmetric stretch	1066	C-O-C aliphatic ether
1726	C=O stretching urethane Hbonded	1017	C-H aromatic ring
1601	N-H bending urethane	925	C-H aromatic ring
1535	C-N stretch, N-H bending, C-H aromatic ring	853	C-H aromatic ring
1508	N-H bending urea	804	C-H aromatic ring
1459	C-H bend aliphatic		
1404	C-C stretching aromatic	766	C-C aliphatic skeleton

3.37 Summary of MDI-TMP-PPG-DEPD Formulation

From the analysis collected from MDI-TMP-PPG-DEPD based PU-U it was apparent that diol chain-extension had little effect on the overall properties of the material when compared to MDI-TMP-PPG. The $T_g$ss of the cured adhesive was too high for the intended application and in this instance was above 0°C. MALDI-MS highlighted that getting such elastomeric polymers of chain-extended molecular weight to successfully ionise is difficult. Next identified by MALDI-MS was the increase to Mn, Mw and PDI following chain-extension with DEPD. It highlighted that forming fully chain-extended prepolymer in the absence of catalyst will require longer reaction times. 180° T-peel testing highlights that PU-U adhesive based on MDI and PPG have an affinity for the PC interface but are incompatible with TAc interface unless treated. Finally the most promising result from this formulation is that chain-extension has a positive impact on the haze of the final cured adhesive.

3.40 Analysis of MDI-TMP-PPG-BD

3.41 Synthesis Information

The effect that diol chain-extension has on the optical clarity of the final cured adhesive requires further investigation following the marked improvement in haze observed when using DEPD. Next 1,3-butane diol was used to determine its effect on the final optical properties of the adhesive. 1,3-butane diol (BD) was selected instead of 1,4-butane diol as the latter is often used to encourage the development of hard-segments.[13] Introducing a sterically hindering methyl group should in theory allow for sufficient disruption of the hard-segment packing and lead to greater optical clarity following moisture cure.

To ensure that any effects observed were a result of the new chain-extender, the synthetic procedure was kept the same as previously used within section 3.31. The initial prepolymer formulation was mixed for three hours following final addition of MDI at 85°C – 95°C. Chain-extension was performed for five hours and the reaction was kept within the same temperature range. Following the chain-extension step, a large amount of entrapped bubbles were visible within the reaction mixture which was a consequence of the viscosity increase. Following five hours of stirring the dual catalyst system was added (TEA and DBTDL) and to ensure the mixture would flow

into the aluminium storage container the temperature was increased to 130°C for a short time. Once transferred the formulation was capped, degassed then placed within a fridge at 0°C for storage. Degassing was performed for six hours once a vacuum of one atmosphere was obtained. Analysis of the prepolymer material was performed using NMR, MALDI-MS and DSC.

Lamination was performed using the six laminate combinations (same as section 3.31) which were then cured at room temperature. MDI-TMP-PPG-BD adhesive was applied at a temperature of 130°C. 180° T-peel testing was recorded at both 7 and 30 days to determine the strength of the laminate and also the mode of failure. A further adhesive sample was prepared as a TAc/TAc laminate, which once cured could be removed for DSC and TGA analysis. The 30 day tensile test samples were also analysed by ATR to characterise the bulk cure material.

Analysis of the chain-extended material only will be presented within this section. MDI-TMP-PPG is considered as representative of the reactive intermediate obtained after step one of this chain-extended reaction and therefor will not be covered (see section 3.21-3.27).

3.42 NMR Analysis

Proton NMR was used to investigate if the polymerisation of the diol chain-extended prepolymer had been a success and to identify the new peaks added from the BD molecule. The peaks of MDI and PPG are discussed within section 3.22 and it can be agreed that they are all present within the spectrum presented in figure 3.17.

Evidence of BD within the ^{1}H spectrum is firstly observed at 1.75 ppm by observation of the additional methylene group **15'** now present. It would also be expected that a methyl signal would be present to represent **17'** however; it is convoluted together with the TMP methyl signal at 1.47 ppm. Methine protons **14'** are present as a shoulder peak at 4.18 ppm and the position shows that the hydroxyl group has been consumed. Reaction of the more sterically hindered secondary group has also occurred and is visible by a shoulder peak at 4.99 ppm from the adjacent **CH** proton **16'**. Again the presence of the **N-H** urethane peaks (**7'** and **13'**) at 7.29 ppm show successful

polymerisation. The large peak present at 2.15 ppm can be discounted as it is an acetone impurity from cleaning of the NMR tube.
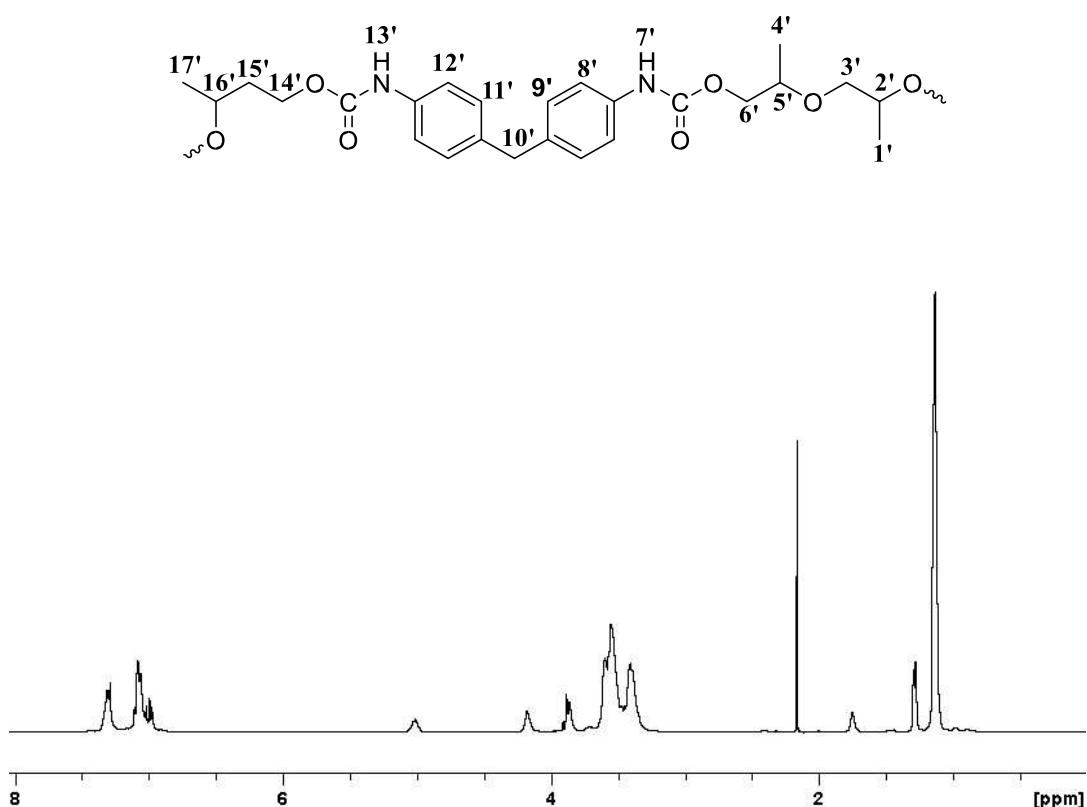
Figure 3.17: ^{1}H NMR spectrum obtained following reaction of MDI-TMP-PPG with BD.

Chain-extender peaks are also present within the ^{13}C spectrum obtained of the MDITMP-PPG-BD prepolymer. Firstly the methyl carbon **21** is visible as a small peak (downfield from the PPG methyl peaks a **1** + **4**) at 17.5 ppm. Methylene carbon **19** is visible at 25.7 ppm and tertiary carbon **20** is also visible at 64.7 ppm. PPG plus the peaks from MDI within the prepolymer backbone as synthesised in step one are still visible between 70 – 80 ppm and 110 – 140 ppm respectively. Carbonyl functionality inherent of the two types of urethane is visible at 152.5 ppm (urethane groups from a secondary hydroxyl) and 153 ppm (urethane groups from a primary hydroxyl). The peak at 30 ppm can be discounted as it corresponds to the methyl groups from the acetone impurity.
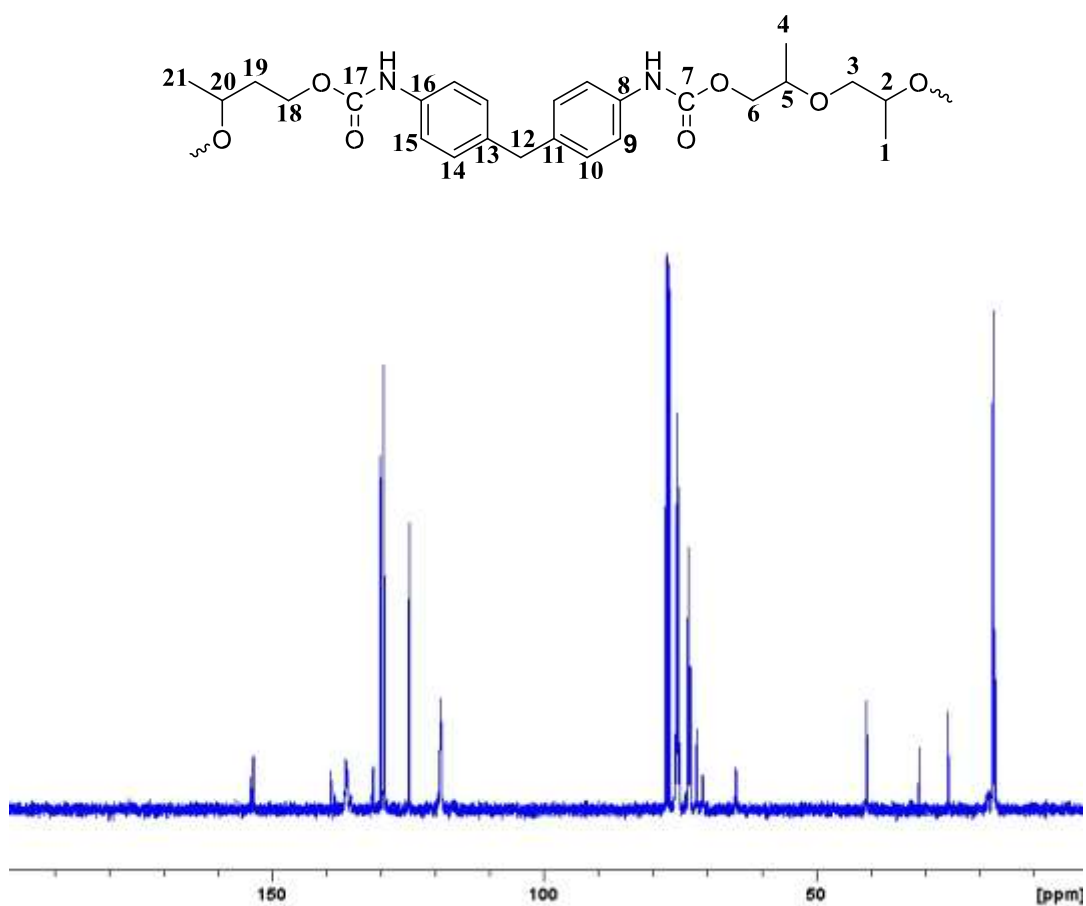
Figure 3.18: ¹³C NMR spectrum obtained following reaction of MDI-TMP-PPG with BD.

NMR has again displayed that the synthetic technique is producing an isocyanate end capped prepolymer that is very similar in nature to those synthesised previously. Also both ¹H and ¹³C spectra are needed as they show that the chain-extender has indeed reacted and been incorporated into the PU prepolymer.

3.43 MALDI-MS Analysis

To quantify the effect that BD has on the higher molecular weight of the prepolymer MALDI-MS was again used. The matrix used for the MALDI-MS analysis was dithranol which contained a cationising agent NaTFA (see section 3.23 for more matrix information).
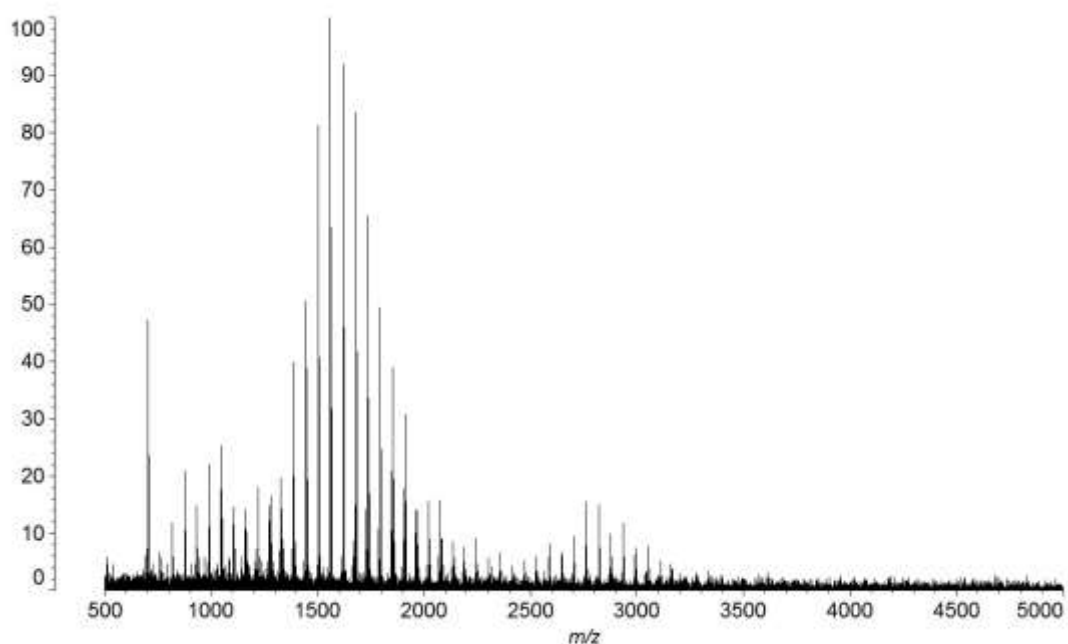
Figure 3.19: **MALDI-MS spectrum of MDI-TMP-PPG-BD chain-extended prepolymer collected in dithranol/NaTFA.**

A 40 mg ml^{-1} solution of MDI-TMP-PPG-BD was prepared in THF and mixed with the matrix (1:8 sample:matrix). 1 µl portions of this sample were then spotted and dried for analysis. Four different molecular weight distributions were observed within the spectrum of the MDI-TMP-PPG-BD.

Confirmation of some unreacted PPG starting material was again evident by the mass distribution centred on 1044 m/z. Tailing on from the first distribution is that of the prepolymer MDI-TMP-PPG formed during the first synthetic step. An end capped prepolymer of this type positioned at 1547 m/z has a composition of two ethanol end capped MDI units, one Na$^+$ cation and 17 PPG repeat units. Persistence of a proportion of non-chain extended prepolymer would be expected due to the high viscosity of the bulk polymerisation process reducing the effectiveness of the mixing (could require longer mixing time). Present at 1045 m/z is the chain-extender TMP that has reacted with three MDI units which are ethanol end-capped (plus one sodium cation). These molecules will contribute to the hard segment microstructure within the adhesive and their observation was possible as all the starting material was consumed.

The higher molecular weight distributions observed within the spectrum accounts for two lengths of chain-extended polymer; firstly MDI-PPG-MDI-PPG-MDI (2200 to 3200) and secondly MDI-PPG-MDI-BD-MDI-PPG-MDI (3200 to 5000). Prepolymers of structure MDI-PPG-MDI-PPG-MDI are produced during the first step of synthesis. Analysis of the upper region shows that a proportion of the prepolymer molecules have reacted with BD but it was difficult to identify the fully chain-extended prepolymer due to the signal to noise ratio.

Similar numbers are obtained for Mn, Mw and PDI compared with the previous chain-extended formulation MDI-TMP-PPG-DEPD. The value calculated for Mn is 1993 m/z which is a slight decrease compared to MDI-TMP-PPG-DEPD. The same trend is observed for the calculated value of Mw with the calculated value 2521 m/z. A minimal increase to the PDI value is obtained with the calculated value 1.26. Comparing this value with that obtained for MDI-TMP-PG-DEPD (1.27) it displays that the chain-extension step itself increases the polydispersity and not the chainextender molecule. Confirmation of this observation will be possible following analysis of the final sample (see section 3.53)

3.44 DSC and TGA Analysis

Previous formulations based on MDI and PPG were rendered unusable as the final material has a $T_g$ss of around 0°C following moisture cure. To determine the effect that BD has on the thermal properties of the prepolymer, DSC analysis was performed. Inspection of the thermogram obtained of the prepolymer PU formulation (MDI-TMP-PPG-BD) displayed two thermal events. Of most interest was the lower temperature thermal event shown by on the thermogram to be a $T_g$ss, which occurs at a temperature of -16°C (over a range of -21°C to -10°C). As was observed for previous formulations based on MDI and PPG the $T_g$ss has already moved above the maximum -20°C set point making this material out with specification. Also a higher temperature exothermic peak was recorded during the DSC experiment at 200°C with and onset of 192°C, this sharp peak was predicted to be the curing of the free isocyanate groups with one another.

The final $T_g$ss for the cured PU-U adhesive was determined by using a heat-coolreheat experiment between -80°C and 140°C within a nitrogen atmosphere (see figure 3.21)

on the first cycle and up to 300°C on the second. On the first heating cycle a T$_g$ss of -3°C was recorded and spanned a range of -13°C to 5°C. Following on from cooling which returned the sample to -80°C, the second heating cycle was performed. As with the previous diol chain-extended formulation, the T$_g$ss recorded on the second heating cycle moves to an elevated temperature. A now centred T$_g$ss at 6°C (which is an increase of +7°C from the first cycle) was visible over a range of -7°C to 15°C. As previously discussed, the increased T$_g$ss is a real event and is believed to be caused by the first heating cycle acting as an annealing type process to the cured PU-U adhesive.
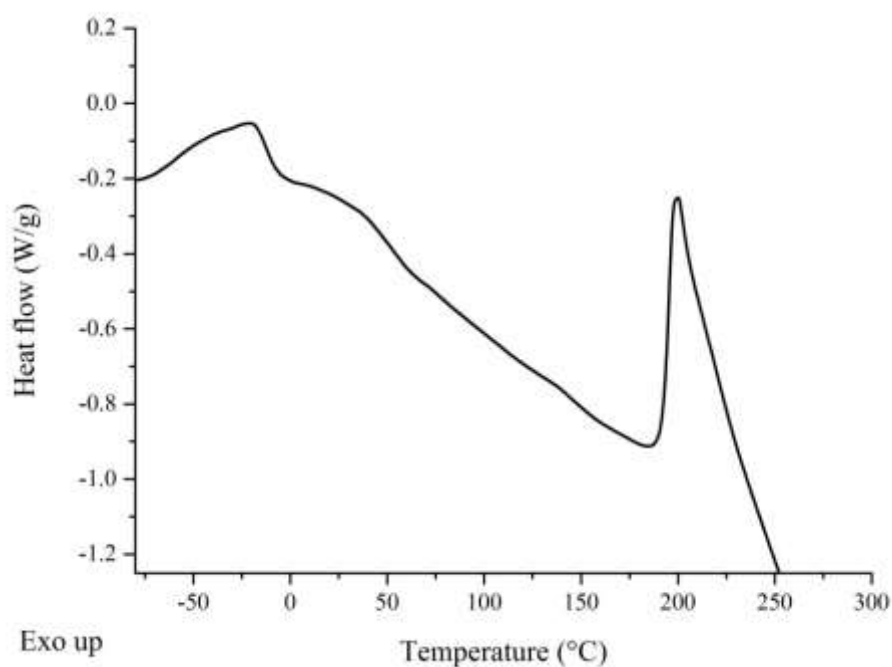
Figure 3.20:   DSC thermogram of MDI-TMP-PPG-BD chain-extended prepolymer formulation.

As the T$_g$ss obtained from the cured PU-U adhesive of formulation MDI-TMP-PPGBD appears above -20°C it shows that the diol chain-extender used is not the reason for the T$_g$ss being pushed to a higher temperature (high with respect to this application). From this observation it shows that the material used in the formulation (MDI and PPG) are the reason for the T$_g$ss moving above -20°C. This could possibly be a result of the soft-segment molecular weight being too low giving an overall greater hard-segment concentration, which even following chain-extension still sufficiently cross-links to elevate the T$_g$ss.
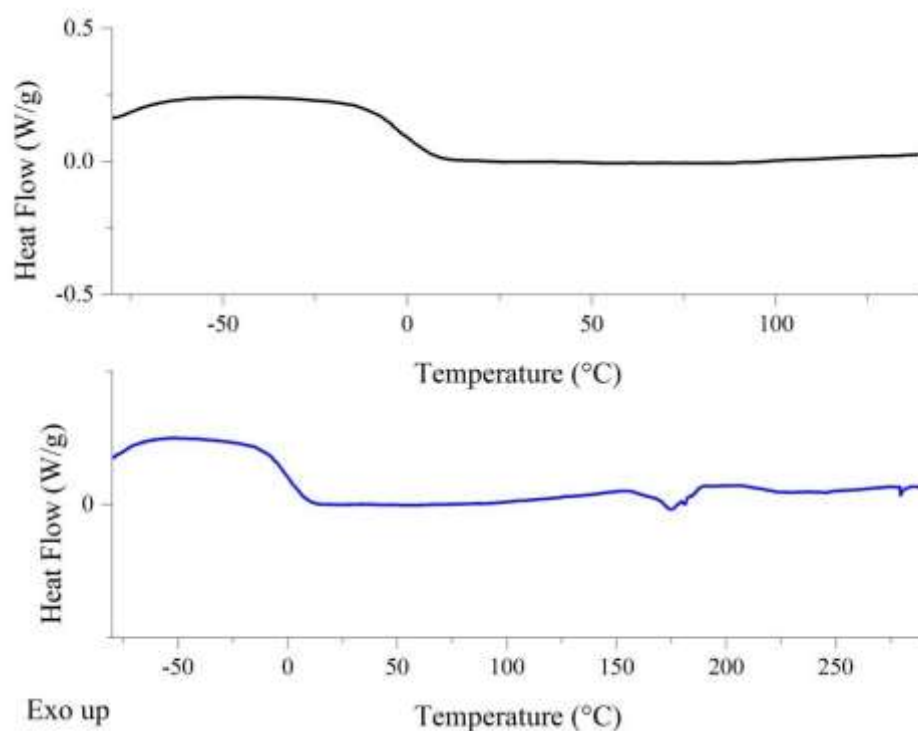
Figure 3.21: **DSC thermogram of fully cured MDI-TMP-PPG-BD adhesive, following removal from TAc/TAc laminate. [First heating cycle *top* in black and second heating cycle *bottom* in blue].**

The overall thermal stability was again determined by the onset of degradation (temperature where 5% of initial mass lost) obtained by TGA analysis. Figure 3.22 displays both a TGA and DTG curve of the cured PU-U adhesive removed for the TAc/TAc laminate. An onset of degradation for MDI-TMP-PPG-BD was recorded at 301°C from the TGA curve and was the only degradation process recorded. This was confirmed by the DTG curve which displayed a single peak at 367°C. The breaking of hard-segment urethane/urea bonds is followed by the degradation of the soft-segment and molecular fragments liberated are contained within this step. As a single step degradation profile was obtained following diol chain-extension it would suggest better phase mixing when compared with the base MDI-TMP-PPG formulation. With a temperature difference of only 6°C between DEPD and BD chain-extended PU-Us, the degradation profiles can be assumed to be essentially the same (within experimental error). From the obtained onset of degradation it can be confirmed that this formulation would be stable well above the 100°C threshold value.
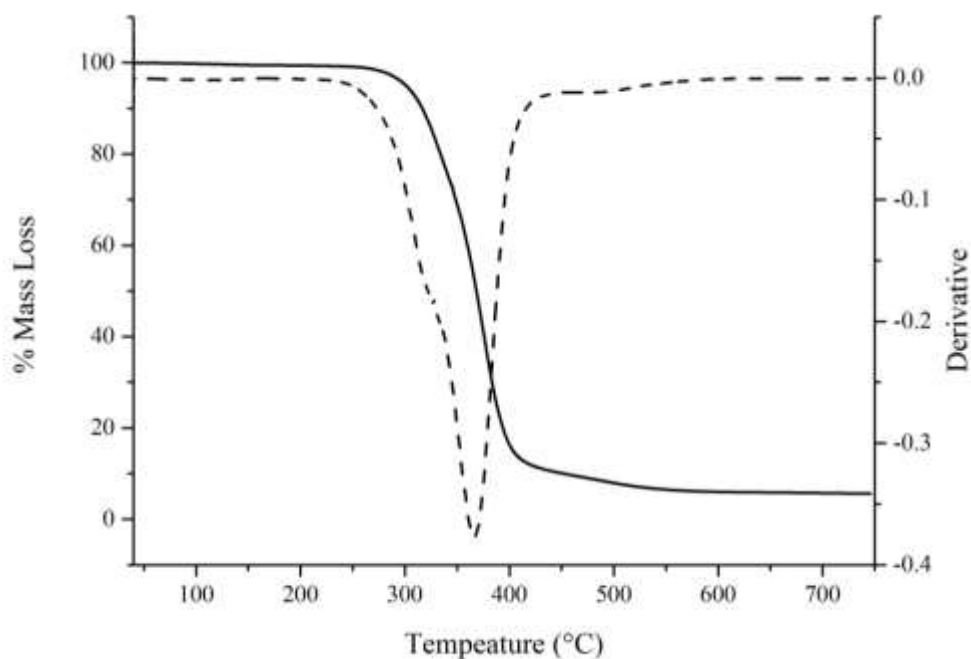
Figure 3.22: TGA and DTG curves of fully cured MDI-TMP-PPG-BD adhesive. [TGA solid line and DTG dashed line].

The merit of using appropriate thermal analysis techniques DSC and TGA for thermal characterisation of adhesive are again justified. DSC analysis allows for accurate recording and following of the $T_g$ss during synthesis and after moisture cure. TGA allows for the thermal stability of the cured adhesive to be determined through the calculated onset of degradation.

3.45 180° T-peel Test and Haze

To quantify the interactions with the ply materials TAc and PC tensile testing was performed. 180° T-peel testing was performed on six laminates, with measurements recorded after both 7 and 30 days of cure. The laminates used for this study were TAc/TAc, TAc(t)/TAc(t), TAc(t)/PC, TAc(t)/PC(t), PC(t)/PC(t) and PC/PC. These six combinations would evaluate the compatibility with the untreated materials and also the treated materials. Due to an application problem encountered during lamination, the tensile testing data obtained for TAc(t)/PC and PC/PC is not reported.

Table 3.05: Peel, haze and mode of failure data for MDI-TMP-PPG-BD cured PU-U adhesive. [The data in bold will be discussed within this section].

Cured Adhesive	Laminate	Peel 1* $(N\ mm^{-1})$	Peel 2^x $(N\ mm^{-1})$	Failure mode	Haze (%)
MDI-TMP-PPG	TAc/TAc	0.2	0.6	Adhesive TAc	<1.1
	TAc(t)/TAc(t)	3.3	3.3	Cohesive	
	TAc(t)/PC	ND	ND	ND	
	TAc(t)/PC(t)	3.6	2.7	Cohesive	
	PC(t)/ PC(t)	3.8	2.7	Cohesive	
	PC/PC	4.5	4.0	Cohesive	
MDI-TMP-PPG-DEPD	TAc/TAc	0.3	0.0	Adhesive TAc	<0.4
	TAc(t)/TAc(t)	2.0	3.0	Adhesive TAc(t)	
	TAc(t)/PC	3.1	3.8	Adhesive TAc(t)	
	TAc(t)/PC(t)	2.3	2.7	Adhesive TAc(t)	
	PC(t)/ PC(t)	2.6	3.3	Adhesive PC(t)	
	PC/PC	4.1	5.4	Adhesive/Cohesive PC	
MDI-TMP-PPG-BD	**TAc/TAc**	**0.5**	**ND**	**Adhesive TAc**	**>1.5**
	TAc(t)/TAc(t)	**2.6**	**4.2**	**Adhesive TAc(t)**	
	TAc(t)/PC	**ND**	**ND**	**ND**	
	TAc(t)/PC(t)	**2.5**	**2.5**	**Adhesive TAc(t)**	
	PC(t)/ PC(t)	**4.7**	**5.3**	**Adhesive PC**	
	PC/PC	**ND**	**ND**	**ND**	
MDI-TMP-PPG-PD	**TAc/TAc**	ND	ND	Adhesive TAc	>1.5
	TAc(t)/TAc(t)	ND	0.6	Adhesive TAc(t)	
	TAc(t)/PC	ND	3.0	Adhesive TAc(t)	
	TAc(t)/PC(t)	ND	0.5	Adhesive TAc(t)	
	PC(t)/ PC(t)	ND	1.1	Adhesive PC	
	PC/PC	ND	1.0	Adhesive PC	

The mentioned application problem resulted in streaks of adhesive and not a consistent layer making analysis of the data non-representative. TAc/TAc could not be tested after 30 days as the adhesive layer foamed. Poor adhesion for TAc/TAc would have been anticipated from the performance of previous formulations. This was confirmed by the 7 day cure peel measurement which recorded an adhesive failure of 0.55 N mm^{-1} (30 day cure data is not available due to adhesive foaming). Improved strength following saponification was observed, which was expected based on previous analysis (see section 3.21 and 3.31). After 7 days the strength was 2.64 N mm^{-1} and this climbed to 4.22 N mm^{-1} following 30 days of cure. Reaching the 3

N mm^{-1} benchmark was an indication of the surface treatment's enhancement to the adhesion. However, the adhesive failure still highlights an inherent incompatibility.

As there was an application issue with PC/PC only the treated laminate was tested for this formulation. Following trends that are emerging from previous experiments within this adhesive set, it would be expected that PC(t)/PC(t) would yield a peel strength around 3 N mm^{-1}. Analysis of the laminate after 7 days of cure resulted in a value of 4.72 N mm^{-1} which further increased to 5.32 N mm^{-1} after 30 days. Using BD as a chain-extender delivers improved results from those obtained by DEPD.

An adhesive failure was recorded with deformation of the PC(t) ply also noted. The compatibility between the MDI based adhesive and PC(t) is far greater than with TAc. For this adhesive, the final laminate tested was TAc(t)/PC(t). An adhesive failure was obtained for both the 7 day test and 30 days with the strengths reading 2.50 N mm^{-1} and 2.53 N mm^{-1} respectively. Failure at the TAc interface was consistent with previous results. It also further supports the interface incompatibility between the adhesive and TAc even after surface treatment.

Finally the haze measured for the final cured PU-U was > 1.5% which is out with the desired specifications. Hazing normally indicated that the material has large hardsegment domains that are not well phased mixed. Such hard block formation could occur during moisture cure as the chain ends will be mobile and free to move with the adhesive being above the $T_g$ss. Upon moisture cure the urea groups will

encourage hard-segment formation through H-bonding between the carbonyl and NH groups. The orientating effect these H-bonds have will also encourage π-π stacking of the aromatic rings. Both these bonding modes will most likely contribute to the observed haze.

180° T-peel testing data for MDI-TMP-PPG-BD has highlighted the incompatibility of this aromatic adhesive with TAc, however, the observed performance with PC(t) was above benchmark. The hybrid laminate was an effective way to display the difference in compatibility as the weakest interface (TAc(t)) always failed first.

3.46 ATR of Peeled Samples

Characterisation of the bulk cured adhesive was performed using ATR analysis. Analysis of the bulk materials was performed on all three of the laminates after 30 day tensile testing.
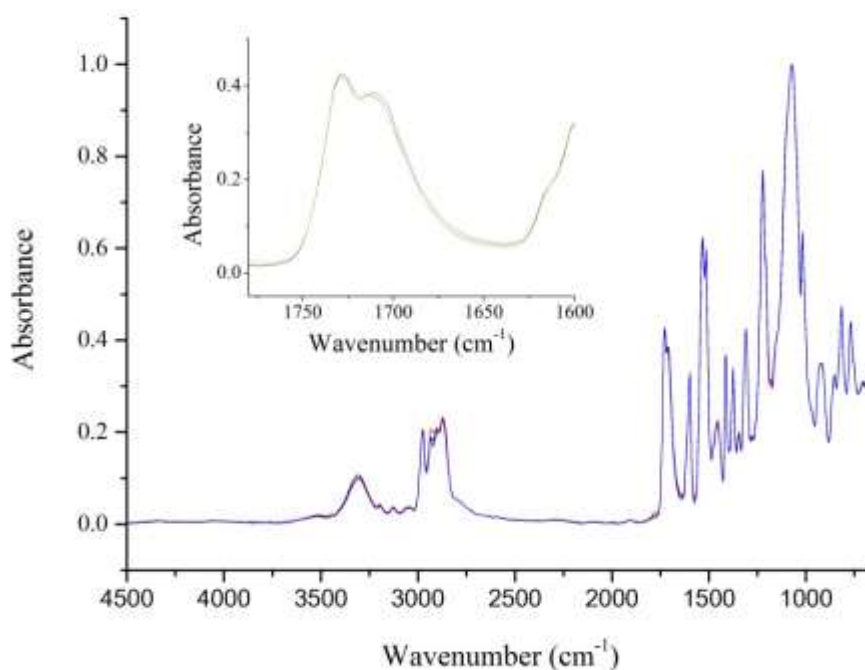
Figure 3.23: ATR spectra of cured MDI-TMP-PPG-BD sampled in-situ after tensile testing with inset expanded carbonyl region. [TAc(t)/TAc(t) in black, TAc(t)/PC(t) in red, and PC(t)/PC(t) in blue. Data collected for each laminate at

nine random positions with each spectrum consisting of 128 scans at 8 cm^{-1} resolution. These were then averaged and plotted as the above spectra].

ATR analysis will determine the chemical functionality of the final cured materials and allow for any distinct differences in curing chemistry to be observed. Discussed within this section will be peaks that indicate either the PU of the prepolymer or PUU obtained after 30 days of cure. For discussion of the peaks inherent of the starting materials see section 3.26 and for all characteristic peaks see table 3.06.

Table 3.06: Characteristic peaks of MDI-TMP-PPG-BD cured PU-U adhesive from all five laminate combinations.

Wavenumber (cm^{-1})	Vibration	Wavenumber (cm^{-1})	Vibration
3534	N-H stretching	1372	C-H methyl deformation
3305	N-H stretching Hbonded	1330	C-N urea
2976	C-H stretching	1300	C-N urethane
2931	C-H asymmetric stretch	1217	C-H aliphatic skeleton
2879	C-H symmetric stretch	1074	C-O-C aliphatic ether
1726	C=O stretching urethane Hbonded	1007	C-H aromatic ring
1598	N-H bending urethane	923	C-H aromatic ring
1534	C-N stretch, N-H bending, C-H aromatic ring	855	C-H aromatic ring
1511	N-H bending urea	814	C-H aromatic ring
1458	C-H bend aliphatic		
		768	C-C aliphatic

| 1413 | C-C stretching aromatic | skeleton |

The characteristic signs of a fully moisture cured PU-U were obtained and are presented in figure 3.23. Bands that show urethane functionality within the spectra are **N-H** stretching at 3534 cm^{-1} plus 3305 cm^{-1}, **C=O** stretching at 1726 cm^{-1}, **N-H** bending at 1598 cm^{-1} and **C-N** stretch at 1300 cm^{-1}. Evidence of urea functionality is also shown within the spectra by **N-H** stretching at 3534 cm^{-1} plus 3305 cm^{-1}, **C=O** stretching at 1726 cm^{-1} (again has urea shoulder), **N-H** bending at 1511 cm^{-1} and **C-N** stretch at 1330 cm^{-1}. For all other characteristic bands found for MDI-TMP-PPG-BD refer to table 3.06.

ATR has successfully displayed that the cured adhesive of formulation MDI-TMPPPG-BD is a PU-U. Analysis of the spectra obtained shows that moisture cure occurs across all laminate types whether they are TAc, PC or a hybrid for the two is the same. Finally the adhesive is fully cured after 30 days as there was no isocyanate band detected.

3.47 Summary of MDI-TMP-PPG-BD Formulation

MDI-TMP-PPG-BD was successfully synthesised and used to form laminated materials. Synthesis of a prepolymer PU was confirmed via NMR and also by evidence of urethane bonds within the final ATR spectrum. Characterisation of the molecular weight distribution by MALDI-MS confirmed the presence of MDI-PPGMDI-BD-MDI-PPG-MDI but also displayed unreacted PPG, MDI-PPG-MDI and MDI-PPG-MDI-PPG-MDI from the first step of synthesis. MALDI-MS displayed that the increase to Mn, Mw and PDI occurs as a result of the chain-extension step.

DSC confirmed that the $T_g$ss of the cured PU-U adhesive was above -20°C making it fall within the processing window of the laminate. The overall thermal stability of the MDI-TMP-PPG-BD cured PU-U was confirmed at being well above the 100°C set point with the recorded onset of degradation not occurring until 301°C. ATR was used to prove the final material was indeed a PU-U as a result of the moisture curing process and that the material after 30 days was fully cured. 180° T-peel testing displayed the continued theme for this family of adhesives that they have an affinity for the PC interface but are incompatible with TAc. To obtain strengths approaching or exceeding

3 N mm^{-1} for TAc requires the saponification surface treatment. Finally the BD chain-extender had a poor effect on clarity as the haze value was >

1.5% whereas, DEPD was only <0.4% and the base formulation (MDI-TMP-PPG) was also lower at < 1.1%.

3.50 Analysis of MDI-TMP-PPG-PD

3.51 Synthesis Information

The final diol chain-extender trailed within this study using MDI with PPG was 1,2propane diol (PD). Selection of this chain-extender was based on the success of DEPD which is also propane diol based. This chain-extender does not possess the same steric bulk as DEPD which contains two ethyl groups, PD contains only a sole methyl as the disruptive group. Introducing a sterically hindered methyl group in theory should allow for sufficient disruption of hard-segment packing and lead to greater optical clarity following moisture cure. It is also aimed to improve the overall phase mixing of the final cured material through the disruption of hardsegment aggregation.

To better ensure that any effect observed was a result of the new chain-extender, the synthetic procedure was kept the same as previously used within section 3.31. Synthesis of the prepolymer was performed as detailed within previous sections in this chapter (see sections 3.21, 3.31, and 3.41). Next addition of PD was carried out, with no change to the reaction temperature which was kept between 85°C – 95°C. Reaction with the small molecular weight diol increased the viscosity but the prepolymer mixture was still clear and contained fewer bubbles than the previous BD based formulation. Following five hours of stirring the dual catalyst system was added (TEA and DBTDL) and to ensure the mixture would flow into the aluminium storage container the temperature was increased to 130°C for a short time. Once transferred the formulation was capped, degassed then placed within a fridge at 0°C for storage. Degassing was performed for six hours once a vacuum of one atmosphere was obtained. Analysis of the prepolymer material was performed using NMR, MALDI-MS and DSC.

Lamination was performed using the six laminate combinations (same as section 3.21) which were then cured at room temperature. MDI-TMP-PPG-PD adhesive was applied at a temperature of 130°C. 180° T-peel testing was recorded at both 7 and 30 days to determine the strength of the laminate and also the mode of failure. A sample was prepared as a TAc/TAc laminate, which once cured could be removed for DSC and TGA analysis. The 30 day peel test samples were also analysed by ATR to characterise the bulk cure material.

Analysis of the chain-extended materials only will be presented within this section. MDI-TMP-PPG is considered as representative of the reactive intermediate obtained after step one of this chain-extended reaction and therefor will not be covered (see section 3.21-3.27).

3.52 NMR Analysis

Proton NMR was used to investigate if the polymerisation of the chain-extended prepolymer had been a success and to identify the new peaks added from the PD molecule. The peaks of MDI and PPG are discussed within section 3.22 and it can be agreed that they are all present within the spectrum presented in figure 3.24.
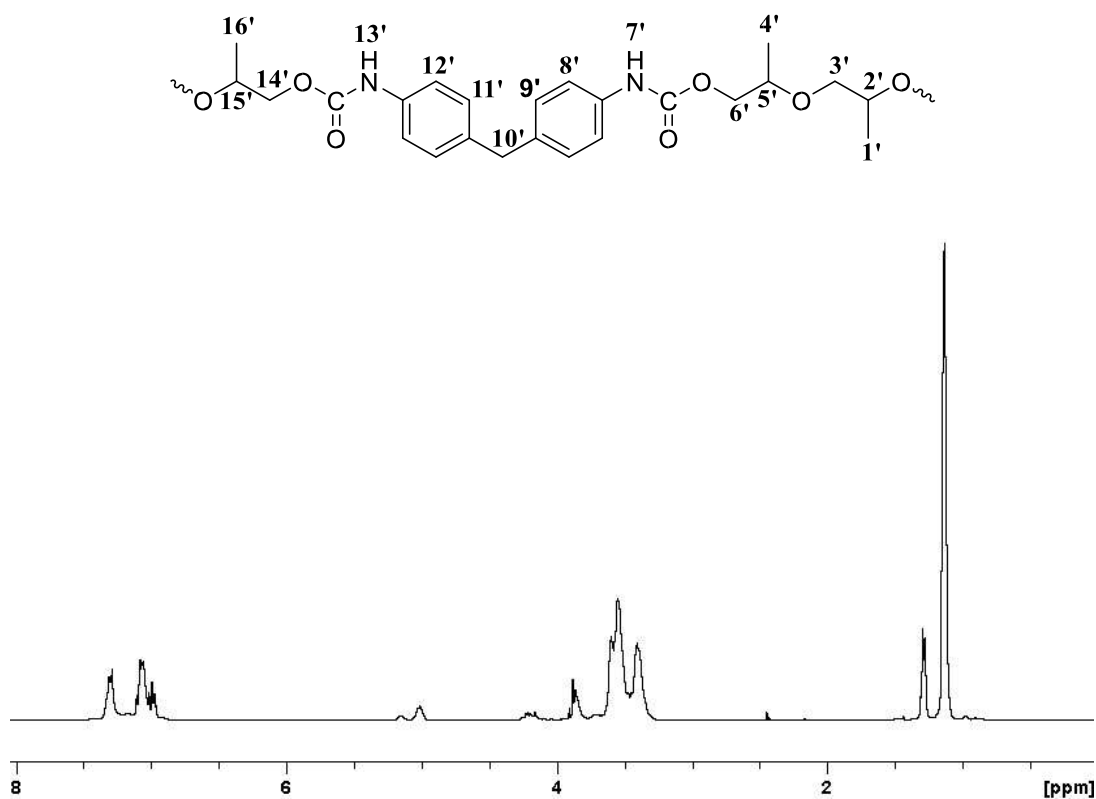
Figure 3.24: ^{1}H NMR spectrum obtained following reaction of MDI-TMP-PPG with PD.

Peaks within the ^{1}H spectrum of the diol chain-extended prepolymer do not display any of the PD peaks as they are convoluted in with the PPG peaks of the polyol. This is a consequence of the chain-extender having the same 1,2-substitution pattern as PPG. PD incorporation has occurred and the evidence can be seen firstly by the broadened peak of the methylene group **14'** adjacent to a urethane group at 4.21 ppm. The second piece of evidence that shows PD incorporation is visible from the **C-H** signal of protons **15'** adjacent to a urethane group at 5.16 ppm. Again the **N-H** protons at 7.29 ppm are evidence that urethane and prepolymer formation.
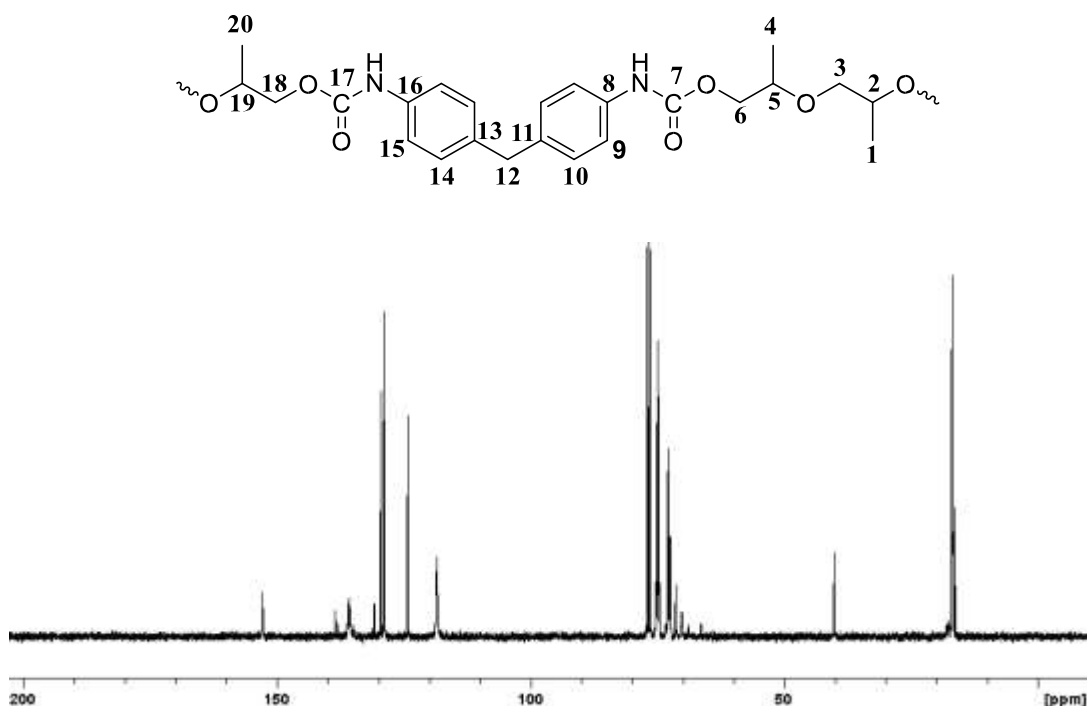
Figure 3.25: ^{13}C NMR spectrum obtained following reaction of MDI-TMP-PPG with BD.

The same detection problem was also encountered using ^{13}C NMR as the peaks of the diol chain-extender are visible within the same region as the PPG soft-segment. Within the spectrum methyl carbons of the chain-extender are visible at a downfield position of 18 ppm compared to the PPG methyl group. Confirmation of urethane formation is shown by the carbonyl peak at 153.8 ppm. For full characterisation of region 60 – 80 ppm and 110 – 140 ppm see section 3.22 and 3.32.

3.53 MALDI-MS Analysis

To quantify the effect diol chain-extension has on the molecular weight of the prepolymer MALDI-MS was used. Mass spectrometry analysis was also used to determine if the synthetic process was producing polymers of similar composition. The matrix used for the MALDI-MS analysis was dithranol which contained a cationising agent NaTFA (see section 3.23 for more matrix information). A 40 mg ml^{-1} solution of MDI-TMP-PPG-PD was prepared in THF and mixed with the matrix (1:8 sample:matrix). 1 μl portions of this sample were then spotted and dried for analysis. Four different molecular weight distributions were observed within the spectrum of the MDI-TMP-PPG-BD prepolymer formulation.
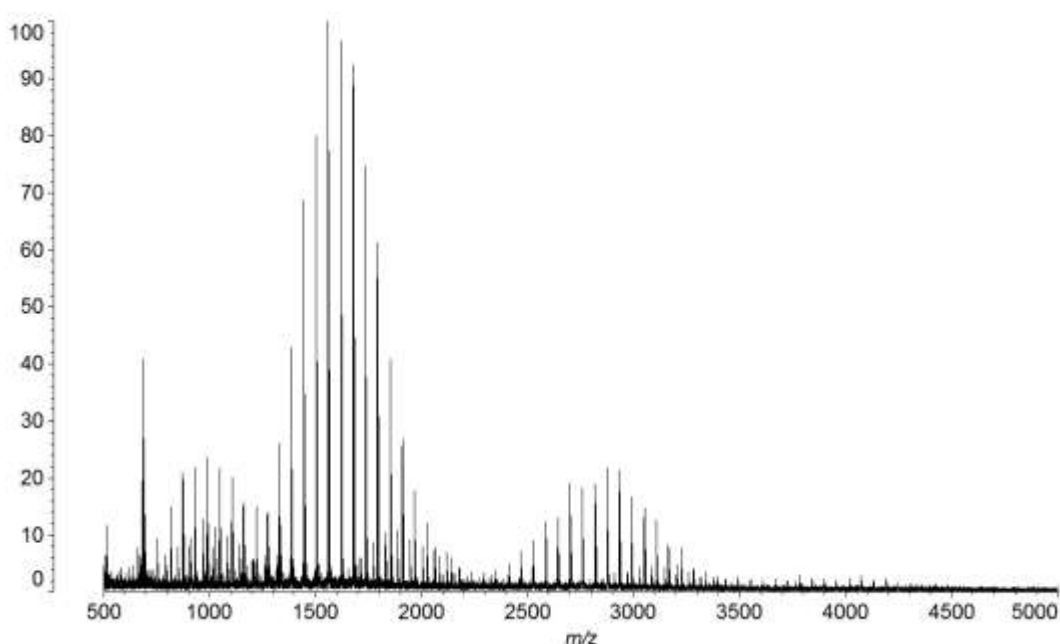
Figure 3.26: MALDI-MS spectrum of MDI-TMP-PPG-PD chain-extended prepolymer collected in dithranol/NaTFA.

Confirmation of some unreacted PPG starting material was again evident by the mass distribution centred on 1044 m/z. Tailing on from the first distribution is that of the prepolymer MDI-TMP-PPG formed during the first synthetic step. An end capped prepolymer of this type with the distribution peaking at 1570 m/z has a composition of two ethanol end capped MDI units, two Na$^+$ cations and 17 PPG repeat units. Persistence of prepolymers which do not contain any chain-extender would be expected due to the high viscosity of the bulk polymerisation process reducing the

179

effectiveness of the mixing (require longer mixing time and possibly catalyst addition). Also present at 1045 m/z is the chain-extender TMP that has reacted with three MDI units which are ethanol end-capped (plus one sodium cation). These molecules will contribute to the hard segment microstructure within the adhesive and their observation was possible as all the starting material was consumed.

The higher molecular weight end of the distribution shows two chain-extended polymer lengths; MDI-PPG-MDI-PPG-MDI (2200 to 3200) and MDI-PPG-MDIPD-MDI-PPG-MDI (3200 to 5000). Prepolymers of structure MDI-PPG-MDI-PPGMDI are produced during the first step of synthesis and have a peak centred on 2876 m/z. Analysis of the upper region shows that a proportion of the prepolymer molecules have reacted with PD and coupling of two prepolymers is displayed by peaks such as 3221 m/z. The mass spectrum obtained for chain-extension of MDITMP-PPG with PD is the first example where diol chain-extended prepolymers are clearly visible and is a result of an improved signal-to-noise. Such structures should result in the inhibiting of hard-segment formation and a clearer cured adhesive.

MALDI-MS has shown the structure of interest MDI-PPG-MDI-PD-MDI-PPG-MDI is present within the PU adhesive formulation. The small size of the peaks could result from a number of reasons e.g. not fully co-crystallising with the matrix resulting in power ionisation, synthesis time needing increased, catalyst needed during synthesis, poor flight in mass spectrometer etc. Similar values were obtained for Mn, Mw and PDI which confirms that the chain-extension step increases the polydispersity. The calculated value of Mn is 1948 m/z and the calculated value of Mw is 2459 m/z giving a PDI of 1.26.

3.54 DSC and TGA Analysis

The PU prepolymer chain-extended with PD has a $T_g$ss of -11°C which spanned a range of -16°C to -4°C. Recording the $T_g$ss further supports the need for thermal analysis to ensure that the adhesive is within specification.

More importantly the $T_g$ss of the cured PU-U adhesive was recorded to determine the properties that would be present within the final material. Analysis was again recorded using a heat-cool-reheat experiment from -80°C to 140°C on the first cycle and -80°C

to 300°C on the second, with the two heating cycles presented in figure 3.28. The $T_g$ss obtained on the first heating cycle was 0°C and was over a range of 12°C to 7°C. Following on from previous cycle, the second $T_g$ss was present at an elevated temperature of 6°C which covered a range of -8°C to 16°C. Elevation of the second $T_g$ss will most likely result from the first process acting as an annealing process.[13] Collection of the final $T_g$ss following diol chain-extension shows that the hard-segments are of a high enough abundance to push the transition to higher temperature. This would suggest that any following synthesis should use a higher molecular weight soft-segment to reduce the hard-segment concentration.
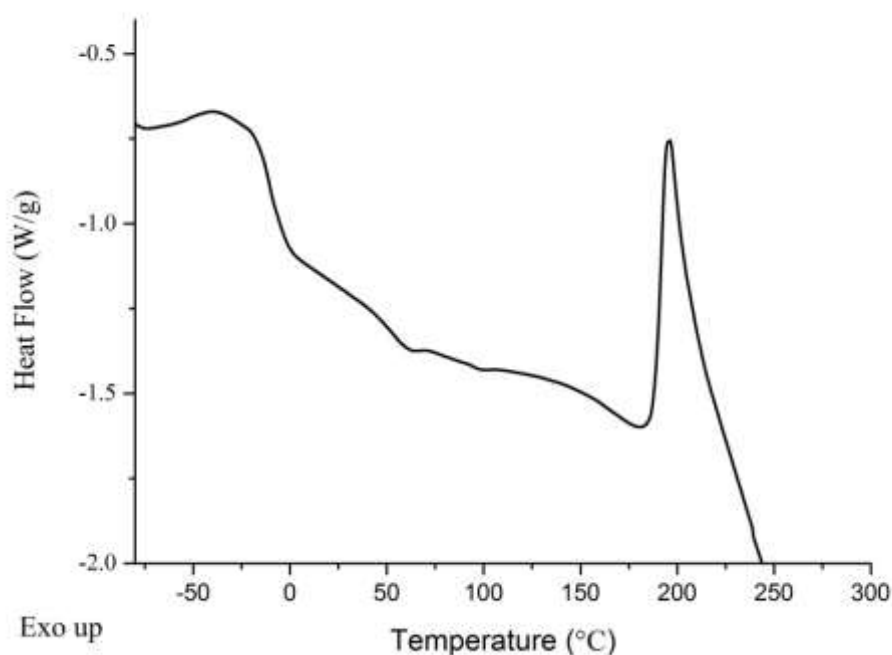
Figure 3.27:   DSC thermogram of MDI-TMP-PPG-PD chain-extended prepolymer formulation.

TGA and DTG curves for MDI-TMP-PPG-PD PU-U cured adhesive are presented within figure 3.29. From the TGA curve the single step degradation profile observed is consistent with the other chain-extended PU-U analysed previously (small initial degradation process also visible). An onset of 294°C was calculated from the TGA curve and the peak rate of degradation at 368°C was calculated form the DTG curve.

Single stage degradation was present within the TGA curve of MDI-TMP-PPG-PD. This would suggest that diol chain-extension step encourages phase mixing and reduces hard-segment aggregation, not the chain-extender selected. Such a conclusion can be drawn from the marked similarity of the three chain-extended curves obtained by TGA and how they are all different form the base prepolymer PU. The data collected using DSC plus TGA analysis of both the prepolymer PU and the cured PU-U are also consistent through the set.
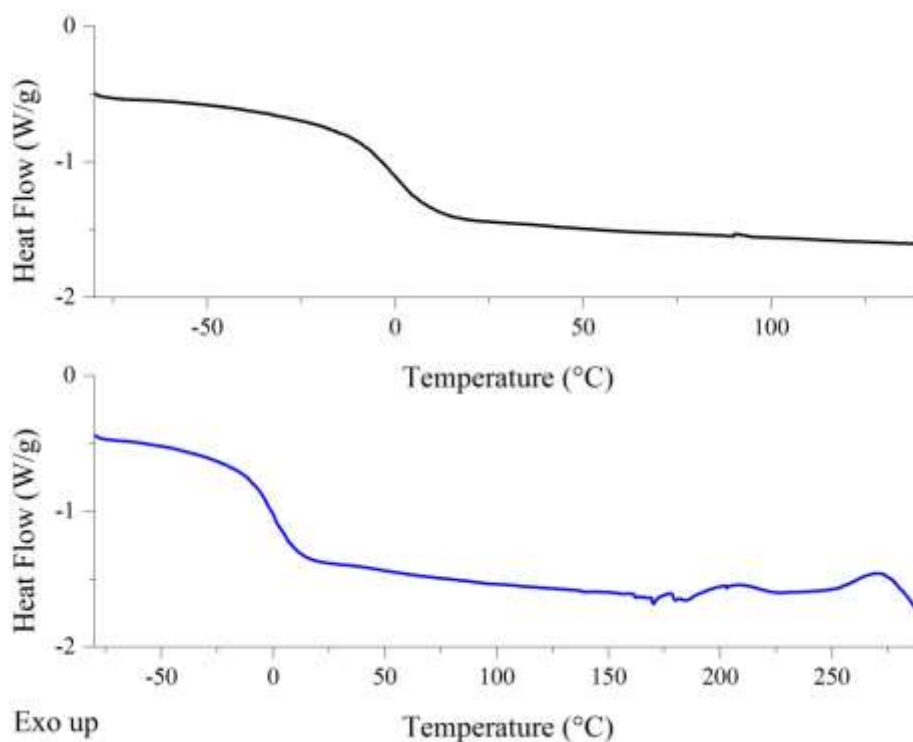
Figure 3.28: DSC thermogram of fully cured MDI-TMP-PPG-PD adhesive, following removal from TAc/TAc laminate. [First heating cycle *top* in black and second heating cycle *bottom* in blue].
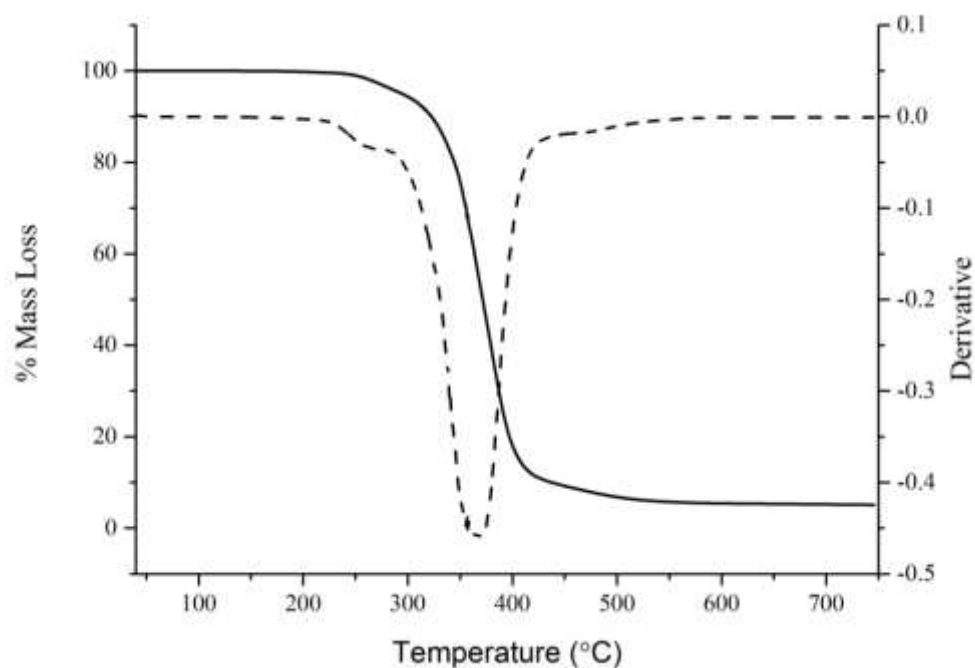
Figure 3.29: TGA and DTG curves of fully cured MDI-TMP-PPG-PD adhesive. [TGA solid line and DTG dashed line].

3.55 180° T-peel Test and Haze

During application of the reactive PU adhesives a lamination problem was encountered for MDI-TMP-PPG-PD. Following lamination the adhesive proceeded to gel almost instantly and failed to wet the surface. Even with time the degree of surface wetting was poor and as a result after 7 days the laminates were untestable due to such poor adhesion. The values obtained following 30 days of cure may be used with caution as they are not truly representative of the adhesive strength or consistent with previous laminations. Lamination was performed in the order presented within the table with the gelling problem getting worse with each combination. It would be expected based on the consistency of all other analysis on MDI-TMP-PPG based prepolymers that the same adhesion trends would be observed. The haze measurement was untestable as a direct result of the uneven surface presented and was >1.5%.

Analysis of TAc/TAc after 30 days resulted in a highly unstable adhesive failure at the interface with a strength of 0.6 N mm^{-1}. Poor peel strengths here will be a combination of mostly the application issue but also the incompatibility of this PU system with the TAc interface. Data collected from TAc(t)/TAc(t) displayed again an adhesive failure

but with a greater strength of 3.0 N mm^{-1}. This data point further clarifies the need for surface treatment to gain benchmark strength with TAc. Next both TAc(t)/PC and TAc(t)/PC(t) were both tested however, they displayed poor results as application was now a real issue. Highly unstable adhesive failures of strength 0.5 N mm^{-1} and 0.6 N mm^{-1} were obtained respectively. If application had been carried out without any issue these laminates would be anticipated to have strength values of ≥ 3 N mm^{-1} (see table 3.07). Finally both PC(t)/PC(t) and PC/PC were tested after 30 days of curing and both displayed highly unstable adhesives failures at the interface. PC/PC had a reduced peel strength of 1.0 N mm^{-1} and this was also observed by the low peel strength of PC(t)/PC(t) which measured in at 1.1 N mm^{-1}. The very low values obtained are a direct result of the problem encountered during application.

From the data obtained it can be observed that similar trends were not observed but the strengths obtained should be accepted with caution as a result of the application issue. Even with the application issue encountered with this formulation, enough data has been collected from previous experiments to discount MDI-TMP-PPG based formulations as the route to high strength and clarity.

Characterisation of the bulk cured adhesive was performed using ATR analysis and was performed to see if any abnormalities could be observed. Analysis of the bulk materials was performed on five of the laminates after 30 day tensile testing (PC(t)/PC(t) was not tested). ATR analysis will determine the chemical functionality of the final cured adhesive. Discussed within this section will be peaks that indicate the PU-U adhesive peaks obtained after 30 days of cure. For discussion of the peaks inherent of the starting materials see section 3.26 and for all characteristic peaks see table 3.08.

Table 3.07: Peel, haze and mode of failure data for MDI-TMP-PPG-PD cured PU-U adhesive. [The data in bold will be discussed within this section].

Cured Adhesive	Laminate	Peel 1* (N mm^{-1})	Peel 2^x (N mm^{-1})	Failure mode	Haze (%)
MDI-TMP-PPG	TAc/TAc	0.2	0.6	Adhesive TAc	<1.1
	TAc(t)/TAc(t)	3.3	3.3	Cohesive	
	TAc(t)/PC	ND	ND	ND	
	TAc(t)/PC(t)	3.6	2.7	Cohesive	
	PC(t)/ PC(t)	3.8	2.7	Cohesive	
	PC/PC	4.5	4.1	Cohesive	
MDI-TMP-PPG-DEPD	TAc/TAc	0.3	0.0	Adhesive TAc	<0.4
	TAc(t)/TAc(t)	2.0	3.0	Adhesive TAc(t)	
	TAc(t)/PC	3.1	3.8	Adhesive TAc(t)	
	TAc(t)/PC(t)	2.3	2.7	Adhesive TAc(t)	
	PC(t)/ PC(t)	2.6	3.3	Adhesive PC(t)	
	PC/PC	4.1	5.4	Adhesive/Cohesive PC	
MDI-TMP-PPG-BD	TAc/TAc	0.5	ND	Adhesive TAc	>1.5
	TAc(t)/TAc(t)	2.6	4.2	Adhesive TAc(t)	
	TAc(t)/PC	ND	ND	ND	
	TAc(t)/PC(t)	2.5	2.5	Adhesive TAc(t)	
	PC(t)/ PC(t)	4.7	5.3	Adhesive PC	
	PC/PC	ND	ND	ND	
MDI-TMP-PPG-PD	**TAc/TAc**	**ND**	**0.6**	**Adhesive TAc**	**>1.5**
	TAc(t)/TAc(t)	**ND**	**3.0**	**Adhesive TAc(t)**	
	TAc(t)/PC	**ND**	**0.5**	**Adhesive TAc(t)**	
	TAc(t)/PC(t)	**ND**	**0.6**	**Adhesive TAc(t)**	
	PC(t)/ PC(t)	**ND**	**1.1**	**Adhesive PC**	
	PC/PC	**ND**	**1.0**	**Adhesive PC**	

peel 1 collected within 7 days of room temperature cure, ^{x} peel 2 collected after 30 days of room temperature cure, ND = No Data

3.36 ATR of Peeled Samples

Previous analysis displays that after moisture cure the final adhesive is a PU-U and that the bulk material observed over each laminate is very similar (see figure 3.30). Therefore, the key peaks of interest are those that display either urethane or urea within the spectra and also the absence of an isocyanate peak. Bands that show urethane functionality within the spectra are **N-H** stretching at 3534 cm^{-1} plus 3305 cm^{-1}, **C=O** stretching at 1726 cm^{-1} (again displays urea shoulder), **N-H** bending at 1598 cm^{-1} and **C-N** stretch at 1300 cm^{-1}.

Figure 3.30:   ATR spectra of cured MDI-TMP-PPG-PD sampled in-situ after tensile testing with inset expanded carbonyl region. [TAc(t)/TAc(t) in black, TAc(t)/PC(t) in red, TAc(t)/PC in blue, TAc(t)/PC(t) in pink and PC/PC in green. Data collected for each laminate at nine random positions with each spectrum consisting of 128 scans at 8 cm^{-1} resolution. These were then averaged and plotted as the above spectra].

Evidence of urea functionality is also shown within the spectra by **N-H** stretching at 3534 cm^{-1} plus 3305 cm^{-1}, **C=O** stretching at 1726 cm^{-1}, **N-H** bending at 1511 cm^{-1} and **C-N** stretch at 1330 cm^{-1}. For all other characteristic bands found for MDITMP-

PPG-PD refer to table 3.08. Also evident is the absence of a free isocyanate band which confirms the adhesive is fully cured after 30 days.

Table 3.08: Characteristic peaks of MDI-TMP-PPG-PD cured PU-U adhesive from all five laminate combinations.

Wavenumber (cm^{-1})	Vibration	Wavenumber (cm^{-1})	Vibration
3538	N-H stretching	1379	C-H methyl deformation
3301	N-H stretching Hbonded	1338	C-N urea
2980	C-H stretching	1304	C-N urethane
2936	C-H asymmetric stretch	1221	C-H aliphatic skeleton
2868	C-H symmetric stretch	1070	C-O-C aliphatic ether
1730	C=O stretching urethane Hbonded	1018	C-H aromatic ring
1594	N-H bending urethane	924	C-H aromatic ring
1534	C-N stretch, N-H bending, C-H aromatic ring	856	C-H aromatic ring
1507	N-H bending urea	818	C-H aromatic ring
1458	C-H bend aliphatic		
1410	C-C stretching aromatic	769	C-C aliphatic skeleton

3.37 Summary of MDI-TMP-PPG-PD Formulation

Successful synthesis of PU adhesive MDI-TMP-PPG-PD was carried out.

Application of the prepolymer however, was not so successful and an issue was encountered with gel formation during lamination. Synthesis of a prepolymer PU was

confirmed via NMR and also by evidence of urethane bonds within the final ATR spectrum. ATR was also used to prove the final adhesive was indeed a PU-U as a result of the moisture curing process and that the adhesive after 30 days was fully cured. Characterisation of the molecular weight distribution by MALDI-MS confirmed the presence of MDI-PPG-MDI-PD-MDI-PPG-MDI but also displayed unreacted PPG, MDI-PPG-MDI and MDI-PPG-MDI-PPG-MDI formed during the first step synthetic step. Similar values for Mn, Mw and PDI were recorded compared with the other diol chain-extended formulations

Thermal analysis by DSC confirmed that the $T_g$ss of the cured PU-U adhesive was above -20°C making it fall within the processing working window of the laminate. The overall thermal stability of the MDI-TMP-PPG-PD cured PU-U was confirmed at well above the 100°C set point with the recorded onset of degradation not occurring until 294°C. 180° T-peel testing data was not considered very valid as a direct result of the poor application. Finally PD effect on the clarity could not be gauged as the application issue made the data collected not valid.

3.60 Summary and Conclusions of Aromatic Polyurethane Adhesives Based on Poly(propylene glycol)

Synthesis of all four adhesive formulations was successfully carried out and the products were confirmed using NMR followed by MALDI-MS analysis. MALDIMS displayed a large increase to the PDI following prepolymer synthesis with the value increasing from 1.02 for PPG to 1.24 for MDI-TMP-PPG. A further increase to the PDI was observed following diol chain-extension. Urethane linkages were also visible within the ATR spectra obtained along with urea bands which confirmed the final fully cured adhesive was a PU-U. Each adhesive was used to perform lamination on six different laminate combinations, which once cured could be tested to determine the 180° T-peel strength, mode of failure and final haze measurement of each laminate. TGA analysis was also collected on each of the cured adhesives and it displayed that for each the onset of degradation was around 300°C. This result confirmed that PU-U based adhesive would be stabile well above the set maximum that these laminate would see within normal processing (set at 100°C). 180° T-peel testing confirmed that all these adhesives have an affinity for the PC interface but for reasonable bond strength

with TAc saponification surface treatment was essential. The overall result however, for formulations based on MDI and PPG is that they cannot be used any further as they were not able to deliver all the aims set out at the beginning of the project. The main two shortcomings will be discussed briefly here.

The first issue highlighted was the $T_g$ss of the each adhesive was within what was specified as the processing window of the laminate. In absence of a chain-extender the observed $T_g$ss was -13°C and this climbed to a final reading of -8°C after the second heating. When chain-extension was implemented the $T_g$ss obtained was further elevated to above 0°C. After the second heating cycle the obtained $T_g$ss for DEPD was 8°C, for BD was 6°C and finally for PD was 6°C. Each value obtained after chain-extension was at least 25°C inside the processing window set for the final laminate. This would lead to stiffening of the lens below 0°C and due to the high hard-segment concentration could result in the adhesive layer hazing.

The second and most important issue was the peel behaviour obtained from formulations based on MDI and PPG. For all formulation regardless of composition the value obtain when using untreated TAc was < 1 N mm^{-1}, meaning each adhesive does not even reach one third of the minimum set strength value. Also for each TAc laminate of this kind the mode of failure was adhesive at the interface suggesting an incompatibility. Finally even with PC, a large proportion of the failure modes were adhesive (all base formulation laminates cohesive except TAc/TAc) which suggests that a new soft-segment is required to obtained greater interaction with the interface.

References

(1)   Engels, H.-W.; Pirkl, H.-G.; Albers, R.; Albach, R. W.; Krause, J.; Hoffmann, A.; Casselmann, H.; Dormish, J. *Angewandte Chemie International Edition* **2013**, *52*, 9422.

(2)   Sawai, M.; Miyamoto, K.; Takemura, K.; Mori, M.; Kiuchi, K. *Journal of Cellular Plastics* **2000**, *36*, 286.

(3)   da Silva, A. L. D.; Martín-Martínez, J. M.; Carlos Moura Bordado, J. *International Journal of Adhesion and Adhesives* **2008**, *28*, 29.

(4)   Wang, P.-S.; Chiu, W.-Y.; Chen, L.-W.; Denq, B.-L.; Don, T.-M.; Chiu, Y.S. *Polymer Degradation and Stability* **1999**, *66*, 307.

(5)   Petrović, Z. S.; Zavargo, Z.; Flyn, J. H.; Macknight, W. J. *Journal of Applied Polymer Science* **1994**, *51*, 1087.

(6)   Grassie, N.; Zulfiqar, M. *Journal of Polymer Science: Polymer Chemistry Edition* **1978**, *16*, 1563.

(7)   Herrera, M.; Matuschek, G.; Kettrup, A. *Polymer Degradation and Stability* **2002**, *78*, 323.

(8)   Poljanšek, I.; Fabjan, E.; Moderc, D.; Kukanja, D. *International Journal of Adhesion and Adhesives* **2014**, *51*, 87.

(9)   Burattini, S.; Greenland, B. W.; Merino, D. H.; Weng, W.; Seppala, J.; Colquhoun, H. M.; Hayes, W.; Mackay, M. E.; Hamley, I. W.; Rowan, S. J. *Journal of the American Chemical Society* **2010**, *132*, 12051.

(10)   Li, C.; Wilkes, G. *Journal of Inorganic and Organometallic Polymers* **1997**, *7*, 203.

(11)   Daniel-da-Silva, A. L.; Bordado, J. C. M.; Martín-Martínez, J. M. *Journal of Applied Polymer Science* **2008**, *107*, 700.

(12)   Randall, D. *The Polyurethane Handbook*; J. Wiley & sons, LTD, 2002.

(13)   Martin, D. J.; Meijs, G. F.; Renwick, G. M.; McCarthy, S. J.; Gunatillake, P. A. *Journal of Applied Polymer Science* **1996**, *62*, 1377.

(14)   Šebenik, U.; Krajnc, M. *International Journal of Adhesion and Adhesives* **2007**, *27*, 527.

(15)   Chen, J.-H.; Ruckenstein, E. *Journal of Colloid and Interface Science* **1990**, *135*, 496.

Chapter 4 Aromatic Polyurethane Adhesives based on Poly(caprolactone diol)

4.10 Polymers Synthesis Introduction

In previous analysis it was identified that the functionality of the soft-segment has a significant influence on the microstructure and adhesive strength. Poly(propylene glycol) (PPG) based formulations (with methylene diphenyl diisocyanate (MDI)) performed well with polycarbonate (PC) giving above benchmark strength irrespective of whether the surface was treated or not. Conversely the same formulations performed poorly with cellulose triacetate (TAc) and a deacetylation surface treatment (saponification) was essential to obtain acceptable bond strengths (3 N mm^{-1}). These findings suggest an inherent incompatibility between the TAc substrate and the PPG based formulations. Furthermore, the adhesive mode of failure which resulted during 180° T-peel testing at the TAc interface was further evidence of this observation.

To increase the measured bond strength and improve the compatibility with the TAc interface the soft-segment was changed to poly(caprolactone diol) (PCD). PCD is an ester based material which will increase the functionality of the soft-segment portion of the polyurethane (PU). Having a more functionalised soft-segment such as PCD should assist with two things: firstly the carbonyl groups of the PCD backbone can form H-bonds with the TAc surface resulting in a stronger interface and secondly Hbonds can form between polymer chains within the polyester giving a tougher crosslinked adhesive matrix. Such polyester based adhesives are commonly used in reactive PU hot melt adhesives, with the polyester soft-segment giving the final adhesive good compatibility with a variety of substrates, high solvent resistance and high matrix strength.[1]

As the soft-segment is crystalline, sufficient disruption of the polyester cross-linking must also be considered if an optically clear final adhesive is to be obtained. Considering this four PU prepolymer adhesives were synthesised: a one-step prepolymer PU of formulation MDI-TMP-PCD (polymer has MDI,TMP and PCD in formulation) and three two-step chain-extended prepolymer formulations MDI-TMPPCD-DEPD (initial step chain-extended with 2,2-diethyl-1,3-propane diol),

MDITMP-PCD-BD (BD = 1,3-butane diol) and MDI-TMP-PCD-PD (PD = 1,2-propane diol).
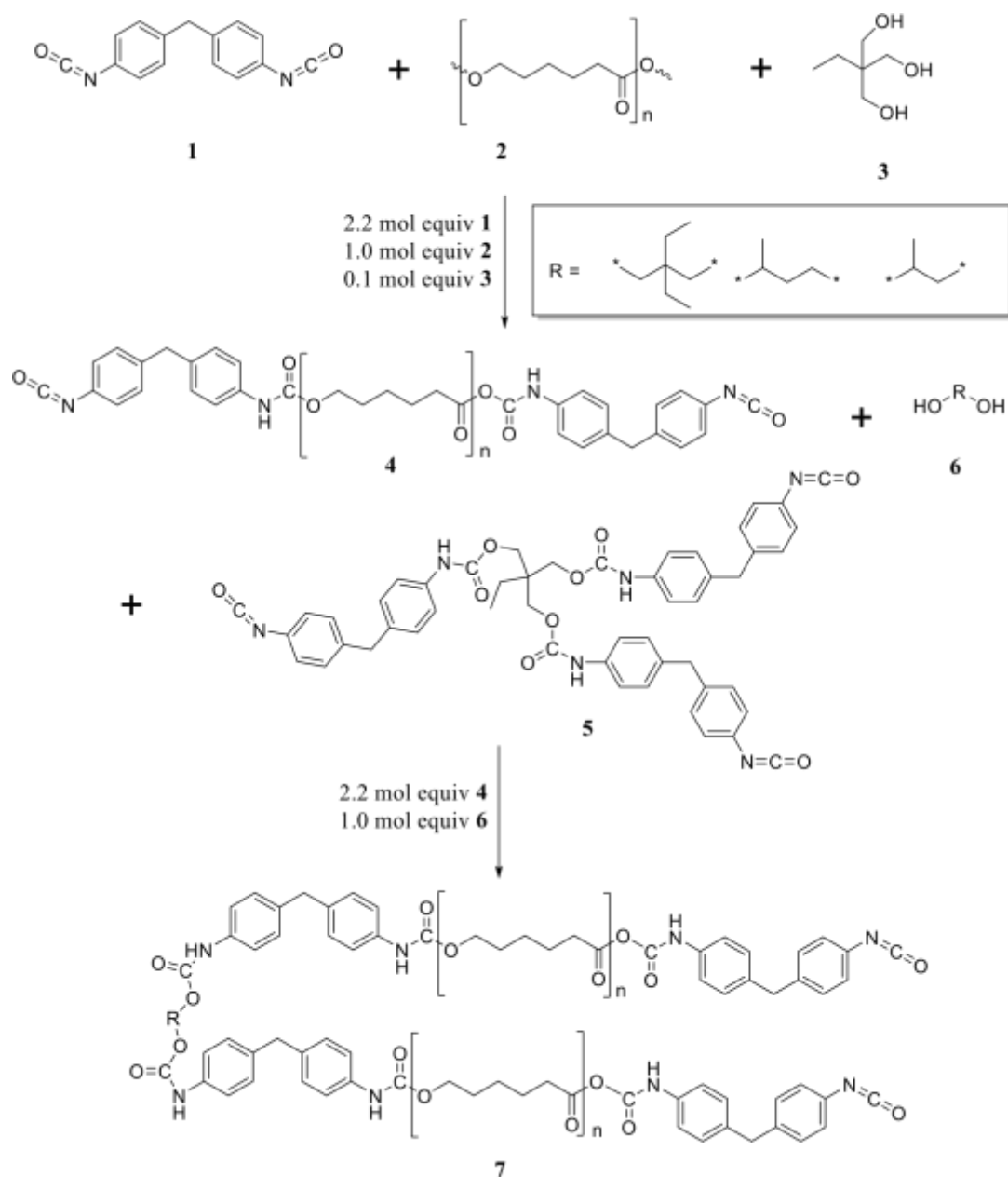
Figure 4.01: General reaction scheme for the synthesis MDI-TMP-PCD based chain-extended polyurethanes adhesives. 1 = MDI, 2 = PCD, 3 = TMP, 4 = MDIPCD prepolymer, 5 = end capped MDI-TMP, 6 = chain-extender and 7 = chainextended prepolymer.

Again the curing chemistry employed will be a two stage process of initial catalyst cure (0.05 wt% of both dibutyltin dilaurate and triethylamine) followed by final moisture

cure of any remaining free isocyanate. Each synthesised prepolymer material was analysed using NMR and MALDI-MS before application. Thermal transition and stability of each fully cured PU-U was analysed by DSC and TGA. The final characteristics of each PU-U were analysed by ATR to obtain functionality information and 180° T-peel testing to determine laminate strength.

4.20 Analysis of MDI-TMP-PCD

4.21 Synthesis Information

Prior to synthesis, PCD (2000 Mw) was dried to remove water by placing within a vacuum oven at 80°C for at least 48 hours. Synthesis was performed using reaction set-up as detailed in section 2.03 with the reaction being performed in the temperature window of 85°C – 95°C for three hours. The reaction time was started after the last addition of MDI to the polyol containing reaction vessel. MDI was melted (50°C – 60°C within a three necked round bottom flask see section 2.03) and degassed before being put under a nitrogen atmosphere. To ensure that the exothermic reaction did not exceeded 95°C, MDI was added drop wise in 1 ml portions. The final prepolymer obtained was clear but visually thicker than the starting mixture as a consequence of the molecular weight increase. Prior to catalyst addition samples of the reaction were taken for NMR, MALDI-MS and DSC analysis. After the elapsed reaction times of three hours 0.05 wt% of dibutyltin dilaurate and 0.05 wt% of triethylamine were added as curing catalysts (calculated from batch weight). Following catalyst addition the formulation was transferred to an aluminium holding tube which was placed in a vacuum desiccator and kept at 0°C within a fridge until being used during lamination (typically not exceeding 7 days). Degassing was performed for six hours once a vacuum of one atmosphere was obtained.

The prepolymer adhesive was applied to six different laminates that were of interest:

- TAc/TAc
- TAc(t)/TAc(t)

- TAc(t)/PC
- TAc(t)/PC(t)
- PC(t)/PC(t)

- PC/PC

Where TAc is cellulose triacetate, PC is bisphenol-A polycarbonate and (t) denotes that the surface of the polymer film has been treated (see section 2.01 and 2.02). MDI-TMP-PCD was applied at 160°C to ensure good surface coverage. The lamination process was carried out as detailed in section 2.04, followed by cure at room temperature. 180° T-peel testing was carried out initially after 7 days and then after 30 days to determine the peel strength of each laminate, with the mode of failure monitored by visual inspection. The cured laminates from the 30 day peel testing were used in the ATR analysis of the fully cured adhesive.

4.22 NMR Analysis

To observe the PU prepolymer formation between MDI with PCD, both ^{1}H and ^{13}C were recorded. The hydroxyl end-groups of the 2000 molecular weight (Mw) PCD are both primary as determined by previous analysis (PCD polymerisation initiated with neopentyl glycol).

Presented below the ^{1}H spectrum of MDI-TMP-PCD isocyanate end-capped prepolymer PU used as the first adhesive for lamination. At 0.95 ppm protons from the methyl group of TMP and the adjacent **CH₂** are visible at 1.6 ppm. Observation of the **CH₂**-O protons of TMP is not possible as they are convoluted with the signal from the MDI methylene bridge **10'** at 3.9 ppm. Next centred on 1.37 ppm is the peak of backbone methylene groups **3'**, with the broad signal inherent of the PCD soft-segment. Further backbone methylene groups **2'** and **4'** are also visible from PCD at 1.64 ppm. Next methylene groups **1'** adjacent to the ester carbonyl group in PCD can be observed at 2.31 ppm. Situated more downfield are the methylene group connected to the oxygen in urethane linkages **5'** at 3.89 ppm. The methylene protons situated next to the oxygen in ester groups in the PCD backbone are also visible further downfield at 4.04 ppm. The triplet signal visible at 4.13 ppm represents the methylene bridge protons **9'** of the MDI molecule.
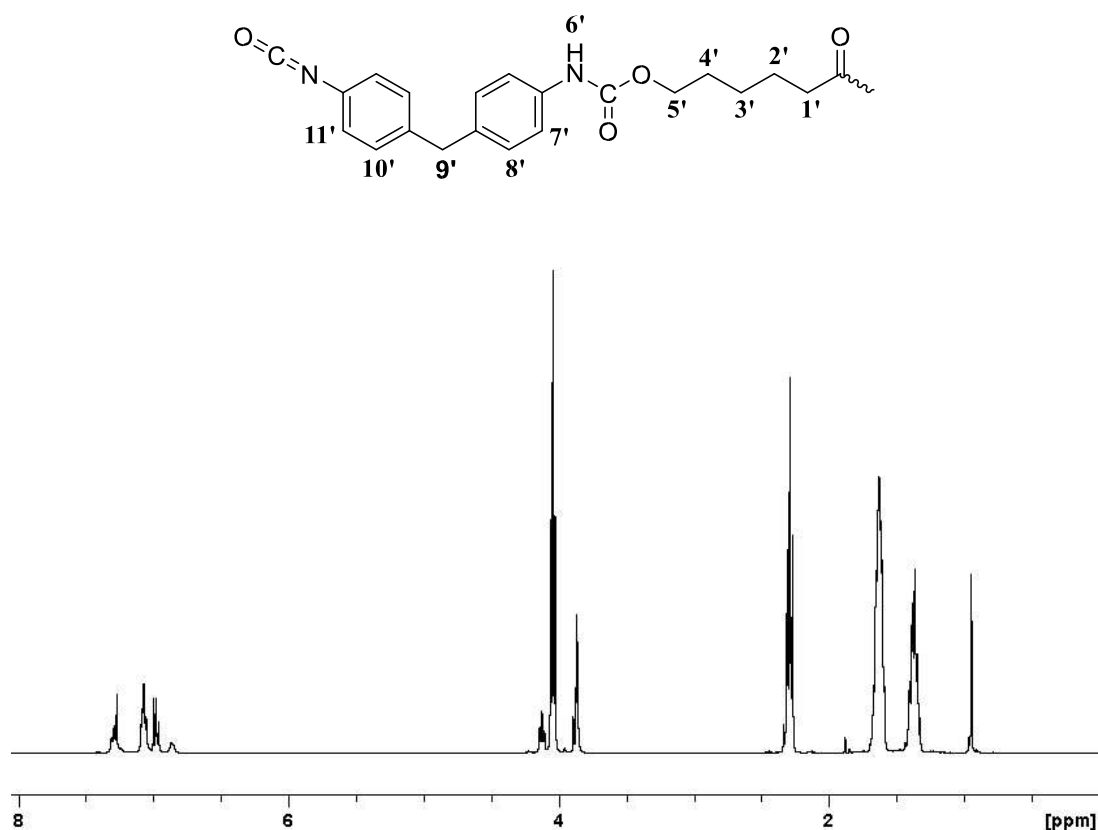
Figure 4.02: **^{1}H NMR spectrum of MDI-TMP-PCD polyurethane prepolymer in deuterated chloroform.**

Further MDI signals from the aromatic **CH** protons are visible at 7.0 ppm **10'** and 7.1 ppm **11'** on the unreacted ring. As these signal are still visible it shows that there is still the presence of free isocyanate groups, which are essential for a reactive adhesive. These peaks have become broadened when compared to unreacted MDI (two sharp peaks at 7.0 and 7.1 ppm); this results from there being a convoluted contribution of the **CH** protons **7'** and **8'** due to the urethane linkages influence on the ring. At 7.3 ppm the broad peak represents the **NH** protons **6'** which are further evidence of the urethane linkage being formed.[2] Its formation is direct evidence that urethane linkages are present.

Further characterisation of the PU prepolymer material was next carried out using ^{13}C analysis. Previous analysis displayed that both terminal hydroxyl groups are primary as the polymerisation was initiated by neopentyl glycol. The methyl carbons positioned at 22 ppm are present due to the neopentyl glycol initiator used during the synthesis of the Capa2201A soft-segment material. Further initiator peaks are also

present at 40.7 ppm (also contains **12** of MDI methylene bridge) for the tertiary carbon and 69 ppm which represents the methylene groups within the propane backbone of neopentyl glycol. Methylene carbon peaks **2**, **3**, **4** and **5** from the PCD backbone are visible at 34 ppm, 24.7 ppm, 25.6 ppm and 24.8 ppm respectively. The final backbone peaks are **6** the methylene group connected to an oxygen atom at 64.3 ppm and also the carbonyl **1** of the ester peak at 174 ppm. The large triplet at 77.23 ppm can be ignored as this signal is from the deuterated chloroform solvent.
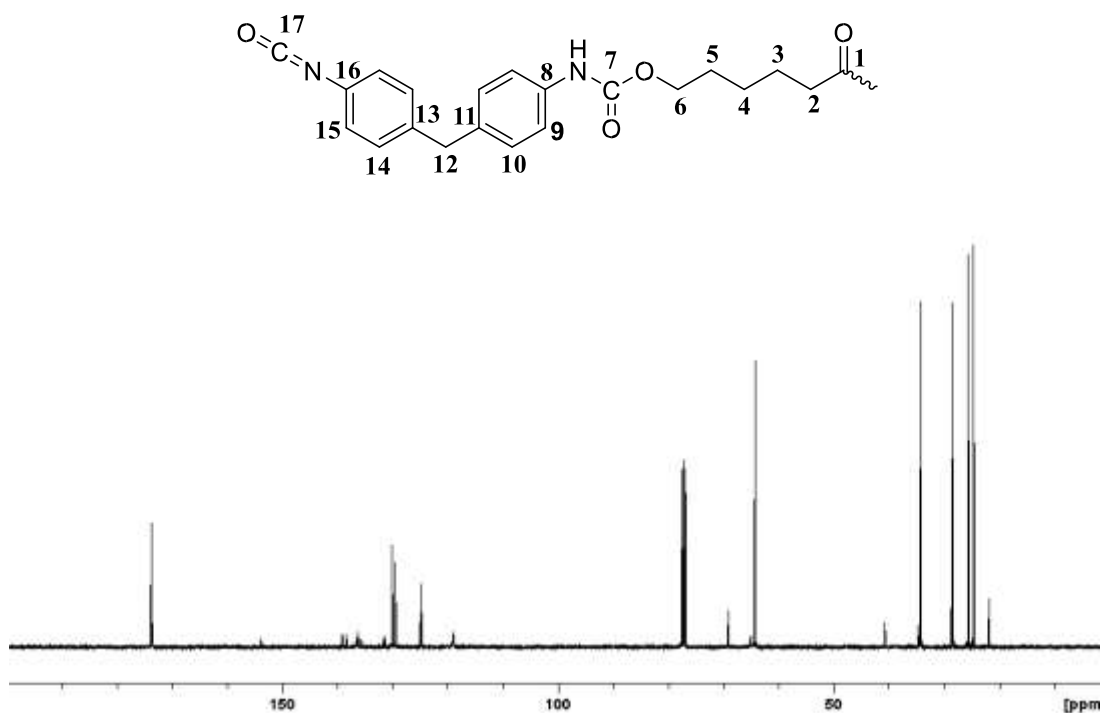
Figure 4.03: ¹³C NMR spectrum of MDI-TMP-PCD prepolymer in deuterated chloroform.

If MDI is in its unreacted state only five different carbons are expected in the aromatic region (ipso, ortho, meta, para and carbonyl in N=C=O) but as urethane bonds are present the molecule is now asymmetric and additional peaks are observed. Carbon atoms positioned ortho to the reacted urethane linkage **9** have a signal at 119 ppm which is an up field shift from 124 ppm for the carbons ortho to the unreacted isocyanate group **15**. At 129 ppm the signal represents the carbon connected to the methylene bridge on the ring that has the urethane linkage **11**. Observed at 130 ppm are two peaks that account for the meta carbons for the reacted ring **10** and **14** of the unreacted ring. The two peaks at 131 ppm are representing the carbonyl carbon **17** of

free isocyanate groups and the ring carbon **16** that the isocyanate groups are attached. Following on at 135 ppm the ring carbon that is connected to the NH of the urethane link **8** is observed. The presence of both peaks **8** and **17** display that not all isocyanate groups have not been consumed which must be true if a prepolymer were formed. Further evidence of urethane formation is given by the peak at 136 ppm which represents the ring carbon connected to the NH of the urethane linkage **8**. The peak at 139 ppm represents the ring carbon attached to the methylene bridge **13** on the unreacted ring. A final piece of evidence of the urethane reaction is shown at 153 ppm and represents the carbonyl within the urethane bond **7**.

4.23 MALDI-MS Analysis

The previous section was able to show both reacted and unreacted isocyanate groups and the presence of urethane linkages. In order to fully understand the structure of the prepolymer, mass spectrometry data is required. To serve this purpose matrix assisted laser desorption ionisation time-of-flight mass spectrometry (MALDI-MS) analysis was employed to determine the molecular mass of the starting polyol and then the prepolymer adhesive.
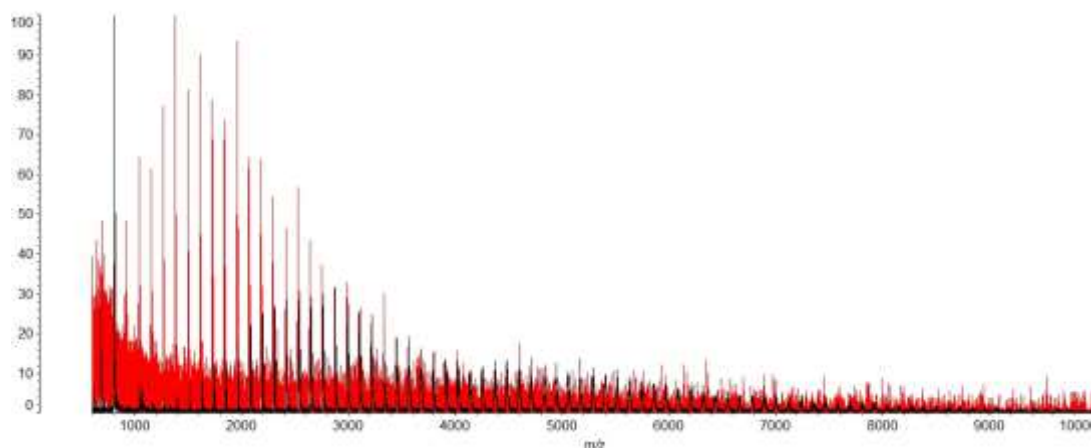
Figure 4.04: MALDI-MS spectra of PCD starting material in red and the prepolymer MDI-TMP-PCD in black. Both were mixed with the matrix material of HABA and NaTFA in a 1:8 sample:matrix mixture.

The matrix used was 2-(4-Hydroxyphenylazo) benzoic acid (HABA) which was prepared as a 20 mg ml^{-1} solution in tetrahydrofuran (THF), this was then mixed with a 1 mg ml^{-1} solution of sodiated trifluoroacetic acid (NaTFA) in a 7:1 ratio respectively.

MDI-TMP-PCD sample was prepared as a 40 mg ml^{-1} solution in THF which was then mixed with the matrix in a 1:8 ratio of sample to matrix. 1 µl aliquots of the solution were then spotted and dried before analysis.

Present at 1045 m/z is the chain-extender TMP that has reacted with three MDI units which are ethanol end-capped (plus one sodium cation). These molecules will contribute to the hard-segment microstructure within the adhesive and their observation was possible as all the starting material was consumed. The mass spectrum of PCD in figure 4.04 displays the sodiated adduct of the polyol material with the sodium coming from the small amount of a cationising (NaTFA) agent added to obtain spectra.

From the MALDI-MS spectrum it is possible to calculate Mn, Mw and PDI. For soft-segment PCD, the calculated Mn is 1695 m/z and Mw is 1824 m/z giving a PDI of 1.08 (see section 2.132 for formulae). This low PDI value displays that the molecular weight distribution of PCD is narrow. Following prepolymer synthesis an increase is observed for all three parameters. Mn is calculated at 3290 m/z and Mw is 4088 m/z giving a PDI for this formulation of 1.24. This noticeable increase to the PDI value following polymerisation displays that the mass distribution is now broader.

For the prepolymer material an observed shift of the distribution by 592 m/z was observed which corresponds to the addition of two MDI units that have had their free isocyanate groups end capped with ethanol to maintain the molecular weight (black distribution). This peak centred at 2325 m/z contains two ethanol end capped MDI units one sodium ion and 14 caprolactone repeat units. From this spectrum it displays that using a 2.2:1.0 excess of isocyanate to polyol makes it possible to obtain an MDI-PCD-MDI end capped prepolymer PU. Also evident are higher molecular weight prepolymer molecules of the structure MDI-PCD-MDI-PCD-MDI. MALDI-MS has allowed for characterisation of the structure of the molecules present in conjunction with the previous NMR analysis.

4.24 DSC and TGA Analysis
Determining the thermal behaviour of the prepolymer and cured adhesive is important as it will give information on the performance of the adhesive within a laminate during

normal processing temperatures. Two techniques, differential scanning calorimetry (DSC) and thermal gravimetric analysis (TGA) were selected to investigate if the adhesives were capable of being stable either side of the set functional processing window of -20°C – 100°C.
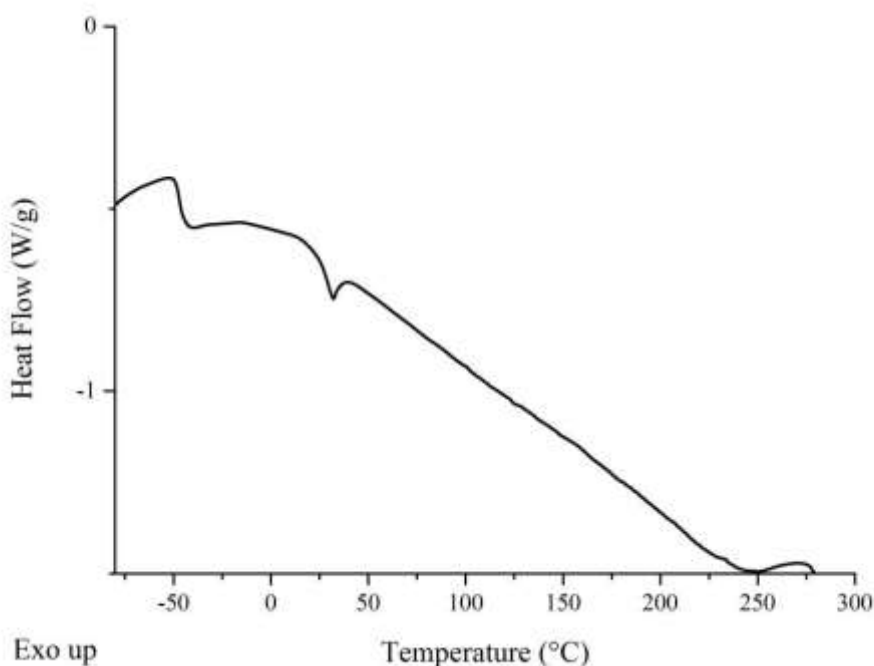
Figure 4.05: DSC thermogram of catalyst free MDI-TMP-PCD prepolymer sampled directly after synthesis.

Understanding the position of the soft-segment glass transition ($T_g$ss) for each formulation was outlined as an important piece of information to collect. For the prepolymer material, the initial aim was to keep the $T_g$ss as low as possible in an attempt to keep the final cured $T_g$ss out with the identified processing window. Any increase in $T_g$ss will come from the increase in molecular weight as expected during cure and also any increase in cross-linking. In the current formulation cross-linking could operate via the TMP molecule within the hard-segment and through H-bonding between the ester chains of the PCD soft-segment.

Hard-segment cross-linking could be enhanced with moisture cure as urea is formed and thus provides two available NH protons for H-bonding (only one in the urethane linkage). When the hard-segments are well organised they may be further crosslinked

through π-π ring stacking of the MDI molecules. Finally, when the adhesive is operating above its $T_g$ss it will ensure that the matrix remains flexible and will not compromise the impact resistance of the laminate. The prepolymer adhesive will be investigated first and the cured adhesive second.

Figure 4.05 contains the DSC thermogram for the MDI-TMP-PCD prepolymer. From the thermogram, the recorded $T_g$ss occurs at -47°C (range -49°C to -45°C) which at this point is outside the specified processing window. Also present on the thermogram of MDI-TMP-PCD is an endothermic peak at 32°C which is melting of the crystalline ester soft-segment. DSC of MDI-TMP-PCD has confirmed that the $T_g$ss is out with the processing window. Also identified is that the prepolymer contains crystalline material this may affect the haze.

After 30 days of room temperature cure between two plies of TAc a portion of the adhesive was removed for DSC analysis. The function of this measurement was to obtain the $T_g$ss of the final PU-U to ensure that it had not entered the functional processing window. The experiment performed was a heat from -80°C to 140°C, then cool back to -80°C and then a second heat to 300°C. Figure 4.06 displays the thermogram obtained from the DSC analysis of both the first and second heating cycles. The broadened $T_g$ss acquired on the first heating cycle occurs at -40°C which is a shift of +7°C compared to the prepolymer adhesive. Also present within the first heating cycle is a melting endotherm of the crystalline PCD soft-segment at 46°C. After subsequent cooling, the second heating cycle displays a $T_g$ss at -38°C (range 45°C to -31°C). The material is now fully amorphous as no melting endotherm was observed. As the $T_g$ss falls out with the functional processing window it displays that based on the DSC analysis this formulation will be of possible use. Conversely it has identified that crystalline domains are present within the soft-segment of the microstructure and this crystallinity may have an adverse effect on the clarity.
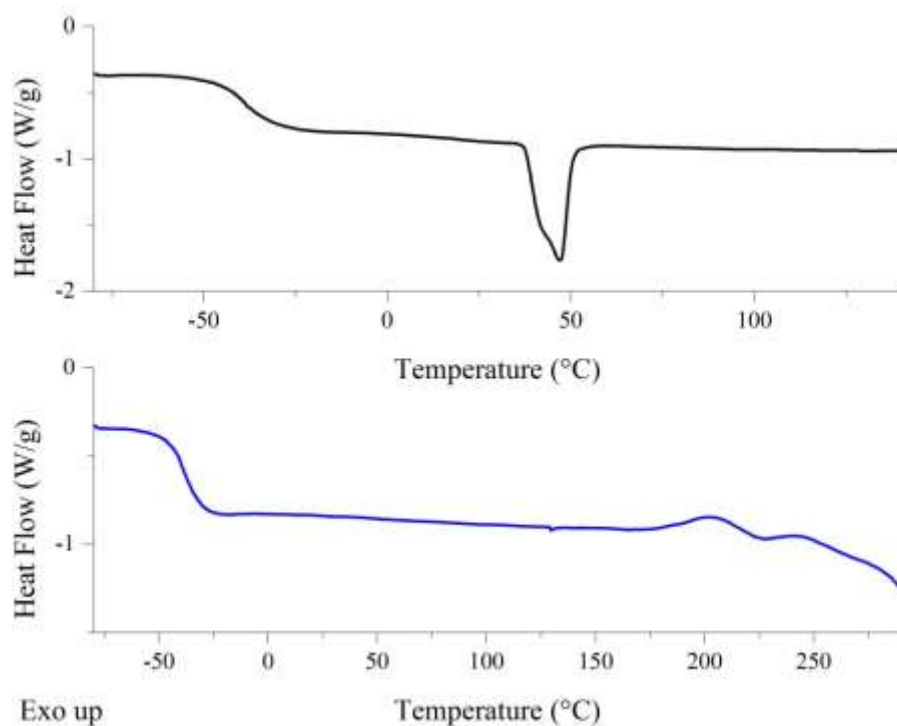
Figure 4.06: DSC thermogram of fully cured MDI-TMP-PCD adhesive, following removal from TAc/TAc laminate. [First heating cycle *top* in black and second heating cycle *bottom* in blue].

Finally to determine that the thermal stability does not fall within the processing window and the subsequent degradation behaviour TGA was used. The experiment performed was a ramped heat from $40 - 750°C$ at $10°C$ min^{-1} under nitrogen. Figure 4.07 displays the collected degradation curve and the derivative thermal gravimetric (DTG) curve of the mass loss. The calculated onset of degradation (calculated as the temperature where 5% of the total mass is lost) of MDI-TMP-PCD occurs at 316°C which is well outside the processing window. Three degradation processes are visible from inspection of the DTG curve, with the peak rates at 358°C, 405°C and 463°C respectively. Firstly degradation by depolymerisation within the hardsegments will dominate and this is present as the peak centred at 358°C.[3-5] The second and third degradation processes occurring at higher temperatures may be explained by the known occurrence of MDI based adhesives undergoing aromatic ring fusion which forms thermally more stable char materials through reaction of reactive degradation products which then require higher temperatures to degrade

(DTG peak 463°C).[6,7] This will also be accompanied with the degradation of the PCD soft-segment and other fragments produced during degradation (DTG peak 405°C).[4,8,9] Such behaviour was also observed in a similar study by Poljanšek when he was investigating the effect that the free NCO content had on the adhesive properties in one-component polyurethane adhesive.[10]
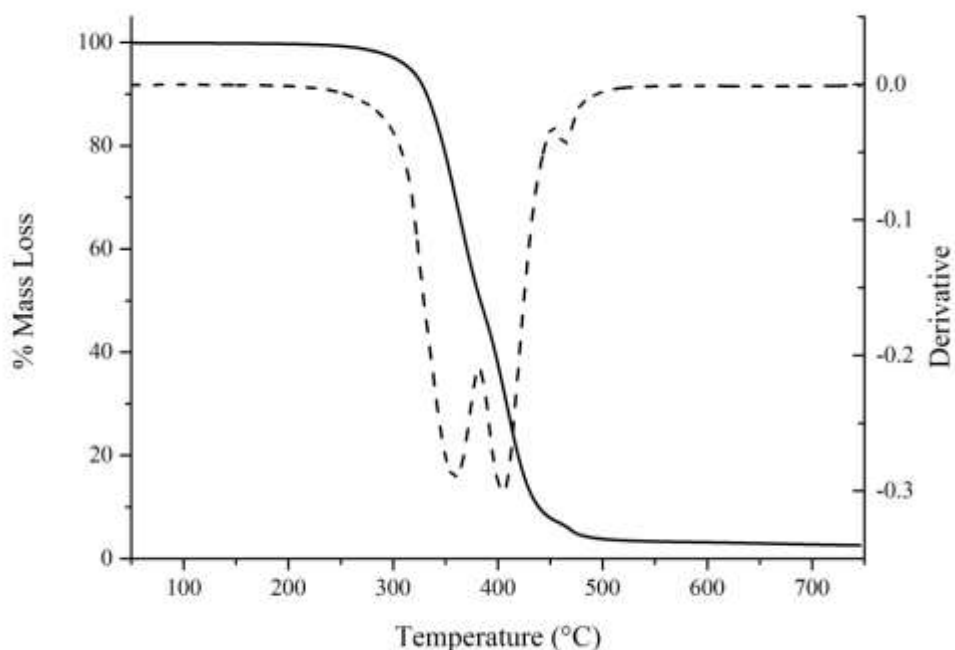
Figure 4.07: TGA and DTG curves of fully cured MDI-TMP-PCD adhesive. [TGA solid line and DTG dashed line].

Based on its thermal character, MDI-TMP-PCD will be suitable for use within the intended laminate application. Following cure, the observed $T_g$ss was -38°C which is well outside the processing window and ensures that the adhesive will remain flexible during processing. Also highlighted within the DSC analysis was that the soft–segment has a crystalline component and this may affect the haze. Finally the fully cured PU-U adhesive has an onset of degradation that occurs well out with the processing window making this formulation acceptable for use within the intended laminate application.

4.25 180° T-peel Test and Haze

Another key parameter that this PU-U adhesive must fulfil is that once cured it must form a high peak strength laminate with TAc and PC (greater than 3 N mm^{-1} is considered high for the intended application). To screen the adhesion potential of MDI-TMP-PCD six different laminates were constructed namely TAc/TAc, TAc(t)/TAc(t), TAc(t)/PC, Tac(t)/PC(t), PC(t)/PC(t) and PC/PC (laminate TAc(t)/PC(t) was untestable). Each laminate was peeled at 100 mm min^{-1} for an extension of at least 150 mm, with the first 50 mm discarded from the strength value as this is where a stable crack was formed. The haze of each cured laminate was also characterised at this point along with the failure mode.

The purpose of performing 180° T-peel tests was to determine the compatibility of MDI-TMP-PCD with the four different surface chemistries. Three different interface scenarios were present within the test set: untreated (e.g. TAc/TAc or PC/PC), treated (TAc(t)/TAc(t) or PC(t)/PC(t)), and a hybrid (TAc(t)/PC). These sets of laminates will allow for characterisation of the affinity of MDI-TMP-PCD towards TAc and PC, but will also confirm if surface treatment is required. Visual inspection was used to determine the mode of failure as this would identify which part of each laminate was the weakest.

Data collected for the five laminate combinations tested is presented within table 4.01 complete with mode of failure and haze. First tested was the TAc/TAc laminate which produced an adhesive failure at the TAc interface and also gave low peel strengths (0.2 N mm^{-1} for peel 1 and 0.6 N mm^{-1} for peel 2). The adhesive failure confirms that the surface chemistries at the TAc – adhesive interface have low compatibility. Possible modes of adhesion that may occur are interaction of the aromatic rings with the surface or possible H-bonding by the urethane linkage and Hbonding of the PCD carbonyl groups. As the values are low this would suggest that most of the aromatic rings and urethane hydrogens are involved in forming hardsegments within the polyurethane microstructure. Furthermore as the adhesive has a crystalline component which consumes carbonyl groups of PCD, H-bonding opportunities will further be limited. The low peel strength displays that adhesion between MDI-TMP-PCD with untreated TAc is very poor and that adhesion does not show a significant improvement with time.

Table 4.01: Peel, haze and mode of failure data for MDI-TMP-PCD cured PUU adhesive. [The data in bold will be discussed within this section].

Cured Adhesive	Laminate	Peel 1* (N mm^{-1})	Peel 2^x (N mm^{-1})	Failure mode	Haze (%)
MDI-TMP-PCD	**TAc/TAc**	**0.2**	**0.6**	**Adhesive TAc**	**Milky White >1.5**
	TAc(t)/TAc(t)	**3.5**	**4.3**	**Adhesive TAc**	
	TAc(t)/PC	**3.8**	**4.4**	**Adhesive TAc**	
	TAc(t)/PC(t)	**ND**	**ND**	**Adhesive TAc**	
	PC(t)/ PC(t)	**7.7**	**8.3**	**Adhesive PC**	
	PC/PC	**7.6**	**8.2**	**Adhesive PC**	
MDI-TMP-PCD-DEPD	TAc/TAc	0.3	0.9	Adhesive TAc	Clear <1.5%
	TAc(t)/TAc(t)	1.5	2.1	Adhesive TAc	
	TAc(t)/PC	1.6	2.4	Adhesive TAc	
	TAc(t)/PC(t)	1.8	3.0	Adhesive TAc	
	PC(t)/ PC(t)	3.2	4.0	Adhesive PC	
	PC/PC	4.6	4.8	Adhesive PC	
MDI-TMP-PCD-BD	TAc/TAc	0.3	0.7	Adhesive TAc	Clear <1.5%
	TAc(t)/TAc(t)	1.2	1.9	Adhesive TAc	
	TAc(t)/PC	1.1	2.3	Adhesive TAc	
	TAc(t)/PC(t)	1.2	2.7	Adhesive TAc	
	PC(t)/ PC(t)	5.5	4.6	Adhesive PC	
	PC/PC	6.3	6.6	Adhesive PC	
MDI-TMP-PCD-PD	TAc/TAc	0.3	0.9	Adhesive TAc	Clear <1.5%
	TAc(t)/TAc(t)	1.1	1.4	Adhesive TAc	
	TAc(t)/PC	1.3	2.4	Adhesive TAc	
	TAc(t)/PC(t)	1.2	2.2	Adhesive TAc	
	PC(t)/ PC(t)	4.4	4.6	Adhesive PC	
	PC/PC	5.3	5.7	Adhesive PC	

Next the saponified TAc(t) laminate (see section 2.01) which has a regenerated cellulose surface was tested to determine the bond strength and mode of failure. Deacetylation will leave hydroxyl groups at the surface which can react with the free isocyanate of the adhesive forming covalent bonds.[11] Covalent bond formation is favourable as it will add physical anchor points between the adhesive and substrate. Inspection of the collected data confirms that regeneration of cellulose at the surface does boost the interface as after 7 days the recorded tensile strength was 3.5 N mm^{-1}. The mode of failure was again consistent with an adhesive failure at the TAc interface. Following 30 days of cure, the same adhesive failure mode was recorded but at an increased peel strength of 4.3 N mm^{-1}.

Next PC was tested to determine the affinity of the interface with the MDI-TMPPCD adhesive. After 7 days of curing the recorded strength was 7.6 N mm^{-1} and this value increased marginally to 8.2 N mm^{-1} after 30 days cure. An adhesive failure at the PC interface was observed and this was accompanied by strong deformation of each PC ply. The greater adhesion observed for PC compared to TAc results from a greater surface compatibility at the substrate – adhesive interface. As there is a high density of carbonate linkages along the PC backbone, many opportunities for Hbonding with the adhesive are available. This coupled with the possible adhesion through ☐-☐ aromatic ring stacking interactions will explain the strong adhesion.[12]

Treatment of the PC interface using an ethanolamine in isopropyl alcohol solution was next performed (see section 2.02 for procedure) to determine its effect on the measured adhesion. The proposed mechanism for the surface treatment of PC is nucleophilic attack of the carbonate linkage by the amine of ethanolamine to leave a phenol and a hydroxyl terminated urethane although the precise mechanism is not known at this time.[13] In theory this should leave OH functional groups at the surface which should boost adhesion through the formation of covalent bonds with the free isocyanate groups. Peel strength data collected after 7 days displayed an adhesive failure 7.7 N mm^{-1} in strength which increased to 8.3 N mm^{-1} after 30 days.

Data collected from the hybrid TAc(t)/PC followed what was observed with the previous four laminates that surface treatment is essential for good adhesion between MDI-TMP-PCD with TAc. After 7 days an adhesive failure with peel strength of 3.8 N mm^{-1} was recorded which increased to 4.4 N mm^{-1} after 30 days. Considering the error associated with the measurement of plastic substrates these values would be considered as being very close to one another. An adhesive failure at the TAc interface identifies that this is the weakest part of the laminate. It would also appear that with time the strength of each laminate increases and this could possibly result from the reorganisation of carbonyl groups to form H-bonds with the substrate as the adhesive is above its $T_g$ss temperature.

180° T-peel testing has shown for formulation MDI-TMP-PCD that surface treatment of TAc is essential whereas PC can be either treated or untreated to reach the threshold measurement of 3 N mm^{-1}. For all five laminates tested the mode of failure was adhesive at the substrate interface with PC > TAc. This mode of failure is not ideal as it shows that there is an incompatibility with the interfaces, however, the strengths at which the adhesive fails is above 3 N mm^{-1} making it less of an issue. Increasing the number of hard blocks before application through chain-extension may help to improve peel strength and reduce the crystalline domains in the softsegment; however, chain-extended prepolymer adhesives based on MDI-TMP-PCD will be discussed in the following sections 4.30, 4.40 and 4.50.

The haze data for the collected laminates was >1.5% which is out with the 1.5% threshold value as the adhesive was opaque and milky white in colour. This was highlighted as a possible problem during the thermal analysis, which identified that the fully cured material had a crystalline component.

4.26 ATR of Peeled Samples

ATR was used to determine two parameters about the final adhesive: (a) if the adhesive after 30 days was cured and (b) if once cured was the bulk adhesive the same final material across each laminate. Investigation of the final bulk material was carried out using ATR as it is a quick and non-destructive way to test the adhesive. Analysis was carried out on the five different laminates once they had been peeled after 30 days of curing.
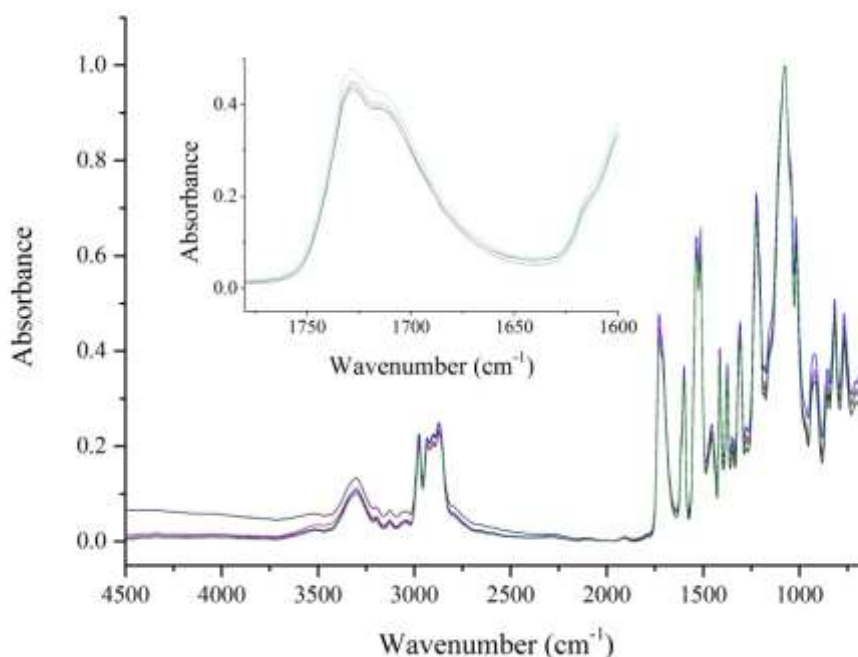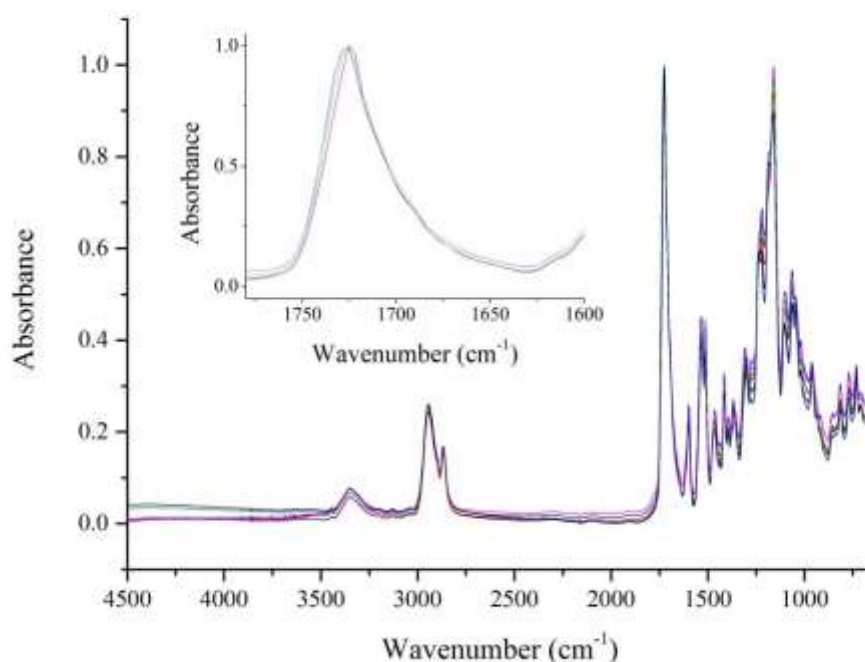
Figure 4.08: ATR spectra of cured MDI-TMP-PCD sampled in-situ after tensile testing with inset expanded carbonyl region. [TAc/TAc in black, TAc(t)/TAc(t) in red, TAc(t)/PC in light blue, TAc(t)/PC(t) in pink, PC(t)/PC(t) in green and PC/PC in orange. Data collected for each laminate at nine random positions with each spectrum consisting of 128 scans at 8 cm^{-1} resolution. These were then averaged and plotted as the above spectra].

Characterisation of the in-situ cured MDI-TMP-PCD by ATR after 30 days for each laminated material is shown in figure 4.08. **N-H** stretching vibrations are positioned at 3551 cm^{-1} with the position of the vibration indicating that the N-H groups are absent of H-bonding.[2] Following are the aliphatic **C-H** stretching vibrations from PCD with both the asymmetric and symmetric bands present at 2943 cm^{-1} and 2867 cm^{-1} respectively. As there is no clear peak between 2260 – 2280 cm^{-1}, the isocyanate has fallen below the detection limit and it can be assumed that the adhesive is fully cured.

A large signal for the **C=O** stretch of the ester carbonyl is present at 1724 cm^{-1}. The size of this carbonyl signal has masked the urea peak (expected around 1700 – 1640

cm^{-1}) which would be expected as urea moieties are introduced during moisture cure (see shoulder in expanded carbonyl peak in figure 4.08).[14] Evidence of urethane linkages are shown by the **N-H** bending vibration at 1601 cm^{-1}.[14] Further evidence of cure (either urea or urethane functionality) appears at 1534 cm^{-1} which corresponds to **C-N** stretching and **N-H** bending vibrations. It would also be expected to see a weak aromatic **C-H** signal; however, it is convoluted in with these previous vibrations. Next the first clear sign of urea formation during moisture cure is observed by the **N-H** bending signal at 1511 cm^{-1}.[14]

Table 4.02: Characteristic peaks of MDI-TMP-PCD cured PU-U adhesive from all five laminate combinations.

Wavenumber (cm^{-1})	Vibration	Wavenumber (cm^{-1})	Vibration
3551	N-H stretching	1307	C-N urethane
2943	C-H asymmetric stretch	1221	C-H aliphatic skeleton
2867	C-H symmetric stretch	1164	C-C stretching
1724	C=O stretching ester	1098	C-O-C aliphatic ether
1601	N-H bending urethane	1060	C-H aromatic ring
1534	C-N stretch, N-H bending, C-H aromatic ring	965	C-H aromatic ring
1515	N-H bending urea	871	C-H aromatic ring
1463	C-H bend aliphatic	808	C-H aromatic ring
1411	C-C stretching aromatic	771	C-C aliphatic skeleton
1373	C-N urea		

Aliphatic **C-H** stretching from the PCD and aromatic **C-C** stretching vibrations of MDI are also present at 1463 cm^{-1} and 1411 cm^{-1} respectively. Confirmation that the cured adhesive is a PU-U can be seen by the urethane and urea **C-N** bands at 1373 cm^{-1} and 1307 cm^{-1}. PCD vibrations for the **C-H** skeleton vibration, **C-C** stretching and the **C-O-C** ester groups are next observed at 1221 cm^{-1}, 1164 cm^{-1} and 1098 cm^{-1} respectively. The position of the **C-H** aromatic ring vibrations are at 1060 cm^{-1}, 985 cm^{-1}, 871 cm^{-1} and 808 cm^{-1} are characteristic of the 1,4 + 1,2 di-substitution mixture of the monomeric MDI. The final peak at 771 cm^{-1} shows the **C-C** skeleton vibrations of the aliphatic backbone and there will also be a contribution of an aromatic **C-H** convoluted in with the signal.

ATR analysis displayed that the final cured MDI-TMP-PCD adhesive is a PU-U, with both urethane and urea groups present. It has also shown that the bulk material across the five laminate combinations is very similar which means that any differences in peel strength can be attributed to differences in adhesion at the interface. Finally the adhesive was fully cured as there was no sign of any unreacted isocyanate in the final spectrum for any of the laminates.

4.27 Summary of MDI-TMP-PCD Formulation

Synthesis of the MDI-TMP-PCD prepolymer was successfully confirmation by ^{1}H and ^{13}C NMR. MALDI-MS displayed that the expected molecular weight distribution of the end-capped prepolymer MDI-PCD-MDI was obtained (2.2:1.0 NCO:OH ratio) as shown by the peak centred at 2325 m/z. DSC was able to highlight that the prepolymer $T_g$ss did not fall within the processing window which makes the adhesive suitable for use, however, it highlighted that there is a crystalline component to the adhesives microstructure. This has an adverse effect on the clarity (>1.5%) as it makes the bulk adhesive milky white in colour. TGA analysis displayed that the adhesive when fully cured was stable well outside the processing window, with the onset of degradation not until 316°C and peak rate not occurring until 358°C. 180° T-peel testing identified two things about the MDI-TMP-PCD adhesive; (a) TAc laminates gave very poor strength values unless the saponification surface treatment was used and (b) PC gave high strength with or without surface treatment. Also observed for this adhesive was that the peel strength increased with time. This would suggest that a more

functionalised soft-segment can lead to greater strength. Finally ATR was able to confirm that the final cured material was indeed a PU-U.

4.30 Analysis of MDI-TMP-PCD-DEPD

4.31 Synthesis Information

MDI-TMP-PCD-DEPD was next synthesised with three intentions: firstly disruption of the packing within the hard-segment through using a sterically hindered chainextender, secondly to disrupt the crystallisation of the soft-segment and thirdly encourage phase mixing. This was achieved by firstly synthesising the MDI-TMPPCD base prepolymer using the same reaction conditions as detailed with section 4.21 and then performing an additional reaction set. The additional step was performed by adding a hydroxyl terminated chain-extender using a 2.2:1.0 isocyanate:hydroxyl ratio based on the calculated amount of free NCO remaining after step one. The chain-extension step was also used to lower the free isocyanate content of the adhesive, which would reduce the opportunity for excessive bubbling by CO_2 liberation during urea formation.

Step one was performed as previously detailed in section 4. After addition of 2,2diethyl-1,3-propane diol (DEPD) to the reaction vessel, the mixture was stirred at 85°C – 95°C for 5 hours before the dual DBTDL and TEA catalyst system was added. Following chain-extension a visual increase in viscosity was observed and was associated with the molecular weight increase caused by the coupling chainextension step. To compensate for the molecular weight increase, the reaction mixture was slowly heated to 130°C to sufficiently lower the viscosity as this would facilitate flow and allow for the formulation to be poured. Once at temperature the formulation was poured into an aluminium tube, which was then capped and degassed as previously outlined in section 2.03. The desiccator containing the adhesive filled tube was then placed within a 0°C fridge for storage. Degassing was performed for six hours once a vacuum of one atmosphere was obtained. Samples of the prepolymer reaction were again taken before catalysed addition, these were analysed by DSC, NMR and MALDI-MS analysis.

MDI-TMP-PCD-DEPD was heated to 180°C before being applied to six laminates which were cured at room temperature. These samples were 180° T-peel tested at 7 days and 30 days to determine the peel strength. A further lamination was performed using two plies of TAc which would allow for the adhesive to be removed for analysis by DSC and TGA once fully cured. The 30 day tensile test samples were also analysed by ATR to characterise the bulk cured material. Analysis of the chainextended materials only will be presented within the remaining sections of this chapter. MDI-TMP-PCD is considered as representative of the reactive intermediate obtained after step one of each chain-extended reaction.

4.32 NMR Analysis

For full spectral characterisation of peaks from MDI and PCD see section 4.22 as this section will only detail peaks that are important to show prepolymer formation or peaks from the chain-extender.
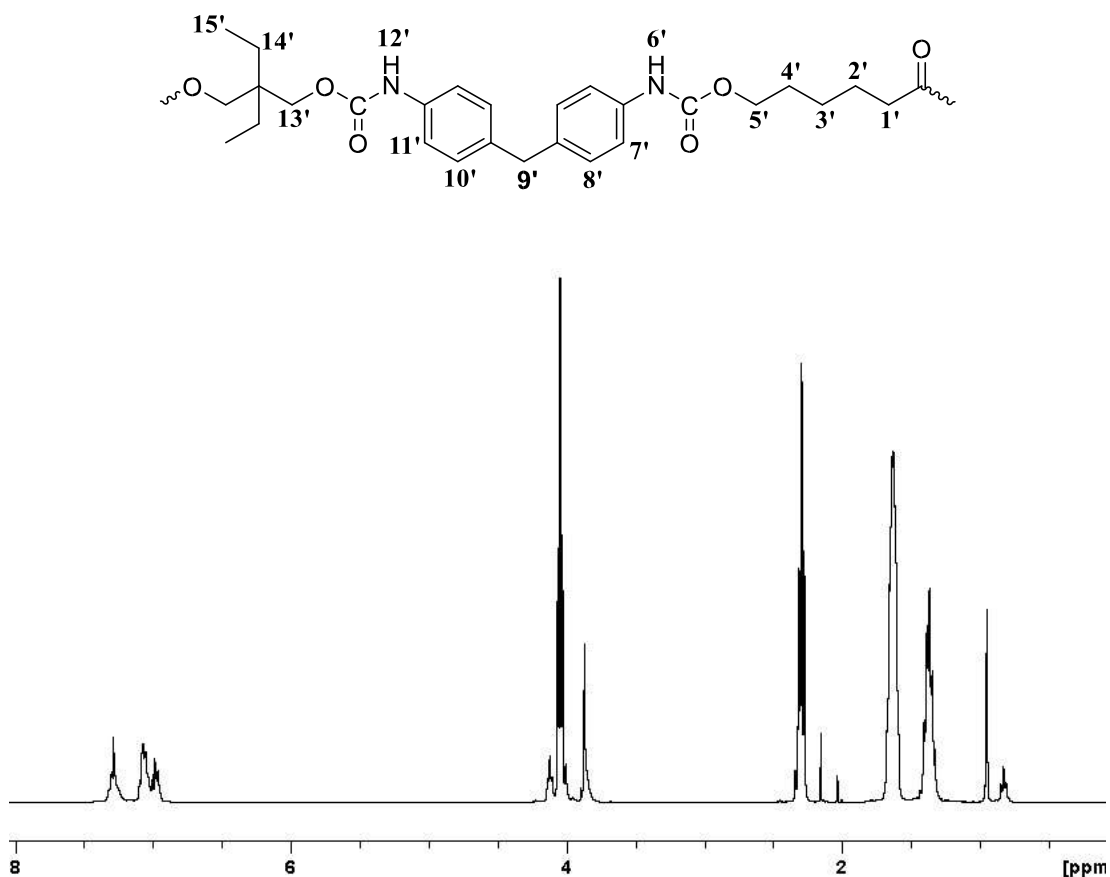
Figure 4.09: ^{1}H NMR spectrum obtained following reaction of MDI-TMP-PCD with DEPD.

DEPD chain-extender contains two steric ethyl groups at the 2 position, evidence of these groups can only be observed by the addition of the CH$_3$ signal **15'** at 0.81 ppm. Evidence that the primary hydroxyl groups from DEPD have reacted is confirmed by the position of CH$_2$-O- group **13'** at 3.89 ppm. Also contained within the spectrum is evidence from the first step of the synthesis. The primary hydroxyl groups of PCD which have been coupled to form urethane linkages can be observed by the position of the CH$_2$ group's **5'** at 4.13 ppm.
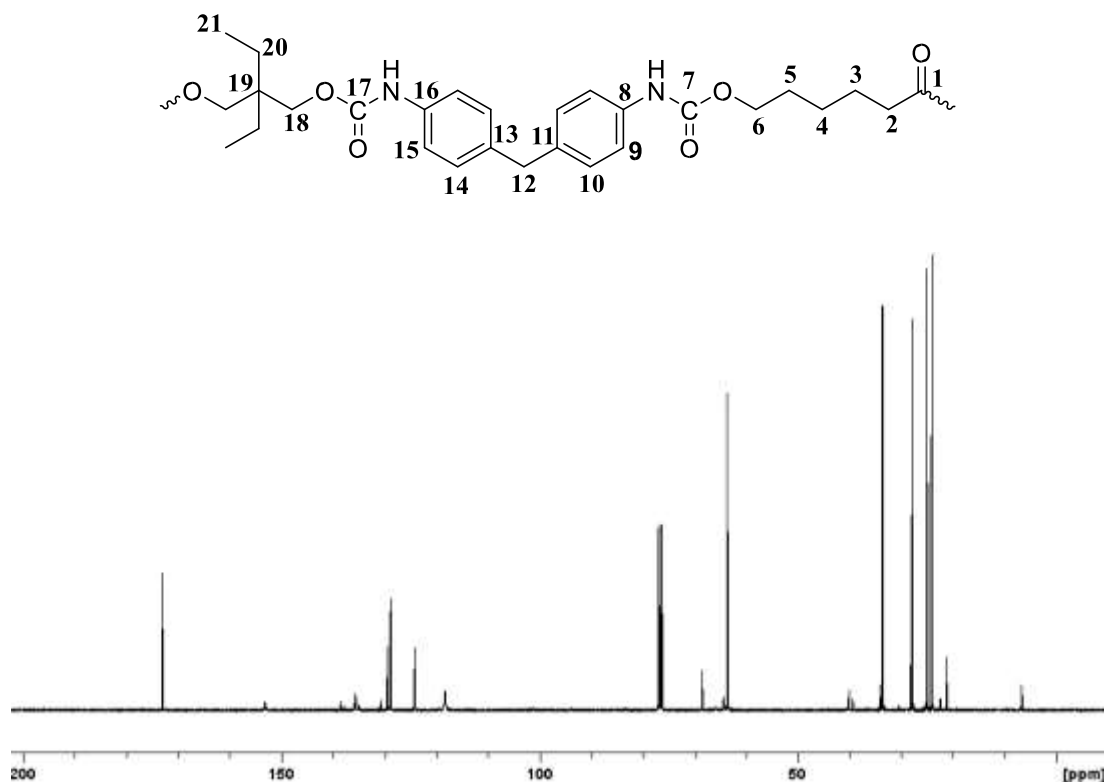
Figure 4.10: ^{13}C NMR spectrum obtained following reaction of MDI-TMP-PCD with DEPD.

Broader aromatic signals are encountered at 7.1 (**8'** and **10'**) and 7.2 ppm (**7'** and **11'**) when compared to MDI or the previous step one prepolymer MDI-TMP-PCD. This would suggest that reaction of the isocyanate groups with hydroxyl groups of PCD and DEPD. Retention of peaks that correspond to unreacted rings are still present at 7.0 ppm, this shows that the material is still a prepolymer with reactive chain ends however, ^{13}C NMR will give a better indication of free N=C=O groups. Finally the NH protons visible at 7.3 ppm **6'** and **12'** are direct evidence of the formation of urethane bonds.

Evidence of the ethyl groups of DEPD are shown in ^{13}C by the methyl carbon **21** signal at 7.2 ppm and the methylene carbons signal **20** at 23.0 ppm. The tertiary carbon **19** of the chain-extender is present within the carbon spectrum at 39 ppm. Evidence of the carbonyl of both urethane (**7** + **17**) and free N=C=O are visible within the ^{13}C spectrum at 155 ppm and 131 ppm respectively (all other peaks within the aromatic region are described within section 4.22).

4.33 MALDI-MS Analysis

To determine if chain-extension has given rise to higher molecular weight prepolymers MALDI-MS was used. The matrix used for the MALDI-MS analysis was HABA which contained a cationising agent NaTFA (see section 4.23 for more matrix information). A 40 mg ml^{-1} solution of MDI-TMP-PCD-DEPD was prepared in THF and mixed with the matrix (1:8 sample:matrix). 1 µl portions of this sample were then spotted and dried for analysis.
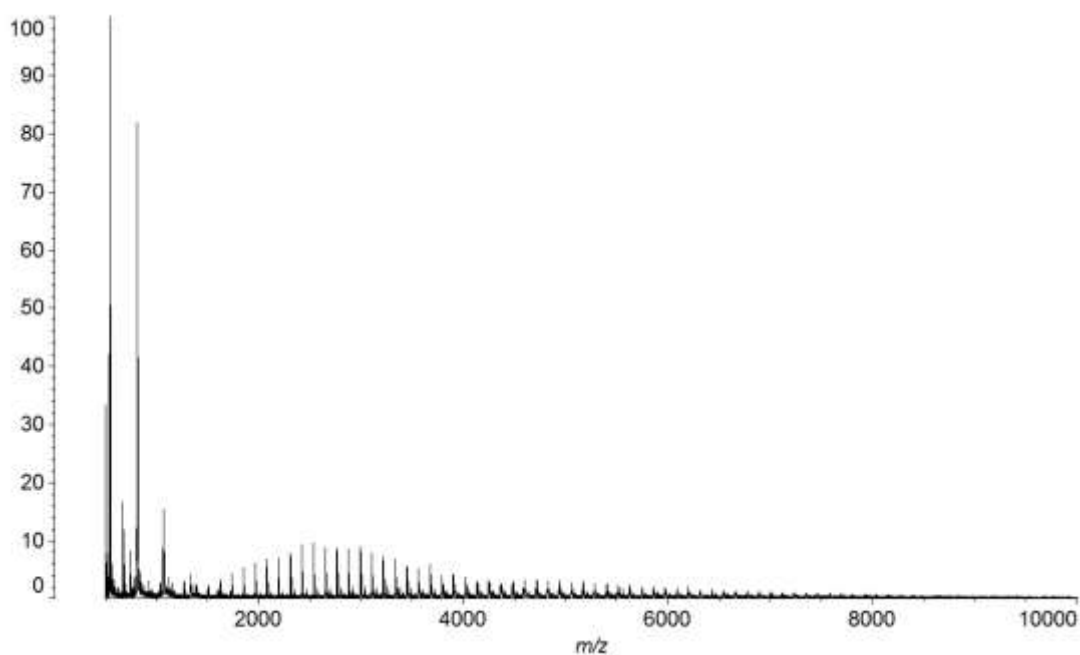
Figure 4.11: MALDI-MS spectrum of MDI-TMP-PCD-DEPD chain-extended prepolymer collected in HABA/NaTFA.

MALDI-MS analysis of the prepolymer adhesive displayed that there was two molecular weight distributions present. The first distribution was for the first synthesised MDI-PCD-MDI prepolymer which was the intermediate produced in-situ

213

prior to chain-extension. The appearance of this distribution suggests that the reaction time from the second step of synthesis requires a review. Evidence of this prepolymer would be expected due to the high viscosity of the bulk polymerisation process reducing the effectiveness of the mixing. Also to limit the possibility of isocyanate based side reactions the temperature of synthesis could not exceed 95°C. At temperatures of 120°C – 140°C where the viscosity of the prepolymer mixture is lower, cross-linking by reaction of the active NH of the urethane with free N=C=O is encouraged forming allophanate groups.[15]

Following diol chain-extension with DEPD a small change in Mn is observed but significant changes to Mw and PDI are observed. The calculated value of Mn is 3305 m/z which is a slight increase compared to the previous formulation (MDITMP-PCD). A noticeable increase in Mw is observed with the calculated value 4435 m/z obtained. This results in a greater PDI value of 1.34 and displays that chainextension with DEPD has broadened the polymer mass distribution.

Present at 1045 m/z is the chain-extender TMP that has reacted with three MDI units which are ethanol end-capped (plus one sodium cation). These molecules will contribute to the hard-segment microstructure within the adhesive and their observation was possible as all the starting material was consumed. Also detected in the MALDI-MS analysis was evidence of the chain-extended prepolymer MDI-PCDMDI-DEPD-MDI-PCD-MDI and also some of the residual higher molecular weight distribution observed previously (MDI-PCD-MDI-PCD-MDI). This collected analysis would suggest that HABA/NaTFA is a good matrix for polyester based polyurethanes but the recipe still required further optimisation which is out with the aims of this thesis.

4.34 DSC and TGA Analysis

Following synthesis of the prepolymer material, the thermal characteristics of the adhesive formulation were investigated to determine the $T_g$ss and if any remaining crystalline component from the soft-segment was present. As previously mentioned, the $T_g$ss of the material was considered important as it had to be lower than -20°C to be suitable for the processing window of the laminated material.

Analysis of the DSC thermogram of MDI-TMP-PCD-DEPD gives a $T_g$ss of -38°C (range of -42°C to -34°C) which is outside the processing window. The broadened $T_g$ss increased by +9°C compared to the prepolymer, however, it still remains suitable for use. Within the range of the experiment no other thermal transitions were observed within the thermogram.
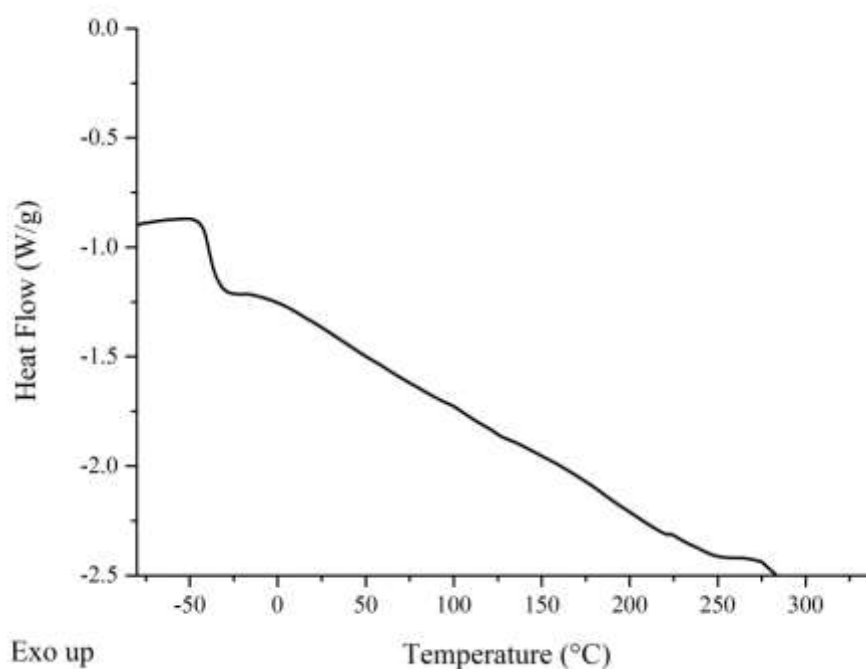
Figure 4.12:   DSC thermogram of MDI-TMP-PCD-DEPD prepolymer formulation.

Following 30 day of curing a portion of the cured material was removed from the TAc/TAc laminate for DSC analysis. The sample was analysed using a heat-coolreheat experiment to determine the final $T_g$ss of the chain-extended adhesive within each heating cycle as shown in figure 4.12. After the first heating cycle a $T_g$ss of 33°C was recorded, which spanned a range of -39°C to -27°C. Following a second heating cycle a $T_g$ss of -32°C was recorded which occurred over a similar range of 37°C to -25°C. The slight increase in $T_g$ss between first and second heating cycles could be due to the experimental temperature range acting as an annealing process.[16]

Also the observation of only one glass transition would suggest that there is a high degree of phase mixing between the hard and soft-segments induced by the

215

chainextender.[10,17] The $T_g$ss obtained even after the second heating was out with the set processing window that the adhesive is likely to meet. As PCD has double the molecular weight of PPG, the number of possible hard-segments within the PU microstructure will be effectively halved. This reduction in hard-segment makes the $T_g$ss closer to the unreacted PCD (recorded at -64°C).
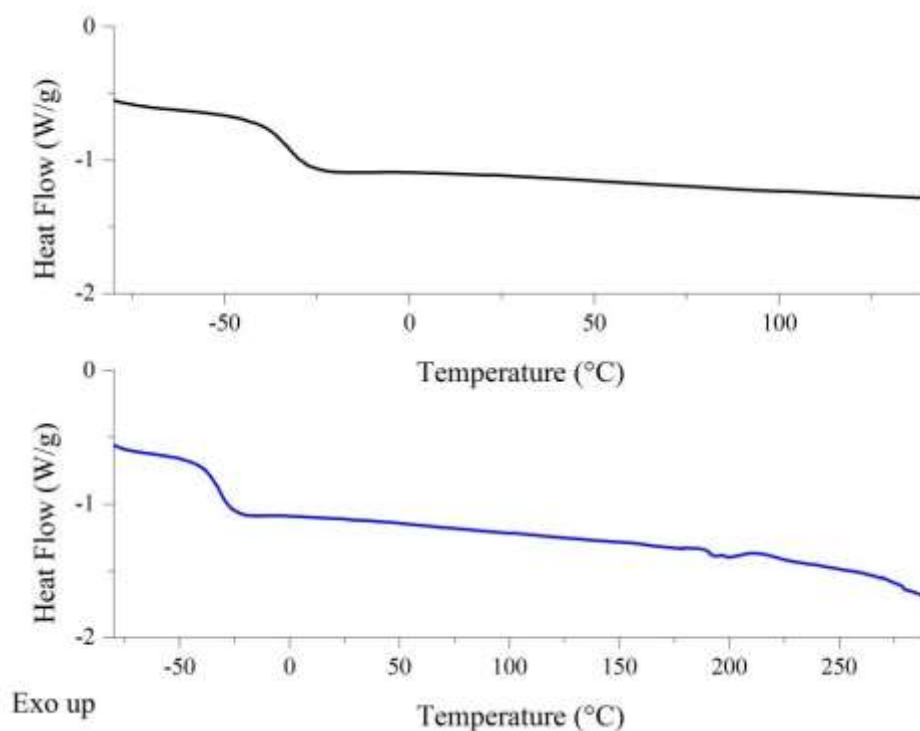
Figure 4.13: DSC thermogram of fully cured MDI-TMP-PCD-DEPD adhesive, following removal from TAc/TAc laminate. [First heating cycle *top* in black and second heating cycle *bottom* in blue].

TGA was then performed to determine what the onset of degradation was for the PUU cured adhesive. The experiment was carried out over the same range as outline in section 2.10 and the data is presented in figure 4.14. From the TGA curve, the onset of degradation was 298°C which is 19°C lower than previous formulation where chain-extension was not performed. This would suggest that chain-extension does have an effect on the onset temperature just not a significant one. Inspection of the DTG curve however, does show some differences in the degradation behaviour of this PU-U. Degradation occurs in three steps which is similar to the previous cured material which also displays three processes.

The distribution of the peaks however, is different from MDI-TMP-PCD with the first degradation process dominating. This main degradation process is clearer in the DTG curve (peak rate at 353°C) and corresponds to the breaking of the hard-segment bonds.[3,4] Subsequent degradation process which occur at 396°C and 458°C account for the breaking of the PCD soft-segment molecules and more stable cross-linked structures formed during degradation respectively.[2,7]
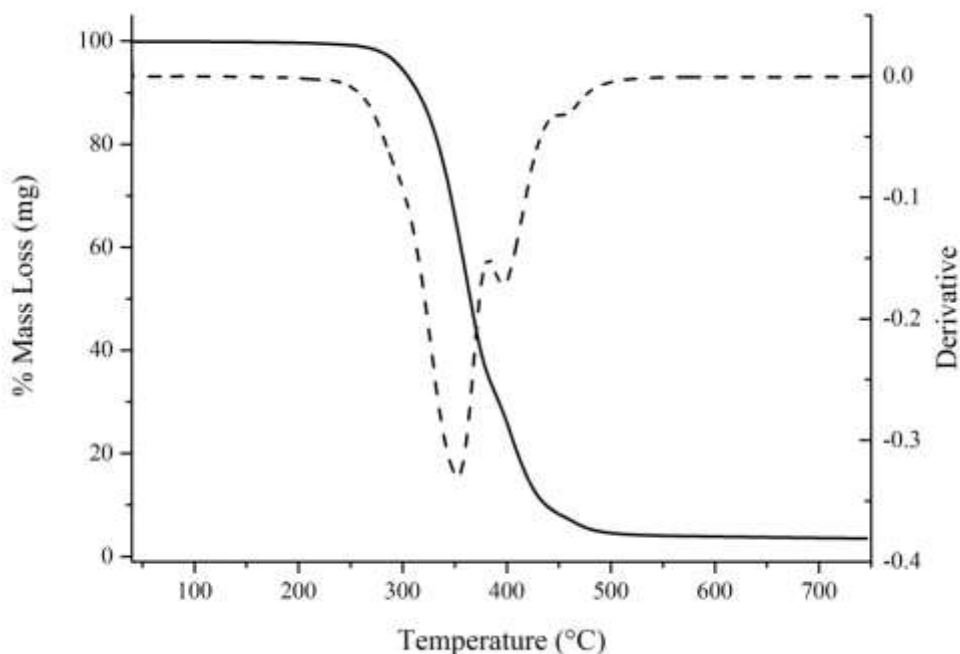
Figure 4.14: TGA and DTG curves of fully cured MDI-TMP-PCD-DEPD adhesive. [TGA solid line and DTG dashed line].

Thermal analysis of this PU-U formulation have identified that the material has a T_gss which will not interfere with the temperatures of the set processing window. The overall thermal stability of the adhesive when fully cured is well outside the temperature that the laminate will meet during processing.

4.35 180° T-peel Test and Haze

To quantify the interactions with the ply materials TAc and PC, peel testing was performed. 180° T-peel testing was performed on six laminates, which were measured after both 7 and 30 days of cure. The laminates used for this study were

TAc/TAc, TAc(t)/TAc(t), TAc(t)/PC, TAc(t)/PC(t), PC(t)/PC(t) and PC/PC. These six combinations would evaluate the compatibility of the adhesive with the untreated materials, with the treated materials and what interface had the greatest compatibility.

Testing of the first laminate TAc/TAc displayed poor compatibility between MDITMP-PCD-DEPD and the interface. Low peel strengths of 0.3 N mm^{-1} and 0.9 N mm^{-1} were recorded for the 7 and 30 day tests respectively. An adhesive failure at the TAc interface was the only mode of failure encountered in both tests. Such poor performance with this untreated material is an indication of the lack of active groups at the surface for covalent bonding, however, it would be expected that the ester softsegment would boost the peel strengths obtained through H-bonding. Following treatment of the TAc interface by saponification, the peel strength of the interface was improved. At 7 days the recorded tensile strength was 1.5 N mm^{-1} which is an improvement on the untreated surface and this increased to 2.1 N mm^{-1} after 30 days. The 30 day measurement has increased compared to the 7 day measurement, indicating that the strength does increase with time. Unfortunately in this case the final peel strength did not reach the 3 N mm^{-1} target (unlike MDI-TMP-PCD).

Untreated PC/PC was next tested and the performance was much improved compared to untreated TAc. Following 7 days of cure the peel strength was 4.56 N mm^{-1} and this further increased to 4.85 N mm^{-1} after 30 days. The high strength obtained can be explained by the high compatibility of the adhesive with the PC by two main processes: firstly both contain aromatic rings which will encourage π-π stacking at the interface and secondly the large number of carbonate groups present in both materials will facilitate H-bonding. Adhesive failures were still observed but these were accompanied by strong deformation of both PC plies.

When the surface treatment was performed it results in a net decrease in the peel strength obtained. After 7 days the strength was 3.2 N mm^{-1} which increased to 4.0 N mm^{-1} after 30 days. This reduction in the strength could be the result of chain scission performed during surface treatment affecting the surface adsorption chemistry (e.g. through surface roughening). The reduction in peel strength was not considered a major issue as all PC laminates have peel strengths > 3 N mm^{-1}.

Finally to fully understand the possible adsorption chemistry occurring hybrid laminates were tested to determine which interface had the greatest compatibility. After 7 days a peel strength of 1.57 N mm^{-1} was observed for the TAc(t)/PC laminate and this increased to 2.4 N mm^{-1} after 30 days. For the fully treated hybrid laminate (TAc(t)/PC(t)), the numbers were similar with 1.85 N mm^{-1} recorded after 7 days and this increased to 3.0 N mm^{-1} after 30 days. Both laminates failed adhesively at the TAc(t) face but with deformation to the PC substrate. The adhesive failure at the TAc(t) interface also further supports that even after treatment the interface compatibility is still poorer than with PC.

Following peel measurements it was observed that TAc could only be used following surface treatment. Chain-extension with DEPD has an overall reducing effect on the peel strength obtained, with untreated PC performing the best. Finally the improved peel strength observed after 30 days for all laminates could suggest that the adhesive is reorganising itself to maximise attractive forces. As the adhesive is curing at room temperature it is above the recorded $T_g$ss making mobility of the polymer groups possible and it has been suggested elsewhere in the literature to occur.[18]

Finally and most significantly the haze measurement recorded for this PU-U adhesive was < 1.5%. When compared to MDI-TMP-PCD this is a marked improvement with the previous material being milky white in colour. The marked improvement in clarity through reduced haze is a result of disruption to the softsegment crystallisation, the cause of this disruption will be discussed in more detail within chapter 8. Such a significant reduction in the haze confirms that using sterically hindered chain-extenders does lead to clearer PU-U adhesives. However, the reduction in crystallinity of the soft-segment does not provide more ester functional groups for surface adhesion as shown by the peel strength. The reduction in crystallinity appears to be coupled with a reduction in peel strength compared to MDI-TMP-PCD (see section 4.25).

Table 4.03: Peel, haze and mode of failure data for MDI-TMP-PCD-DEPD cured PU-U adhesive. [The data in bold will be discussed within this section].

Cured Adhesive	Laminate	Peel 1* (N mm^{-1})	Peel 2^x (N mm^{-1})	Failure mode	Haze (%)
MDI-TMP-PCD	TAc/TAc	0.2	0.6	Adhesive TAc	Milky White >1.5
	TAc(t)/TAc(t)	3.5	4.3	Adhesive TAc	
	TAc(t)/PC	3.8	4.4	Adhesive TAc	
	TAc(t)/PC(t)	ND	ND	Adhesive TAc	
	PC(t)/ PC(t)	7.7	8.3	Adhesive PC	
	PC/PC	7.6	8.2	Adhesive PC	
MDI-TMP-PCD-DEPD	**TAc/TAc**	**0.3**	**0.9**	**Adhesive TAc**	**Clear <1.5%**
	TAc(t)/TAc(t)	**1.5**	**2.1**	**Adhesive TAc**	
	TAc(t)/PC	**1.6**	**2.4**	**Adhesive TAc**	
	TAc(t)/PC(t)	**1.8**	**3.0**	**Adhesive TAc**	
	PC(t)/ PC(t)	**3.2**	**4.0**	**Adhesive PC**	
	PC/PC	**4.6**	**4.8**	**Adhesive PC**	
MDI-TMP-PCD-BD	**TAc/TAc**	0.3	0.7	Adhesive TAc	Clear <1.5%
	TAc(t)/TAc(t)	1.2	1.9	Adhesive TAc	
	TAc(t)/PC	1.1	2.3	Adhesive TAc	
	TAc(t)/PC(t)	1.2	2.7	Adhesive TAc	
	PC(t)/ PC(t)	5.5	4.6	Adhesive PC	
	PC/PC	6.3	6.6	Adhesive PC	
MDI-TMP-PCD-PD	**TAc/TAc**	0.3	0.9	Adhesive TAc	Clear <1.5%
	TAc(t)/TAc(t)	1.1	1.4	Adhesive TAc	
	TAc(t)/PC	1.3	2.4	Adhesive TAc	
	TAc(t)/PC(t)	1.2	2.2	Adhesive TAc	
	PC(t)/ PC(t)	4.4	4.6	Adhesive PC	
	PC/PC	5.3	5.7	Adhesive PC	

peel 1 collected within 7 days of room temperature cure, ^{x} peel 2 collected after 30 days of room temperature cure, ND = No Data

4.36 ATR of Peeled Samples

Characterisation of the bulk cured adhesive was performed using ATR analysis. Analysis of the bulk adhesive was performed on all six of the laminates after the 30 day tensile test. ATR analysis will determine the chemical functionality of the final cured material and allow for any distinct differences in curing chemistry to be observed. Discussed within this section will be peaks that indicate either the PU of the prepolymer or PU-U peaks obtained after 30 days of cure. For discussion of the peaks inherent of the starting materials see section 4.15 or table 4.04.
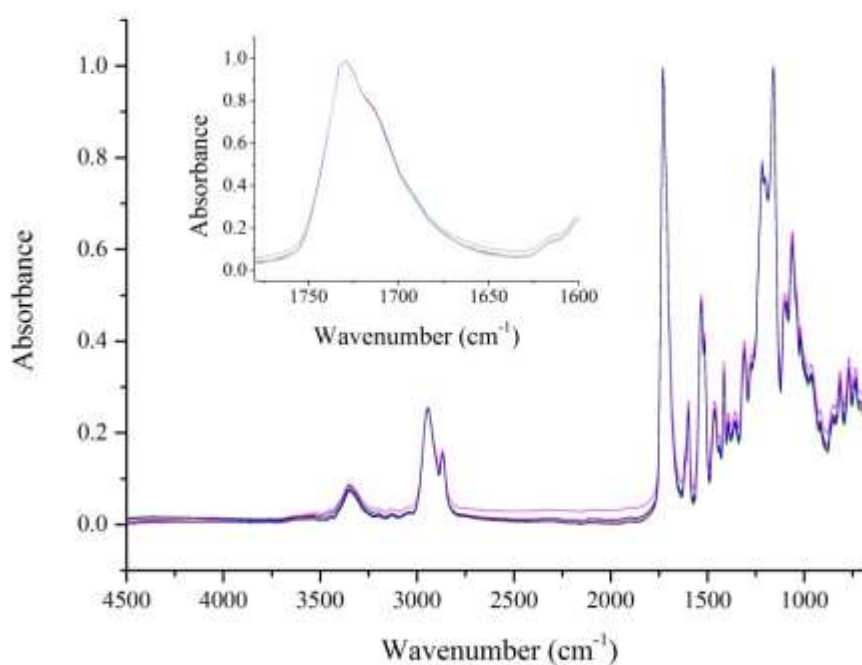
Figure 4.15: ATR spectra of cured MDI-TMP-PCD-DEPD sampled in-situ after tensile testing with inset expanded carbonyl region. [TAc/TAc in black, TAc(t)/TAc(t) in red, TAc(t)/PC in blue, TAc(t)/PC(t) in pink, PC(t)/PC(t) in green and PC/PC in orange. Data collected for each laminate at nine random positions with each spectrum consisting of 128 scans at 8 cm^{-1} resolution. These were then averaged and plotted as the above spectra].

As there is an **N-H** stretching band at 3346 cm^{-1} this displays that the cured adhesive contains urethane and urea groups. The positon of the **N-H** band is characteristic for

H-bonded network, which is consistent with previous analysis and the literature.[2] Carbonyl groups of the ester soft-segment are visible at 1727 cm^{-1} but with a more noticeable shoulder from the formation of urea (see figure 4.15).[14] Confirmation of urethane formed during prepolymer synthesis is shown by the **N-H** bending at 1597 cm^{-1}. Urea formed during moisture cure of the adhesive is shown by the **N-H** bending band at 1508 cm^{-1}. The **C-N** stretching band for both these groups can also be observed at 1535 cm^{-1}. Further **C-N** bands are again visible further into the finger print region with both urethane at 1312 cm^{-1} and urea at 1365 cm^{-1} present.

Table 4.04: Characteristic peaks of MDI-TMP-PCD-DEPD cured PU-U adhesive from all six laminate combinations.

Wavenumber (cm^{-1})	Vibration	Wavenumber (cm^{-1})	Vibration
3346	N-H stretching	1312	C-N urethane
2940	C-H asymmetric stretch	1218	C-H aliphatic skeleton
2864	C-H symmetric stretch	1163	C-C stretching
1727	C=O stretching ester	1102	C-O-C aliphatic ether
1597	N-H bending urethane	1063	C-H aromatic ring
1535	C-N stretch, N-H bending, C-H aromatic ring	964	C-H aromatic ring
1508	N-H bending urea	852	C-H aromatic ring
1459	C-H bend aliphatic	822	C-H aromatic ring
1410	C-C stretching aromatic	772	C-C aliphatic skeleton
1365	C-N urea		

ATR analysis has allowed for the characterisation of the fully cured PU-U adhesive. The presence of both urethane and urea bands display that the prepolymer urethane has cured through moisture uptake consuming the free isocyanate groups. As there was no band for free isocyanate the adhesive was fully cured after 30 days. A noticeable shoulder on the carbonyl peak between 1700 cm^{-1} – 1640 cm^{-1} corresponds to the carbonyl within a urea linkage which are not as clear within the MDI-TMP-PCD based systems. Finally the ply combination appears to have little effect on the final cure of the bulk adhesive.

4.37 Summary of MDI-TMP-PCD-DEPD Formulation

From the analysis collected from MDI-TMP-PCD-DEPD based PU-U it was observed that chain-extension has a significant effect on the properties of the final adhesive. The $T_g$ss of the cured adhesive was measured at -32°C which is out with the processing window of the laminate. TGA displayed that the thermal stability was also greater than the processing window with the onset of degradation occurring at 298°C. MALDI-MS highlighted that getting such elastomeric polymers of chainextended molecular weight to successfully ionise is difficult however, chainextended prepolymers were observed. 180° T-peel testing highlighted that PU-U adhesives based on MDI and PCD have an affinity for the PC interface but are incompatible with TAc interface unless treated. It also highlighted that chainextension has a reducing effect on the peel strength recorded. Finally the most promising result from this formulation is that chain-extension has a positive impact on the haze of the final cured adhesive by disrupting the crystallisation of the PCD soft-segment.

4.40 Analysis of MDI-TMP-PCD-BD

4.41 Synthesis Information

MDI-TMP-PCD-BD was next synthesised with the intention of disrupting the hardsegment packing through use of a sterically hindered chain-extender, disrupt the crystallisation of the soft-segment and encourage phase mixing. This was achieved by firstly synthesising the MDI-TMP-PCD base prepolymer using the same reaction conditions as detailed with section 4.21 and then performing an additional reaction set. The additional step was performed by adding a hydroxyl terminated chainextender using a 2.2:1.0 isocyanate:hydroxyl ratio based on the calculated amount of free NCO

remaining after step one. The chain-extension step was also used to lower the free isocyanate content of the adhesive, which would reduce the opportunity for excessive bubbling by CO_2 liberation during urea formation.

Step one was performed as previously detailed in section 4.21 and was a clear liquid which has an observed increase in viscosity from the starting mixture. After addition of 1,3-butane diol (BD) to the reaction it was stirred at 85°C – 95°C for 5 hours before the dual DBTDL and TEA catalyst system was added. Following chainextension a visual increase in viscosity was observed and was associated with the molecular weight increase caused by the coupling step. To compensate for the molecular weight increase, the reaction mixture was slowly heated to 130°C to sufficiently lower the viscosity as this would facilitate flow and allow for the formulation to be poured. Once at temperature, the formulation was poured into an aluminium tube, which was then capped and degassed as previously outlined in section 2.03. The desiccator containing the adhesive filled tube was then placed within a 0°C fridge for storage. Degassing was performed for six hours once a vacuum of one atmosphere was obtained. Samples of the reaction were again taken before catalysed addition, these were analysed by DSC, NMR and MALDI-MS analysis.

MDI-TMP-PCD-BD was heated to 180°C before being applied to six laminates (same as section 4.21) which were then allowed to cure at room temperature. These samples were 180° T-peel tested at 7 days and 30 days to determine the peel strength. A further lamination was performed using two plies of TAc which would allow for the adhesive to be removed for analysis by DSC and TGA once fully cured. The 30 day tensile test samples were also analysed by ATR to characterise the bulk cure material.

Analysis of the chain-extended materials only will be presented within the remaining sections of this chapter. MDI-TMP-PCD is considered as representative of the reactive intermediate obtained after step one of each chain-extended reaction.

4.42 NMR Analysis

For full spectral characterisation of peaks from MDI and PCD see section 4.22 as this section will only detail peaks that are important to show prepolymer formation or peaks from the BD chain-extender.
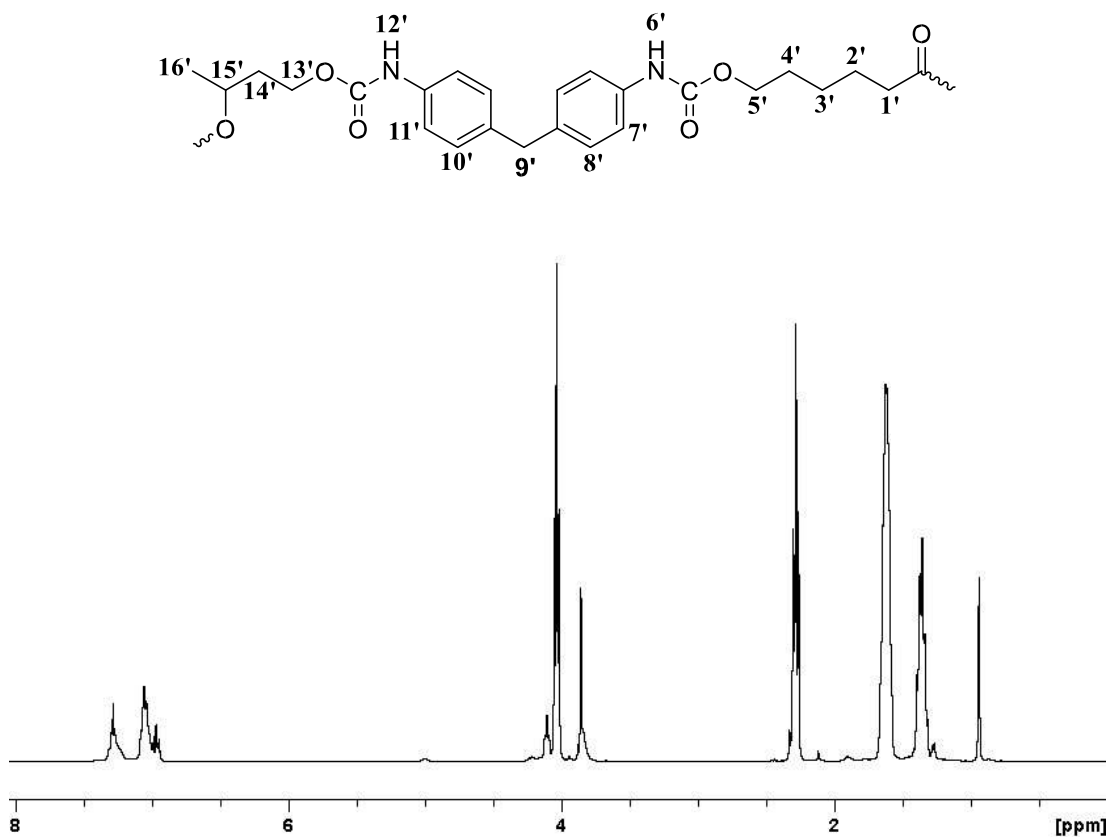
Figure 4.16: ^{1}H NMR spectrum obtained following reaction of MDI-TMP-PCD with BD.

BD chain-extender contains a single steric methyl group at the 3 position, evidence of this group can be observed by the addition of the **CH₃** signal **16'** at 1.29 ppm. The position of the **CH** proton **15'** at 4.99 ppm displays that the secondary hydroxyl groups within BD have been consumed. Evidence that the primary hydroxyl groups from BD have reacted is confirmed by the position of **CH₂-O-** group **13'** at 3.93 ppm. Also contained within the spectrum is evidence from the first step of the synthesis.

The primary hydroxyl groups of PCD which have been coupled to form urethane linkages can be observed by the position of the **CH₂** group **5'** at 4.11 ppm.

Broader aromatic signals are encountered at 7.1 (**8'** and **10'**) and 7.2 ppm (**7'** and **11'**) when compared to MDI or the previous step one prepolymer MDI-TMP-PCD.

Broader peaks suggest that reaction of the isocyanate groups with hydroxyl groups of PCD and BD. Retention of peaks that correspond to unreacted rings are also still present at 7.0 ppm, this shows that the material is still a prepolymer with reactive chain ends, however, ^{13}C NMR will give a better indication of free N=C=O groups. Finally the NH protons visible at 7.3 ppm **6'** and **12'** are direct evidence of the formation of urethane bonds.
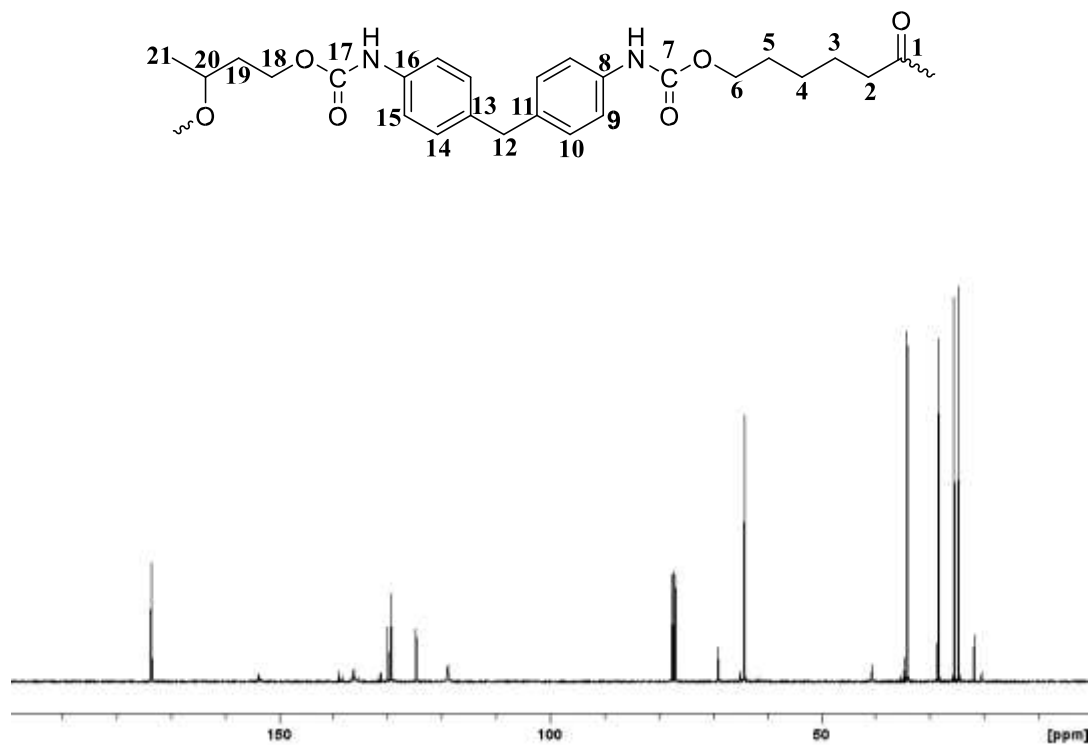
Figure 4.17: ^{13}C NMR spectrum obtained following reaction of MDI-TMP-PCD with BD.

Evidence of the methyl group **21** of BD is visible by the peak at 20 ppm in the ^{13}C soectrum. The tertiary carbon atom **20** of BD is also visible at 65 ppm and the adjacent methylene carbon **19** is visible at 35 ppm. It would be expected to observe carbon **18** of the primary hydroxyl group from BD at ~56 ppm however, it was not detected within the sample (reacted or unreacted). Evidence of the carbonyl group of both urethane (**7** + **17**) and free N=C=O are visible within the ^{13}C spectrum at 154 ppm and 131 ppm respectively (all other peaks within the aromatic region are described within section 4.22).

4.43 MALDI-MS Analysis

To measure the chain-extenders effect on the molecular weight of the prepolymers MALDI-MS was used. The matrix used for the MALDI-MS analysis was HABA which contained a cationising agent NaTFA (see section 4.23 for more matrix information). A 40 mg ml^{-1} solution of MDI-TMP-PCD-BD was prepared in THF and mixed with the matrix (1:8 sample:matrix). 1 µl portions of this sample were then spotted and dried for analysis.
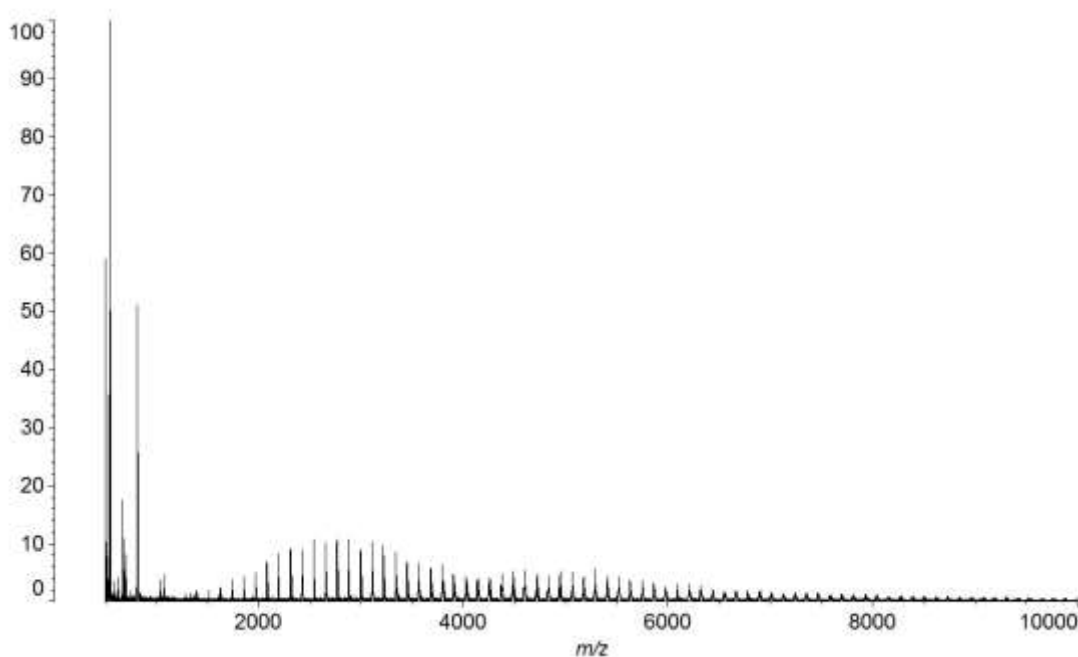
Figure 4.18: MALDI-MS spectrum of MDI-TMP-PCD-BD chain-extended prepolymer collected in HABA/NaTFA.

MALDI-MS analysis of the prepolymer adhesive displayed that there are three molecular weight distributions present. The first synthesised MDI-PCD-MDI prepolymer which was the intermediate produced in-situ prior to chain-extension is displayed by the first distribution. This peak centred at 2211 m/z contains the two ethanol end capped MDI units, one sodium ion and 13 caprolactone repeat units. Evidence of this prepolymer would be expected due to the high viscosity of the bulk polymerisation process reducing the effectiveness of the mixing. Also to limit the possibility of isocyanate based side reactions, the temperature of synthesis could not exceed 95°C. At temperatures of 120°C – 140°C where the viscosity of the prepolymer

227

mixture is lower, cross-linking by reaction of the active NH of the urethane with free N=C=O is encouraged forming allophanate groups.[15]

Diol chain-extension with BD has resulted in a greater amount of higher molecular weight prepolymers. This is evident in the higher Mn and Mw values of 4098 m/z and 4916 m/z respectively. Interestingly the PDI value of 1.20 is the lowest of all the polyurethane prepolymers synthesised within this section. This narrower mass distribution compared to the other formulations displays a more complete reaction.

Present at 1045 m/z is the chain-extender TMP that has reacted with three MDI units which are ethanol end-capped (plus one sodium cation). These molecules will contribute to the hard-segment microstructure within the adhesive and their observation was possible as all the starting material was consumed. Also detected in the MALDI-MS analysis was evidence of the chain-extended prepolymer MDI-PCDMDI-BD-MDI-PCD-MDI and also some of the residual higher molecular weight distribution observed previously in step one (MDI-PCD-MDI-PCD-MDI).

4.44 DSC and TGA Analysis

Following synthesis of the prepolymer material, the thermal characteristics of the adhesive formulation were investigated to determine the $T_g$ss and if any remaining crystalline component from the soft-segment was present. As previously mentioned the $T_g$ss of the material was considered important as it had to be lower than -20°C to be suitable for the processing window of the laminated material. From the DSC thermogram of MDI-TMP-PCD-BD, a $T_g$ss of -40°C (range of -44 to -37°C) was recorded which is out with the processing window. The broadened $T_g$ss increased by +7°C compared to the base prepolymer, however, it still remains suitable for use. Within the range of the experiment, the only other noticeable thermal transition was an exothermic peak at 276°C and this is proposed to be curing of the remaining free isocyanate groups. Also evident from the DSC thermogram was the absence of an endothermic melting peak which displays that chain-extension with BD had disrupted the soft-segment crystallisation.
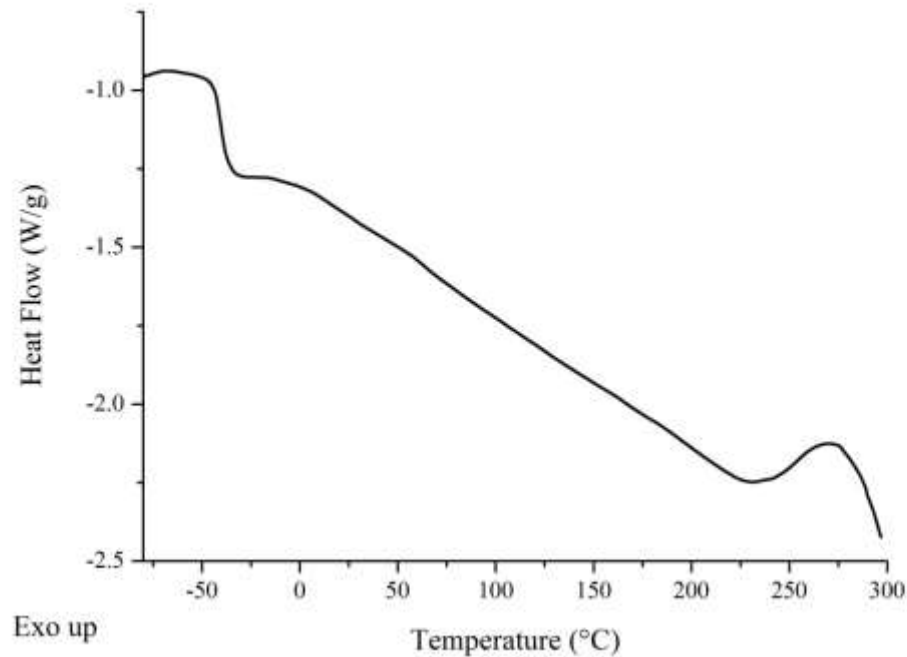
Figure 4.19: DSC thermogram of MDI-TMP-PCD-BD prepolymer formulation.
Following 30 day of curing a portion of the cured material was removed from the TAc/TAc laminate for DSC analysis. The sample was analysed using a heat-coolreheat experiment to determine the final $T_g$ss of the chain-extended adhesive as shown in figure 4.20. After the first heating cycle, a $T_g$ss of -36°C was recorded that spanned a range of -41°C to -29°C. Following a second heating cycle, a $T_g$ss of 32°C was recorded which occurred over a similar range of -39°C to -25°C. The slight increase in $T_g$ss between first and second heating cycles could be due to the experimental temperature range acting as an annealing process.[16] Also the observation of only one glass transition would suggest that there is a high degree of phase mixing between the hard and soft-segments induced by the chain-extender.[10,17] The $T_g$ss obtained even after the second heating was out with the set processing window that the adhesive is likely to meet. The DSC analysis recorded displays that even once fully cured the adhesive will be flexible within the processing window and will also be free of crystallisation.

Figure 4.20: **DSC thermogram of fully cured MDI-TMP-PCD-BD adhesive, following removal from TAc/TAc laminate. [First heating cycle *top* in black and second heating cycle *bottom* in blue].**

TGA was then performed to determine what the onset of degradation was for the PUU adhesive. The experiment was carried out over the same range as outline in section 2.10 and the data is presented in figure 4.21. From the TGA curve, the onset of degradation was 298°C which is 19°C lower than base formulation where chainextension was not performed. This would suggest that chain-extension does have an effect on the onset temperature just not a significant one. The reduction in onset of degradation may be from the introduction of more urethane bonds due to the chainextension step. Inspection of the DTG profile however, does show some differences in the degradation behaviour of this PU-U. Degradation occurs in two major steps and one minor step which are similar to the previous cured material which also displayed three processes.
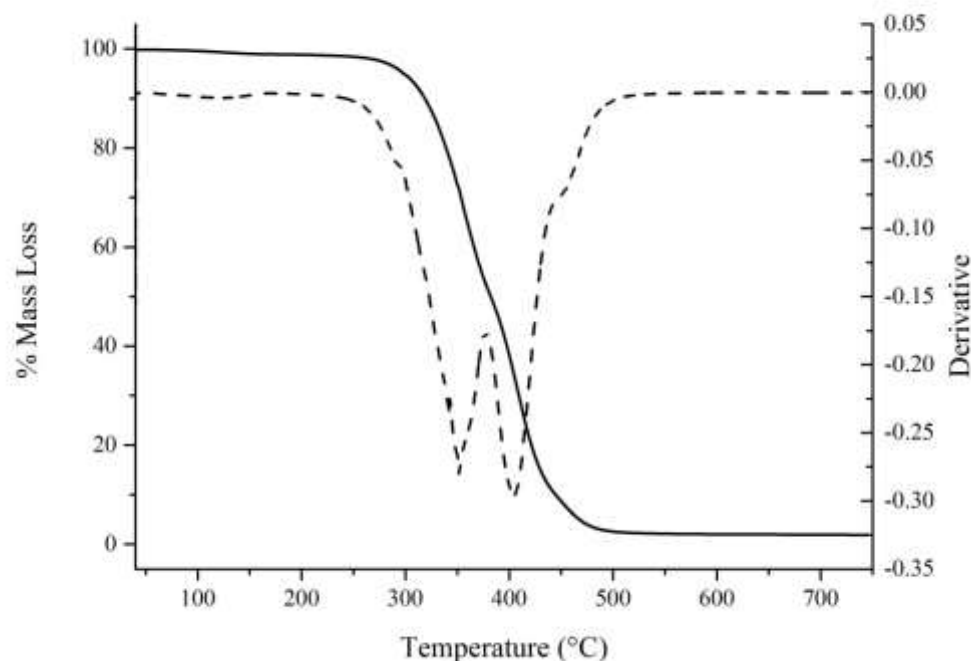
Figure 4.21: TGA and DTG curves of fully cured MDI-TMP-PCD-BD adhesive. [TGA solid line and DTG dashed line].

These peaks within the DTG curve show the different degradation processing that are occurring with the first peak at 352°C displaying the breaking of the hard-segment urethane/urea bonds.[3,4] Subsequent degradation process which occur at 403°C and 458°C account for the breaking of the PCD soft-segment molecules and more stable cross-linked structures formed during degradation respectively.[2,7]

Thermal analysis of this PU-U formulation have identified that the material has a $T_g$ss which will not interfere with the temperatures of the set processing window. The overall thermal stability of the adhesive when fully cured is well outside the temperature that the laminate will meet during processing.

4.45 180° T-peel Test and Haze

Quantifying the peel strength of the interactions with the ply materials TAc and PC by 180° T-peel testing was again performed. All six laminates were constructed; these were then tested after 7 and then 30 days of cure. These six combinations would evaluate the compatibility of the adhesive with untreated materials, with treated

231

materials and identify what interface had the greatest compatibility in the hybrid systems.

Testing of the first laminate TAc/TAc displayed poor compatibility between MDITMP-PCD-BD and the interface. Low peel strengths of 0.3 N mm^{-1} and 0.7 N mm^{-1} were recorded for the 7 and 30 day tests respectively. An adhesive failure at the TAc interface was the only mode of failure encountered in both tests. Such poor performance with this untreated material was an indication of the lack of active groups at the surface for covalent bonding, however, it would be expected that the ester soft-segment would boost the peel strengths obtained through H-bonding between the substrate and the available ester groups of PCD.

Following treatment of the TAc interface by saponification, the peel strength of the interface was improved. At 7 days the recorded tensile strength was 1.2 N mm^{-1} which is an improvement on the untreated surface and this increased to 1.9 N mm^{-1} after 30 days. The 30 day measurement has increased compared to the 7 day measurement again indicating that the strength does increase with time. Unfortunately in this case the final peel strength did not reach the 3 N mm^{-1} target. Previously 3 N mm^{-1} was reached after 7 days of cure using the base prepolymer adhesive MDI-TMP-PCD indicating for this system that chain-extension has a nonfavourable effect on the peel strength with TAc.

PC/PC was next tested and the performance was much improved compared to TAc. Following 7 days of cure, the peel strength was 6.3 N mm^{-1} which further increased to 6.6 N mm^{-1} after 30 days. The high strength obtained can be explained by the high compatibility of the adhesive with the PC by two main processes: firstly both contain aromatic rings which will encourage π-π stacking at the interface and secondly the large numbers of carbonate groups presents many opportunities for H-bonding with the ester groups of PCD. Adhesive failures were still observed but these were accompanied by strong deformation of the PC ply. When the surface treatment was performed it resulted in a decrease in the peel strength obtained. After 7 days an adhesive failure of strength 5.5 N mm^{-1} was recorded which then decreased to 4.6 N mm^{-1} after 30 days.

Table 4.05: Peel, haze and mode of failure data for MDI-TMP-PCD-BD cured PU-U adhesive. [The data in bold will be discussed within this section].

Cured Adhesive	Laminate	Peel 1* (N mm^{-1})	Peel 2^x (N mm^{-1})	Failure mode	Haze (%)
MDI-TMP-PCD	TAc/TAc	0.2	0.6	Adhesive TAc	Milky White >1.5
	TAc(t)/TAc(t)	3.5	4.3	Adhesive TAc	
	TAc(t)/PC	3.8	4.4	Adhesive TAc	
	TAc(t)/PC(t)	ND	ND	Adhesive TAc	
	PC(t)/ PC(t)	7.7	8.3	Adhesive PC	
	PC/PC	7.6	8.2	Adhesive PC	
MDI-TMP-PCD-DEPD	TAc/TAc	0.3	0.9	Adhesive TAc	Clear <1.5%
	TAc(t)/TAc(t)	1.5	2.1	Adhesive TAc	
	TAc(t)/PC	1.6	2.4	Adhesive TAc	
	TAc(t)/PC(t)	1.8	3.0	Adhesive TAc	
	PC(t)/ PC(t)	3.2	4.0	Adhesive PC	
	PC/PC	4.6	4.8	Adhesive PC	
MDI-TMP-PCD-BD	**TAc/TAc**	**0.3**	**0.7**	**Adhesive TAc**	**Clear <1.5%**
	TAc(t)/TAc(t)	**1.2**	**1.9**	**Adhesive TAc**	
	TAc(t)/PC	**1.1**	**2.3**	**Adhesive TAc**	
	TAc(t)/PC(t)	**1.2**	**2.7**	**Adhesive TAc**	
	PC(t)/ PC(t)	**5.5**	**4.6**	**Adhesive PC**	
	PC/PC	**6.3**	**6.6**	**Adhesive PC**	
MDI-TMP-PCD-PD	TAc/TAc	0.3	0.9	Adhesive TAc	Clear <1.5%
	TAc(t)/TAc(t)	1.1	1.4	Adhesive TAc	
	TAc(t)/PC	1.3	2.4	Adhesive TAc	
	TAc(t)/PC(t)	1.2	2.2	Adhesive TAc	
	PC(t)/ PC(t)	4.4	4.6	Adhesive PC	
	PC/PC	5.3	5.7	Adhesive PC	

*peel 1 collected within 7 days of room temperature cure, ^x peel 2 collected after 30 days of room temperature cure, ND = No Data

The values obtained are similar to the untreated test and considering experimental error can be considered as the same. The recovery in strength due to the use of BD will most likely result from the microstructure created being less hindered and of greater compatibility with PC (when compared with the previous DEPD formulation).

Finally hybrid laminates were tested to determine which interface had the greatest compatibility. After 7 days a peel strength of 1.1 N mm^{-1} was observed for the TAc(t)/PC laminate and this increased to 2.3 N mm^{-1} after 30 days. For the fully treated hybrid laminate (TAc(t)/PC(t)), the numbers were similar with 1.2 N mm^{-1} recorded after 7 days and this increased to 2.7 N mm^{-1} after 30 days. Both laminates failed adhesively at the TAc(t) face but with a slight deformation to the PC substrate. The adhesive failure at the TAc(t) face, further supports that even after treatment the interface compatibility is still poorer than with PC.

Following peel measurements it was observed that TAc could only be used following surface treatment. BD chain-extension has a negative effect on the peel strength obtained for TAc but has no effect on the performance with PC when compared to MDI-TMP-PCD. Finally the improved peel strength observed after 30 days for all laminates displays that the adhesive is reorganising itself to maximise attractive forces (equilibrium with repulsive adhesive forces). As the adhesive is curing at room temperature it is above the recorded $T_g$ss making mobility of the polymer groups possible, also this phenomenon has been observed elsewhere in the literature to occur.[18]

Finally the haze measurement recorded for this PU-U adhesive was < 1.5%. When compared to MDI-TMP-PCD, this is a marked improvement as that adhesive formulation was milky white in colour when fully cured. The marked improvement in haze is a result of disruption to the soft-segment crystallisation. Equally important is that diol chain-extension has encouraged phase mixing which has prevented softsegment crystallisation. Such a significant reduction in the haze confirms that using sterically hindered chain-extenders does lead to clearer PU-U adhesives. Reducing the crystallisation of the soft-segment will also free up more ester functional

groups for surface adhesion. The reduction in crystallinity appears to be coupled with a reduction in peel strength compared to MDI-TMP-PCD in TAc and hybrid systems (see section 4.25) however, PC values have recovered.

4.46 ATR of Peeled Samples

Characterisation of the bulk cured adhesive was performed using ATR analysis. Analysis of the bulk adhesive was performed on all six of the laminates after the 30 day tensile test. ATR analysis will determine the chemical functionality of the final cured material and allow for any distinct differences in curing chemistry to be observed. Discussed within this section will be peaks that indicate either the PU of the prepolymer or PU-U peaks obtained after 30 days of cure. For discussion of the peaks inherent of the starting materials see section 4.22 or table 4.06.
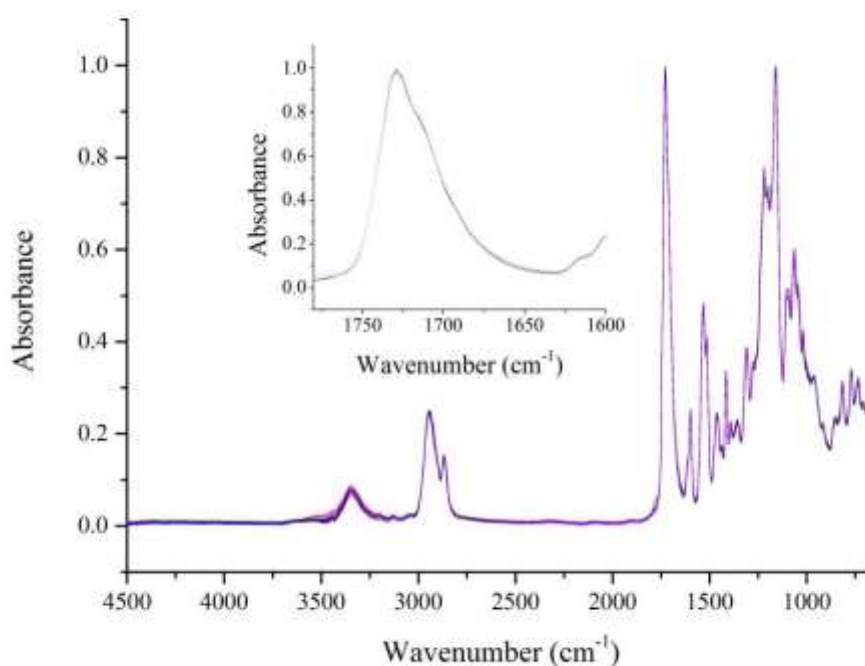
Figure 4.22: ATR spectra of cured MDI-TMP-PCD-BD sampled in-situ after tensile testing with inset expanded carbonyl region. [TAc/TAc in black, TAc(t)/TAc(t) in red, TAc(t)/PC in blue, TAc(t)/PC(t) in pink, PC(t)/PC(t) in green and PC/PC in orange. Data collected for each laminate at nine random positions with each spectrum consisting of 128 scans at 8 cm^{-1} resolution. These were then averaged and plotted as the above spectra].

Table 4.06: Characteristic peaks of MDI-TMP-PCD-BD cured PU-U adhesive from all six laminate combinations.

Wavenumber (cm⁻¹)	Vibration	Wavenumber (cm⁻¹)	Vibration
3345	N-H stretching	1306	C-N urethane
2942	C-H asymmetric stretch	1214	C-H aliphatic skeleton
2871	C-H symmetric stretch	1154	C-C stretching
1726	C=O stretching ester	1094	C-O-C aliphatic ether
1595	N-H bending urethane	1061	C-H aromatic ring
1535	C-N stretch, N-H bending, C-H aromatic ring	969	C-H aromatic ring
1513	N-H bending urea	860	C-H aromatic ring
1470	C-H bend aliphatic	821	C-H aromatic ring
1416	C-C stretching aromatic	777	C-C aliphatic skeleton
1355	C-N urea		

As there is an **N-H** stretching band at 3345 cm⁻¹ this displays that the cured adhesive has urethane and urea groups within the final composition. The positon of the **N-H** band is characteristic for a H-bonded network, which is consistent with previous analysis and the literature.[2] Carbonyl groups of the ester soft-segment are again visible at 1726 cm⁻¹ but with a more noticeable shoulder from the formation of urea (see figure 4.22).[14] Confirmation of urethane formed during prepolymer synthesis is shown by the **N-H** bending at 1595 cm⁻¹. Urea formed during moisture cure of the adhesive is shown by the **N-H** bending band at 1513 cm⁻¹. The **C-N** stretching band for both these groups can also be observed at 1535 cm⁻¹. Further **C-N** bands are visible further into the finger print region with both urethane at 1306 cm⁻¹ and urea at 1355 cm⁻¹ present.

ATR analysis has allowed for the characterisation of the fully cured PU-U adhesive. The presence of both urethane and urea bands display that the prepolymer urethane has cured through moisture uptake to consume the free isocyanate groups. As there was no band for free isocyanate, the adhesive was fully cured after 30 days. A noticeable shoulder on the carbonyl peak between 1700 cm^{-1} – 1640 cm^{-1} corresponds to carbonyl groups within a urea linkage. Finally the ply combination appears to have little effect on the final cure of the bulk adhesive.

4.47 Summary of MDI-TMP-PCD-BD Formulation

From the analysis collected from MDI-TMP-PCD-BD based PU-U it was observed that chain-extension has no significant effect on the properties of the final adhesive except for the haze measurement. The T$_g$ss of the cured adhesive was measured at 32°C which is out with the processing window of the laminate. TGA displayed that the thermal stability was also greater than the processing window with the onset of degradation occurring at 298°C. MALDI-MS highlighted that getting such elastomeric polymers of chain-extended molecular weight to successfully ionise is difficult but it is possible to observe the chain-extended prepolymers. 180° T-peel testing highlighted that PU-U adhesives based on MDI and PCD have an affinity for the PC interface but are incompatible with TAc interface unless treated. Peel testing data collected for both PC laminates displayed peel strength values on par with those of the base system. It also highlighted that chain-extension has a reducing effect on the peel strength recorded for the other four laminates tested which can be correlated to the fact that they all contain TAc or TAc(t). Finally the most promising result from this formulation is that chain-extension has a positive impact on the haze of the final cured adhesive by disrupting the crystallisation of the PCD soft-segment through phase mixing which yields an improved haze value.

4.50 Analysis of MDI-TMP-PCD-PD

4.51 Synthesis Information

MDI-TMP-PCD-PD was next synthesised with the intention of disrupting the hardsegment packing through using a sterically hindered chain-extender, continued disruption of the crystallisation within the soft-segment and to encourage phase mixing. This was achieved by firstly synthesising the MDI-TMP-PCD base

prepolymer using the same reaction conditions as detailed with section 4.21 and then performing an additional reaction set. The additional step was performed by adding a hydroxyl terminated chain-extender using a 2.2:1.0 isocyanate:hydroxyl ratio based on the calculated amount of free NCO remaining after step one. The chain-extension step was used to lower the free isocyanate content of the adhesive, which would reduce the opportunity for excessive bubbling by CO_2 liberation during urea formation.

Step one was performed as previously detailed in section 4.21 and was a clear liquid which had an observed increase in viscosity from the starting mixture. After addition of 1,2-propane diol (PD) to the reaction it was stirred at 85°C – 95°C for 5 hours before the dual DBTDL and TEA catalyst system was added. Following chainextension a visual increase in viscosity was observed and was associated with the molecular weight increase caused by the coupling step. To compensate for the molecular weight increase, the reaction mixture was slowly heated to 130°C to sufficiently lower the viscosity as this would facilitate flow and allow for the formulation to be poured. Once at temperature the formulation was poured into an aluminium tube, which was then capped and degassed as previously outlined in section 2.03. The desiccator containing the adhesive filled tube was then placed within a 0°C fridge for storage. Degassing was performed for six hours once a vacuum of one atmosphere was obtained. Samples of the reaction were taken before catalysed addition, these were analysed by DSC, NMR and MALDI-MS analysis.

MDI-TMP-PCD-PD was heated to 180°C before being applied to six laminates (same as section 4.21) which were the cured at room temperature. These samples were 180° T-peel tested at 7 days and 30 days to determine the peel strength. A further lamination was performed using two plies of TAc which would allow for the adhesive to be removed for analysis by DSC and TGA once fully cured. The 30 day tensile test samples were also analysed by ATR to characterise the bulk cured material.

Analysis of the chain-extended materials only will be presented within the remaining sections of this chapter. MDI-TMP-PCD is considered as representative of the reactive intermediate obtained after step one of each chain-extended reaction.

4.52 NMR Analysis

For full spectral characterisation of peaks from MDI and PCD see section 4.22 as this section will only detail peaks that are important to show prepolymer formation or peaks from the BD chain-extender.
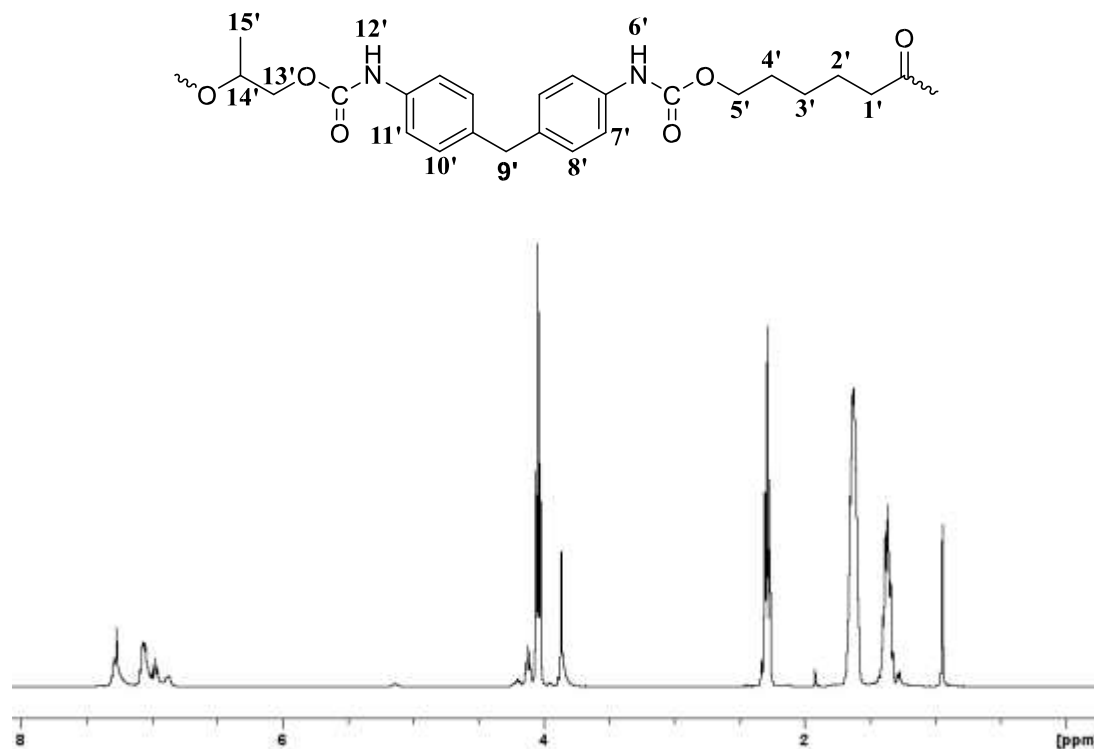
Figure 4.23: ^{1}H NMR spectrum obtained following reaction of MDI-TMP-PCD with PD.

PD chain-extender contains a single steric methyl group at the 2 position, evidence of this group can be observed by the addition of the **CH$_3$** signal **15'** at 1.29 ppm. The position of the **CH** proton **14'** at 5.30 ppm displays that the secondary hydroxyl groups within PD have been consumed. Evidence that the primary hydroxyl groups from PD have reacted is confirmed by the position of **CH$_2$**-O- group **13'** at 4.19 ppm. Also contained within the spectrum is evidence from the first step of the synthesis. The primary hydroxyl groups of PCD which have been coupled to form urethane linkages can be observed by the position of the **CH$_2$** group's **5'** at 4.11 ppm.
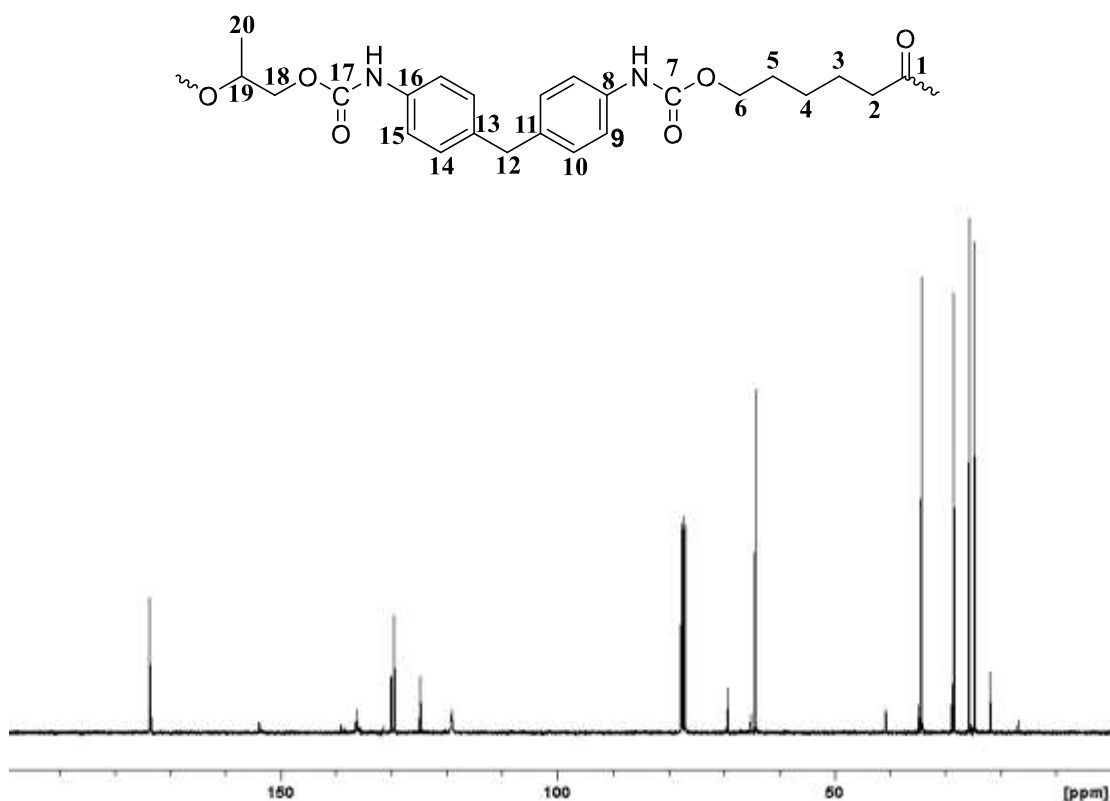
Figure 4.24: ^{13}C NMR spectrum obtained following reaction of MDI-TMP-PCD with PD.

Broader aromatic signals are encountered at 7.1 (**8'** and **10'**) and 7.2 ppm (**7'** and **11'**) when compared to MDI or the previous step one prepolymer MDI-TMP-PCD. Broader peaks suggest that reaction of the isocyanate groups with hydroxyl groups of PCD and PD. Retention of peaks that correspond to unreacted rings are also still present at 7.0 ppm, this shows that the material is still a prepolymer as there are still reactive chain ends however, ^{13}C NMR will give a better indication of free N=C=O groups. Finally the **NH** protons visible at 7.3 ppm **6'** and **12'** are direct evidence of the formation of urethane bonds.

Evidence of the methyl group of PD is visible in the ^{13}C spectrum by peak **20** at 17 ppm. The tertiary and secondary carbon atoms **19** + **18** of PD are also visible at 65ppm. Evidence of the carbonyl group of both urethane (**7** + **17**) and free N=C=O are visible within the ^{13}C spectrum at 154 ppm and 131 ppm respectively (all other peaks within the aromatic region are described within section 4.22).

To measure the chain-extenders effect on the molecular weight of the prepolymers MALDI-MS was again used. The matrix used for the MALDI-MS analysis was HABA which contained a cationising agent NaTFA (see section 4.23 for more matrix information). A 40 mg ml^{-1} solution of MDI-TMP-PCD-PD was prepared in THF and mixed with the matrix (1:8 sample:matrix). 1 µl portions of this sample were then spotted and dried for analysis.

Figure 4.25: MALDI-MS spectrum of MDI-TMP-PCD-PD chain-extended prepolymer collected in HABA/NaTFA.

MALDI-MS analysis of the prepolymer adhesive displayed that there were two molecular weight distributions present. The first and clearest distribution was for the first synthesised MDI-PCD-MDI prepolymer which was the intermediate produced in-situ prior to chain-extension. This peak centred at 2211 m/z contains the two ethanol end capped MDI units, one sodium ion and 13 caprolactone repeat units. Evidence of this prepolymer would be expected due to the high viscosity of the bulk polymerisation process reducing the effectiveness of the mixing. To limit the possibility of isocyanate based side reactions the temperature of synthesis could not exceed 95°C.

Present at 1045 m/z is the chain-extender TMP that has reacted with three MDI units which are ethanol end-capped (plus one sodium cation). These molecules will

contribute to the hard-segment microstructure within the adhesive and there observation was possible as all the starting material was consumed. Within the MALDI-MS spectrum, the origin of the second distribution is less clear. This collected analysis would suggest that HABA/NaTFA may not be the best matrix for the analysis of polyester based polyurethanes.

Using PD as the diol chain-extender results in similar Mn, Mw and PDI values to those obtained for MDI-TMP-PCD. Mn is calculated as 3216 m/z and Mw is calculated as 4012 m/z giving a PDI of 1.25. This data displays that the molecular mass distribution obtained is similar in breath to that of MDI-TMP-PCD.

4.54 DSC and TGA Analysis

Following synthesis of the prepolymer material, the thermal characteristics of the adhesive formulation were investigated to determine the $T_g$ss and if any remaining crystalline component from the soft-segment was present. As previously mentioned the $T_g$ss of the adhesive was considered important as it had to be lower than -20°C to be suitable for the processing window of the laminated material. From the DSC thermogram of MDI-TMP-PCD-PD, a $T_g$ss of -38°C (range of -42 to -34°C) which is out with the processing window. The broadened $T_g$ss increased by +9°C compared to the prepolymer, however, it still remains suitable for use. Within the range of the experiment no other significant thermal transitions were visible.

Following 30 day of curing a portion of the cured adhesive was removed from the TAc/TAc laminate for DSC analysis. The sample was analysed using a heat-coolreheat experiment to determine the final $T_g$ss of the chain-extended adhesive as shown in figure 4.27. After the first heating cycle a $T_g$ss of -33°C was recorded that spanned a range of -40°C to -25°C. Following a second heating cycle a $T_g$ss of 30°C was recorded which occurred over a similar range of -38°C to -23°C. The slight increase in $T_g$ss between first and second heating cycles could be due to the experimental temperature range acting as an annealing process.[16] Also the observation of only one glass transition would suggest that there is a high degree of phase mixing between the hard and soft-segments induced by the chain-extender.[10,17] The $T_g$ss obtained even after the second heating was out with the set processing window that the adhesive is likely to meet. The DSC analysis recorded displays that even once fully

cured the adhesive will be flexible within the processing window and will also be free of crystallisation.

Figure 4.26: DSC thermogram of MDI-TMP-PCD-PD prepolymer formulation. TGA was then performed to determine what the onset of degradation was for the PUU cured adhesive. The experiment was carried out over the same range as outline in section 2.10 and the data is presented in figure 4.28. From the TGA curve the onset of degradation was 297°C which is 20°C lower than the base formulation where chain-extension was not performed. This would suggest that chain-extension does affect the onset temperature just not significantly. Inspection of the DTG curve however, does show some differences in the degradation behaviour of this PU-U. Degradation occurs in two major steps, with the minor step viewed previously displaying a reduced contribution. These peaks within the DTG curve display the different degradation processing that are occurring, with the first peak at 350°C corresponds to the breaking of the hard-segment urethane and urea bonds.[3,4] The subsequent degradation that occurs at 398°C accounts for the breaking of the PCD soft-segment molecules.[2]
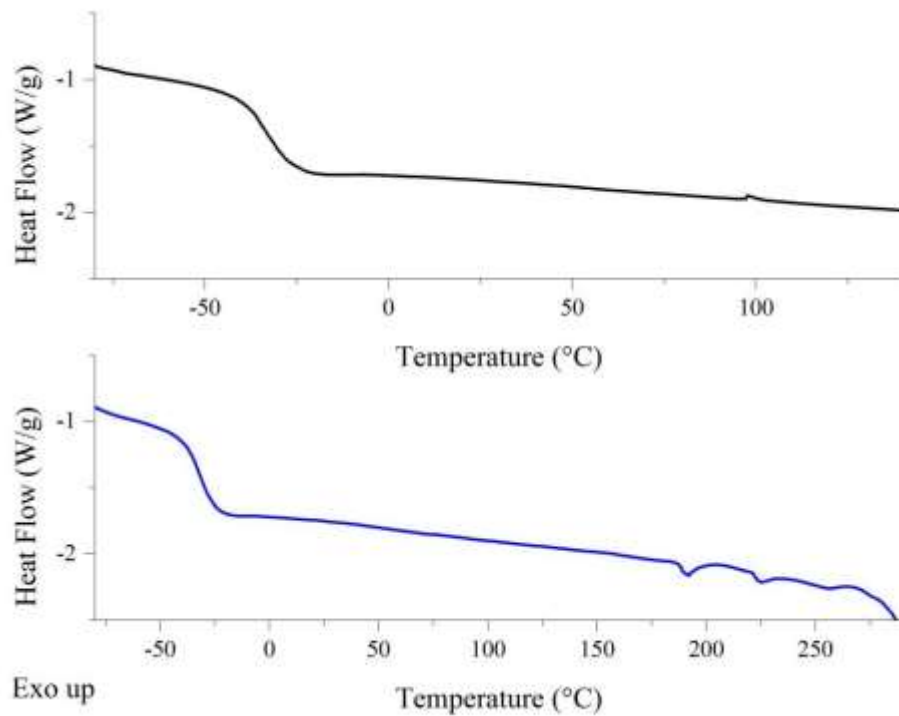
Figure 4.27: **DSC thermogram of fully cured MDI-TMP-PCD-PD adhesive, following removal from TAc/TAc laminate. [First heating cycle *top* in black and second heating cycle *bottom* in blue].**

Thermal analysis of this PU-U formulation have identified that the adhesive has a T_{gss} which will not interfere with the temperatures of the set processing window. The overall thermal stability of the adhesive when fully cured is well outside the temperature that the laminate will meet during processing.
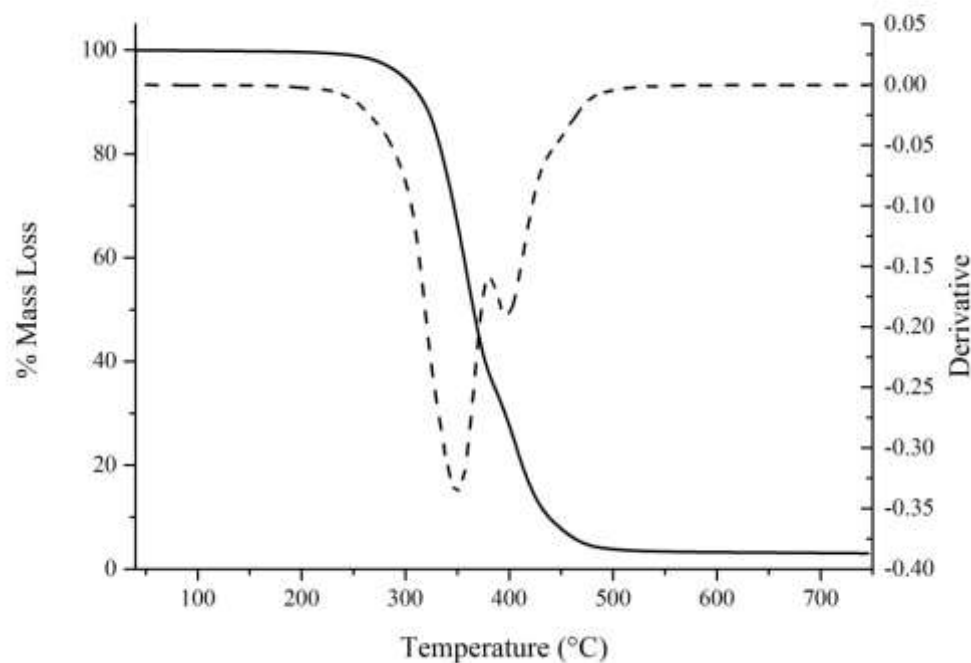
Figure 4.28: TGA and DTG curves of fully cured MDI-TMP-PCD-PD adhesive. [TGA solid line and DTG dashed line].

4.55 180° T-peel Test and Haze

Quantifying the peel strength of the interactions with the ply materials TAc and PC by 180° T-peel testing was performed to complete this set of PCD based formulations. All six laminates were constructed, with each tested after 7 and then 30 days of cure (see section 4.25 for laminates). These six combinations would evaluate the compatibility of the adhesive with untreated materials, with treated materials and determine what interface had the greatest compatibility in the hybrid systems.

Testing of the first laminate TAc/TAc displayed poor compatibility between MDITMP-PCD-PD and the interface. Low peel strengths of 0.3 N mm^{-1} and 0.9 N mm^{-1} were recorded for the 7 and 30 day tests respectively. An adhesive failure at the TAc interface was the only mode of failure encountered in both tests. Such poor performance with this untreated material was an indication of the lack of active groups at the surface for covalent bonding, however, it would be expected that the ester soft-segment would boost the peel strengths obtained through H-bonding between the substrate and the available ester groups of PCD.

245

Following treatment of the TAc interface by saponification, the peel strength of the interface was only marginally improved. At 7 days the recorded peel strength was 1.1 N mm^{-1} which is an improvement on the untreated surface and this increased to 1.4 N mm^{-1} after 30 days. The 30 day measurement has increased compared to the 7 day measurement again indicating that the strength does increase with time. Unfortunately in this case, the final peel strength did not reach the 3 N mm^{-1} benchmark. Previously 3 N mm^{-1} was reached after 7 days of cure using the base prepolymer adhesive MDI-TMP-PCD-BD, indicating for this system that chainextension has a non-favourable effect on the peel strength.

PC was next tested and the performance was much improved compared to TAc. Following 7 days of cure the peel strength was 5.3 N mm^{-1} which further increased to 5.7 N mm^{-1} after 30 days. The high strength obtained can be explained by the high compatibility of the adhesive with the PC by two main processes: firstly both contain aromatic rings which will encourage π-π stacking at the interface and secondly, the large numbers of carbonate groups will present many opportunities for H-bonding with the ester groups. Adhesive failures were still observed but these were accompanied by strong deformation of the PC ply.

Finally hybrid laminates were tested to determine which interface had the greatest compatibility. After 7 days a peel strength of 1.3 N mm^{-1} was observed for the TAc(t)/PC laminate and this increased to 2.4 N mm^{-1} after 30 days. For the fully treated hybrid laminate TAc(t)/PC(t), the numbers were similar with 1.2 N mm^{-1} recorded after 7 days and this increased to 2.2 N mm^{-1} after 30 days. Both laminates failed adhesively at the TAc(t) interface but with a slight deformation to the PC substrate. The adhesive failure at the TAc(t) interface further supports that even after treatment the interface compatibility is still poorer than with PC.

Table 4.07: Peel, haze and mode of failure data for MDI-TMP-PCD-PD cured PU-U adhesive. [The data in bold will be discussed within this section].

Cured Adhesive	Laminate	Peel 1* (N mm^{-1})	Peel 2^x (N mm^{-1})	Failure mode	Haze (%)

		*	x		
MDI-TMPPCD	TAc/TAc	0.2	0.6	Adhesive TAc	Milky White >1.5
	TAc(t)/TAc(t)	3.5	4.3	Adhesive TAc	
	TAc(t)/PC	3.8	4.4	Adhesive TAc	
	TAc(t)/PC(t)	ND	ND	Adhesive TAc	
	PC(t)/ PC(t)	7.7	8.3	Adhesive PC	
	PC/PC	7.6	8.2	Adhesive PC	
MDI-TMP-PCD-DEPD	**TAc/TAc**	0.3	0.9	Adhesive TAc	Clear <1.5%
	TAc(t)/TAc(t)	1.5	2.1	Adhesive TAc	
	TAc(t)/PC	1.6	2.4	Adhesive TAc	
	TAc(t)/PC(t)	1.8	3.0	Adhesive TAc	
	PC(t)/ PC(t)	3.2	4.0	Adhesive PC	
	PC/PC	4.6	4.8	Adhesive PC	
MDI-TMP-PCD-BD	**TAc/TAc**	0.3	0.7	Adhesive TAc	Clear <1.5%
	TAc(t)/TAc(t)	1.2	1.9	Adhesive TAc	
	TAc(t)/PC	1.1	2.3	Adhesive TAc	
	TAc(t)/PC(t)	1.2	2.7	Adhesive TAc	
	PC(t)/ PC(t)	5.5	4.6	Adhesive PC	
	PC/PC	6.3	6.6	Adhesive PC	
MDI-TMP-PCD-PD	**TAc/TAc**	**0.3**	**0.9**	**Adhesive TAc**	**Clear <1.5 %**
	TAc(t)/TAc(t)	**1.1**	**1.4**	**Adhesive TAc**	
	TAc(t)/PC	**1.3**	**2.4**	**Adhesive TAc**	
	TAc(t)/PC(t)	**1.2**	**2.2**	**Adhesive TAc**	
	PC(t)/ PC(t)	**4.4**	**4.6**	**Adhesive PC**	
	PC/PC	**5.3**	**5.7**	**Adhesive PC**	

* peel 1 collected within 7 days of room temperature cure, ^x peel 2 collected after 30

Following peel measurements it was observed that TAc could only be used following surface treatment. Also chain-extension has a negative effect on the peel strength obtained for TAc and PC when compared to MDI-TMP-PCD, however, PC is still

above benchmark. Finally, the improved peel strength observed after 30 days for all laminates displays that the adhesive is reorganising itself to maximise attractive forces (equilibrium with repulsive adhesive forces). As the adhesive is curing at room temperature it is above the recorded $T_g$ss making mobility of the polymer groups possible, also this phenomenon has been observed elsewhere in the literature to occur.[18]

Finally the haze measurement recorded for this PU-U adhesive was < 1.5%. When compared to MDI-TMP-PCD this is a marked improvement as the previous adhesive was milky white in colour. The marked improvement through reduced haze is a result of disruption to hard-segments within the microstructure of the adhesive by the steric methyl group of the chain-extender. Equally important for this system (MDI and PCD based) is that chain-extension has prevented soft-segment crystallisation. Such a significant reduction in the haze confirms that using sterically hindered chainextenders does lead to clearer PU-U adhesives. Reducing the crystallisation of the soft-segment will also free up more ester functional groups for surface adhesion.

4.56 ATR of Peeled Samples

Characterisation of the bulk cured adhesive was performed using ATR analysis. Analysis of the bulk adhesive was performed on all six of the laminates after the 30 day tensile test. ATR analysis will determine the chemical functionality of the final cured material and allow for any distinct differences in curing chemistry to be observed.

Discussed within this section will be peaks that indicate either the PU of the prepolymer or PU-U peaks obtained after 30 days of cure. For discussion of the peaks inherent of the starting materials see section 4.29 or table 4.08. As there is an **N-H** stretching band at 3350 cm^{-1} this displays that the cured adhesive will contain urethane and urea groups within the final composition. The positon of the **N-H** band is characteristic of a H-bonded network, which is consistent with previous analysis and the literature.[2] Carbonyl groups of the ester soft-segment are again visible at 1727 cm^{-1} but with a more noticeable shoulder from the formation of urea (see figure 4.29).[14]
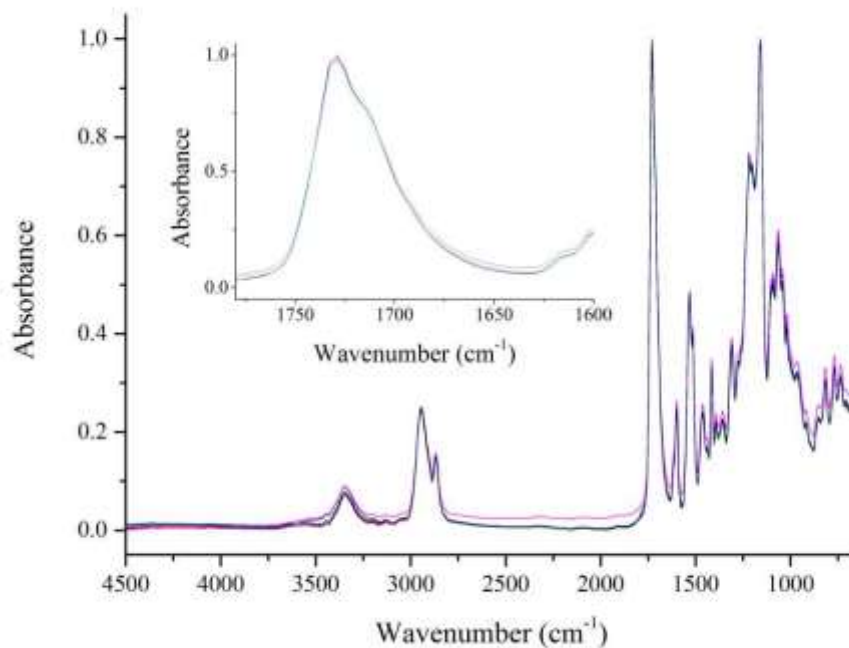
Figure 4.29: ATR spectra of cured MDI-TMP-PCD-PD sampled in-situ after tensile testing with inset expanded carbonyl region. [TAc/TAc in black, TAc(t)/TAc(t) in red, TAc(t)/PC in blue, TAc(t)/PC(t) in pink, PC(t)/PC(t) in green and PC/PC in orange. Data collected for each laminate at nine random positions with each spectrum consisting of 128 scans at 8 cm⁻¹ resolution. These were then averaged and plotted as the above spectra].

Confirmation of urethane formed during prepolymer synthesis is shown by the **N-H** bending at 1602 cm⁻¹. Urea formed during moisture cure of the adhesive is shown by the **N-H** bending band at 1512 cm⁻¹. The **C-N** stretching band for both these groups can also be observed at 1526 cm⁻¹. Further **C-N** bands are visible further into the finger print region with both urethane at 1312 cm⁻¹ and urea at 1361 cm⁻¹ present.

ATR analysis has allowed for the characterisation of the fully cured PU-U adhesive. The presence of both urethane and urea bands display that the prepolymer urethane has cured through moisture uptake to consume the free isocyanate groups. As there was no detectable band for free isocyanate the adhesive was fully cured after 30 days. A noticeable shoulder on the carbonyl peak between 1700 cm⁻¹ – 1640 cm⁻¹ corresponds

to carbonyl groups within a urea linkage. Finally the ply combination appears to have little effect on the final cure of the bulk adhesive.

Table 4.08: Characteristic peaks of MDI-TMP-PCD-PD cured PU-U adhesive from all six laminate combinations.

Wavenumber (cm^{-1})	Vibration	Wavenumber (cm^{-1})	Vibration
3350	N-H stretching	1312	C-N urethane
2944	C-H asymmetric stretch	1223	C-H aliphatic skeleton
2868	C-H symmetric stretch	1156	C-C stretching
1727	C=O stretching ester	1102	C-O-C aliphatic ether
1602	N-H bending urethane	1067	C-H aromatic ring
1526	C-N stretch, N-H bending, C-H aromatic ring	964	C-H aromatic ring
1512	N-H bending urea	853	C-H aromatic ring
1463	C-H bend aliphatic	812	C-H aromatic ring
1419	C-C stretching aromatic	777	C-C aliphatic skeleton
1361	C-N urea		

4.57 Summary of MDI-TMP-PCD-PD Formulation

From the analysis collected from MDI-TMP-PCD-PD based PU-U it was observed that chain-extension has no significant effect on the properties of the final adhesive except for the haze measurement. The $T_g$ss of the cured adhesive was measured at 30°C which is out with the processing window of the laminate. TGA displayed that the thermal stability was also greater than the processing window with the onset of degradation occurring at 297°C. MALDI-MS highlighted that getting such elastomeric polymers of chain-extended molecular weight to successfully ionise is difficult and more

complex spectrum was obtained for this formulation. 180° T-peel testing highlighted that PU-U adhesives based on MDI and PCD have an affinity for the PC interface but are incompatible with TAc interface unless treated. Peel testing data collected for both PC laminate gave values lower than the base PU-U adhesive but were still above benchmark. It also highlighted that chain-extension has a reducing effect on the peel strength recorded for the remaining laminates tested which can be correlated the presence of TAc. Finally the most promising result from this formulation is that chain-extension has a positive impact on the haze of the final cured adhesive by disrupting the crystallisation of the PCD soft-segment through phase mixing of the materials microstructure.

4.60 Summary of Aromatic Polyurethane Adhesives based on Poly(caprolactone diol)

Synthesis of all four different adhesive formulations was successfully carried out and the products were confirmed using NMR followed by MALDI-MS analysis. Urethane linkages were visible within the ATR spectra obtained along with urea bands which confirm that each final fully cured adhesive was a PU-U. Each adhesive was used to perform lamination on six different combinations (MDI-TMPPCD only had five), each once cured could be tested to determine the 180° T-peel strength, mode of failure and final haze measurement of each laminate. TGA analysis was also collected on each of the cured adhesives and it displayed that for each the onset of degradation was higher for the base adhesive (MDI-TMP-PCD onset at 316°C) than for the chain-extended adhesives (DEPD = 298°C, BD = 298°C and PD = 297°C). This result confirmed that PU-U based adhesive would be stable well above the set maximum temperature that the adhesive would see within normal processing (set at 100°C). Peel testing confirmed that all these adhesives have an affinity for the PC interface but for reasonable bond strength with TAc saponification surface treatment was essential. The overall result however, for formulations based on MDI and PCD is that the chain-extended formulations may be of use but ideally the performance with untreated TAc should be around benchmark. For all formulation regardless of composition, the value obtain when using untreated TAc was < 1 Nmm^{-1}, meaning each adhesive does not even reach one third of the minimum set strength value. Also for each TAc laminate the mode of failure was adhesive at the interface suggesting an incompatibility. Finally

even with PC, all failures were also adhesive which suggests full compatibility with the interface has not yet been reached.

4.70 Comparison of Polyol Functionality on Adhesion in MDI Based Polyurethanes

MDI based formulations have been structured around synthesising one base adhesive and three diol chain-extended version of the original base material. The base material is used to determine the properties of the main system. Next use of different chain-extenders will determine if the properties of the main system can be changed and if so can they be improved. PPG based formulations were based on a 1000 molecular weight soft-segment whereas the PCD based formulations were based on a 2000 molecular weight material. During application, the lower molecular weight PPG prepolymers required application temperatures of 50°C for the base prepolymer which was then increase to 130°C for the larger molecular weight chain-extended prepolymers. For application of the larger base PCD prepolymer adhesive, an application temperature of 160°C was required which had to be increased to 180°C for the subsequent chain-extended materials. The high application temperature required especially for the PCD materials is not ideal as the substrate materials may be damaged during application. Before and after application the thermal properties of the adhesives were of interest.

Investigation of the thermal characteristic of both adhesive sets identified some interesting data. Prepolymers based on PPG have a higher hard-segment concentration compared to the PCD based prepolymers. This is reflected in the $T_g$ss of the PPG prepolymer base material which is -29°C but this then climbs for the chain-extended prepolymers to -16°C for DEPD, -16°C for BD and -11°C for PD. In contrast PCD based material have a $T_g$ss much closer to the soft-segment material. The base material has a $T_g$ss of -47°C which then climbs for each chain-extended material to -38°C for DEPD, -40°C for BD and -38°C for PD. Accompanied by the doubling of the molecular weight of the PCD is the reduction in the $T_g$ss by around 20°C. The significance of the relationship between the $T_g$ss and the microphase morphology will be discussed in chapter 8.

When formulating the hard-segment concentration is important to consider. If a short soft-segment is used the hard-segment concentration will be high which will result in the PU microstructure becoming mixed.[17] The longer the soft-segment, the more dilute the hard-segments will become which results in greater phase separation. When phase mixing is high only one $T_g$ss will be observed, its positon will be a temperature in between the glass transition of the hard and soft-segments. The inherent value of the $T_g$ss is influenced by such things as the microstructure induced during formulation, on the degree of cross-linking and the degree of phase mixing.

Upon moisture cure, the number of possible hard-segments within the PU-U microstructure will be increased with the formation of urea groups. Considering the PPG based PU-U adhesives which uses a 1000 molecular weight soft-segment, the base formulation has a $T_g$ss of -8°C which again climbs for the chain-extended materials to 8°C for DEPD, 6°C for BD and 6°C for PD. From the data it can be observed that it is the chain-extension step that yields this increase in final $T_g$ss and not the choice of chain-extender. Moving to the 2000 molecular weight PCD based PU-U adhesives, the base formulation has a $T_g$ss of -38°C which then increases for the chain-extended formulation to -32°C for DEPD, -42°C for BD and -32°C for PD. The reduction in hard-segment concentration through increasing the molecular weight of the soft-segment has resulted in a higher degree of phase separation which has weighted the $T_g$ss more towards that of the soft-segment.

The thermal degradation of the fully cured PU-U adhesives for both set boast very similar results. The base PU-U adhesive formulation for PPG has an onset of degradation of 312°C which following chain-extension decreases to a lower temperature with DEPD at 297°C, BD at 301°C and PD at 294°C. A very similar trend was observed for the PCD based PU-U adhesives with the base formulation having an onset of degradation of 316°C which reduced after chain-extension to 298°C for DEPD, 298°C for BD and 297°C for PD. For PPG based formulations the DTG curve displayed only one peak which corresponded to the breaking of hardsegment bonds, however, the broadness of the peak in each case would suggest that degradation of the soft-segment is also occurring and they are convoluted into one peak. For PCD up to three processes where observed. The first in each case was the breaking of hard-

segment bonds, this was followed by the degradation of the PCD soft-segment and the final process was the breaking of more stable char materials formed by reactive species created during degradation.

During the 180° peel test studies it was identified that for both sets of adhesives that TAc performed poorly unless it was surface treated. For the base PPG formulation all laminates except TAc/TAc performed above the benchmark value of 3 N mm^{-1}. Of these laminates, the best performer was PC/PC which gave a 30 day peel test of 4.1 N mm^{-1} and also a noticeable mention must be given to the TAc(t)/TAc(t) laminate which after 30 days recorded a peel test of 3.3 N mm. Following chainextension with DEPD and after 30 days of cure, the laminate of greatest peel strength was PC/PC with strength of 5.2 N mm^{-1}. Also of interest was the TAc(t)/TAc(t) value which performed above benchmark after 30 days recording a value of 3.0 N mm^{-1}. Similar data was observed of chain-extension with BD by which PC(t)/PC(t) was the highest strength at 5.3 N mm^{-1}. Again TAc(t)/TAc(t) performed above benchmark recording a value of 4.2 N mm^{-1}. Due to an application issue the values obtained for PD are not considered valid as the surface contact was limited.

Moving to data obtained using PCD as the soft-segment a very similar trend is observed. The base PCD PU-U adhesive performed best with PC/PC and the recorded adhesive failure was 8.3 N mm^{-1}. The TAc(t) laminate was also above benchmark recording a peel strength of 4.3 N mm^{-1}. Following chain-extension the same trend was apparent with PC/PC delivering the greatest peel strengths in each case (DEPD = 4.8 N mm^{-1}, BD = 6.6 N mm^{-1} and PD = 5.7 N mm^{-1}). Data collected for the TAc(t) laminate was not as encouraging after chain-extension with all peel strengths below benchmark (DEPD = 2.1 N mm^{-1}, BD = 2.3 N mm^{-1} and PD = 1.4 N mm^{-1}). Regardless of the soft-segment functionality or length, the higher strength values obtained with PC result from the compatibility of the aromatic rings in both the adhesive - substrate. Additional strength will be also be added through Hbonding between the large number of carbonate linkages and the adhesive polymers.

Finally one of the most important properties that changed following chain-extension was the haze of the laminated material. PPG adhesives performed well for the base PU-U which had a haze value of < 1.1% and this more than halved to 0.4% after chain

extension with DEPD. In opposition to these haze measurements, chainextension with both BD and PD took the overall laminate haze to > 1.5% and out with useable specification. For PCD, the base PU-U was milky white in colour and had a haze value > 1.5% however, in all cases after chain-extension the value of the laminated material fell to < 1.5%. These haze measurements display that the use of sterically hindered diol chain-extenders can lead to higher clarity PU-U adhesives. Based on haze and the T-peel data the best formulation thus far is MDI-TMP-PCDDEPD as it gives high strength values coupled with low haze. To further improve upon this greater compatibility with the TAc interface is required.

References

(1)   Cui, Y.; Chen, D.; Wang, X.; Tang, X. *International Journal of Adhesion and Adhesives* **2002**, *22*, 317.
(2)   da Silva, A. L. D.; Martín-Martínez, J. M.; Carlos Moura Bordado, J. *International Journal of Adhesion and Adhesives* **2008**, *28*, 29.
(3)   Wang, P.-S.; Chiu, W.-Y.; Chen, L.-W.; Denq, B.-L.; Don, T.-M.; Chiu, Y.S. *Polymer Degradation and Stability* **1999**, *66*, 307.

(4)   Petrović, Z. S.; Zavargo, Z.; Flyn, J. H.; Macknight, W. J. *Journal of Applied Polymer Science* **1994**, *51*, 1087.

(5)   Dominguez-Rosado, E.; Liggat, J. J.; Snape, C. E.; Eling, B.; Pichtel, J. *Polymer Degradation and Stability* **2002**, *78*, 1.

(6)   Levchik, S. V.; Weil, E. D. *Polymer International* **2004**, *53*, 1585.

(7)   Dick, C.; Dominguez-Rosado, E.; Eling, B.; Liggat, J. J.; Lindsay, C. I.; Martin, S. C.; Mohammed, M. H.; Seeley, G.; Snape, C. E. *Polymer* **2001**, *42*, 913.

(8)   Grassie, N.; Zulfiqar, M. *Journal of Polymer Science: Polymer Chemistry Edition* **1978**, *16*, 1563.

(9)   Herrera, M.; Matuschek, G.; Kettrup, A. *Polymer Degradation and Stability* **2002**, *78*, 323.

(10)   Poljanšek, I.; Fabjan, E.; Moderc, D.; Kukanja, D. *International Journal of Adhesion and Adhesives* **2014**, *51*, 87.

(11)   Venkataraman, A.; Subramanian, D. R.; Soosamma, P. C. *Textile Research Journal* **1982**, *52*, 506.

(12)   Burattini, S.; Greenland, B. W.; Merino, D. H.; Weng, W.; Seppala, J.; Colquhoun, H. M.; Hayes, W.; Mackay, M. E.; Hamley, I. W.; Rowan, S. J. *Journal of the American Chemical Society* **2010**, *132*, 12051.

(13)   Li, C.; Wilkes, G. *Journal of Inorganic and Organometallic Polymers* **1997**, *7*, 203.

(14)   Daniel-da-Silva, A. L.; Bordado, J. C. M.; Martín-Martínez, J. M. *Journal of Applied Polymer Science* **2008**, *107*, 700.

(15)   Randall, D. *The Polyurethane Handbook*; J. Wiley & sons, LTD, 2002.

(16)   Martin, D. J.; Meijs, G. F.; Renwick, G. M.; McCarthy, S. J.; Gunatillake, P. A. *Journal of Applied Polymer Science* **1996**, *62*, 1377.

(17)   Šebenik, U.; Krajnc, M. *International Journal of Adhesion and Adhesives* **2007**, *27*, 527.

(18)   Chen, J.-H.; Ruckenstein, E. *Journal of Colloid and Interface Science* **1990**, *135*, 496.

Chapter 5 Aliphatic Polyurethane Adhesives based on Poly(propylene glycol)

5.10 Polymers Synthesis Introduction

Preceding synthesis and application has been based on methylene diphenyl diisocyanate (MDI). Implementation of MDI into the formulation was to gain high strength within the adhesive matrix through the formation of strongly adhered hardsegments. The strength along with the compatibility of the adhesive was investigated using two different soft-segments, namely poly(propylene glycol) (PPG) and poly(caprolactone diol) (PCD). The introduction of PPG was to determine the effect to the clarity of the formulation and PCD was implemented in an attempt to improve the compatibility towards both substrate materials (bisphenol-A polycarbonate (PC) and cellulose triacetate (TAc)). Using 180° T-peel testing it was evident that MDI based formulations have a greater affinity for PC than for TAc. Also observed was when using PCD (more functionalised) the peel strength increased for PC, PC(t) and TAc(t) laminates but not for untreated TAc.

Within this chapter, the focus was shifted from an aromatic MDI based isocyanate to an aliphatic isocyanate, namely isophorone diisocyanate (IPDI). The main reasons behind this shift are: MDI undergoes colouration by UV degradation which will affect the adhesives clarity, IPDI has greater UV resistance and should aid clarity.[1] In normal applications of MDI based adhesives such as wood glues the colouration of the adhesive is not a major issue however, in the current application the adhesive requires to be clear. It was also of interest to determine if changing the hardsegments within the adhesive would have any effect on the peel strength of the final cured adhesive within a laminate.

Again four PU prepolymer adhesives were synthesised: a one-step prepolymer PU of formulation IPDI-TMP-PPG (polymer has IPDI, TMP and PPG in its formulation) and three chain-extended prepolymer formulations IPDI-TMP-PPG-DEPD (initial step chain-extended with DEPD = 2,2-diethyl-1,3-propane diol), IPDI-TMP-PPGBD (BD = 1,3-butane diol) and IPDI-TMP-PPG-PD (PD = 1,2-propane diol).

Again the curing chemistry employed will be a two stage process of initial catalyst cure (0.05 wt% of both dibutyltin dilaurate (DBTDL) and triethylamine(TEA)) followed by final moisture cure of any remaining free isocyanate. Each prepolymer material was analysed using NMR, DSC and MALDI-MS prior to application.
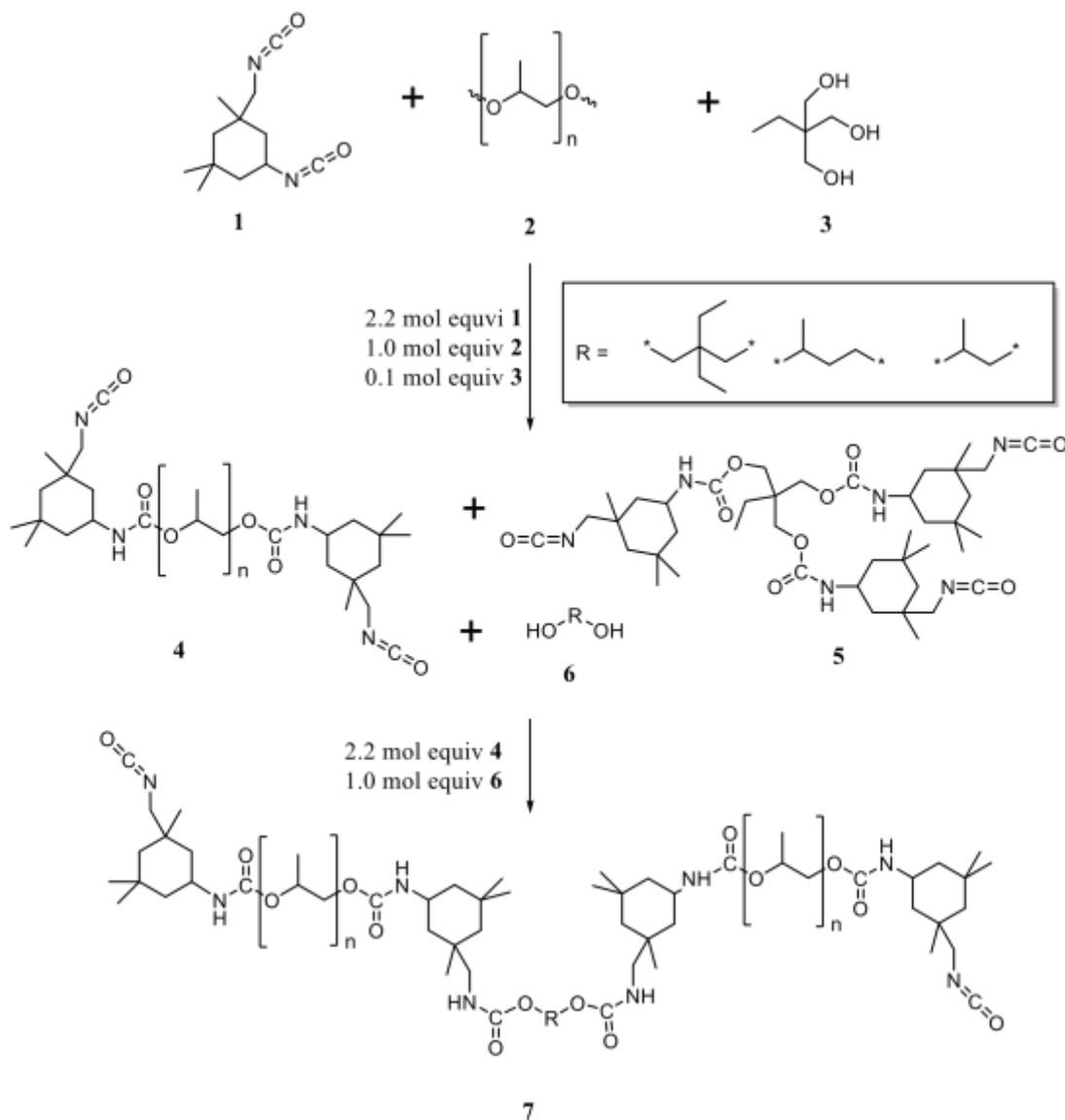
Figure 5.01: General reaction scheme for the synthesis IPDI-TMP-PPG based chain-extended polyurethanes adhesives. 1 = IPDI, 2 = PPG, 3 = IPDI-PPG prepolymer, 4 = chain-extender and 5 = chain-extended prepolymer.

Thermal transitions and stability of each fully cured PU-U were characterised by DSC and TGA. The final chemical characteristics of each PU-U were investigated by ATR

to obtain functionality information and 180° T-peel testing to determine laminate peel strength.

5.20 Analysis of IPDI-TMP-PPG

5.21 Synthesis Information

Prior to synthesis, PPG (molecular weight 1000) was dried to remove water by placing within a vacuum oven at 80°C for at least 48 hours. The synthesis was performed using the reaction set-up as detailed in section 2.03, with the reaction being performed in the temperature window of 85°C – 95°C for seven hours. The reaction time was started after the last addition of IPDI to the polyol containing reaction vessel. IPDI was degassed within a three necked round bottom flask before being put under a nitrogen atmosphere. To ensure that the exothermic reaction did not exceeded 95°C, IPDI was added drop wise in 1 ml portions. The final prepolymer obtained was clear but with a slight visually increase in viscosity compared to the starting mixture (consequence of the molecular weight increase). Prior to catalyst addition, samples of the reaction were taken for NMR, MALDI-MS and DSC analysis. After the elapsed reaction time of seven hours, 0.05 wt% of DBTDL and 0.05 wt% of TEA were added as curing catalysts (calculated from batch weight). Following catalyst addition, the formulation was transferred to an aluminium holding tube and placed within a vacuum desiccator. The adhesive was kept at 0°C within a fridge until being used during lamination (typically not exceeding 7 days). Degassing was performed for six hours once a vacuum of one atmosphere was obtained.

The prepolymer adhesive was applied to six different laminates that were of interest:

- TAc/TAc
- TAc(t)/TAc(t)
- TAc(t)/PC
- TAc(t)/PC(t)
- PC(t)/PC(t)
- PC/PC

Where TAc is cellulose triacetate, PC is bisphenol-A polycarbonate and (t) denotes that the surface of the polymer film has been treated (see section 2.01 and 2.02). As

IPDI-TMP-PPG was of low viscosity even after synthesis only a low application temperature of 50°C was required to ensure good surface coverage. The lamination process was carried out as detailed in section 2.04 and the laminated materials were left to cure at room temperature. 180° T-peel testing was carried out initially within 7 days and then after 30 days to determine the peel strength of each laminate, with the mode of failure monitored by visual inspection. The cured laminates from the 30 day peel testing were used in the ATR analysis of the fully cured adhesive.

5.22 NMR Analysis

To follow the reaction between the hydroxyl end groups of the PPG soft-segment and the isocyanate groups of IPDI hard-segment NMR was again used. The two nuclei investigated were ^{1}H and ^{13}C as both would be able to monitor the formation of polyurethane linkages within the prepolymer material. From previous analysis it had been determined that the PPG polyol has both primary and secondary hydroxyl groups as the end groups (primary methylene group at 3.51 ppm and secondary methine at 3.91 ppm). Both these groups will react but the primary hydroxyl groups will be expected to be consumed quicker than the secondary groups.

Figure 5.02 displays the ^{1}H spectrum for the isocyanate end-capped prepolymer (IPDI-TMP-PPG) synthesised as the base prepolymer to be used for lamination. As the reaction was un-catalysed between 85°C - 95°C a mixture of both primary and secondary free isocyanate groups would be expected.[2] With both IPDI and PPG being aliphatic, coupled with the broad signals inherent of the atactic soft-segment, some regions within the spectrum are rather complex (especially 0.84 ppm - 1.21 ppm). Table 5.01 displays all the chemical shifts of the prepolymer molecules in deuterated chloroform for both nuclei. At 0.95 ppm protons from the methyl group of TMP and the adjacent **CH₂** are visible at 1.6 ppm. Observation of the **CH₂-O** protons of TMP is not possible as they are convoluted with the signal from the MDI methylene bridge **10'** at 3.9 ppm.

Inspection of the ^{1}H spectrum displays a mixture of both primary and secondary urethane linkages as would be expect from the catalyst free synthesis within this temperature range.[3] Reaction of primary hydroxyl groups of PPG are shown by the

shift of the methylene protons **6** adjacent to the urethane linkage from 3.51 ppm to 3.79 ppm. Also visible is reaction of the secondary hydroxyl groups of PPG as shown by the shift of the methine peak adjacent to the urethane linkage from 3.89 ppm to 4.84 ppm.
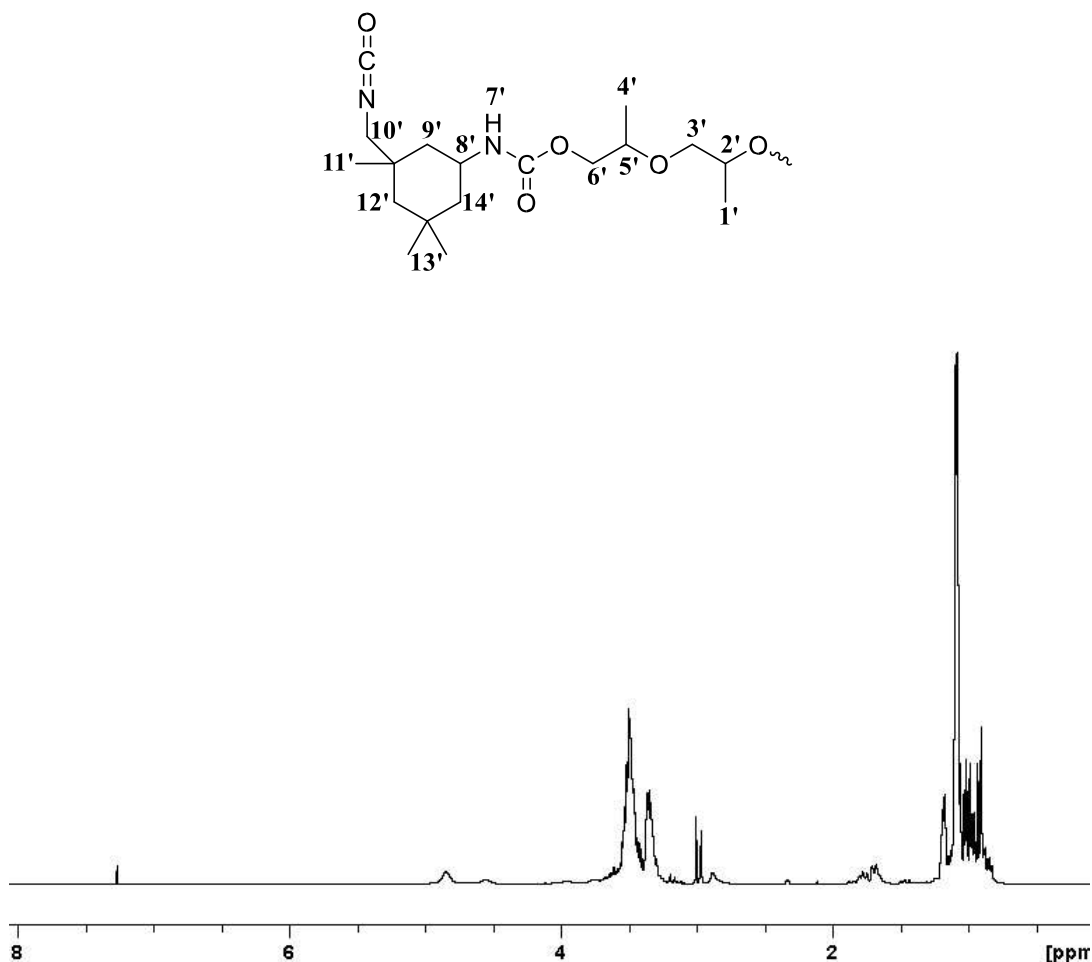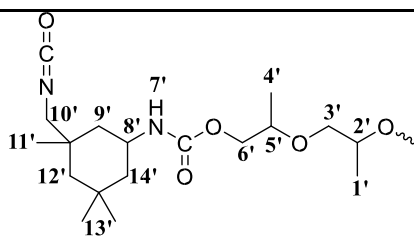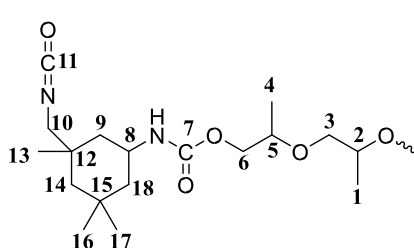
Figure 5.02: ¹H NMR spectrum of IPDI-TMP-PPG polyurethane prepolymer in deuterated chloroform.

Signals from the methyl protons **1'** and **4'** of PPG are present between 1.00 ppm – 1.20 ppm (along with a contribution from TMP chain-extender at 1.20 ppm). Other signals from the PPG soft-segment are present between 3.35 ppm - 3.65 ppm, which are represented by methylene groups **3'** and methine groups **2'** in the structure presented in figure 5.02. Signals from the methyl protons **11'** and **13'** present within IPDI are present between 0.84 ppm – 1.00 ppm. IPDI signals for methylene protons

9' and **14'** of the aliphatic ring are also present at 1.71 ppm – 1.84 ppm. Methylene signal **12'** of the aliphatic ring would also be expect at 1.19 ppm (determine by

previous analysis), however, it has been convoluted with PPG signals.   **Table 5.01:**
^{1}H and ^{13}C chemical shift for IPDI-TMP-PPG collected in CDCl$_3$.

IPDI-TMP-PPG	Position	^{1}H Chemical Shift (ppm)	Position	$_{13}$C Chemical Shift (ppm)
	1'	1.21	1	17.5
	2'	3.61	2	75.7
	3'	3.23	3	73.5
	4'	1.21	4	17.5
	5'	3.98	5	72.1
	6'	4.10	6	70.1
	7'	NDT	7	156.6$_p$/154.4$_s$
	8'	3.54	8	42.6
	9'	1.41/1.71	9	43.5
	10'	3.00/3.21	10	56.9
	11'	0.94	11	123$_p$/121.8$_s$
	12'	1.09/1.30	12	18.6
	13'	0.91	13	23.4
	14'	1.39/1.68	14	48.7
			15	23.2
			16	27.1
			17	31.7
			18	46.7

$_p$ = primary, $_s$ = secondary, NDT = not detected

Next presented at 2.89 ppm are methylene protons adjacent to the primary isocyanate group now part of a urethane bond. Also observed within this region of the spectrum are two sharp signals at 3.00 ppm which represent methylene proton which are adjacent to an unreacted primary isocyanate **10'**. Evidence of methine protons connected to the nitrogen of free secondary isocyanate groups is also visible at 3.19 ppm.

Unfortunately evidence of methine ring protons **8'** (connected to NH in secondary reacted isocyanates) are not observed as they occur at 3.55 ppm meaning they are obscured by the PPG signals. ^{1}H NMR analysis has highlighted that both primary and secondary free isocyanate groups are present within the prepolymer and that both are involved within urethane linkages. Next ^{13}C analysis of the same sample was carried out to further characterise the prepolymer formed. Table 5.01 displays all the chemical shifts and assignment of position for the carbons atoms within the prepolymer formulation.
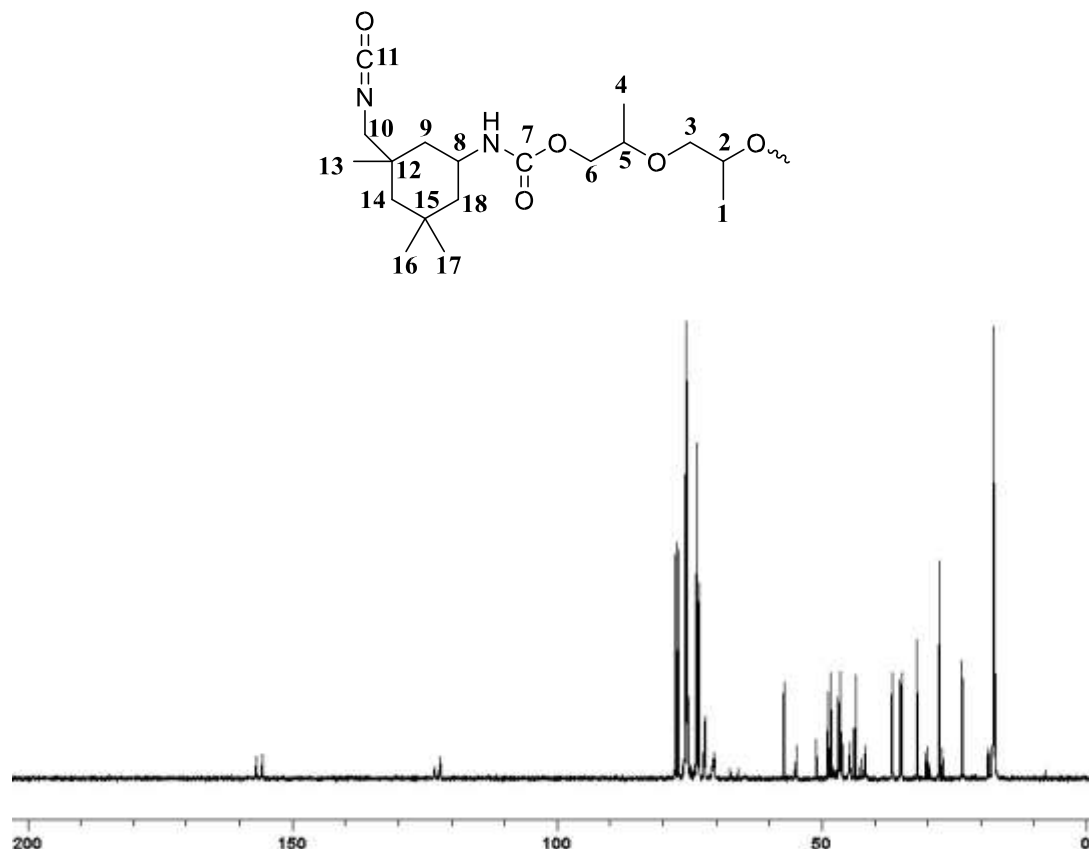
Figure 5.03: ^{13}**C NMR spectrum of IPDI-TMP-PPG prepolymer in deuterated chloroform.**

Within figure 5.03 it is evident that the free isocyanates at the terminus of the prepolymer are a mixture of both primary and secondary groups. As the prepolymer reaction was non-catalysed and between 85°C – 95°C this would be expected.[3] Reaction of the primary isocyanate groups to form urethane linkages is displayed by the carbonyl shift at 157 ppm and the evidence of the remaining free primary isocyanates **11** are also visible at 122 ppm. Urethane linkages containing secondary

isocyanate groups **7** can be observed at 155 ppm and free secondary isocyanate groups are still present at 123 ppm. This data displays that there are varying free isocyanate groups at the terminus and varying urethane linkages within the prepolymer structure.

Further evidence of urethane linkage formation can be observed by the shift of the carbon peaks from adjacent PPG end groups. Consumption of primary PPG end groups is visible by the shift of the adjacent methylene carbons from 67 ppm to 72 ppm. Secondary PPG groups have also been consumed as is evident from the shift of the methine carbons from 68 ppm to 71 ppm. As both these end groups are still visible (at 67 ppm and 68 ppm) it may suggest that there is a proportion of unreacted starting material still present but this will be further investigated within section 5.23.

5.23 MALDI-MS Analysis

To further solve the structure of the prepolymer molecules matrix assisted laser desorption ionisation time-of-flight mass spectrometry (MALDI-MS) analysis was used. The molecular mass of both the starting soft-segment and the synthesised prepolymer were measured.

The matrix used was dithranol which was prepared as a 20 mg ml^{-1} solution in tetrahydrofuran (THF), this was then mixed with a 1 mg ml^{-1} solution of sodiated trifluoroacetic acid (NaTFA) in a 7:1 ratio respectively. IPDI-TMP-PPG sample was prepared as a 40 mg ml^{-1} solution in THF which was then mixed with the matrix in a 1:8 ratio of sample to matrix. 1 μl aliquots of the solution were then spotted and dried before analysis.

As was previously recorded using MALDI-MS (see section 3.23), the PPG softsegment was observed to be the di-sodiated adduct (sodium ion from NaTFA) centred at 974 m/z, with a composition of 16 repeat units and two sodium ions. In the previous section it was highlighted that there may be some unreacted PPG starting material and from inspection of the spectrum obtained (figure 5.04) the ^{13}C NMR analysis was accurate. Mono end-capped polymers (IPDI-PPG) are visible within the spectrum and results in a shift of 268 m/z. It is possible from the MALDIMS spectrum to calculate Mn, Mw and PDI (see section 2.132 for formulae). Softsegment PPG has a Mn of 1008 m/z and ha a Mw of 1033 m/z giving a PDI of 1.02. Following prepolymer synthesis an

increase in all three of these parameters is observed for formulation IPDI-TMP-PPG. The value of Mn increases to 1262 m/z and the value of Mw increases to 1531 m/z. This results in an increased PDI value of 1.21 and displays that the bulk polymerisation broadens the mass distribution.
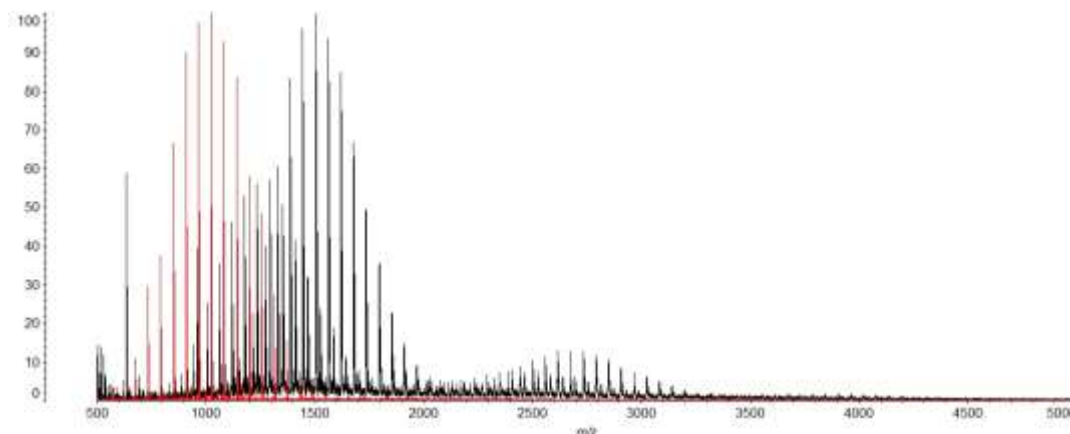
Figure 5.04: MALDI-MS spectra of PPG starting material in red and the prepolymer IPDI-TMP-PPG in black. Both were mixed with the matrix material of dithranol and sodiated trifluoroacetic acid in a 1:8 sample:matrix mixture.

Also evident within this distribution was a peak at 961 m/z which corresponds to a TMP chain-extender molecule which has three ethanol quenched IPDI groups. The molecular distribution which has the greatest intensity within the spectrum corresponds to the target isocyanate end-capped prepolymer molecule and is centred at 1572 m/z a further shift of 268 m/z. Prepolymers IPDI-PPG-IPDI contained within this peak will consist of two ethanol end-capped IPDI groups, two sodium ions and 13 PPG repeat unit. Evidence of this peak confirms that using a 2.2:1.0 NCO:OH ratio results in formation of isocyanate end-capped prepolymer molecules. Also visible within the spectrum was a higher molecular mass distribution which corresponds to IPDI-PPG-IPDI-PPG-IPDI polymers centred at 2780 m/z. MALDIMS has confirmed that the target isocyanate end-capped prepolymer is within the formulation.

5.24 DSC and TGA Analysis

Following the thermal behaviour of the prepolymer and cured adhesive is important to determine if the current formulation will be appropriate for the likely temperatures that each laminate will be exposed to during manufacture. Two techniques that were

selected to investigate if the material (prepolymer and cured adhesive) were capable of being stable within the set functional working window of -20°C – 100°C where differential scanning calorimetry (DSC) and thermal gravimetric analysis (TGA). The thermal behaviour of the prepolymer directly after synthesis will be discussed first and fully cured adhesive (adhesive removed from a TAc/TAc laminate) will be discussed second.
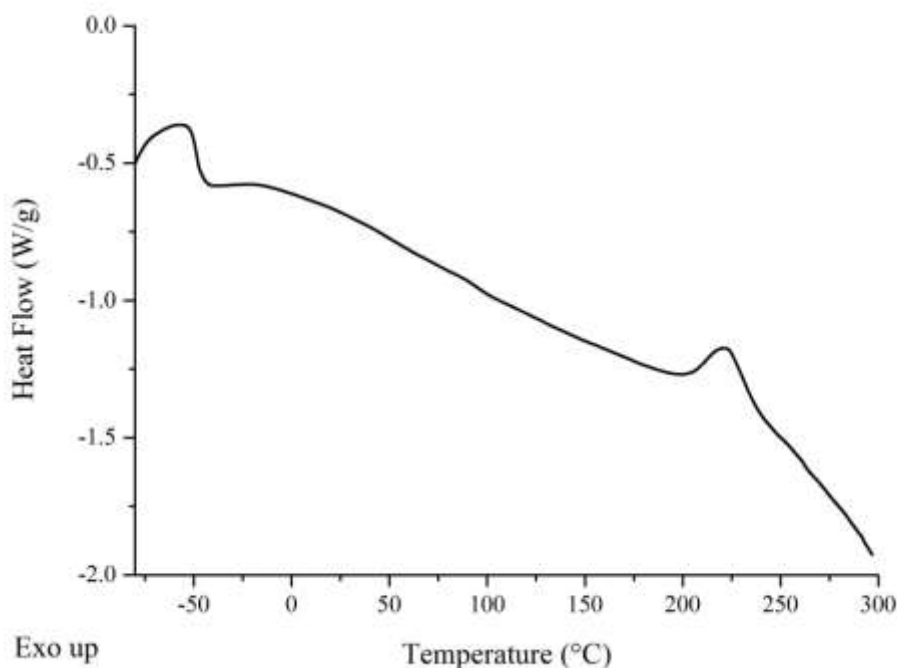
Figure 5.05: DSC thermogram of catalyst free IPDI-TMP-PPG prepolymer sampled directly after synthesis.

Recording the soft-segment glass transition ($T_g$ss) temperature of the prepolymer material will determine if the formulation is performing out with the identified processing window. Also the position of the $T_g$ss compared to the unreacted softsegment will give an indication about the morphology, if the molecular weight has changed, if cross-linking has occurred within the matrix and the compatibility of the two segments. The DSC experiment was recorded within an inert nitrogen atmosphere from -90°C to 300°C at a ramp rate of 10°C min^{-1}. For the prepolymer IPDI-TMP-PPG, the recorded $T_g$ss was -49°C which covered a range of -51°C to 46°C. When in its unreacted state the PPG soft-segment has a $T_g$ss of -63°C, the polymerisation has

resulted in a shift of +14°C. As a molecular weight increase has occurred from the end capping of both the PPG plus TMP molecules, the viscosity of the system will have increased resulting in an elevated $T_g$ss. Within the thermogram also observed is a small exothermic peak (enthalpy 8.2 J g^{-1}) at 224°C which is believed to be cure of residual isocyanate groups via isocyanate based reactions such as isocyanurate formation.
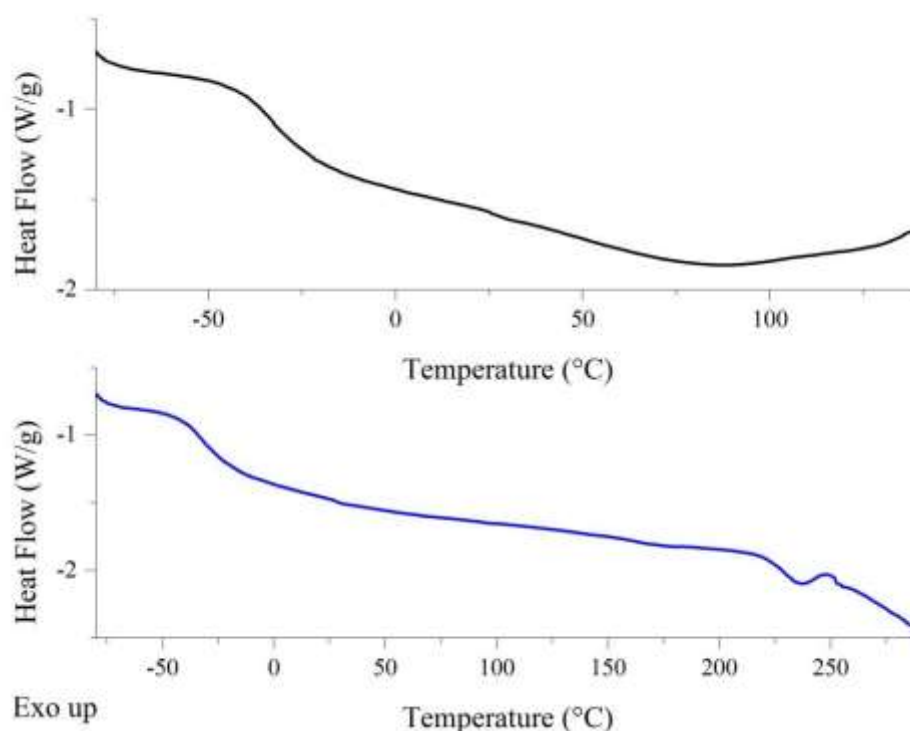
Figure 5.06: DSC thermogram of fully cured IPDI-TMP-PPG adhesive, following removal from TAc/TAc laminate. [First heating cycle *top* in black and second heating cycle *bottom* in blue].

Recording the $T_g$ss following 30 days of moisture cure at room temperature is much more informative as it indicates the final properties of the cured adhesive. The cured adhesive sample was removed from a pre-made test laminate consisting of two TAc plies and put through a cool-heat-cool-reheat experiment. The first heating cycle was recorded from -80°C to 140°C at 10°C min^{-1} and was used to remove any thermal history from the sample. The second heating cycle was recorded from -80°C to 300°C to investigate if any information on hard and soft domains was available.
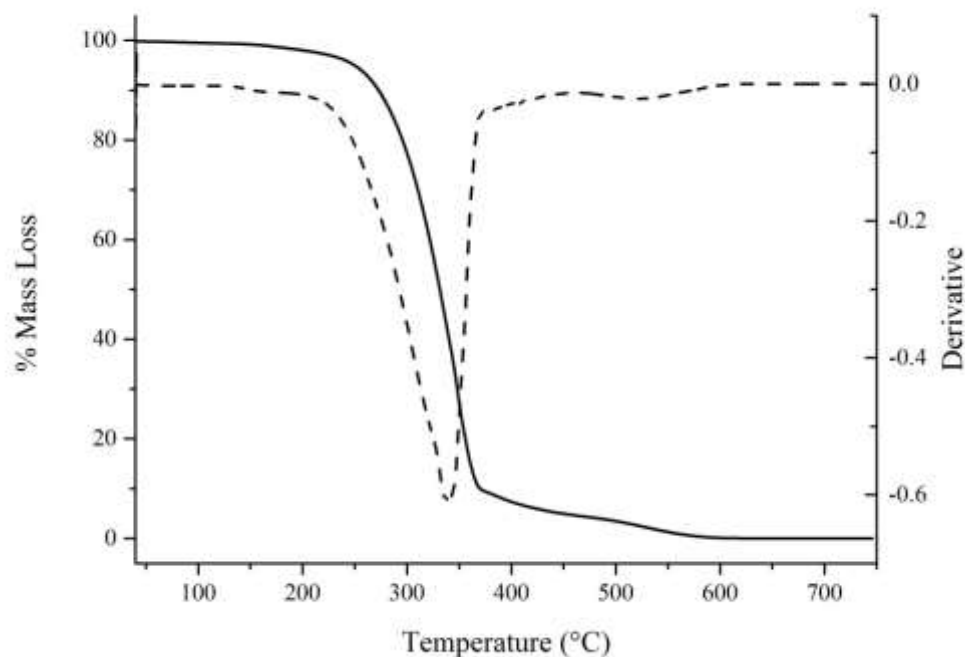
Figure 5.07: TGA and DTG curves of fully cured IPDI-TMP-PPG adhesive. [TGA solid line and DTG dashed line].

Following the first heating cycle, a $T_g$ss of -33°C was obtained and now covered a broadened range of -41°C to -23°C (compared to prepolymer which only spanned a range of 7°C). This first heating cycle $T_g$ss is now +30°C higher than the PPG softsegment (prepolymer was only +14°C). After a second heating cycle was performed, a $T_g$ss of -33°C was recorded which spanned a range of -41°C to -20°C. On this same cycle a melting endotherm was observed at 233°C (onset 222°C with enthalpy of 2.5 J g^{-1}) and was assigned to breaking of H-bonds within hard-segments of the PU-Us microstructure. The elevated $T_g$ss displays that mixing of the hard and softsegments has occurred within the cured matrix (will be discussed further with chapter 8).[4] This would suggest, that following moisture cure the compatibility between hard and soft-segments has sufficiently increased but not to the extent as previously observed for MDI based materials (see section 3.24). Also the upper end of the $T_g$ss range has almost entered the processing window of the laminate, however, it has not yet breached this pre-set window making it a pass. Evidence of hard-segment melting also confirms that there is a degree of phase separation within the adhesives

268

microstructure. DSC analysis has displayed that the current formulation based on IPDI and PPG has the potential to be used in the intended laminate application.

Characterisation of the overall thermal stability of the fully cured adhesive was carried out using TGA. To ensure that the degradation of the adhesive sample was consistent, the experiment was again performed under nitrogen from 40°C to 750°C at 10°C min^{-1}. From inspection of figure 5.07 it is evident that degradation occurs in two steps which can be observed from TGA and DTG curves. It is widely accepted that the degradation profile of polyurethanes is complex due to the difference in thermal stabilities of the hard and soft-segments within polyurethane microstructure.[5,6]

The dominant degradation process shown in figure 5.07 has an onset of 250°C, with the peak rate occurring at 339°C. As this process is relatively broad it will contain both the hard and soft-segment degradation processes. Degradation through depolymerisation within the hard-segment will occur first as these bonds are thermally the weakest within the matrix structure.[7,8] Degradation of the hardsegment occurs from the thermal breakdown of either urethane or urea bonds. Also contained within this broad peak will be the thermal break down of the soft-segment ether groups.[5] Another much smaller degradation peak at 523°C is visible and will most likely be the result of the breakdown of cross-linked products formed by reactive intermediates produced during degradation or a small amount of residual soft-segment.[7] For the intended application, the onset of thermal degradation is well out with the temperature range that the laminate will experience during manufacture. This makes the formulation in question based on IPDI and PPG suitable for consideration as a possible adhesive based on the thermal characteristics obtained from both DSC and TGA.

5.25 180° T-peel Test and Haze

In order to screen the adhesion potential of IPDI-TMP-PPG, six different laminates were constructed (as detailed in section 2.04) namely TAc/TAc, TAc(t)/TAc(t), TAc(t)/PC, TAc(t)/PC(t), PC(t)/PC(t) and PC/PC. Each laminate was peeled at a rate of 100 mm min^{-1} for an extension of at least 150 mm, with the first 50 mm discarded from the peel strength value as this is where a stable crack was formed. The haze of

the fully cured laminate was also characterised prior to testing and the mode of failure for each laminate investigated following testing. 180° T-peel testing was performed to determine the compatibility of the adhesive (IPDI-TMP-PPG) with different surface chemistries and to determine if it would perform to the desired strength (> 3 N mm^{-1}). Three different interface scenarios were present within the test set: untreated (e.g. TAc/TAc or PC/PC), treated (TAc(t)/TAc(t) or PC(t)/PC(t)), and hybrid (TAc(t)/PC or TAc(t)/PC(t)). Visual inspection was used to determine the mode of failure and to highlight the weakest part of the laminate.

A laminate combination that was becoming of major interest was TAc/TAc due the consistent poor performance (see sections 3.25, 3.35, 3.45, 3.55 in chapter 3 and 4.25, 4.35, 4.45, 4.55 in chapter 4) with all previous adhesives. The inherent poor strength that was previously obtained displayed that the untreated surface has a very poor compatibility with the adhesive formulation. Upon inspection of table 5.02 it is apparent that changing the isocyanate to an aliphatic block has had no significant effect on the compatibility with the untreated surface as an adhesive mode of failure was recorded at the TAc interface.

Following 7 days of cure, the peel strength obtain for TAc/TAc was 0.77 N mm^{-1} and this slightly increased to 0.9 N mm^{-1} after 30 days of cure. Low strength values coupled with an adhesive mode of failure display that the TAc – Adhesive interface is very poor and will only be operating by very weak (Van der Waals) adsorption forces.

Table 5.02: Peel, haze and mode of failure data for IPDI-TMP-PPG cured PUU adhesive. [The data in bold will be discussed within this section].

Cured Adhesive	Laminate	Peel 1* (N mm^{-1})	Peel 2^x (N mm^{-1})	Failure mode	Haze (%)
IPDI-TMP-PPG	**TAc/TAc**	**0.8**	**0.9**	**Adhesive TAc**	**<0.3 %**
	TAc(t)/TAc(t)	**4.7**	**9.6**	**Adhesive TAc**	
	TAc(t)/PC	**6.5**	**7.7**	**Adhesive PC**	
	TAc(t)/PC(t)	**3.8**	**4.4**	**Adhesive PC**	

	PC(t)/ PC(t)	**4.8**	**6.0**	**Adhesive PC**	
	PC/PC	**3.0**	**3.9**	**Adhesive PC**	
IPDI-TMP-PPG-DEPD	TAc/TAc	0.8	0.7	Adhesive TAc	<0.5%
	TAc(t)/TAc(t)	8.2	6.6	Cohesive	
	TAc(t)/PC	5.0	3.8	Adhesive PC	
	TAc(t)/PC(t)	4.1	3.3	Adhesive PC	
	PC(t)/ PC(t)	6.1	6.0	Adhesive PC	
	PC/PC	4.7	3.2	Adhesive PC	
IPDI-TMP-PPG-BD	TAc/TAc	0.6	0.8	Adhesive TAc	<0.8%
	TAc(t)/TAc(t)	0.8	3.3	Cohesive	
	TAc(t)/PC	0.9	1.7	Adhesive PC	
	TAc(t)/PC(t)	1.0	2.3	Adhesive PC	
	PC(t)/ PC(t)	1.5	3.4	Cohesive	
	PC/PC	0.8	2.3	Cohesive	
IPDI-TMP-PPG-PD	TAc/TAc	0.8	1.0	Adhesive TAc	<0.8%
	TAc(t)/TAc(t)	5.3	5.7	Ply	
	TAc(t)/PC	3.7	4.9	Adhesive PC	
	TAc(t)/PC(t)	3.1	3.7	Adhesive PC	
	PC(t)/ PC(t)	3.4	4.1	Adhesive PC	
	PC/PC	2.9	3.4	Adhesive PC	

* peel 1 collected within 7 days of room temperature cure, ˣ peel 2 collected after 30 days of room temperature cure, ND = No Data

Saponification of the TAc surface was next performed (see section 2.01) to leave a regenerated cellulose surface and as displayed by previous testing this increases the compatibility between the reactivity adhesive and the substrate during cure. Deacetylation will leave hydroxyl groups at the surface which can react with the free isocyanate of the adhesive forming covalent bonds. Thus covalent bonds should form anchor points between the adhesive and substrate creating a strong interface. Peel strengths recorded following this treatment show a significant improvement while the mode of failure remains consist being adhesive at the interface.

After 7 days of cure, the peel strength recorded was 4.7 N mm^{-1} which more than doubled to 9.6 N mm^{-1} after 30 days of curing. Both measurements registered above the 3 N mm^{-1} set point which displays that the surface treatment has had the intended effect of increasing the compatibility between the adhesive and the TAc interface. The strength increase will be initially inhibited once the adhesive reaches the gel point during cure. When the matrix is above the gel point the mobility of the of both reacted hard blocks and reactive isocyanate groups will be influenced. This will in turn effect the microphase structure and ability to chemically bond with the interface.

Next the focus was moved to PC laminates, in previous testing these laminates consistently performed above benchmark following 30 days of cure. For untreated PC, the mode of failure encountered during 180° T-peel testing was adhesive at the PC interface but this was coupled with strong deformation of the PC substrate. Following 7 days of cure a peel strength of 2.9 N mm^{-1} was recorded and this increased to 3.9 N mm^{-1} after 30 days of curing. As untreated PC gives a greater peel strengths than untreated TAc, it shows that it has a better inherent compatibility with the cured adhesive. At the PC interface a greater number of H-bonding sites are available when compared to TAc and this will contribute towards the increased peel strengths obtained.

Next the surface treated PC(t)/PC(t) laminate was tested. Treatment of the PC surface was performed using an ethanolamine in isopropyl alcohol solution (see section 2.02 for procedure) to further improve the surface compatibility with the reactive adhesive. The proposed mechanism for the surface treatment of the PC is nucleophilic attack of the carbonate linkage by the amine of ethanolamine to leave a phenol and a hydroxyl terminated urethane, although the precise mechanism is not known at this time.[9] If the proposed mechanism is correct then the surface treatment should leave OH functional groups at the surface that are available for covalent bonding with the free isocyanate groups. Peel strength data collected after 7 days of cure displayed an adhesive mode of failure that was 4.8 N mm^{-1} in strength, this value increased to 6.0 N mm^{-1} after 30 days of cure. After collection of the peel strength data the PC(t) substrate also displayed signs of strong substrate deformation. Compared to untreated PC, the affinity for the surface has been increased by the surface treatment. The greater affinity

with the surface of the treated PC is based on the peel data and observed mode of failure. As the measured peel strength is significantly improved following surface treatment it would support the proposed mechanism. If free hydroxyl groups are available it will allow for the formation of covalent bonds to the interface which will increase the strength of the substrate – adhesive interface. Another possible mechanism for the improved strength is that a weak boundary layer has been removed leaving a cleaner and more accessible surface for bonding.

Finally to determine which substrate was most compatible with the current formulation hybrid laminates were tested. First tested was TAc(t)/PC which displayed an adhesive mode of failure at the PC interface. For 7 days of curing, the peel strength was 6.5 N mm^{-1} and this increased following 30 days of cure to 7.7 N mm^{-1}. Next the fully treated hybrid was tested (TAc(t)/PC(t)) and it also displayed an adhesive mode of failure at the PC interface. After 7 days of cure, a peel strength of 3.8 N mm^{-1} was recorded and following 30 days of cure the strength further improved to 4.4 N mm^{-1}. These two laminate combinations display that TAc(t) forms a stronger interface with the adhesive than PC or PC(t). Encouragingly the strength at which the PC or PC(t) interface fails is still above the set benchmark. Considering all the data collected for this current formulation, the substrate interfaces can be ranked as TAc(t) > PC(t) or PC > TAc. Once fully cured the adhesive displayed an exceptionally low haze value with the average value for the six laminates being < 0.3%.

5.26 ATR of Peeled Samples

Due to the varying peel strengths obtained it was essential to characterise if (a) the adhesive after 30 days was fully cured and (b) if once cured was the bulk adhesive the same final material. To investigate the bulk material ATR was used as it is a non-destructive way to sample the adhesive. ATR was carried out on the six different laminates once they had been peeled after 30 days of curing. The purpose of this analysis was to characterise the bulk material following 30 days of cure and to identify if there was any residual free isocyanate following this period of cure.

Figure 5.08: ATR spectra of cured IPDI-TMP-PPG sampled in-situ after peel testing with inset expanded carbonyl region. [TAc/TAc in black, TAc(t)/TAc(t) in red, TAc(t)/PC in blue, TAc(t)/PC(t) in pink, PC(t)/PC(t) in green and PC/PC in orange. Data collected for each laminate at nine random positions with each spectrum consisting of 128 scans at 8 cm^{-1} resolution. These were then averaged and plotted as the above spectra].

The spectra collected from the in-situ characterisation of the cured adhesive are shown within figure 5.08 with the spectra for all six laminates displayed. All characteristic peaks for the fully cured PU-U are shown within table 5.03.

Observation of the band positioned at 3341 cm^{-1} displays that H-bonds involving **NH** groups are present within the network. Possible domains where H-bonding would occur are between urea or urethane groups in the formation of hard-segments or with soft-segment chains when the two domains are intermixed. Also evident are **N-H** stretching vibrations that are not involved within the H-bonded network as shown by the shoulder to the previous peak at around ~3500 cm^{-1}. Next aliphatic **C-H** stretching vibrations from PPG are present with the methyl group stretching at 2981 cm^{-1} followed by both the asymmetric and symmetric bands at 2960 cm^{-1} and 2865 cm^{-1}

respectively. No detectable isocyanate peak was visible between 2260 cm^{-1} – 2280 cm^{-1} which displays that the adhesive is fully cured after 30 days.

Next the carbonyl region of the spectrum will be investigated to determine if any further morphological information on the adhesive can be observed. From the position of the carbonyl peak, the order (or disorder) of hard-segment domains can be interpreted complete with the functional groups responsible. From the position of the carbonyl at 1715 cm^{-1} it is clear that urethane groups are part of ordered domain as it confirms H-bonding (will be discussed within chapter 8). It would be expected that H-bonds within hard-segment will account for the shift of the carbonyls position as a free urethane carbonyl would appear around 1740 cm^{-1} – 1730 cm^{-1}.[8,10]

Also within the carbonyl region there appears to be three different kinds of urea formed during the moisture cure of the free isocyanate groups (see inset expanded carbonyl region in figure 5.08). First encountered at 1699 cm^{-1} is the carbonyl peak of free or unordered urea possible residing in areas of the soft-segment.[10] Evidence of monodentate H-bonded urea within the cured adhesive is visible by the broad shoulder attached to the previous peak between 1675 cm^{-1} – 1660 cm^{-1}.[8] Finally evidence of fully ordered bidentate urea groups are observed by the carbonyl peak at 1648 cm^{-1}. From the urea region alone it is clear that there are regions of high order, low order and regions of disorder. The ordered regions will contribute to the strength of the cured matrix through the formation of cross-links within hard-segments, whereas the disordered region will contribute towards phase mixing of the cured adhesive and reduce haze.

Table 5.03: Characteristic peaks of IPDI-TMP-PPG cured PU-U adhesive from all six laminate combinations.

Wavenumber (cm^{-1})	Vibration	Wavenumber (cm^{-1})	Vibration
3341	N-H stretching Hbonded	1340	C-N Urea
2981	C-H stretching	1307	C-N Urethane

2934	C-H asymmetric stretch	1231	Asymmetric N-CO-O, C-H aliphatic skeleton
2876	C-H symmetric stretch	1093	C-O-C stretch aliphatic ether
1715	C=O stretch Urethane Hbonded	1016	Symmetric N-CO-O
1699	C=O stretch free Urea	932	C-O-C stretch aliphatic ether
1648	C=O stretch Urea Bidentate Hbonded	866	C-C skeleton vibration
1530	C-N stretch, N-H bend	833	C-C skeleton vibration
1463	C-H bend aliphatic		
1378	C-H methyl deformation	775	C-C skeleton rocking

Further bands of urethane and urea formation are evident with in the spectrum. At 1530 cm^{-1} both **C-N** stretching and **N-H** stretching can be observed from either urethane or urea. Adjacent to this peak are **C-H** bending vibrations inherent of the aliphatic nature of the IPDI and PPG based formulation. Methyl **C-H** deformation are visible at 1378 cm^{-1} from the soft-segment PPG. Evidence of urea within the finger print region is shown by the C-N stretching vibration at 1340 cm^{-1}, with the urethane also shown at 1307 cm^{-1}. Further urethane vibrations within the spectrum display the asymmetric and symmetric **N-CO-O** stretching vibrations at 1231 cm^{-1} and 1016 cm^{-1} respectively. Aliphatic ether **C-O-C** stretching vibrations of the PPG soft-segment are present at 1093 cm^{-1} and 932 cm^{-1}. The final absorption peaks within the spectrum are **C-C** skeleton vibrations at 866 cm^{-1} and 833 cm^{-1} with the final peak at 775 cm^{-1} corresponding to the **C-C** skeleton rocking.

ATR analysis has displayed that following 30 of days of moisture cure (at room temperature), the adhesive is fully cured. In keeping with previous analysis, the fully cured adhesive was shown to be a PU-U with urethane formed during synthesis and the urea formed during subsequent moisture cure. As the material is fully cured it confirms that the mode of failure recorded during T-peel testing is a result of it being the weakest part of the laminate.

5.27 Summary of IPDI-TMP-PPG Formulation

From the above analysis it can be confirmed from both ^{1}H and ^{13}C NMR that the end-capped polyurethane prepolymer was successfully synthesised. This was further confirmed by MALDI-MS analysis which also highlighted that there was unreacted polyol, mono end-capped polyurethanes and a higher molecular weight distribution that consisted of IPDI-PPG-IPDI-PPG-IPDI structured molecules. MALDI displayed an increase in Mn, Mw and PDI compared to PPG.

Thermal analysis performed using DSC displayed that the prepolymer material had a $T_g$ss of -49°C which is a shift of +14°C compared to the PPG soft-segment. Following moisture cure, the $T_g$ss of the cured adhesive shifted to -33°C for the first heating cycle and was -33°C for the second heating cycle. This shift to higher temperature, displays that following cure the affinity of the hard and soft-segments have increased, resulting in greater phase mixing. The increase in $T_g$ss will also be influenced by the increased viscosity of the fully cured system and any cross-linking. Of greater significance is that the final $T_g$ss of the fully cured adhesive was out with the processing window. Also observed was a melting endotherm characteristic of the breakdown of hard-segments, displaying that there is also a degree of phase separation within the adhesives morphology. The thermal stability following moisture cure of the cured adhesive was evaluated using TGA which displayed an onset of degradation at 250°C with the peak rate occurring at 339°C.

Analysis carried out using 180° T-peel testing displayed that the best laminate combination was TAc(t)/TAc(t) which boasted a peel strength of 9.6 N mm^{-1} following 30 days of cure. The worst laminate was TAc/TAc, which registered a peel strength of 0.9 N mm^{-1} after 30 day of cure which is one tenth of the treated TAc laminate. PC

based laminates also performed well, with every combination involving PC or PC(t) giving a peel strength above the 3 N mm^{-1} benchmark. Finally ATR analysis displayed that following 30 days of curing, the adhesive was fully cured and was a PU-U. It also displayed that ordered regions were present as shown by the H-bonding in **N-H** and **C=O** stretching of urethane and urea. Also highlighted was that there are regions of free urea absent of any H-bonding. These groups may result due to greater disorder observed within the hard-segments which has removed the opportunity for H-bonding.

5.30 Analysis of IPDI-TMP-PPG-DEPD

5.31 Synthesis Information

IPDI-TMP-PPG-DEPD was next synthesised with the intention of disrupting the close packing of hard-segment through using a less conventional chain-extender which should aid with phase mixing of the different domains. This was achieved by firstly synthesising the IPDI-TMP-PPG prepolymer using the same reaction conditions as detailed with section 5.21 and then performing an addition reaction set. The additional step was performed by adding a hydroxyl terminated chain-extender using a 2.2:1.0 isocyanate:hydroxyl ratio based on the calculated amount of free NCO remaining after step one. The chain-extension step was used to lower the free isocyanate content of the adhesive, which would reduce the opportunity for excessive bubbling by CO_2 liberation from urea formation during cure.

Step one was performed as previously detailed in section 5.21 with the exception of the reaction time which was seven hours. A clear liquid which had an observed increase in viscosity from the starting mixture was observed. After addition of 2,2diethyl-1,3-propane diol (DEPD), the reaction was allowed to stir at 85°C – 95°C for seventeen hours before the dual DBTDL and TEA catalyst system was added. Following chain-extension a visual increase in viscosity was observed and was associated with the molecular weight increase caused by the coupling step. The viscosity of the system was low enough that it did not require the temperature to be increased before transfer. Once the reaction was complete, the material was poured into an aluminium tube, which was then capped and degassed as previously outlined in section 2.03. The desiccator containing the adhesive filled tube was then placed

within a 0°C fridge for storage. Degassing was performed for six hours once a vacuum of one atmosphere was obtained. Samples of the reaction were again taken before catalysed addition, these were analysed by DSC, NMR and MALDI-MS analysis.

IPDI-TMP-PPG-DEPD was heated to 95°C before being applied to six laminates which are cured at room temperature. These samples were 180° T-peel tested at 7 days and 30 days to determine the peel strength. A further lamination was performed using two plies of TAc which would allow for the fully cured adhesive to be removed for analysis by DSC and TGA. The 30 day peel test samples were also analysed by ATR to characterise the final adhesive and determine the extent of cure.

Analysis of the chain-extended material only will be presented within the remaining sections of this chapter. IPDI-TMP-PPG (sections 5.21-5.26) is considered as representative of the reactive intermediate obtained after step one of each chainextended reaction.

5.32 NMR Analysis

For full spectral characterisation of peaks from IPDI and PPG see section 5.22 (or table 5.04) as this section will only detail peaks that show prepolymer formation or peaks from the chain-extender.

Previous analysis displayed that the synthetic procedure used is not selective towards either the primary or secondary isocyanate. During the chain-extension step there will be both isocyanate groups available for reaction with the primary hydroxyl groups of DEPD. Reaction of methylene protons **16'** is shown by the shift of the peak from 3.39 ppm to 3.94 ppm. Also evident are protons of the adjacent methylene groups of PPG formed during step one of synthesis at 3.79 ppm. Methylene protons **17'** within the ethyl side group are visible at 1.67 ppm and the methyl protons **18'** are visible at 0.83 ppm.
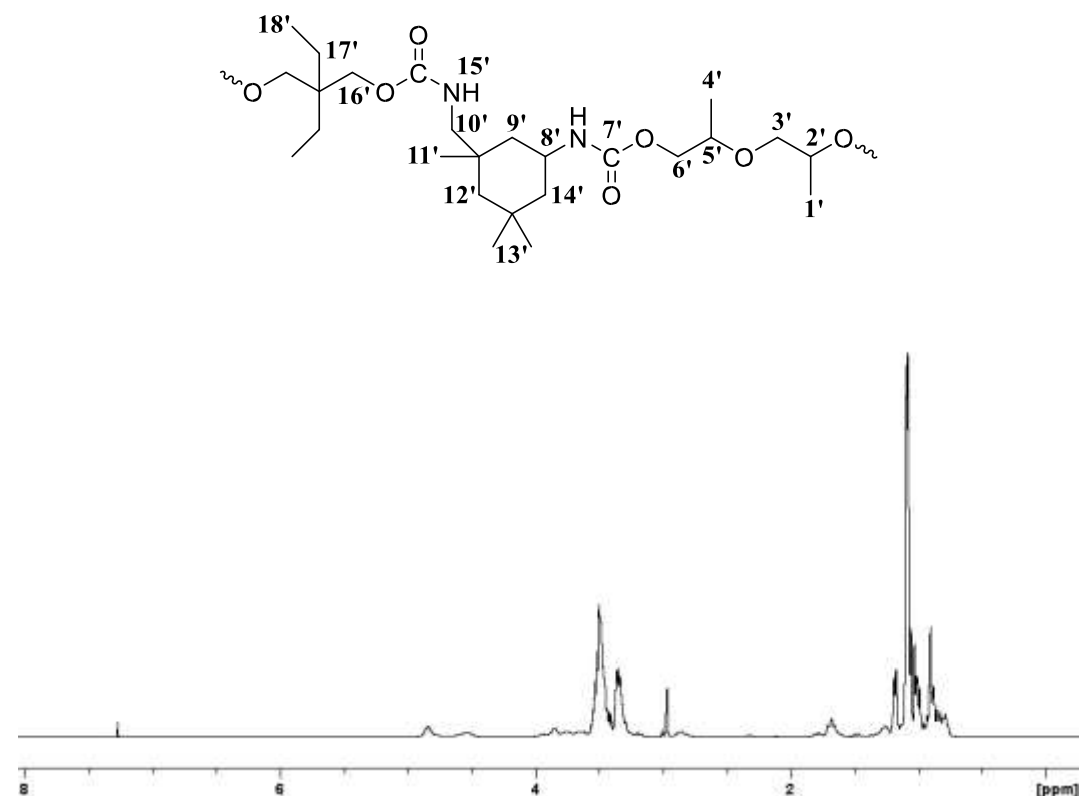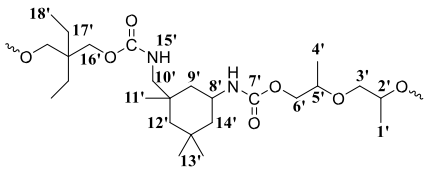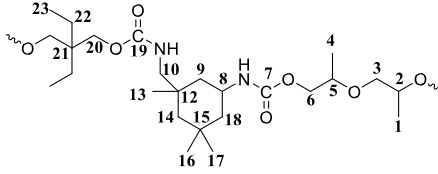
Figure 5.09: **¹H NMR spectrum obtained following reaction of IPDI-TMP-PPG with DEPD.**

Evidence of the chain-extenders incorporation into the prepolymer molecule was also observed by ¹³C NMR analysis. Methyl carbons **23** of the ethyl side group are observed at 7.2 ppm and the methylene carbons **22** of this group are visible at 23 ppm. Next the tertiary carbon **21** of DEPD appears at 39 ppm and the adjacent methylene group **19** appears at 66 ppm. Carbon peaks that correspond to the end groups within PPG are observed at 71 ppm for the methylene carbons (primary) and 72 ppm for the methine carbons (secondary). Also present are the peaks which correspond to the carbonyl of reactive isocyanate groups that still remain within the prepolymer formulation with primary group observed at 123 ppm and secondary at 122 ppm. Finally peaks which display the carbonyl within urethane groups appear at 156 ppm for a primary isocyanate within the urethane and 157 ppm for urethanes formed with secondary isocyanates.

Table 5.04: **¹H and ¹³C chemical shift for IPDI-TMP-PPG-DEPD collected in CDCl₃.**

IPDI-TMP-PPG-DEPD	Position	^{1}H Chemical Shift (ppm)	Position	^{13}C Chemical Shift (ppm)
	1'	1.21	1	17.5
	2'	3.61	2	75.7
	3'	3.23	3	73.5
	4'	1.21	4	17.5
	5'	3.98	5	72.1
	6'	4.10	6	70.1
	7'	NDT	7	156.6p/155.4s
	8'	3.54	8	42.6
	9'	1.41/1.71	9	43.5
	10'	3.00/3.21	10	56.9
	11'	0.94	11	123p/122s
	12'	1.09/1.30	12	18.6
	13'	0.91	13	23.4
	14'	1.39/1.68	14	48.7
	15'	NDT	15	23.2
	16'	3.84	16	27.1
	17'	1.68	17	31.7
	18'	0.83	18	46.7
			19	156.6p/154.4s

		20	66
		21	39
		22	23
		23	7.2

p = primary, s = secondary, NDT = not detected
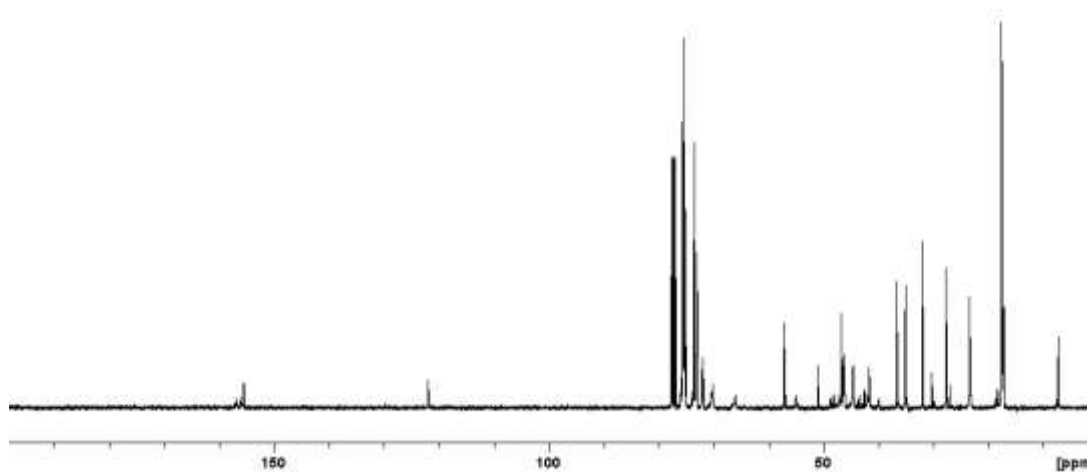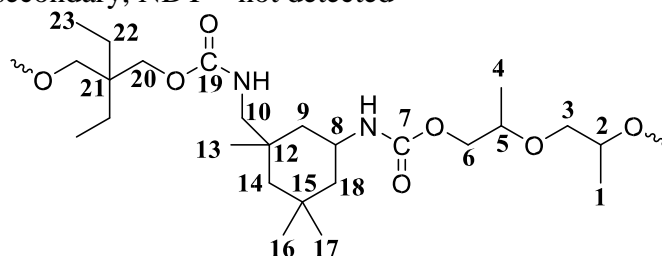
Figure 5.10: ^{13}C NMR spectrum obtained following reaction of MDI-TMP-PPG with DEPD.

5.33 MALDI-MS Analysis

To determine the molecular weight increase within the chain-extended prepolymer MALDI-MS was used. The matrix used for analysis was dithranol which contained a cationising agent NaTFA (see section 3.23 for more matrix information). A 40 mg ml⁻¹ solution of IPDI-TMP-PPG-DEPD was prepared in THF and mixed with the matrix (1:8 sample:matrix). 1 μl portions of this sample were then spotted and dried for analysis.

The peak situated at 691 m/z corresponds to the chain-extender DEPD coupled with two ethanol end-capped IPDI units and one sodium cation. Also present is the

chainextender TMP that has reacted with three IPDI unit which are in this sample also ethanol end-capped at 961 m/z (plus a sodium cation). Identification of these end capped molecules confirms that both TMP and DEPD will be involved in the hardsegments which upon cure will have an influence on the hard-segments packing arrangement.

Mn, Mw and PDI were calculated from the MALDI-MS spectrum to determine the influence that chain extension with DEPD has on the mass distribution. Diol chainextension results in an increase to all three of these parameters. Mn is calculated at 2032 m/z and Mw is calculated at 2526 m/z giving a PDI of 1.24. Using DEPD as the chain-extender has shifted and broadened the mass distribution.
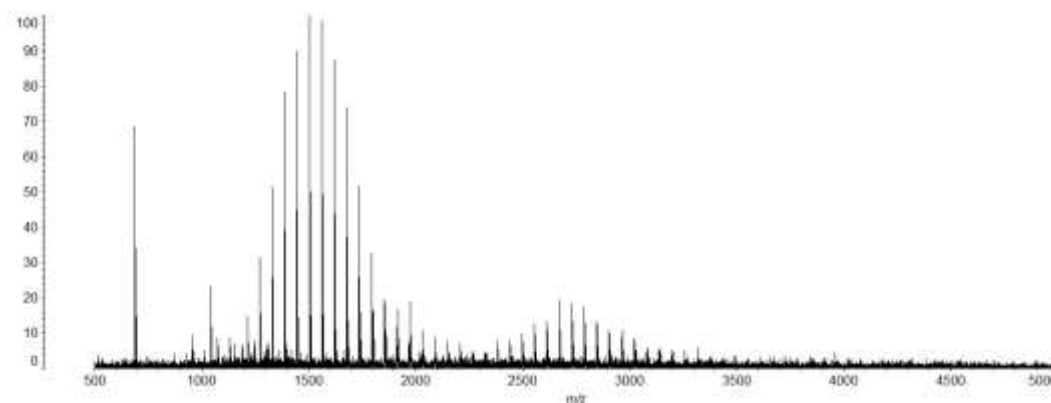
Figure 5.11: MALDI-MS spectrum of IPDI-TMP-PPG-DEPD chain-extended prepolymer collected in dithranol/NaTFA.

The most intense distribution centred at 1573 m/z corresponds to the PPG softsegment that is isocyanate end-capped (IPDI-PPG-IPDI). Prepolymers of this type are formed during step one of the synthetic process and a contribution of this prepolymer would be expected to remain. The next molecular weight distribution centred at 2780 m/z is a prepolymer of IPDI-PPG-IPDI-PPG-IPDI and is also produced during the first step of synthesis. A final mass distribution is visible, however it is very weak. This distribution corresponds to the chain-extended prepolymer and is centred around 4025 m/z. Identification of chain-extended prepolymers would be expected based on the synthetic procedure adopted coupled with previous NMR analysis. To obtain better signal to noise in this upper region of the mass spectrum may require altering the matrix recipe or a new matrix all together. Finally it must be noted that the size of the peaks

in MALDI-MS should not be mistaken as being a quantitative measurement and only serves to show that each polymer is present.

5.34 DSC and TGA Analysis

Following synthesis of the chain-extended prepolymer, the thermal characteristics of the formulation were investigated to determine the $T_g$ss (and any other physical processes occurring). As previously mentioned the $T_g$ss of the material was considered important as it had to be lower than -20°C to be suitable for the intended laminate application. Within figure 5.12 the DSC thermogram for the DEPD chainextended prepolymer is displayed. Analysis of the thermogram obtained for the chain-extended prepolymer (IPDI-TMP-PPG-DEPD) results in a $T_g$ss of -32°C which cover a broadened range of -36°C to -22°C. A shift in the $T_g$ss of +31°C can be observed compared of the unreacted PPG soft-segment and +13°C with reference to the base prepolymer (IPDI-TMP-PPG). Such a significant shift of the $T_g$ss would suggest that the polymer has increased in molecular weight, has a degree of crosslinking or has mixing of the hard and soft-segments. Also observed was an exothermic peak at 153°C with an enthalpy of 54 J g^{-1} from the curing of free isocyanate molecules via isocyanate based reactions as the system is moisture free.

Figure 5.12:   DSC thermogram of IPDI-TMP-PPG-DEPD chain-extended prepolymer formulation.

Following 30 day of curing a portion of the adhesive was removed from the TAc/TAc laminate for DSC analysis. The adhesive was analysed using a cool-heatcool-reheat experiment to determine the final $T_g$ss within each heating cycle as shown in figure 5.13 (same experiment procedure as detail in section 5.24). A broad $T_g$ss which observed at -30°C with the thermal transition covering a range of 32°C from -41°C to -23°C. After a second heating cycle, the $T_g$ss was recorded at -28°C and covered a broad range from -41°C to -16°C. Going by the $T_g$ss value alone the laminates are out with the -20°C set point, however, the range of the $T_g$ss goes +4°C inside the processing window. At the extreme limit of -20°C the adhesive will not perform as expected due the adhesive still going through its glass transition and this will have a direct effect on the flexibility of the adhesive. Observed on the second heating cycle was a melting endotherm corresponding to hard domains within the microstructure at 202°C.

285
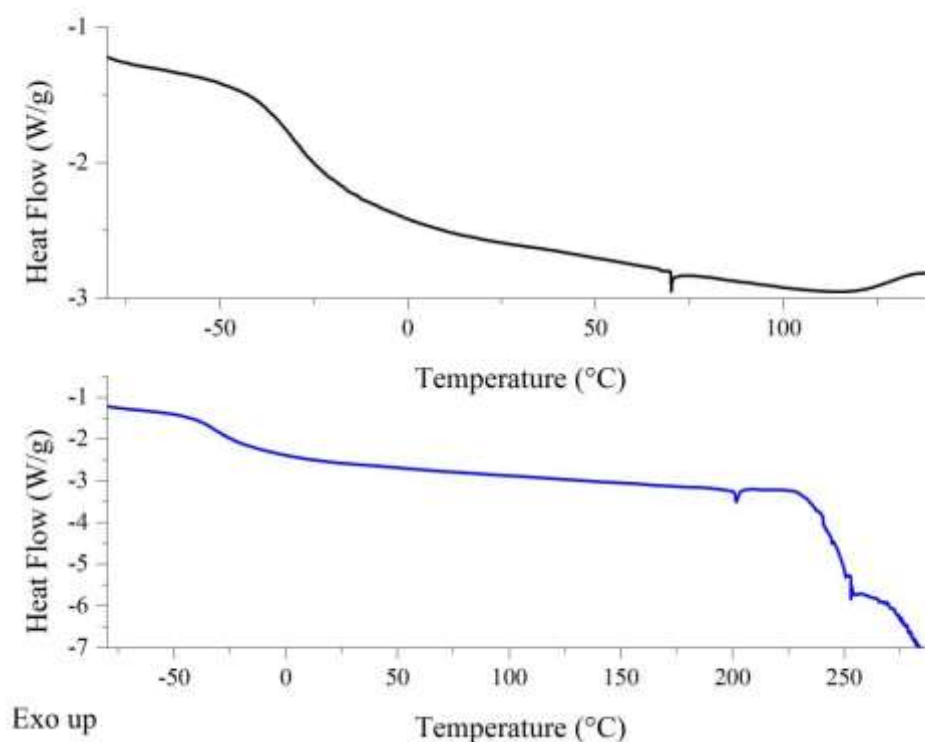
Figure 5.13: DSC thermogram of fully cured IPDI-TMP-PPG-DEPD adhesive, following removal from TAc/TAc laminate. [First heating cycle *top* in black and second heating cycle *bottom* in blue].

The enthalpy of this peak is very weak at 0.01 J g^{-1}, however, this is expected for polyurethanes which contain TMP within the hard-segment.[11] From DSC of the fully cured adhesive it was observed that the $T_g$ss range has been shifted to within the processing window (discussion of the morphology will be presented within chapter 8).
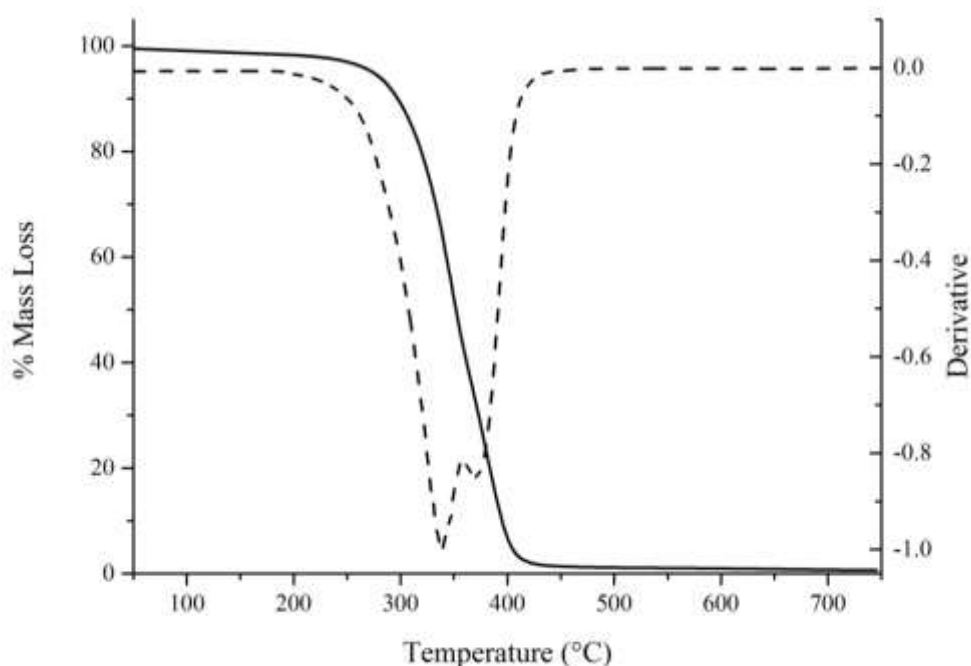
Figure 5.14: TGA and DTG curves of fully cured IPDI-TMP-PPG-DEPD adhesive. [TGA solid line and DTG dashed line].

Following moisture cure TGA was carried out to determine if chain-extension with DEPD had any effect on the overall thermal stability. Within figure 5.14 the TGA and DTG curves for the fully cured adhesive are displayed. From the TGA curve the onset of degradation was calculated to be 275°C which is 25°C higher than the base prepolymer (IPDI-TMP-PPG).   This slight increase was not considered to be significant. The previous comment is reinforced by inspection of the DTG curve which displayed that the maximum rate of degradation occurs at 338°C (IPDI-TMPPPG occurred at 339°C). Thermal cleavage of both urethane and urea hard-segment bonds within the hard block are the primary degradation pathway.[7,8] A second degradation

peak at 372°C is also observed within the DTG curve which displays the breakdown of the soft-segment PPG.[5]

From the TGA data collected it is apparent that the thermal stability of the chainextended adhesive was comparable to the previous formulation (IPDI-TMP-PPG) and that the onset of degradation is well outside the processing temperature of the laminate.

5.35 180° T-peel Test and Haze

The influence of chain-extension by DEPD on the performance as an adhesive was next tested using 180° T-peel testing. For the previous formulation which is absent of chain-extender, it was established that untreated TAc performs poorly, however, every other laminate (TAc(t), PC or PC(t) based) performed above 3 N mm^{-1}. Following 7 days of moisture cure, the observed mode of failure for TAc/TAc was adhesive at the TAc interface, the failure was very unstable and of low strength (0.83 N mm^{-1}). Following 30 days of cure, the peel strength had not change significantly and was recorded at 0.7 N mm^{-1}, again the mode of failure was adhesive at the TAc interface. As was observed in all previous formulation TAc/TAc performs very poorly and is well outside the 3 N mm^{-1} target peel strength following 30 days of cure.

Highlighted in previous formulations was that saponification of the TAc interface was essential to obtain a high peel strength. Data collected using the fully cured adhesive of formulation IPDI-TMP-PPG-DEPD was consistent with all previous analysis. Following 7 days of moisture cure, the peel strength recorded was 8.2 N mm^{-1} which decreased to 6.6 N mm^{-1} after 30 days of curing. Unlike previous analysis the mode of failure was cohesive within the adhesive layer (MDI-TMP-PPG exception), all other tests fail adhesively at TAc(t) interface. Also accompanying the cohesive failure was strong ply deformation and for one sample a cohesive failure of the TAc(t) substrate. Data collected from this cured adhesive further confirms that saponification is essential for high peel strength.

Further investigation of the effect that chain-extension has on the peel strength was now extended to PC laminates. In previous MDI based formulations, PC performed the best and for MDI-TMP-PCD a peel strength of around 8 N mm^{-1} was reached.

Table 5.05: Peel, haze and mode of failure data for IPDI-TMP-PPG-DEPD cured PU-U adhesive. [The data in bold will be discussed within this section].

Cured Adhesive	Laminate	Peel 1* (N mm^{-1})	Peel 2^x (N mm^{-1})	Failure mode	Haze (%)
IPDI-TMP-PPG	TAc/TAc	0.8	0.9	Adhesive TAc	<0.3%
	TAc(t)/TAc(t)	4.7	9.6	Adhesive TAc	
	TAc(t)/PC	6.5	7.7	Adhesive PC	
	TAc(t)/PC(t)	3.8	4.4	Adhesive PC	
	PC(t)/ PC(t)	4.8	6.0	Adhesive PC	
	PC/PC	3.0	3.9	Adhesive PC	
IPDI-TMP-PPG-DEPD	**TAc/TAc**	**0.8**	**0.7**	**Adhesive TAc**	**<0.5%**
	TAc(t)/TAc(t)	**8.2**	**6.6**	**Cohesive**	
	TAc(t)/PC	**5.0**	**3.8**	**Adhesive PC**	
	TAc(t)/PC(t)	**4.1**	**3.3**	**Adhesive PC**	
	PC(t)/ PC(t)	**6.1**	**5.9**	**Adhesive PC**	
	PC/PC	**4.7**	**3.2**	**Adhesive PC**	
IPDI-TMP-PPG-BD	**TAc/TAc**	0.6	0.8	Adhesive TAc	<0.8%
	TAc(t)/TAc(t)	0.8	3.3	Cohesive	
	TAc(t)/PC	0.9	1.7	Adhesive PC	
	TAc(t)/PC(t)	1.0	2.3	Adhesive PC	
	PC(t)/ PC(t)	1.5	3.4	Cohesive	
	PC/PC	0.8	2.3	Cohesive	
IPDI-TMP-PPG-PD	**TAc/TAc**	0.8	1.0	Adhesive TAc	<0.8%
	TAc(t)/TAc(t)	5.3	5.7	Ply	
	TAc(t)/PC	3.7	4.9	Adhesive PC	
	TAc(t)/PC(t)	3.1	3.7	Adhesive PC	
	PC(t)/ PC(t)	3.4	4.1	Adhesive PC	
	PC/PC	2.9	3.4	Adhesive PC	

Switching to an aliphatic isocyanate will forfeit the potential for π-π stacking between the hard blocks within the hard domains, potentially lowering the interdomain adhesion.[12] Removing the aromatic functional groups also has the potential to affect the adsorption chemistry at the PC interface.

Peel strength data acquired following 7 days of cure on PC was 4.7 N mm^{-1}, a slight reduction to 3.2 N mm^{-1} was observed after 30 days. Both experiments displayed an adhesive mode of failure at the interface and strong deformation of the PC substrate. These strength values collected using this current formulation are above benchmark and display that high strength can still be obtained when π-π interactions are absent.

Treatment of the PC interface was performed and the peel strength measured. After 7 days of cure, the peel strength of the fully treated PC(t) laminate was 6.1 N mm^{-1} which depreciated to 5.9 N mm^{-1} after 30 days. An adhesive mode of failure at the interface was recorded for both experiments and was accompanied by strong deformation of the substrate. Following PC surface treatment an increase in the overall peel strength is observed and supports the treatment mechanism which promotes the formation of covalent bonds to the substrate.

Analysis thus far has identified that the adhesive has an affinity for the treated TAc(t) interface over either PC or PC(t). In order to support this hypothesis, hydride laminates were next tested at they would display the weakest interface or component of the laminate. Discussed first is the laminate of composition TAc(t)/PC which recorded a peel strength of 5.0 N mm^{-1} following 7 days and 3.8 N mm^{-1} after 30 days of cure. Strong deformation of both substrate plies was observed, coupled with an adhesive mode of failure at the PC interface. For the fully treated laminate a 7 day peel strength of 4.1 N mm^{-1} was recorded which reduced to 3.4 N mm^{-1} after 30 days. Again strong deformation of both substrates was observed and the mode of failure recorded was adhesive at the PC(t) interface. Both experiments have identified that the PC interface is weakest as both have adhesive failure modes at the interface. It was also noted that each laminate combination performed above the set 3 N mm^{-1} benchmark.

Finally the overall haze for the fully cured adhesive across all six laminates was < 0.5%. Such low haze displays that chain-extension has minimal effect on the haze. This is in agreement with the previous adhesive (formulation IPDI-TMP-PPG) which was free of chain-extender and also displayed a low haze value of < 0.3%. *5.36 ATR of Peeled Samples*
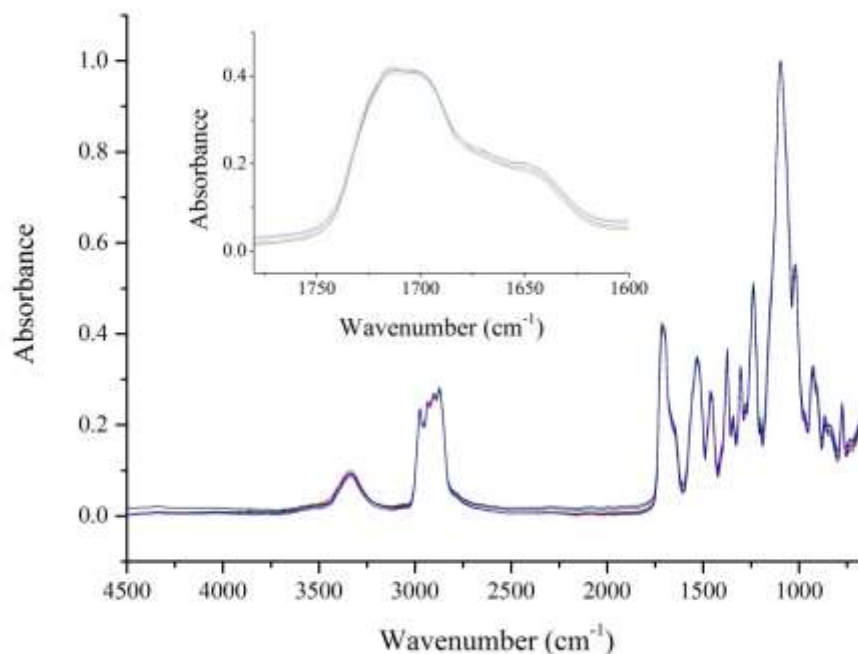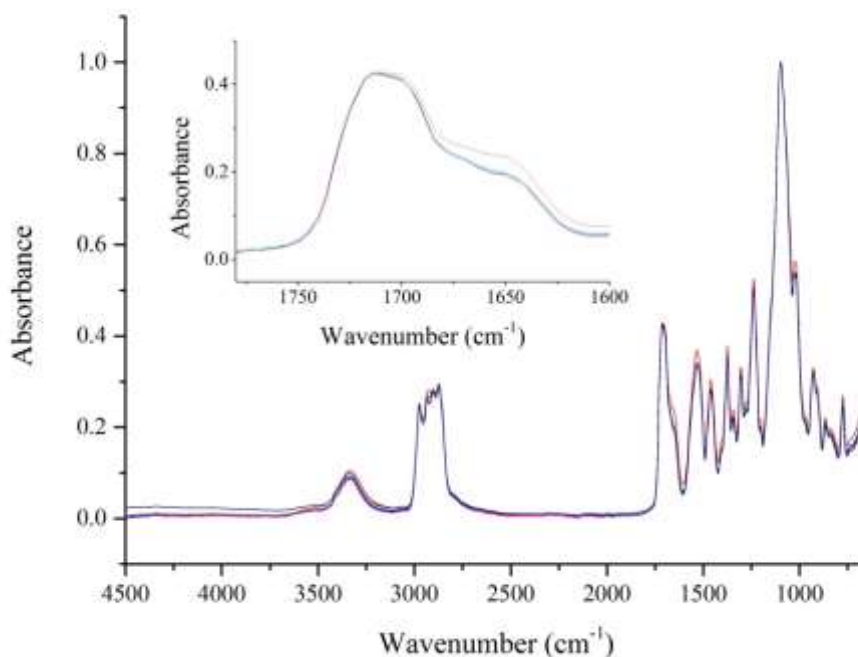

Figure 5.15: ATR spectra of cured IPDI-TMP-PPG-DEPD sampled in-situ after tensile testing with inset expanded carbonyl region. [TAc/TAc in black, TAc(t)/TAc(t) in red, TAc(t)/PC in blue, TAc(t)/PC(t) in pink, PC(t)/PC(t) in green and PC/PC in orange. Data collected for each laminate at nine random positions with each spectrum consisting of 128 scans at 8 cm⁻¹ resolution. These were then averaged and plotted as the above spectra].

Analysis of the bulk materials was performed on all six of the laminates after the 30 day tensile test. ATR analysis will determine the chemical functionality of the final cured material and allow for any distinct differences in curing chemistry to be observed. ATR will give some indication of the inherent morphology of the fully cured adhesive. Discussed within this section will be peaks that indicate either the

PU of the chain-extended prepolymer or PU-U peaks obtained after 30 days of cure.

For discussion of the peaks inherent of the starting materials see section 5.26 and for all characteristic peaks see table 5.06.

Table 5.06: Characteristic peaks of IPDI-TMP-PPG-DEPD cured PU-U adhesive from all six laminate combinations.

Wavenumber (cm^{-1})	Vibration	Wavenumber (cm^{-1})	Vibration
3336	N-H stretching Hbonded	1340	C-N urea
2971	C-H stretching	1307	C-N urethane
2928	C-H asymmetric stretch	1230	Asymmetric N-CO-O, C-H aliphatic skeleton
2871	C-H symmetric stretch	1102	C-O-C aliphatic ether
1710	C=O stretching urethane H-bonded	1022	Symmetric N-CO-O
1700	C=O stretch free Urea	922	C-O-C aliphatic ether
1640	C=O stretching Urea Bidentate Hbonded	870	C-C skeleton vibration
1530	C-N stretch, N-H bending	841	C-C skeleton vibration
1463	C-H bend aliphatic	775	C-C skeleton rocking
1373	C-H methyl deformation		

From the spectra present with figure 5.15 it is visible that there are two different **N-H** vibrations within the above cured PU-U. **N-H** stretching vibrations occurring at 3336 cm^{-1} show that H-bonded domains are present in the microstructure, whereas, the shoulder peak at around 3500 cm^{-1} correspond to free **N-H** stretching vibrations. The corresponding bending vibrations are visible in the fingerprint region of the spectra for

N-H at 1530 cm^{-1}, also present within this peak will be the **C-N** stretch. **C-N** bending vibrations are observed for urea at 1340 cm^{-1} and urethane at 1307 cm^1. No detectable isocyanate peak was visible between 2260 cm^{-1} – 2280 cm^{-1} which displays that the adhesive is fully cured after 30 days.

Further information on the inherent microstructure following moisture cure is available within the carbonyl region. Evidence of H-bonded urethane carbonyl stretching is visible at 1710 cm^{-1} which would indicate the formation of hardsegments within the microstructure. An immediate shoulder to this peak displays the occurrence of free urea carbonyl stretching at 1690 cm^{-1}. Further evidence of structured regions within the microstructure of the cured adhesive is shown by the bidentate H-bonded urea stretching vibration at 1640 cm^{-1}. As these peaks are beginning to convolute together it also displays that there will be proportion of monodentate urea groups which have characteristic vibrations of 1675 cm^{-1} – 1660cm^{-1}. The overall morphology observed from ATR will be discussed in greater detail within chapter 8.

5.37 Summary of IPDI-TMP-PPG-DEPD Formulation

Synthesis of the DEPD chain-extended prepolymer was followed using NMR which displayed successful synthesis. This was confirmed using MALDI-MS to characterise the molecular mass distributions present within the chain-extended prepolymer formulation. MALDI-MS identified chain-extended prepolymers, prepolymer which were absent of any chain-extension from step one and a molecular distribution that was formed during step one (IPDI-PPG-IPDI-PPG-IPDI) of a higher molecular weight. Following chain-extension with DEPD Mn, Mw and PDI increased compared to formulation MDI-TMP-PPG.

Investigation of the thermal transition by DSC recorded a $T_g$ss for the chain-extended prepolymer of -32°C which is an elevation of +32°C compared to PPG. Once fully cured the $T_g$ss was further elevated to -30°C on the first heating cycle and -28°C after the second. Although the $T_g$ss quoted is out with the processing range the thermal event was broad and finished almost +4°C inside this range. Detection of hard-segment melting was also much reduced compared to the previous formulation. The overall thermal stability was determined by TGA with the onset of degradation

occurring at 275°C. From the DTG curve visible deconvolution of the two main degradation pathways through hard and soft-segment bond breaking was visible.

Using 180° T-peel testing it was identified that untreated TAc performed very poorly (0.8 N mm^{-1}), however, following surface treatment the values performed 10 fold greater (8.2 N mm^{-1}). Laminates based on PC performed above benchmark regardless of treatment or not. From hybrid laminates it was identified that the PC or PC(t) interface was weaker than TAc(t). This is confirmed by the adhesive mode of failure at the PC interface on both these tests. Haze values recorded for the six laminates were very low at < 0.5% making the cured laminate very high clarity. Finally using ATR the adhesive material was observed to be fully cured following 30 days of curing. Also observed was that the fully cured adhesive was a PU-U and that there were H-bonding domains within the cured network.

5.40 Analysis of IPDI-TMP-PPG-BD

5.41 Synthesis Information

IPDI-TMP-PPG-BD was next synthesised with the intention of continuing the disruption of hard-segment packaging through using a less conventional chainextender which should aid with phase mixing of the different domains. This was achieved by firstly synthesising the IPDI-TMP-PPG prepolymer using the same reaction conditions as detailed with section 5.21 followed by an addition reaction set. The additional step was performed by adding a hydroxyl terminated chain-extender using a 2.2:1.0 isocyanate:hydroxyl ratio based on the calculated amount of free NCO remaining after step one. The chain-extension step was used to lower the free isocyanate content of the adhesive, which would reduce the opportunity for excessive bubbling by CO_2 liberation due to urea formation during cure.

Step one was performed as previously detailed in section 5.21 and was a clear liquid which had an observed increase in viscosity from the starting mixture. After addition of 1,3-butane diol (BD), the reaction was allowed to stir at 85°C – 95°C for seventeen hours before the dual DBTDL and TEA catalyst system was added. Following chain-extension a visual increase in viscosity was observed and was associated with the molecular weight increase caused by the coupling step. The viscosity of the system

was low enough that it did not require the temperature to be increased before transfer. Once the reaction was complete the materials was poured into an aluminium tube, which was then capped and degassed as previously outlined in section 2.03. The desiccator containing the adhesive filled tube was then placed within a 0°C fridge for storage. Degassing was performed for six hours once a vacuum of one atmosphere was obtained. Samples of the reaction were taken before catalysed addition, these were analysed by DSC, NMR and MALDI-MS analysis.

IPDI-TMP-PPG-BD was heated to 95°C before being applied to six laminates (same as section 5.31) which were cured at room temperature. These samples were 180° Tpeel tested at 7 days and 30 days to determine the peel strength. A further lamination was performed using two plies of TAc which would allow for the fully cured adhesive to be removed for analysis by DSC and TGA. The 30 day peel test samples were analysed by ATR to characterise the final adhesive and determine its extent of cure.

Analysis of the chain-extended material only will be presented within the remaining sections of this chapter. IPDI-TMP-PPG (sections 5.21-5.26) is considered as representative of the reactive intermediate obtained after step one of each chainextended reaction.

5.42 NMR Analysis

For full spectral characterisation of peaks from IPDI and PPG see section 5.22 as this section will only detail peaks that are important to show prepolymer formation or peaks from the chain-extender. Within figure 5.16, the ^{1}H spectrum of the BD chainextended prepolymer is presented in deuterated chloroform. The asymmetric chainextender molecule has both primary and secondary hydroxyl groups available for reaction with free isocyanate groups.

Urethane formation via the primary alcohol groups is visible by the position of the adjacent methylene group **16'** that have shifted from 3.80 ppm to 4.00 ppm. Also visible within the spectra are the methylene protons **17'** within BD at 1.86 ppm, however, these show no significant shift before or after reaction. Inclusion of secondary hydroxyl groups within urethane linkages are shown by the shift of the methine protons **18'** from 4.03 ppm to 4.55 ppm. The final shift from BD which

represents the methyl protons **19'** is visible at 1.27 ppm. Full ^{1}H peak assignment can be observed within table 5.07.
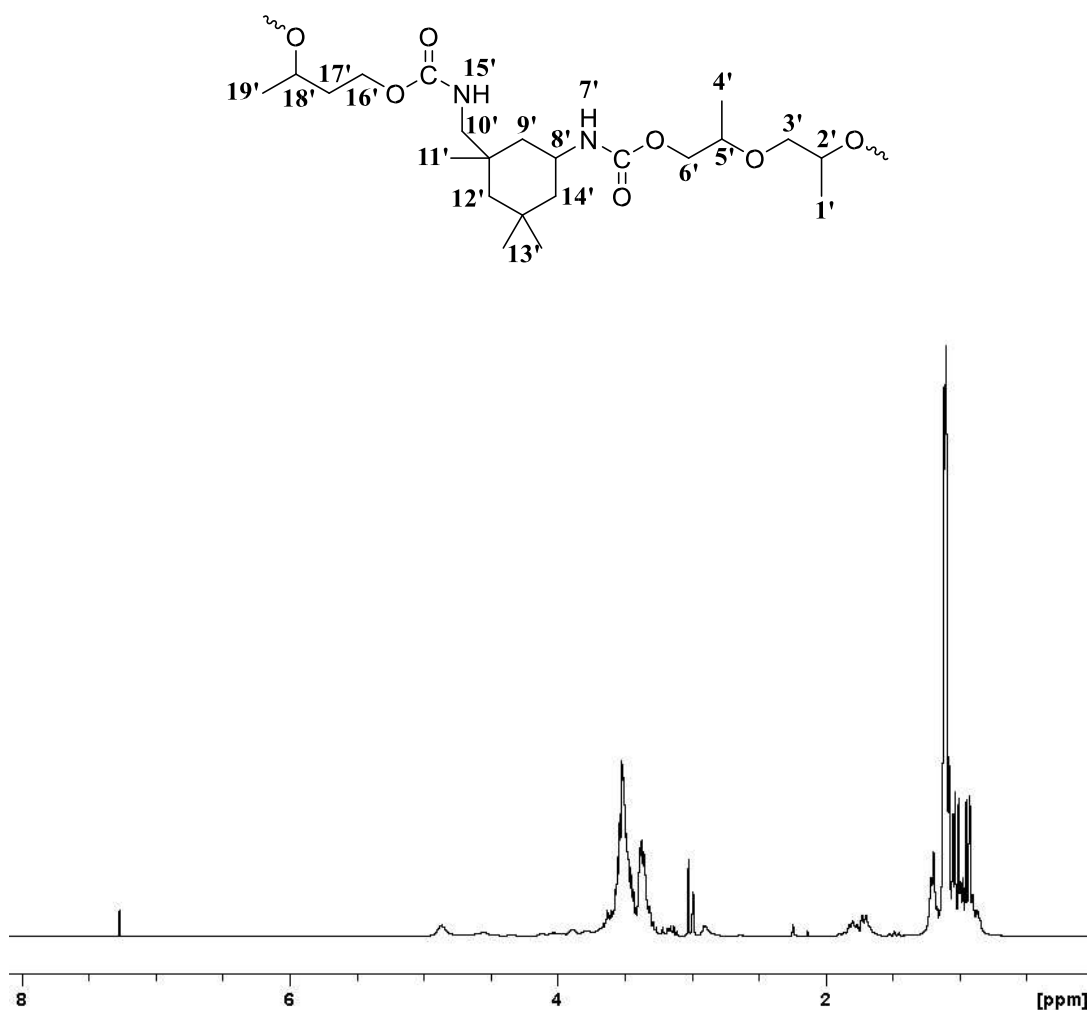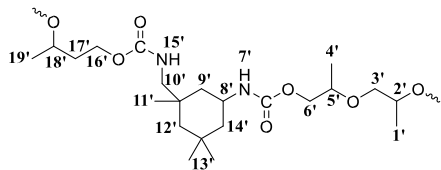
Figure 5.16: ^{1}H NMR spectrum obtained following reaction of IPDI-TMP-PPG with BD.

Further evidence that BD chain-extension has occurred, along with retention of free isocyanate groups was observed using ^{13}C NMR. Consumption of the primary hydroxyl groups within BD is confirmed by the position of the methylene carbon **20** at 56.9 ppm. Methine carbons of the secondary hydroxyl group **22** once reacted are also visible at 65 ppm. Also observed within figure 5.17 are methylene carbons **21** at 35 ppm and methyl carbons **23** at 20.8 ppm. Carbonyl shifts characteristic of urethane bonds are again visible at 156.7 ppm and 155.4 ppm following reaction of primary and secondary isocyanate groups respectively.

Table 5.07: ^{1}H and ^{13}C chemical shift for IPDI-TMP-PPG-BD collected in CDCl$_3$.

IPDI-TMP-PPG-DEPD	Position	^{1}H Chemical Shift (ppm)	Position	^{13}C Chemical Shift (ppm)
	1'	1.21	1	17.5
	2'	3.61	2	75.7
	3'	3.23	3	73.5
	4'	1.21	4	17.5
	5'	3.98	5	72.1
	6'	4.10	6	70.1
	7'	NDT	7	156.6$_p$/155.4$_s$
	8'	3.54	8	42.6
	9'	1.41/1.71	9	43.5
	10'	3.00/3.21	10	56.9
	11'	0.94	11	123$_p$/122$_s$
	12'	1.09/1.30	12	18.6
	13'	0.91	13	23.4
	14'	1.39/1.68	14	48.7
	15'	NDT	15	23.2
	16'	4.03	16	27.1
	17'	1.86	17	31.7
	18'	4.56	18	46.7
	19'	1.27	19	156.7$_p$/155.4$_s$

		20	56.9
		21	35
		22	65
		23	20.8

p = primary, s = secondary, NDT = not detected

Confirmation that the polymers within solution still contain free reactive groups can be observed by the remaining carbonyl shifts from primary and secondary isocyanate groups at 123 ppm and 122 ppm respectively.
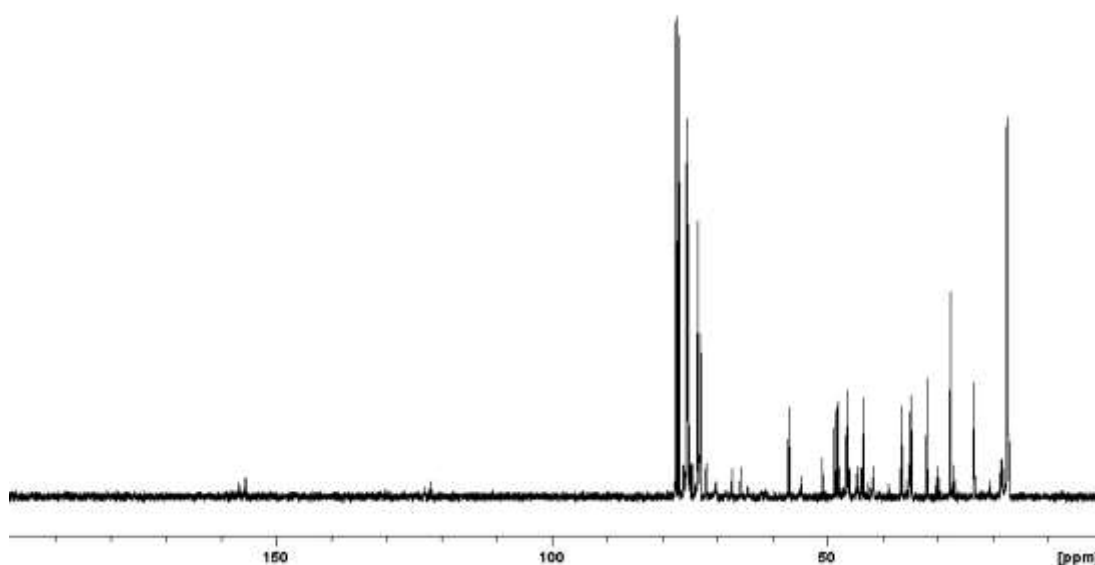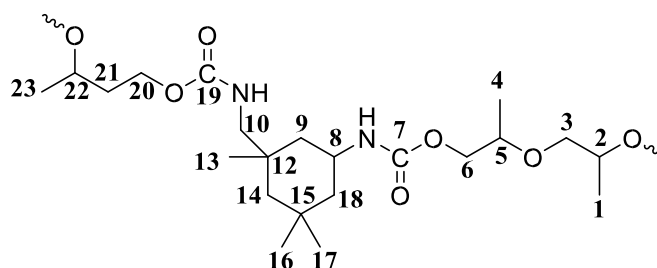
Figure 5.17: ^{13}C NMR spectrum obtained following reaction of MDI-TMP-PPG with BD.

5.43 MALDI-MS Analysis

To determine the molecular weight increase within the chain-extended prepolymer formulation MALDI-MS was used. The matrix used for analysis was dithranol which contained a cationising agent NaTFA (see section 3.23 for more matrix information). A 40 mg ml^{-1} solution of IPDI-TMP-PPG-BD was prepared in THF and mixed with

the matrix (1:8 sample:matrix). 1 µl portions of this sample were then spotted and dried for analysis.

Inspection of the MALDI-MS spectrum collected of the chain-extended prepolymer IPDI-TMP-PPG-BD was complex. Evidence of consumption of chain-extender with free IPDI can be observed by the peak at 649 m/z, which corresponds to BD coupled with two ethanol end-capped IPDI units and one sodium cation. Also present is the chain-extender TMP with three ethanol end capped IPDI units and one sodium cation at 961 m/z. Identification of these end capped molecules confirms that both TMP and BD will be involved in the hard-segments and will influence the packing arrangement. Within figure 5.18 there is also evidence of unreacted PPG.
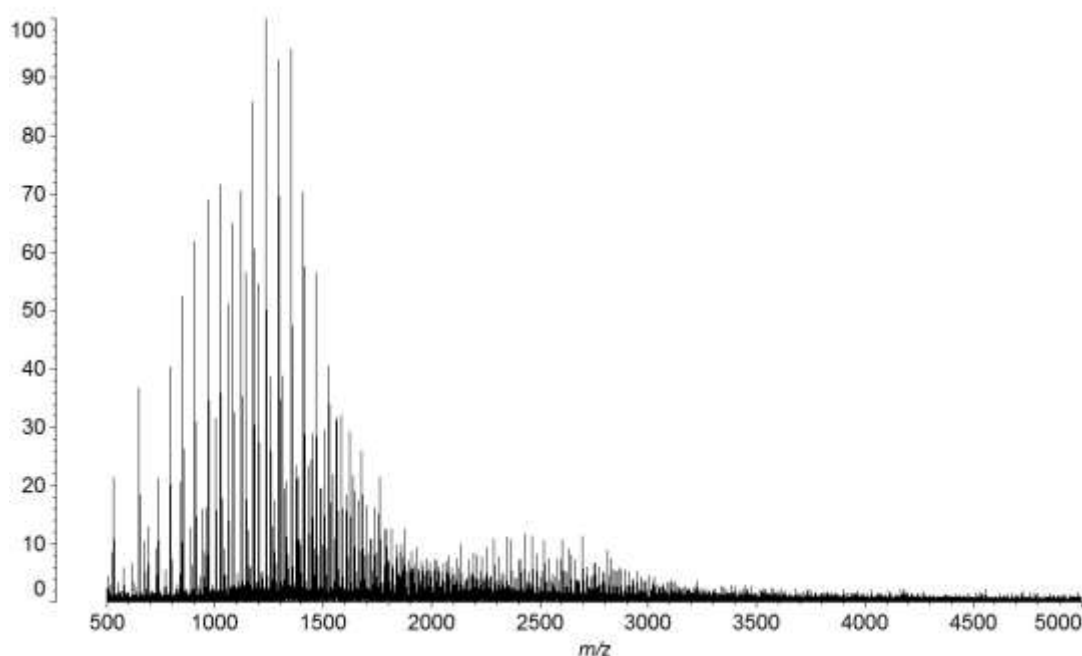
Figure 5.18: MALDI-MS spectrum of IPDI-TMP-PPG-BD chain-extended prepolymer collected in dithranol/NaTFA.

Mn, Mw and PDI were calculated from the MALDI-MS spectrum to determine the influence that chain-extension with BD has on the mass distribution. The calculated value of Mn is 1698 m/z and the calculated value of Mw is 2062 m/z giving a PDI of 1.21. Using BD as the chain-extender has reduced the shift to molecular weight distribution as shown by the lower values of Mn and Mw. This is coupled with a narrower distribution compared to IPDI-TMP-PPG-DEPD as shown by the lower PDI

value. The smaller shift in Mn and Mw compared to the DEPD chain-extended formulation may be result from BD containing both primary and secondary hydroxyl groups whereas the former only contains primary.

Following next is mono IPDI end capped polymers (IPDI-PPG) which are observed by the distribution centred on 1237 m/z. Next centred on 1471 m/z this distribution corresponds to the PPG soft-segment that has become isocyanate end-capped at both ends giving rise to prepolymers of type IPDI-PPG-IPDI. These polymers are formed during step one of the synthetic process and a contribution would be expected to remain. This region of the spectrum also displays the di-sodiated adduct of this prepolymer which is offset from this distribution by 23 m/z. Also to further complicate the spectrum there are peaks which are offset by 90 m/z from polymers that have reacted with BD but not yet coupled with another prepolymer molecule.

The next molecular weight distribution centred at 2529 m/z displays polymers of type IPDI-PPG-IPDI-PPG-IPDI, with these polymers produced during the first step of synthesis. On inspection of this region there is a further distribution offset by 23 m/z as the di-sodiated adduct is also present. A further mass distribution that is offset by 90 m/z was observed from polymer which have reacted with BD and have not yet coupled with another prepolymer (from step one).

A final mass distribution is also visible, however it is very weak. This distribution corresponds to the BD chain-extended prepolymers and is centred around 4195 m/z. Identification of chain-extended prepolymers would be expected based on the synthetic procedure adopted coupled with previous NMR analysis. To obtain better signal to noise in this upper region of the mass spectrum may require that the matrix recipe is improved or a new matrix is found all together. Finally it must be noted that the size of the peaks in MALDI-MS should not be mistaken as being a quantitative measurement and only serves to show that it is present. Also observed within this formulation was that it is possible to have both mono and di-sodiated adducts of the PU polymer within the same sample.

5.44 DSC and TGA Analysis

As previously mentioned the $T_g$ss of the material was considered important as it had to be lower than -20°C to be suitable for the intended laminate application. Within figure 5.19, the DSC thermogram for the BD chain-extended prepolymer is displayed. Analysis of the thermogram obtained for the chain-extended prepolymer shows a $T_g$ss of -54°C which covers a range of -57°C to -51°C. A shift in the $T_g$ss of +9°C can be observed compared to the unreacted PPG soft-segment. When only a small shift of the $T_g$ss is encountered it would suggest that the polymer has only slightly increased in molecular weight or is not sufficiently phased mixed. Also visible was an exothermic peak at 161°C which has an enthalpy of 81 J g^{-1}, this peak is believed to represent the curing of free isocyanate groups via isocyanate based reactions. From the data collected it was apparent that this uncured prepolymer formulation was thermally different from the previous formulation which used DEPD (see section 5.34).
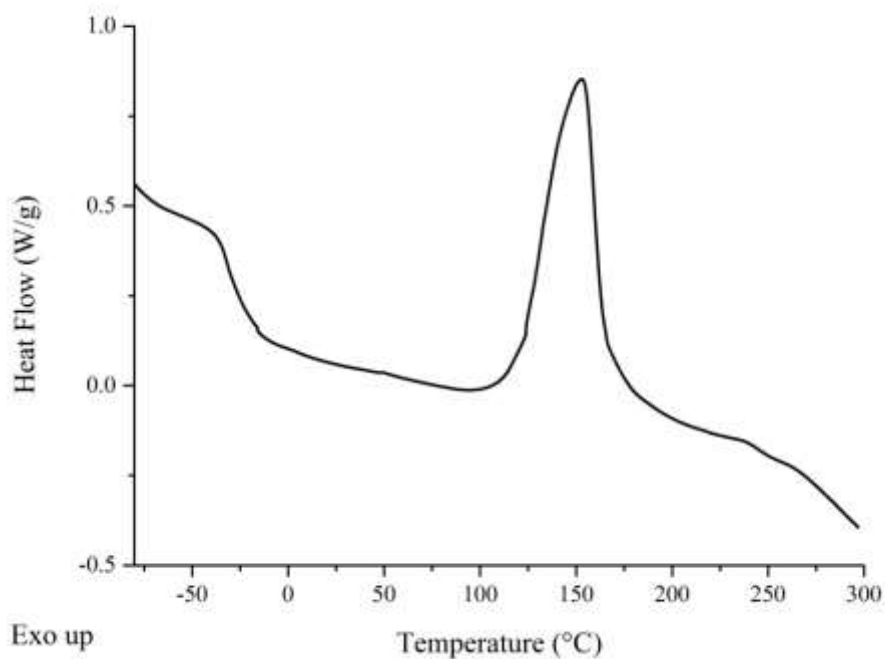

Figure 5.19: **DSC thermogram of IPDI-TMP-PPG-BD chain-extended prepolymer formulation.**

Following 30 day of curing a portion of the cured adhesive was removed from the TAc/TAc laminate for DSC analysis. The fully cured adhesive was analysed using a

cool-heat-cool-reheat experiment to determine the final $T_g$ss within each heating cycle as shown in figure 5.20 (same experiment procedure as detail in section 5.24). A broad $T_g$ss was observed at -30°C with the thermal transition covering a range of 23°C from -40°C to -17°C. After a second heating cycle, the $T_g$ss was recorded at 32°C and covered a broad range from -42°C to -21°C. Following a second heating cycle, the collected $T_g$ss has shifted by -2°C which is an indication of greater phase separation. Also evident from the second heating cycle was the absence of any melting peak of hard domains. In both heating cycles a broad $T_g$ss was recorded and in the first heating cycle this transition entered the processing window. Based on the DSC analysis of the fully cured adhesive it is apparent that the microphase morphology within this system is different from the previous two polymers within this section (discussion of the morphology will be presented within chapter 8).

Figure 5.20: DSC thermogram of fully cured IPDI-TMP-PPG-BD adhesive, following removal from TAc/TAc laminate. [First heating cycle *top* in black and second heating cycle *bottom* in blue].

TGA analysis was next performed to assess the effect that BD has on the overall thermal stability of the PU-U. Within figure 5.21, the TGA and DTG curves for the fully cured adhesive are displayed. From the TGA curve, the onset of degradation was

calculated to be 267°C which is 8°C lower than the previous formulation (IPDITMP-PPG-DEPD). This slight decrease was not considered to be significant. The previous comment is reinforced by inspection of the DTG curve which displayed that the maximum rate of degradation occurs for this first peak at 346°C (IPDI-TMPPPG-DEPD occurred at 338°C) which is similar to previous adhesives within this set.

Thermal cleavage of both urethane and urea hard-segment bonds within the adhesives microstructure are the primary degradation pathway represented by this first peak.[7,8] A second degradation peak at 375°C was also observed within the DTG curve which displays the breakdown of the soft-segment PPG.[5] From the TGA data collected it was apparent that the thermal stability of this chain-extended adhesive using BD was comparable with previous formulations within this chapter. It also further displays that PU-U adhesives based on IPDI and PPG are stable within the processing window of the laminate.

Figure 5.21: TGA and DTG curves of fully cured IPDI-TMP-PPG-BD adhesive. [TGA solid line and DTG dashed line].

5.45 180° T-peel Test and Haze

The influence of chain-extension using BD on the performance of the fully cured PU-U adhesive was next investigated using 180° T-peel testing. Following 7 days of moisture cure the observed mode of failure for TAc/TAc was adhesive at the TAc interface, the failure was very unstable and of low strength (0.6 N mm^{-1}). Following 30 days of cure, the peel strength had not changed significantly and was recorded at 0.8 N mm^{-1}, again with the mode of failure was adhesive at the TAc interface.

Table 5.08: Peel, haze and mode of failure data for IPDI-TMP-PPG-BD cured PU-U adhesive. [The data in bold will be discussed within this section].

Cured Adhesive	Laminate	Peel 1* (N mm^{-1})	Peel 2^x (N mm^{-1})	Failure mode	Haze (%)
IPDI-TMP-PPG	TAc/TAc	0.8	0.9	Adhesive TAc	<0.3%
	TAc(t)/TAc(t)	4.7	9.6	Adhesive TAc	
	TAc(t)/PC	6.5	7.7	Adhesive PC	
	TAc(t)/PC(t)	3.8	4.4	Adhesive PC	
	PC(t)/ PC(t)	4.8	6.0	Adhesive PC	
	PC/PC	3.0	3.9	Adhesive PC	
IPDI-TMP-PPG-DEPD	**TAc/TAc**	0.8	0.7	Adhesive TAc	<0.5%
	TAc(t)/TAc(t)	8.2	6.6	Cohesive	
	TAc(t)/PC	5.0	3.8	Adhesive PC	
	TAc(t)/PC(t)	4.1	3.3	Adhesive PC	
	PC(t)/ PC(t)	6.1	5.9	Adhesive PC	
	PC/PC	4.7	3.2	Adhesive PC	
IPDI-TMP-PPG-BD	**TAc/TAc**	**06**	**0.8**	**Adhesive TAc**	**<0.8 %**
	TAc(t)/TAc(t)	**0.8**	**3.3**	**Cohesive**	
	TAc(t)/PC	**0.9**	**1.7**	**Adhesive PC**	
	TAc(t)/PC(t)	**1.0**	**2.3**	**Adhesive PC**	
	PC(t)/ PC(t)	**1.5**	**3.4**	**Cohesive**	
	PC/PC	**0.8**	**2.3**	**Cohesive**	

IPDI-TMP-PPG-PD	**TAc/TAc**	0.8	1.0	Adhesive TAc	<0.8%
	TAc(t)/TAc(t)	5.3	5.7	Ply	
	TAc(t)/PC	3.7	4.9	Adhesive PC	
	TAc(t)/PC(t)	3.1	3.7	Adhesive PC	
	PC(t)/ PC(t)	3.4	4.1	Adhesive PC	
	PC/PC	2.9	3.4	Adhesive PC	

* peel 1 collected within 7 days of room temperature cure, ^x peel 2 collected after 30 days of room temperature cure, ND = No Data

As has been observed in all previous formulations, TAc/TAc performs extremely poorly and is well outside the 3 N mm⁻¹ target peel strength. Also highlighted from previous formulations was that saponification of the TAc interface was essential to obtain high peel strengths. Data collected using the fully cured adhesive of formulation IPDI-TMP-PPG-BD, is consistent but the peel strength was lower than previous adhesives due to a curing issue. Following 7 days of moisture cure the peel strength recorded was 0.8 N mm⁻¹ which increased to 3.3 N mm⁻¹ after 30 days of curing. The cohesive mode of failure observed during both tests was extremely unstable which resulted in the strength recorded being very variable. At the 7 days stage of curing, the adhesive was still very liquid like and displayed little evidence of matrix formation (matrix was gelled at this point in previous formulations). After 30 days of curing the adhesive displayed greater matrix strength and this was reflected by the strength value reacting benchmark after this time. A cohesive mode of failure was still observed after 30 days which highlight that the adhesive matrix was still weak (compared to previous formulations) as a direct result of the highlighted curing issue.

Data was next acquired for PC/PC, after 7 days of cure the peel strength recorded was 0.8 N mm⁻¹ which increased to 2.3 N mm⁻¹ after 30 days. Both experiments displayed a cohesive mode of failure in the adhesive along with large variations in peel strength. Both strength values collected are below benchmark and the low strength is attributed to the curing issue already highlighted. Treatment of the PC interface was again performed and the peel strength measured. After 7 days of cure the peel strength of the fully treated PC laminate was 1.5 N mm⁻¹ which increased to 3.4 N mm⁻¹ after 30

days. A cohesive mode of failure within the adhesive was recorded for both experiments and was accompanied again by high variation in peel strength.

Previous analysis has identified that IPDI and PPG based adhesives have an affinity for the treated TAc(t) interface over either PC or PC(t). In order to further test this conclusion hydride laminates were next tested as they would display the weakest interface or component of the laminate. Discussed first is the laminate of composition TAc(t)/PC which recorded a peel strength of 0.9 N mm^{-1} following 7 days and 1.7 N mm^{-1} after 30 days of cure. An adhesive mode of failure at the PC interface was observed and was coupled with large variations in peel strength. For the fully treated laminate a 7 day peel strength of 1.0 N mm^{-1} was recorded which increased to 2.3 N mm^{-1} after 30 days. Again an adhesive mode of failure at the PC(t) interface was observed with large variations in peel strength. Both experiments have identified that the PC interface is weakest component, as an adhesive mode of failure is obtained. From this formulation it can be observed that any issues with the curing chemistry will have an adverse effect on the final peel strength. Only two laminates (TAc(t)/TAc(t) and PC(t)/PC(t)) reached 3 N mm^{-1} and confirms the overall poor performance of this adhesive. In the previous two adhesives (IPDI-TMP-PPG and IPDI-TMP-PPG-DEPD) all laminate excluding TAc/TAc reached benchmark.

Finally the overall haze for the fully cured adhesive across all six laminates was < 0.8%. The data collected displays that using non-conventional chain-extender has a positive impact on the clarity PU-U adhesives.

5.46 ATR of Peeled Samples

Analysis of the bulk material was performed on all six of the laminates after the 30 day tensile test. ATR analysis will determine the chemical functionality of the final cured material and allow for any distinct differences in curing chemistry to be observed. ATR will give some indication of the inherent morphology of the fully cured adhesive. Discussed within this section will be peaks that indicate either the PU of the chain-extended prepolymer or PU-U peaks obtained after 30 days of cure and any peaks which will have an influence on the morphology within the microstructure. For

discussion of the peaks inherent of the starting materials see section 5.26 and for all characteristic peaks see table 5.09.

From the spectra present within figure 5.22 it is visible there are two different **N-H** vibrations present following cure. **N-H** stretching vibrations occurring at 3334 cm^{-1} show that H-bonded domains are present in the cured PU-U adhesives microstructure whereas, the shoulder peak at around 3500 cm^{-1} correspond to free **N-H** stretching vibrations. Corresponding bending vibrations are visible in the fingerprint region of the spectra for **N-H** at 1535 cm^{-1}, also present within this peak is the **C-N** stretch. **CN** bending vibrations are observed for urea at 1350 cm^{-1} and urethane at 1306 cm^{-1}.

Figure 5.22: **ATR spectra of cured IPDI-TMP-PPG-BD sampled in-situ after tensile testing with inset expanded carbonyl region. [TAc/TAc in black, TAc(t)/TAc(t) in red, TAc(t)/PC in blue, TAc(t)/PC(t) in pink, PC(t)/PC(t) in green and PC/PC in orange. Data collected for each laminate at nine random positions with each spectrum consisting of 128 scans at 8 cm^{-1} resolution. These were then averaged and plotted as the above spectra].**

Again no detectable isocyanate peak was visible between 2260 cm^{-1} – 2280 cm^{-1} which displays that the adhesive is fully cured after 30 days. Further information on the

inherent microstructure following moisture cure is available within the carbonyl region. Evidence of H-bonded urethane carbonyl stretches are visible at 1710 cm^{-1} which is an indication that urethane linkages are ordered within the microstructure. An immediate shoulder to this peak displays the carbonyl stretching of free urea at 1699 cm^{-1}. Further evidence of structured regions within the microstructure of the cured adhesive is shown by the bidentate H-bonded urea stretching vibration at 1644 cm^{-1}. As the two previous peaks are beginning to convolute together it also displays that there will be proportion of monodentate urea groups which have characteristic vibration range of 1675 cm^{-1} – 1660cm^{-1}. The overall morphology observed from ATR will be discussed in greater detail within chapter 8.

Table 5.09: Characteristic peaks of IPDI-TMP-PPG-BD cured PU-U adhesive from all six laminate combinations.

Wavenumber (cm^{-1})	Vibration	Wavenumber (cm^{-1})	Vibration
3334	N-H stretching Hbonded	1350	C-N urea
2974	C-H stretching	1306	C-N urethane
2936	C-H asymmetric stretch	1246	Asymmetric N-CO-O, C-H aliphatic skeleton
2871	C-H symmetric stretch	1094	C-O-C aliphatic ether
1710	C=O stretching urethane Hbonded	1017	Symmetric N-CO-O
1699	C=O stretch free Urea	925	C-O-C aliphatic ether
1644	C=O stretching Urea Bidentate Hbonded	870	C-C skeleton vibration
1535	C-N stretch, N-H bending	832	C-C skeleton vibration

1453	C-H bend aliphatic		
		778	C-C skeleton rocking
1372	C-H methyl deformation		

5.47 Summary of IPDI-TMP-PPG-BD Formulation

Synthesis of the BD chain-extended prepolymer was followed using NMR which displayed successful synthesis. This was confirmed using MALDI-MS which characterised the molecular mass distributions present within the chain-extended prepolymer formulation. MALDI-MS identified chain-extended prepolymers, prepolymers which were absent of any chain-extension from step one, mono end capped polymers and a molecular distribution that was formed during step one (IPDI-PPG-IPDI-PPG-IPDI) of a higher molecular weight. Compared to MDI-TMpPPG and increase in Mn, Mw and PDI is observed. The shift to mass distribution is smaller than when DEPD is used and a narrow profile is mass obtained.

Investigation of the thermal transition by DSC recorded a $T_g$ss for the chain-extended prepolymer of -54°C which is an elevation of +9°C compared to PPG. Once fully cured, the $T_g$ss was further elevated to -30°C on the first heating cycle and -32°C after the second. For this formulation unlike was measured previously after chainextension, the $T_g$ss finished out with the processing window. The overall thermal stability was determined by TGA with the onset of degradation occurring at 267°C. From the DTG curve visible deconvolution of the two main degradation pathways through hard and soft-segment bond breaking was visible which made for more accurate calculation of the breakdown temperatures.

Using 180° T-peel testing it was identified that untreated TAc performed very poorly. After 30 days of curing with TAc(t) however, an above benchmark value was recorded. Lower than anticipated peel strength values were recorded on all laminates which was explained by the curing time being longer than expected. The slow rate of cure obtained is believed to due to a reduction in the activity of DBTDL. Of all the laminates that contained PC, only the fully treated PC(t)/PC(t) laminate performed above benchmark and it required 30 days of cure to obtain (only required 7 days for IPDI-TMP-PPG and IPDI-TMP-PPG-DEPD). From the hybrid laminates it was

identified that the PC or PC(t) interfaces were weaker than the TAc(t) interface (displayed by adhesive mode of failure at the PC/PC(t) interface). The poor curing chemistry is shown by both laminates displaying an adhesive failure after 30 days and the unstable peel observed during testing. Haze values recorded for the six laminates were very low at < 0.8% making the cured laminate very high clarity.

Finally ATR displayed that the adhesive was fully cured following 30 days which is in contrast to other results. Also observed was that the fully cured adhesive was a PU-U and that there was a considerable degree of H-bonding occurring within the cured network. ATR was not able to identify any significant difference in composition after 30 days that would help explain the very poor peel strengths.

5.50 Analysis of IPDI-TMP-PPG-PD

5.51 Synthesis Information

IPDI-TMP-PPG-PD was next synthesised with the intention of continuing the disrupting of hard-segment packing through using a less conventional chain-extender and this should aid with phase mixing of the different domains. This was achieved by firstly synthesising the IPDI-TMP-PPG prepolymer using the same reaction conditions as detailed with section 5.21 followed by an addition reaction set. The additional step was performed by adding a hydroxyl terminated chain-extender using a 2.2:1.0 isocyanate:hydroxyl ratio based on the calculated amount of free NCO remaining after step one. The chain-extension step was used to lower the free isocyanate content of the adhesive, which would reduce the opportunity for excessive bubbling by CO_2 liberation produced during urea formation as the adhesive cures.

Step one was performed as previously detailed in section 5.21 and was a clear liquid which had an observed increase in viscosity from the starting mixture. After addition of 1,2-propane diol (PD), the reaction was allowed to stir at 85°C – 95°C for seventeen hours before the dual DBTDL and TEA catalyst system was added. Following chain-extension a visual increase in viscosity was observed and was associated with the molecular weight increase caused by the coupling step. The viscosity of the system was low enough that it did not require the temperature to be increased before transfer. Once the reaction was complete, the material was poured into an aluminium tube,

which was then capped and degassed as previously outlined in section 2.03. The desiccator containing the adhesive filled tube was then placed within a 0°C fridge for storage. Degassing was performed for six hours once a vacuum of one atmosphere was obtained. Samples of the reaction were again taken before catalysed addition, these were analysed by DSC, NMR and MALDI-MS analysis.

IPDI-TMP-PPG-PD was heated to 95°C before being applied to six laminates (same as section 5.31) which were cured at room temperature. These samples were 180° Tpeel tested at 7 days and 30 days to determine the peel strength. A further lamination was performed using two plies of TAc which would allow for the fully cured adhesive to be removed for analysis by DSC and TGA. The 30 day peel test samples were also analysed by ATR to characterise the final adhesive and determine its extent of cure. Analysis of the chain-extended material only will be presented within the remaining sections of this chapter. IPDI-TMP-PPG (sections 5.21-5.26) is considered as representative of the reactive intermediate obtained after step one of each chain-extended reaction.

5.52 NMR Analysis
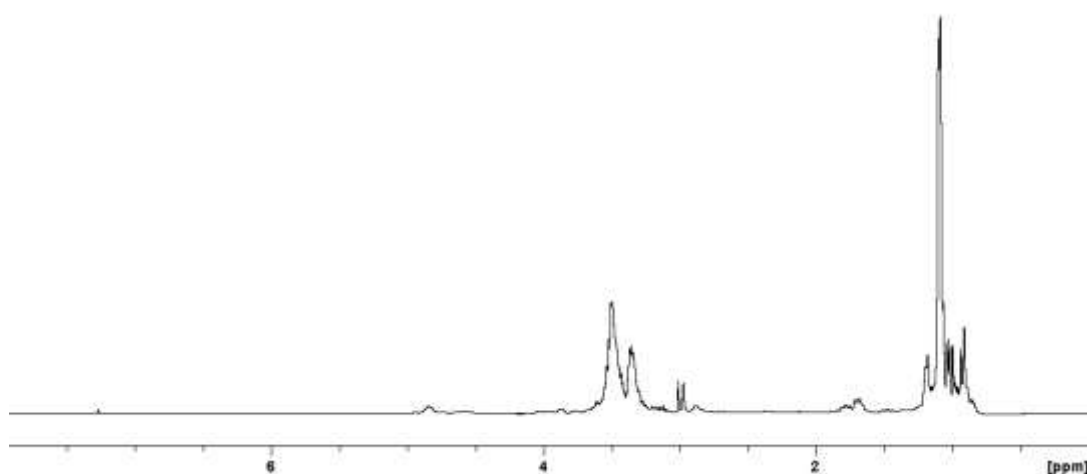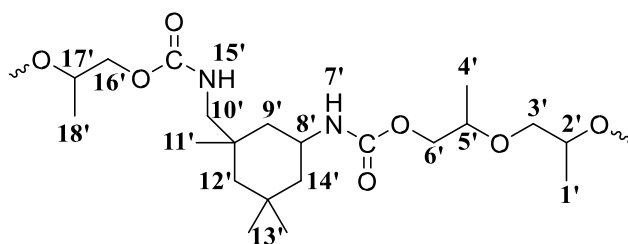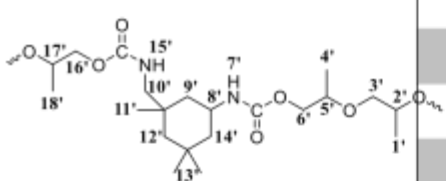
Figure 5.23: ^{1}H NMR spectrum obtained following reaction of IPDI-TMP-PPG with PD.

Table 5.10: ^{1}H and ^{13}C chemical shift for IPDI-TMP-PPG-PD collected in CDCl$_3$.

IPDI-TMP-PPG-DEPD	Position	^{1}H Chemical Shift (ppm)	Position	^{13}C Chemical Shift (ppm)
	1'	1.21	1	17.5
	2'	3.61	2	75.7
	3'	3.23	3	73.5
	4'	1.21	4	17.5
	5'	3.98	5	72.1
	6'	4.10	6	70.1
	7'	NDT	7	156.6$_p$/155$_s$
	8'	3.54	8	42.6
	9'	1.41/1.71	9	43.5
	10'	3.00/3.21	10	56.9
	11'	0.94	11	123$_p$/122$_s$
	12'	1.09/1.30	12	18.6
	13'	0.91	13	23.4
	14'	1.39/1.68	14	48.7
	15'	NDT	15	23.2
	16'	4.03	16	27.1
	17'	4.96	17	31.7
	18'	1.2 – 1.3	18	46.7
			19	156.7$_p$/155$_s$
			20	67.2
			21	66.4
			22	19

$_p$ = primary, $_s$ = secondary, NDT = not detected

For full spectral characterisation of peaks from IPDI and PPG see section 5.22 as this section will only detail peaks that are important to show prepolymer formation or peaks from the chain-extender. Within figure 5.23 the ^{1}H spectrum of the PD chainextended prepolymer is presented in deuterated chloroform. Urethane formation via the primary alcohol groups is visible by the position of the adjacent methylene protons **16'** that have shifted from 3.60 ppm to 4.03 ppm.

Inclusion of secondary hydroxyl groups within urethane linkages is shown by the shift of the methine proton **17'** from 3.70 ppm to 4.96 ppm. As previously mention in section 5.22, the methyl region is complex within the ^{1}H spectrum and as a consequence observation of methyl protons **18'** of the PD chain-extender was not possible, however, the peak would be expected to appear between 1.20 ppm – 1.30 ppm. Full ^{1}H peak assignment can be observed within table 5.10.
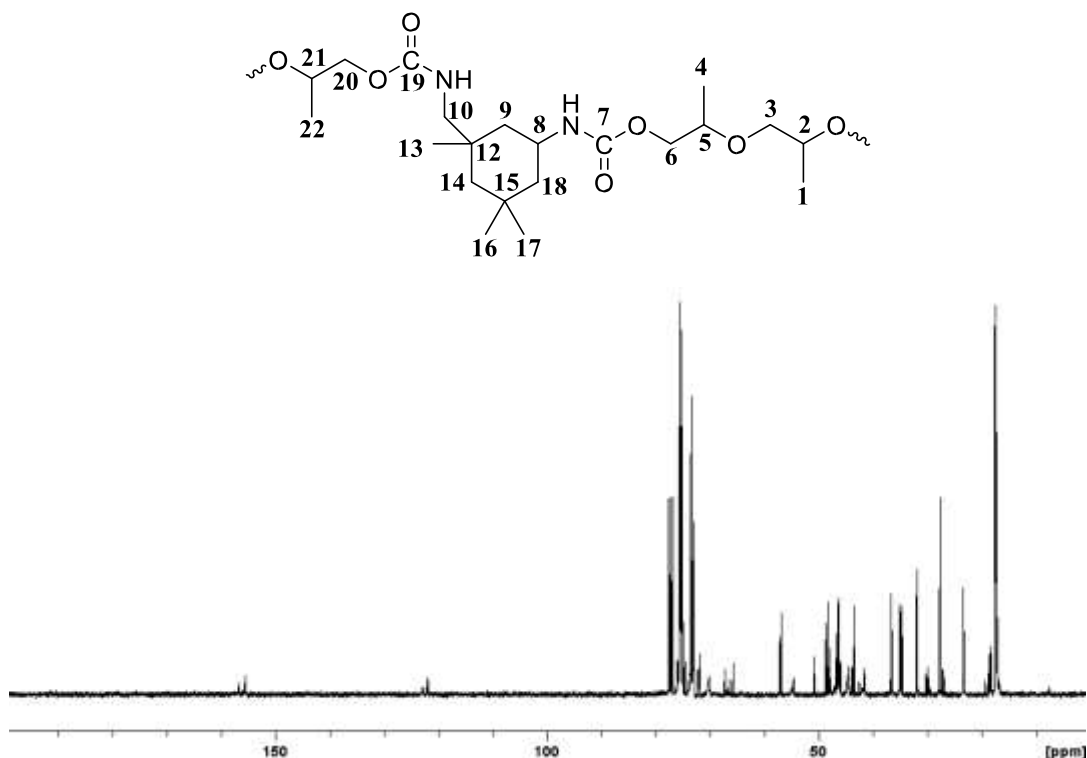
Figure 5.24: ^{13}C **NMR spectrum obtained following reaction of MDI-TMP-PPG with PD.**

Further evidence that PD chain-extension has occurred, along with retention of free isocyanate groups was observed using ^{13}C NMR. Consumption of the primary hydroxyl groups within PD is confirmed by the position of the methylene carbon **20** at

67.2 ppm. Methine carbons of the secondary hydroxyl group **21** once reacted are also visible at 66.4 ppm. The methyl carbons **23** for the PD chain-extender can be observed at 19 ppm. Carbonyl shifts characteristic of urethane bonds are visible at 156.7 ppm and 155.5 ppm following reaction of primary and secondary isocyanate groups respectively. Confirmation that the prepolymers within solution still contain free reactive groups can be observed by the remaining carbonyl shifts from primary and secondary isocyanates at 123 ppm and 122 ppm respectively.

5.53 MALDI-MS Analysis

To confirm that chain-extension by PD has occurred MALDI-MS was used. The matrix used for analysis was dithranol which contained a cationising agent NaTFA (see section 3.23 for more matrix information). A 40 mg ml^{-1} solution of IPDI-TMPPPG-PD was prepared in THF and mixed with the matrix (1:8 sample:matrix). 1 μl portions of this sample were then spotted and dried for analysis.
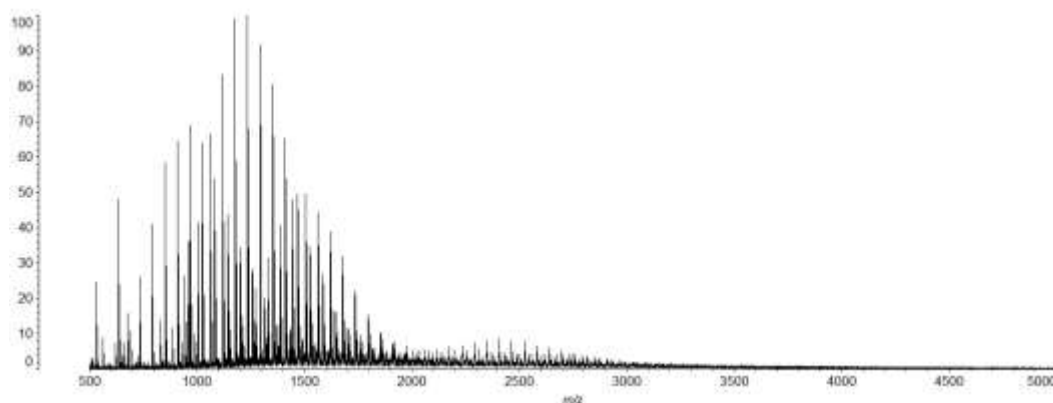
Figure 5.25: MALDI-MS spectrum of IPDI-TMP-PPG-PD chain-extended prepolymer collected in dithranol/NaTFA.

Figure 5.25 displays the MALDI-MS spectrum collected of the chain-extended prepolymer IPDI-TMP-PPG-PD and it can be seen that it is rather complex. Evidence of consumption of the chain-extender PD by free IPDI can be observed by the peak at 635 m/z, which corresponds to PD coupled with two ethanol end-capped IPDI units and one sodium cation. Present next is the chain-extender TMP that has reacted with three IPDI units which are in this sample are also ethanol end-capped plus a sodium cation at 961 m/z. Identification of these end capped molecules confirms that TMP and PD will be involved in the hard-segments and will influence the packing

arrangement. Also evident is some unreacted starting material centred at 958 m/z which is a polymer of 12 propylene glycol repeat units and two sodium cations (mono-sodiated distribution also present).

Following next is mono IPDI end capped polymers (IPDI-PPG) which are observed by the distribution centred on 1237 m/z. Centred on 1494 m/z is the distribution that corresponds to the PPG soft-segment that has become isocyanate end-capped at both ends giving rise to prepolymers of type IPDI-PPG-IPDI. These polymers are formed during step one of the synthetic process and a contribution would be expected to remain. This region of the spectrum displays the mono-sodiated adduct of this prepolymer which offset the distribution by -23 m/z. Also to further complicate the spectrum there are peaks which are offset by +76 m/z as a result of some prepolymers that have reacted with PD but not yet coupled with another prepolymer molecule.

The next molecular weight distribution centred at 2486 m/z displays polymers of type IPDI-PPG-IPDI-PPG-IPDI, with these polymers produced during the first step of synthesis. On inspection of the region there is a further distribution offset by -23 m/z as the mono-sodiated adduct is also present. A mass distribution centred on 2846 m/z corresponds to chain-extension of mono end capped polymers. The composition of this peak would be twenty two PPG repeat units one fully reacted IPDI, two ethanol end-capped IPDI units and two sodium cations.

A final mass distribution is also visible, however it is very weak. This distribution corresponds to PD chain-extended prepolymers and is centred around 3870 m/z. Identification of chain-extended prepolymer would be expected based on the synthetic procedure adopted coupled with previous NMR analysis. To obtain better signal to noise in this upper region of the mass spectrum may require that the matrix recipe is improved or a new matrix is found all together.

Finally Mn, Mw and PDI are calculated from the MALDI-MS spectrum to determine PD influence on the mass distribution. The calculated value for Mn is 1558 m/z and the calculated value for Mw is 1975 m/z giving a PDI of 1.27. Using PD as a chainextender has both shifted the mass distribution to higher mass and broadened its profile.

5.54 DSC and TGA Analysis

Within figure 5.26, the DSC thermogram for the PD chain-extended prepolymer is displayed. Analysis of the thermogram obtained for the chain-extended prepolymer shows a $T_g$ss of -54°C which covers a range of -56°C to -51°C. A shift in the $T_g$ss of +9°C can be observed compared of the unreacted PPG soft-segment (results very similar to previous formulation). When only a small shift of the $T_g$ss is encountered it would suggest that the polymer has only slightly increased in molecular weight or has very little cross-links. Also observed is an exothermic peak at 127°C with an enthalpy of 66 J g^{-1} and this will most likely account for the curing of free isocyanate groups within the prepolymer. From the data collected it was apparent that this uncured prepolymer formulation was thermally similar to previous formulation (see section 5.44).
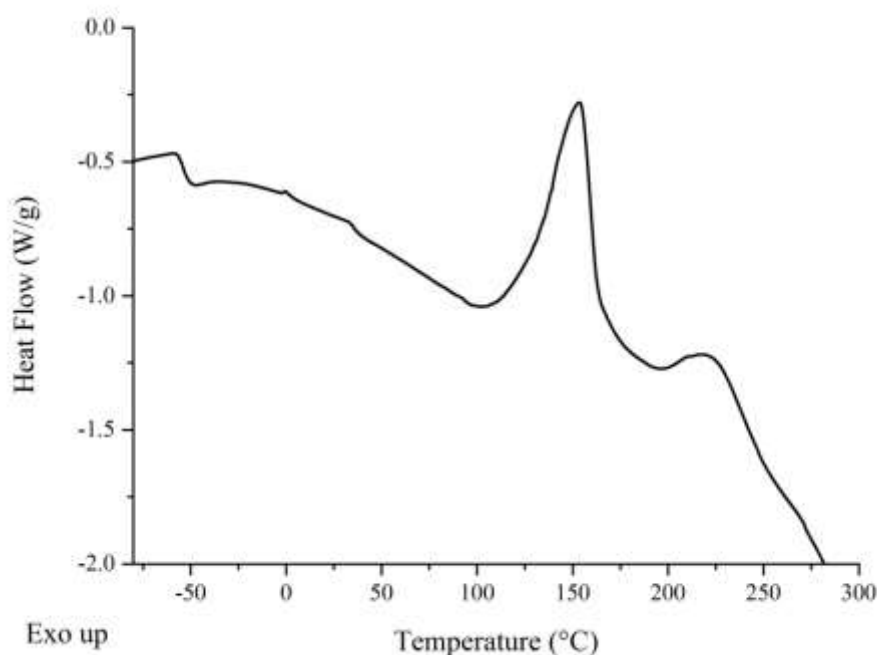
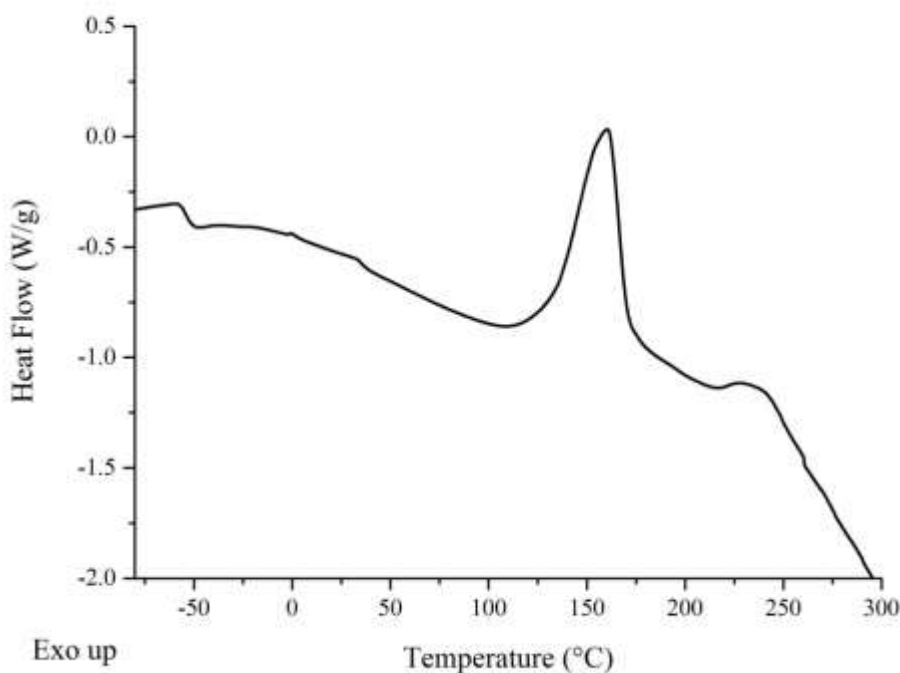**Figure 5.26: DSC thermogram of IPDI-TMP-PPG-PD chain-extended prepolymer formulation.**

Following 30 day a portion of the cured adhesive was removed from the TAc/TAc laminate for DSC analysis. The fully cured adhesive was analysed using a cool-heatcool-reheat experiment to determine the final $T_g$ss within each heating cycle as

shown in figure 5.27 (same experiment procedure as detail in section 5.24). A broad $T_g$ss was observed at -34°C with the thermal transition covering a range of 17°C from -42°C to -25°C. After a second heating cycle, the $T_g$ss was recorded at -33°C and covered a broad range from -42°C to -23°C. Following a second heating cycle the collected $T_g$ss has only shifted by +2°C and can be considered the same. On the second heating cycle it was observed that no melting endotherm for hard-segments was observed. As this peak was absent it would suggest that the material has good mixing of both hard and soft-segments within its microstructure. DSC analysis of the fully cured adhesive and the microphase morphology within this system will be discussed in greater detail within chapter 8.
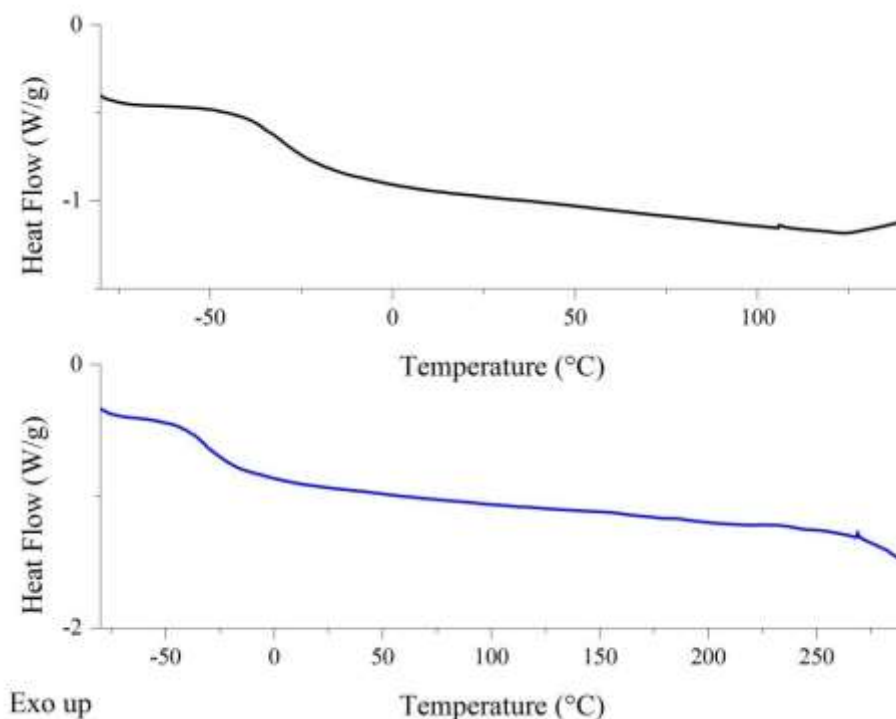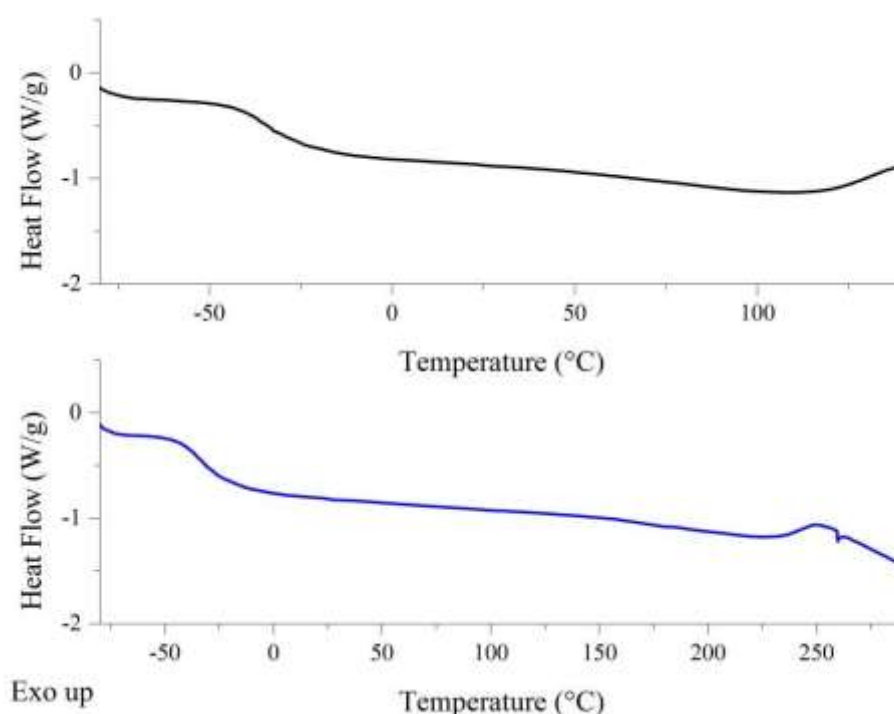

Figure 5.27: DSC thermogram of fully cured IPDI-TMP-PPG-PD adhesive, following removal from TAc/TAc laminate. [First heating cycle *top* in black and second heating cycle *bottom* in blue].

TGA analysis was also collected to assess the effect that PD has on the overall thermal stability of the PU-U. Within figure 5.28, the TGA and DTG curves for the fully cured adhesive are displayed. From the TGA curve, the onset of degradation was calculated to be 278°C which is in keeping with previous formulations within this chapter. The DTG curve displayed that the maximum rate of degradation occurs for this cured

adhesive at 352°C (IPDI-TMP-PPG occurred at 338°C) which again is consistent with other formulations within this set. Thermal cleavage of both urethane and urea hard-segment bonds within the adhesives microstructure are the initial degradation pathway.[7,8] A second degradation peak at 379°C was also observed within the DTG curve and this peak will account for the breakdown of the softsegment PPG.[5] From the TGA data collected it was apparent that the thermal stability of this chain-extended adhesive using PD was comparable the previous formulations within this set. It also further displays that PU-U adhesives based on IPDI and PPG are stable within the processing window of the laminate.
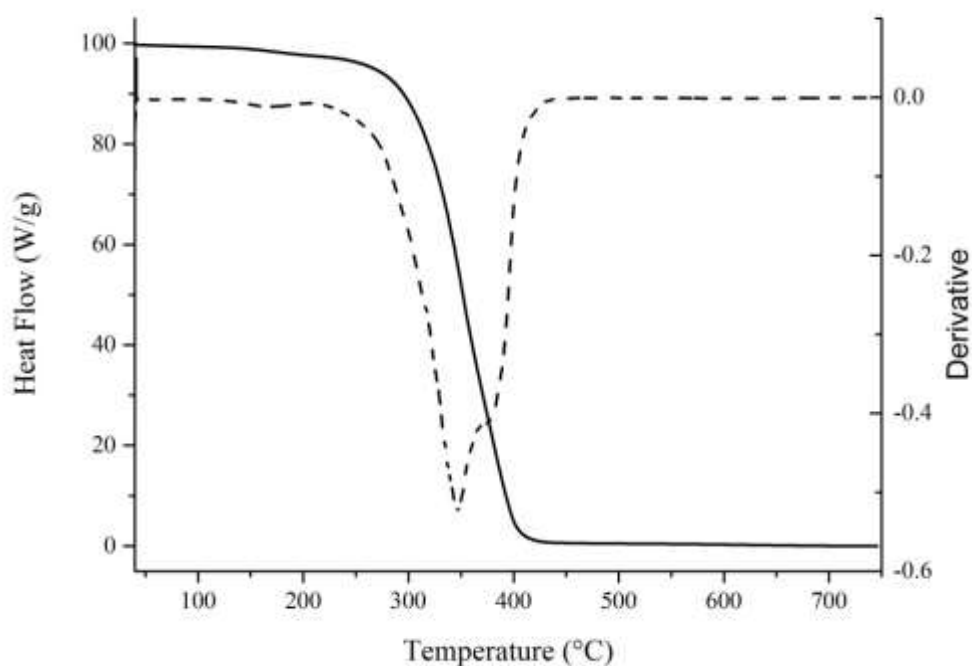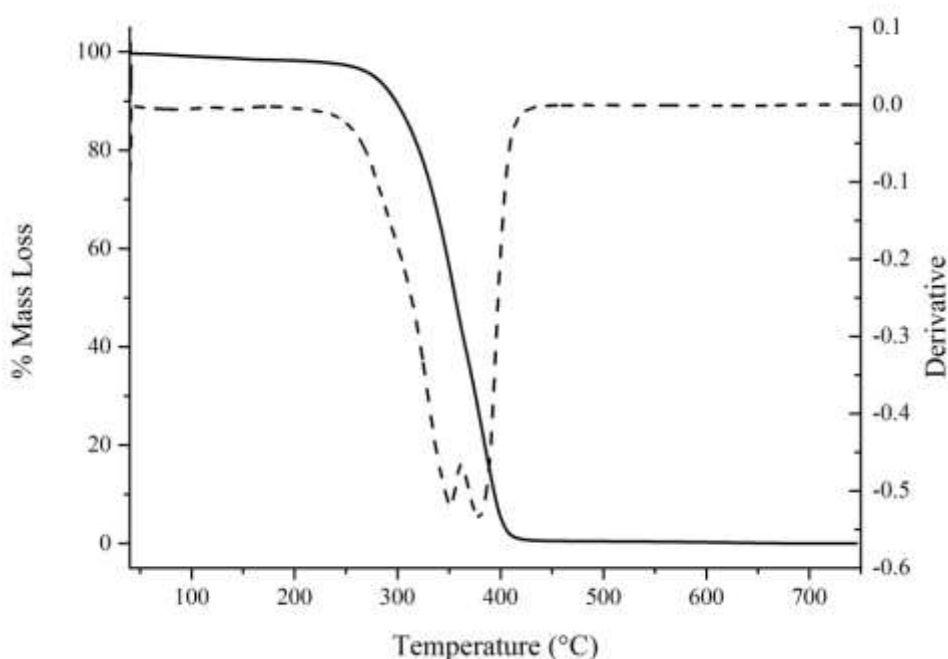

Figure 5.28: TGA and DTG curves of fully cured IPDI-TMP-PPG-PD adhesive. [TGA solid line and DTG dashed line].

5.55 180° T-peel Test and Haze

To gauge the influence of chain-extension using PD on the peel strength of each laminate, 180° T-peel testing was performed after 7 and 30 days. Following 7 days of moisture cure, the observed mode of failure for TAc/TAc was adhesive at the interface, the failure was very unstable and of low strength (0.9 N mm^{-1}).

Table 5.11: Peel, haze and mode of failure data for IPDI-TMP-PPG-PD cured PU-U adhesive. [The data in bold will be discussed within this section].

Cured Adhesive	Laminate	Peel 1* (N mm⁻¹)	Peel 2ˣ (N mm⁻¹)	Failure mode	Haze (%)
IPDI-TMP-PPG	TAc/TAc	0.8	0.9	Adhesive TAc	<0.3%
	TAc(t)/TAc(t)	4.7	9.6	Adhesive TAc	
	TAc(t)/PC	6.5	7.7	Adhesive PC	
	TAc(t)/PC(t)	3.8	4.4	Adhesive PC	
	PC(t)/ PC(t)	4.8	6.0	Adhesive PC	
	PC/PC	3.0	3.9	Adhesive PC	
IPDI-TMP-PPG-DEPD	TAc/TAc	0.8	0.7	Adhesive TAc	<0.5%
	TAc(t)/TAc(t)	8.2	6.6	Cohesive	
	TAc(t)/PC	5.0	3.8	Adhesive PC	
	TAc(t)/PC(t)	4.1	3.3	Adhesive PC	
	PC(t)/ PC(t)	6.1	5.9	Adhesive PC	
	PC/PC	4.7	3.2	Adhesive PC	
IPDI-TMP-PPG-BD	TAc/TAc	0.6	0.8	Adhesive TAc	<0.8%
	TAc(t)/TAc(t)	0.8	3.3	Cohesive	
	TAc(t)/PC	0.9	1.7	Adhesive PC	
	TAc(t)/PC(t)	1.0	2.3	Adhesive PC	
	PC(t)/ PC(t)	1.5	3.4	Cohesive	
	PC/PC	0.8	2.3	Cohesive	
IPDI-TMP-PPG-PD	TAc/TAc	0.8	1.0	Adhesive TAc	<0.8 %
	TAc(t)/TAc(t)	5.3	5.7	Ply	
	TAc(t)/PC	3.7	4.9	Adhesive PC	
	TAc(t)/PC(t)	3.1	3.7	Adhesive PC	
	PC(t)/ PC(t)	3.4	4.1	Adhesive PC	
	PC/PC	2.9	3.4	Adhesive PC	

Following 30 days of cure the peel strength has not changed significantly and was recorded at 1.0 N mm^{-1}, again with the mode of failure was adhesive at the TAc interface. As has been observed in all previous formulations, TAc/TAc performs extremely poorly and is well outside the 3 N mm^{-1} target peel strength. The results obtained are again consistent with all other formulation based on IPDI and PPG. This result confirms the incompatibility at the interface between the fully cured adhesive and untreated TAc.

Previous experiments displayed that following saponification, there is a marked improvement in peel strength. After 7 days of moisture cure, the peel strength recorded was 5.3 N mm^{-1} which increased to 5.7 N mm^{-1} after 30 days of curing. A cohesive mode of failure in the TAc(t) ply was observed during both tests. As a cohesive mode of failure was observed for both tests within the substrate ply, it highlights that the adhesive strength is now reaching the limits of the TAc(t) substrate.

Data was next acquired for PC/PC, after 7 days of cure a peel strength of 2.9 N mm^{-1} was recorded which increased to 3.4 N mm^{-1} after 30 days. Both experiments displayed an adhesive mode of failure at the PC interface with deformation of the substrate. After 7 days the peel strength recorded is just below benchmark, however, following 30 days an above benchmark value was obtained. Treatment of the PC interface was again performed and the peel strength measured. After 7 days of cure, the peel strength of the fully treated PC(t) laminate was 3.4 N mm^{-1} which increased to 4.1 N mm^{-1} after 30 days. An adhesive mode of failure at the interface was recorded for both experiments and was accompanied by deformation of the substrate plies.

Analysis thus far has identified that the adhesive has an affinity for the treated TAc(t) interface over PC or PC(t). In order to confirm this statement, hydride laminates were next tested to identify the weakest interface or component of the laminate. Discussed first is the laminate of composition TAc(t)/PC which recorded a peel strength of 3.7 N mm^{-1} following 7 days and 4.9 N mm^{-1} after 30 days of cure. Strong deformation of

both substrates was observed and the mode of failure was adhesive at the PC interface. For the fully treated laminate, a 7 day peel strength of

3.1 N mm^{-1} was recorded which increased to 3.7 N mm^{-1} after 30 days. Again strong deformation of both substrates was observed and the mode of failure recorded was adhesive at the PC interface. Both experiments have identified that the PC interface is the weakest component, as identified by the adhesive failure modes at the PC interface in both cases. It was also noted that each laminate combination performed above the set 3 N mm^{-1} benchmark.

Finally the overall haze for the fully cured adhesive across all six laminates was < 0.8%. Such high clarity displays that chain-extension has had minimal effect on the haze within this adhesive formulation compared to IPDI-TMP-PPG which is absent of any diol chain-extender as the haze value recorded was < 0.3%.

5.56 ATR of Peeled Samples

Analysis of the bulk materials was performed on all six of the laminates after the 30 day tensile test. ATR analysis will determine the chemical functionality of the final cured material and allow for any distinct differences in curing chemistry to be observed. Also ATR analysis will give some indication of the inherent morphology of the fully cured adhesive.

Discussed within this section will be peaks that indicate either the PU of the chainextended prepolymer or PU-U peaks obtained after 30 days of cure. Any peaks which yield information on the microphase morphology will be discussed. For discussion of the peaks inherent of the starting materials see section 5.29 and for all characteristic peaks see table 5.12.

From the spectra present with figure 5.29 it is visible that there are two different **N-H** vibrations within the cured PU-U. **N-H** stretching vibrations occurring at 3335 cm^{-1} show that H-bonded domains are present in the cured PU-U adhesives microstructure whereas, the shoulder peak at around 3500 cm^{-1} correspond to free **N-H** stretching vibrations. Corresponding bending vibrations are visible in the fingerprint region of the spectra for **N-H** at 1535 cm^{-1}, also present within this peak is the **C-N** stretch. **CN**

bending vibrations are observed for urea at 1345 cm^{-1} and urethane at 1301 cm^{-1}. Again no detectable isocyanate peak was visible between 2260 cm^{-1} – 2280 cm^{-1} which displays that the adhesive is fully cured after 30 days.
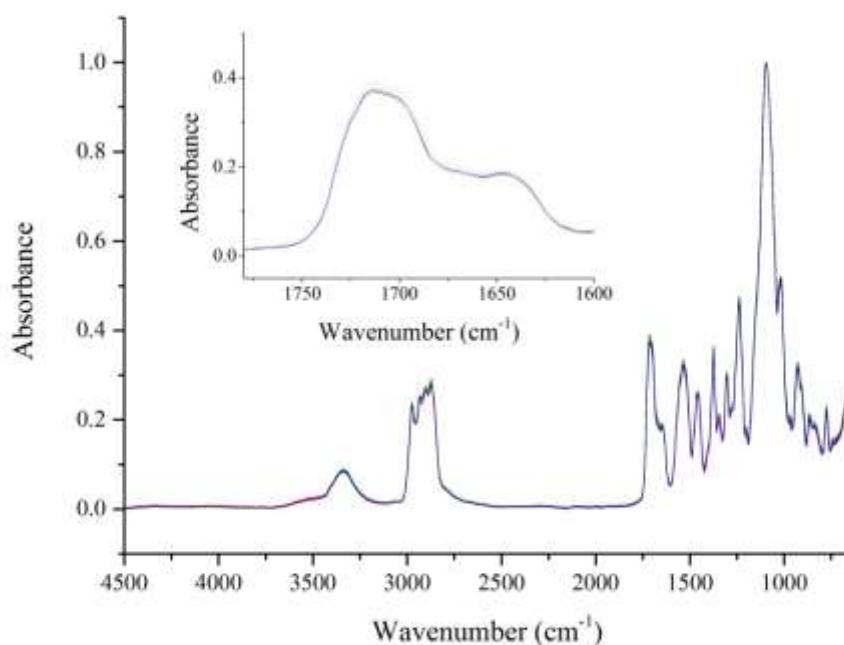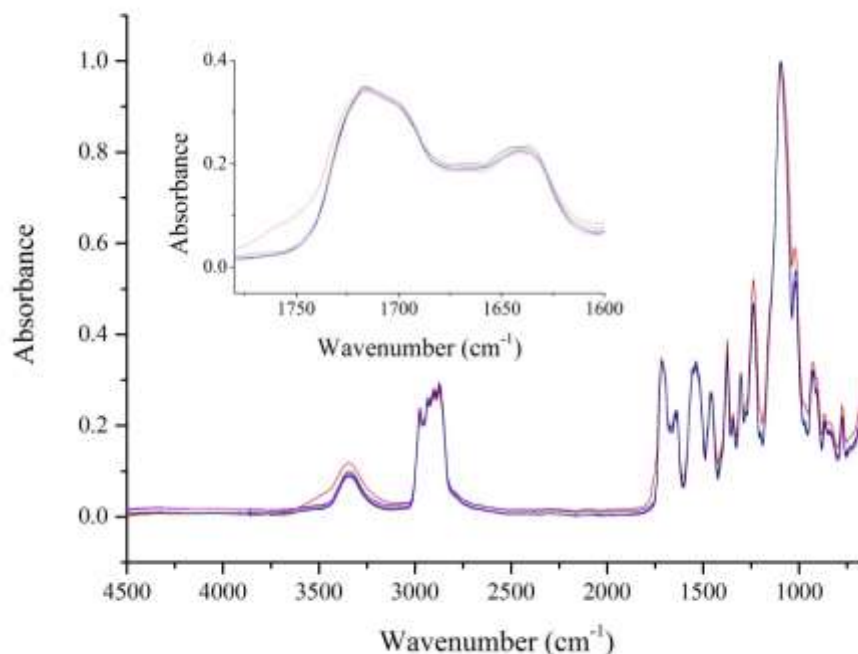

Figure 5.29: ATR spectra of cured IPDI-TMP-PPG-PD sampled in-situ after tensile testing with inset expanded carbonyl region. [TAc/TAc in black, TAc(t)/TAc(t) in red, TAc(t)/PC in blue, TAc(t)/PC(t) in pink, PC(t)/PC(t) in green and PC/PC in orange. Data collected for each laminate at nine random positions with each spectrum consisting of 128 scans at 8 cm^{-1} resolution. These were then averaged and plotted as the above spectra].

Further information on the inherent microphase structure following moisture cure is available within the carbonyl region. Evidence of H-bonded urethane carbonyl stretching is visible at 1715 cm^{-1} which shows the formation of ordered urethane domains within the microstructure. An immediate shoulder to this peak displays the occurrence of free urea carbonyl stretching at 1700 cm^{-1}. Further evidence of structured regions within the microstructure of the cured adhesive is shown by the bidentate H-bonded urea stretching vibration at 1644 cm^{-1}. As these peaks are beginning to convolute together it also displays that there will be proportion of

monodentate urea groups which have characteristic vibrations of 1675 cm^{-1} – 1660cm^{-1}. The overall morphology observed from ATR will be discussed in greater detail within chapter 8.

Table 5.12: Characteristic peaks of IPDI-TMP-PPG-PD cured PU-U adhesive from all six laminate combinations.

Wavenumber (cm^{-1})	Vibration	Wavenumber (cm^{-1})	Vibration
3345	N-H stretching Hbonded	1345	C-N urea
2980	C-H stretching	1301	C-N urethane
2936	C-H asymmetric stretch	1241	Asymmetric N-CO-O, C-H aliphatic skeleton
2877	C-H symmetric stretch	1094	C-O-C aliphatic ether
1715	C=O stretching urethane Hbonded	1012	Symmetric N-CO-O
1700	C=O stretch free Urea	925	C-O-C aliphatic ether
1644	C=O stretching Urea Bidentate Hbonded	865	C-C skeleton vibration
1535	C-N stretch, N-H bending	832	C-C skeleton vibration
1453	C-H bend aliphatic	772	C-C skeleton rocking
1367	C-H methyl deformation		

5.57 Summary of IPDI-TMP-PPG-PD Formulation

Synthesis of the PD chain-extended prepolymer was followed using NMR which displayed successful synthesis. This was confirmed using MALDI-MS which

characterised the molecular mass distributions present within the chain-extended prepolymer formulation. MALDI-MS identified chain-extended prepolymers, prepolymers which were absent of any chain-extension from step one, mono end capped polymers and a molecular distribution that was formed during step one (IPDI-PPG-IPDI-PPG-IPDI) of a higher molecular weight. Compared to MDI-TMPPPG an increase in Mn, Mw and PDI is observed using PDI as the chain-extender. The PDI value obtained for this formulation was the highest of all the formulations within this section at 1.27.

Investigation of the thermal transition by DSC recorded a $T_g$ss for the chain-extended prepolymer of -54°C which is an elevation of +9°C compared to PPG suggests reduced phase mixing compared to previous formulations. Once fully cured the $T_g$ss was further elevated after the first heating to -34°C on and was -33°C after the second cycle. This formulation was similar to previous PPG based formulation as the $T_g$ss never entered the processing window (only second heating cycle in IPDITMP-PPG-BD). The overall thermal stability was determined by TGA with the onset of degradation occurring at 278°C. From the DTG curve visible deconvolution of the two main degradation pathways through hard and soft-segment bond breaking was visible which made calculation of the breakdown temperatures more accurate.

Using 180° T-peel testing it was identified that untreated TAc performed very poorly (1.0 N mm^{-1}) however, with TAc(t) an above benchmark reading was recorded (5.7 N mm^{-1} after 30 days). For PC based laminates good performance was also observed, with 3.4 N mm^{-1} recorded for PC/PC after 30 days. Following surface treatment of the PC substrate, the peel strength after 30 days elevated to 4.1 N mm^{-1}. On both these laminates, the mode of failure was adhesive at the PC interface and this was accompanied by strong deformation of the substrate ply. Both hybrid laminate performed above 3 N mm^{-1} (TAc(t)/PC 4.9 N mm^{-1} and TAc(t)/PC(t) 3.7 N mm^{-1}) and displayed that the PC interface (treated or non-treated) was weaker than the TAc(t) interface. Haze values recorded for the six laminates were very low at < 0.8% making the cured laminate very high clarity. Finally using ATR the adhesive material was observed to be fully cured following 30 days of curing. Also clarification that the fully cured adhesive was indeed a PU-U was determined by ATR.

5.60 Summary of Aliphatic Polyurethane Adhesives based on Poly(propylene glycol)

Synthesis of all four different adhesive formulations was successfully carried out with prepolymer formation confirmed using NMR and MALDI-MS analysis. MALDI-MS identified that the target molecules were present in each formulation e.g. end capped prepolymer in IPDI-TMP-PPG and chain-extended prepolymers in each of the following three adhesives. Also identified was a higher molecular weight polymer of composition IPDI-PPG-IPDI-PPG-IPDI in all formulations. Exclusive to BD and PD chain-extended formulations was evidence of mono end capped polymers. MALDI-MS identified an increase to Mn, Mw and PDI following synthesis of formulation MDI-TMP-PPG compared with soft-segment PPG. These parameters further increased following chain-extension. Urethane linkages formed during synthesis were visible within the ATR spectra along with urea bonds, confirming that each fully cured adhesive was a PU-U. Investigation of **N-H** and carbonyl regions displayed that within the microstructure of each adhesive are regions of order as a result of H-bonding and region of disorder. The carbonyl region displayed that H-bonding was occurring within both urethane and urea domains.

Each adhesive was used to perform lamination on six different combinations, which were tested at two different curing times to determine the 180° T-peel strength, mode of failure and final haze measurement of each laminate. Identified from each adhesive was that every material has an inherent incompatibility with TAc and only after saponification will benchmark peel strengths be obtained. Also observed was that both treated and untreated PC (BD material exception) performed to give above benchmark peel strengths. Hybrid laminates identified that saponification of TAc will improve the peel strength more than ethanolamine treatment of PC. This observation is confirmed by the adhesive failure recorded at the PC interface for TA(t)/PC(t). Following chain-extension the haze value recorded was not significantly altered. The cured base material displayed a haze value of $< 0.3\%$, this value increased to $< 0.5\%$ following DEPD chain-extension and $< 0.8\%$ following chain-extension with BD or PD.

TGA analysis was also collected on each of the cured adhesives and it displayed that the onset of degradation was similar in all materials (base adhesive IPDI-TMP-PPG = 250°C, DEPD = 275°C, BD = 267°C and PD = 278°C). This result confirmed that PU-U based adhesive are stable well above the set maximum temperature that the adhesive would see within normal laminate processing (set at 100°C). DSC analysis displayed that the $T_g$ss recorded was out with the -20°C set point (glass transition range entered this window for DEPD and BD chain extenders). Evidence of hardsegment melting endotherms were visible in the TMP only and DEPD chainextended formulations, however, this transition was absent in both BD and PD formulations. This results displays that chain-extension does have a disruptive effect on hard-segment formation (DEPD melting endotherm small in comparison to IPDITMP-PPG). Considering all the analysis collected from this set of adhesives the only criteria that was not passed was obtaining a benchmark peel strength laminate with TAc.

References

(1)   Umemura, K.; Yamauchi, H.; Ito, T.; Shibata, M.; Kawai, S. *J Wood Sci* **2008**, *54*, 289.
(2)   Prabhakar, A.; Chattopadhyay, D. K.; Jagadeesh, B.; Raju, K. V. S. N. *Journal of Polymer Science Part A: Polymer Chemistry* **2005**, *43*, 1196.
(3)   Lomölder, R.; Plogmann, F.; Speier, P. *Journal of Coatings Technology* **1997**, *69*, 51.
(4)   Chattopadhyay, D. K.; Sreedhar, B.; Raju, K. V. S. N. *Industrial & Engineering Chemistry Research* **2005**, *44*, 1772.
(5)   Rath, S. K.; Ishack, A. M.; Suryavansi, U. G.; Chandrasekhar, L.; Patri, M. *Progress in Organic Coatings* **2008**, *62*, 393.
(6)   Zhang, J.; Tu, W.; Dai, Z. *J Coat Technol Res* **2013**, *10*, 887.
(7)   García-Pacios, V.; Jofre-Reche, J. A.; Costa, V.; Colera, M.; MartínMartínez, J. M. *Progress in Organic Coatings* **2013**, *76*, 1484.
(8)   Cakic, S. M.; Stamenkovic, J. V.; Djordjevic, D. M.; Ristic, I. S. *Polymer Degradation and Stability* **2009**, *94*, 2015.
(9)   Li, C.; Wilkes, G. *Journal of Inorganic and Organometallic Polymers* **1997**, *7*, 203.
(10)   García-Pacios, V.; Iwata, Y.; Colera, M.; Miguel Martín-Martínez, J. *International Journal of Adhesion and Adhesives* **2011**, *31*, 787.
(11)   Petrović, Z. S.; Javni, I.; Divjaković, V. *Journal of Polymer Science Part B: Polymer Physics* **1998**, *36*, 221.
(12)   Burattini, S.; Greenland, B. W.; Merino, D. H.; Weng, W.; Seppala, J.; Colquhoun, H. M.; Hayes, W.; Mackay, M. E.; Hamley, I. W.; Rowan, S. J. *Journal of the American Chemical Society* **2010**, *132*, 12051.

Chapter 6 Aliphatic Polyurethane Adhesives based on Poly(caprolactone diol)

6.10 Polymers Synthesis Introduction

From previous analysis some consistent trends in the peel strength obtained using 180° T-peel testing of laminates based on TAc or PC are emerging. All three formulation sets have identified that TAc performs poorly and only after saponification could benchmark peel strength be reached (> 3 N mm^{-1}). PC based laminates perform above benchmark both when treated and untreated for all adhesive sets (except in isolated instances when curing was an issue). Highlighted in the previous adhesive sets was that changing the isocyanate increased the compatibility towards TAc(t), as was displayed by the adhesive mode of failure recorded at the PC interface in hybrid laminates. In chapters 3 and 4 where MDI was the isocyanate used, the mode of failure in hybrid laminates was exclusively at the TAc(t) interface.

Within this chapter, PU's based on IPDI and PCD will be presented to determine the soft-segments effect on the overall peel strength. In theory as this formulation is based on a reactive PU hot melt it should lead to higher peel strengths through additional H-bonding in the microstructure and at the interface.[1]

As the soft-segment is crystalline, sufficient disruption of the polyester cross-linking must also be considered if an optically clear final adhesive is to be obtained. Considering this four PU prepolymer adhesives were synthesised: a one-step prepolymer PU of formulation IPDI-TMP-PCD (polymer has IPDI,TMP and PCD in formulation) and three two-step chain-extended prepolymer formulations IPDI-TMPPCD-DEPD (initial step chain-extended DEPD = 2,2-diethyl-1,3-propane diol), IPDI-TMP-PCD-BD (BD = 1,3-butane diol) and IPDI-TMP-PCD-PD (PD = 1,2-propane diol). Again the curing chemistry employed will be a two stage process of initial catalyst cure (0.05 wt% of both dibutyltin dilaurate and triethylamine) followed by final moisture cure of any remaining free isocyanate. Each synthesised prepolymer material was analysed using DSC, NMR and MALDI-MS before application. Thermal transitions and stability of each fully cured PU-U was analysed by DSC and TGA. The

final characteristics of each PU-U were analysed by ATR to obtain functionality information and 180° T-peel testing to determine laminate strength.
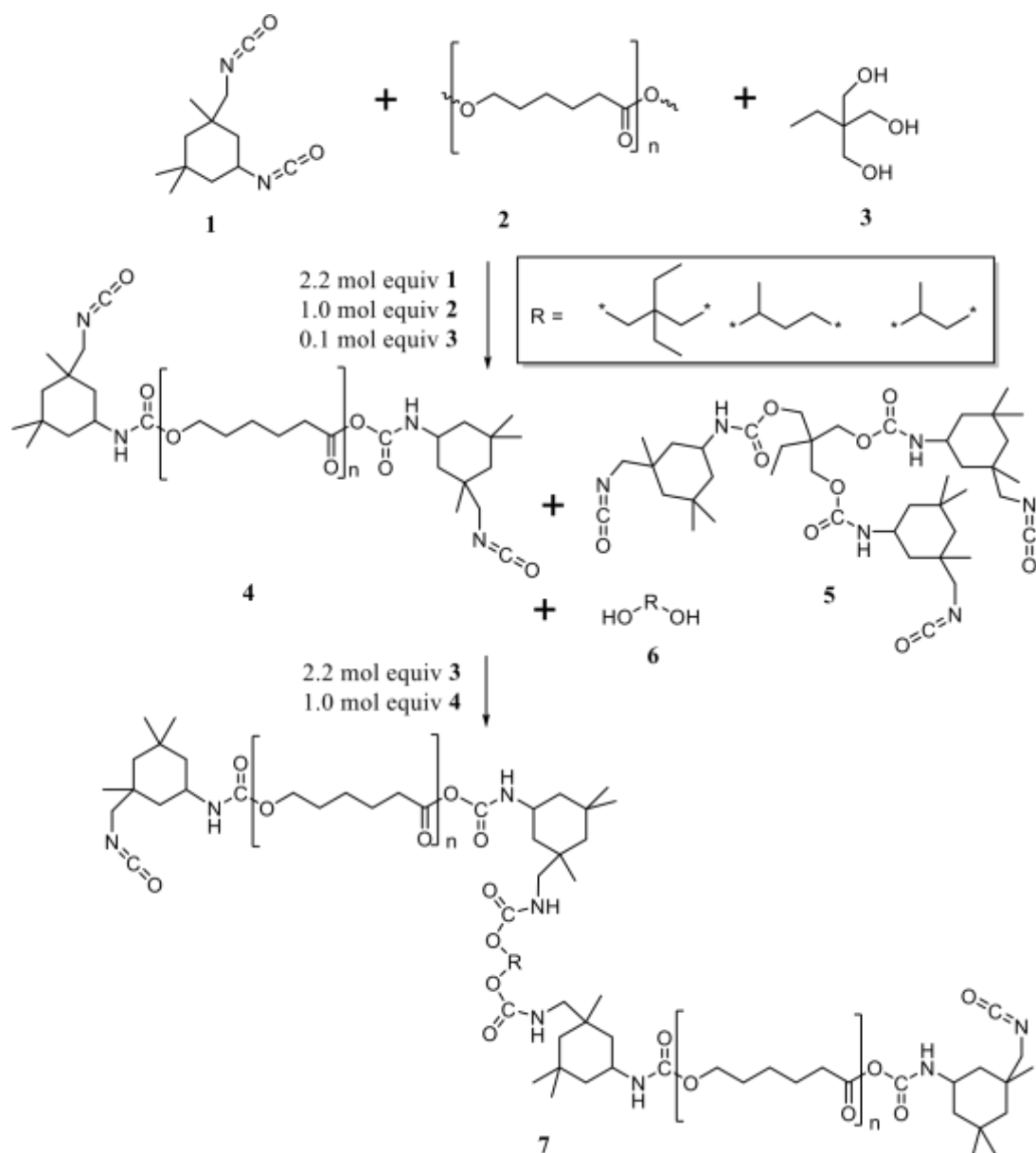
Figure 6.01: General reaction scheme for the synthesis IPDI-TMP-PCD based chain-extended polyurethanes adhesives. 1 = IPDI, 2 = PCD, 3 = TMP, 4 = IPDIPCD prepolymer, 5 = end capped IPDI-TMP, 6 = chain-extender and 7 = chainextended prepolymer.

6.20 Analysis of IPDI-TMP-PCD

6.21 Synthesis Information

Prior to synthesis PCD (molecular weight 2000) was dried to remove water by placing within a vacuum oven at 80°C for at least 48 hours. The synthesis was performed using the reaction set-up as detailed in section 2.03, with the reaction being performed in the temperature window of 85°C – 95°C for seven hours. The reaction time was started after the last addition of IPDI to the polyol containing reaction vessel. IPDI was degassed within a three necked round bottom flask before being put under a nitrogen atmosphere. To ensure that the exothermic reaction did not exceeded 95°C, IPDI was added drop wise in 1 ml portions. The final prepolymer obtained was clear but with a slight visually increase in viscosity compared to the starting mixture (consequence of the molecular weight increase). Prior to catalyst addition samples of the reaction were taken for NMR, MALDI-MS and DSC analysis. After the elapsed reaction time of seven hours 0.05 wt% of dibutyltin dilaurate and 0.05 wt% of triethylamine were added as curing catalysts (calculated from total batch weight). Following catalyst addition the formulation was transferred to an aluminium holding tube and placed within a vacuum desiccator. The adhesive was stored at 0°C within a fridge until being used during lamination (typically not exceeding 7 days). Degassing was performed for six hours once a vacuum of one atmosphere was obtained.

The prepolymer adhesive was applied to six different laminates that were of interest:

- TAc/TAc
- TAc(t)/TAc(t)
- TAc(t)/PC
- TAc(t)/PC(t)
- PC(t)/PC(t)
- PC/PC

Where TAc is cellulose triacetate, PC is bisphenol-A polycarbonate and (t) denotes that the surface of the polymer film has been treated (see section 2.01 and 2.02). IPDI-TMP-PCD was applied at 95°C to ensure good surface coverage. The lamination process was carried out as detailed in section 2.04, followed by cure at room

temperature. 180° T-peel testing was carried out initially after 7 days and then after 30 days to determine the peel strength of each laminate, with the mode of failure monitored by visual inspection. The cured laminates from the 30 day peel testing were used in the ATR analysis of the fully cured adhesive.

6.22 NMR Analysis

Investigation of the urethane reaction between PDI and PCD was carried out using both ^{1}H and ^{13}C NMR. A mixture of both primary and secondary free isocyanate groups is expected within the prepolymer based on the synthesis procedure plus previous analysis. Both end groups of the PCD soft-segment are primary. The initiator used for synthesis of PCD was neopentyl glycol which results in two proton signals. Firstly the methyl protons are visible at 0.89 ppm and the methylene groups adjacent to the hydroxyl end groups are visible at 3.94 ppm. As the position of these methylene protons has shifted from 3.39 ppm it displays that the hydroxyl groups have reacted.

Figure 6.02 displays the ^{1}H spectrum for the isocyanate end capped prepolymer (IPDI-TMP-PCD) synthesised as the base prepolymer to be used for lamination. The reaction conditions were catalyst free, with a synthesis temperature of between 85°C - 95°C. Both these condition contribute towards the mixture of both primary and secondary free isocyanate groups being present as the end groups.[2] With both IPDI and PCD being aliphatic, coupled with the broad signals inherent of the soft-segment it results in the methyl region within the spectrum being rather complex (0.88 ppm - 1.30 ppm). Table 6.01 displays all the chemical shifts of the prepolymer molecules in deuterated chloroform for both nuclei.

The ^{1}H spectrum is dominated by the peaks from the PCD soft-segment which is 2000 molecular weight. Peaks inherent of the PCD soft-segment are visible at 2.26 ppm for methylene protons **1'** which are adjacent to ester carbonyls. Further backbone methylene protons in groups **2'**, **3'** and **4'** are visible at 1.66 ppm, 1.29 ppm and 1.60 ppm respectively. The final signals inherent of the soft-segment are the methylene protons adjacent to the ether oxygen at 4.01 ppm or within urethanes **5'** at 4.65 ppm.
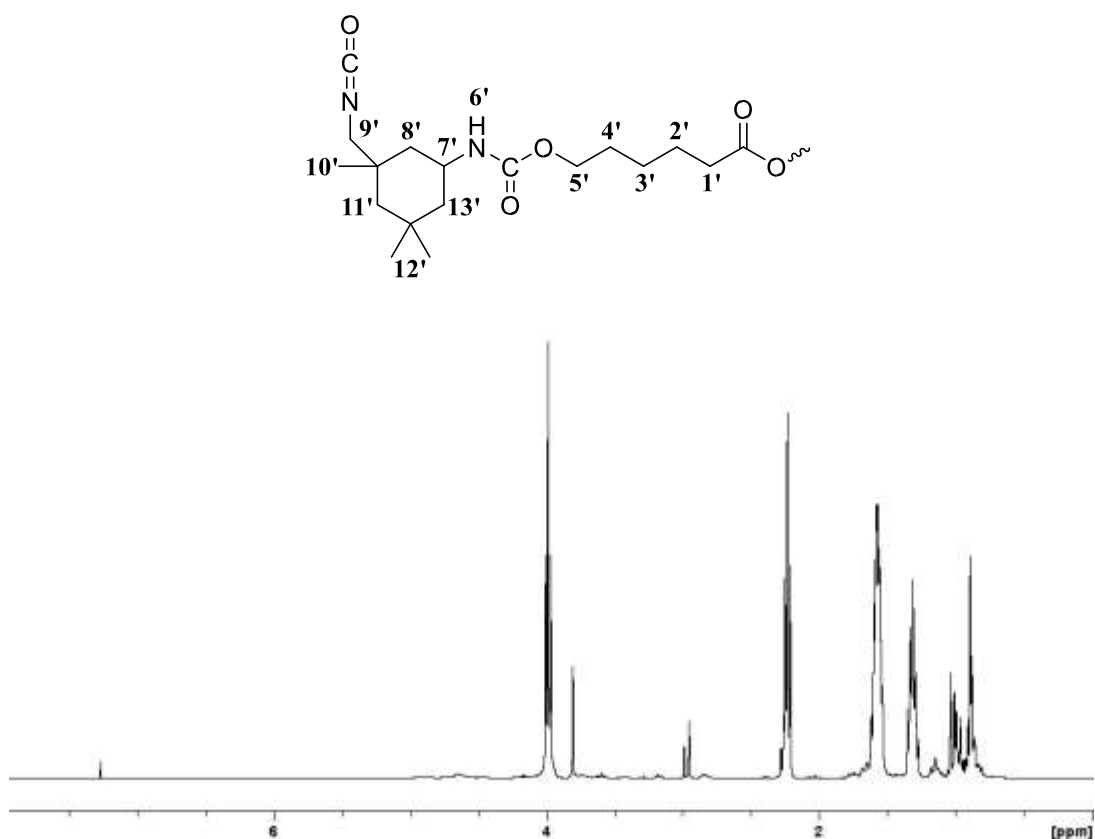
Figure 6.02: ¹H NMR spectrum of IPDI-TMP-PCD polyurethane prepolymer in deuterated chloroform.
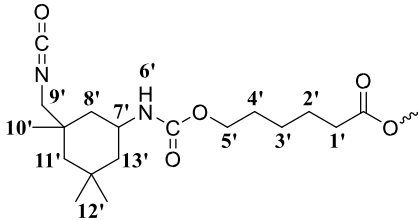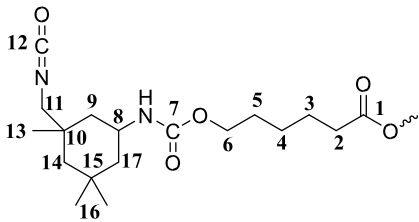
Evidence that primary isocyanate groups are retained within the prepolymer formulation is shown by the methylene protons **9'** at 2.98 ppm. Also visible is the consumption of a proportion of these primary isocyanate groups in the formation of urethane linkages which is shown by the upfield shift of these methylene protons to 2.71 ppm. This is also visible for the secondary isocyanate groups with the unreacted isocyanate groups shown by the adjacent methine protons at 3.19 ppm. Urethane linkages which contain secondary isocyanate groups are shown by the position of adjacent methine protons **7'** which have shifted downfield to 3.59 ppm.

For full assignment of peaks inherent of IPDI hard block see table 6.01.

¹³C NMR was next used to further investigate the prepolymer and confirm what was observed in ¹H NMR. Methyl carbons from neopentyl glycol which is used as the initiator are visible at 21.8 ppm and tertiary carbons can also be observed at 31.9 ppm. The methylene carbons adjacent to the urethane linkages occur at 77.1 ppm but are masked by the solvent peak. Peaks inherent of the PCD soft-segment are observed by

the carbonyl **1** of the ester linkage at 173.5 ppm. Backbone methylene carbons **2**, **3**, **4** and **5** are visible at 34.1 ppm, 24.5 ppm, 25.5 ppm and 24.8 ppm respectively. Methylene protons adjacent to the oxygen in ester linkages are visible in the backbone at 64 ppm. When adjacent to a urethane linkage theses groups appear more downfield at 69 ppm.

Table 6.01: ^{1}H and ^{13}C chemical shift for IPDI-TMP-PCD collected in CDCl$_3$.

IPDI-TMP-PCD	Position	^{1}H Chemical Shift (ppm)	Position	$_{13}$C Chemical Shift (ppm)
	1'	2.26	1	173.5
	2'	1.63	2	34.1
	3'	1.27	3	24.5
	4'	1.59	4	25.5
	5'	4.65	5	24.8
	6'	NDT	6	69
	7'	3.59	7	156.2$_p$/155.0$_s$
	8'	1.62/1.35	8	42.5
	9'	3.19/2.95	9	43.4
	10'	0.96	10	20.9
	11'	1.33/1.04	11	46.8
	12'	0.88	12	123$_p$/122s
	13'	1.62/1.35	13	23.4
			14	48.8
			15	21.7

| | | 16 | 31.9 |
| | | 17 | 48.1 |
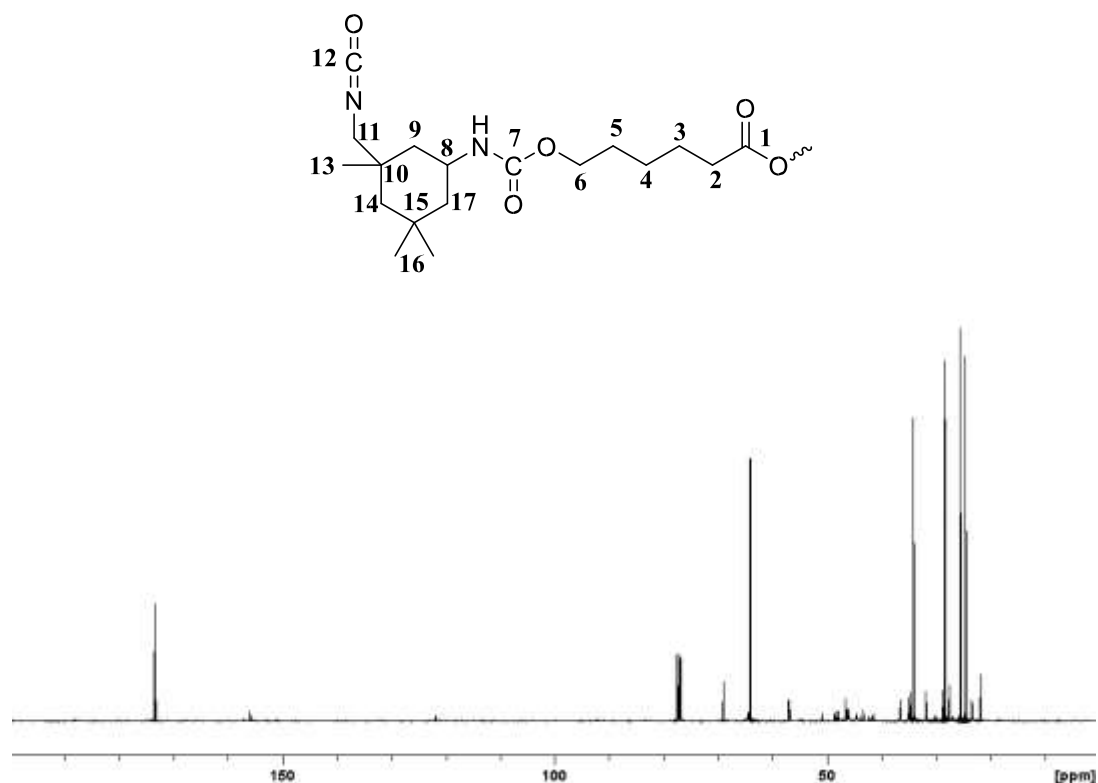
Figure 6.03: **¹³C NMR spectrum of IPDI-TMP-PCD prepolymer in deuterated chloroform.**

Complementary to what was observed for ¹H NMR evidence of both free isocyanate groups and urethane linkages are also visible in ¹³C NMR. Free primary isocyanate groups were observed at 123 ppm with secondary isocyanates shown at 122 ppm. Evidence that both groups are contained within urethane linkages is shown by two carbon signals at 155 ppm and 156.2 ppm for secondary and primary groups respectively. All carbon peaks inherent of IPDI are presented within table 6.01.

6.23 MALDI-MS Analysis

For a further insight into the structure of the prepolymer molecules, matrix assisted laser desorption ionisation time-of-flight mass spectrometry (MALDI-MS) analysis

was used. The molecular mass of both the starting soft-segment and the synthesised prepolymer were measured. The matrix used was 2-(4-Hydroxyphenylazo)benzoic acid (HABA) which was prepared as a 20 mg ml^{-1} solution in tetrahydrofuran (THF), this was then mixed with a 1 mg ml^{-1} solution of sodiated trifluoroacetic acid (NaTFA) in a 7:1 ratio respectively. IPDI-TMP-PCD was prepared as a 40 mg ml^{-1} solution in THF which was then mixed with the matrix in a 1:8 ratio of sample to matrix. 1 μl aliquots of the solution were then spotted and dried before analysis.
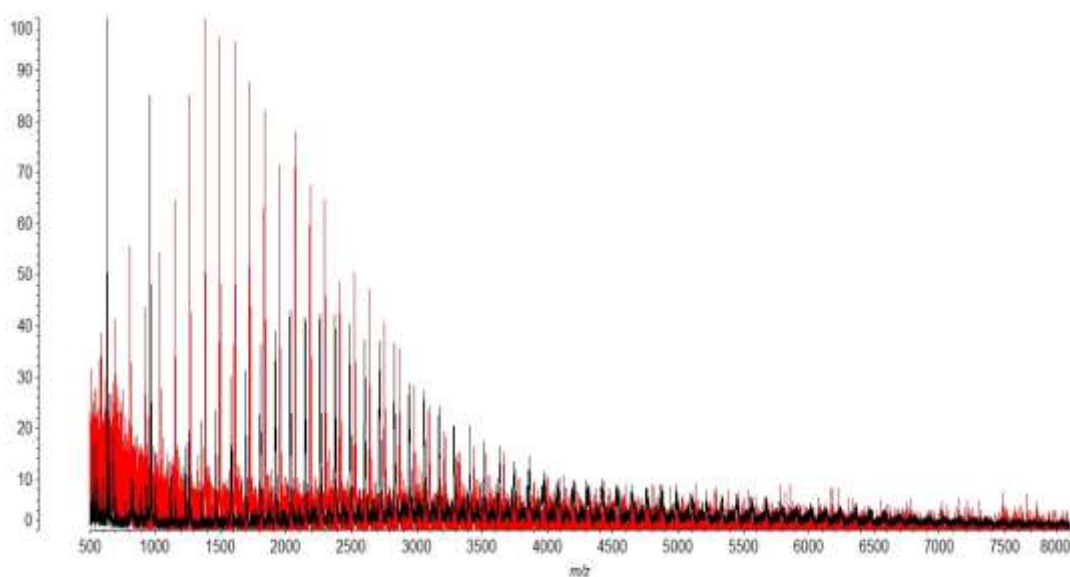
Figure 6.04: MALDI-MS spectra of PCD starting material in red and the prepolymer IPDI-TMP-PCD in black. Both were mixed with the matrix material of HABA and sodiated trifluoroacetic acid in a 1:8 sample:matrix mixture.

The mass spectrum of PCD in figure 6.04 displays the sodiated adduct of the softsegment with the sodium coming from the small amount of a cationising agent (NaTFA) added to enhance spectral quality. The molecular weight distribution for PCD has a peak mass of 1619 m/z which is 14 repeat units and one sodium ions. For the prepolymer material an observed shift of the distribution by 536 m/z was observed which correspond to the addition of two IPDI units that have had their free isocyanate groups end capped with ethanol to maintain the molecular weight. This peak centred at 2155 m/z contains the two ethanol end capped IPDI units one sodium ion and 14 caprolactone repeat units.

Present at 961 m/z is the chain-extender TMP that has reacted with three IPDI units which are also ethanol end-capped (plus a sodium cation). These molecules will contribute to the hard-segment microstructure and will interfere with the packing arrangement. From this spectrum it is clear that using a 2.2:1.0 excess of isocyanate to polyol makes it possible to obtain an IPDI-PCD-IPDI end capped prepolymer PUs.

MALDI-MS has allowed for characterisation of the structure of the molecules present in conjunction with the previous NMR analysis.

From the MALDI-MS spectrum it is possible to calculate Mn, Mw and PDI (see section 2.132 for formulae). For the soft-segment PCD, the value of Mn is 1695 m/z and the value of Mw is 1824 m/z giving a PDI of 1.08. Following polymerisation there is an increase to all three of these parameters. For IPDI-TMP-PCD, the calculated value of Mn is 3222 m/z and the calculated value of Mw is 3943 m/z giving a PDI of 1.22. Two things are visible from the data obtained for formulation IPDI-TMP-PCD; firstly the distribution shifts to higher mass following reaction with IPDI and secondly the mass profile becomes broader compared to PCD.

6.24 DSC and TGA Analysis

Monitoring the thermal behaviour of the prepolymer and cured adhesive is important to determine if the current formulation will be appropriate for the likely temperatures that each laminate will be exposed to during manufacture and use. Two techniques that were selected to investigate if the materials (prepolymer or cured adhesive) were capable of being stable within the set processing window of -20°C to 100°C were differential scanning calorimetry (DSC) and thermal gravimetric analysis (TGA). The thermal behaviour of the prepolymer directly after synthesis will be discussed first and the fully cured adhesive (adhesive removed from a TAc/TAc laminate) will be discussed second.

Recording the soft-segment glass transition temperature ($T_g$ss) of the prepolymer material will determine if the formulation is performing out with the identified processing window. Also the position of the $T_g$ss compared to the unreacted softsegment will give an indication about the morphology, molecular weight changes, cross-linking within the matrix and the compatibility of the two segments. The DSC

experiment was recorded within an inert nitrogen atmosphere from -90°C to 300°C at a ramp rate of 10°C min^{-1}. For the prepolymer IPDI-TMP-PCD the recorded $T_g$ss was -55°C which covered a range of -57°C to -52°C. When in its unreacted state, the PCD soft-segment has a $T_g$ss of -64°C which shows that the polymerisation has resulted in a shift of +9°C. From the molecular weight increase due to the end capping of PCD (plus trifunctional TMP molecules) the viscosity of the system will also have increased leading to an elevated $T_g$ss.
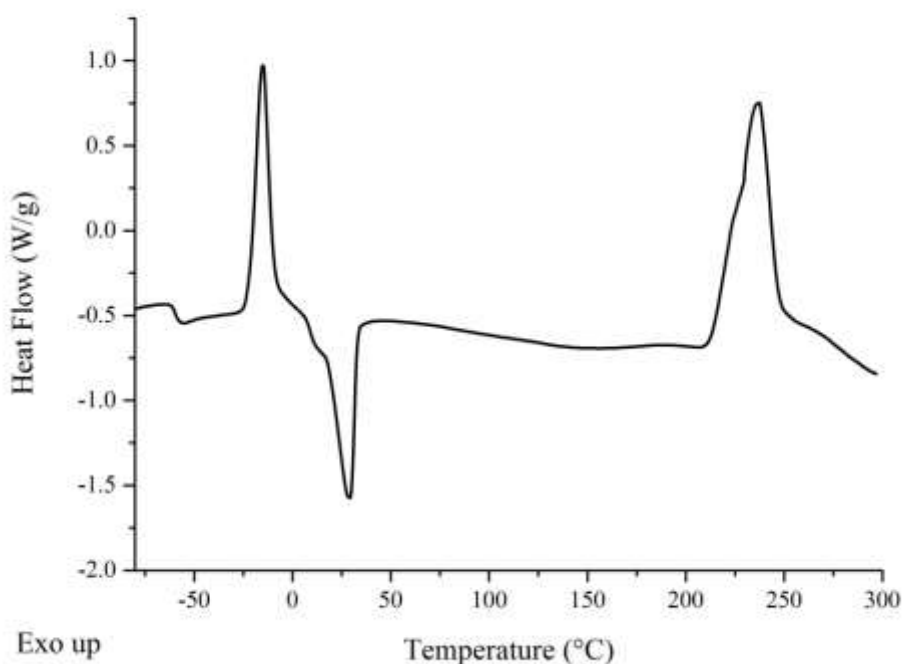
Figure 6.05: DSC thermogram of catalyst free IPDI-TMP-PCD prepolymer sampled directly after synthesis.

Crystallisation of the soft-segment is also observed and is shown by the sharp exothermic peak in the DSC thermogram of the prepolymer. The onset of this exothermic peak occurs at -5°C with peak temperature occurring at 10°C for a crystallisation enthalpy of 11 J g^{-1}. Following is the subsequent melting endotherm of the PCD soft-segment with an onset at 16°C, peak at 29°C which accounts for a melting enthalpy of 27 J g^{-1}. As the melting endotherm occurs around room temperature it displays a reduction in the melting temperature of the pure softsegment which occurs at 50°C. This reduction in melting temperature displays that there is a degree of phase

mixing within the prepolymers microstructure, thus depressing the melting temperature. A final exothermic peak was observed at 231°C with and enthalpy of 55 J g^{-1}. This peak is believed to be a curing of the free isocyanate groups via isocyanate based reactions. To fully understand the sure process further analysis would be required to determine the chemistry occurring.
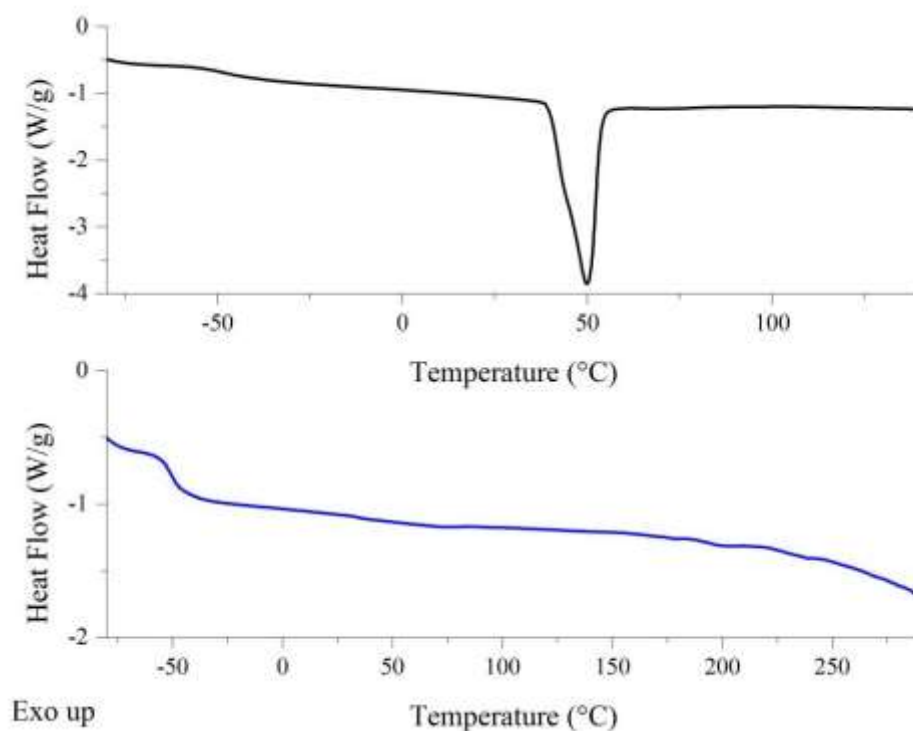
Figure 6.06: DSC thermogram of fully cured IPDI-TMP-PCD adhesive, following removal from TAc/TAc laminate. [First heating cycle *top* in black and second heating cycle *bottom* in blue].

Recording the $T_g$ss following 30 days of moisture cure at room temperature is much more informative as it indicates the final properties of the cured adhesive. The cured adhesive sample was removed from a pre-made test laminate consisting of two TAc plies and put through a heat cool-heat-cool-reheat experiment. The first heating cycle was recorded from -80°C to 140°C at 10°C min^{-1} and was used to both remove any thermal history from the sample plus investigate the soft-segment. The second heating cycle was recorded form -80°C to 300°C and was used to investigate the hard domains within the matrix.

In the first heating cycle two thermal transitions were visible a glass transition and a melting endotherm. A temperature of -46°C was recorded for the $T_g ss$, which covered a range from -50°C to -40°C. Next the melting endotherm recorded an onset at 40°C with peak at 49°C for a melting enthalpy of 28 J g^{-1}. From the position of the melting endotherm within this thermogram it would suggest that the soft-segment is phase segregated from the hard-segment as minimal depression of the melt temperature is observed.

In the second cycle again two thermal transitions were observed in the form of a glass transition and a melting endotherm. The melting endotherm of the softsegment was not observed upon the second heat scan as recrystallisation did not occur within the time frame of the experiment. A Tg_{ss} of -52°C was recorded on the second heating scan and covered a range of -55°C to -45°C. A second weak transition was observed with an onset of 191°C and peaked at 197°C. The recorded enthalpy of melting for this small peak was 0.3 J g^{-1} and was considered to be the thermal breakdown of the H-bonded hard-segments within the adhesives microstructure (urethane and urea).[3-5]
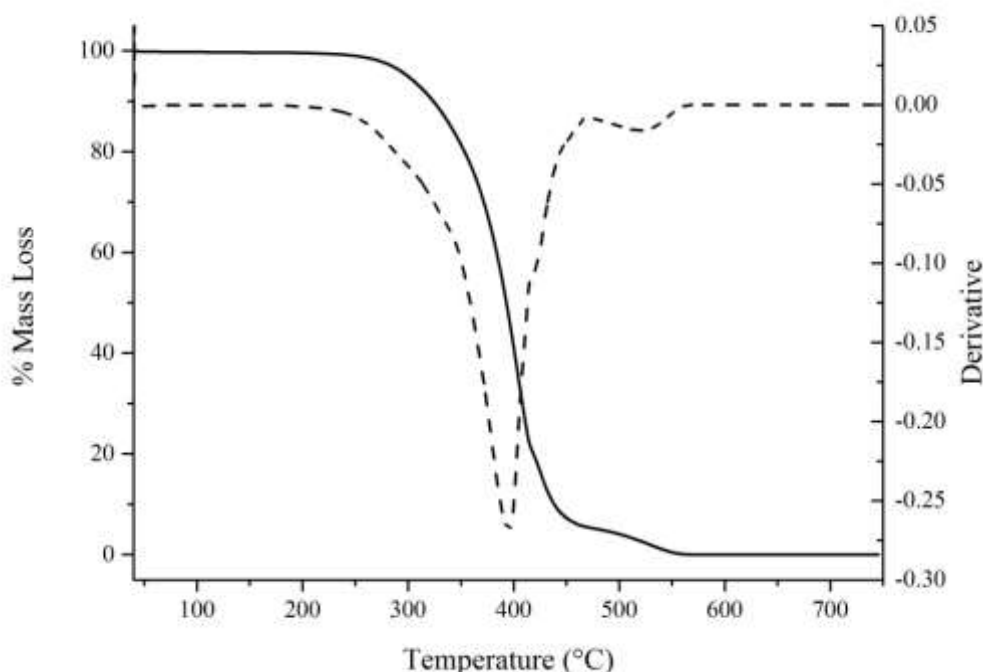
Figure 6.07: TGA and DTG curves of fully cured IPDI-TMP-PCD adhesive.

[TGA solid line and DTG dashed line].

Characterisation of the overall thermal stability of the fully cured adhesive was carried out using TGA. To ensure that the degradation of the adhesive was consistent the experiment was again performed under nitrogen from 40°C to 750°C at 10°C min^{-1}. From inspection of figure 6.07 it is evident that degradation occurs in two steps, as can be observed from TGA and DTG curves. It is widely accepted that the degradation profile of polyurethanes is complex due to the difference in thermal stabilities of the hard and soft-segment within the polyurethane microstructure.[3,6]

The dominant degradation process (shown in figure 6.07) has an onset of 300°C, with the peak rate occurring at 395°C. As this process is relatively broad it will contain both the hard and soft-segment degradation processes. Degradation through depolymerisation within the hard-segment will occur first as these bonds are thermally the weakest within the microstructure.[7,8] Degradation of the hard-segment occurs from the thermal breakdown of either urethane or urea bonds. Also contained within this broad peak will be the thermal break down of the soft-segment ester groups.[3] Another much smaller degradation peak at 521°C is visible and will most likely be the result from the breakdown of cross-linked products formed by reactive intermediates during degradation or a small amount of residual soft-segment.[7] For the intended application the onset of thermal degradation is well out with the temperature range that the laminate will experience during manufacture or use. This makes the formulation in question based on IPDI and PCD suitable for consideration as an adhesive for the intended application, however, the soft-segment crystallisation may be problematic.

6.25 180° T-peel Test and Haze

Recording the peel strength of the laminate has been an effective tool in gauging if the formulation will result in a high peel strength laminate with TAc or PC (greater than 3 N mm^{-1} is considered high for the intended application) once fully cured. In order to screen the adhesion potential of IPDI-TMP-PCD, six different laminates were constructed (as detailed in section 2.04), namely, TAc/TAc, TAc(t)/TAc(t), TAc(t)/PC, TAc(t)/PC(t), PC(t)/PC(t) and PC/PC. Each laminate was peeled at a rate of 100 mm min^{-1} for an extension of at least 150 mm, with the first 50 mm discarded from the peel strength value as this is where a stable crack was formed.

The haze of the fully cured laminate was also characterised prior to testing and the mode of failure for each laminate investigated following testing. 180° T-peel testing was performed to determine the compatibility of the adhesive with different surface chemistries and to determine if it would perform to the desired strength (> 3 N mm^{-1}). Three different interface scenarios were present within the test set: untreated (e.g. TAc/TAc or PC/PC), treated (TAc(t)/TAc(t) or PC(t)/PC(t)), and hybrid (TAc(t)/PC or TAc(t)/PC(t)).

Table 6.02: Peel, haze and mode of failure data for IPDI-TMP-PCD cured PUU adhesive. [The data in bold will be discussed within this section].

Cured Adhesive	Laminate	Peel 1* (N mm^{-1})	Peel 2^x (N mm^{-1})	Failure mode	Haze (%)
IPDI-TMP-PCD	TAc/TAc	0.9	0.6	Adhesive TAc	>1.5 %
	TAc(t)/TAc(t)	6.0	4.3	Ply	
	TAc(t)/PC	3.0	3.8	Adhesive Both	
	TAc(t)/PC(t)	2.8	2.9	Adhesive Both	
	PC(t)/ PC(t)	5.5	5.1	Adhesive Both	
	PC/PC	8.1	10.5	Adhesive Both	
IPDI-TMP-PCD-DEPD	TAc/TAc	0.8	0.7	Adhesive TAc	>1.5%
	TAc(t)/TAc(t)	5.0	5.6	Cohesive TAc	
	TAc(t)/PC	3.7	3.5	Cohesive TAc	
	TAc(t)/PC(t)	5.0	4.4	Cohesive TAc	
	PC(t)/ PC(t)	5.5	5.3	Adhesive Both	
	PC/PC	2.5	2.3	Adhesive Both	
IPDI-TMP-PCD-BD	TAc/TAc	1.1	1.0	Adhesive TAc	>1.5%
	TAc(t)/TAc(t)	0.8	ply	Cohesive	
	TAc(t)/PC	0.5	2.7	Adhesive PC	
	TAc(t)/PC(t)	0.6	4.1	Cohesive	
	PC(t)/ PC(t)	0.4	4.7	Cohesive	
	PC/PC	0.5	9.2	Adhesive PC	

IPDI-TMP-PCD-PD	TAc/TAc	1.0	0.7	Adhesive TAc	>1.5%
	TAc(t)/TAc(t)	0.7	4.8	Cohesive	
	TAc(t)/PC	0.5	3.3	Cohesive	
	TAc(t)/PC(t)	0.4	6.4	Cohesive	
	PC(t)/ PC(t)	0.3	7.8	Cohesive	
	PC/PC	0.4	9.9	Adhesive PC	

* peel 1 collected within 7 days of room temperature cure, ˣ peel 2 collected after 30 days of room temperature cure, ND = No Data

A laminate combination that is becoming of major interest is TAc/TAc due the consistent poor performance observed with all previous adhesives. The poor strength that was previously obtained displayed that the untreated surface has a very poor compatibility with each previous adhesive formulation. Results collected with the current formulation (as displayed in table 6.02) which now contains an ester based soft-segment has had no significant effect on the compatibility with the untreated surface. Following 7 days of cure the peel strength obtain for TAc/TAc was 0.9 N mm^{-1} and this slightly decreased to 0.6 N mm^{-1} after 30 days of cure. An unstable peel coupled with an adhesive mode of failure displays that the TAc – Adhesive interface is very poor and will only be operating by very weak (Van der Waals) adsorption forces.

Saponification of the TAc surface was next performed (see section 2.01) as this would present a more active regenerated cellulose surface and as displayed by previous testing this increases the compatibility at the adhesive - substrate interface. Deacetylation will leave hydroxyl groups at the surface which can react with the free isocyanate of the adhesive forming covalent bonds. Thus forming anchor points between the adhesive and substrate creating a strong interface. After 7 days of cure the peel strength recorded was 6.0 N mm^{-1} which decreased to 4.3 N mm^{-1} after 30 days of curing. These values were collected before cohesive failure of the TAc(t) ply occurred (full 150 mm displacement not possible). Both measurements register above the 3 N mm^{-1} set point which displays that the surface treatment has had the intended effect of increasing the compatibility between the adhesive and TAc(t). As possible explanation for the reduction in strength observed could be a result of the crystallisation of the soft-segment (observed in DSC first scan and white adhesive

colour) consuming ester groups that have previously been H-bonded at the interface. Another possible explanation is that upon becoming fully cured shrinkage of the adhesive layer has resulted and reduced the overall contact.

Previous testing has shown that PC laminates consistently perform above benchmark following 30 days of cure when there are no issues with curing or application. Untreated PC displayed an adhesive mode of failure at both PC interfaces which was coupled with strong deformation of the PC substrate. Following 7 days of cure, a peel strength of 8.1 N mm^{-1} was recorded and this increased to 10.5 N mm^{-1} after 30 days of curing. As untreated PC gives greater peel strengths than untreated TAc, it shows there is a better inherent compatibility with the cured adhesive. PC has a greater number of H-bonding sites available compared to TAC at the interface and this may account for the increased peel strengths being obtained.

Next PC(t) was tested to determine the effect of the treatment on peel strength. Treatment of the PC surface was performed using an ethanolamine in isopropyl alcohol solution (see section 2.02 for procedure) to further improve the surface compatibility with the reactive adhesive. The proposed mechanism for the surface treatment of the PC is nucleophilic attack of the carbonate linkage by the amine of ethanolamine to leave a phenol and a hydroxyl terminated urethane, although the precise mechanism is not known at this time.[9] If the proposed mechanism is correct then the surface treatment should leave OH functional groups at the surface that are available for covalent bonding with the free isocyanate groups. Data collected after 7 days recorded the peel strength at 5.5 N mm^{-1} which slightly decreased to 5.1 N mm^{-1} after 30 days of cure although this reduction was not considered significant. Each sample displayed an adhesive mode of failure at the PC(t) interface, this was also paired with strong substrate deformation. Compared to the untreated PC the affinity for the surface has been decreased by almost 50% following the surface treatment. As the recorded peel strength is decreased as a result of the surface treatment it would display that disruption of the adsorption chemistry at the interface has occurred. As the peel strengths recorded were well above benchmark the reduction in strength was not considered an issue.

Finally to determine which substrate was most compatible with the current formulation hybrid laminates were tested. First tested was TAc(t)/PC which displayed an adhesive mode of failure at both interfaces. For 7 days of curing the peel strength was 3.0 N mm^{-1} and this increased following 30 days of cure to 3.8 N mm^{-1}. Next the fully treated hybrid was tested (TAc(t)/PC(t)) and it also displayed an adhesive mode of failure at both interfaces. After 7 days of cure, a peel strength of 2.8 N mm^{-1} was recorded and following 30 days of cure the strength only marginally improved to 2.9 N mm^{-1}. These two laminate combinations display the affinity of the adhesive is not selective to one interface. Considering all the data collected for this current formulation then the substrate interfaces can be ranked as TAc(t) = PC = PC(t) > TAc. Once fully cured the adhesive displayed poor clarity as the average haze for the six laminate materials was > 1.5%. The high haze value was a result of the crystallisation of the PCD soft-segment which results in the adhesive becoming an opaque white colour.

6.26 ATR of Peeled Samples

Due to the varying peel strengths obtained it was essential to characterise if (a) the adhesive after 30 days was fully cured and (b) if once cured was the bulk adhesive the same final material.
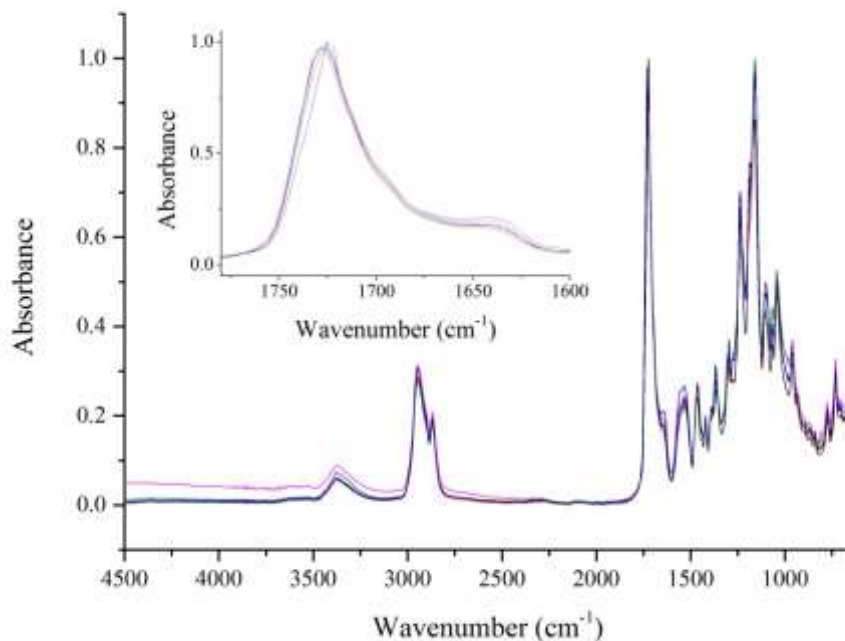
Figure 6.08: ATR spectra of cured IPDI-TMP-PCD sampled in-situ after peel testing with inset expanded carbonyl region. [TAc/TAc in black, TAc(t)/TAc(t) in red, TAc(t)/PC in blue, TAc(t)/PC(t) in pink, PC(t)/PC(t) in green and PC/PC in orange. Data collected for each laminate at nine random positions with each spectrum consisting of 128 scans at 8 cm^{-1} resolution. These were then averaged and plotted as the above spectra].

To investigate the bulk material ATR was used as it is a non-destructive way to sample the adhesive. ATR was carried out on the six different laminates once they had been peel tested after 30 days of curing. The purpose of this analysis was to characterise the bulk material following 30 days of cure and also to identify if there was any residual free isocyanate following this period of cure.

The spectra collected from the in-situ characterisation of the cured adhesive are shown within figure 6.08 for all six laminates. All characteristic peaks for the fully cured PU-U are shown within table 6.03. Observation of the band positioned at 3372 cm^{-1} displays that H-bonding between **N-H** groups within the network is occurring. Possible domains where H-bonding would occur are between urea or urethane groups in the formation of hard-segments or with soft-segment ester groups when the two

domains are intermixed. Also evident are **N-H** stretching vibrations that are not involved within the H-bonded network as shown by the shoulder to the previous peak at around 3500 cm^{-1}. Next aliphatic **C-H** stretching vibrations from PCD are present for both the asymmetric and symmetric bands at 2946 cm^{-1} and 2870 cm^{-1} respectively. No detectable isocyanate peak was visible between 2260 cm^{-1} – 2280 cm^{-1} which displays that the adhesive is fully cured after 30 days.

Next the carbonyl region of the spectrum will be investigated to determine if any further morphological information on the adhesive can be observed. The position of the carbonyl peak will show the order/disorder of the domain in which the carbonyl group resides and it will also indicate the type of functional group. From the position of the carbonyl at 1726 cm^{-1} it displays that ester groups are part of ordered domain as it confirms H-bonding (will be discussed within chapter 8). It would be expected that H-bonds within hard-segment will occur for urethane carbonyl groups but they are not visible due to the large intensity of the H-bonded ester carbonyl peak.[8,10]

Also within the carbonyl region there appears to be three different kinds of urea formed during the moisture cure of the free isocyanate groups (see inset expanded carbonyl region in figure 6.08). First encountered is a shoulder peak at 1697 cm^{-1} for carbonyl groups of free or unordered urea.[10] Evidence of monodentate H-bonded urea within the cured adhesive is visible by the broad shoulder attached to the previous peak between 1675 cm^{-1} – 1660 cm^{-1}.[8] Fully ordered bidentate urea groups are observed by the carbonyl peak at 1644 cm^{-1}. From the urea region alone it is clear that there are regions of high order, low order and regions of disorder. The ordered regions will contribute to the strength of the cured matrix through the formation of cross-links, whereas the disordered region will increase the phase mixing of the cured adhesive and clarity. Also within this formulation the order within the soft-segment as a consequence of the crystallisation will also contribute to the strength of the adhesive.[5]

Table 6.03: Characteristic peaks of IPDI-TMP-PCD cured PU-U adhesive from all six laminate combinations.

Wavenumber (cm^{-1})	Vibration	Wavenumber (cm^{-1})	Vibration

3372	N-H stretching Hbonded	1387	C-H symmetric deformation
2946	C-H asymmetric stretch	1360	C-N Urea
2870	C-H symmetric stretch	1295	C-N Urethane
1726	C=O stretch Hbonded Ester	1159	Asymmetric N-CO-O, C-H aliphatic skeleton
1697	C=O stretch free Urea	1093	C-O-C stretch aliphatic ester
1644	C=O stretch Urea Bidentate Hbonded	1055	Symmetric N-CO-O
1535	C-N stretch, N-H bend	968	C-O-C stretch aliphatic ester
1464	C-H bend aliphatic	777	C-C skeleton rocking
1426	C-H asymmetric deformation	725	C-C skeleton rocking

Further bands of urethane and urea formation are evident within the spectrum. At 1535 cm^{-1} both **C-N** stretching and **N-H** stretching can be observed from either urethane or urea. Aliphatic **C-H** bending vibrations inherent of both the hard and soft-segments within the PU-U microstructure are visible at 1464 cm^{-1}. Asymmetric and symmetric **C-H** deformations from the PCD soft-segment are visible at 1426 cm^{-1} and 1387 cm^{-1}. Evidence of urea within the finger print region is shown by the **C-N** stretching vibration at 1360 cm^{-1} with the urethane vibration also shown at 1295 cm^{-1}. Further urethane vibrations within the microstructure for the asymmetric and symmetric **N-CO-O** stretching are shown at 1159 cm^{-1} and 1055 cm^{-1} respectively. Aliphatic ester **C-O-C** stretching vibrations of the PCD soft-segment are present at 1093 cm^{-1} and 968 cm^{-1}. The final absorption peaks within the spectrum are **C-C** skeleton rocking vibrations at 777 cm^{-1} and 725 cm^{-1}.

ATR analysis has displayed that following 30 of days of moisture cure (at room temperature) that the adhesive is fully cured. In keeping with previous analysis the fully cured adhesive was again shown to be a PU-U with urethane formed during synthesis and the urea formed during subsequent moisture cure. As the material is fully cured it confirms that the mode of failure recorded during 180° T-peel testing is a result of it being the weakest part of the laminate.

6.27 Summary of IPDI-TMP-PCD Formulation

From the above analysis it can be confirmed from both ^{1}H and ^{13}C NMR that the end-capped polyurethane prepolymer was successfully synthesised. This was further confirmed by MALDI-MS analysis which also highlighted that the expected prepolymer IPDI-PPG-IPDI structure was obtained. MALDI-MS displayed than Mn, Mw and PDI increased following prepolymer synthesis.

Thermal analysis performed using DSC displayed that the prepolymer material had a $T_g$ss of -55°C which is a shift of +9°C compared to the PCD soft-segment. This was accompanied by both a crystallisation and melting peak of the soft-segment. Following moisture cure the $T_g$ss of the cured adhesive shifted to -47°C for the first heating cycle which also displayed a melting endotherm at -50°C. The shift of the $T_g$ss displays that the molecular weight has increased following cure. On the second heating cycle a glass transition and higher temperature melt were observed. The $T_g$ss recorded was -52°C and the small melting endotherm occurred at 197°C. From the position of the glass transition it displays that little mixing of the phases has occurred which is reinforced by the melting temperature of the soft-segment recorded in the first heating cycle. Breaking of H-bonds that hold hard-segments together within the microstructure are displayed by the high temperature melt, however, the small enthalpy value would suggest that these domains are not highly organised.[11] The increase in $T_g$ss will also be influenced by the increased viscosity of the fully cured system along with any cross-linking. More important however, was that the final $T_g$ss of the fully cured adhesive was out with the processing window. The thermal stability following moisture cure of the adhesive was evaluated using TGA which displayed an onset of degradation at 300°C with the peak rate occurring at 395°C.

Analysis carried out using 180° T-peel testing displayed that the best laminate combination was PC/PC which boasted a peel strength of 10.5 N mm^{-1} following 30 days of cure (greatest strength recorded so far). The worst laminate was TAc/TAc which registered 0.6 N mm^{-1} after 30 day of cure which is one tenth of the treated TAc laminate. PC based laminates also performed well with every combination involving PC or PC(t) resulting in peel strengths that were above the 3 N mm^{-1} benchmark. Finally ATR analysis displayed that following 30 days the adhesive was fully cured and a PU-U. It also displayed that ordered regions were present as shown by the H-bonding in **N-H** and **C=O** region. Also highlighted was that there are regions of free urea absent of any H-bonding. These groups may result from phase mixing between the different domains as a result of the more polar urea groups, but as the PCD soft-segments melting temperature has not shifted considerably, it displays that phase mixing is minimal.

6.30 Analysis of IPDI-TMP-PCD-DEPD

6.31 Synthesis Information

IPDI-TMP-PCD-DEPD was next synthesised with the intention of disrupting the close packing of hard-segments by using a less conventional chain-extender which should aid with phase mixing of the different domains. This was achieved by firstly synthesising the IPDI-TMP-PCD prepolymer using the same reaction conditions as detailed with section 6.21 and then performing an addition reaction set. The additional step was performed by adding a hydroxyl terminated chain-extender using a 2.2:1.0 isocyanate:hydroxyl ratio based on the calculated amount of free NCO remaining after step one. The chain-extension step was also used to lower the free isocyanate content of the adhesive, which would reduce the opportunity for excessive bubbling by CO_2 liberation produced during urea formation.

Step one was performed as previously detailed in section 6.21 and was a clear liquid which had an observed increase in viscosity from the starting mixture. After addition of 2,2-diethyl-1,3-propane diol (DEPD), the reaction was allowed to stir at 85°C – 95°C for seventeen hours before the dual DBTDL and TEA catalyst system was added. Following chain-extension a visual increase in viscosity was observed and was

associated with the molecular weight increase caused by the coupling step. The viscosity of the system was low enough that it did not require the temperature to be increased before transfer. Once the reaction was complete, the formulation was poured into an aluminium tube, which was then capped and degassed as previously outlined in section 2.03. The desiccator containing the adhesive filled tube was then placed within a 0°C fridge for storage. Degassing was performed for six hours once a vacuum of one atmosphere was obtained. Samples of the reaction were again taken before catalysed addition, these were analysed by DSC, NMR and MALDI-MS analysis.

IPDI-TMP-PCD-DEPD was heated to 105°C before being applied to six laminates which were cured at room temperature. These samples were 180° T-peel tested at 7 days and 30 days to determine the peel strength. A further lamination was performed using two plies of TAc which would allow for the fully cured adhesive to be removed for analysis by DSC and TGA. The 30 day peel test samples were also analysed by ATR to characterise the final adhesive and determine the extent of cure. Analysis of the chain-extended adhesive only will be presented within the remaining sections of this chapter. IPDI-TMP-PCD (sections 6.21-6.26) is considered as representative of the reactive intermediate obtained after step one of each chainextended reaction.

6.32 NMR Analysis

For full spectral characterisation of peaks from IPDI and PCD see section 6.22 (or table 6.04) as this section will only detail peaks that show prepolymer formation or peaks from the chain-extender.
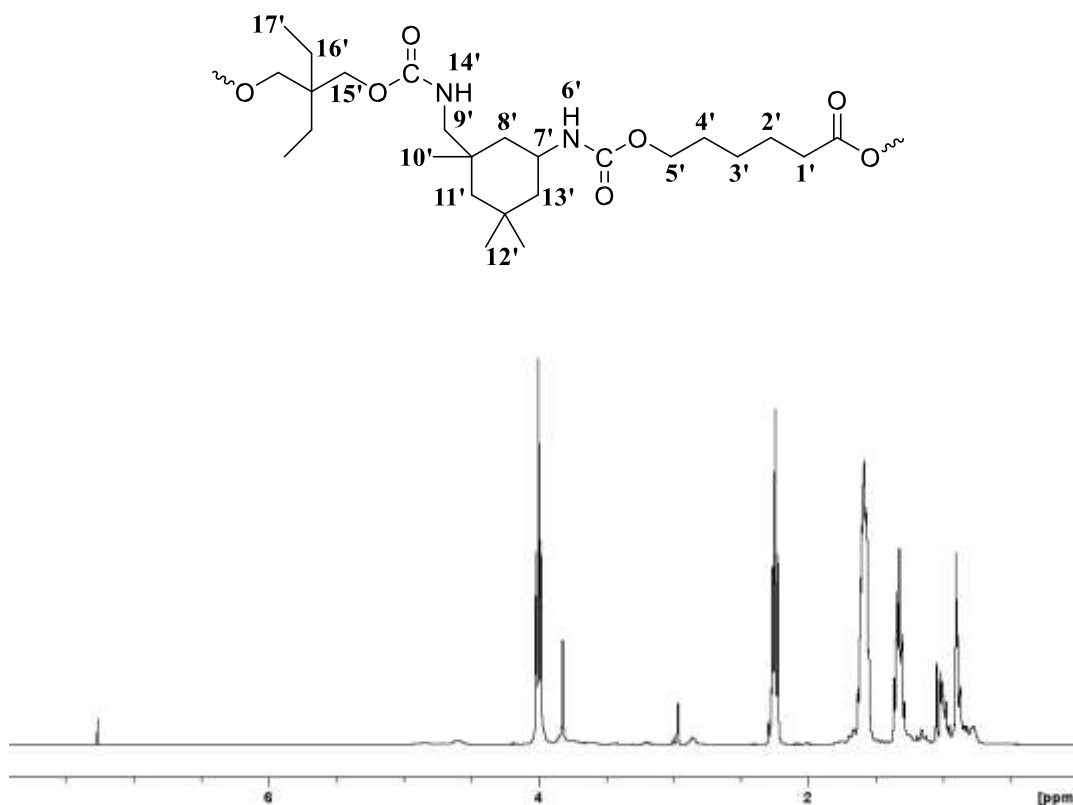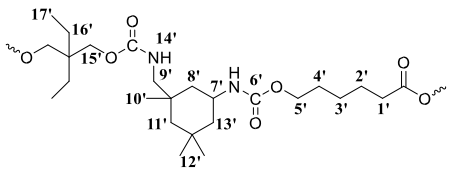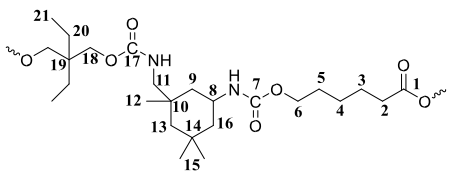
Figure 6.09: ¹H NMR spectrum obtained following reaction of IPDI-TMP-PCD with DEPD.

Previous analysis displayed that the synthetic procedure used is not selective towards either the primary or secondary isocyanate. During the chain-extension step there will be both isocyanate groups available for reaction with the primary hydroxyl groups of DEPD. Reaction of methylene protons **16'** are shown by the shift of the peak from 3.39 ppm to 3.96 ppm. Also evident are protons of the adjacent methylene groups of PCD formed during step one of synthesis at 4.65 ppm. Methylene protons **17'** within the ethyl side group are visible at 1.69 ppm and the methyl proton **18'** are visible at 0.79 ppm.

Table 6.04: ¹H and ¹³C chemical shift for IPDI-TMP-PCD-DEPD collected in CDCl₃.

IPDI-TMP-PCD-DEPD	Position	^{1}H Chemical Shift (ppm)	Position	^{13}C Chemical Shift (ppm)
	1'	2.26	1	173.5
	2'	1.63	2	34.1
	3'	1.27	3	24.5
	4'	1.59	4	25.5
	5'	4.65	5	24.8
	6'	NDT	6	69
	7'	3.59	7	157.2_p/156.0_s
	8'	1.62/1.35	8	42.5
	9'	2.97/2.71	9	43.4
	10'	0.96	10	21.0
	11'	1.33/1.04	11	46.3
	12'	0.88	12	25.6
	13'	1.62/1.35	13	48.8
	14'	NDT	14	21.8
	15'	3.96	15	31.9
	16'	1.70	16	48.2
	17'	0.79	17	157.2_p/156_s
			18	64.9
			19	34.1

		20	23.4
		21	7.2

Evidence of the chain-extenders incorporation into the prepolymer molecule was also observed by ^{13}C NMR analysis. Methyl carbons **23** of the ethyl side group are observed at 7.2 ppm and the methylene carbons **22** of this group are visible at 23.4 ppm. Next the tertiary carbon **21** of DEPD appears at 34.1 ppm and the adjacent methylene group **19** appears at 64.9 ppm. Carbon peaks that correspond to both end groups from end capping of PCD (step one of synthesis) appear at 69 ppm for adjacent methylene carbons in caprolactone end groups and 77.1 ppm for adjacent methylene carbons in the neopentyl glycol initiator (masked by solvent peak). Also present are the peaks which correspond to the carbonyl from reactive isocyanates still remaining within the formulation at 123 ppm for primary and 122 ppm for secondary. Finally peaks which display carbonyl groups within urethane linkages appear at 157.2 ppm for primary isocyanate groups within the urethane and 156 ppm for secondary isocyanate groups within a urethane.
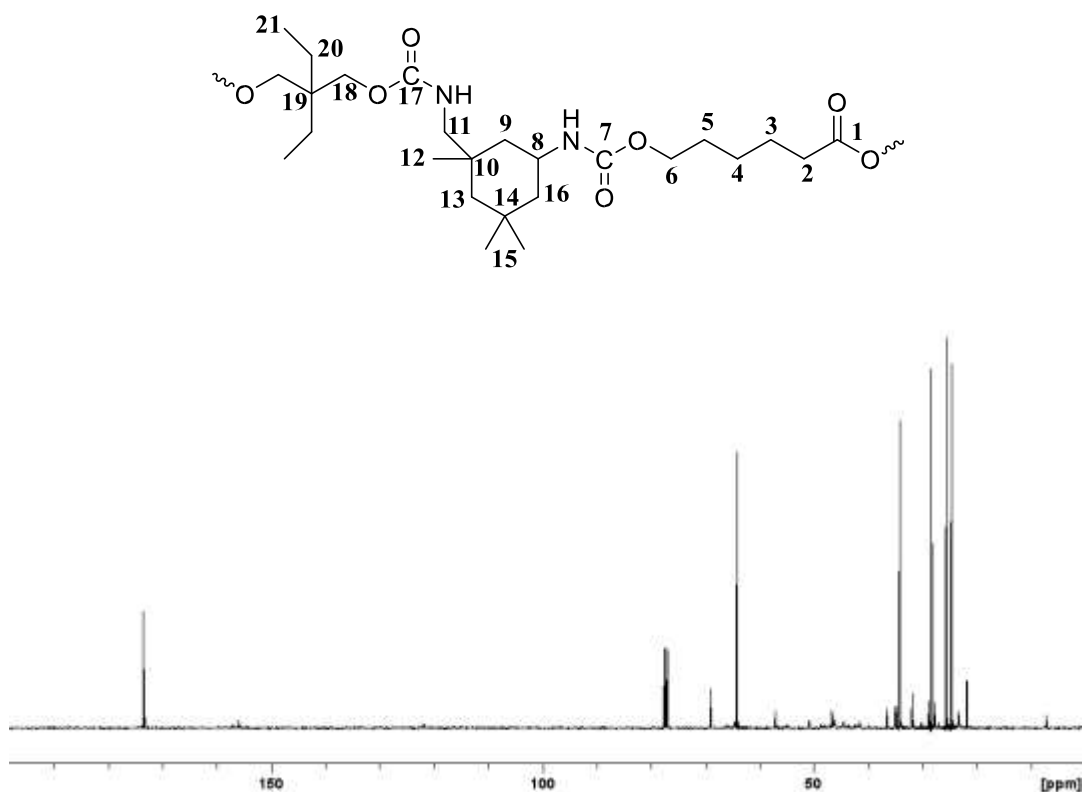
Figure 6.10: ^{13}C NMR spectrum obtained following reaction of MDI-TMP-PCD with DEPD.

6.33 MALDI-MS Analysis

To determine the molecular weight increase within the chain-extended prepolymer MALDI-MS was used. The matrix used for analysis was HABA which contained a cationising agent NaTFA (see section 3.23 for more matrix information). A 40 mg ml^{-1} solution of IPDI-TMP-PCD-DEPD was prepared in THF and mixed with the matrix (1:8 sample:matrix). 1 μl portions of this sample were then spotted and dried for analysis.

---

[1] H and ^{13}C NMR analysis of the chain-extended prepolymer of formulation IPDITMP-PCD-DEPD has been successfully, however, molecular weight data is required to gain further structure information.
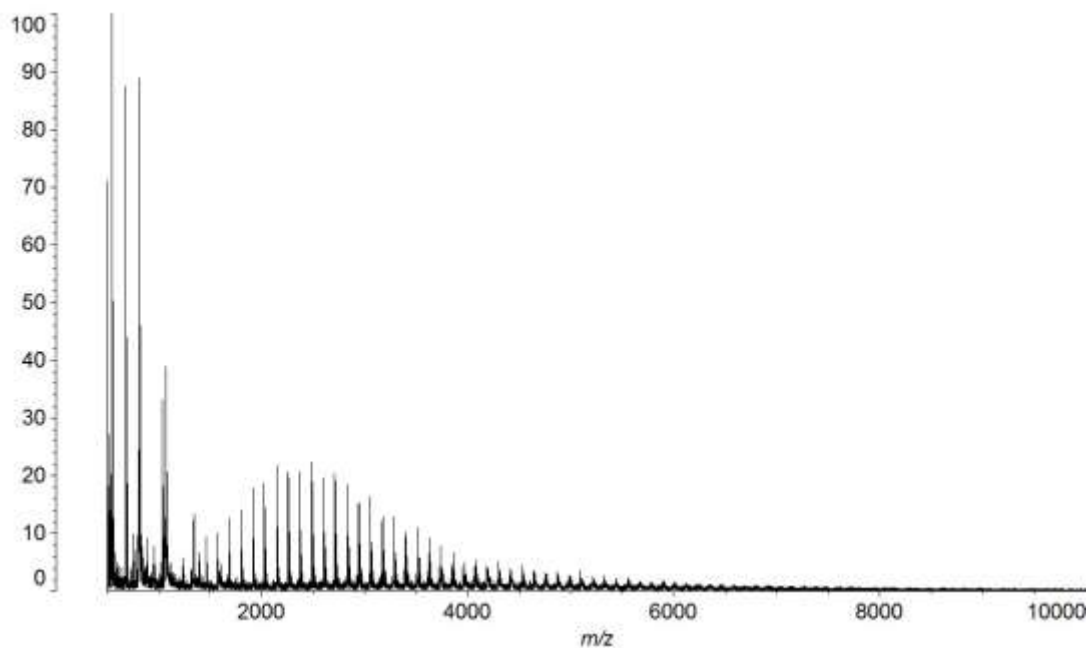
Figure 6.11: MALDI-MS spectrum of IPDI-TMP-PCD-DEPD chain-extended prepolymer collected in HABA/NaTFA.

The peak situated at 691 m/z corresponds to the chain-extender DEPD coupled with two ethanol end-capped IPDI units and one sodium cation. Also present is the crosslinking agent TMP that has reacted with three IPDI units which are also ethanol endcapped at 961 m/z (plus a sodium cation). These molecules will contribute to the hard-segment microstructure and will interfere with the packing arrangement.

The observed distribution centred on 2269 m/z corresponds to the PCD soft-segment that is isocyanate end-capped IPDI-PPG-IPDI. Prepolymer of this type are formed during step one of the synthetic process and a contribution of this prepolymer would be expected to remain. A further two distributions are visible which are off set from this distribution by 23 m/z due to the di-sodiated adduct and 132 m/z for prepolymers that have reacted with DEPD but have not yet coupled with another molecule. Evidence of chain-extended prepolymers of type IPDI-PCD-IPDI-DEPD-IPDI-PCDIPDI are shown within the spectrum but with lower resolution with an example peak of these prepolymers is visible at 5695 m/z. The weak response of these higher molecular weight prepolymers is believed to result from their poorer ability to ionise meaning fewer will reach the mass spectrometer.

Mn, Mw and PDI are then calculated to determine the influence that DEPD has on these parameters. The calculated value for Mn is 4248 m/z and the calculated value of Mw is 5162 m/z giving a PDI of 1.22. Chain-extension with DEPD has resulted in an increase to Mn and Mw while retaining the same breadth of distribution compared to IPDI-TMP-PCD.

6.34 DSC and TGA Analysis
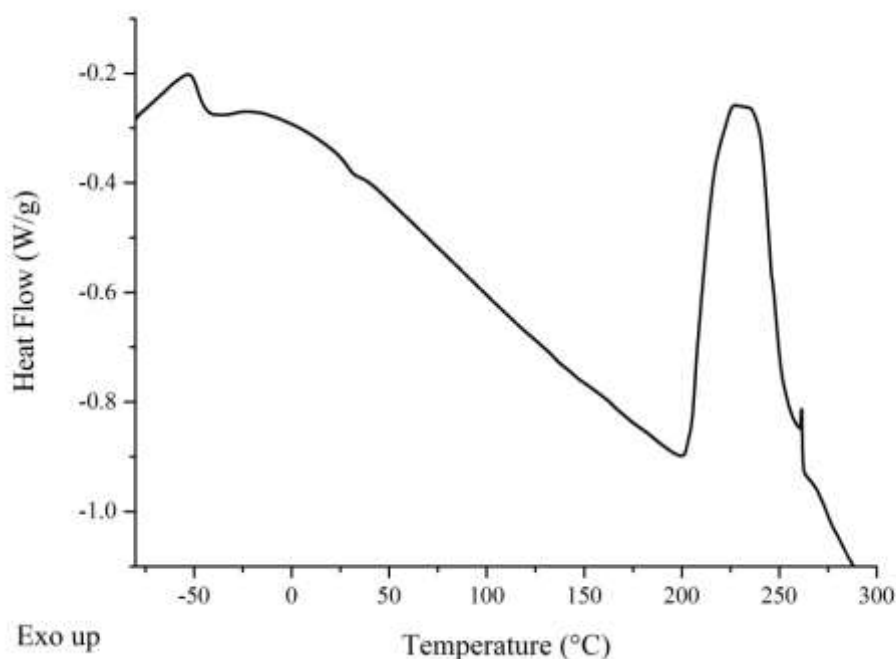
Figure 6.12:   DSC thermogram of IPDI-TMP-PCD-DEPD prepolymer formulation.

Following synthesis of the chain-extended prepolymer, the thermal characteristics of the formulation were investigated to primarily determine the $T_g$ss and to determine if a melting endotherm from the hard or soft-segments was visible. As previously mentioned the $T_g$ss of the material was considered important as it had to be lower than -20°C to be suitable for the intended laminate application. Within figure 6.12 the DSC thermogram for the DEPD chain-extended prepolymer is presented. Analysis of the thermogram obtained for the chain-extended prepolymer displays a $T_g$ss of -48°C

which cover a range of -51°C to -44°C. A shift in the $T_g$ss of +16°C can be observed compared to the unreacted PCD soft-segment and +7°C with reference to the base prepolymer (IPDI-TMP-PCD).
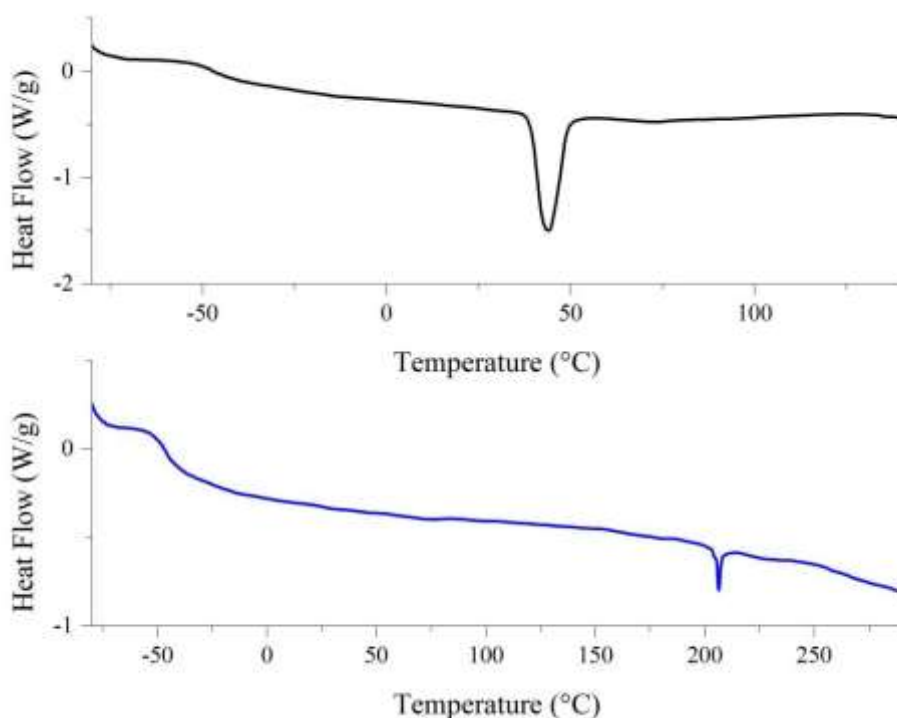
Figure 6.13: DSC thermogram of fully cured IPDI-TMP-PCD-DEPD adhesive, following removal from TAc/TAc laminate. [First heating cycle *top* in black and second heating cycle *bottom* in blue].

This shift in the $T_g$ss would suggest that the prepolymer has increased in molecular weight, has a degree of cross-linking or has ordered domains within the microstructure. Also observed was an exothermic peak at 235°C with an enthalpy of 84 J g^{-1}, this peak displays the curing of the residual free isocyanate groups within the sample. Following 30 day of curing a portion of the adhesive was removed from the TAc/TAc laminate for DSC analysis. The adhesive was analysed using a coolheat-cool-reheat experiment to determine the $T_g$ss within each heating cycle as shown in figure 6.13 (same experiment procedure as detail in section 6.24). From the first heating cycle a $T_g$ss was observed at -47°C, with the thermal transition covering a narrow range of 11°C from -51°C to -40°C. A melting endotherm from the soft-segment was also visible at 44°C with the enthalpy of the melting peak 9 J g^1. The depreciation in melt temperature and reduction in enthalpy would suggest that following moisture cure the morphology

has become more phased mixed. After a second heating cycle, the $T_g$ss was recorded at -47°C and covered a broad range from -51°C to -38°C.
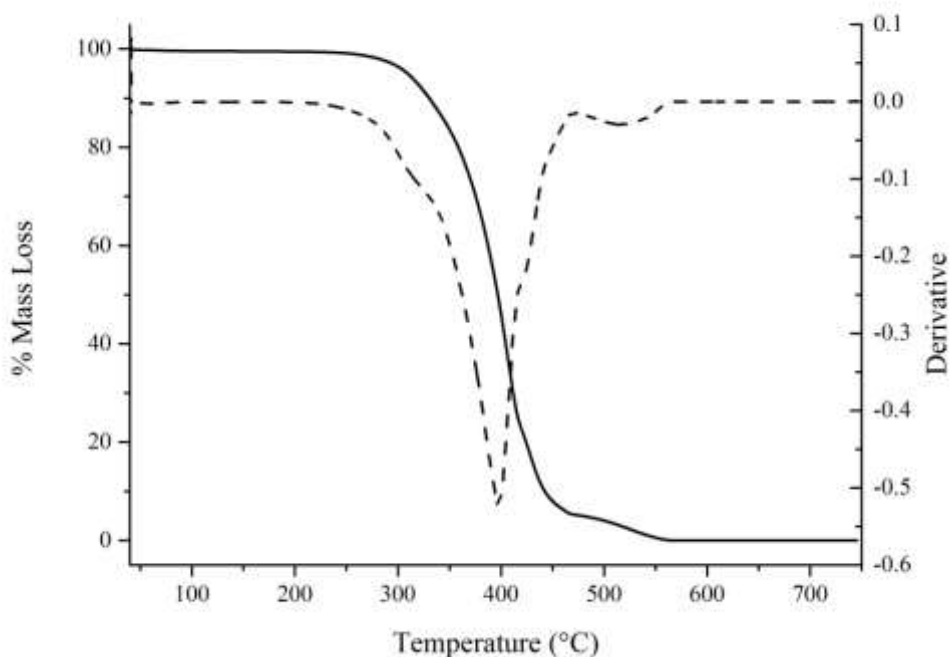
Figure 6.14: TGA and DTG curves of fully cured IPDI-TMP-PCD-DEPD adhesive. [TGA solid line and DTG dashed line].

Also observed on the second heating cycle was a melting endotherm of the hardsegments within the microstructure at 206°C with the enthalpy of melt 1 J g⁻¹. From DSC of the fully cured adhesive it was observed that the $T_g$ss is well outside the processing window. Also observed were melting endotherms for both soft and hardsegments within the PU-U microstructure (discussion of the morphology will be presented within chapter 8).

Following moisture cure TGA was carried out to determine if chain-extension with DEPD had any effect on the overall thermal stability. Within figure 6.14 the TGA and DTG curves for the fully cured adhesive are displayed. From the TGA curve the onset of degradation (calculated as 5% of the total mass lost) was calculated to be 309°C which is 9°C higher that the base prepolymer material (IPDI-TMP-PCD). This slight increase was not considered to be significant. The previous comment is reinforced by inspection of the DTG curve which displayed that the maximum rate of degradation

occurs at 397°C (IPDI-TMP-PCD occurred at 395°C). This main degradation process will be a combination of the thermal cleavage of both urethane and urea hard-segment bonds within the adhesives microstructure coupled with breakdown of the soft-segment PCD.[3,7,8] A secondary more thermally stable process is also observed by the degradation peak at 517°C which will be the breakdown of cross-linked materials formed during degradation.[7]

From the TGA data collected it was apparent that the thermal stability of the chainextended adhesive was comparable to the previous formulation (IPDI-TMP-PCD) and that the onset of degradation is well outside the processing temperature of the laminate.

6.35 180° T-peel Test and Haze

Previous analysis for the cured adhesive which was absent of any diol chain-extender displayed that TAc performed poorly whereas TAc(t), PC and PC(t) performed above 3 N mm^{-1} . Following 7 days of moisture cure the observed mode of failure for TAc/TAc was adhesive at the TAc interface with a peel strength of 0.8 N mm^{-1} recorded. Following 30 days of cure the peel strength did not change significantly and was recorded at 0.7 N mm^{-1}, again the mode of failure was adhesive at the TAc interface. As was observed in all previous formulations, TAc/TAc performs extremely poorly and is well outside the 3 N mm^{-1} target peel strength. Also highlighted in previous formulations was that saponification of the TAc interface was essential to obtain high peel strengths. Data collected using the fully cured adhesive of formulation IPDI-TMP-PCD-DEPD was consistent with previous analysis. Following 7 days of moisture cure the peel strength recorded was 5.0 N mm^{-1} which increased to 5.6 N mm^{-1} after 30 days of curing.

Table 6.05: Peel, haze and mode of failure data for IPDI-TMP-PCD-DEPD cured PU-U adhesive. [The data in bold will be discussed within this section].

Cured Adhesive	Laminate	Peel 1* (N mm^{-1})	Peel 2^x (N mm^{-1})	Failure mode	Haze (%)
IPDI-TMPPCD	TAc/TAc	0.9	0.6	Adhesive TAc	>1.5%
	TAc(t)/TAc(t)	6.0	4.3	Ply	

	TAc(t)/PC	3.0	3.8	Adhesive Both	
	TAc(t)/PC(t)	2.8	2.9	Adhesive Both	
	PC(t)/ PC(t)	5.5	5.1	Adhesive Both	
	PC/PC	8.1	10.5	Adhesive Both	
IPDI-TMP-PCD-DEPD	**TAc/TAc**	**0.8**	**0.7**	**Adhesive TAc**	**>1.5 %**
	TAc(t)/TAc(t)	**5.0**	**5.6**	**Cohesive TAc**	
	TAc(t)/PC	**3.7**	**3.5**	**Cohesive TAc**	
	TAc(t)/PC(t)	**5.0**	**4.4**	**Cohesive TAc**	
	PC(t)/ PC(t)	**5.5**	**5.3**	**Adhesive Both**	
	PC/PC	**2.5**	**2.3**	**Adhesive Both**	
IPDI-TMP-PCD-BD	TAc/TAc	1.1	1.0	Adhesive TAc	>1.5%
	TAc(t)/TAc(t)	0.8	ply	Cohesive	
	TAc(t)/PC	0.5	2.7	Adhesive PC	
	TAc(t)/PC(t)	0.6	4.1	Cohesive	
	PC(t)/ PC(t)	0.4	4.7	Cohesive	
	PC/PC	0.5	9.2	Adhesive PC	
IPDI-TMP-PCD-PD	TAc/TAc	1.0	0.7	Adhesive TAc	>1.5%
	TAc(t)/TAc(t)	0.7	4.8	Cohesive	
	TAc(t)/PC	0.5	3.3	Cohesive	
	TAc(t)/PC(t)	0.4	6.4	Cohesive	
	PC(t)/ PC(t)	0.3	7.7	Cohesive	
	PC/PC	0.4	9.9	Adhesive PC	

* peel 1 collected within 7 days of room temperature cure, ˣ peel 2 collected after 30 days of room temperature cure, ND = No Data

The observed mode of failure was different from previous analysis as a cohesive mode of failure in the TAc(t) substrate ply was obtained (adhesive failure mode at the interface the most common failure in previous analysis see chapters 3,4 and 5). Also accompanying the cohesive failure was strong ply deformation of the TAc(t) substrate.

Data collected from this cured adhesive further confirms the need for surface treatment of TAc to gain high peel strength.

The peel strength recorded following 7 days of cure on PC was 2.5 N mm^{-1}, a slight reduction to 2.3 N mm^{-1} was observed after 30 days. Both experiments displayed an adhesive mode of failure at the interface and slight deformation of the PC substrate. These strength values collected using this current formulation are below benchmark and lower than anticipated (IPDI-TMP-PCD 10.5 N mm^{-1} after 30 days).

Treatment of the PC interface was again performed and the peel strength measured. After 7 days of cure the peel strength of the fully treated PC laminate was 5.5 N mm^{-1} which depreciated to 5.3 N mm^{-1} after 30 days. An adhesive mode of failure at the interface was recorded for both experiments and was accompanied by strong deformation of the substrate. Following PC surface treatment an increase in the overall peel strength is observed and supports the treatment mechanism which allows for formation of covalent bonds to the substrate.

Analysis so far in this chapter has identified that the adhesive has an affinity for the TAc(t), PC(t) or PC over TAc. To identify the weakest interface or component of the laminate, hybrid systems were next tested. Discussed first is the laminate of composition TAc(t)/PC which recorded a peel strength of 3.7 N mm^{-1} following 7 days and 3.5 N mm^{-1} after 30 days of cure. The mode of failure was cohesive in the TAc(t) substrate with deformation of the PC layer. For the fully treated laminate a 7 day peel strength of 5.0 N mm^{-1} was recorded which reduced to 4.4 N mm^{-1} after 30 days. Again the mode of failure was cohesive in the TAc(t) substrate layer with deformation of the PC substrate. Both experiments have identified that the TAc(t) substrate is the weakest component of the laminate as evident by the TAc(t) cohesive failure. It was also noted that each laminate combination performed above the set 3 N mm^{-1} benchmark.

Finally the overall haze for the fully cured adhesive across all six laminates was > 1.5% and the adhesive layer within each laminate was milky white in colour. This haze value displays that chain-extension has not significantly improved the clarity of the adhesive layer by disruption of soft-segment crystallisation. A high haze value would

have been anticipated due to the large melting endotherm recorded during the first heating scan in DSC analysis.

6.36 ATR of Peeled Samples

Characterisation of the bulk material was performed on all six of the laminates after the 30 day tensile test. ATR analysis will determine the chemical functionality of the final cured material and allow for any distinct differences in curing chemistry to be observed. Also ATR will give some indication of the inherent morphology of the fully cured adhesive. Discussed within this section will be peaks that indicate the PU functionality of the chain-extended prepolymer or PU-U peaks obtained after 30 days of moisture cure. For discussion of the peaks inherent of the starting materials see section 6.26 and for all characteristic peaks see table 6.06.

From the spectra present with figure 6.15 it is visible there are two different **N-H** vibrations within the above cured PU-U. **N-H** stretching vibrations occurring at 3374 cm^{-1} show that H-bonded domains are present in the microstructure whereas, the shoulder peak at around 3500 cm^{-1} correspond to free **N-H** stretching vibrations. Corresponding bending vibrations are visible in the fingerprint region of the spectra for **N-H** at 1531 cm^{-1}, also present within this peak is the **C-N** stretch. **C-N** bending vibrations are also observed for urea at 1363 cm^{-1} and urethane at 1296 cm^{-1}. Again no detectable isocyanate peak was visible between 2260 cm^{-1} – 2280 cm^{-1} which displays that the adhesive is fully cured after 30 days.
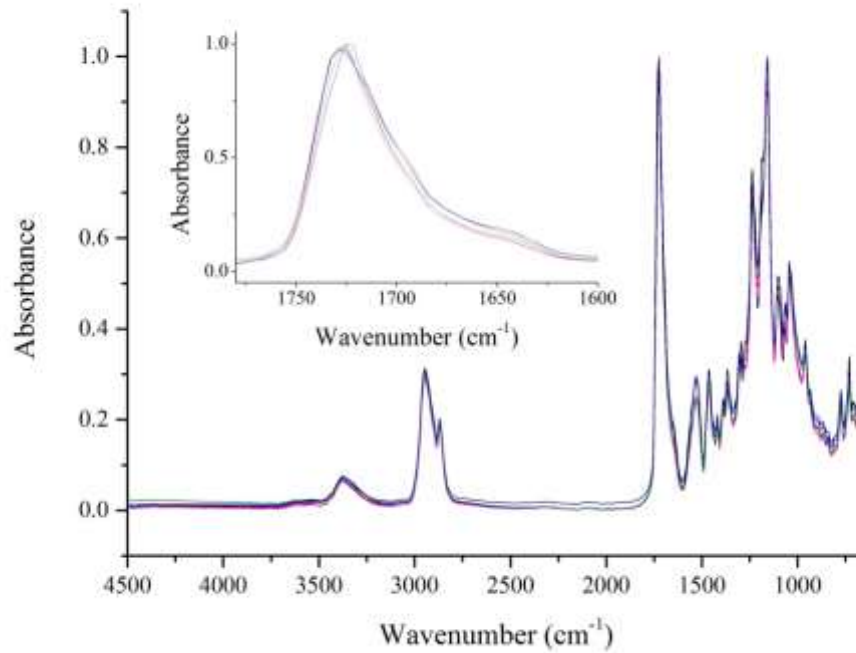
Figure 6.15: ATR spectra of cured IPDI-TMP-PCD-DEPD sampled in-situ after tensile testing with inset expanded carbonyl region. [TAc/TAc in black, TAc(t)/TAc(t) in red, TAc(t)/PC in blue, TAc(t)/PC(t) in pink, PC(t)/PC(t) in green and PC/PC in orange. Data collected for each laminate at nine random positions with each spectrum consisting of 128 scans at 8 cm^{-1} resolution. These were then averaged and plotted as the above spectra].

Further information on the inherent microstructure following moisture cure is available within the carbonyl region. Evidence of H-bonded ester carbonyl stretching is visible at 1725 cm^{-1} which would indicate the formation H-bonds within the soft-segments of the microstructure. An immediate shoulder to this peak displays the occurrence of free urea carbonyl stretching at 1696 cm^{-1}. Further evidence of structured regions within the microstructure of the cured adhesive is shown by the bidentate H-bonded urea stretching vibration at 1644 cm^{-1}. As these peaks are beginning to convolute together it also displays that there will be proportion of monodentate urea groups which has a characteristic vibration of 1675 cm^{-1} – 1660cm^{-1}. The overall morphology observed from ATR will be discussed in greater detail within chapter 8.

Table 6.06: Characteristic peaks of IPDI-TMP-PCD-DEPD cured PU-U adhesive from all six laminate combinations.

Wavenumber (cm^{-1})	Vibration	Wavenumber (cm^{-1})	Vibration
3374	N-H stretching Hbonded	1389	C-H symmetric deformation
2948	C-H asymmetric stretch	1363	C-N Urea
2867	C-H symmetric stretch	1296	C-N Urethane
1725	C=O stretch Hbonded Ester	1158	Asymmetric N-CO-O, C-H aliphatic skeleton
1696	C=O stretch free Urea	1103	C-O-C stretch aliphatic ester
1644	C=O stretch Urea Bidentate Hbonded	1043	Symmetric N-CO-O
1531	C-N stretch, N-H bend	961	C-O-C stretch aliphatic ester
1464	C-H bend aliphatic	775	C-C skeleton rocking
1419	C-H asymmetric deformation	730	C-C skeleton rocking

6.37 Summary of IPDI-TMP-PCD-DEPD Formulation

Synthesis of the DEPD chain-extended prepolymer was followed using NMR which displayed successful synthesis. MALDI-MS was used to characterise the molecular mass distributions present within the chain-extended prepolymer formulation. MALDI-MS identified prepolymers from step one as the main molecular weight distribution. Also encountered were two further distributions which are off set from

the main distribution by 23m/z for the di-sodiated adduct and 132 m/z for prepolymers that have reacted with DEPD. Most importantly evidence of fully chain-extended prepolymers were also observed

Investigation of the thermal transition by DSC recorded a $T_g$ss for the chain-extended prepolymer of -48°C which is an elevation of +16°C compared to PCD. Once fully cured the $T_g$ss was recorded -47°C on both heating cycles. Observed on the first heating cycle was a melting endotherm from the soft-segment at 44°C. As the melting temperature was lower than PCD (50°C), it highlights that the crystalline soft-segment domains are less pure and suggests some phase mixing is occurring. Observed on the second heating cycle was melting of the hard-segments within the PU-U which display that region of phase segregation are present. The overall thermal stability was determined by TGA with the onset of degradation occurring at 309°C. From the DTG curve a single degradation peak was observed which represented the decomposition of both the hard and soft-segment.

Using 180° T-peel testing it was identified that untreated TAc performed very poorly (0.7 N mm^{-1}), however, following surface treatment the values performed 7 fold greater (5.6 N mm^{-1}). Untreated PC performed unexpectedly poor and only exceeded the 3 N mm^{-1} benchmark following surface treatment. From hybrid laminates it was identified that the TAc(t) substrate was the weakest component as was displayed by the cohesive mode of failure within this substrate.

The haze values recorded for each of the six laminates was > 1.5% and the adhesive layer was milky white in colour. This value would have been expected based on the data obtained on the first heating cycle using DSC which displayed a melting endotherm of the soft-segment. Finally using ATR, the adhesive material was observed to be fully cured following 30 days of curing. Also observed was that the fully cured adhesive was a PU-U and that there were H-bonding domains within the cured network.

6.40 Analysis of IPDI-TMP-PCD-BD

6.41 Synthesis Information

IPDI-TMP-PCD-BD was next synthesised with the intention of disrupting the close packing of hard-segments through using a less conventional diol chain-extender which should aid with phase mixing of the different domains. This was achieved by firstly synthesising the IPDI-TMP-PCD prepolymer using the same reaction conditions as detailed with section 6.21 and then performing an addition reaction set. The additional step was performed by adding a hydroxyl terminated diol chainextender using a 2.2:1.0 isocyanate:hydroxyl ratio based on the calculated amount of free NCO remaining after step one. The chain-extension step was also used to lower the free isocyanate content of the adhesive, which would reduce the opportunity for excessive bubbling by CO_2 liberation produced by the formation of urea during moisture cure.

Step one was performed as previously detailed in section 6.21 and was a clear liquid which had an observed increase in viscosity from the starting mixture. After addition of 1,3-butane diol (BD), the reaction was allowed to stir at 85°C – 95°C for seventeen hours before the dual DBTDL and TEA catalyst system was added. Following chain-extension a visual increase in viscosity was observed and was associated with the molecular weight increase caused by the coupling step. The viscosity of the system was low enough that it did not require the temperature to be increased before transfer. Once the reaction was complete the formulation was poured into an aluminium tube, which was then capped and degassed as previously outlined in section 2.03. The desiccator containing the adhesive filled tube was then placed within a 0°C fridge for storage. Degassing was performed for six hours once a vacuum of one atmosphere was obtained. Samples of the reaction were again taken before catalysed addition, these were analysed by DSC, NMR and MALDI-MS analysis.

IPDI-TMP-PCD-BD was heated to 105°C before being applied to six laminates which was followed by room temperature cure. These samples were 180° T-peel tested at 7 days and 30 days to determine the peel strength. A further lamination was performed using two plies of TAc which would allow for the fully cured adhesive to be removed

for analysis by DSC and TGA. The 30 day peel test samples were also analysed by ATR to characterise the final adhesive and determine the extent of cure.

Analysis of the chain-extended materials only will be presented within the remaining sections of this chapter. IPDI-TMP-PCD (sections 5.21-5.26) is considered as representative of the reactive intermediate obtained after step one of each chainextended reaction.

6.42 NMR Analysis

For full spectral characterisation of peaks from IPDI and PCD see section 6.22 (or table 6.07) as this section will only detail peaks that show prepolymer formation or peaks from the chain-extender.
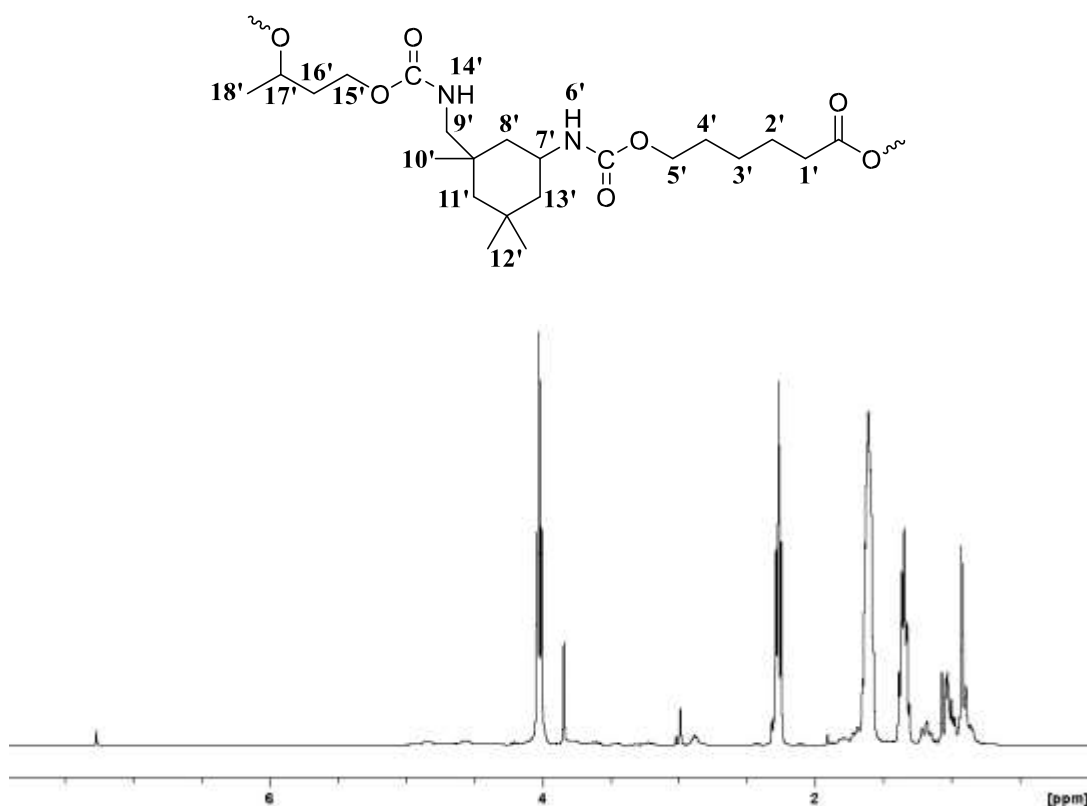
Figure 6.16: ¹H NMR spectrum obtained following reaction of IPDI-TMP-PCD with BD.

Urethane formation via the primary alcohol groups is visible by the position of the adjacent methylene group **15'** that has shifted from 3.80 ppm to 4.05 ppm. Also visible within the spectra are the methylene protons **16'** within BD at 1.91 ppm, however, there is no significant shift before or after reaction. Inclusion of secondary hydroxyl

groups within urethane linkages are shown by the shift of the methine protons **17'** from 4.03 ppm to 4.64 ppm. The final shift from BD which represents the methyl protons **18'** is also visible at 1.31 ppm.
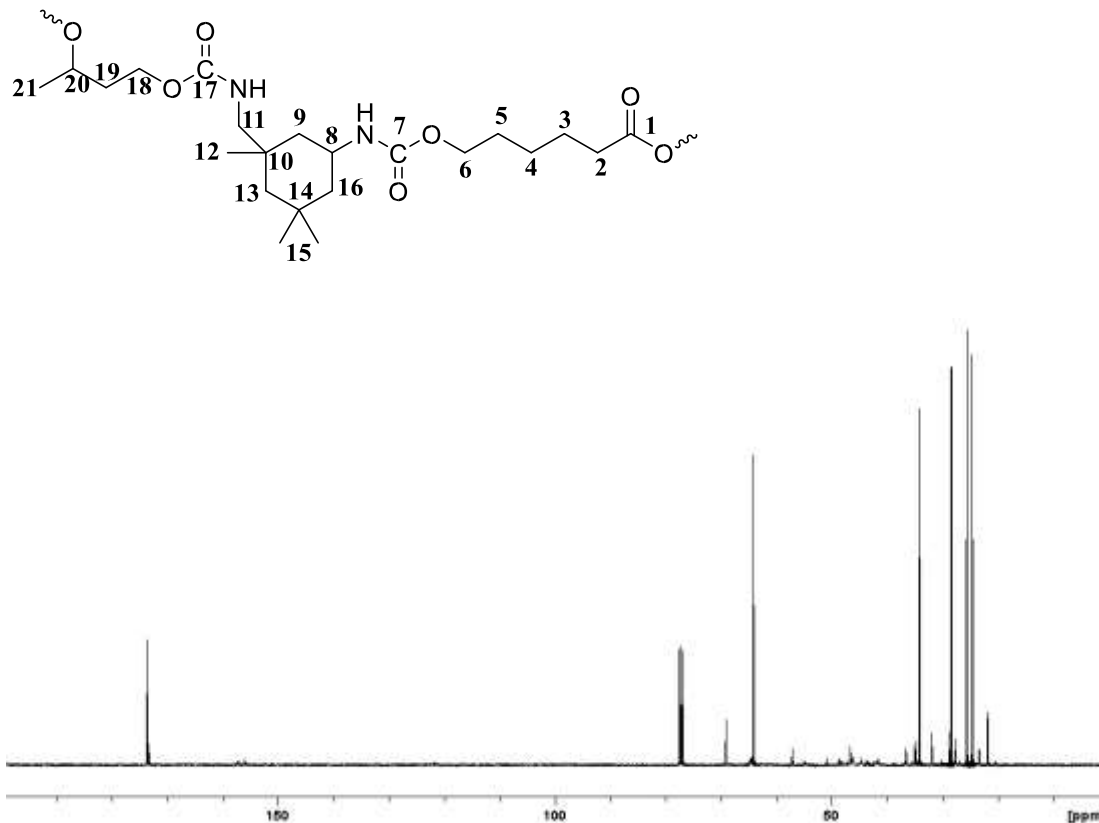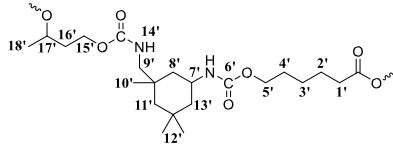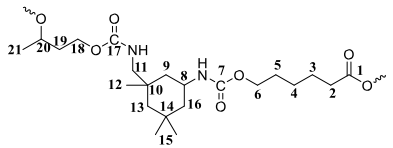
Figure 6.17: **^{13}C NMR spectrum obtained following reaction of MDI-TMP-PCD with BD.**

Further evidence that BD chain-extension has occurred, along with retention of free isocyanate groups was observed using ^{13}C NMR. Consumption of the primary hydroxyl groups within BD is confirmed by the position of the methylene carbon 18 at 57.1 ppm. Methine carbons of the secondary hydroxyl group 20 once reacted are also visible at 65.1 ppm. Also observed within figure 6.17 are methylene carbons 19 at 34.7 ppm and methyl carbons 21 at 20.1 ppm.

Carbonyl shifts characteristic of urethane bonds are again visible at 157.2 ppm and 156 ppm following reaction of primary and secondary isocyanate groups respectively. Confirmation that the prepolymers within solution still contain free reactive groups can be observed by the remaining carbonyl shifts from primary and secondary isocyanate groups at 123 ppm and 122 ppm respectively.

Table 6.07: ^{1}H and ^{13}C chemical shift for IPDI-TMP-PCD-BD collected in CDCl$_3$.

IPDI-TMP-PCD-BD	Position	^{1}H Chemical Shift (ppm)	Position	^{13}C Chemical Shift (ppm)
	1'	2.26	1	173.5
	2'	1.63	2	34.1
	3'	1.27	3	24.5
	4'	1.59	4	25.5
	5'	4.65	5	24.8
	6'	NDT	6	69
	7'	3.59	7	157.2$_p$/156.0$_s$
	8'	1.62/1.35	8	42.5
	9'	2.97/2.71	9	43.4
	10'	0.96	10	21.0
	11'	1.33/1.04	11	46.3
	12'	0.88	12	25.6
	13'	1.62/1.35	13	48.8
	14'	NDT	14	21.8
	15'	4.05	15	31.9
	16'	1.91	16	48.2
	17'	4.68	17	157.2$_p$/156$_s$
	18'	4.05	18	57.1
			19	34.7

		20	65.1
		21	20.1

p = primary, s = secondary, NDT = not detected

6.43 MALDI-MS Analysis

To determine the molecular weight increase within the chain-extended prepolymer MALDI-MS was used. The matrix used for analysis was HABA which contained a cationising agent NaTFA (see section 3.23 for more matrix information). A 40 mg ml⁻¹ solution of IPDI-TMP-PCD-BD was prepared in THF and mixed with the matrix (1:8 sample:matrix). 1 µl portions of this sample were then spotted and dried for analysis.

The peak situated at 649 m/z corresponds to the chain-extender BD coupled with two ethanol end-capped IPDI units and one sodium cation. Also present is the crosslinking agent TMP that also had reacted with three IPDI units which are in this sample also ethanol end-capped at 961 m/z (plus a sodium cation). These molecules will contribute to the hard-segment microstructure within the adhesive and they will disrupt the packing arrangement within this domain.
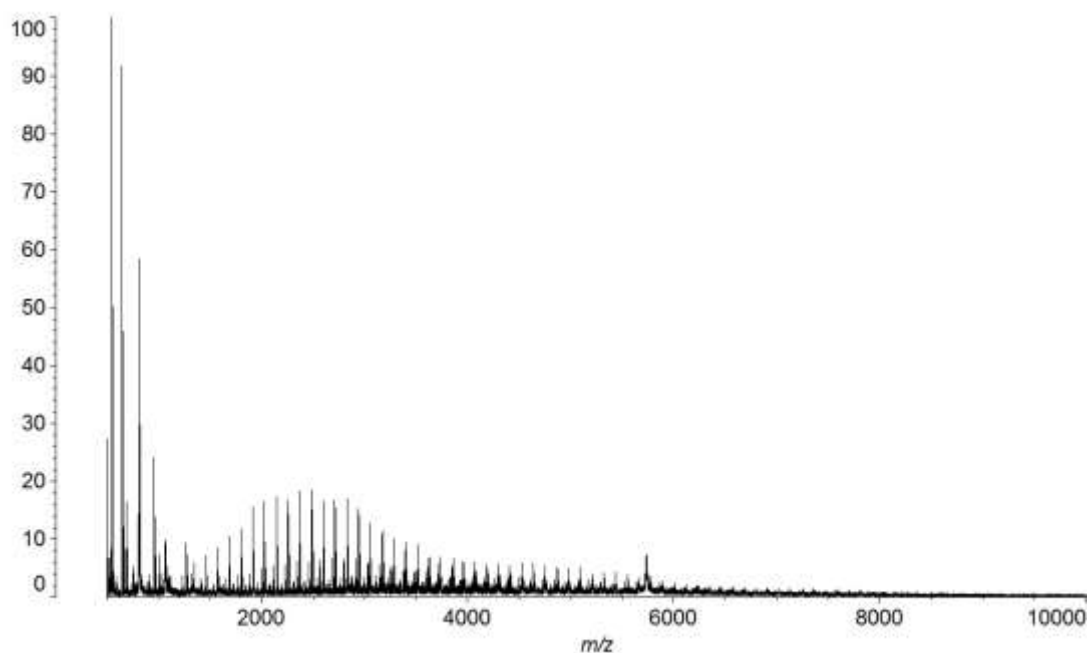
Figure 6.18: MALDI-MS spectrum of IPDI-TMP-PCD-BD chain-extended prepolymer collected in HABA/NaTFA.

The observed distribution centred on 2269 m/z corresponds to the PCD soft-segment that is isocyanate end-capped IPDI-PPG-IPDI. Prepolymer of this type are formed during step one of the synthetic process and a contribution of this prepolymer would be expected to remain. A further two distributions are visible which are off set from this distribution by 23 m/z due to the di-sodiated adduct and 90 m/z for prepolymers that have reacted with BD but have not yet coupled with another molecule. Evidence of chain-extended prepolymers of type IPDI-PCD-IPDI-BD-IPDI-PCD-IPDI is shown within the spectrum but with lower resolution. An example peak of these prepolymers is visible at 5695 m/z.

Calculation of Mn, Mw and PDI of formulation IPDI-TMP-PCD-BD is performed to determine the influence of BD on the mass distribution. The calculated value of Mn is 3607 m/z and the calculated value of Mw is 4491 m/z giving a PDI of 1.25. Chain-extension with BD results in an increase to both Mn and Mw compared to IPDI-TMP-PCD but it also results in a broader mass distribution.

6.44 DSC and TGA Analysis

Previous analysis within this chapter displayed that chain-extension has little effect on the thermal transitions of formulations based on PCD with IPDI and even following cure, the $T_g$ss obtained was well out with the processing window. Within figure 6.19 the DSC thermogram for the BD chain-extended prepolymer is presented.
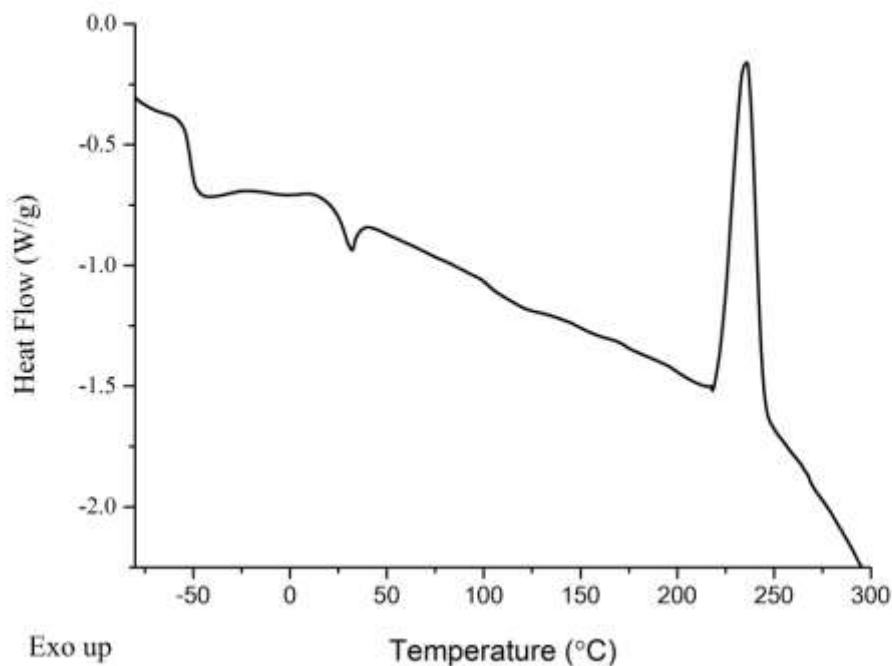
Figure 6.19: DSC thermogram of IPDI-TMP-PCD-BD prepolymer formulation.

Analysis of the thermogram obtained for the chain-extended prepolymer displays a $T_g$ss at -51°C which covers a range of -55°C to -49°C. A shift in the $T_g$ss of +13°C can be observed compared of the unreacted PCD soft-segment and +4°C with reference to the base prepolymer (IPDI-TMP-PCD). This shift in the $T_g$ss would suggest that the polymer has increased in molecular weight, has a degree of crosslinking or has ordered domains within the microstructure. Following was a melting endotherm at 31°C of enthalpy 2 J g^{-1} from the PCD soft-segment. As the melting value is 19°C lower than the value of PCD it displays that crystalline domains within the prepolymer are not pure. Also observed was an exothermic peak at 236°C with an enthalpy of 27 J g^{-1} which accounts for the cure of the residual isocyanate groups within the sample.
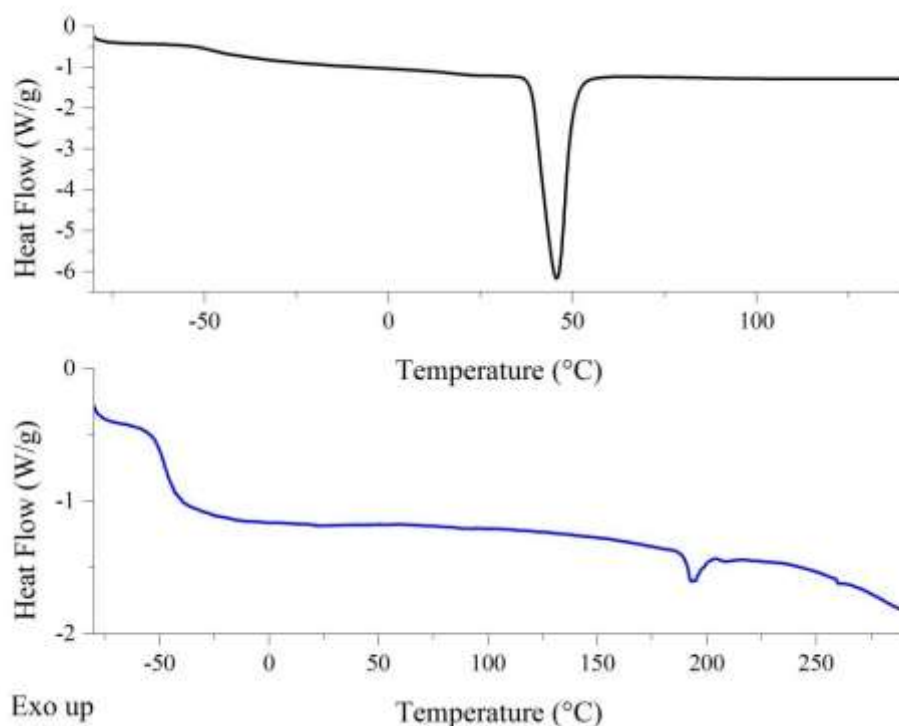
Figure 6.20: DSC thermogram of fully cured IPDI-TMP-PCD-BD adhesive, following removal from TAc/TAc laminate. [First heating cycle *top* in black and second heating cycle *bottom* in blue].

Following 30 day of curing a portion of the adhesive was removed from the TAc/TAc laminate for DSC analysis. The adhesive was analysed using a cool-heatcool-reheat experiment to determine the final $T_g$ss within each heating cycle as shown in figure 6.20 (same experiment procedure as detail in section 6.24) and to look for any other morphological information. A $T_g$ss was observed at -46°C in the first heat scan, with the thermal transition covering a range of 16°C from -53°C to 36°C. A melting endotherm from the soft-segment was also visible at 46°C with the enthalpy of the peak 23 J g^{-1}. The recovery in melt temperature and in enthalpy would suggest that following moisture cure, there is less phase mixing within the microstructure. After a second heating cycle, the $T_g$ss was recorded at -48°C and covered a range from -52°C to -40°C. Also observed on the second heating cycle was a melting endotherm of the hard-segments within the microstructure at 193°C, with the enthalpy of melt 1.4 J g^{-1}. From DSC of the fully cured adhesive it was observed that the $T_g$ss is well outside the processing window. Also observed were melting endotherms for both soft and hard-

segments within the PU-U microstructure (discussion of the morphology will be presented within chapter 8).
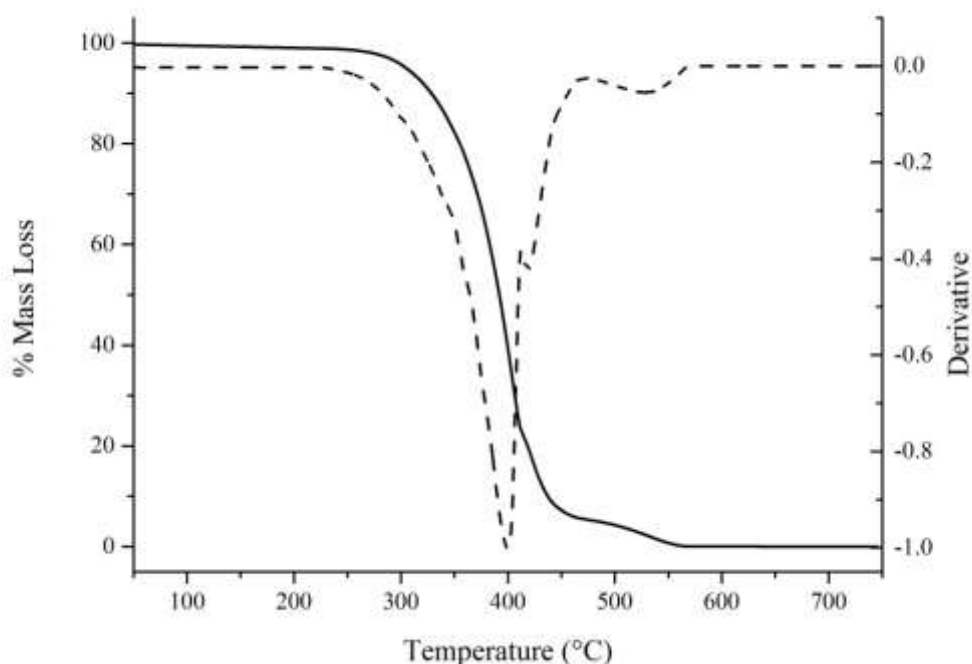
Figure 6.21: TGA and DTG curves of fully cured IPDI-TMP-PCD-BD adhesive. [TGA solid line and DTG dashed line].

Following moisture cure TGA was carried out to determine if chain-extension with BD had any effect on the overall thermal stability (based on previous analysis effect would be expected to be minimal). Within figure 6.21 the TGA and DTG curves for the fully cured adhesive are displayed. From the TGA curve the onset of degradation (calculated as 5% of the total mass lost) was calculated to be 305°C which is 5°C higher that the base prepolymer material (IPDI-TMP-PCD). This slight increase was not considered to be significant and is consistent with the previous two adhesives within this chapter. The previous comment is reinforced by inspection of the DTG curve which displayed that the maximum rate of degradation occurs at 394°C (IPDITMP-PCD occurred at 395°C). The main degradation process will be a combination of the thermal cleavage of both urethane and urea hard-segment bonds within the adhesives microstructure coupled with breakdown of the soft-segment PCD.[3,7,8] A secondary more thermally stable process is also observed by the degradation process at 523°C

which will be the breakdown of cross-linked materials formed during degradation and possibly some residual soft-segment.[7]

From the TGA data collected it was apparent that the thermal stability of the chainextended adhesive was comparable to the previous formulation (IPDI-TMP-PCDDEPD) and that the onset of degradation is well outside the processing temperature of the laminate.

6.45 180° T-peel Test and Haze

Adhesives within this chapter based on IPDI and PCD have this far been following the same trends as observed for previous systems. The consistent observations are that: none of the formulations have obtained benchmark for untreated TAc, saponification is essential to obtain benchmark values for TAc and PC performs above benchmark regardless of the surface chemistry (in the most part).

Following 7 days of moisture cure the observed mode of failure for TAc/TAc was adhesive at the TAc interface with a peel strength of 1.1 N mm^{-1}. Following 30 days of cure the peel strength did not change significantly and was recorded at 1.0 N mm^{1}, again the mode of failure was adhesive at the TAc interface. As was observed in all previous formulations, TAc/TAc performs extremely poorly and is well outside the 3 N mm^{-1} target peel strength.

Also highlighted in previous formulations was that saponification of the TAc interface was essential to obtain high peel strengths. Following 7 days of moisture cure the peel strength recorded was low at 0.8 N mm^{-1}. Following 30 days of cure a value could not be obtain as a cohesive substrate failure was encountered before a stable peel could be obtained. The observed mode of failure displays that the adhesive strength is now reaching the strength limits of the TAc(t) substrate. Data collected from this cured adhesive further confirms the need for surface treatment of TAc to gain high peel strength.

Further investigation of the effect that chain-extension has on the peel strength was now extended to PC laminates. The peel strength data acquired following 7 days of cure on PC was low at 0.5 N mm^{-1} however following 30 days the peel strength value

significantly increased to 9.2 N mm^{-1}. Both experiments displayed an adhesive mode of failure at the interface and the 30 day test displayed very strong deformation of the PC substrate. These strength values collected using this current formulation are well above benchmark and at the level anticipated based on IPDI-TMP-PCD base material.

Treatment of the PC interface was again performed and the peel strength measured. After 7 days of cure the peel strength of the fully treated PC laminate was 0.4 N mm^{1} which increased to 4.7 N mm^{-1} after 30 days. A cohesive mode of failure within the adhesive was encountered for this laminate. Following PC surface treatment a decrease in the overall peel strength was observed, however, as it was above benchmark it was still acceptable.

To identify the weakest interface or component of the laminate hybrid systems were next tested. Discussed first is the laminate of composition TAc(t)/PC which recorded a peel strength of 0.5 N mm^{-1} following 7 days and 2.7 N mm^{-1} after 30 days of cure.

The mode of failure was adhesive at the PC interface and this was coupled with deformation of the PC substrate (second test only). For the fully treated laminate peel strength was 0.6 N mm^{-1} after 7 days which increased to 4.1 N mm^{-1} after 30 days. A cohesive mode of failure within the adhesive layer was observed for this laminate. From the first experiment the PC interface was identified as the weakest component however, following surface treatment the mode of failure moved to cohesive within the adhesive layer.

Table 6.08: Peel, haze and mode of failure data for IPDI-TMP-PCD-BD cured PU-U adhesive. [The data in bold will be discussed within this section].

Cured Adhesive	Laminate	Peel 1* (N mm^{-1})	Peel 2^x (N mm^{-1})	Failure mode	Haze (%)
IPDI-TMPPCD	TAc/TAc	0.	0.6	Adhesive TAc	>1.5%
	TAc(t)/TAc(t)	6.0	4.3	Ply	
	TAc(t)/PC	3.0	3.8	Adhesive Both	

	TAc(t)/PC(t)	2.8	2.9	Adhesive Both	
	PC(t)/ PC(t)	5.5	5.1	Adhesive Both	
	PC/PC	8.1	10.5	Adhesive Both	
IPDI-TMP-PCD-DEPD	TAc/TAc	0.8	0.7	Adhesive TAc	>1.5%
	TAc(t)/TAc(t)	5.0	5.6	Cohesive TAc	
	TAc(t)/PC	3.7	3.5	Cohesive TAc	
	TAc(t)/PC(t)	5.0	4.4	Cohesive TAc	
	PC(t)/ PC(t)	5.5	5.3	Adhesive Both	
	PC/PC	2.5	2.3	Adhesive Both	
IPDI-TMP-PCD-BD	**TAc/TAc**	**1.1**	**1.0**	**Adhesive TAc**	**>1.5%**
	TAc(t)/TAc(t)	**0.8**	**ply**	**Cohesive**	
	TAc(t)/PC	**0.5**	**2.7**	**Adhesive PC**	
	TAc(t)/PC(t)	**0.6**	**4.1**	**Cohesive**	
	PC(t)/ PC(t)	**0.4**	**4.7**	**Cohesive**	
	PC/PC	**0.5**	**9.2**	**Adhesive PC**	
IPDI-TMP-PCD-PD	TAc/TAc	1.0	0.7	Adhesive TAc	>1.5%
	TAc(t)/TAc(t)	0.7	4.8	Cohesive	
	TAc(t)/PC	0.5	3.3	Cohesive	
	TAc(t)/PC(t)	0.4	6.4	Cohesive	
	PC(t)/ PC(t)	0.3	7.8	Cohesive	
	PC/PC	0.4	9.9	Adhesive PC	

* peel 1 collected within 7 days of room temperature cure, ˣ peel 2 collected after 30 days of room temperature cure, ND = No Data

Finally the overall haze for the fully cured adhesive across all six laminates was > 1.5% and within each laminate a milky white adhesive layer was observed. This haze value displays that chain-extension with BD has not significantly improved the clarity of the adhesive layer by disruption of soft-segment crystallisation. Such a haze value would have been anticipated due to the large melting endotherm visible within the first heating scan during DSC analysis of the cured adhesive.

6.46 ATR of Peeled Samples

Characterisation of the bulk material was performed on all six of the laminates after the 30 day tensile test. ATR analysis will determine the chemical functionality of the final cured material and allow for any distinct differences in curing chemistry to be observed. Also ATR will give some indication of the inherent morphology of the fully cured adhesive. Discussed within this section will be peaks that indicate either the PU of the BD chain-extended prepolymer or PU-U peaks obtained after 30 days of moisture cure. For discussion of the peaks inherent of the starting materials see section 6.26 and for all characteristic peaks see table 6.09.

From the spectra present within figure 6.22 it is visible there are two different **N-H** vibrations within the above cured PU-U. **N-H** stretching vibrations occurring at 3376 cm^{-1} show that H-bonded domains are present in the microstructure whereas, the shoulder peak at around 3500 cm^{-1} correspond to free **N-H** stretching vibrations. Corresponding bending vibrations are visible within the fingerprint region of the spectra for **N-H** at 1527 cm^{-1}, also present within this peak is the **C-N** stretch. **C-N** bending vibrations are also observed for urea at 1367 cm^{-1} and urethane at 1295 cm^{-1}. Again no detectable isocyanate peak was visible between 2260 cm^{-1} – 2280 cm^{-1} which displays that the adhesive is fully cured after 30 days.
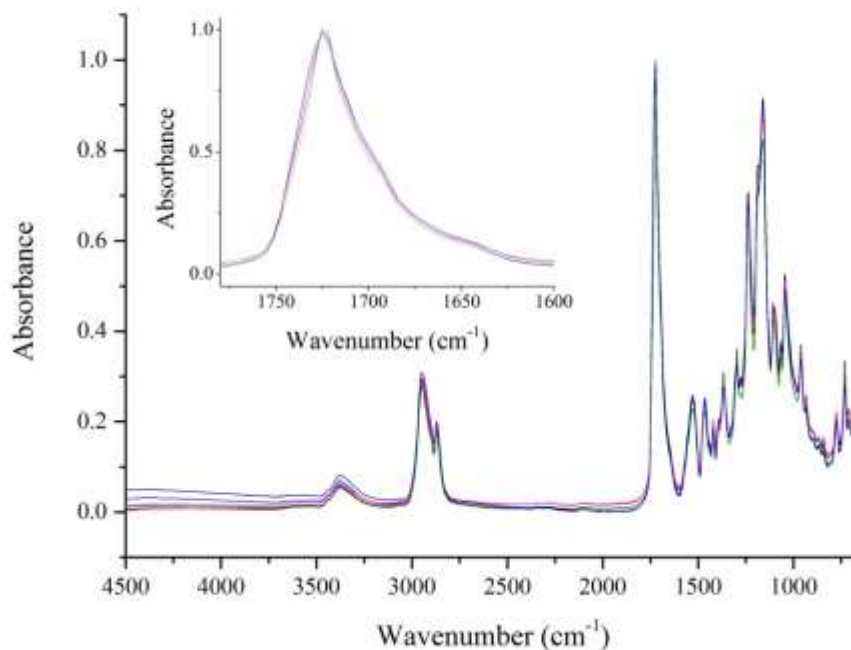
Figure 6.22: **ATR spectra of cured IPDI-TMP-PCD-BD sampled in-situ after tensile testing with inset expanded carbonyl region. [TAc/TAc in black, TAc(t)/TAc(t) in red, TAc(t)/PC in blue, TAc(t)/PC(t) in pink, PC(t)/PC(t) in green and PC/PC in orange. Data collected for each laminate at nine random positions with each spectrum consisting of 128 scans at 8 cm^{-1} resolution. These were then averaged and plotted as the above spectra].**

Further information on the inherent microstructure following moisture cure is available within the carbonyl region. Evidence of H-bonded ester carbonyl stretching is visible at 1725 cm^{-1} which would indicate crystallisation of softsegments. An immediate shoulder to this peak displays the occurrence of free urea carbonyl stretching at 1697 cm^{-1}. Further evidence of structured regions within the microstructure of the cured adhesive is shown by the bidentate H-bonded urea stretching vibration at 1646 cm^{-1}. As these peaks are beginning to convolute together it also displays that there will be proportion of monodentate urea groups which has a characteristic vibration of 1675 cm^{-1} – 1660cm^{-1}. The overall morphology observed from ATR will be discussed in greater detail within chapter 8.

Table 6.09: Characteristic peaks of IPDI-TMP-PCD-BD cured PU-U adhesive from all six laminate combinations.

Wavenumber (cm⁻¹)	Vibration	Wavenumber (cm⁻¹)	Vibration
3376	N-H stretching Hbonded	1367	C-H symmetric deformation
2947	C-H asymmetric stretch		C-N Urea
2867	C-H symmetric stretch	1295	C-N Urethane
1725	C=O stretch Hbonded Ester	1158	Asymmetric N-CO-O, C-H aliphatic skeleton
1697	C=O stretch free Urea	1106	C-O-C stretch aliphatic ester
1646	C=O stretch Urea Bidentate Hbonded	1065	Symmetric N-CO-O
1527	C-N stretch, N-H bend	961	C-O-C stretch aliphatic ester
1464	C-H bend aliphatic	775	C-C skeleton rocking
1418	C-H asymmetric deformation	730	C-C skeleton rocking

6.47 Summary of IPDI-TMP-PCD-BD Formulation

Synthesis of the BD chain-extended prepolymer was followed using NMR which displayed successful synthesis. MALDI-MS was used to characterise the molecular mass distributions present within the chain-extended prepolymer formulation. MALDI-MS identified prepolymers from step one as the main molecular weight distribution. Also encountered were two further distributions which are off set from

the main distribution by 23m/z for the di-sodiated adduct and 90 m/z for prepolymers that have reacted with BD but not yet coupled with another prepolymer molecule to become fully chain-extended. Direct observation of chain-extended prepolymer molecules was also possible. It was identified that using BD as chain-extender results in greater values of Mn and Mw compared to IPDI-TMP-PCD but it also results in a larger PDI value.

Investigation of the thermal transition by DSC recorded a $T_g$ss for the chain-extended prepolymer of -51°C which is an elevation of +13°C compared to PCD. A melting endotherm of the PCD soft-segment at 31°C was also observed within the prepolymers thermogram. Once fully cured the $T_g$ss was recorded at -46°C on the first heating cycle and this decreased to -48°C on the second heating cycle. Observed on the first heating cycle was a melting endotherm for the PCD softsegment at 46°C. As the melting temperature was lower than pure PCD (50°C) and this highlights that the crystalline soft-segment domains are less ordered. Observed on the second heating cycle was melting of the hard-segment (at 193°C) within the PU-U which displays that regions of phase segregation are present. The overall thermal stability was determined by TGA with the onset of degradation occurring at 305°C. From the DTG curve two degradation peaks at 394°C and 524°C were observed which represent the decomposition of both the hard and soft-segment followed by degradation of more stable cross-linked materials formed during degradation.

Using 180° T-peel testing it was identified that untreated TAc performed very poorly (1.0 N mm^{-1}), however, following surface treatment the values greatly improved with a cohesive mode of failure within the TAc(t) substrate recorded. Untreated PC performed exceptionally well reaching 9.2 N mm^{-1} after 30 days. For treated PC a similar result was obtained with an above benchmark value of 4.7 N mm^{-1} recorded following 30 days of cure. Two different components were identified as being weakest from analysis using hybrid laminates. The observed mode of failure for TAc(t)/PC was adhesive at the PC substrate interface whereas, for TAc(t)/PC(t) the observed mode of failure was cohesive within the adhesive layer.

Finally the haze value recorded for each of the six laminates was > 1.5% and the adhesive layer was milky white in colour. This value would have been expected based on the data obtained on the first heating cycle using DSC which displayed a melting endotherm of the soft-segment. Finally using ATR the adhesive material was observed to be fully cured following 30 days of curing. Also observed was that the fully cured adhesive was a PU-U and contained H-bonding domains within the cured network.

6.50 Analysis of IPDI-TMP-PCD-PD

6.51 Synthesis Information

IPDI-TMP-PCD-PD was next synthesised with the intention of disrupting the close packing of hard-segments through using a less conventional diol chain-extender which should aid with phase mixing of the different domains. This was achieved by firstly synthesising the IPDI-TMP-PCD prepolymer using the same reaction conditions as detailed with section 6.21 and then performing an addition reaction set. The additional step was performed by adding a hydroxyl terminated chain-extender using a 2.2:1.0 isocyanate:hydroxyl ratio based on the calculated amount of free NCO remaining after step one. The chain-extension step was also used to lower the free isocyanate content of the adhesive, which would reduce the opportunity for excessive bubbling by CO_2 liberation produced by the formation of urea during moisture cure.

Step one was performed as previously detailed in section 6.21 and was a clear liquid which had an observed increase in viscosity from the starting mixture. After addition of 1,2-propane diol (PD), the reaction was allowed to stir at 85°C – 95°C for seventeen hours before the dual DBTDL and TEA catalyst system was added. Following chain-extension a visual increase in viscosity was observed and was associated with the molecular weight increase caused by the coupling step. The viscosity of the system was low enough that it did not require the temperature to be increased before transfer. Once the reaction was complete the formulation was poured into an aluminium tube, which was then capped and degassed as previously outlined in section 2.03. The desiccator containing the adhesive filled tube was then placed within a 0°C fridge for storage. Degassing was performed for six hours once a vacuum of one atmosphere

was obtained. Samples of the reaction were again taken before catalysed addition, these were analysed by DSC, NMR and MALDI-MS analysis.

IPDI-TMP-PCD-PD was heated to 105°C before being applied to six laminates (same as section 5.21) which was followed by room temperature cure. These samples were 180° T-peel tested at 7 days and 30 days to determine the peel strength. A further lamination was performed using two plies of TAc which would allow for the fully cured adhesive to be removed for analysis by DSC and TGA. The 30 day peel test samples were also analysed by ATR to characterise the final adhesive and determine the extent of cure.

Analysis of the chain-extended materials only will be presented within the remaining sections of this chapter. IPDI-TMP-PCD (sections 5.21-5.26) is considered as representative of the reactive intermediate obtained after step one of each chainextended reaction.

6.52 NMR Analysis

For full spectral characterisation of peaks from IPDI and PCD see section 6.22 (or table 6.10) as this section will only detail peaks that show prepolymer formation or peaks from the chain-extender.

Urethane formation via the primary alcohol groups is visible by the position of the adjacent methylene group **15'** that have shifted from 3.80 ppm to 4.20 ppm. Also visible within the spectra are the methine protons **16'** within PD at 5.18 ppm with these protons shifted from 3.80 ppm. The final shift from PD which represents the methyl protons **17'** is also visible at 1.31 ppm.

Further evidence that PD chain-extension has occurred, along with retention of free isocyanate groups was observed using ^{13}C NMR. Consumption of the primary hydroxyl groups within PD is confirmed by the position of the methylene carbon 18 at 64.6 ppm.   Methine carbons of the secondary hydroxyl groups 19 once reacted are also visible at 65 ppm. Also observed within figure 6.24 are methyl carbons 20 at 21 ppm for the chain-extender.
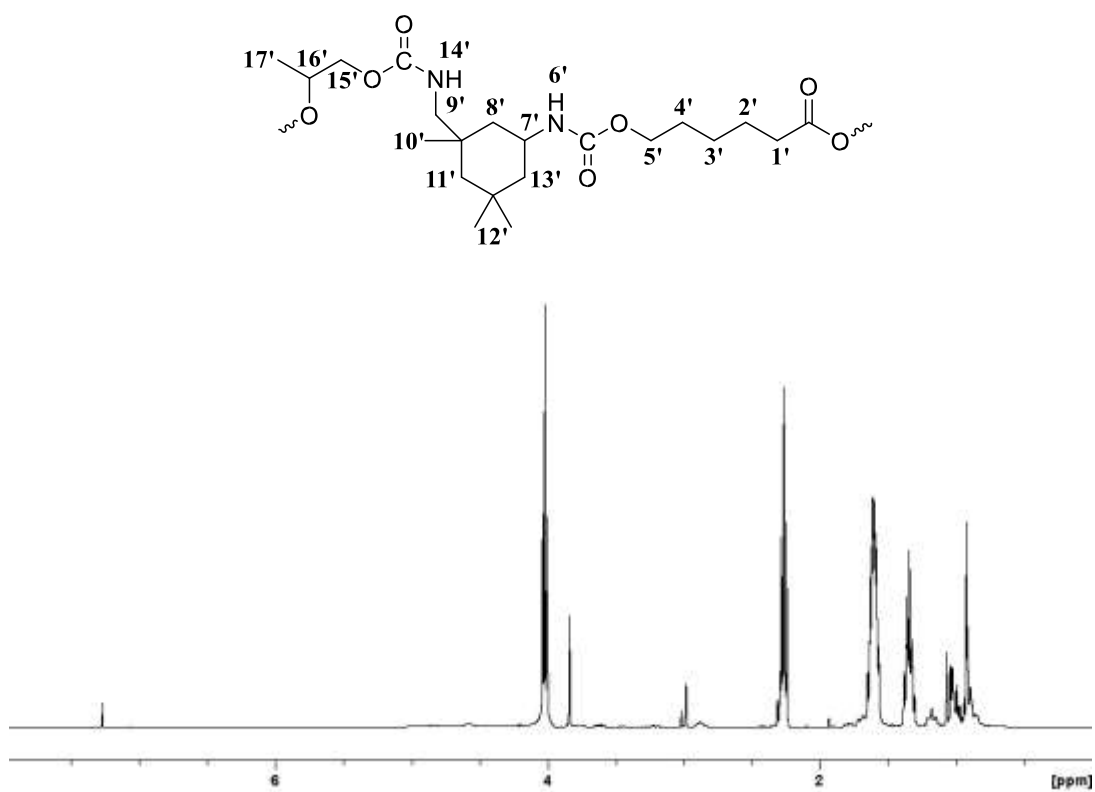
Figure 6.23: ^{1}H NMR spectrum obtained following reaction of IPDI-TMP-PCD with PD.
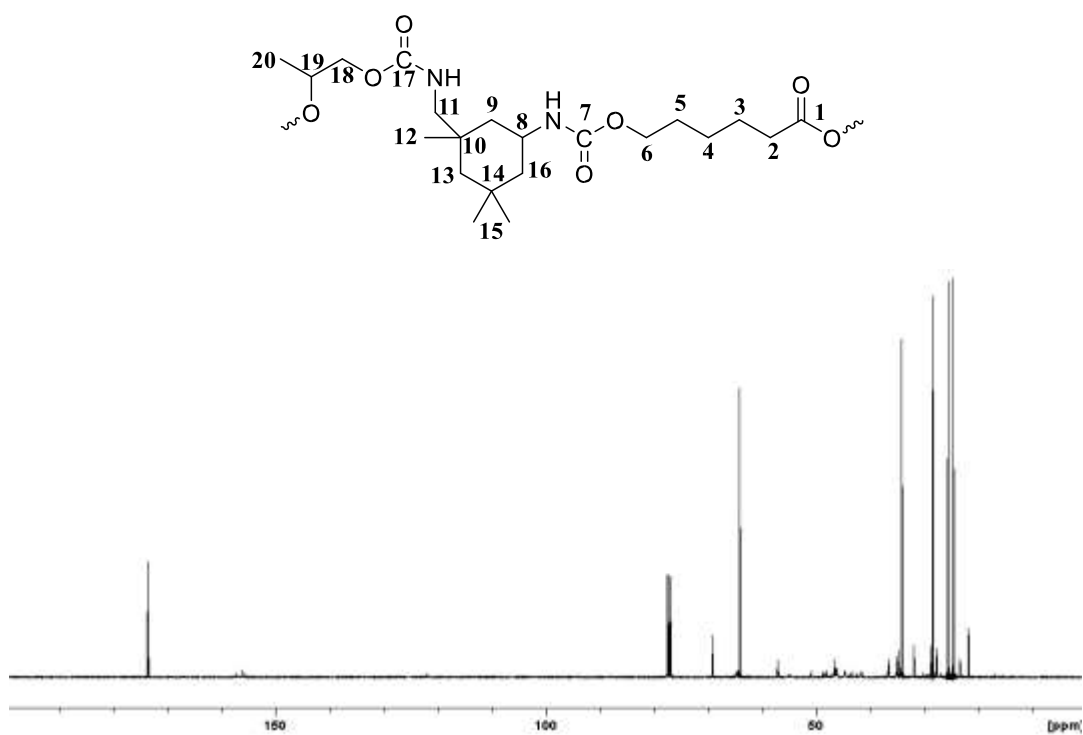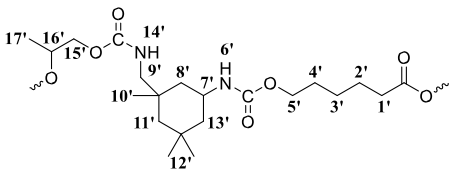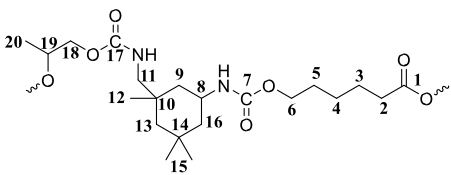
Figure 6.24: ^{13}C NMR spectrum obtained following reaction of MDI-TMP-PCD with PD.

Table 6.10: ^{1}H and ^{13}C chemical shift for IPDI-TMP-PCD-PD collected in CDCl$_3$.

IPDI-TMP-PCD-PD	Position	^{1}H Chemical Shift (ppm)	Position	^{13}C Chemical Shift (ppm)
	1'	2.26	1	173.5
	2'	1.63	2	34.1
	3'	1.27	3	24.5
	4'	1.59	4	25.5
	5'	4.65	5	24.8
	6'	NDT	6	69
	7'	3.59	7	157.2$_p$/156$_s$
	8'	1.62/1.35	8	42.5
	9'	2.97/2.71	9	43.4
	10'	0.96	10	21.0
	11'	1.33/1.04	11	46.3
	12'	0.88	12	25.6
	13'	1.62/1.35	13	48.8
	14'	NDT	14	21.8
	15'	4.20	15	31.9
	16'	5.18	16	48.2
	17'	1.31	17	157.2$_p$/156$_s$
			18	64.6
			19	65

			20	21

p = primary, s = secondary, NDT = not detected

Carbonyl shifts characteristic of urethane bonds are visible at 157.2 ppm and 156.1 ppm following reaction of primary and secondary isocyanate groups respectively. Confirmation that the prepolymers within solution still contain free reactive groups can be observed by the remaining carbonyl shifts from primary and secondary isocyanate at 123 ppm and 122 ppm respectively.

6.53 MALDI-MS Analysis

To determine the molecular weight increase within the chain-extended prepolymer MALDI-MS was used. The matrix used for analysis was HABA which contained a cationising agent NaTFA (see section 3.23 for more matrix information). A 40 mg ml^{-1} solution of IPDI-TMP-PCD-PD was prepared in THF and mixed with the matrix (1:8 sample:matrix). 1 µl portions of this sample were then spotted and dried for analysis.

The peak situated at 635 m/z corresponds to the chain-extender PD coupled with two ethanol end-capped IPDI units and one sodium cation. Also present is the crosslinking agent TMP that also had reacted with three IPDI units which are in this sample also ethanol end-capped at 961 m/z (plus a sodium cation). These molecules will contribute towards the hard-segment microstructure and will interfere with the packaging arrangement of the hard domain.
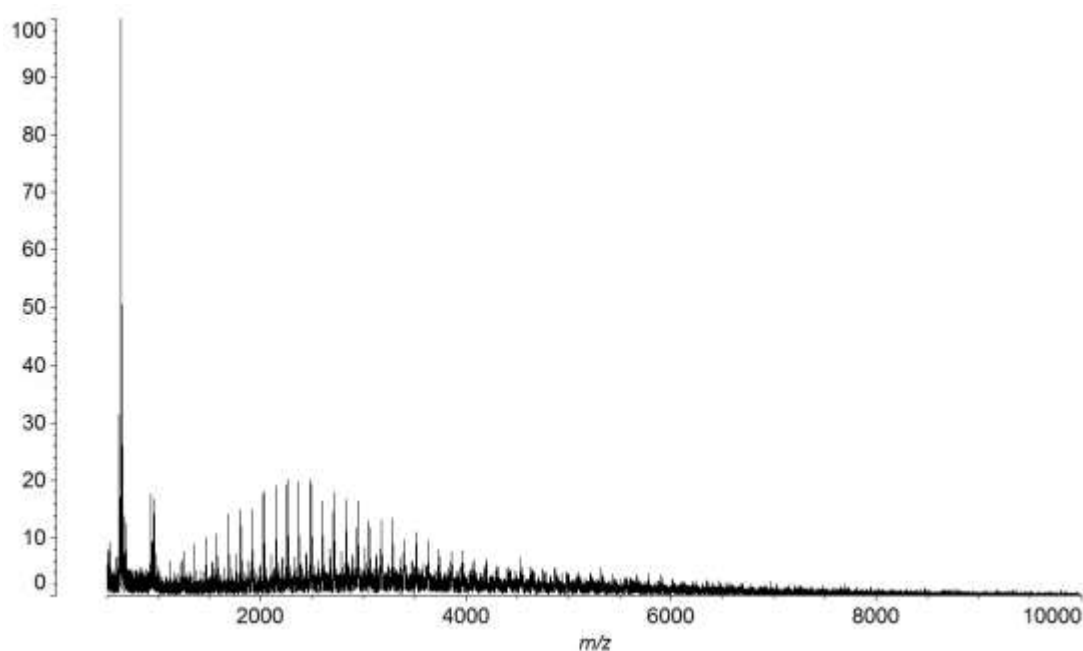
Figure 6.25: **MALDI-MS spectrum of IPDI-TMP-PCD-PD chain-extended prepolymer collected in HABA/NaTFA.**

The observed distribution centred on 1927 m/z corresponds to the PCD soft-segment that is isocyanate end-capped IPDI-PPG-IPDI. The prepolymer within this peak will be composed of thirteen PCD repeat units, two ethanol end-capped IPDI units and one sodium cation. Prepolymer of this type are formed during step one of the synthetic process and a contribution of this prepolymer would be expected to remain. A further two distributions are visible which are off set from this distribution by 23 m/z due to the di-sodiated adduct and 76 m/z for prepolymers that have reacted with PD but have not yet coupled with another molecule. Evidence of chain-extended prepolymers of type IPDI-PCD-IPDI-PD-IPDI-PCD-IPDI is shown within the spectrum but with lower resolution. An example peak of these prepolymers is visible at 5695 m/z.

Following calculation of Mn, Mw and PDI it was clear that PD as a chain-extender has no influence on these parameters with respect to IPDI-TMP-PCD. The calculated value of Mn is 3230 m/z and the calculated value of Mw is 3911 m/z giving a PDI of 1.21. From the numbers obtained it would appear that PD has resulted in no change to the position or breadth of the mass distribution when compared to IPDI-TMP-PCD.

6.54 DSC and TGA Analysis

Previous analysis within this chapter displayed that diol chain-extension has little effect on the thermal transitions of formulations based on PCD with IPDI and even following cure the $T_g$ss obtained was well out with the processing window. Within figure 6.26 the DSC thermogram for the PD chain-extended prepolymer is presented. Analysis of the thermogram obtained a $T_g$ss of -52°C which cover a range of -55°C to -49°C. A shift in the $T_g$ss of +12°C can be observed compared of the unreacted PCD soft-segment and +3°C with reference to the base prepolymer (IPDI-TMPPCD). This shift in the $T_g$ss would suggest that the prepolymer has increased in molecular weight or has a degree of cross-linking. Following was a melting endotherm of the PCD soft-segment at 30°C of enthalpy 2 J g^{-1}. As the melting value is 19°C lower than the value of PCD it displays that crystalline domains with the prepolymer are not well arranged. Also observed was an exothermic peak at 212°C with an enthalpy of 20 J g^{-1} which displays cure of the residual free isocyanate groups.
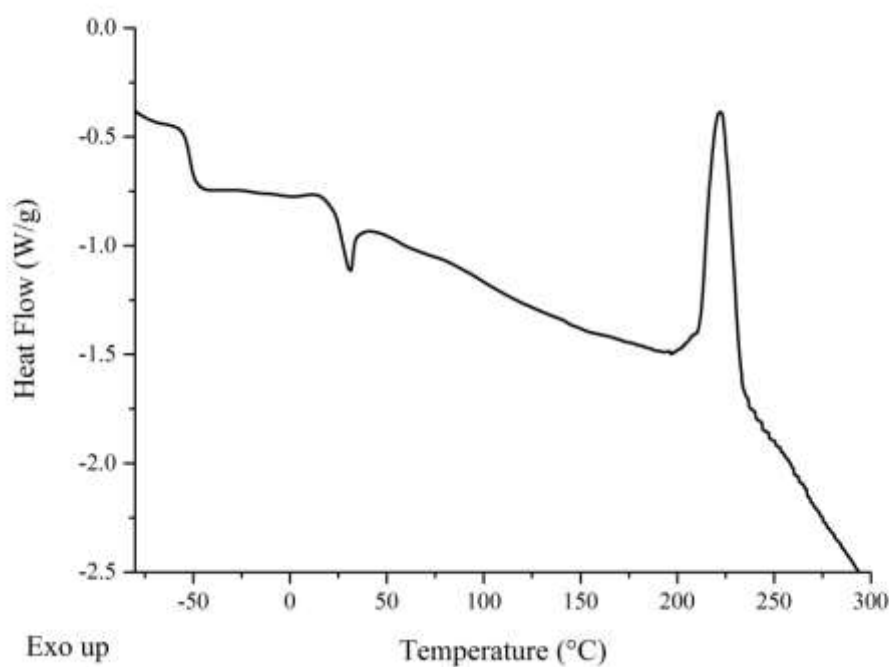
Figure 6.26: DSC thermogram of IPDI-TMP-PCD-PD prepolymer formulation.

Following 30 day a sample of the adhesive was analysed using a cool-heat-coolreheat experiment to determine the final $T_g$ss within each heating cycle (as shown in figure

6.27) and to identify any other morphological information. A $T_g$ss was observed at -48°C, with the thermal transition covering a range of 12°C from -53°C to -41°C. A melting endotherm from the soft-segment was also visible at 45°C (onset 28°C) with the enthalpy of the melting peak 18 J g^{-1}. The recovery in melt temperature and in enthalpy would suggest that following moisture cure the degree of phase mixing has reduced. After a second heating cycle, the $T_g$ss was recorded at -48°C and covered a range from -52°C to -41°C. Also observed on the second heating cycle was a melting endotherm of the hard-segments within the microstructure at 196°C with the enthalpy of melt 1 J g^{-1}. From DSC of the fully cured adhesive it was observed that the $T_g$ss is well outside the processing window. Also observed were melting endotherms for both soft and hard-segments within the

PU-U microstructure (discussion of the morphology will be presented within chapter 8).
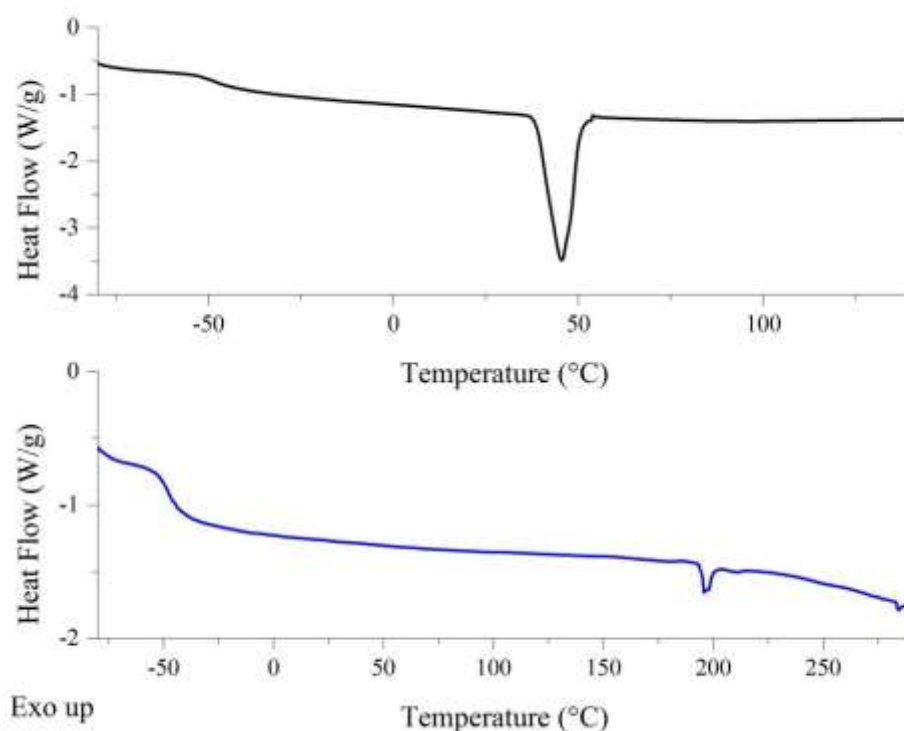
Figure 6.27: DSC thermogram of fully cured IPDI-TMP-PCD-PD adhesive, following removal from TAc/TAc laminate. [First heating cycle *top* in black and second heating cycle *bottom* in blue].

Following moisture cure TGA was carried out to determine if chain-extension with PD had any effect on the overall thermal stability (based on previous analysis effect would

388

be expected to be minimal). Within figure 6.28 the TGA and DTG curves for the fully cured adhesive are displayed. From the TGA curve the onset of degradation (calculated as 5% of the total mass lost) was calculated to be 299°C which is 1°C lower that the base prepolymer material (IPDI-TMP-PCD). This slight decrease was not considered to be significant and is consistent with the previous two chainextended materials within this chapter. The previous comment is reinforced by inspection of the DTG curve which displayed that the maximum rate of degradation occurs at 399°C (IPDI-TMP-PCD occurred at 395°C). The main degradation process will be a combination of the thermal cleavage of both urethane and urea hardsegment bonds within the adhesives microstructure coupled with breakdown of the soft-segment PCD.[3,7,8] A secondary more thermally stable process is also observed by the degradation process at 532°C which will be the breakdown of cross-linked materials formed during degradation and possible some residual soft-segment.[7]
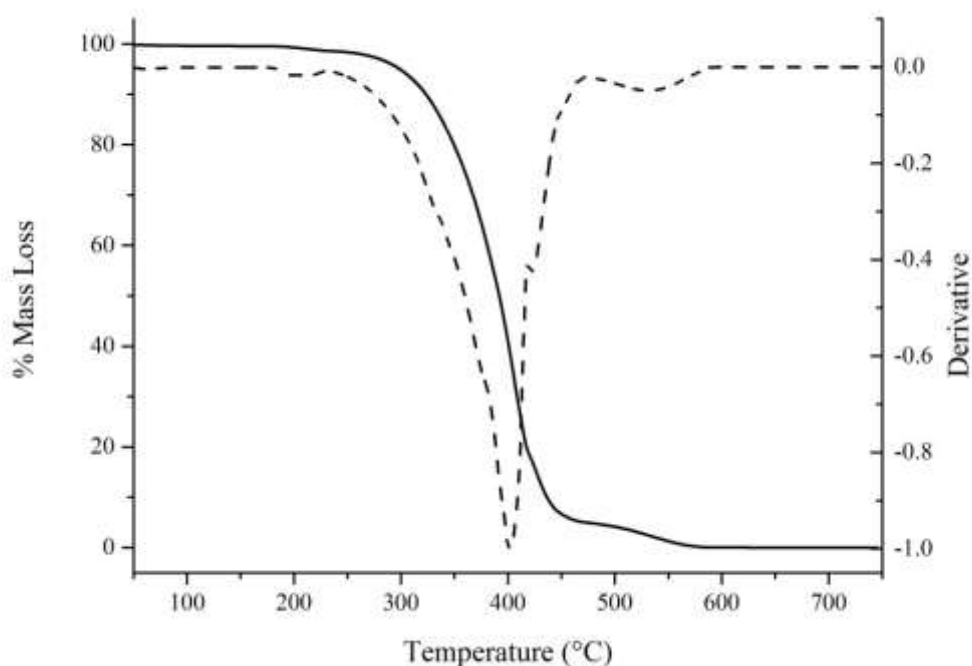
Figure 6.28: TGA and DTG curves of fully cured IPDI-TMP-PCD-PD adhesive. [TGA solid line and DTG dashed line].

From the TGA data collected it was apparent that the thermal stability of the chainextended adhesive was comparable to the previous formulation (IPDI-TMP-

PCDBD) and that the onset of degradation is well outside the processing temperature of the laminate.

6.55 180° T-peel Test and Haze

Adhesives within this chapter based on IPDI and PCD have this far been following the same trends as observed for previous systems. The consistent observations are: firstly none of the formulations have obtained a benchmark for untreated TAc, secondly saponification is essential to obtain benchmark values with TAc and PC performs above benchmark regardless of the surface chemistry (in the most cases).

Following 7 days of moisture cure the observed mode of failure for TAc/TAc was adhesive at the TAc interface with a peel strength of 1.0 N mm^{-1} recorded. Following 30 days of cure the peel strength dropped to 0.7 N mm^{-1} and the mode of failure was again adhesive at the TAc interface. Consistent with all previous formulations, TAc/TAc performs extremely poorly and is well outside the 3 N mm^{-1} target peel strength.

Also highlighted in previous formulations was that saponification of the TAc interface was essential to obtain high peel strengths. Following 7 days of moisture cure the peel strength recorded was 0.7 N mm^{-1}. Following 30 days of cure the value jumped to 4.8 N mm^{-1} with the observed mode of failure cohesive within the adhesive layer. Data collected from this adhesive formulation further confirms the need for surface treatment of TAc to gain high peel strength.

Further investigation of the effect that chain-extension has on the peel strength was now extended to PC laminates. The peel strength data acquired following 7 days of cure on PC was low at 0.4 N mm^{-1} however, following 30 days the peel strength value significantly increased to 9.9 N mm^{-1}. Both experiments displayed an adhesive mode of failure at the PC interface and the 30 day test display very strong deformation of the PC substrate. The 30 day strength values collected using this current formulation is well above benchmark and at a level as would have been anticipated based on IPDI-TMP-PCD material. Treatment of the PC interface was again performed and the peel strength measured. After 7 days of cure the peel strength of the fully treated PC laminate was 0.3 N mm^{-1} which increased to 7.8 N mm^{-1} after 30 days. A cohesive

mode of failure within the adhesive was encountered for this laminate. Following PC surface treatment a decrease in the overall peel strength was observed, however, as it was above benchmark it was still acceptable.

To identify the weakest interface or component of the laminate, hybrid systems were next tested. Discussed first is the laminate of composition TAc(t)/PC which recorded a peel strength of 0.4 N mm^{-1} following 7 days and 3.3 N mm^{-1} after 30 days of cure. The mode of failure was cohesive within the adhesive layer and this was coupled with deformation of the PC substrate. For the fully treated laminate, the peel strength was recorded at 0.4 N mm^{-1} after 7 days which increased to 6.4 N mm^{-1} after 30 days. A cohesive mode of failure within the adhesive layer was observed for this laminate. Both experiments have identified that the weakest component of the laminate is the adhesive layer as evident by the cohesive failure within this layer.

Table 6.11: Peel, haze and mode of failure data for IPDI-TMP-PCD-PD cured PU-U adhesive. [The data in bold will be discussed within this section].

Cured Adhesive	Laminate	Peel 1* (N mm^{-1})	Peel 2^x (N mm^{-1})	Failure mode	Haze (%)
IPDI-TMPPCD	TAc/TAc	0.9	0.6	Adhesive TAc	>1.5%
	TAc(t)/TAc(t)	6.0	4.3	Ply	
	TAc(t)/PC	3.0	3.8	Adhesive Both	
	TAc(t)/PC(t)	2.8	2.9	Adhesive Both	
	PC(t)/ PC(t)	5.5	5.1	Adhesive Both	
	PC/PC	8.1	10.5	Adhesive Both	
IPDI-TMP-PCD-DEPD	TAc/TAc	0.8	0.7	Adhesive TAc	>1.5%
	TAc(t)/TAc(t)	5.0	5.6	Cohesive TAc	
	TAc(t)/PC	3.7	3.5	Cohesive TAc	
	TAc(t)/PC(t)	5.0	4.4	Cohesive TAc	
	PC(t)/ PC(t)	5.5	5.3	Adhesive Both	
	PC/PC	2.5	2.3	Adhesive Both	
IPDI-TMP-	TAc/TAc	1.1	1.0	Adhesive TAc	>1.5%

PCD-BD	TAc(t)/TAc(t)	0.8	ply	Cohesive	
	TAc(t)/PC	0.5	2.7	Adhesive PC	
	TAc(t)/PC(t)	0.6	4.1	Cohesive	
	PC(t)/ PC(t)	0.4	4.7	Cohesive	
	PC/PC	0.5	9.2	Adhesive PC	
IPDI-TMP-PCD-PD	**TAc/TAc**	**1.0**	**0.7**	**Adhesive TAc**	**>1.5%**
	TAc(t)/TAc(t)	**0.7**	**4.8**	**Cohesive**	
	TAc(t)/PC	**0.5**	**3.3**	**Cohesive**	
	TAc(t)/PC(t)	**0.4**	**6.4**	**Cohesive**	
	PC(t)/ PC(t)	**0.3**	**7.8**	**Cohesive**	
	PC/PC	**0.4**	**9.9**	**Adhesive PC**	

* peel 1 collected within 7 days of room temperature cure, ˣ peel 2 collected after 30 days of room temperature cure, ND = No Data

Finally the overall haze for the fully cured adhesive across all six laminates was > 1.5% and within each laminate a milky white adhesive layer was observed. This haze value displays that chain-extension with PD has not significantly improved the clarity of the adhesive layer by disruption of soft-segment crystallisation. Such a haze value would have been anticipated due to the large melting endotherm visible within the first heating scan of DSC analysis. This haze value is also consistent with the previous two diol chain-extended formulations.
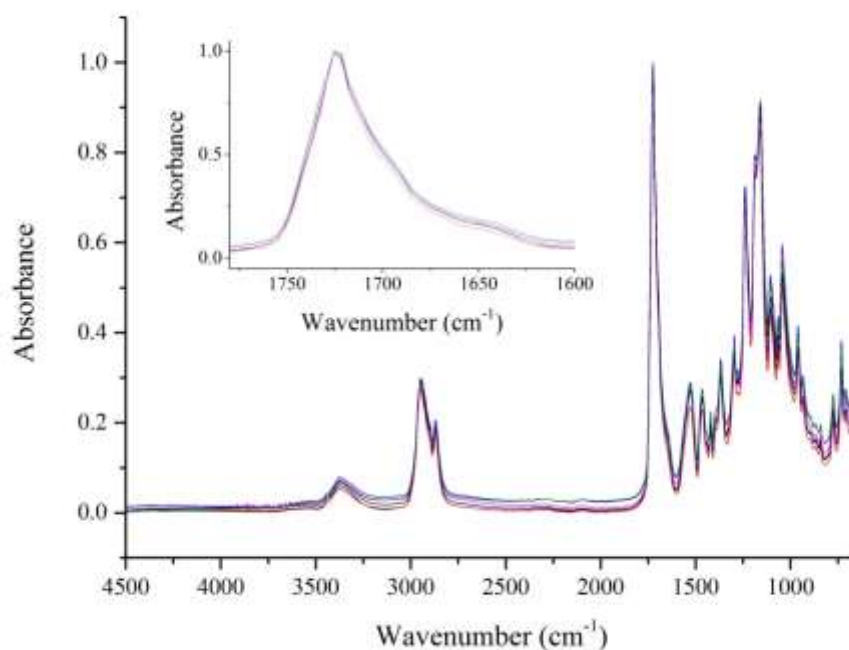
Figure 6.29: **ATR spectra of cured IPDI-TMP-PCD-PD sampled in-situ after tensile testing with inset expanded carbonyl region. [TAc/TAc in black, TAc(t)/TAc(t) in** red**, TAc(t)/PC in** blue**, TAc(t)/PC(t) in** pink**, PC(t)/PC(t) in** green **and PC/PC in** orange**. Data collected for each laminate at nine random positions with each spectrum consisting of 128 scans at 8 cm^{-1} resolution. These were then averaged and plotted as the above spectra].**

Characterisation of the bulk material was performed on all six of the laminates after the 30 day tensile test. ATR analysis will determine the chemical functionality of the final cured material and allow for any distinct differences in curing chemistry to be observed. Discussed within this section will be peaks that indicate either the PU of the chain-extended prepolymer or PU-U peaks obtained after 30 days of cure. For discussion of the peaks inherent of the starting materials see section 6.26 and for all characteristic peaks see table 6.12.

Table 6.12: **Characteristic peaks of IPDI-TMP-PCD-PD cured PU-U adhesive from all six laminate combinations.**

Wavenumber (cm^{-1})	Vibration	Wavenumber (cm^{-1})	Vibration
3368	N-H stretching Hbonded	1390	C-H symmetric deformation
2947	C-H asymmetric stretch	1368	C-N Urea
2870	C-H symmetric stretch	1297	C-N Urethane
1725	C=O stretch Hbonded Ester	1159	Asymmetric N-CO-O, C-H aliphatic skeleton
1698	C=O stretch free Urea	1107	C-O-C stretch aliphatic ester
1645	C=O stretch Urea Bidentate Hbonded	1066	Symmetric N-CO-O
1527	C-N stretch, N-H bend	961	C-O-C stretch aliphatic ester
1464	C-H bend aliphatic	775	C-C skeleton rocking
1420	C-H asymmetric deformation	730	C-C skeleton rocking

From the spectra present with figure 6.29 it is visible there are two different **N-H** vibrations within the above cured PU-U. **N-H** stretching vibrations occurring at 3368 cm^{-1} show that H-bonded domains are present in the microstructure whereas, the shoulder peak at around 3500 cm^{-1} correspond to free **N-H** stretching vibrations. Corresponding bending vibrations are visible in the fingerprint region of the spectra for **N-H** at 1527 cm^{-1}, also present within this peak is the **C-N** stretch. **C-N** bending vibrations are also observed for urea at 1368 cm^{-1} and urethane at 1297 cm^{-1}. Again no detectable isocyanate peak was visible between 2260 cm^{-1} – 2280 cm^{-1} which displays that the adhesive is fully cured after 30 days.

Further information on the inherent microstructure following moisture cure is available within the carbonyl region. Evidence of H-bonded ester carbonyl stretching is visible at 1725 cm^{-1} which would indicate that crystallisation is occurring within the soft-segments. An immediate shoulder to this peak displays the occurrence of free urea carbonyl stretching at 1698 cm^{-1}. Further evidence of structured regions within the microstructure of the cured adhesive is shown by the bidentate H-bonded urea stretching vibration at 1644 cm^{-1}. As these peaks are beginning to convolute together it also displays that there will be proportion of monodentate urea groups which has a characteristic vibration of 1675 cm^{-1} – 1660cm^{-1}. The overall morphology observed from ATR will be discussed in greater detail within chapter 8.

6.57 Summary of IPDI-TMP-PCD-PD Formulation

Synthesis of the PD chain-extended prepolymer was followed using NMR which displayed successful synthesis. MALDI-MS was used to characterise the molecular mass distributions present within the chain-extended prepolymer formulation. MALDI-MS identified prepolymers from step one as the main molecular weight distribution. Also encountered were two further distributions which are off set from the main distribution by 23m/z for the di-sodiated adduct and 76 m/z for prepolymers that have reacted with PD but not yet coupled with another prepolymer molecule to become fully chain-extended. Direct observation of chain-extended prepolymer molecules was also possible. The values calculated for Mn, Mw and PDI were almost identical to IPDI-TMP-PCD.

Investigation of the thermal transition by DSC recorded a T$_g$ss for the chain-extended prepolymer of -52°C which is an elevation of +12°C compared to PCD. A melting endotherm of the PCD soft-segment at 30°C was also observed in the prepolymers thermogram. Once fully cured the T$_g$ss was recorded at -48°C on the first heating cycle and this remained consistent at -48°C on the second heating cycle. Observed on the first heating cycle was a melting endotherm for the PCD soft-segment at 45°C. As the melting temperature was lower than pure PCD (50°C) it highlights that the crystalline soft-segment domains are less organised and suggests some phase mixing is occurring. Observed on the second heating cycle was melting of the hardsegment (at 196°C) within the PU-U which displays that regions of phase segregation are present. The

overall thermal stability was determined by TGA with the onset of degradation occurring at 299°C. From the DTG curve two degradation peaks at 399°C and 5324°C were observed which represent the decomposition of both the hard and soft-segment followed by degradation of more stable cross-linked materials formed during degradation.

Using 180° T-peel testing it was identified that untreated TAc performed very poorly (0.7 N mm^{-1}), however, following surface treatment the values greatly improved with a cohesive mode of failure within the TAc(t) substrate recorded (peel strength 4.8 N mm^{-1}). Untreated PC performed exceptionally well reaching 9.9 N mm^{-1} after 30 days. For treated PC a similar result was obtained with an above benchmark value of 7.8 N mm^{-1} recorded following 30 days of cure. For the hybrid laminate the observed weakest component was the adhesive layer which in both cases resulted in a cohesive mode of failure within this layer.

The haze values recorded for each of the six laminates was > 1.5% and the adhesive layer was milky white in colour. This value would have been expected based on the data obtained on the first heating cycle using DSC which displayed a melting endotherm of the soft-segment. Finally using ATR the adhesive material was observed to be fully cured following 30 days of curing. Also observed was that the fully cured adhesive was a PU-U and that there were H-bonding domains within the cured network.

6.60 Summary of Aliphatic Polyurethane Adhesives based on Poly(caprolactone diol)

NMR analysis using both ^{1}H and ^{13}C was able to follow the synthesis of the prepolymer PU. NMR was used to identify the incorporation of the chain-extender molecules into the formulation through the following the shift the appropriate end groups in the soft-segment molecules. ^{13}C was especially useful at showing the asymmetric reaction which did not favour either isocyanate group during synthesis. This was displayed by two peaks in the urethane region which showed both primary and secondary groups involved within the newly formed linkages. Confirmation that the prepolymers in solution were still reactive was also confirmed by ^{13}C NMR which displayed both primary and secondary free isocyanates in solution. MALDIMS analysis was used to

characterise the molecular weight of the prepolymer and chain-extended prepolymers. For IPDI-TMP-PCD the target molecular weight was successfully obtained along with isocyanate end capped TMP molecules. For the chain-extended formulations the target molecules were observed however, the peaks were less intense.

Characterisation of the thermal stability of each fully cured adhesive was carried out using TGA analysis. The observed onset of degradation and the subsequent degradation profile was similar for all four formulations. For each formulation the onset of degradation occurs around 300°C and (base formulation = 300°C, DEPD = 309°C, BD = 305°C and PD = 299°C) no significant enhancement or depreciation of the thermal stability was observed as a result of diol chain-extension. Each formulation displayed one major degradation step (base formulation = 395°C, DEPD = 397°C, BD = 394°C and PD = 399°C) which corresponds to the degradation of firstly urethane/urea bonds followed by the subsequent degradation of the softsegment. The second and minor degradation step (base formulation = 521°C, DEPD = 517°C, BD = 524°C and PD = 532°C) will account for the degradation of either thermally more stable materials formed during degradation or degradation of residual soft-segment. Evident in each of these formulations is that there thermal degradation is well above the maximum processing temperature of 100°C.

Thermal transitions of each formulation were followed by DSC analysis for both the prepolymer material directly after synthesis and the fully cured system. The $T_g$ss was considered an important data point as it had to be out with the set processing range and likely temperature of application. At the prepolymer step a small increase of around 5°C was observed in the $T_g$ss between the base material and each of the chain-extended prepolymers (base formulation = -55°C, DEPD = -48°C, BD = -51°C and PD = -52°C). Also observed within each thermogram was a melting endotherm inherent of the crystalline PCD soft-segment (base formulation = 29°C, DEPD = none, BD = 31°C and PD = 30°C). This crystallisation signature observed in the prepolymer was also evident in the first heating cycle of each cured adhesive (base formulation = 49°C, DEPD = 44°C, BD = 46°C and PD = 45°C). Observed on each of the second heating scans was an endotherm at an elevated temperature which corresponded to melting of

hard-segments (base formulation = 197°C, DEPD = 206°C, BD = 193°C and PD = 196°C).

The previous data collected in thermal analysis was used to help explain the high haze values recorded for each adhesive. All four formulations gave a haze value of > 1.5% which was a result of the soft-segment crystallisation and resulted in each adhesive layer being milky white in colour. Although crystallisation of the softsegment had an adverse effect on the adhesive clarity it appears to have had a positive impact on the peel strength.

The high peel strengths obtained on each of the formulation was attributed to the high degree of cross-linking through H-bonding in both hard and soft-segments. On average each material performed above benchmark (base formulation = 5.3 N mm^{-1}, DEPD = 4.2 N mm^{-1}, BD = 5.1 N mm^{-1} and PD = 6.4 N mm^{-1} average peel strength for 5 laminate excluding TAc/TAc after 30 days) with TAc/TAc again being the exception (base formulation = 0.6 N mm^{-1}, DEPD = 0.7 N mm^{-1}, BD = 1.0 N mm^{-1} and PD = 0.7 N mm^{-1} peel strength of TAc/TAc). Of the six laminates tested PC/PC gave the highest strength (base formulation = 10.5 N mm^{-1}, DEPD = 2.2 N mm^{-1}, BD = 9.2 N mm^{-1} and PD = 9.9 N mm^{-1}) which are the highest values recorded of any set to present (DEPD exception).

Following all the analysis collected the formulations based on IPDI and PCD are not going to be used for the proposed application as the adhesive layer does not remain clear or bond TAc/TAc. Excluding these two major downfalls this set of adhesive passes the other two criteria of being able to form high peel strength laminates while retaining a $T_g$ss well out with the processing or usage temperatures and being thermally stable well above processing temperatures.

References

(1)   Cui, Y.; Chen, D.; Wang, X.; Tang, X. *International Journal of Adhesion and Adhesives* **2002**, *22*, 317.
(2)   Prabhakar, A.; Chattopadhyay, D. K.; Jagadeesh, B.; Raju, K. V. S. N. *Journal of Polymer Science Part A: Polymer Chemistry* **2005**, *43*, 1196.
(3)   Rath, S. K.; Ishack, A. M.; Suryavansi, U. G.; Chandrasekhar, L.; Patri, M. *Progress in Organic Coatings* **2008**, *62*, 393.

(4)   Chattopadhyay, D. K.; Prasad, P. S. R.; Sreedhar, B.; Raju, K. V. S. N. *Progress in Organic Coatings* **2005**, *54*, 296.

(5)   Korley, L. T. J.; Pate, B. D.; Thomas, E. L.; Hammond, P. T. *Polymer* **2006**, *47*, 3073.

(6)   Zhang, J.; Tu, W.; Dai, Z. *J Coat Technol Res* **2013**, *10*, 887.

(7)   García-Pacios, V.; Jofre-Reche, J. A.; Costa, V.; Colera, M.; MartínMartínez, J. M. *Progress in Organic Coatings* **2013**, *76*, 1484.

(8)   Cakic, S. M.; Stamenkovic, J. V.; Djordjevic, D. M.; Ristic, I. S. *Polymer Degradation and Stability* **2009**, *94*, 2015.

(9)   Li, C.; Wilkes, G. *Journal of Inorganic and Organometallic Polymers* **1997**, *7*, 203.

(10)   García-Pacios, V.; Iwata, Y.; Colera, M.; Miguel Martín-Martínez, J. *International Journal of Adhesion and Adhesives* **2011**, *31*, 787.

(11)   Petrović, Z. S.; Javni, I.; Divjaković, V. *Journal of Polymer Science Part B: Polymer Physics* **1998**, *36*, 221.

Chapter 7 Polyurethane Adhesives based on Poly[di(ethylene glycol) adipate]

7.10 Polymers Synthesis Introduction

Visible in chapters 3, 4, 5, and 6 was that there are two main factors that benefit the peel strength. The first and most influential was removing MDI from the formulation and replacing it with IPDI. Two advantages of this switch are that the aliphatic isocyanate has better UV stability, also its lower viscosity aids synthesis and application (lower viscosity that versus MDI based formulations).[1] The second observation was that using an ester based soft-segment leads to better peel strengths compared to an ether soft-segment. It must be noted that when using a crystalline soft-segment with MDI a clear adhesives could still be obtained following chainextension but phase separation occurred in IDPI based formulations resulting in high haze within the adhesive layer. Ether based adhesives were always of low haze regardless of the hard-segment used. Considering the two previous highlighted points it was decided to move to an adipate based soft-segment namely poly(di(ethyleneglycol) adipate) (PDEGA) which displays both ester and ether functionality.

As the soft-segment is non-crystalline an optically clear final adhesive should be obtain, with the addition advantage of still having a degree of H-bonding in the softsegment. Considering this two MDI based PU prepolymer adhesives were synthesised: a one-step prepolymer PU of formulation MDI-TMP-PDEGA (polymer has MDI, TMP and PDEGA in formulation) and a two-step chain-extended prepolymer formulation MDI-TMP-PDEGA-DEPD (initial step chain-extended DEPD = 2,2-diethyl-1,3-propane diol). To prove that the increased performance is a result of the isocyanate hard-segment two IPDI based PU prepolymer adhesives were also synthesised: a one-step prepolymer PU of formulation IPDI-TMP-PDEGA and a two-step chain-extended prepolymer formulation IPDI-TMP-PDEGA-DEPD.

Again the curing chemistry employed will be a two stage process of initial catalyst cure (0.05 wt% of both dibutyltin dilaurate and triethylamine) followed by final moisture cure of any remaining free isocyanate.
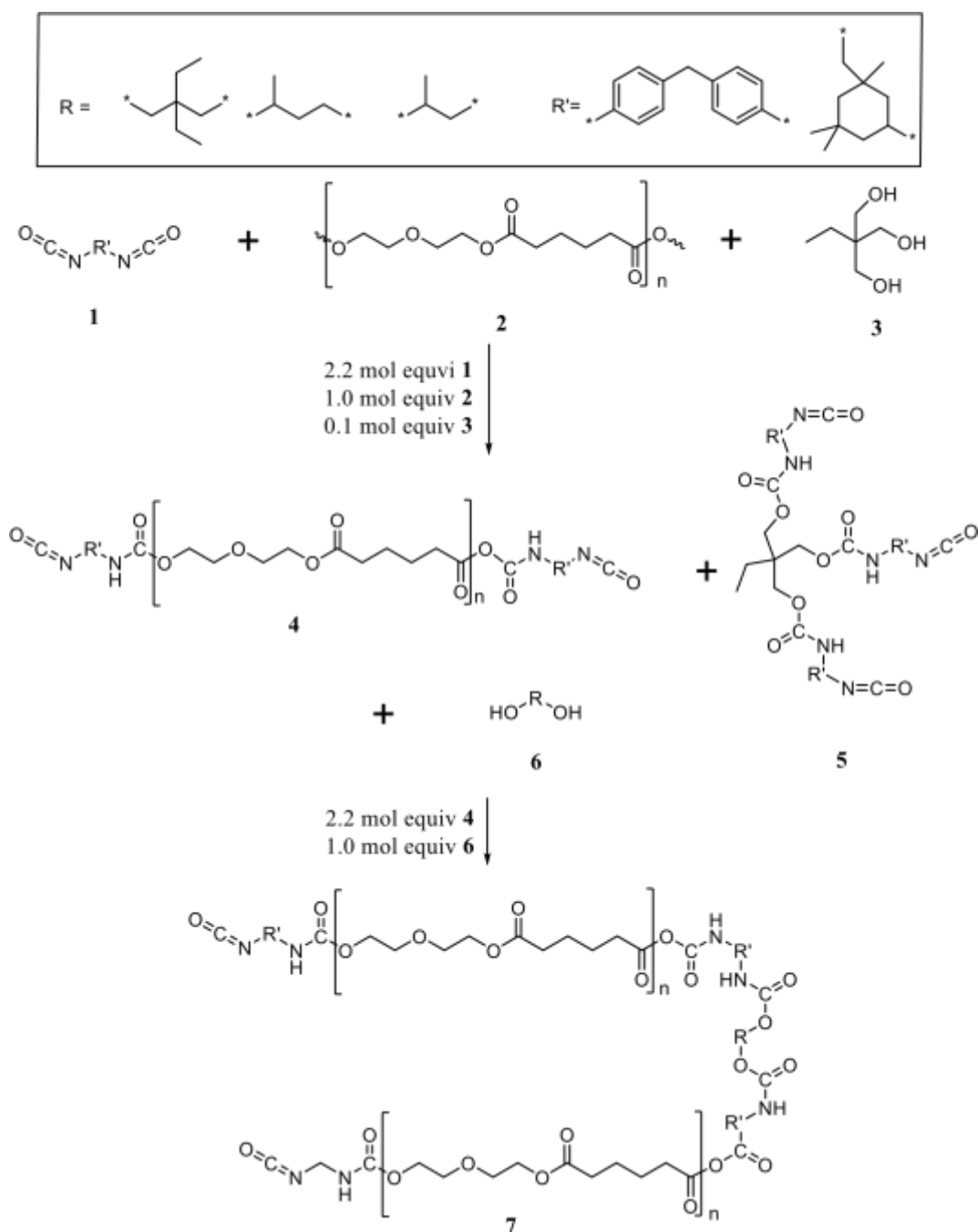
Figure 7.01: General reaction scheme for the synthesis IPDI/MDI-TMPPDEGA chain-extended polyurethanes adhesives. 1 = IPDI/MDI, 2 = PDEGA, 3 = TMP, 4 = isocyanate end capped PDEGA prepolymer, 5 end capped IPDI/MDI-TMP, 6 = chain-extender and 7 = chain-extended prepolymer.

Each synthesised prepolymer material was analysed using DSC, NMR and MALDIMS before application. Thermal transitions and stability of each fully cured PU-U was analysed by DSC and TGA. The final characteristics of each PU-U were analysed by

ATR to obtain functionality information and 180° T-peel testing to determine laminate peel strength.

7.20 Analysis of MDI-TMP-PDEGA

7.21 Synthesis Information

Prior to synthesis PDEGA (2500 Mw) was dried to remove water by placing within a vacuum oven at 80°C for at least 48 hours. Synthesis was performed using reaction set-up as detailed in section 2.03 with the reaction being performed in the temperature window of 85°C – 95°C for three hours. The reaction time was started after the last addition of MDI to the soft-segment containing reaction vessel. MDI was melted (50°C – 60°C within a three necked round bottom flask see section 2.03) and degassed before being put under a nitrogen atmosphere. To ensure that the exothermic reaction did not exceeded 95°C, MDI was added drop wise in 1 ml portions. The final prepolymer obtained was clear but visually thicker than the starting mixture as a consequence of the molecular weight increase. Prior to catalyst addition samples of the reaction were taken for NMR, MALDI-MS and DSC analysis. After the elapsed reaction time of three hours 0.05 wt% of dibutyltin dilaurate and 0.05 wt% of triethylamine were added as curing catalysts (calculated from batch weight). Following catalyst addition the formulation was transferred to an aluminium holding tube and placed within a vacuum desiccator. The adhesive was then kept at 0°C within a fridge until lamination (typically not exceeding 7 days). Degassing was performed for six hours once a vacuum of one atmosphere was obtained.

The prepolymer adhesive was applied to six different laminates that were of interest:

- TAc/TAc
- TAc(t)/TAc(t)
- TAc(t)/PC
- TAc(t)/PC(t)

- PC(t)/PC(t)
- PC/PC

Where TAc is cellulose triacetate, PC is bisphenol-A polycarbonate and (t) denotes that the surface of the polymer film has been treated (see section 2.01 and2.02). MDI-

TMP-PDEGA was applied at 180°C to ensure good surface coverage. The lamination process was carried out as detailed in section 2.04, followed by cure at room temperature. 180° T-peel testing was carried out initially after 7 days and then after 30 days to determine the peel strength of each laminate, with the mode of failure monitored by visual inspection. The cured laminates from the 30 day peel testing were used in the ATR analysis of the fully cured adhesive.

7.22 NMR Analysis

To observe the PU prepolymer formation between MDI with PDEGA, both ^{1}H and ^{13}C were both recorded. The hydroxyl end-groups of the 2500 molecular weight (Mw) PDEGA were both primary as determined by previous analysis (diethylene glycol terminated hydroxyl groups at 5.4 ppm).

Presented in figure 7.02 is the ^{1}H spectrum of MDI-TMP-PDEGA which displays the end capping of PDEGA with MDI. The below spectrum is dominated by peaks of the soft-segment PDEGA which makes observation of the TMP chain-extender difficult however, the signals are still present. The methyl group from TMP molecules appear at 0.89 ppm are visible and the adjacent methylene groups are visible at 1.69 ppm. Once fully reacted with MDI, the methylene protons adjacent to the urethane linkage shift from 3.49 ppm (when hydroxyl) to 4.01 ppm which displays that end capped TMP polymers are present within the formulation.

Peaks inherent of the PDEGA soft-segment as mentioned dominate the ^{1}H spectrum. Within the soft-segment there are both ester based blocks from adipic acid and ether based blocks from diethylene glycol. ^{1}H signals from the adipic acid segments appear at 1.63 ppm (**2'** and **3'**) and 2.32 ppm (**1'** and **4'**). Two proton signals inherent of the diethylene glycol blocks are visible at 3.63 ppm (**6'** and **7'**) and 4.19 ppm (**5'**). A further downfield shift of the methylene protons of the end groups attached to the urethane linkages **8'** is visible at 4.24 ppm (free primary hydroxyl end groups observed at 5.4 ppm).
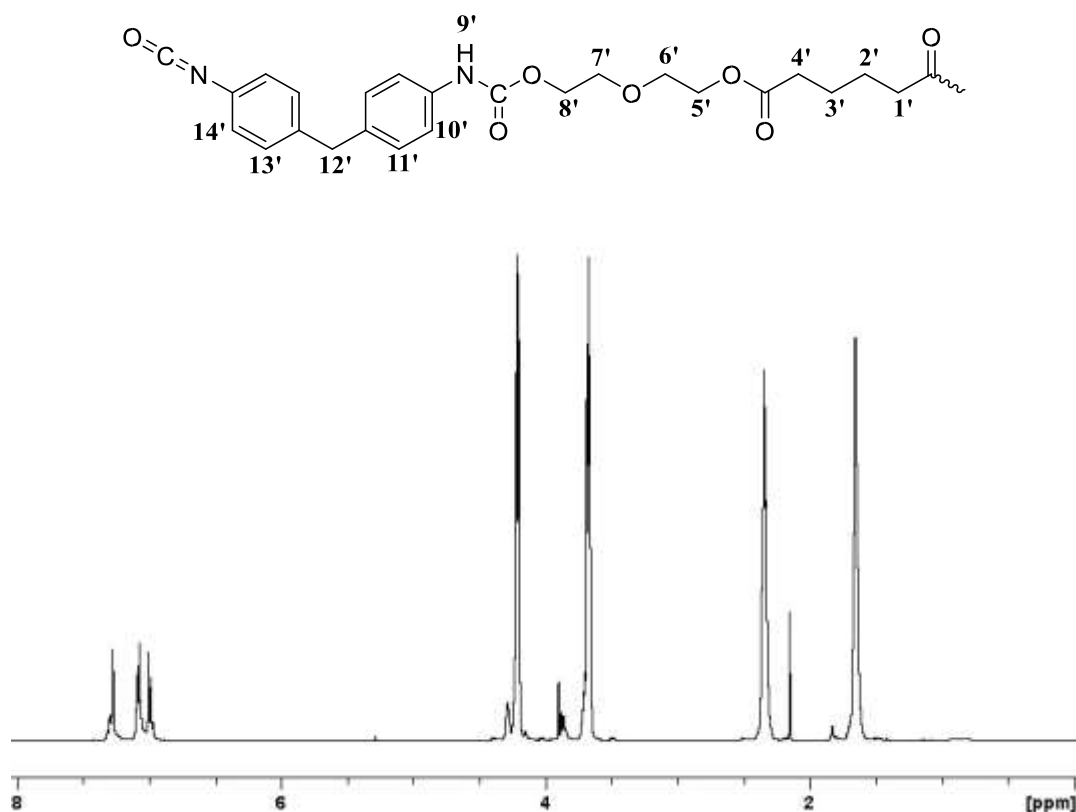
Figure 7.02: ¹H NMR spectrum of MDI-TMP-PDEGA polyurethane prepolymer in deuterated chloroform.

The signal visible at 3.87 ppm represents the methylene bridge protons **12'** of the MDI molecule. Further MDI signals from the aromatic **CH** protons are visible at 7.09 ppm **13'** and 7.15 ppm **14'** on the unreacted ring. As these signal are visible it infers displays the presence of free isocyanate groups. Further aromatic peaks at 7.09 **11'** and 7.00 ppm **10'** are within the aromatic ring which is attached to the urethane linkage. At 7.29 ppm **14'** the broad peak corresponds to the **CH** protons which have shifted downfield due to the presence of the urethane linkage and these are further evidence of the urethane fromation.[2]

Further evidence of urethane formation is visible within the ¹³C NMR spectrum presented within figure 7.03. At 153.5 ppm a weak carbonyl shift is observed which is characteristic for a urethane linkage **11** followed and at 131.3 ppm the carbonyl for free isocyanate group **21** is displayed. For characterisation of all ¹³C peaks present within figure 7.03 consult table 7.01.

Table 7.01: ¹H and ¹³C chemical shift for MDI-TMP-PDEGA collected in CDCl₃.

MDI-TMP-PDEGA	Position	¹H Chemical Shift (ppm)	Position	13C Chemical Shift (ppm)
	1'	2.32	1	173.2
	2'	1.63	2	33.7
	3'	1.63	3	24.4
	4'	2.32	4	24.4
	5'	4.20	5	33.7
	6'	3.65	6	173.2
	7'	3.65	7	64.1
	8'	4.24	8	69.4
	9'	7.29	9	69.0
	10'	7.09	10	63.3
	11'	7.00	11	153.5
	12'	3.87	12	135.6
	13'	7.09	13	124.8
	14'	7.15	14	129.9
			15	128.9
			16	40.7
			17	138.9
			18	131.5
			19	124.2
			20	131.5
			21	131.3

401
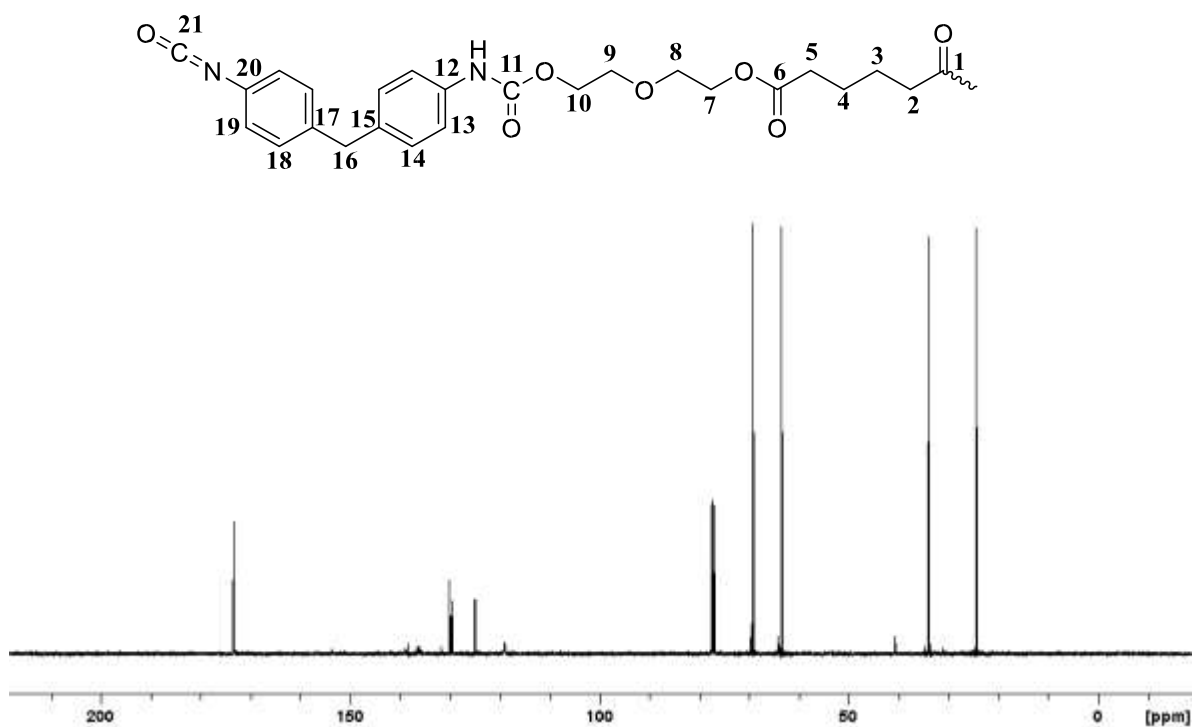
Figure 7.03: ^{13}C NMR spectrum of MDI-TMP-PDEGA prepolymer in deuterated chloroform.

7.23 MALDI-MS Analysis

Within the previous section, evidence of both urethane and free isocyanate were observed using NMR. In order to fully understand the structure of the prepolymer, mass spectrometry data is required. To serve this purpose MALDI-MS analysis was employed to determine the molecular mass of the starting polyol and then the prepolymer adhesive. The matrix used was 2-(4-hydroxyphenlazo)benzoic acid) (HABA) which was prepared as a 20 mg ml^{-1} solution in tetrahydrofuran (THF), this was then mixed with a 1 mg ml^{-1} solution of sodiated trifluoroacetic acid (NaTFA) in a 7:1 ratio respectively. MDI-TMP-PDEGA was prepared as a 40 mg ml^{-1} solution in THF which was then mixed with the matrix in a 1:8 ratio of sample to matrix. 1 μl aliquots of the solution were then spotted and dried before analysis.

The mass spectrum of PDEGA in figure 7.04 displays the sodiated adduct of the softsegment (with the sodium coming from the small amount of a cationising (NaTFA) agent added to obtain spectra). The molecular weight distribution for PDEGA has a peak mass of 2397 m/z which is 9 adipic acid blocks, 10 diethylene glycol blocks and one sodium ion. For the prepolymer material an observed shift of the distribution by

592 m/z was observed which correspond to the addition of two MDI units that have had their free isocyanate groups end capped with ethanol to maintain the molecular weight. This peak centred at 2989 m/z contains two ethanol end capped MDI units, one sodium ion, 9 adipic acid blocks and 10 diethylene glycol blocks.
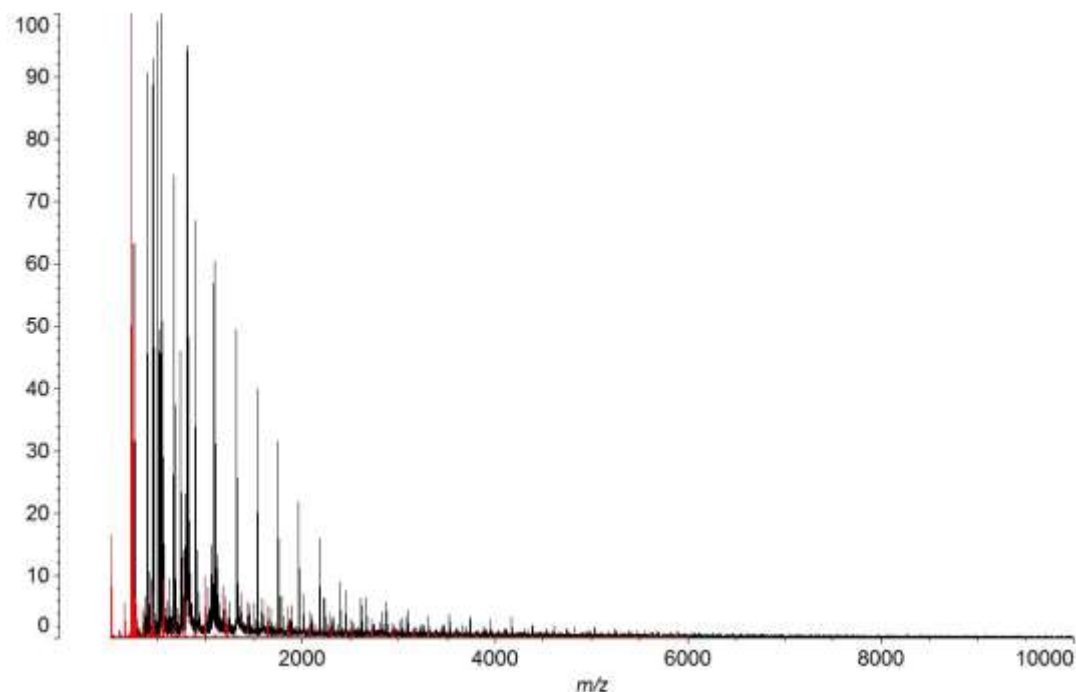
Figure 7.04: MALDI-MS spectra of PDEGA starting material in red and the prepolymer MDI-TMP-PDEGA in black. Both were mixed with the matrix material of 2-(4-hydroxyphenlazo)benzoic acid) and sodiated trifluoroacetic acid in a 1:8 sample:matrix mixture.

Also present is the chain-extender TMP that has reacted with three MDI unit which are ethanol end-capped at 1045 m/z (plus a sodium cation). These molecules will contribute to the hard-segment microstructure and will interfere with the packing arrangement. This spectrum confirms that using a 2.2:1.0 excess of isocyanate to polyol makes it possible to obtain an MDI-PDEGA-MDI end capped prepolymer PU. MALDI-MS has allowed for characterisation of the structure of the molecules present in conjunction with the previous NMR analysis.

From the MALDI-MS spectrum it is possible to calculate Mn, Mw and PDI (see section 2.132 for formulae). For soft-segment PDEGA, the calculated value of Mn is 1443

m/z and the calculated value of Mw is 1923 m/z giving a PDI of 1.33. It is noted that the calculated value of Mn from MALDI-MS is lower than the value quoted by the supplier (Mn ~ 2500) and that the mass distribution of the starting polymer is rather broad. Following prepolymer synthesis with MDI, the calculated value of Mn is 2374 m/z and the calculated Mw value is 3417 m/z giving a PDI of 1.44. Synthesis with MDI has shifted the distribution to a higher mass and increased the distributions width as shown by the increased PDI.

7.24 DSC and TGA Analysis

Characterising the thermal behaviour of both the prepolymer and cured adhesive is important to determine if the current formulation will be appropriate for the temperatures of manufacture. Two techniques that were selected to investigate if the materials were both free of unfavourable thermal transition and stable between -20°C – 100°C were DSC and TGA. The thermal behaviour of the prepolymer as analysed directly after synthesis will be discussed first and the fully cured adhesive will be discussed second.
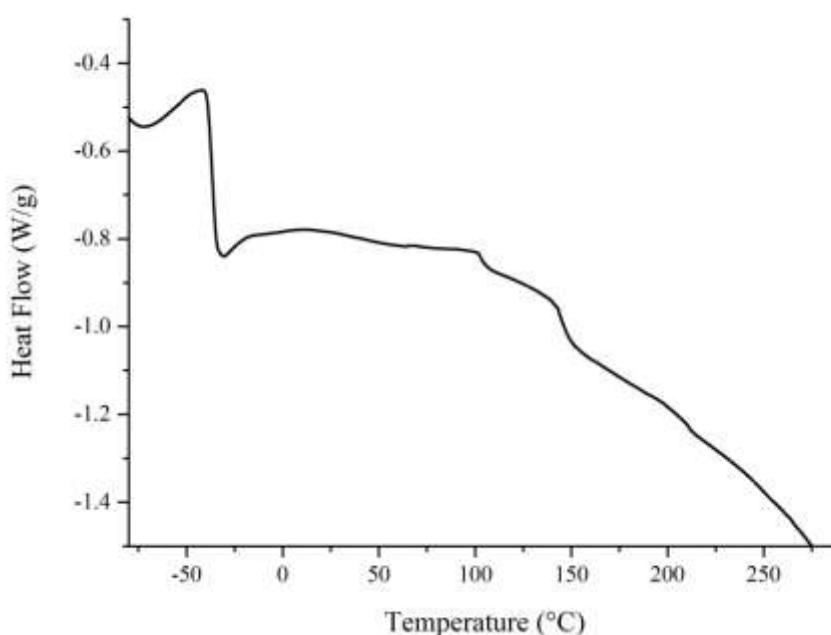
Figure 7.05: DSC thermogram of catalyst free MDI-TMP-PDEGA prepolymer sampled directly after synthesis.

Recording the soft-segment glass transition temperature ($T_g$ss) of the prepolymer material will determine if the formulation is performing out with the identified processing window. Also the position of the $T_g$ss compared to the unreacted softsegment will give an indication about the morphology and the compatibility of the two segments. The DSC experiment was recorded within an inert nitrogen atmosphere from -90°C to 300°C at a ramp rate of 10°C min^{-1}. For the prepolymer MDI-TMP-PDEGA the recorded $T_g$ss was -41°C which covered a narrow range of 45°C to -39°C. Within the thermogram also observed are two small exothermic peaks at 101°C and 143°C which will be curing peaks of the free isocyanate. As the analysis is carried out within a dry nitrogen atmosphere, the reactions will most likely be dimer formation, trimer formation or the reaction for free isocyanate groups with the acid hydrogen situated on the nitrogen within the urethane linkage forming an allophonate however, twould require further investigation.
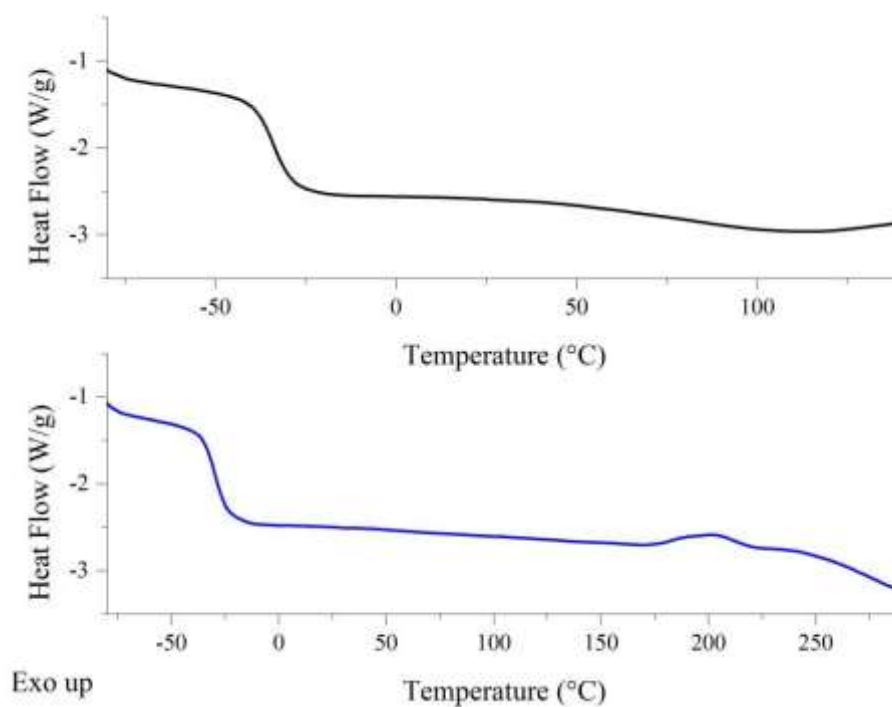
Figure 7.06: DSC thermogram of fully cured MDI-TMP-PDEGA adhesive, following removal from TAc/TAc laminate. [First heating cycle *top* in black and second heating cycle *bottom* in blue].

After 30 days of room temperature cure between two plies of TAc a portion of the adhesive was removed for DSC analysis. The function of this measurement was to

obtain the $T_g$ss of the final PU-U and to ensure that it had not entered the functional working window. The first heating cycle was recorded from -80°C to 140°C at 10°C min^{-1} and was used to remove any thermal history within the soft-segment of the sample. The second heating cycle was recorded from -80°C to 300°C to investigate if any information on hard and soft domains was available. Figure 7.06 displays the thermogram obtained from the DSC analysis of both the first and second heating cycles. The broadened $T_g$ss acquired on the first heating cycle occurs at -34°C (range from -39°C to -28°C) which has shift +8°C compared to the prepolymer material. Following on from the cooling cycle is the second heating cycle which displayed a $T_g$ss at -30°C which ranged from -35°C to -24°C. The shift observed within the glass transition in the second heating cycle could result from the first heating cycle increasing the phase mixing. On the second heating cycle there is a broad endothermic peak at 221°C which may correspond to hard-segment melting (transition is weak with the enthalpy of melting 0.3 J g^{-1}).[3]
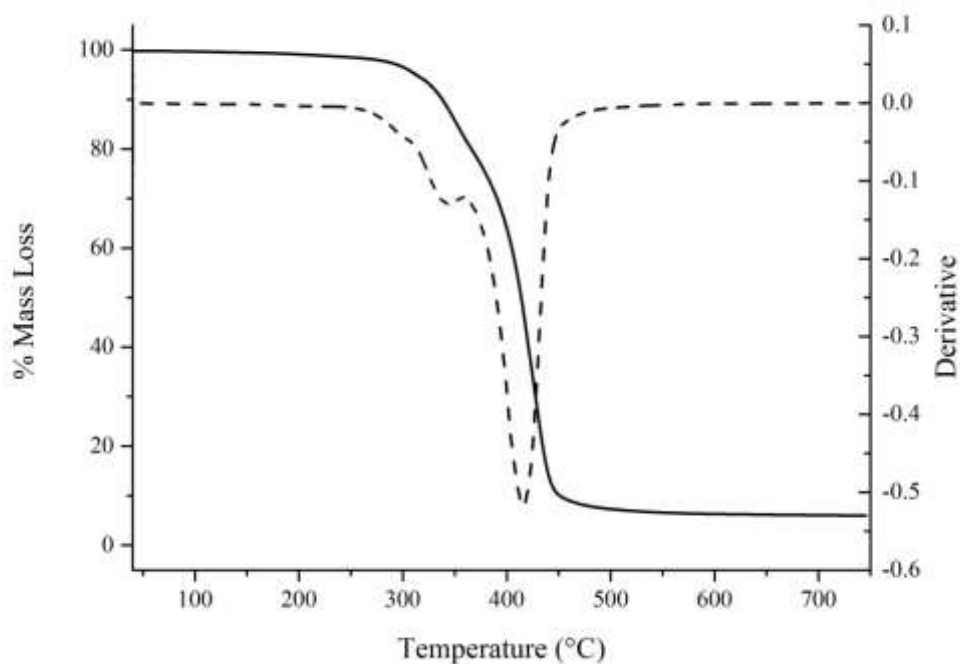
Figure 7.07: TGA and DTG curves of fully cured MDI-TMP-PDEGA adhesive. [TGA solid line and DTG dashed line].

Finally to determine that the thermal onset of degradation is out with the processing window TGA was used. A ramped heating experiment was performed from 40 – 750°C

at 10°C min^{-1} under nitrogen. Figure 7.07 displays the collected degradation curve and the derivative thermal gravimetric (DTG) curve of the mass loss. The calculated onset of degradation (calculated as the temperature where 5% of the total mass is lost) of MDI-TMP-PDEGA occurs at 313°C which is well outside the processing window. Two degradation processes are visible from inspection of the DTG curve, with the peak rates at 342°C and 416°C respectively. Firstly degradation within the hard-segments is shown by the peak centred at 342°C and will result from the breaking of urethane/urea bonds.[4-6] The second degradation process which occurs at a higher temperature corresponds to decomposition of the PDEGA soft-segment and other fragments produced during degradation (DTG peak 416°C).[5,7,8]

From the thermal analysis performed on MDI-TMP-PDEGA, it has identified that this formulation will be suitable for use within the intended laminate application. Following cure the observed T$_g$ss was -30°C which is well out with the processing window and will ensure that the adhesive will remain flexible during processing. Finally the fully cured adhesive has an onset of degradation which occurs well outside the processing window, again making this formulation acceptable for use within the intended laminate application.

7.25 180° T-peel Test and Haze

To screen the adhesion potential of MDI-TMP-PDEGA, six different laminates were constructed (as detailed in section 2.04) namely TAc/TAc, TAc(t)/TAc(t), TAc(t)/PC, TAc(t)/PC(t), PC(t)/PC(t) and PC/PC. This set of laminates will allow for characterisation of the affinity of MDI-TMP-PDEGA towards TAc and PC, but will also confirm if surface treatment is required. Three different interface scenarios are present within the test set: untreated (e.g. TAc/TAc or PC/PC), treated (TAc(t)/TAc(t) or PC(t)/PC(t)), and a hybrid (TAc(t)/PC or Tac(t)/PC(t)). Each laminate was peeled at 100 mm min^{-1} for an extension of at least 150 mm, with the first 50 mm discarded from the peel strength value as this is where a stable crack was formed. The haze of each cured laminate was also characterised at this point along with the failure mode. Visual inspection was used to determine the mode of failure as this would identify which part of each laminate was the weakest.

First tested was the TAc/TAc laminate which had an unstable adhesive mode of failure at the interface (0.2 N mm^{-1} for 7 days and 1.3 N mm^{-1} after 30 days). The adhesive failure confirms that the surface chemistries at the TAc – adhesive interface have low compatibility. Possible adhesion mechanisms present will be a combination of Van der Waals forces between the adhesive and interface. Also Hbonding would be expected between the interface - adhesive as the soft-segment contains carbonyl groups and ethers linkages which will interact with the TAc surface. Possible H-bonding sites for the TAc are the acetate side groups and the ether linkages which are situated in or between the glycosidic rings.

Next the saponified TAc(t)/TAc(t) laminate (see section 2.01), which has a regenerated cellulose surface was tested to determine the peel strength and mode of failure. Deacetylation will leave hydroxyl groups at the surface which can react with the free isocyanate of the adhesive forming covalent bonds.[9] Covalent bond formation is favourable as it will form physical anchor points between the adhesive and substrate. Inspection of the collected data is not in keeping with previous data as the regeneration of cellulose at the surface did not show any significant increase in the peel strength after 7 days which was 0.8 N mm^{-1}. The mode of failure however, was consistent with an adhesive failure at the TAc interface observed. A peel strength value could not be obtained after 30 days due to adhesive layer foaming. For this current formulation surface treatment has made no significant improvement, this may result from the lower isocyanate content (result of soft-segment molecular weight increase).

Next untreated PC was tested to determine the affinity of the interface with the MDITMP-PDEGA adhesive. After 7 days of curing, the recorded strength was 4.2 N mm^{-1} and this value increased to 5.6 N mm^{-1} after 30 days of cure. An adhesive failure at the PC interface was observed and this was accompanied by strong deformation of each PC substrate. The greater adhesion observed for untreated PC compared to untreated TAc is due to a greater surface compatibility at the substrate – adhesive interface. As there is a high density of carbonate linkages along the PC backbone, many opportunities for H-bonding with the adhesive are available. This coupled with the possible adhesion through ▯-▯ aromatic ring stacking interactions will explain the strong adhesion.[10]

Treatment of the PC using an ethanolamine in isopropyl alcohol solution was next performed (see section 2.02 for procedure) to determine its effect on the measured adhesion. The proposed mechanism for the surface treatment of the PC is nucleophilic attack of the carbonate linkage by the amine of ethanolamine to leave a phenol and a hydroxyl terminated urethane, although the precise mechanism is not known at this time.[11] In theory this should leave OH functional groups at the surface which should boost adhesion through the formation of covalent bonds with the free isocyanate groups. Peel strength data collected after 7 days displayed an adhesive mode of failure that was 6.2 N mm^{-1} in strength and this value increased to 7.6 N mm^{-1} after 30 days. From the above data the surface treatment for PC had a positive effect on the peel strength between the adhesive and substrate. Treatment of the PC had a significant effect on the recorded peel strength however, both PC/PC and PC(t)/PC(t) were above benchmark.

Data collected from the hybrid laminates TAc(t)/PC and TAc(t)/PC(t) followed the trends observed for the previous four laminates (PC has a greater affinity with the adhesive than either TAc or TAc(t)). For the hybrid laminate TAc(t)/PC after 7 days an adhesive mode of failure at the TAc(t) interface was observed with the peel strength recorded at 0.9 N mm^{-1} (30 day value not available due to adhesive foaming). For the fully treated hybrid system TAc(t)/PC(t) a very similar scenario was presented with both tests resulting in an adhesive mode of failure at the TAc(t) interface. Both tests displayed an unstable peel which was 0.8 N mm^{-1} after 7 days of cure and this marginally increased to 1.1 N mm^{-1} after 30 days of cure.

The average haze collected across the six laminates was > 1.5% which is out with the 1.5% benchmark value. This high value was unexpected as the soft-segment does not crystallise however, it can be explained by the large amount of bubbles which are visible within the adhesive layer. These bubbles are either CO_2 produced during the moisture cure which become trapped as the viscosity increases or liberation of air that has dissolved into the formulation (this would not be expected due to the degassing step).

Table 7.02: Peel, haze and mode of failure data for MDI-TMP-PDEGA cured PU-U adhesive. [The data in bold will be discussed within this section].

Cured Adhesive	Laminate	Peel 1* (N mm^{-1})	Peel 2^x (N mm^{-1})	Failure mode	Haze (%)
MDI-TMP-PDEGA	**TAc/TAc**	**0.2**	**1.3**	**Adhesive TAc**	**>1.5 %**
	TAc(t)/TAc(t)	**0.8**	**ND**	**Adhesive TAc**	
	TAc(t)/PC	**0.9**	**ND**	**Adhesive TAc**	
	TAc(t)/PC(t)	**0.8**	**1.1**	**Adhesive TAc**	
	PC(t)/ PC(t)	**6.2**	**7.6**	**Adhesive PC**	
	PC/PC	**4.2**	**5.6**	**Adhesive PC**	
MDI-TMP-PDEGA-DEPD	TAc/TAc	1.3	ND	Adhesive TAc	>1.5%
	TAc(t)/TAc(t)	0.9	ND	Adhesive TAc	
	TAc(t)/PC	1.1	1.4	Adhesive TAc	
	TAc(t)/PC(t)	1.0	1.1	Adhesive TAc	
	PC(t)/ PC(t)	2.3	ND	Adhesive PC	
	PC/PC	3.6	ND	Adhesive PC	
IPDI-TMP-PDEGA	TAc/TAc	0.9	Ply	Cohesive	<0.7%
	TAc(t)/TAc(t)	1.0	Ply	Cohesive	
	TAc(t)/PC	0.8	4.7	Cohesive	
	TAc(t)/PC(t)	0.9	4.7	Cohesive	
	PC(t)/ PC(t)	0.5	9.1	Cohesive	
	PC/PC	0.9	11.5	Cohesive	
IPDI-TMP-PDEGA-DEPD	TAc/TAc	1.4	6.4	Cohesive	<0.7%
	TAc(t)/TAc(t)	1.7	6.0	Cohesive	
	TAc(t)/PC	1.4	6.5	Cohesive	
	TAc(t)/PC(t)	1.1	6.1	Cohesive	
	PC(t)/ PC(t)	0.6	10.3	Cohesive	
	PC/PC	0.7	10.6	Cohesive	

peel 1 collected within 7 days of room temperature cure, ^{x} peel 2 collected after 30 days of room temperature cure, ND = No Data

7.26 ATR of Peeled Samples

Due to the varying peel strengths obtained it was essential to characterise if (a) the adhesive after 30 days was fully cured and (b) once cured was the bulk adhesive the same final material. To investigate the bulk MDI-TMP-PDEGA material, ATR was used as it is a non-destructive way to sample the adhesive. ATR was carried out on all six different laminates once they had been peel tested after 30 days of curing. The purpose of this analysis was to characterise the bulk material following 30 days of cure and also to identify if any residual isocyanate was visible following this period of cure.
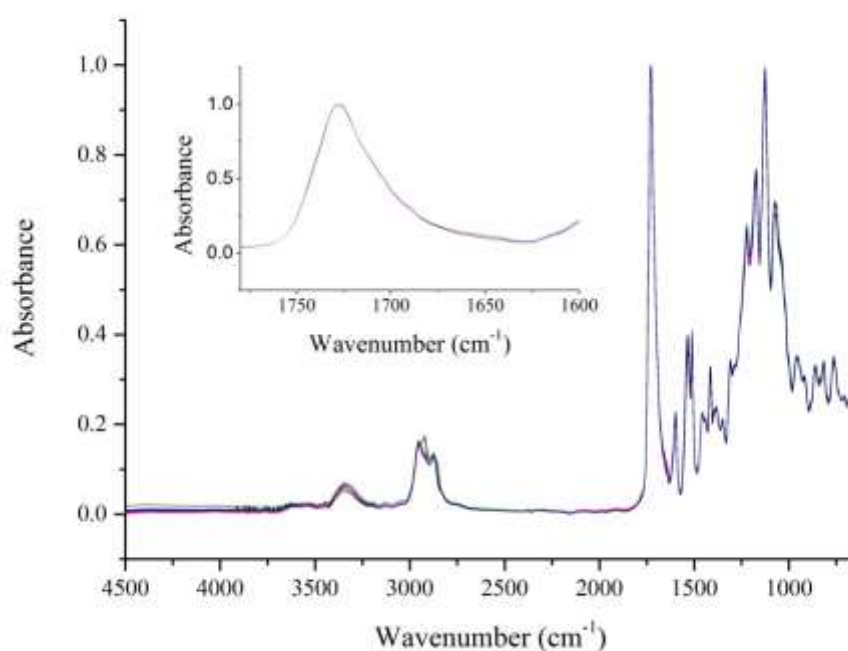
Figure 7.08: ATR spectra of cured MDI-TMP-PDEGA sampled in-situ after peel testing with inset expanded carbonyl region. [TAc/TAc in black, TAc(t)/TAc(t) in red, TAc(t)/PC in blue, TAc(t)/PC(t) in pink, PC(t)/PC(t) in green and PC/PC in orange. Data collected for each laminate at nine random positions with each spectrum consisting of 128 scans at 8 cm^{-1} resolution. These were then averaged and plotted as the above spectra].

The spectra collected from the in-situ characterisation of the cured adhesive are shown within figure 7.08 for all six laminates. All characteristic peaks for the fully cured PU-U are shown within table 7.03. Observation of the band positioned at 3342 cm^{-1}

displays that H-bonding between **N-H** groups within the network is occurring. Possible domains where H-bonding would occur for **N-H** groups are between urea or urethane groups of hard-segments or with soft-segment ester/ether groups when the two domains are mixed. Also evident are **N-H** stretching vibrations which display no H-bonded as shown by the shoulder to the previous peak at 3500 cm^{-1}.

Next aliphatic **C-H** stretching vibrations from PDEGA are present for both the asymmetric and symmetric bands at 2954 cm^{-1} and 2878 cm^{-1} respectively. No detectable isocyanate peak was visible between 2260 cm^{-1} – 2280 cm^{-1} which displays that the adhesive is fully cured after 30 days. A large signal for the **C=O** stretch of the ester from the soft-segment is present at 1727 cm^{-1}. The size of this carbonyl signal has masked the urethane/urea peaks (expected around 1710 – 1640 cm^{-1}) which would be expected as both urethane and urea moiety's are introduced during synthesis and moisture cure (see shoulder in expanded carbonyl peak in figure 7.08).[12] Evidence of urethanes is shown by the **N-H** bending vibration at 1594 cm^{-1}.[12] Further evidence of cure (either urea or urethane functionality) appears at 1538 cm^{-1} which corresponds to **C-N** stretching and **N-H** bending vibrations. It would also be expected to see a weak aromatic **C-H** signal; however, it is convoluted in with these previous vibrations. Next the first clear sign of urea formation during moisture cure is observed by the **N-H** bending signal at 1505 cm^{-1}.[12]

Aliphatic **C-H** stretching from the PDEGA and aromatic **C-C** stretching vibrations of MDI are also present at 1452 cm^{-1} and 1415 cm^{-1} respectively. Confirmation that the cured adhesive is a PU-U can be seen by the urethane and urea **C-N** bands at 1353 cm^{-1} and 1317 cm^{-1}. PDEGA vibrations for the **C-H** skeleton vibration, **C-C** stretching plus asymmetric **N-CO-O** and the **C-O-C** ester groups are next observed at 1220 cm^{-1}, 1178 cm-1 and 1074 cm^{-1} respectively. The position of the **C-H** aromatic ring vibrations are at 960 cm^{-1}, 927 cm^{-1}, 861 cm^{-1} and 827 cm^{-1} are characteristic of the 1,4- + 1,2- di-substitution mixture of the monomeric MDI. The final peak at 771 cm^{-1} shows the **C-C** skeleton vibrations of the aliphatic backbone and there will also be a contribution of an aromatic **C-H** convoluted in with the signal.

Table 7.03: Characteristic peaks of MDI-TMP-PDEGA cured PU-U adhesive from all six laminate combinations.

Wavenumber (cm⁻¹)	Vibration	Wavenumber (cm⁻¹)	Vibration
3342	N-H stretching H-Bonded	1317	C-N urethane
2954	C-H asymmetric stretch	1220	C-H aliphatic skeleton
2878	C-H symmetric stretch	1178	C-C stretching
1727	C=O stretching ester	1121	Asymmetric N-CO-O
1594	N-H bending urethane	1074	C-H aromatic ring, C-O-C stretch aliphatic ester/ether, symmetric N-CO-O
1538	C-N stretch, N-H bending, C-H aromatic ring	960	C-H aromatic ring, C-O-C stretch aliphatic ester/ether
1505	N-H bending urea	927	C-H aromatic ring
1452	C-H bend aliphatic	861	C-H aromatic ring
1415	C-C stretching aromatic	827	C-H aromatic ring
1353	C-N urea	771	C-C aliphatic skeleton

ATR analysis displayed that the final cured MDI-TMP-PDEGA adhesive is a PU-U, with both urethane and urea groups present. It has also shown that the bulk adhesive across the six laminate combinations is very similar. This displays that any differences in peel strength can be attributed to differences in adhesion at the interface. Finally

the adhesive was fully cured as there was no sign of any unreacted isocyanate in the final spectrum for any of the laminates.

7.27 Summary of MDI-TMP-PDEGA Formulation

From the above analysis it can be confirmed from both ^{1}H and ^{13}C NMR that the end capped PU prepolymer was successfully synthesised. This was further confirmed by MALDI-MS analysis which also highlighted that the expected prepolymer MDIPDEGA-MDI structure was obtained. The value calculated by MALDI-MS for PDEGA was lower than that quoted by the supplier and of all the soft-segments tested it has the greatest PDI. Following prepolymer synthesis with MDI the values obtained for Mn, Mw and PDI all increased.

Thermal analysis performed using DSC displayed that the prepolymer material had a $T_g$ss of -41°C which covered a narrow range (-45°C to -39°C). This was accompanied by a curing peak of the free isocyanate at 143°C. Following moisture cure, the $T_g$ss of the cured adhesive shifted to -33°C for the first heating cycle (this cycle displayed no other clear thermal features). On the second heating cycle the $T_g$ss recorded was -30°C and this was accompanied by a small melting endotherm which occurred at 201°C. From the position of the glass transition it would display that mixing of the phases has occurred. Breaking of H-bonds that hold hardsegments together within the microstructure are displayed by the high temperature melt, however, the small enthalpy value would suggest that these domains are not highly organised. The increase in $T_g$ss will also be influenced by the increased viscosity of the fully cured system along with any cross-linking. More important however, was that the final $T_g$ss of the fully cured adhesive was out with the processing window. The thermal stability following moisture cure of the adhesive was evaluated using TGA which displayed an onset of degradation at 313°C with the peak rate occurring at 343°C for degradation of the hard-segment and 416°C for degradation of the soft-segment.

Analysis carried out using 180° T-peel testing displayed that the best laminate combination was PC(t)/PC(t) which boasted a peel strength of 7.6 N mm^{-1} following 30 days of cure. The worst laminate was TAc/TAc which registered 1.3 N mm^{-1} after 30 day of cure and displayed a very unstable peel. ATR analysis displayed that

following 30 days the adhesive was fully cured and was a PU-U. It also displayed that ordered regions were present as shown by the H-bonding in **N-H** region (also in the **C=O** region but less clear due to large soft-segment peak). Finally the haze value of the fully cured laminates were > 1.5% as a result of the large amount of bubble trapped within the adhesive layer. These bubbles could be the result of CO_2 liberation during the urea reaction or the trapping of gases contained within the formulation.

7.30 Analysis of MDI-TMP-PDEGA-DEPD

7.31 Synthesis Information

MDI-TMP-PDEGA-DEPD was next synthesised with the intention of disrupting the hard-segment formation through use of a sterically hindered diol chain-extender and encourage good phase mixing. This was achieved by firstly synthesising the prepolymer MDI-TMP-PDEGA using the same reaction conditions as detailed with section 7.21 and then performing an addition reaction set. The additional step was performed by adding a hydroxyl terminated chain-extender using a 2.2:1.0 isocyanate:hydroxyl ratio based on the calculated amount of free NCO remaining after step one. The chain-extension step was used to lower the free isocyanate content of the adhesive, which would reduce the opportunity for excessive bubbling by CO_2 liberation from urea formation during moisture cure.

Step one was performed as previously detailed in section 7.21 and was a clear liquid which had an observed increase in viscosity from the starting mixture. After addition of 2,2-diethyl-1,3-propane diol (DEPD), the reaction was allowed to stir at 85°C – 95°C for 5 hours before the dual DBTDL and TEA catalyst system was added. Following chain-extension a visual increase in viscosity was observed and was associated with the molecular weight increase caused by the coupling step. To compensate for the molecular weight increase, the reaction mixture was slowly heated to 130°C to sufficiently lower the viscosity as this would facilitate flow and allow for the formulation to be poured. Once at temperature, the formulation was poured into an aluminium tube, which was then capped and degassed as previously outlined in section 2.03. The desiccator containing the adhesive filled tube was then placed within a 0°C fridge for storage until lamination. Degassing was performed for six hours once

a vacuum of one atmosphere was obtained. Samples of the reaction were again taken before catalysed addition, these were analysed by DSC, NMR and MALDI-MS analysis.

MDI-TMP-PDEGA-DEPD was heated to 190°C before being applied to six laminates (same as section 3.21), this was followed by room temperature cure. These samples were 180° T-peel tested at 7 days and 30 days to determine the peel strength. A further lamination was performed using two plies of TAc which would allow for the fully cured adhesive to be removed for analysis by DSC and TGA. The 30 day peel test samples were also analysed by ATR to characterise the final adhesive and determine its extent of cure.

Analysis of the chain-extended materials only will be presented within the remaining sections of this chapter. MDI-TMP-PDEGA is considered as representative of the reactive intermediate obtained after step one of each chain-extended reaction. *7.32 NMR Analysis*
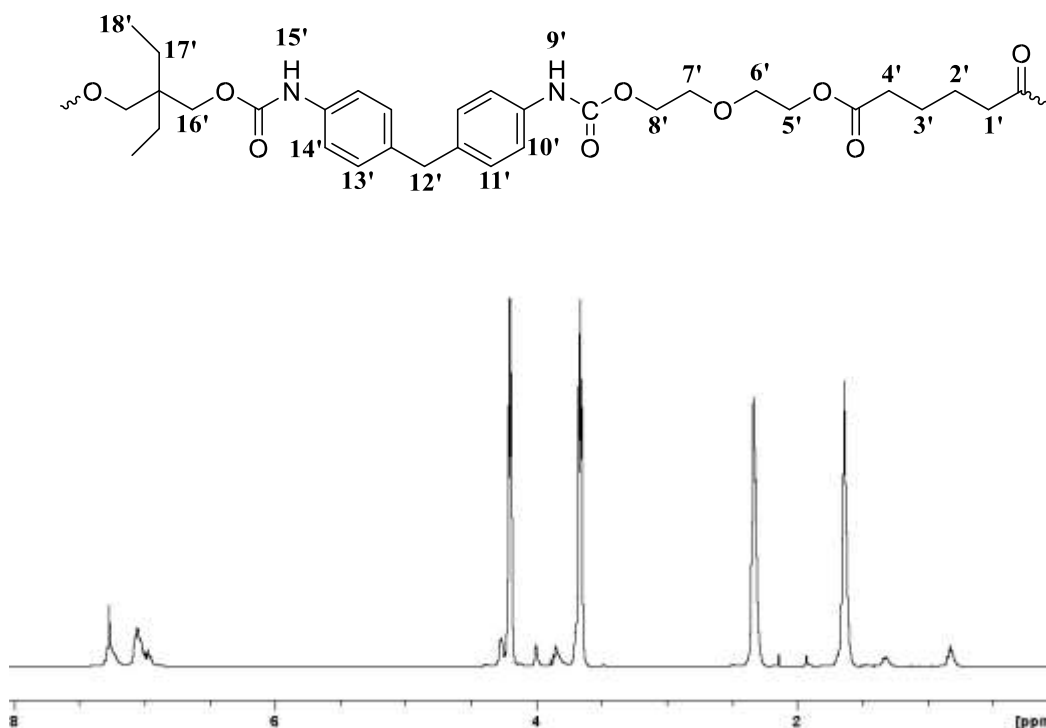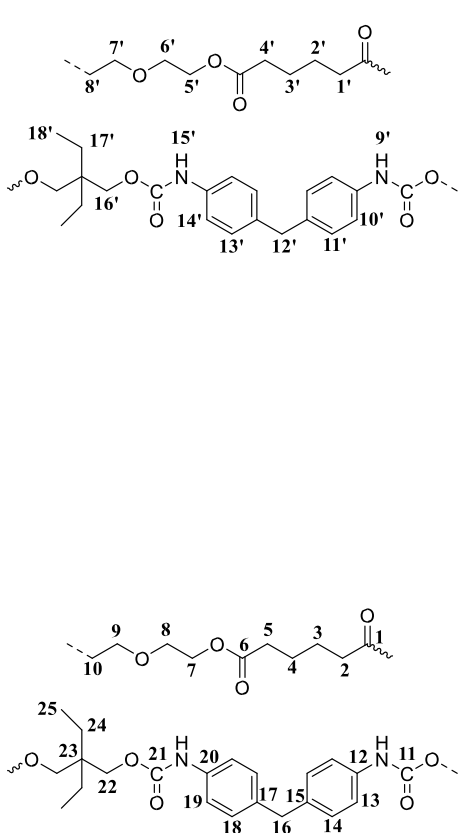
Figure 7.09: **¹H NMR spectrum obtained following reaction of MDI-TMPPDEGA with DEPD.**

Table 7.04: ^{1}H and ^{13}C chemical shift for MDI-TMP-PDEGA-DEPD in CDCl$_3$.

MDI-TMP-PDEGA-DEPD	Position	^{1}H Chemical Shift	Position	^{13}C Chemical Shift
	1'	2.32	1	173.2
	2'	1.63	2	33.7
	3'	1.63	3	24.4
	4'	2.32	4	24.4
	5'	4.20	5	33.7
	6'	3.65	6	173.2
	7'	3.65	7	64.1
	8'	4.24	8	69.4
	9'	7.29	9	69.0
	10'	7.09	10	63.3
	11'	6.99	11	153.5
	12'	3.87	12	135.6
	13'	7.05	13	124.8
	14'	7.07	14	129.9
	15'	7.29	15	128.9
	16'	4.00	16	40.7
	17'	1.90	17	138.9
	18'	0.85	18	131.5
			19	124.2
			20	136.2

		21	153.5
		22	64.1
		23	40.1
		24	23.9
		25	7.2

For full spectral characterisation of peaks from MDI and PDEGA see section 7.22 (or table 7.04) as this section will only detail peaks that show prepolymer formation or peaks from the chain-extender.

The chain-extension step is carried out by reaction of the free isocyanate end groups from two prepolymers with the primary hydroxyl groups of DEPD. Reaction of methylene protons **16'** is shown by the downfield peak shift from 3.39 ppm to 4.00 ppm. Methylene protons **17'** within the ethyl side group are visible at 1.90 ppm and the methyl proton **18'** are visible at 0.85 ppm.
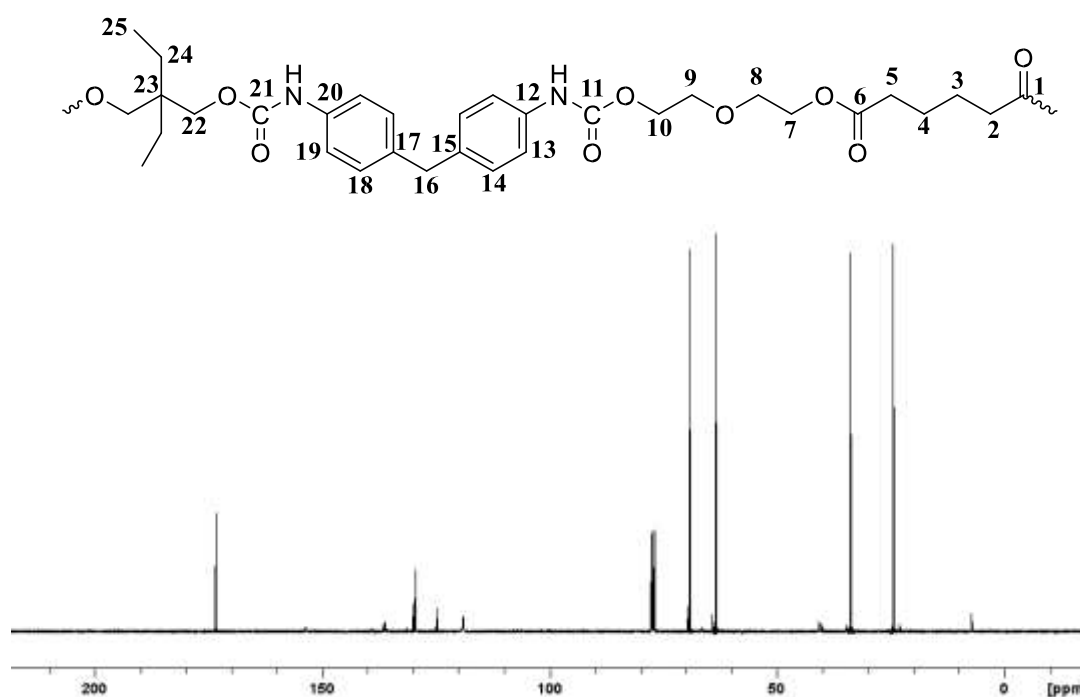
Figure 7.10: ^{13}C NMR spectrum obtained following reaction of MDI-TMPPDEGA with DEPD.

Evidence of the chain-extenders incorporation into the prepolymer molecule was also observed by ^{13}C NMR analysis. Methyl carbons **25** of the ethyl side group are

observed at 7.2 ppm and the methylene carbons **24** of this group are visible at 23.9 ppm. Next the tertiary carbon **21** of DEPD appears at 40.1 ppm and the adjacent methylene group **19** appears at 64.1 ppm. Reaction of the primary end groups of PDEGA is also visible by the position of the adjacent methylene carbons at 69.4 ppm. Also present are the peaks which correspond to the carbonyl from reactive isocyanates still remaining in the formulation at 131 ppm. Finally the carbonyl within urethane linkages appears at 153.5 ppm (this peak represent urethane linkages formed by either PDEGA or DEPD).

^{1}H and ^{13}C NMR analysis of the chain-extended prepolymer of formulation MDITMP-PDEGA-DEPD has been successful, however, molecular weight data is required to gain further structure information.

7.33 MALDI-MS Analysis

To determine the molecular weight increase within the chain-extended prepolymer MALDI-MS was used. The matrix used for analysis was HABA which contained a cationising agent NaTFA (see section 3.23 for more matrix information). A 40 mg ml^{-1} solution of MDI-TMP-PDEGA-DEPD was prepared in THF and mixed with the matrix (1:8 sample:matrix). 1 μl portions of this sample were then spotted and dried for analysis.
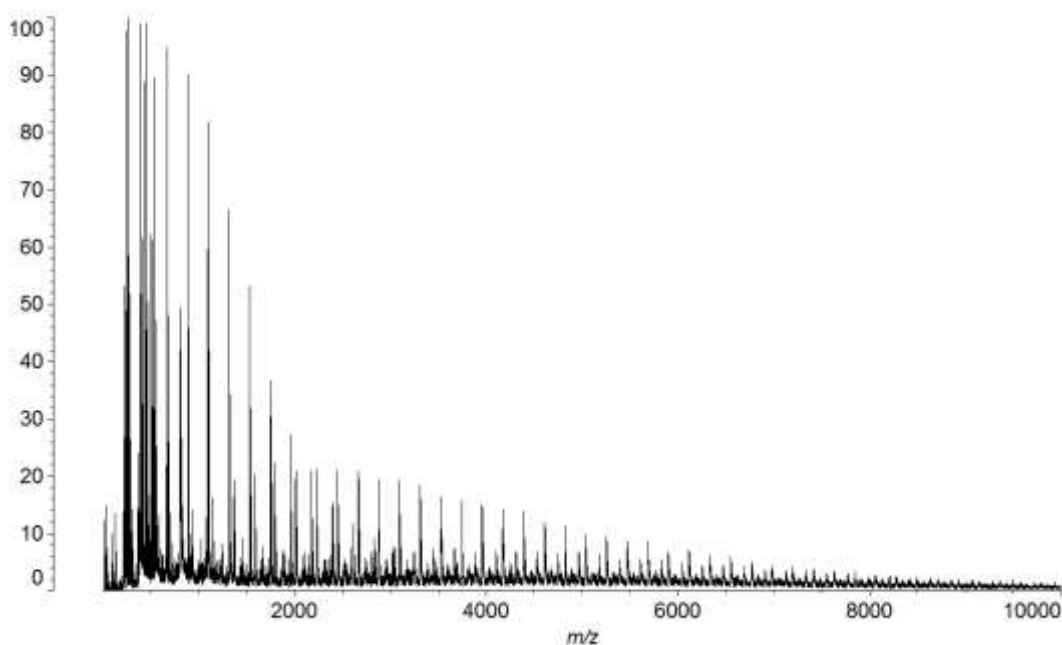
Figure 7.11: MALDI-MS spectrum of MDI-TMP-PDEGA-DEPD chainextended prepolymer collected in HABA/NaTFA.

Present at 1045 m/z is chain-extender TMP that has reacted with three MDI units which are ethanol end-capped (plus one sodium cation). These molecules will contribute to the hard-segment microstructure within the adhesive and their observation was possible as all the starting material was consumed. The observed distribution centred on 2989 m/z corresponds to the PDEGA soft-segment that is isocyanate end-capped MDI-PPG-MDI. The prepolymer within this peak will be composed of 9 adipic acid blocks, 10 diethylene glycol blocks, two ethanol endcapped MDI units and one sodium cation. Prepolymer of this type are formed during step one of the synthetic process and a contribution of this prepolymer would be expected to remain.

Also visible are higher molecular mass polymers which correspond to the chainextended prepolymer molecules. For the previously observed prepolymer (at 2989 m/z), the fully chain-extended prepolymer can be observed at 5995 m/z. Within this polymer there will be four MDI molecules (two of which are ethanol end capped), 18 adipic acid blocks, 20 diethylene glycol blocks, one DEPD molecule and one sodium cation. MALDI-MS has been successful in displaying that it is possible to form chain-extended prepolymer using the mentioned synthetic procedure and it complements the information collected using NMR.

From the spectrum the calculated value of Mn is 4614 m/z and the calculated value of Mw is 5949 m/z giving a PDI of 1.35. Compared to MDI-TMP-PCD, the values of Mn and Mw have increased as would have been anticipated by using a chainextender. Chain-extension with DEPD has reduced the width of the mass distribution with the PDI value nearing that of the starting soft-segment PDEGA.

7.34 DSC and TGA Analysis

Following synthesis of the chain-extended prepolymer, characterisation of the thermal properties was carried out to determine the position of the $T_g$ss and to investigate any other thermal transitions within the formulation. As previously mentioned the $T_g$ss of the material was considered important as it had to be lower than -20°C to be suitable for the intended laminate application.

Within figure 7.12 the DSC thermogram for the DEPD chain-extended prepolymer is presented. Analysis of the thermogram obtained a $T_g$ss of -30°C which covered a range of -35°C to -26°C and this is a shift in the $T_g$ss of +5°C with reference to the base prepolymer (MDI-TMP-PDEGA). This shift in the $T_g$ss would suggest that the polymer has increased in molecular weight and will also have a contribution from the viscosity increase due to the trifunctional TMP prepolymer molecules (observed in MALDI-MS see section 7.33). Also observed was a broad exothermic peak at 170°C (onset 94°C) with an enthalpy of 6.2 J g^{-1} and is a curing peak of the free isocyanate groups. Possible curing reaction will be dimer/trimer formation of the free isocyanate groups or reaction of these free isocyanate groups with the acidic hydrogen in the urethane linkage forming allophonate groups.
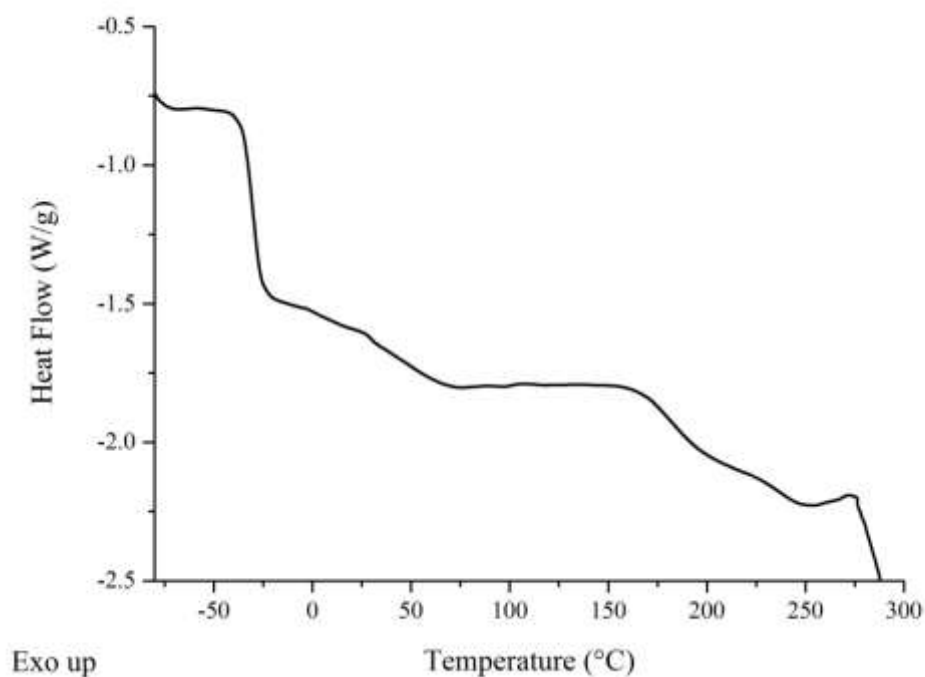
Figure 7.12: **DSC thermogram of MDI-TMP-PDEGA-DEPD prepolymer formulation.**

Following 30 day of curing, a sample of adhesive was removed from the TAc/TAc laminate for DSC analysis. The adhesive was analysed using a cool-heat-cool-reheat experiment to determine the $T_g$ss within each heating cycle as shown in figure 7.13 (same experiment procedure as detail in section 7.24). From the first heating cycle,

the only visible transition is a glass transition which was observed at -31°C and ranged from -37°C to -26°C. After a second heating cycle, the $T_g$ss was recorded at 26°C and covered a range from -33°C to -22°C. Also observed on the second heating cycle was a melting endotherm of the hard-segments within the microstructure at 199°C (onset 197°C) with the enthalpy of melt 0.3 J g^{-1}. From DSC of the fully cured adhesive it was observed that the $T_g$ss is outside the processing window. Also observed was a melting endotherm for the hard-segments within the PU-U microstructure (discussion of the morphology will be presented within chapter 8) which is also out with this window, meaning that hard-segment reinforcement will be operating during manufacture. This will eliminate the potential for ply slippage of the laminate during processing.

TGA was then performed to determine the onset of degradation for the PU-U cured adhesive. The experiment was carried out over the same range as outline in section 2.10 and the data is presented in figure 7.14. From the TGA curve the onset of degradation (temperature at which 5% of the total mass is lost) was 316°C which is 3°C higher than previous formulation where chain-extension was not performed. This would suggest that chain-extension does not have any significant effect on the onset temperature.
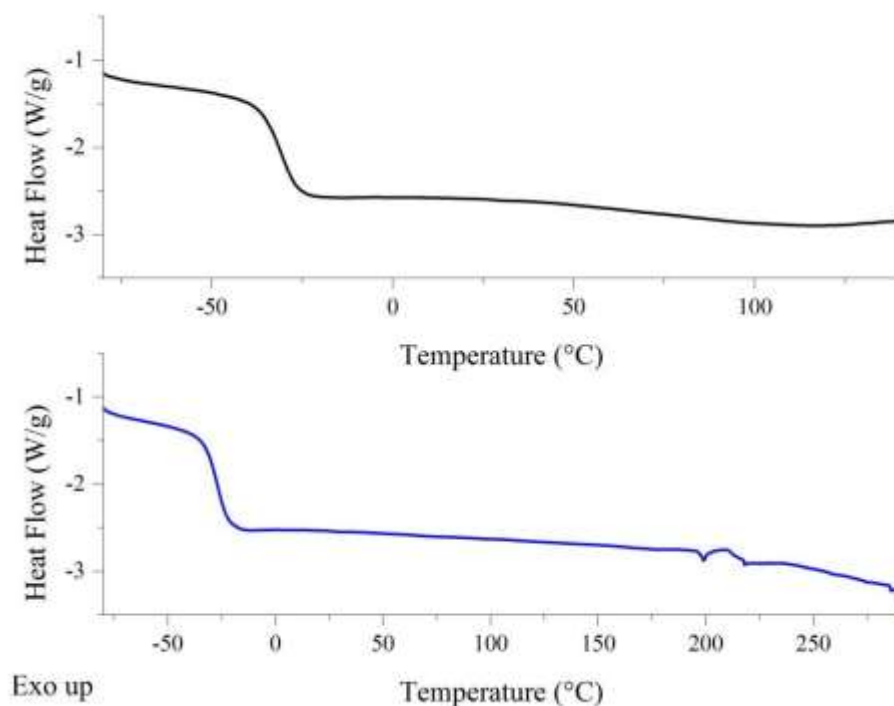
Figure 7.13: DSC thermogram of fully cured MDI-TMP-PDEGA-DEPD adhesive, following removal from TAc/TAc laminate. [First heating cycle *top* in black and second heating cycle *bottom* in blue].

Inspection of the DTG curve however, does show some differences in the degradation behaviour of this PU-U. Degradation occurs in four steps which is different to the previous cured material which displayed only two processes. The main degradation is better viewed on the DTG curve (peak rate at 351°C) and corresponds to the breaking of the hard-segment bonds.[4,5] Subsequent degradation process which occur at 393°C, 419°C and 568°C account for the breaking of the PDEGA soft-segment molecules and more stable cross-linked structures formed during degradation respectively.[2,13]
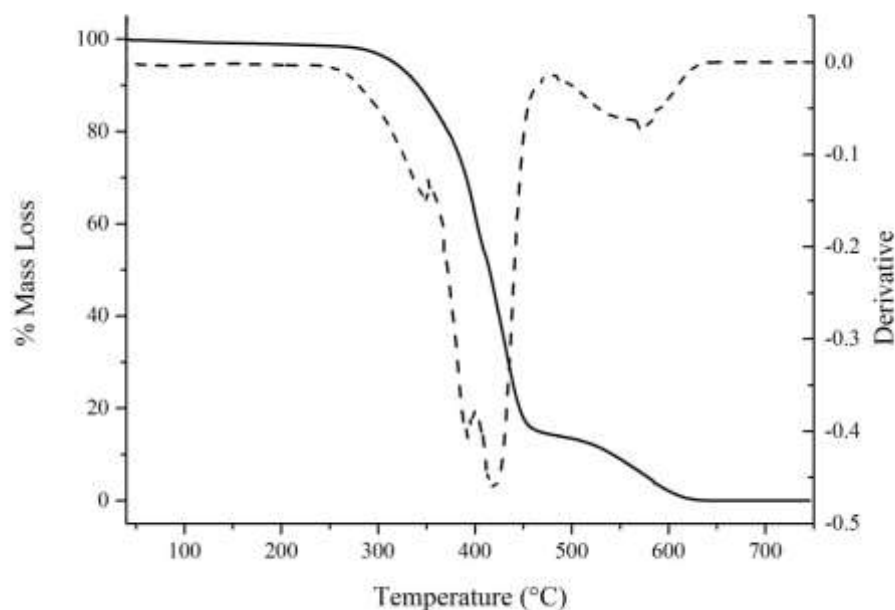
Figure 7.14: TGA and DTG curves of fully cured MDI-TMP-PDEGA-DEPD adhesive. [TGA solid line and DTG dashed line].

7.35 180° T-peel Test and Haze

To quantify the interactions with the ply materials TAc and PC peel testing was again performed. 180° T-peel testing was performed after both 7 and 30 days of cure. The laminates used for this study were TAc/TAc, TAc(t)/TAc(t), TAc(t)/PC, TAc(t)/PC(t), PC(t)/PC(t) and PC/PC. Following 7 days of moisture cure, the observed mode of failure for TAc/TAc was adhesive at the interface with a peel strength of 1.3 N mm^{-1} recorded (equal highest so far). Following 30 days of cure no peel strength value could be collected as the sample was untestable due to a foaming issue within the adhesive layer. As was observed in all previous formulations, TAc/TAc performs extremely poorly and is well outside the 3 N mm^{-1} target peel strength.

Table 7.05: Peel, haze and mode of failure data for MDI-TMP-PDEGA-DEPD cured PU-U adhesive. [The data in bold will be discussed within this section].

Cured Adhesive	Laminate	Peel 1* (N mm^{-1})	Peel 2^x (N mm^{-1})	Failure mode	Haze (%)
MDI-TMPPDEGA	TAc/TAc	0.2	1.3	Adhesive TAc	>1.5%
	TAc(t)/TAc(t)	0.8	ND	Adhesive TAc	

	TAc(t)/PC	0.9	ND	Adhesive TAc	
	TAc(t)/PC(t)	0.8	1.1	Adhesive TAc	
	PC(t)/ PC(t)	6.2	7.6	Adhesive PC	
	PC/PC	4.2	5.6	Adhesive PC	
MDI-TMP-PDEGA-DEPD	**TAc/TAc**	**1.3**	**ND**	**Adhesive TAc**	**>1.5 %**
	TAc(t)/TAc(t)	**0.9**	**ND**	**Adhesive TAc**	
	TAc(t)/PC	**1.1**	**1.4**	**Adhesive TAc**	
	TAc(t)/PC(t)	**1.1**	**1.1**	**Adhesive TAc**	
	PC(t)/ PC(t)	**2.3**	**ND**	**Adhesive PC**	
	PC/PC	**3.6**	**ND**	**Adhesive PC**	
IPDI-TMP-PDEGA	TAc/TAc	0.9	Ply	Cohesive	<0.7%
	TAc(t)/TAc(t)	1.0	Ply	Cohesive	
	TAc(t)/PC	0.8	4.7	Cohesive	
	TAc(t)/PC(t)	0.9	4.7	Cohesive	
	PC(t)/ PC(t)	0.5	9.1	Cohesive	
	PC/PC	0.9	11.5	Cohesive	
IPDI-TMP-PDEGA-DEPD	TAc/TAc	1.4	6.4	Cohesive	<0.7%
	TAc(t)/TAc(t)	1.7	6.0	Cohesive	
	TAc(t)/PC	1.4	6.5	Cohesive	
	TAc(t)/PC(t)	1.1	6.1	Cohesive	
	PC(t)/ PC(t)	0.6	10.3	Cohesive	
	PC/PC	0.7	10.6	Cohesive	

* peel 1 collected within 7 days of room temperature cure, ^x peel 2 collected after 30 days of room temperature cure, ND = No Data

Previous formulations highlighted that saponification of the TAc interface enhanced the peel strength. Data collected using the fully cured adhesive of formulation IPDITMP-PDEGA-DEPD however, is not consistent with previous analysis. Following 7 days of cure, the peel strength recorded was 0.9 N mm^{-1} and no peel could be performed after 30 days of curing. The observed mode of failure was adhesive at

the interface and the peel was very unstable. Data collected from this cured adhesive is not in keeping with previous formulations (see chapter 3,4,5 and 6) but is consistent with the previous formulation within this chapter.

Further investigation of the effect that chain-extension has on the peel strength was now extended to PC laminates. In order to obtain high peel strengths using this formulation adhesion mechanisms such as π-π stacking and H-bonding have to be maximised.[10] The peel strength recorded following 7 days of cure on PC was 3.6 N mm^{-1} and again no data could be collected after 30 days of curing. An adhesive mode of failure at the PC interface was observed and this was coupled with deformation of the PC substrate. This strength value is just above benchmark and it would be expected to remain the same after 30 days of cure.

Treatment of the PC interface was performed and the peel strength measured. After 7 days of cure, the peel strength of the fully treated PC laminate was 2.3 N mm^{-1} again with no value available after 30 days. An adhesive mode of failure at the interface was recorded and was accompanied by slight deformation of the substrate. Following PC surface treatment a slight decrease in the overall peel strength was observed.

Analysis so far in this chapter has identified that the adhesive does not display a great affinity for any one interface (TAc poor). To identify the weakest interface or component of the system hybrid laminates were next tested. Discussed first is the laminate of composition TAc(t)/PC which recorded a peel strength of 1.1 N mm^{-1} following 7 days and 1.4 N mm^{-1} after 30 days of cure. The mode of failure was adhesive at the TAc(t) interface with a slight deformation of the PC substrate. For the fully treated laminate, a 7 day peel strength of 1.1 N mm^{-1} was recorded which increased to 1.1 N mm^{-1} after 30 days. Again the mode of failure was adhesive at the TAc(t) interface with slight deformation of the PC substrate. Both experiments have identified that the TAc(t) substrate is the weakest component of the laminate as evident by the TAc(t) interface failure. It was noted that each hybrid laminate combination performed below the 3 N mm^{-1} benchmark. From the data collect it was observed that no significant increase in strength occurred after 30 days of cure which displays that adhesion has not increased with time for this current formulation.

Finally the overall haze for the fully cured adhesive (across all six laminates) was > 1.5% with the adhesive layer containing a large number of bubbles. The chainextenders effect on the haze could not be measured as the large number of bubbles has influenced the haze reading as they scatter light. To obtain a lower haze the number of bubbles will need to be reduced through increasing the degassing time (high viscosity trapping bubble of air in formulation) or reducing the rate at which urea is formed.

7.36 ATR of Peeled Samples

Characterisation of the bulk material was performed on all six of the laminates after the 30 day peel test. ATR analysis will determine the chemical functionality of the final cured material and allow for any distinct differences in curing chemistry to be observed. ATR will give some indication of the inherent morphology of the fully cured adhesive. Discussed within this section will be peaks that indicate the PU functionality of the chain-extended prepolymer or PU-U peaks obtained after 30 days of moisture cure. For discussion of the peaks inherent of the starting materials see section 7.26 and for all characteristic peaks see table 7.06.

From the spectra presented within figure 7.15 it is visible that there are two different **N-H** vibrations within the cured PU-U. **N-H** stretching vibrations occurring at 3347 cm^{-1} show that H-bonded domains are present in the microstructure whereas, the shoulder peak at around 3500 cm^{-1} correspond to free **N-H** stretching vibrations. Corresponding bending vibrations are visible in the fingerprint region of the spectra for **N-H** at 1533 cm^{-1}, also present within this peak is the **C-N** stretch. **C-N** bending vibrations are also observed for urea at 1386 cm^{-1} and urethane at 1310 cm^{-1}. Again no detectable isocyanate peak was visible between 2260 cm^{-1} – 2280 cm^{-1} which displays that the adhesive is fully cured after 30 days.
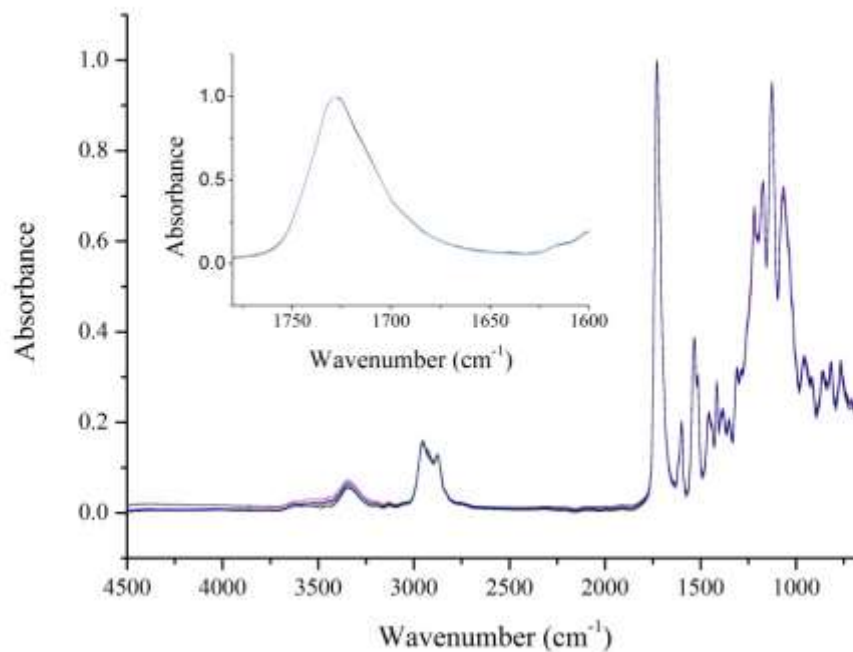
Figure 7.15: ATR spectra of cured MDI-TMP-PDEGA-DEPD sampled in-situ after peel testing with inset expanded carbonyl region. [TAc/TAc in black, TAc(t)/TAc(t) in red, TAc(t)/PC in blue, TAc(t)/PC(t) in pink, PC(t)/PC(t) in green and PC/PC in orange. Data collected for each laminate at nine random positions with each spectrum consisting of 128 scans at 8 cm^{-1} resolution. These were then averaged and plotted as the above spectra].

Further information on the inherent microstructure following cure is available within the carbonyl region. Evidence of H-bonded ester carbonyl stretching is visible at 1727 cm^{-1} which would indicate H-bonding within the soft domains of the microstructure. An immediate shoulder to this peak would be expected which signifies the occurrence of free urea carbonyl stretching (~1700 cm^{-1}) however, as the ester peak of PDEGA dominates the spectrum it was difficult to observe. For this cured adhesive no evidence of any bidentate H-bonded urea stretching vibrations was visible (1660 cm-1 - 1640 cm^{-1}). As there is a tail to the ester peak at the lower wavenumber side, it shows that a proportion of monodentate urea groups are present and these groups have a characteristic vibration range of 1675 cm^{-1} – 1660cm^{-1}. The overall morphology observed from ATR will be discussed in greater detail within chapter 8.

Table 7.06: Characteristic peaks of MDI-TMP-PDEGA-DEPD cured PU-U adhesive from all six laminate combinations.

Wavenumber (cm^{-1})	Vibration	Wavenumber (cm^{-1})	Vibration
3347	N-H stretching H-Bonded	1310	C-N urethane
2949	C-H asymmetric stretch	1216	C-H aliphatic skeleton
2878	C-H symmetric stretch	1173	C-C stretching
1727	C=O stretching ester	1135	Asymmetric N-CO-O
1595	N-H bending urethane	1074	C-H aromatic ring, C-O-C stretch aliphatic ester/ether, symmetric N-CO-O
1533	C-N stretch, N-H bending, C-H aromatic ring	955	C-H aromatic ring, C-O-C stretch aliphatic ester/ether
1514	N-H bending urea	927	C-H aromatic ring
1448	C-H bend aliphatic	856	C-H aromatic ring
1415	C-C stretching aromatic	817	C-H aromatic ring
1348	C-N urea	756	C-C aliphatic skeleton

7.37 Summary of MDI-TMP-PDEGA-DEPD Formulation

Synthesis of the DEPD chain-extended prepolymer was followed using NMR which displayed successful synthesis. MALDI-MS was used to characterise the molecular

mass distributions present within the chain-extended prepolymer formulation. MALDI-MS identified prepolymers from step one as well as higher molecular weight for chain-extended prepolymers. Evidence of the higher molecular weight prepolymer displays that the coupling reaction has been successful. Following chain-extension with DEPD values of Mn and Mw increased compared to MDITMP-PDEGA. The PDI value obtained using DEPD as chain-extender was similar to the PDEGA soft-segment material with values of 1.33 and 1.35 obtained respectively.

Investigation of the thermal transition by DSC recorded a $T_g$ss for the chain-extended prepolymer of -30°C which is an elevation of +11°C compared to MDI-TMPPDEGA. Observed in the prepolymer thermogram was a broad curing peak of the remaining free isocyanate groups. Once fully cured, the $T_g$ss was recorded at -31°C on the first heating cycle and -26°C on the second. Observed on the second heating cycle was melting of the hard-segments within the PU-U which display that region of phase segregation are present (peak at 199°C for a melting enthalpy of 0.3 J g^{-1}). The overall thermal stability was determined by TGA with the onset of degradation occurring at 316°C. From the DTG curve, three main degradation peaks were observed which represent the decomposition of the hard-segments, soft-segments and cross-linked materials formed during degradation.

Using 180° T-peel testing it was identified that untreated TAc performed very poorly (1.3 N mm^{-1}) and following surface treatment no significant improvement in peel strength was recorded (0.9 N mm^{-1}). Untreated PC performance was unexpectedly poor (3.6 N mm^{-1}) but was still above benchmark and after surface treatment the strength value reduced (2.3 N mm^{-1}). From hybrid laminates it was identified that the TAc(t) interface was the weakest component of the system as was evident by the adhesive mode of failure at this substrate interface.

The haze value recorded (from all six laminates) was > 1.5% and the adhesive layer had a large amount of entrapped bubbles. This high value would have been expected from inspection of the adhesive layer prior to testing as the high bubble concentration will promote light scattering. Finally using ATR the adhesive material was observed to be fully cured following 30 days of curing. Also observed was that the fully cured

adhesive was a PU-U and that there were H-bonding domains within the cured network.

7.40 Analysis of IPDI-TMP-PDEGA

7.41 Synthesis Information

Prior to synthesis PDEGA (molecular weight 2500) was dried to remove water by placing within a vacuum oven at 80°C for at least 48 hours. The synthesis was performed using the reaction set-up as detailed in section 2.03, with the reaction being performed in the temperature window of 85°C – 95°C for seven hours. The reaction time was started after the last addition of IPDI to the soft-segment containing reaction vessel. IPDI was degassed within a three necked round bottom flask before being put under a nitrogen atmosphere. To ensure that the exothermic reaction did not exceeded 95°C, IPDI was added drop wise in 1 ml portions. The final prepolymer obtained was clear but with a slight visually increase in viscosity compared to the starting mixture (consequence of the molecular weight increase).

Prior to catalyst addition samples of the reaction were taken for NMR, MALDI-MS and DSC analysis. After the elapsed reaction time of seven hours 0.05 wt% of dibutyltin dilaurate and 0.05 wt% of triethylamine were added as curing catalysts (calculated from total batch weight). Following catalyst addition, the formulation was transferred to an aluminium holding tube and placed within a vacuum desiccator, which was kept at 0°C until lamination (typically not exceeding 7 days). Degassing was performed for six hours once a vacuum of one atmosphere was obtained.

The prepolymer adhesive was applied to six different laminates that were of interest:

- TAc/TAc
- TAc(t)/TAc(t)
- TAc(t)/PC
- TAc(t)/PC(t)
- PC(t)/PC(t)
- PC/PC

Where TAc is cellulose triacetate, PC is bisphenol-A polycarbonate and (t) denotes that the surface of the polymer film has been treated (see section 2.01 and2.02). IPDI-TMP-PDEGA was applied at 95°C to ensure good surface coverage. The lamination process was carried out as detailed in section 2.04, followed by cure at room temperature. 180° T-peel testing was carried out initially after 7 days and then after 30 days to determine the peel strength of each laminate. The mode of failure was monitored by visual inspection. The cured laminates from the 30 day peel testing were used in the ATR analysis of the fully cured adhesive.

7.42 NMR Analysis

Investigation of the urethane reaction between IPDI and PDEGA was carried out using both ^{1}H and ^{13}C NMR. A mixture of both primary and secondary free isocyanate groups is expected within the prepolymer based on the synthesis procedure plus previous analysis. Both end groups of the PDEGA soft-segment are primary as determined by previous analysis which displayed diethylene glycol at the terminus with hydroxyl end groups at 5.4 ppm.

Figure 7.16 displays the ^{1}H spectrum for the isocyanate end capped prepolymer (IPDI-TMP-PDEGA) synthesised as the base adhesive for lamination. The reaction conditions were un-catalysed between 85°C - 95°C which results in a mixture of both primary and secondary free isocyanate groups being present as the end groups.[14] Table 7.07 displays all the chemical shifts of the prepolymer molecules in deuterated chloroform for both nuclei.

The ^{1}H spectrum is dominated by the peaks from the PDEGA soft-segment which is 2500 molecular weight. Peaks inherent of the adipic acid blocks in the soft-segment are visible at 2.24 ppm for methylene protons **1'** plus **4'** and 1.61 ppm for methylene protons **2'** plus **3'**. Further backbone methylene protons from the diethylene glycol blocks are present at 4.10 ppm (**5'**) and 3.57 ppm (**6'** plus **7'**). The signals inherent of the end groups from the soft-segment can be seen at 4.26 ppm (a downfield shift from 3.70 ppm) which corresponds to the adjacent methylene protons.
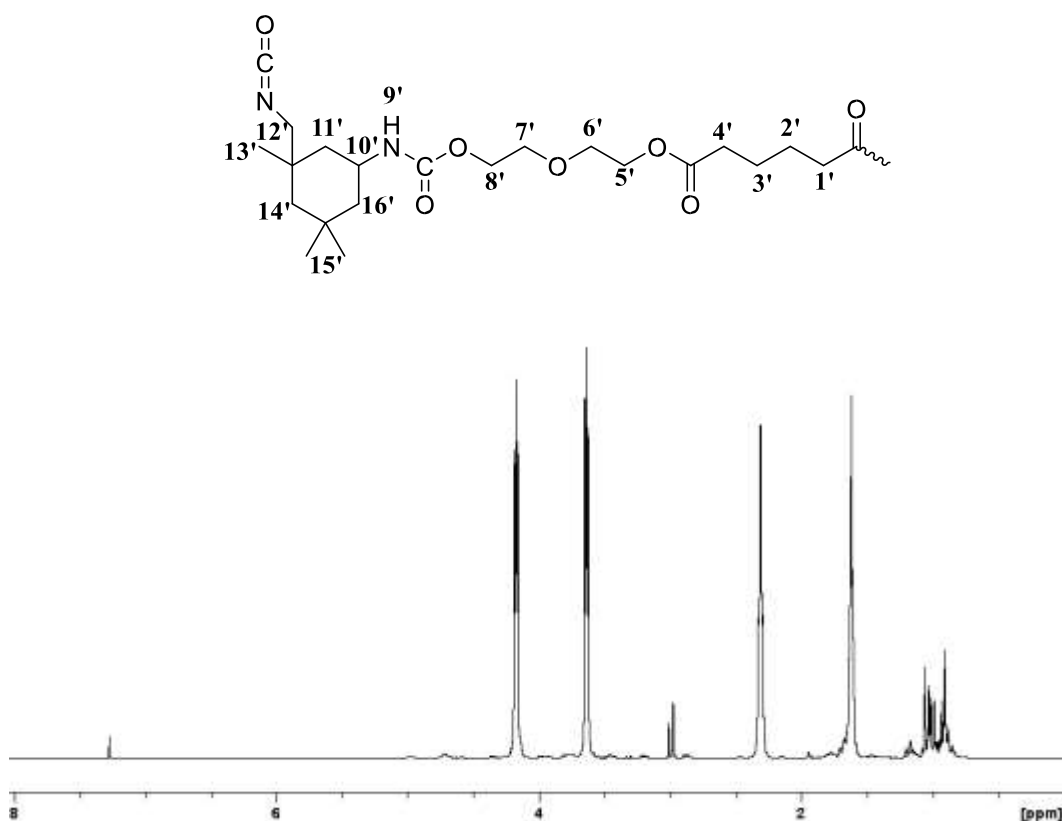
Figure 7.16: ¹H NMR spectrum of IPDI-TMP-PDEGA polyurethane prepolymer in deuterated chloroform.

Evidence that primary isocyanate groups are retained within the prepolymer formulation can be observed by the position of the methylene protons **12'** at 2.94 ppm. Also visible is the consumption of a proportion of these primary isocyanate groups in the formation of urethane linkages, which is shown by the upfield shift of these methylene protons to 2.70 ppm. This is also visible for the secondary isocyanate groups with the unreacted isocyanate shown by the adjacent methine protons at 3.19 ppm. Urethane linkages which contain secondary isocyanate groups are shown by the position of adjacent methine protons **10'** which have shifted downfield to 3.38 ppm. For full assignment of peaks inherent of IPDI hard block see table 7.07.

¹³C NMR was next used to further investigate the prepolymer and confirm what was observed in ¹H NMR. Peaks inherent of the PDEGA soft-segment are observed by the carbonyl peaks (**1** and **6**) of the ester groups at 173.1 ppm. Other peaks within the adipic acid block are visible at 24.5 ppm (**3** + **4**) and 33.6 ppm (**2** + **5**).

Methylene protons from the diethylene glycol blocks are visible at 64.0 ppm (**7**) and 69.0 ppm (**8** + **9**). Reaction of the diethylene glycol end group results in a downfield shift of the adjacent methylene group from 61.3 ppm to 63.3 ppm (**10**).

Table 7.07: ^{1}H and ^{13}C chemical shift for IPDI-TMP-PDEGA collected in CDCl$_3$.

IPDI-TMP-PDEGA	Position	^{1}H Chemical Shift (ppm)	Position	^{13}C Chemical Shift (ppm)
	1'	2.24	1	173.1
	2'	1.61	2	33.6
	3'	1.61	3	24.52
	4'	2.24	4	24.5
	5'	4.10	5	33.6
	6'	3.57	6	173.1
	7'	3.57	7	64
	8'	4.26	8	69.3
	9'	NDT	9	69
	10'	3.38	10	63.3
	11'	1.68/1.41	11	156.7$_p$/155.5$_s$
	12'	2.94/2.21	12	42.2
	13'	0.94	13	43.3
	14'	1.37/1.05	14	56.7
	15'	0.86	15	123$_p$/122$_s$
	16'	1.48/1.41	16	24.3
			17	20.5
			18	48.6
			19	23.1
			20	31.7
			21	48.1

$_p$ = primary, $_s$ = secondary, NDT = not detected
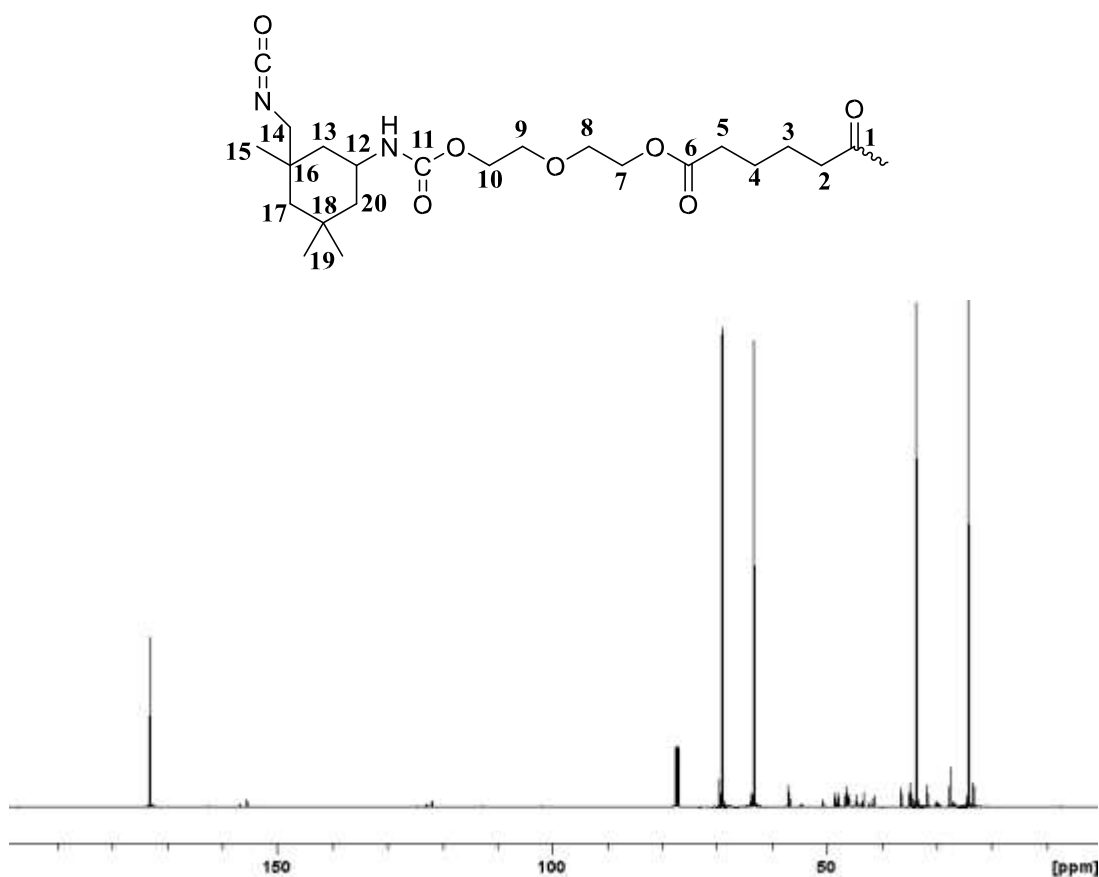
Figure 7.17: ¹³C NMR spectrum of IPDI-TMP-PDEGA prepolymer in deuterated chloroform.

Complementary to what was observed for ^{1}H NMR evidence of both free isocyanate groups and urethane linkages are also visible in ^{13}C NMR. Free primary isocyanate groups were observed at 123 ppm with secondary isocyanates shown at 122 ppm. Evidence that both groups are contained within urethane linkages is shown by two carbon signals at 155 ppm and 156.2 ppm for secondary and primary groups respectively. All carbon peaks inherent of IPDI are presented within table 7.07.

7.43 MALDI-MS Analysis

For a further insight into the structure of the prepolymer molecules matrix assisted MALDI-MS analysis was used. The molecular mass of both the starting softsegment and the synthesised prepolymer were measured. The matrix used was HABA which was prepared as a 20 mg ml^{-1} solution in tetrahydrofuran (THF), this was then mixed with a 1 mg ml^{-1} solution of NaTFA in a 7:1 ratio respectively. IPDI-TMP-PDEGA was prepared as a 40 mg ml^{-1} solution in THF which was then mixed with the matrix

in a 1:8 ratio of sample to matrix. 1 μl aliquots of the solution were then spotted and dried before analysis.
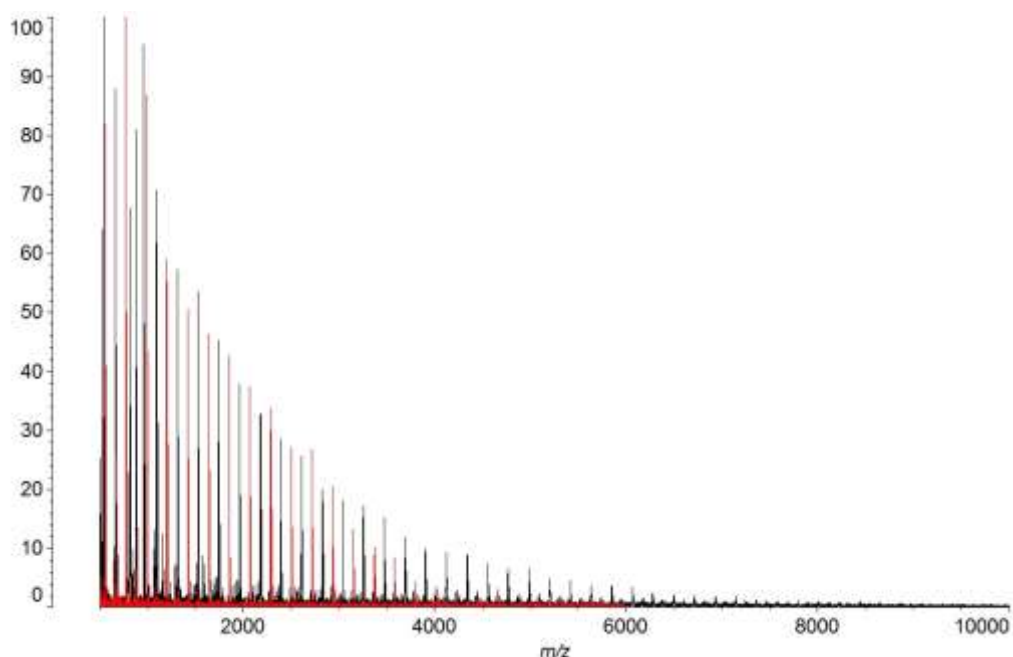
Figure 7.18: MALDI-MS spectra of PDEGA starting material in red and the prepolymer IPDI-TMP-PDEGA in black. Both were mixed with the matrix material of HABA and NaTFA in a 1:8 sample:matrix mixture.

Present within the spectrum is chain-extender TMP that has reacted with three IPDI units which are all ethanol end capped as can be observed at 961 m/z (plus a sodium cation). These molecules will contribute to the hard-segment microstructure within the adhesive and interfere with the packing arrangement within this domain. The mass spectrum of PDEGA in figure 7.18 displays the sodiated adduct of the softsegment with the sodium coming from the small amount of a cationising (NaTFA) agent added to enhance spectral collection. The molecular weight distribution for PDEGA has a peak mass of 2397 m/z which is 9 adipic block and 10 diethylene glycol blocks plus one sodium ion. For the prepolymer material an observed shift of the distribution by 536 m/z was observed which correspond to the addition of two IPDI units that have had their free isocyanate groups end capped with ethanol to maintain the molecular weight. This peak centred at 2933 m/z contains the two ethanol end capped IPDI units, one sodium ion, 9 adipic blocks and 10 diethylene glycol blocks.

From this spectrum it is clear that using a 2.2:1.0 excess of isocyanate to polyol makes it possible to obtain an IPDI-PDEGA-IPDI end capped prepolymer PUs. MALDI-MS has allowed for characterisation of the structure of the molecules present in conjunction with the previous NMR analysis.

From the spectrum it is possible to calculate Mn, Mw and PDI. For the soft-segment PDEGA, the calculated value of Mn is 1443 m/z and the calculated value of Mw is 1923 m/z giving a PDI of 1.33. It is noted that the value of Mn obtained using MALDI-MS is lower that the valued quoted by the supplier (Mn ~2500) and that the starting mass distribution is rather broad. Following prepolymer synthesis with IPDI, the calculated value of Mn is 2854 m/z and the calculated value of Mw is 3859 m/z giving a PDI of 1.35. Following synthesis both values of Mn and Mw have increased as would be expected. The effect to the mass distribution is minimal as only a small increase in PDI is observed.

7.44 DSC and TGA Analysis

Recording the $T_g$ss of the prepolymer material will determine if the formulation is performing out with the identified processing window. Also the position of the $T_g$ss compared to the unreacted soft-segment will give an indication about the morphology e.g. changes in molecular weight, cross-linking within the matrix and the compatibility of the two segments.

The DSC experiment was recorded within an inert nitrogen atmosphere from -90°C to 300°C at a ramp rate of 10°C min^{-1}. For the prepolymer IPDI-TMP-PDEGA the recorded $T_g$ss is -43°C which covered a narrow range of -46°C to -42°C. As a molecular weight increase has occurred from the end capping of both the PDEGA (plus trifunctional TMP molecules). The viscosity of the system will have increased and this will contribute towards the elevated $T_g$ss. Also a large exothermic peak was observed at 184°C with an enthalpy of 17 J g^{-1}. This peak is believed to be moisture free curing of the free isocyanate groups. As the isocyanate is IPDI this will most likely be cured through trimerisation and allophonate formation, however, further investigation will be required to determine the mode of cure.[15]

Recording the $T_g$ss following 30 days of moisture cure at room temperature is much more informative as it indicates the final properties of the cured adhesive. The cured adhesive was removed from a pre-made test laminate consisting of two TAc plies and put through a cool-heat-cool-reheat experiment. The first heating cycle was recorded from -80°C to 140°C at 10°C min^{-1} and was used to remove any thermal history from the soft-segment of the sample. The second heating cycle was recorded form -80°C to 300°C to investigate what information on hard and soft domains was available.
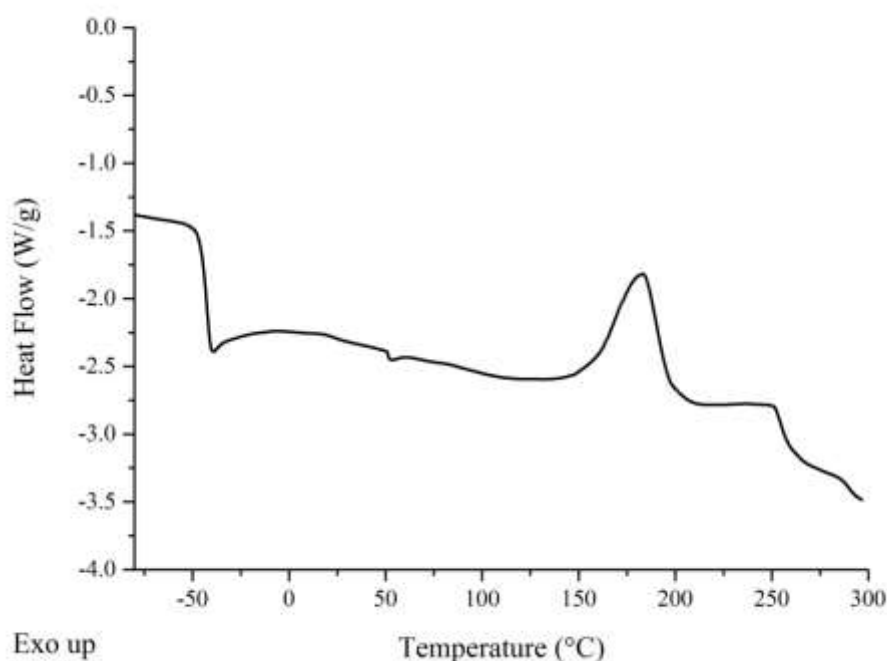
Figure 7.19: DSC thermogram of catalyst free IPDI-TMP-PDEGA prepolymer sampled directly after synthesis.

In the first heating cycle only a single thermal transition was visible in the form of a glass transition. A $T_g$ss of -40°C was recorded which covered a narrow range from 42°C to -36°C. In the second cycle, two thermal transitions were observed in the form of a glass transition and melting endotherm. The $T_g$ss on the second heating scan was -38°C and it covered a narrow range from -42°C to -36°C. A second weak transition was observed with an onset of 162°C and peaked at 198°C. This small peak has a melting enthalpy of 1.8 J g^{-1} and corresponds to the thermal decomposition of H-bonds

within the hard-segments of the adhesives microstructure (urethane and urea groups).[16-18]

Characterisation of the overall thermal stability of the fully cured adhesive was carried out using TGA. To ensure that the degradation of the adhesive was consistent the experiment was performed under nitrogen from 40°C to 750°C at 10°C min^{-1}. From inspection of figure 7.21 it is evident that degradation occurs in four steps which can be observed from TGA and DTG curves. It is widely accepted that the degradation profile of polyurethanes is complex due to the difference in thermal stabilities of the hard and soft-segments within the PU-Us microstructure.[16,19]
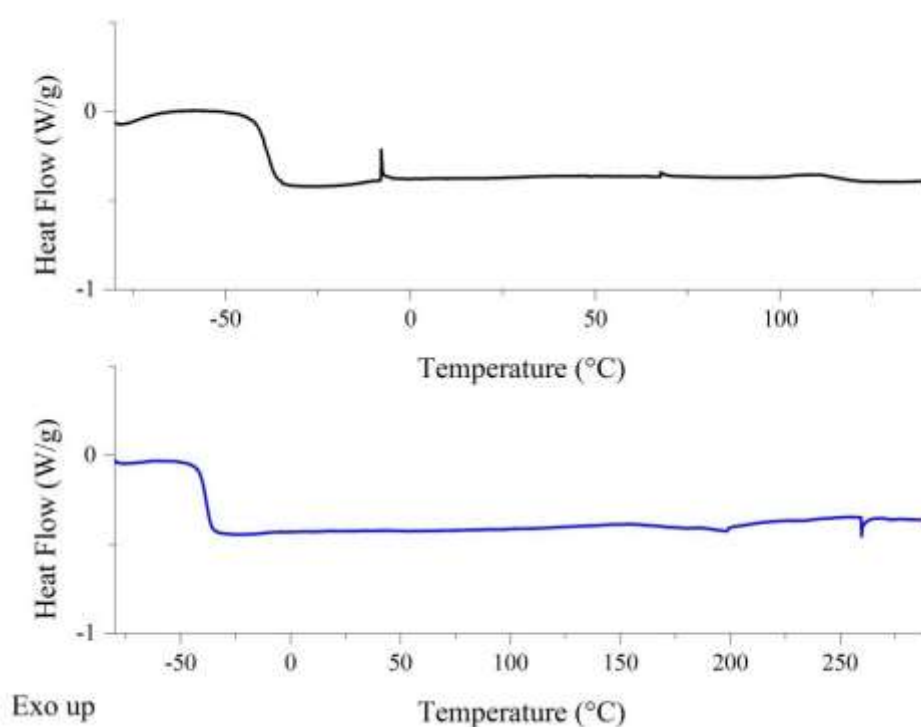
Figure 7.20: DSC thermogram of fully cured IPDI-TMP-PDEGA adhesive, following removal from TAc/TAc laminate. [First heating cycle *top* in black and second heating cycle *bottom* in blue].

The dominant degradation process (shown in figure 7.21) has an onset of 293°C, with the peak rate occurring at 329°C. Degradation through depolymerisation within the hard-segment will occur first as these bonds are thermally the weakest within the microstructure.[20,21] Degradation of the hard-segment occurs from the thermal

breakdown of either urethane or urea bonds. Also contained within this broad peak will be the thermal break down of the soft-segment ester groups.[16]

The peaks which correspond to the decomposition of the soft-segment are visible in the DTG curve at 401°C and 426°C. Another much smaller degradation peak at 543°C is also visible which corresponds to the breakdown of cross-linked products formed by reactive intermediates during degradation.[20] For the intended application the onset of thermal degradation is well out with the temperature range that the laminate will experience during manufacture or use.
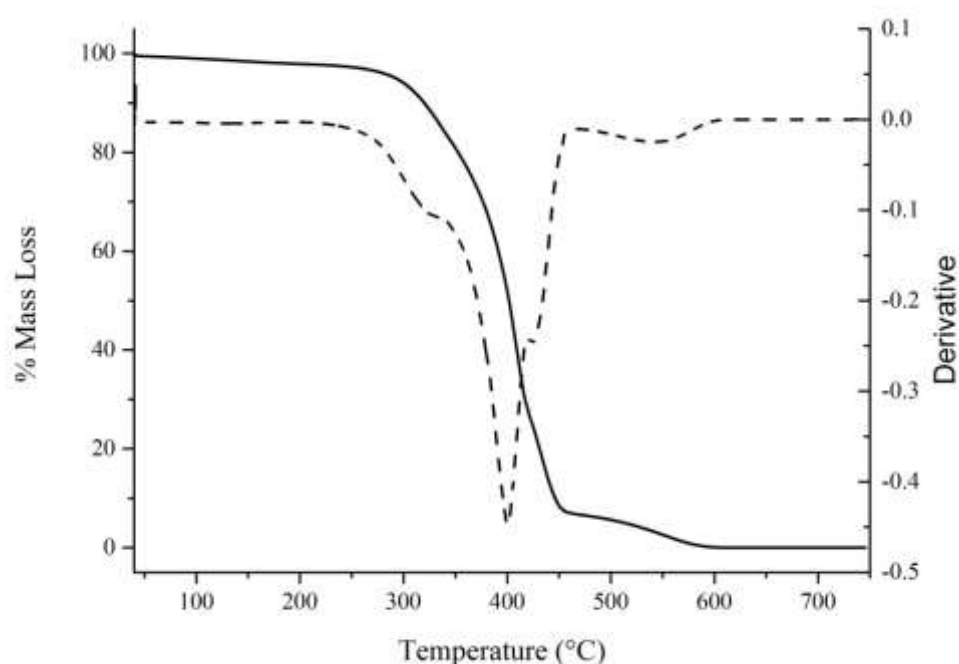
Figure 7.21: TGA and DTG curves of fully cured IPDI-TMP-PDEGA adhesive. [TGA solid line and DTG dashed line].

7.45 180° T-peel Test and Haze

To quantify the interactions with the ply materials TAc and PC peel testing was again performed. The laminates used for this study were TAc/TAc, TAc(t)/TAc(t), TAc(t)/PC, TAc(t)/PC(t), PC(t)/PC(t) and PC/PC. A laminate combination that was becoming of major interest was TAc/TAc due the consistent poor performance with all previous adhesives. The inherent poor strengths obtained displayed that the untreated surface had a very poor compatibility with previous adhesives.

Results collected for the current formulation (as displayed in table 7.08) which has an adipate based soft-segment has had a significant impact on the peel strength. Following 7 days of cure the peel strength obtain for TAc/TAc was 0.9 N mm^{-1} however, following 30 days of cure the TAc substrate cohesively failed before any value could be collected. A cohesive mode of failure within the adhesive was observed following 7 days of cure and this changed to a cohesive TAc substrate failure following 30 days. As the TAc substrate failed after 30 days of curing this would be considered as having an above benchmark peel strength.

Saponification of the TAc surface was next performed (see section 2.01) as this would present a more active regenerated cellulose surface and as displayed by previous testing this increases the compatibility at the adhesive - substrate interface. Deacetylation will leave hydroxyl groups at the surface which can react with the free isocyanate of the adhesive forming covalent bonds. Thus forming anchor points between the adhesive and substrate creating a strong interface. After 7 days of cure the peel strength recorded was 1.0 N mm^{-1} with a cohesive failure in the adhesive was the observed mode of failure. Following 30 days of curing, all samples displayed a cohesive substrate failure of the TAc ply. As the TAc substrate failed after 30 days of curing this would be considered as pass and > 3 N mm^{-1} in peel strength.

Previous testing has shown that PC laminates consistently perform above benchmark following 30 days of cure (when there are no issues with curing or application). Untreated PC displayed a cohesive mode of failure within the adhesive layer which was coupled with deformation of the PC substrate. Following 7 days of cure the peel strength recorded was 0.9 N mm^{-1} and this increased to 11.5 N mm^{-1} after 30 days of curing. It would appear from the data collected, that the current formulation (based on IPDI and PDEGA) has an affinity for both TAc and PC.

Next surface treated PC(t) was tested to determine the effect of the surface treatment on peel strength. Treatment of the PC surface was performed using ethanolamine in an isopropyl alcohol solution (see section 2.02 for procedure) to further improve the surface compatibility with the reactive adhesive.

Table 7.08: Peel, haze and mode of failure data for IPDI-TMP-PDEGA cured PU-U adhesive. [The data in bold will be discussed within this section].

Cured Adhesive	Laminate	Peel 1* (N mm^{-1})	Peel 2^x (N mm^{-1})	Failure mode	Haze (%)
MDI-TMPPDEGA	TAc/TAc	0.2	1.3	Adhesive TAc	>1.5%
	TAc(t)/TAc(t)	0.8	ND	Adhesive TAc	
	TAc(t)/PC	0.9	ND	Adhesive TAc	
	TAc(t)/PC(t)	0.8	1.1	Adhesive TAc	
	PC(t)/ PC(t)	6.2	7.6	Adhesive PC	
	PC/PC	4.2	5.6	Adhesive PC	
MDI-TMP-PDEGA-DEPD	TAc/TAc	1.3	ND	Adhesive TAc	>1.5%
	TAc(t)/TAc(t)	0.9	ND	Adhesive TAc	
	TAc(t)/PC	1.1	1.4	Adhesive TAc	
	TAc(t)/PC(t)	1.1	1.1	Adhesive TAc	
	PC(t)/ PC(t)	2.3	ND	Adhesive PC	
	PC/PC	3.6	ND	Adhesive PC	
IPDI-TMP-PDEGA	**TAc/TAc**	**0.9**	**Ply**	**Cohesive**	**<0.7%**
	TAc(t)/TAc(t)	**1.0**	**Ply**	**Cohesive**	
	TAc(t)/PC	**0.8**	**4.7**	**Cohesive**	
	TAc(t)/PC(t)	**0.9**	**4.7**	**Cohesive**	
	PC(t)/ PC(t)	**0.5**	**9.1**	**Cohesive**	
	PC/PC	**0.9**	**11.5**	**Cohesive**	
IPDI-TMP-PDEGA-DEPD	TAc/TAc	1.4	6.4	Cohesive	<0.7%
	TAc(t)/TAc(t)	1.7	6.0	Cohesive	
	TAc(t)/PC	1.4	6.5	Cohesive	
	TAc(t)/PC(t)	1.1	6.1	Cohesive	
	PC(t)/ PC(t)	0.6	10.3	Cohesive	
	PC/PC	0.7	10.6	Cohesive	

The proposed mechanism for the surface treatment of the PC is nucleophilic attack of the carbonate linkage by the amine of ethanolamine to leave a phenol and a hydroxyl terminated urethane, although the precise mechanism is not known at this time.[11] If the proposed mechanism is correct then the surface treatment should leave OH functional groups at the surface that are available for covalent bonding with the free isocyanate groups. Data collected after 7 days recorded the peel strength of 0.5 N mm^{-1} which greatly increased to 9.5 N mm^{-1} after 30 days of cure. Each sample displayed a cohesive mode of failure within the adhesive layer which was also paired with strong substrate deformation. Surface treatment of PC substrates appears to have no significant effect on the peel strength (reduced by 2 N mm^{-1}). All PC based laminate after 30 days of curing were well above the 3 N mm^{-1} benchmark.

Finally to determine which substrate was most compatible with the current formulation hybrid laminates were tested. First tested was TAc(t)/PC which displayed a cohesive mode of failure within the adhesive layer at both testing times. After 7 days of curing the peel strength was 0.8 N mm^{-1} and this increased following 30 days of cure to 4.7 N mm^{-1}. Next the fully treated hybrid was tested (TAc(t)/PC(t)) and it also displayed a cohesive mode of within the adhesive layer. After 7 days of cure the peel strength recorded was 0.9 N mm^{-1} and following 30 days of cure the strength greatly improved to 4.7 N mm^{-1}. These two laminate combinations display the affinity of the adhesive is not selective to one interface and that the adhesive layer is the weakest component within the system for every laminate.

Once fully cured, the adhesive displayed good clarity as the average haze for the six laminate materials was < 0.7%. The low haze value was attributed to the lack of crystallisation within the PDEGA soft-segment which results in the adhesive becoming a clear colourless layer.

7.46 ATR of Peeled Samples

Due to the varying peel strengths obtained it was essential to characterise if (a) the adhesive after 30 days was fully cured and (b) if once cured was the bulk adhesive the

same final material. To investigate the bulk material ATR was used as it is a non-destructive way to sample the adhesive. ATR was carried out on the six different laminates once they had been peel tested after 30 days of curing. The purpose of this analysis was to characterise the bulk material following 30 days of cure and also to identify if there was any residual free isocyanate following this period of cure.
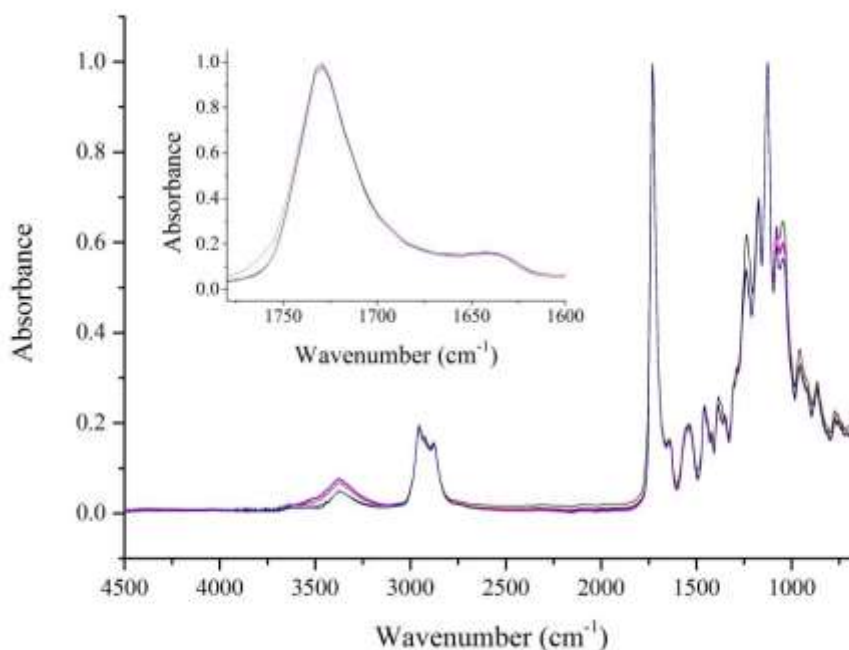
Figure 7.22: ATR spectra of cured IPDI-TMP-PDEGA sampled in-situ after peel testing with inset expanded carbonyl region. [TAc/TAc in black, TAc(t)/TAc(t) in red, TAc(t)/PC in blue, TAc(t)/PC(t) in pink, PC(t)/PC(t) in green and PC/PC in orange. Data collected for each laminate at nine random positions with each spectrum consisting of 128 scans at 8 cm^{-1} resolution. These were then averaged and plotted as the above spectra].

The spectra collected from the in-situ characterisation of the cured adhesive are shown within figure 7.22 for all six laminates. All characteristic peaks for the fully cured PU-U are shown within table 7.09. Observation of the band positioned at 3370 cm^{-1} displays that H-bonding between **N-H** groups within the network is occurring. Also evident is **N-H** stretching vibrations that are not involved within the H-bonded network as shown by the shoulder to the previous at 3500 cm^{-1}. Next aliphatic **C-H** stretching

vibrations from PDEGA are present for both the asymmetric and symmetric bands at 2954 cm^{-1} and 2873 cm^{-1} respectively. No detectable isocyanate peak was visible between 2260 cm^{-1} – 2280 cm^{-1} which displays that the adhesive is fully cured after 30 days.

The carbonyl region of the spectrum was investigated to determine if any further morphological information on the adhesive can be observed. The position of the carbonyl peak will show the order/disorder of the domains in which the carbonyl group resides and it will also indicate the type of functional group. From the position of the carbonyl at 1727 cm^{-1} it displays that ester groups are part of ordered domains as it confirms H-bonding (will be discussed within chapter 8). It would be expected that H-bonds within hard-segment will occur for urethane carbonyl groups but they are not visible due to the large intensity of the H-bonded ester carbonyl peak.[21,22]

Also within the carbonyl region there appears to be three different kinds of urea formed during the moisture cure of the free isocyanate groups (see inset expanded carbonyl region in figure 7.22). First encountered is a shoulder peak at 1696 cm^{-1} for carbonyl groups of free or unordered urea.[22] Evidence of monodentate H-bonded urea within the cured adhesive is visible by the broad shoulder attached to the previous peak between 1675 cm^{-1} – 1660 cm^{-1}.[21] Fully ordered bidentate urea groups are observed by the carbonyl peak at 1647 cm^{-1}. From the urea region it is clear that there are regions of high order, low order and regions of disordered. The ordered regions will contribute to the strength of the cured matrix through the formation of cross-links, whereas the disordered region will increase the phase mixing of the cured adhesive and clarity.

Further bands which display urethane and urea formation are evident within the spectrum. At 1542 cm^{-1} both **C-N** stretching and **N-H** stretching vibrations can be observed from either urethane or urea. Aliphatic **C-H** bending vibrations inherent of both the hard and soft-segments within the PU-U microstructure are visible at 1466 cm^{-1}. Asymmetric and symmetric **C-H** deformations from the PDEGA soft-segment are visible at 1423 cm^{-1} and 1381 cm^{-1}. Evidence of urea within the finger print region is shown by the **C-N** stretching vibration at 1357 cm^{-1} with the urethane vibration also shown at 1287 cm^{-1}. Further urethane vibrations within the microstructure are visible

from the asymmetric and symmetric **N-CO-O** stretching as shown at 1164 cm^{-1} and 1041 cm^{-1} respectively. Aliphatic ester **C-O-C** stretching vibrations of the PDEGA soft-segment are present at 1074 cm^{-1} and 955 cm^{-1}. The final absorption peaks within the spectrum are **C-C** skeleton rocking vibrations at 874 cm^{-1} and 771 cm^{-1}.

Table 7.09: Characteristic peaks of IPDI-TMP-PDEGA cured PU-U adhesive from all six laminate combinations.

Wavenumber (cm^{-1})	Vibration	Wavenumber (cm^{-1})	Vibration
3370	N-H stretching H-Bonded	1381	C-H symmetric deformation
2954	C-H asymmetric stretch	1357	C-N Urea
2873	C-H symmetric stretch	1287	C-N Urethane
1727	C=O stretching ester	1164	Symmetric N-CO-O
1647	C=O stretch Urea Bidentate Hbonded	1074	C-O-C stretch aliphatic ester
1696	C=O free Urea stretch	1041	Symmetric N-CO-O
1542	C-N stretch, N-H bend	955	C-O-C stretch aliphatic ester
1466	C-H bend aliphatic	874	C-C skeleton vibration
1423	C-H asymmetric deformation	771	C-C aliphatic skeleton

ATR analysis has displayed that following 30 of days of moisture cure (at room temperature) that the adhesive is fully cured. In keeping with previous analysis the fully cured adhesive was shown to be a PU-U with urethane formed during synthesis and the urea formed during subsequent moisture cure. As the material is fully cured it

confirms that the mode of failure recorded during 180° T-peel testing is a result of it being the weakest part of the laminate.

7.47 Summary of IPDI-TMP-PDEGA Formulation

From the above analysis it can be confirmed from both ^{1}H and ^{13}C NMR that the end capped PU prepolymer was successfully synthesised. This was further confirmed by MALDI-MS analysis which also highlighted that the expected prepolymer IPDIPDEGA-MDI structure was obtained. End capping of the PDEGA soft-segment was confirmed by the 536 m/z shift with reference to the starting material. Synthesis with IPDI shifts Mn plus, Mw to higher masses and slightly increases the PDI of the sample.

Thermal analysis performed using DSC which displayed that the prepolymer material had a $T_g$ss of -43°C and covered a narrow range (-46°C to -42°C). This was accompanied by a curing peak of the free isocyanate at 184°C. Following cure, the $T_g$ss of the cured adhesive shifted to -40°C for the first heating cycle and within this cycle no other clear thermal features were observed. On the second heating cycle, the $T_g$ss recorded was -38°C and this was accompanied by a small melting endotherm which occurred at 198°C (enthalpy 1.8 J g^{-1}). Breaking of H-bonds within hard-segments of the microstructure are displayed by this high temperature melt, however, the small enthalpy value would suggest that these domains are not highly organised. The increase in $T_g$ss will be influenced by the increased viscosity of the fully cured system along with any cross-linking. More important however, was that the final $T_g$ss of the fully cured adhesive was out with the processing window. Following cure, the thermal stability of the adhesive was evaluated using TGA which displayed an onset of degradation at 293°C with the peak rate occurring at 329°C for degradation of the hard-segment and 426°C for degradation of the softsegment.

Analysis carried out using 180° T-peel testing displayed that the best laminate combination was PC/PC which boasted the peel strength of 11.5 N mm^{-1} following 30 days of cure. The most significant result from peel testing was the improved performance of the TAc/TAc laminate, which after 30 days could not be measured as a cohesive substrate failure resulted before any measurement could be acquired. For all previous formulations TAc/TAc performed nowhere near benchmark and had an

unstable peel which resulted in an adhesive failure at the interface. ATR analysis displayed that following 30 days the adhesive was fully cured and was a PU-U. It also displayed that ordered regions were present as shown by the H-bonding in **N-H** (also in the **C=O** region but less clear due to large soft-segment peak). Finally the haze value of the fully cured laminates was < 0.7% which is half of the set threshold value and a good result.

7.50 Analysis of IPDI-TMP-PDEGA-DEPD

7.51 Synthesis Information
IPDI-TMP-PDEGA-DEPD was synthesised with the intention of disrupting the close packing of hard-segments through using a less conventional diol chain-extender which should aid with phase mixing of the different domains. This was achieved by firstly synthesising the IPDI-TMP-PDEGA prepolymer using the same reaction conditions as detailed with section 7.41 and then performing an addition reaction set. The additional step was performed by adding a hydroxyl terminated chain-extender in a 2.2:1.0 isocyanate:hydroxyl ratio based on the calculated amount of free NCO remaining after step one. The chain-extension step was used to lower the free isocyanate content of the adhesive, which would reduce the opportunity for excessive bubbling by CO_2 produced as a consequence of the moisture cure (urea formation).

Step one was performed as previously detailed in section 7.41 and was a clear liquid which had an observed increase in viscosity from the starting mixture. After addition of DEPD, the reaction was allowed to stir at 85°C – 95°C for seventeen hours before the dual catalyst system (DBTDL and TEA) was added. Following chain-extension a visual increase in viscosity was observed and occurs as consequence of the molecular weight increase caused by the coupling step. The viscosity of the system was low enough that it did not require the temperature to be increased before transfer. Once the reaction was complete, the formulation was poured into an aluminium tube, which was then capped and degassed as previously outlined in section 2.03. The desiccator containing the adhesive filled tube was then placed within a 0°C fridge for storage. Degassing was performed for six hours once a vacuum of one atmosphere was

obtained. Samples of the reaction were again taken before catalysed addition, these were analysed by DSC, NMR and MALDI-MS analysis.

IPDI-TMP-PDEGA-DEPD was heated to 105°C before being applied to six laminates which was followed by room temperature cure. These samples were 180° T-peel tested at 7 days and 30 days to determine the peel strength. A further lamination was performed using two plies of TAc which would allow for the fully cured adhesive to be removed for analysis by DSC and TGA. The 30 day peel test samples were also analysed by ATR to characterise the final adhesive and determine the extent of cure.

Analysis of the chain-extended adhesive only will be presented within the remaining sections of this chapter. IPDI-TMP-PDEGA (sections 7.41-7.46) is considered as representative of the reactive intermediate obtained after step one of each chainextended reaction.

7.52 NMR Analysis
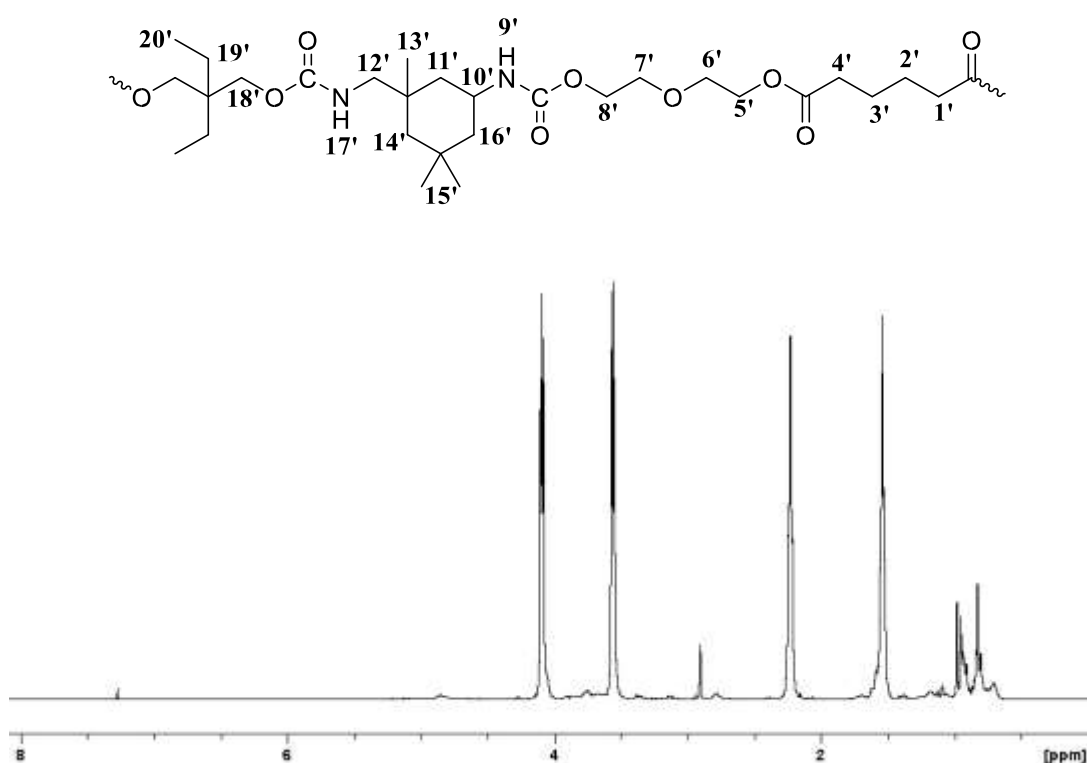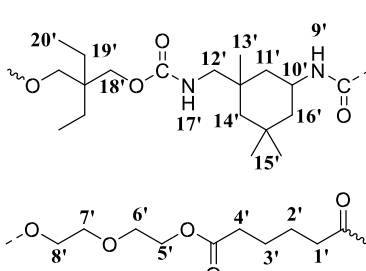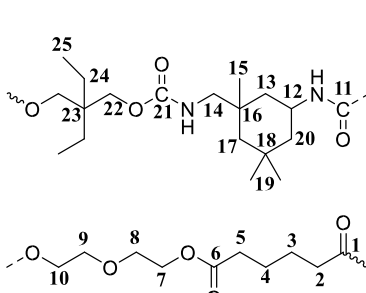
Figure 7.23: ¹H NMR spectrum obtained following reaction of IPDI-TMPPDEGA with DEPD.

Table 7.10: ¹H and ¹³C chemical shift for IPDI-TMP-PDEGA-DEPD collected in CDCl₃.

IPDI-TMP-PDEGA-DEPD	Position	^{1}H Chemical Shift (ppm)	Position	^{13}C Chemical Shift (ppm)
	1'	2.24	1	173.1
	2'	1.61	2	33.6
	3'	1.61	3	24.5
	4'	2.24	4	24.5
	5'	4.10	5	33.6
	6'	3.57	6	173.1
	7'	3.57	7	64.0
	8'	4.28	8	69.3
	9'	NDT	9	69.0
	10'	3.38	10	63.3
	11'	1.68/1.41	11	156.7$_p$/155.5$_s$
	12'	2.94/2.21	12	42.2
	13'	0.94	13	43.3
	14'	1.37/1.05	14	56.7
	15'	0.86	15	24.3
	16'	1.48/1.41	16	20.5
	17'	NDT	17	48.6
	18'	3.91	18	23.1
	19'	1.71	19	31.7
	20'	0.82	20	48.1

		21	156.7$_p$/155.5$_s$
		22	68.2
		23	33.4
		24	22.9
		25	7.1

$_p$ = primary, $_s$ = secondary, NDT = not detected

For full spectral characterisation of peaks from IPDI and PDEGA see section 7.42 (or table 7.10) as this section will only detail peaks that show prepolymer formation or peaks from the chain-extender.

Previous analysis displayed that the synthetic procedure used is not selective towards either the primary or secondary isocyanate groups. During the chain-extension step there will be both isocyanate groups available for reaction with the primary hydroxyl groups of DEPD. Reaction of hydroxyl end groups can be followed by examination of the adjacent methylene protons **18'** which shift downfield from 3.39 ppm to 3.91 ppm once reacted. Examination of the adjacent methylene groups of the hydroxyl groups in PDEGA can be used to monitor the synthesis, as when fully reacted the peak shifts downfield from 3.70 ppm to 4.28 ppm **8'**. Methylene protons **19'** within the ethyl side group are visible at 1.71 ppm and the methyl protons **20'** are visible at 0.82 ppm.
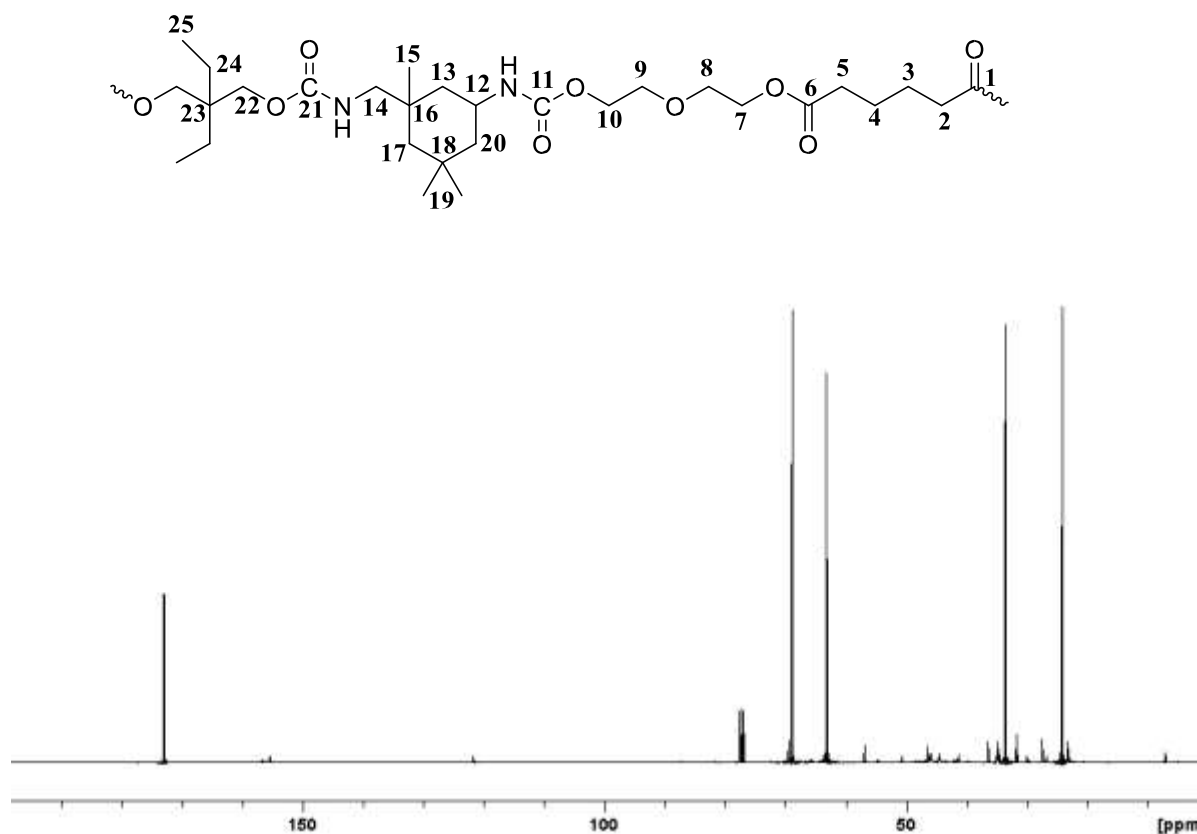
Figure 7.24: **¹³C NMR spectrum obtained following reaction of IPDI-TMPPDEGA with DEPD.**

Evidence of the chain-extenders incorporation into the prepolymer molecule was also observed by ¹³C NMR analysis. Methyl carbons **25** of the ethyl side group of DEPD are observed at 7.1 ppm and the methylene carbons **24** of this group are visible at 22.9 ppm. Next the tertiary carbon **23** of DEPD appears at 33.4 ppm and the adjacent methylene group **22** appears at 68.2 ppm.

Carbon peaks that correspond to reaction of the hydroxyl groups to urethane linkages in the end capping of PDEGA (step one of synthesis) can be observed by monitoring the position of the adjacent methylene carbons which shift upfield from 70.5 ppm to 69.3 ppm once reacted. Also present are peaks which correspond to the carbonyl within reactive isocyanates that are still present within the formulation. Both isocyanate groups are observed (would be expected based on the synthetic procedure) with the primary isocyanate at 123 ppm and secondary isocyanate at 122 ppm. Finally peaks which are characteristic of the carbonyl groups present within a urethane linkage are also observed. Both groups were observed with urethane linkages containing a

primary isocyanate occurring at a shift of 156.7 ppm and urethane linkages containing a secondary isocyanate occurring at 155.5 ppm.

^{1}H and ^{13}C NMR analysis of the chain-extended prepolymer of formulation IPDITMP-PDEGA-DEPD has been successful, however, molecular weight data is required to gain further structure information.

7.53 MALDI-MS Analysis

To determine the molecular weight increase within the chain-extended prepolymer MALDI-MS was used. The matrix used for analysis was HABA which contained a cationising agent NaTFA (see section 7.23 for more matrix information). A 40 mg ml^{-1} solution of IPDI-TMP-PDEGA-DEPD was prepared in THF and mixed with the matrix (1:8 sample:matrix). 1 µl portions of this sample were then spotted and dried for analysis.

The peak situated at 691 m/z corresponds to the chain-extender DEPD coupled with two ethanol end-capped IPDI units and one sodium cation. Also present is chainextender TMP that has reacted with three IPDI units which are ethanol end-capped as shown by the peak at 961 m/z (plus a sodium cation). These molecules will contribute to the hard-segment microstructure within the adhesive and they will also interfere with the packing arrangement within this domain.
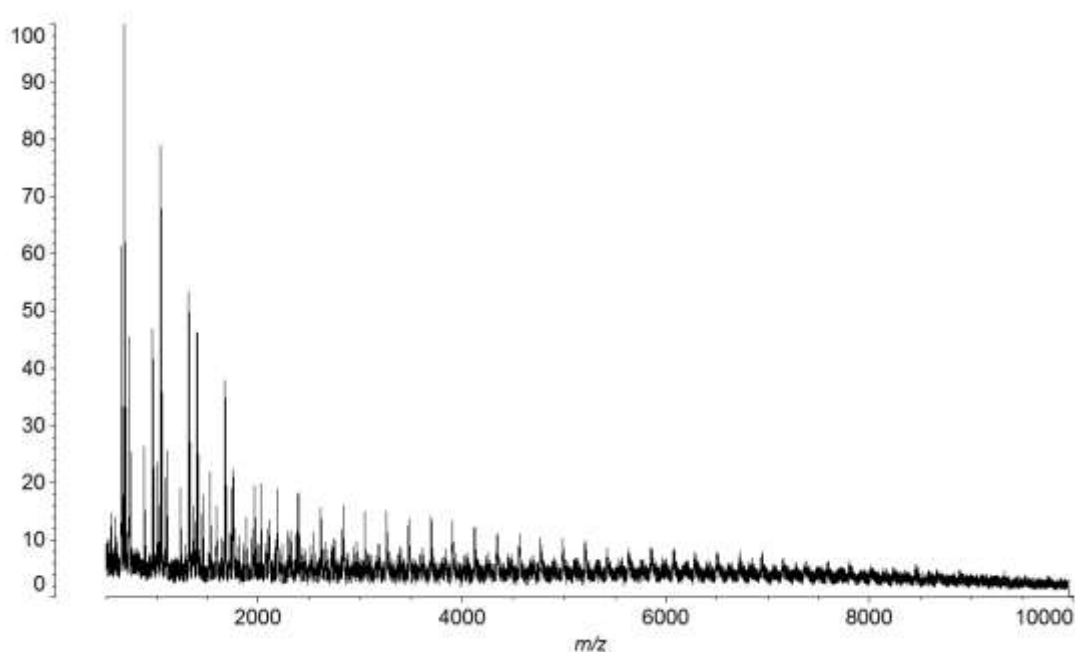
Figure 7.25: MALDI-MS spectrum of IPDI-TMP-PDEGA-DEPD chainextended prepolymer collected in HABA/NaTFA.

The peak centred at 2933 m/z contains the two ethanol end capped IPDI units, one sodium ion, 9 adipic blocks and 10 diethylene glycol blocks. This is a step one prepolymer as observed within section 7.43 and a proportion of this molecular weight would be expected. A chain-extended prepolymer peak is visible at 5860 m/z with the composition of the peak being 18 adipic acid blocks, 20 diethylene glycol blocks, two fully reacted IPDI units, two ethanol end capped IPDI units and one DEPD molecule. The previous peak was the non-sodiated adduct with the sodiated chain-extended prepolymer visible at 5883 m/z.

Calculation of Mn, Mw and PDI is then performed to determine the effect that DEPD has on the mass distribution. The calculated value of Mn is 3825 m/z and the calculated value of Mw is 5132 m/z giving a PDI of 1.34. The data collected displays that DEPD serves to increase the values of Mn and Mw while have a negligible effect on the breadth of the mass distribution with respect to PDEGA (see section 7.43 for PDEGA values).

7.54 DSC and TGA Analysis

Following synthesis of the chain-extended prepolymer, the thermal characteristics of the formulation were investigated to determine the $T_g$ss and to investigate any other thermal transitions within the formulation. As previously mentioned the $T_g$ss of the material was considered important as it had to be lower than -20°C to be suitable for the intended laminate application.
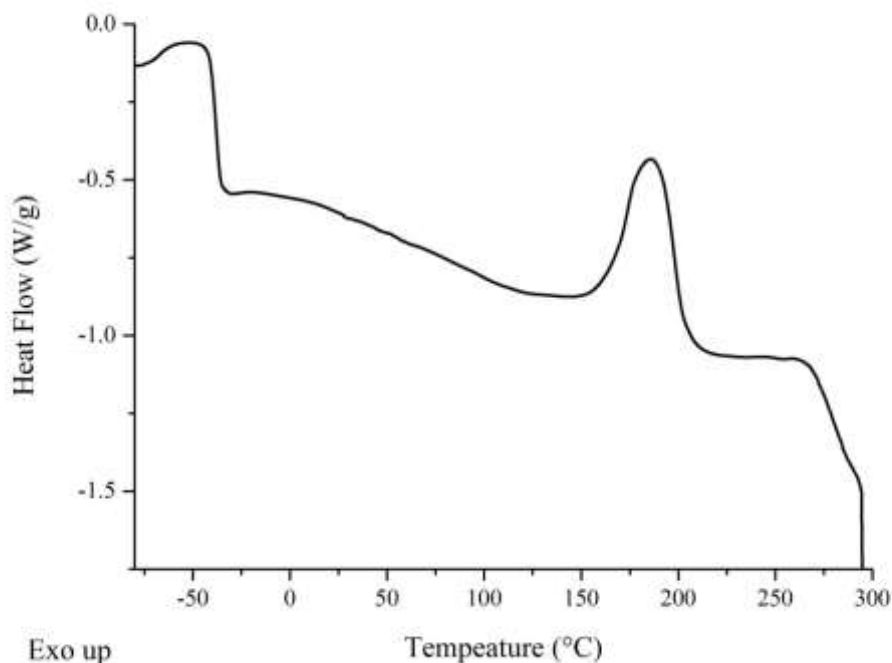
Figure 7.26: **DSC thermogram of IPDI-TMP-PDEGA-DEPD prepolymer formulation.**

Within figure 7.26 the DSC thermogram for the DEPD chain-extended prepolymer is presented. From analysis of the thermogram obtained for the chain-extended prepolymer, a $T_g$ss of -38°C was measured which covers a range of -41°C to -36°C. This is a shift in the $T_g$ss of +5°C with reference to the base prepolymer (IPDI-TMPPDEGA). This shift in the $T_g$ss would suggest that the polymer has increased in molecular weight and will also have a contribution from the viscosity increase due to the trifunctional TMP prepolymer molecules (observed in MALDI-MS see section 7.33). Also observed was a broad exothermic peak for the curing of the free isocyanate groups at 188°C (onset 165°C) with an enthalpy of 17 J g^{-1}. Possible curing reactions will be trimer formation of the free isocyanate groups or reaction of isocyanate groups with the acidic hydrogen present in the urethane linkage to form the cross-linked allophonate group, however, more analysis would be required to confirm.[15]
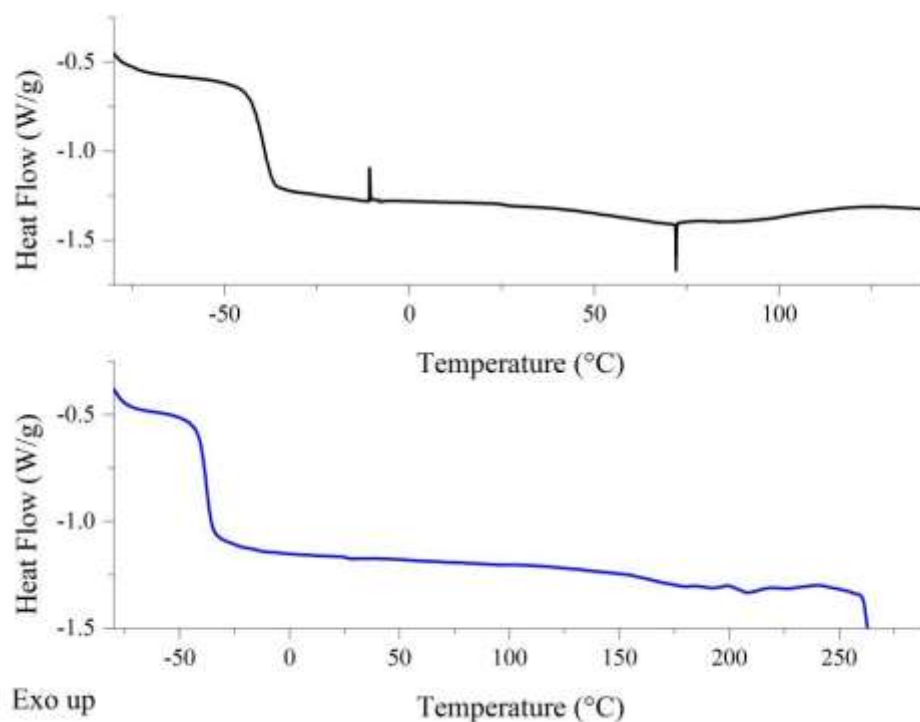
Figure 7.27: DSC thermogram of fully cured IPDI-TMP-PDEGA-DEPD adhesive, following removal from TAc/TAc laminate. [First heating cycle *top* in black and second heating cycle *bottom* in blue].

Recording the $T_g$ss following 30 days of cure (room temperature) is much more informative as it indicates the final properties of the cured adhesive. The cured adhesive was removed from the pre-made test laminate consisting of two TAc plies and put through a cool-heat-cool-reheat experiment (see section 7.44). In the first heating cycle only a single thermal transition was visible in the form of a glass transition. A $T_g$ss of -39°C was recorded which covered a narrow range from -43°C to -37°C. In the second cycle, two thermal transitions were observed in the form of a glass transition and melting endotherm. The $T_g$ss on the second heating scan was 38°C and it covered a narrow range from -41°C to -35°C. A second weak transition was observed with an onset of 201°C and peaked at 208°C. This small peak has a melting enthalpy of 0.3 J g^{-1} and corresponds to the thermal decomposition of Hbonds within the hard-segments of the adhesives microstructure (urethane and urea groups).[16-18]
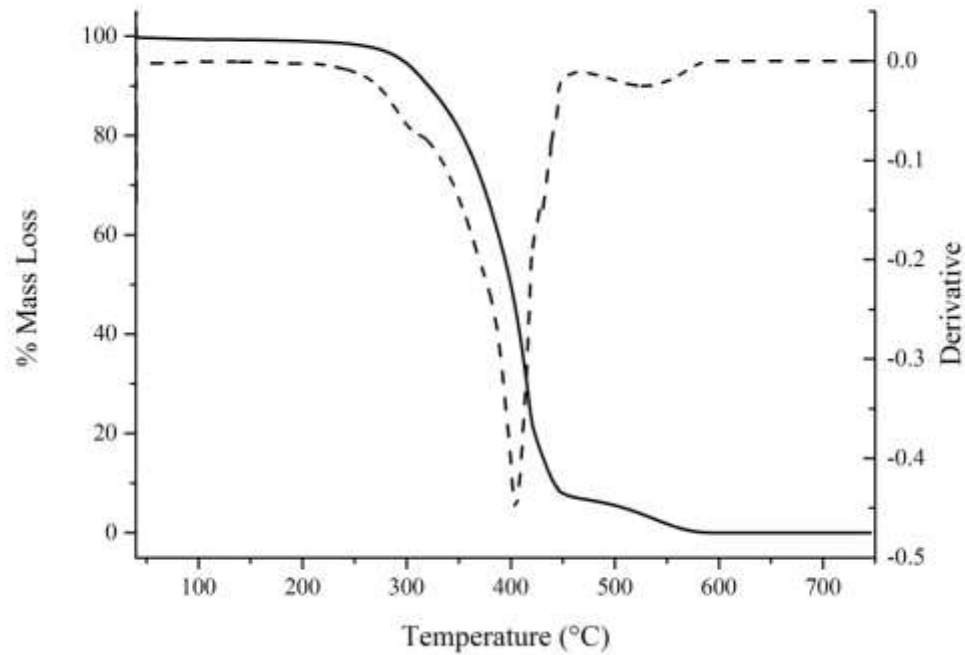
Figure 7.28: TGA and DTG curves of fully cured IPDI-TMP-PDEGA-DEPD adhesive. [TGA solid line and DTG dashed line].

In the TGA curve, the dominant degradation process (shown in figure 7.28) has an onset of 297°C, with the peak rate occurring at 308°C. Degradation through depolymerisation within the hard-segment will occur first as these bonds are thermally the least stable within the microstructure.[20,21] Degradation of the hardsegments occurs through the thermal decomposition of both the urethane and urea linkages. Also contained within this broad peak will be the thermal break down of the soft-segment ester groups.[16] The peak which corresponds to the decomposition of the soft-segment is visible in the DTG curve at 403°C. Another much smaller degradation peak at 530°C is also visible and will correspond to the decomposition of cross-linked products formed by reactive intermediates during degradation.[20]

For the intended application the onset of thermal degradation is well out with the temperature range that the laminate will experience during manufacture or use. This makes the formulation in question based on IPDI and PDEGA suitable for consideration as a possible adhesive based on the thermal characteristics obtained from both DSC and TGA.

7.55 180° T-peel Test and Haze

180° T-peel testing was performed on six laminates, which were measured after both 7 and 30 days of cure. The laminates used for this study were TAc/TAc, TAc(t)/TAc(t), TAc(t)/PC, TAc(t)/PC(t), PC(t)/PC(t) and PC/PC. Each laminate was peeled at a rate of 100 mm min^{-1} for an extension of at least 150 mm, with the first 50 mm discarded from the peel strength value as this is where a stable crack was formed. Previous lamination within this chapter displayed that both MDI based formulations performed very poorly with TAc/TAc whereas, the IPDI based formulation performed extremely well.

Results collected for the current formulation (as displayed in table 7.11) again displayed very strong results. Following 7 days of cure the peel strength obtain for TAc/TAc was 1.4 N mm^{-1} however, following 30 days of cure this value significantly increased to 6.4 N mm^{-1}. A cohesive mode of failure within the adhesive layer was observed for both tests, with the 30 day test also displaying deformation of the substrate. The value collected following 30 days of cure is twice the set benchmark.

Saponification of the TAc surface was next performed (see section 2.01) as this would present a more active regenerated cellulose surface and as displayed by previous testing this increases the compatibility at the adhesive - substrate interface. Deacetylation will leave hydroxyl groups at the surface which can react with the free isocyanate of the adhesive forming covalent bonds, forming anchor points between the adhesive and substrate creating a strong interface. After 7 days of cure, the peel strength recorded was 1.7 N mm^{-1} and the observed mode of failure was cohesive within the adhesive layer. Following 30 days, the peel strength recorded was 6.0 N mm^{-1} which again is a significant increase. Again a cohesive failure within the adhesive layer was observed and this was coupled with strong deformation of the TAc(t) substrate. The data shows that this formulation and IDPI-TMP-PDEGA can be used in the lamination of TAc without the need for surface treatment as peel strength for TAc $\approx$ TAc(t).

Table 7.11: Peel, haze and mode of failure data for IPDI-TMP-PDEGA-DEPD cured PU-U adhesive. [The data in bold will be discussed within this section].

Cured Adhesive	Laminate	Peel 1* (N mm^{-1})	Peel 2^{x} (N mm^{-1})	Failure mode	Haze (%)
MDI-TMPPDEGA	TAc/TAc	0.2	1.3	Adhesive TAc	>1.5%
	TAc(t)/TAc(t)	0.8	ND	Adhesive TAc	
	TAc(t)/PC	0.9	ND	Adhesive TAc	
	TAc(t)/PC(t)	0.8	1.1	Adhesive TAc	
	PC(t)/ PC(t)	6.2	7.6	Adhesive PC	
	PC/PC	4.2	5.6	Adhesive PC	
MDI-TMP-PDEGA-DEPD	TAc/TAc	1.3	ND	Adhesive TAc	>1.5%
	TAc(t)/TAc(t)	0.9	ND	Adhesive TAc	
	TAc(t)/PC	1.1	1.4	Adhesive TAc	
	TAc(t)/PC(t)	1.1	1.1	Adhesive TAc	
	PC(t)/ PC(t)	2.3	ND	Adhesive PC	
	PC/PC	3.6	ND	Adhesive PC	
IPDI-TMP-PDEGA	TAc/TAc	0.9	Ply	Cohesive	<0.7%
	TAc(t)/TAc(t)	1.0	Ply	Cohesive	
	TAc(t)/PC	0.8	4.68	Cohesive	
	TAc(t)/PC(t)	0.9	4.73	Cohesive	
	PC(t)/ PC(t)	0.5	9.1	Cohesive	
	PC/PC	0.9	11.5	Cohesive	
IPDI-TMP-PDEGA-DEPD	**TAc/TAc**	**1.4**	**6.4**	**Cohesive**	**<0.7%**
	TAc(t)/TAc(t)	**1.7**	**6.0**	**Cohesive**	
	TAc(t)/PC	**1.4**	**6.5**	**Cohesive**	
	TAc(t)/PC(t)	**1.1**	**6.1**	**Cohesive**	
	PC(t)/ PC(t)	**0.6**	**10.3**	**Cohesive**	
	PC/PC	**0.7**	**10.6**	**Cohesive**	

peel 1 collected within 7 days of room temperature cure, ^x peel 2 collected after 30 days of room temperature cure, ND = No Data

Previous testing has shown that PC laminates consistently perform above benchmark following 30 days of cure (when there are no issues with curing or application). Untreated PC displayed a cohesive mode of failure within the adhesive layer, which was coupled with deformation of the PC substrate. Following 7 days of cure, the peel strength recorded was 0.7 N mm^{-1} and this increased to 10.6 N mm^{-1} after 30 days of curing. It would appear from the data collected for this current formulation (based on IPDI and PDEGA) that it has an affinity for both TAc and PC.

Data collected after 7 days recorded the peel strength at 0.6 N mm^{-1} which greatly increased to 10.2 N mm^{-1} after 30 days of cure. Each sample displayed a cohesive mode of failure within the adhesive layer and in the 30 day test this was also paired with strong substrate deformation. Comparing these results with untreated PC, the surface treatment has had very little effect on the recorded peel strength. All PC based laminates after 30 days of curing are well above the 3 N mm^{-1} benchmark.

Finally to determine which substrate was most compatible with the current formulation hybrid laminates were tested. First tested was TAc(t)/PC which displayed a cohesive mode of failure within the adhesive layer on both occasions. After 7 days of curing the peel strength was 1.4 N mm^{-1} and this increased following 30 days of cure to 6.5 N mm^{-1}. Next the fully treated hybrid was tested (TAc(t)/PC(t)) and it also displayed a cohesive mode of failure within the adhesive layer. After 7 days of cure the peel strength recorded was 1.1 N mm^{-1} and following 30 days of cure the strength greatly improved to 6.1 N mm^{-1}. These two laminate combinations display the affinity of the adhesive is not selective to one interface and that the adhesive layer is the weakest component within the system for every laminate.

Once fully cured, the adhesive displayed good clarity as the average haze for the six laminates was < 0.7%. The low haze value was a result of the absence of any large scale crystallisation within the PDEGA soft-segment which gives the adhesive a clear colourless appearance.

For discussion of the peaks inherent of the starting materials see section 7.46 and for all characteristic peaks see table 7.12.
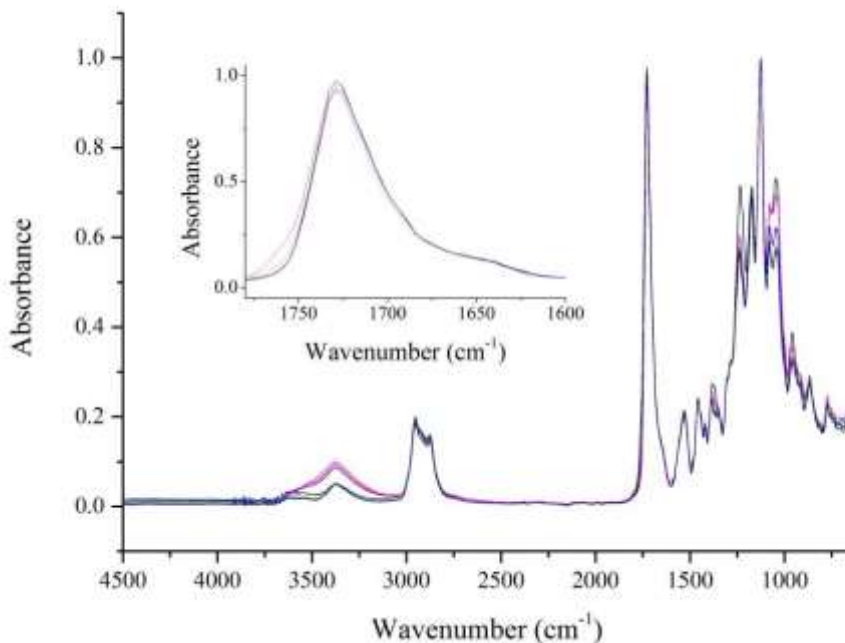
Figure 7.29: ATR spectra of cured IPDI-TMP-PDEGA-DEPD sampled in-situ after peel testing with inset expanded carbonyl region. [TAc/TAc in black, TAc(t)/TAc(t) in red, TAc(t)/PC in blue, TAc(t)/PC(t) in pink, PC(t)/PC(t) in green and PC/PC in orange. Data collected for each laminate at nine random positions with each spectrum consisting of 128 scans at 8 cm^{-1} resolution. These were then averaged and plotted as the above spectra].

The spectra collected from the in-situ characterisation of the cured adhesive are shown within figure 7.29 for all six laminates. All characteristic peaks for the fully cured PU-U are shown within table 7.12. Observation of the band positioned at 3375 cm^{-1} displays that H-bonding with **N-H** groups within the network is occurring. Also evident is **N-H** stretching vibrations that are not involved within the H-bonded network as shown by the shoulder to the previous at 3500 cm^{-1}. Next aliphatic **C-H** stretching vibrations from PDEGA are present for both the asymmetric and symmetric bands at 2954 cm^{-1} and 2873 cm^{-1} respectively. No detectable isocyanate peak was visible

between 2260 cm^{-1} – 2280 cm^{-1} which displays that the adhesive is fully cured after 30 days.

Table 7.12: **Characteristic peaks of IPDI-TMP-PDEGA-DEPD cured PU-U adhesive from all six laminate combinations.**

Wavenumber (cm^{-1})	Vibration	Wavenumber (cm^{-1})	Vibration
3375	N-H stretching H-Bonded	1357	C-N Urea
2954	C-H asymmetric stretch	1284	C-N Urethane
2873	C-H symmetric stretch	1173	Symmetric N-CO-O
1725	C=O stretching ester	1083	C-O-C stretch aliphatic ester
1695	C=O free Urea stretch	1050	Symmetric N-CO-O
1646	C=O stretch Urea Bidentate Hbonded	960	C-O-C stretch aliphatic ester
1533	C-N stretch, N-H bend	861	C-C skeleton vibration
1457	C-H bend aliphatic		
1386	C-H symmetric deformation	775	C-C aliphatic skeleton

Next the carbonyl region of the spectrum was investigated to determine if any further morphological information on the adhesive can be observed. The position of the carbonyl peak will show the order/disorder of the domain in which the carbonyl group resides and it will also indicate the type of functional group. From the position of the carbonyl at 1725 cm^{-1} it displays that the ester groups are part of ordered domain as it confirms H-bonding (will be discussed within chapter 8). It would be expected that

H-bonds within hard-segment will occur for urethane carbonyl groups but they are not visible due to the large intensity of the H-bonded ester carbonyl peak.[21,22]

Also within the carbonyl region there appears to be three different kinds of urea formed during the moisture cure of the free isocyanate groups. First encountered is a shoulder peak at 1695 cm^{-1} for carbonyl groups of free or unordered urea.[22] Evidence of monodentate H-bonded urea within the cured adhesive is visible by the broad shoulder attached to the previous peak between 1675 cm^{-1} – 1660 cm^{-1}.[21] Fully ordered bidentate urea groups are observed by the carbonyl peak at 1646 cm^{-1}. From the urea region alone it is clear that there are regions of high order, low order and regions of disordered. The ordered regions will contribute to the strength of the cured matrix through the formation of cross-links, whereas the disordered region will increase the phase mixing of the cured adhesive and clarity.

Further bands of urethane and urea formation are evident within the spectrum. At 1533 cm^{-1} the **C-N** stretching and **N-H** stretching of both urethane and urea is observed. Evidence of urea within the finger print region is shown by the **C-N** stretching vibration at 1357 cm^{-1} with the urethane vibration shown at 1284 cm^{-1}. Further urethane vibrations within the microstructure are shown by the asymmetric and symmetric **N-CO-O** stretching at 1173 cm^{-1} and 1050 cm^{-1} respectively. Aliphatic ester **C-O-C** stretching vibrations of the PDEGA soft-segment are present at 1083 cm^{-1} and 960 cm^{-1}. The final absorption peaks within the spectrum are **C-C** skeleton rocking vibrations at 861 cm^{-1} and 775 cm^{-1}.

7.57 Summary of IPDI-TMP-PDEGA-DEPD Formulation

From the above analysis it can be confirmed from both ^{1}H and ^{13}C NMR that the end capped PU prepolymer was successfully synthesised. MALDI-MS analysis also highlighted that step one prepolymers of structure IPDI-PDEGA-MDI were still present within the formulation. MALDI-MS also displayed higher molecular weight chain-extended prepolymers which were the target molecules within the bulk polymerisation process.

Thermal analysis performed using DSC displayed that the prepolymer material had a $T_g$ss of -38°C which covered a narrow range (-41°C to -36°C). This was accompanied

by a curing peak of the free isocyanate at 188°C. Following moisture cure, the $T_g$ss of the cured adhesive shifted to -39°C (-43°C to -37°C) for the first heating cycle, with this cycle having no other clear thermal features. On the second heating cycle, the $T_g$ss recorded was -38°C (-41°C to -35°C) and this was accompanied by a small melting endotherm at 208°C (enthalpy 0.3 J/g). Decomposition of H-bonds within hard-segments of the microstructure are displayed by the high temperature melt, however, the small enthalpy value would suggest that these domains are not highly organised. More important however, was that the final $T_g$ss of the fully cured adhesive was out with the processing window. The overall thermal stability following cure of the adhesive was evaluated using TGA which displayed an onset of degradation at 297°C with the peak rate occurring at 308°C for degradation of the hard-segment and 403°C for degradation of the soft-segment.

Analysis carried out using 180° T-peel testing displayed that the best laminate combination was PC/PC which boasted the peel strength of 10.6 N mm^{-1} following 30 days of cure. The most significant result from peel testing was the improved performance of the TAc/TAc laminate which had a peel strength after 30 days of 6.4 N mm^{-1} (TAc(t)/TAc(t) recorded 6.0 N mm^{-1}). For all previous formulations (excluding IPDI-TMP-PDEGA) TAc/TAc performed nowhere near benchmark and had an unstable peel which resulted in an adhesive failure at the interface. For this current formulation the obtained peel strength is twice the set benchmark value.

ATR analysis displayed that following 30 days the adhesive was fully cured and was a PU-U. It also displayed that ordered regions were present as shown by the Hbonding in **N-H** (also in the **C=O** region but less clear due to large soft-segment peak). Finally the haze value of the fully cured laminates was < 0.7% which is half of the set threshold value and a good result.

7.60 Summary of Polyurethane Adhesives based on Poly[di(ethylene glycol) adipate]

NMR analysis using both ^{1}H and ^{13}C was able to follow the synthesis of each PU. NMR was used to identify the incorporation of the chain-extender molecules into the formulation. In ^{1}H NMR chain-extender incorporation was monitored by observing

the shift to the protons adjacent to hydroxyl end groups. [13]C was especially useful at following the reaction of both isocyanate groups in IPDI or the introduction of asymmetry into MDI following reaction. For MDI only a single peak was visible for the urethane carbonyl as both isocyanates are secondary whereas, for IPDI two peaks in the urethane region are visible which allowed for differentiation between urethane linkages which contained primary and secondary isocyanate groups. Confirmation that the prepolymer in solution was still reactive was shown by ^{13}C NMR through monitoring the isocyanate carbonyl groups in all four systems.

MALDI-MS analysis was used to characterise the molecular weight of the prepolymers and chain-extended prepolymers. In all four cases step one end capped prepolymers of structure MDI-PDEGA-MDI and IPDI-PDEGA-IPDI were obtained along with isocyanate end capped TMP molecules. In both chain-extended reactions the target molecules of MDI-PDEGA-MDI-DEPD-MDI-PDEGA-MDI and IPDIPDEGA-IPDI-DEPD- IPDI-PDEGA-IPDI were observed (plus TMP-IPDI/MDI and DEPD-IPDI/MDI).

Characterisation of the thermal stability of each fully cured adhesive was carried out using TGA analysis. The observed onset of degradation and the subsequent degradation curve varied slightly depending on the hard-segment used. For MDI based formulations, the onset of degradation occurred at 313°C in the adhesive which was not chain-extended and 316°C for the DEPD chain-extended adhesive. Degradation occurred in two processes for MDI-TMP-PDEGA with decomposition of the hard-segments occurring first (342°C) followed by decomposition of the softsegments (416°C). Following chain-extension the degradation behaviour was very similar except for the additional higher temperature decomposition at 560°C of thermally more stable cross-linked material formed during degradation (hardsegment decomposition peak at 351°C and soft-segment decomposition peak at 419°C).

In IPDI based formulations the onset of degradation occurred at slightly lower temperatures. The adhesive which was free of chain-extension had an onset of degradation which occurred at 293°C and the chain-extended adhesive had an onset of 297°C. Compared to the MDI based formulations the onset of thermal degradation

was lower but as thermal degradation occurs well above the maximum processing temperature of 100°C it will not impact the intended application. For the IPDI based formulation three decomposition processes were visible: first decomposition of hard-segment bonds is observed (none = 329°C and DEPD = 308°C), next decomposition of the soft domains was observed (none = 401°C and DEPD = 403°C) and the final decomposition process was of thermally more stable cross-linked product formed during degradation (none = 543°C and DEPD = 530°C).

DSC analysis was used to investigation the thermal characteristics of all four formulations. The $T_g$ss was considered an important data point as it had to be out with the set processing range and likely temperatures of application. MDI based prepolymers displayed a greater shift in the $T_g$ss (none = -41°C and DEPD = -30°C) following chain-extension compared to IPDI based prepolymers (none = -43°C and DEPD = -38°C). Once fully cured the observed $T_g$ss for MDI based adhesive appears at a higher temperature (none = -30°C and DEPD = -26°C) when compared to the IPDI based adhesives (none = -38°C and DEPD = -38°C). The greater shift of the $T_g$ss in MDI based adhesive displays that the phase compatibility and mixing is greater that IPDI based materials. Also observed on each of the second heating scans was a melting endotherm which occurred at an elevated temperature. The temperature at which the melt occurred and the enthalpy of the melt were similar in all cases except for IPDI-TMP-PDEGA which had a melting enthalpy six fold larger (MDI-TMP-PDEGA peak = 221°C + enthalpy = 0.3 J g^{-1}, MDI-TMP-PDEGADEPD peak = 199°C + enthalpy = 0.3 J g^{-1}, IPDI-TMP-PDEGA peak = 198°C + enthalpy = 1.8 J g^{-1}, IPDI-TMP-PDEGA-DEPD peak = 208°C + enthalpy = 0.3 J g^{-1}).

Previously data collected in thermal analysis was used to help explain the high haze values recorded for each adhesive. Both MDI based formulations displayed a high haze value which was greater than the 1.5% threshold result as a direct result of the large amount of bubbles within the adhesive layer (bubble trapped due to higher viscosity). Conversely both the IPDI based adhesive have a low haze value of < 0.7% and contained almost no bubbles within the adhesive layer.

The most significant result in this chapter is presented by the peel data collect.

PDEGA adhesives based on MDI performed very poorly on TAc in any combination (TAc or TAc(t)) but reach benchmark for PC (in most cases). IPDI performs well above benchmark on all six laminate combinations including TAc/TAc which until this point recorded average peels strengths of 1 N mm^{-1}. The greater peel strength observed for IPDI based adhesives will be a combination of factors but briefly here are some hypotheses. Firstly the slower curing time and low viscosity will allow for the adhesive to penetrate into the substrate which once cured will form the lock and key type mechanical adhesion. Also as the IPDI based adhesive have less mixing of the phases, the hard-segments will form larger reinforcement point while the larger soft-segment domains will increase the potential for adhesion at the interface through adsorption mechanisms.

Following all the analysis collected on the formulations based on IPDI, MDI and PDEGA it is clear that MDI based adhesives will not be considered any further whereas IPDI based adhesives are the strongest formulations. Not only do IPDI and PDEGA based formulations pass the thermal, haze and peel strength thresholds, the average peel strengths are the highest of all the formulations tested (TMP only formulation average = 7.0 N mm^{-1} and DEPD chain-extended average = 7.8 N mm^{-1}) and eliminate the need for surface treatment. Also apparent is that chain-extension does not significantly improve the haze but it does have a positive impact on the peel strength.

References

(1)   Randall. D, L. S. *The Polyurethanes Handbook*; Wiley, 2003.
(2)   da Silva, A. L. D.; Martín-Martínez, J. M.; Carlos Moura Bordado, J. *International Journal of Adhesion and Adhesives* **2008**, *28*, 29.

(3)   Li, Y.; Gao, T.; Liu, J.; Linliu, K.; Desper, C. R.; Chu, B. *Macromolecules* **1992**, *25*, 7365.

(4)   Wang, P.-S.; Chiu, W.-Y.; Chen, L.-W.; Denq, B.-L.; Don, T.-M.; Chiu, Y.S. *Polymer Degradation and Stability* **1999**, *66*, 307.

(5)   Petrović, Z. S.; Zavargo, Z.; Flyn, J. H.; Macknight, W. J. *Journal of Applied Polymer Science* **1994**, *51*, 1087.

(6)   Dominguez-Rosado, E.; Liggat, J. J.; Snape, C. E.; Eling, B.; Pichtel, J. *Polymer Degradation and Stability* **2002**, *78*, 1.

(7)   Grassie, N.; Zulfiqar, M. *Journal of Polymer Science: Polymer Chemistry Edition* **1978**, *16*, 1563.

(8)   Herrera, M.; Matuschek, G.; Kettrup, A. *Polymer Degradation and Stability* **2002**, *78*, 323.

(9)   Venkataraman, A.; Subramanian, D. R.; Soosamma, P. C. *Textile Research Journal* **1982**, *52*, 506.

(10)   Burattini, S.; Greenland, B. W.; Merino, D. H.; Weng, W.; Seppala, J.; Colquhoun, H. M.; Hayes, W.; Mackay, M. E.; Hamley, I. W.; Rowan, S. J. *Journal of the American Chemical Society* **2010**, *132*, 12051.

(11)   Li, C.; Wilkes, G. *Journal of Inorganic and Organometallic Polymers* **1997**, *7*, 203.

(12)   Daniel-da-Silva, A. L.; Bordado, J. C. M.; Martín-Martínez, J. M. *Journal of Applied Polymer Science* **2008**, *107*, 700.

(13)   Dick, C.; Dominguez-Rosado, E.; Eling, B.; Liggat, J. J.; Lindsay, C. I.; Martin, S. C.; Mohammed, M. H.; Seeley, G.; Snape, C. E. *Polymer* **2001**, *42*, 913.

(14)   Prabhakar, A.; Chattopadhyay, D. K.; Jagadeesh, B.; Raju, K. V. S. N. *Journal of Polymer Science Part A: Polymer Chemistry* **2005**, *43*, 1196.

(15)   Lapprand, A.; Boisson, F.; Delolme, F.; Méchin, F.; Pascault, J. P. *Polymer Degradation and Stability* **2005**, *90*, 363.

(16)   Rath, S. K.; Ishack, A. M.; Suryavansi, U. G.; Chandrasekhar, L.; Patri, M. *Progress in Organic Coatings* **2008**, *62*, 393.

(17)   Chattopadhyay, D. K.; Prasad, P. S. R.; Sreedhar, B.; Raju, K. V. S. N. *Progress in Organic Coatings* **2005**, *54*, 296.

(18)   Korley, L. T. J.; Pate, B. D.; Thomas, E. L.; Hammond, P. T. *Polymer* **2006**, *47*, 3073.

(19)   Zhang, J.; Tu, W.; Dai, Z. *J Coat Technol Res* **2013**, *10*, 887.

(20)   García-Pacios, V.; Jofre-Reche, J. A.; Costa, V.; Colera, M.; MartínMartínez, J. M. *Progress in Organic Coatings* **2013**, *76*, 1484.

(21)   Cakic, S. M.; Stamenkovic, J. V.; Djordjevic, D. M.; Ristic, I. S. *Polymer Degradation and Stability* **2009**, *94*, 2015.

(22)   García-Pacios, V.; Iwata, Y.; Colera, M.; Miguel Martín-Martínez, J. *International Journal of Adhesion and Adhesives* **2011**, *31*, 787.

Chapter 8 Discussion of Adhesive Morphology - The Relationship with Adhesive Strength and Haze

It is well known that the final morphology of polyurethane materials will depend on a variety of factors such as stoichiometry, reaction temperature, curing conditions, thermal history and composition. Careful design of the system is essential to ensure that the final material is optimised for the application of choice. As the planned application of the PU-U in this report was as an adhesive for lamination of TAc and PC the available starting materials were limited to those that could be used in bulk synthesis.

Previous analysis within this report identified some interesting observations. It was identified that greater adhesive strength could be obtained using the aliphatic isocyanate IPDI than was possible with the aromatic isocyanate MDI. Using an aliphatic isocyanate within the adhesive will enhance the UV stability of the adhesive layer as MDI based adhesives are known to degraded when exposed to UV radiation.[1-3] As mentioned, the synthetic procedure used will influence the morphology of the adhesive and will affect the ability of the final material to adhere to the substrate (TAc or PC) interface. The morphology will also have an influence the matrix strength.

Furthermore, the hard-segment content will also influence the morphology. When the hard-segment content is around 50 wt% mixing of the phases will occur however, when below 50 wt% the morphology drives towards phase separation. Phase separations leads to the formation of solid anchoring points which are fixed together by hydrogen bonding. Morphology of this type is termed globular as it consists of a sea of soft-segment containing islands of hard-segment based on similar systems within the literature.[4] In the literature it has been noted that the hard-segment content is a critical parameter to consider when designing any type of adhesion as it will directly affect the properties obtained.[5,6]

Within the remainder of this chapter, each fully cured adhesive set will be discussed in terms of its morphology. Interpretation of the microphase morphology will be based on thermal analysis obtained by DSC and spectroscopic analysis of the N-H and C=O regions using ATR. A relationship will be constructed based on the morphology and the effect it has on the adhesive strength recorded during 180° Tpeel testing.

From DSC it is possible to investigate the morphology of polyurethanes by using some simple relationships: (1) a small increase in the glass transition temperature of the soft-segment identifies that the material is phase separated, (2) a narrow softsegment glass transition also indicates phase separation, (3) a large shift of the softsegment glass transition shows phase mixing and (4) a broad soft-segment glass transition indicates that the morphology is phased mixed. Using these simple relationships it is possible to start the determination of the microphase morphology within the polyurethane.

Establishing the same kind of simple relationships for ATR it is possible to investigate the morphology. If the N-H peak is situated within the range of 33303365 cm^{-1} then the hydrogen bonds are within hard-segments and thus a phase separated morphology. If the N-H peak appears broader and at lower wavenumbers ~3300 cm^{-1} it is an indication of hard-to-soft interaction within the microstructure, this indicates phase mixing. Furthermore the carbonyl region is also used to investigate the phase morphology. Having groups such as bidentate urea and hydrogen bonded urethane display phase separation. When these groups are in low concentration or replaced with free urethane/urea it displays that the phase morphology of the system is mixed. Determination of the polyurethane phase morphology is only possible once both techniques have been consulted.

8.10 Morphology of Polyurethane Adhesives Based on Thermal Analysis

Using DSC as a means of investigating the morphology of polyurethane materials is a well-practiced method with many examples in the literature.[7-12] Successful determination of the morphology in this way requires that it is combined with another analysis method such as FTIR.[13-17] Within this section, the thermal data collected on each adhesive set will be discussed in terms of morphology based on the position of thermal events such as the glass transition and melting endotherms.

8.11 Discussion of the Morphology in Aromatic Polyurethane Adhesives

Investigation of adhesive formulations based on MDI and PPG using DSC will first be discussed. Within table 8.01 the thermal data collected from all four formulations is presented complete with the PPG 1000 molecular weight soft-segment. The $T_g$ss (soft-

segment glass transition temperature) of PPG occurs at -70°C and covers a narrow range of 2°C. Presented within figure 8.01 are the DSC thermograms of each cured adhesive obtained during the second heating cycle. For experimental procedures and selection criteria of higher temperature thermal event see section 2.142 (spectra in appendix A).

For formulation MDI-TMP-PPG, the glass transition has shifted by +62°C to -8°C. This shift is coupled with visible broadening of the glass transition which now covers a range of 14°C from -18°C to -4°C. A further shift in the $T_g$ss is observed for each diol chain-extended adhesive with 7°C reached for DEPD, 1°C reached for BD and 1°C reached for PD. Again accompanying the elevated $T_g$ss was an expansion of the range in which the transition occurs. Elevation of the $T_g$ss in each case following the introduction of each diol chain-extender displays that chain-extension step encourages phase mixing with the polyether based soft-segment. This indicates that each of the diol chain-extenders improves the compatibility or miscibility of the soft and hard-segments. This could be a result of the short hard-segment block length (average 2 MDI units) reducing the ability of the hard-segments to aggregate which will also make it easier for the hard-segments to migrate between soft-segment chains .[18]

The observed shift and broadening of the soft-segment $T_g$ss from phase mixing would be expected based on the literature for PUs containing a polyether softsegment.[19,20] Elevation of the $T_g$ss can be explained by two common processes: (a) when a proportion of the hard-segment dissolves in the soft-segment the net result is elevation in temperature of the $T_g$ss shifts (towards that of the hard-segment glass transition temperature ($T_g$hs)) and (b) chain mobility becomes restricted by the conformational constraints applied by the physical cross-links formed by hydrogen bonds between the hard-segment with the soft-segment in which it is now dispersed.[19]

Table 8.01: Table of DSC data for MDI based PU-U adhesives.

Formulation	HS wt %	$T_g$ss /°C	Range /°C	$T_g$hs /°C	$T_m$ss* /°C	Enthalpy /J g^{-1}	$T_m$hs1 /°C	Enthalpy /J g^{-1}	$T_m$hs2 /°C	Enthalpy /J g^{-1}	$T_m$hs3 /°C	Enthalpy /J g^{-1}
PPG	-	-70	-71to -69	-	-	-	-	-	-	-	-	-
MDI-TMP-PPG	36.4	-8	-18to-4	81	-	-	-	-	203[x]	4.9	-	-
MDI-TMP-PPG-DEPD	41.5	7	-3to17	96	-	-	171	0.3	219	0.6	-	-
MDI-TMP-PPG-BD	40.0	1	-9to9	-	-	-	175	2.6	224	0.5	-	-
MDI-TMP-PPG-PD	39.5	1	-10to9	-	-	-	170	1.9	-	-	247	3.0
PCD	-	-64	-67to-58	-	50	57	-	-	-	-	-	-
MDI-TMP-PCD	22.3	-40	-44to-31	-	47	8.6	-	-	205[x]	2.8	-	-
MDI-TMP-PCD-DEPD	26.1	-31	-39to-26	-	-	-	177	0.2	193	0.7	-	-
MDI-TMP-PCD-BD	25.0	-33	-39to-27	-	-	-	193	0.6	227	0.4	-	-
MDI-TMP-PCD-PD	24.6	-32	-38to-25	-	-	-	192	0.6	223	0.4	255	0.3
PDEGA	-	-49	-51to-48	-	-	-	-	-	-	-	-	-
MDI-TMP-PDEGA	18.7	-30	-35to-24	-	-	-	-	-	202[x]	2.4	-	-
MDI-TMP-PDEGA-DEPD	22.1	-26	-33to-22	-	-	-	174	0.1	199	0.3	218	0.8

*obtained on first heating cycle, $T_g$ss = soft-segment glass transition temperature, $T_g$hs = hard-segment glass transition temperature,

$T_m$ss = melting endotherm soft-segment, $T_m$hs = melting endotherm hard-segment, [x] = curing exotherm
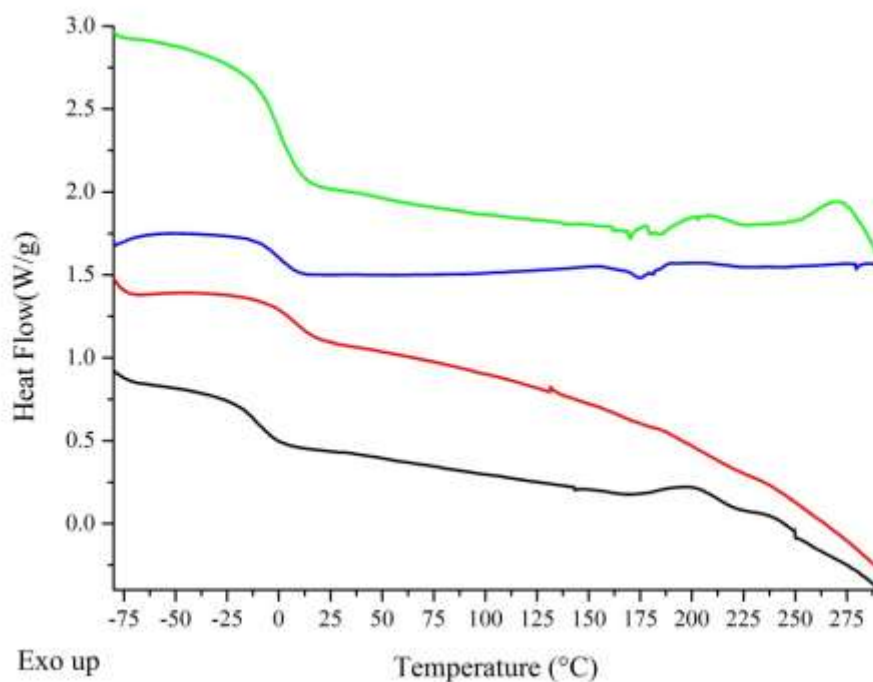
Figure 8.01: Stacked DSC thermograms for PU-U adhesives based on MDI and PPG. [MDI-TMP-PPG in black, MDI-TMP-PPG-DEPD in red, MDI-TMPPPG-BD in blue and MDI-TMP-PPG-PD in green].

Ryan et al. discussed how precipitation of the chain-extender within the hardsegment can affect the packing arrangement and overall segmented structure.[21]

Precipitation in this sense is defined as "upon matrix solidification chain-extender molecules will be segregated or phase separated within the hard-segment only, directly affecting this segments crystalline structure". Therefore the chain-extender is considered miscible with the hard-segment but immiscible with the soft-segment. Sànchez-Adsuar et al. and Gisselfält et al. reported that the chain-extenders length/structure also has an influence on the microphase morphology, with short chain length chain-extenders promoting ordered hard-segment packing along with phase separation.[22,23] Within the Sànchez-Adsuar et al. study ethylene glycol, 1,4butane diol and 1,6-heaxane diol were applied during synthesis. It was shown by following the $T_g$ss using DSC that 1,6-hexane diol displayed the greatest shift of the $T_g$ss as a result of phase mixing. As the diol chain-extenders used within this study contain side groups (ethyl in DEPD and methyl for BD and PD) it is anticipated that these will

472

interfere with the intimate packing of the hard-segments and their ability to crystallise, consistent with the observation of Gisselfält et al.

Based on the literature for segmented block copolymers it would be expected to observe the glass transition of the hard-segment.[7,19,24,25] Within the DSC thermogram of MDI-TMP-PPG two weak higher temperature thermal transitions were observed. The first transition occurs at 32°C and is associated with dissociation/relaxation of hard blocks that are highly disordered which may be a result of the known disruptive effect induced by the triol chain-extender TMP.[4] Observation of these weak transitions is difficult but becomes clearer when the first derivative is plotted of the second heating cycle (see appendix A). Also identified from the first derivative was the $T_g$hs for more ordered hard-segment domains at 81°C. This value is consistent with the literature for formulations of this hardsegment content and short hard-segment block length.[24] Of the diol chain-extended formulations only MDI-TMP-PPG-DEPD displays a $T_g$hs at 96°C which is again consistent with the literature.[19] As the glass transition has shifted to a higher temperature it confirms that the greater hard-segment block length introduced by diol chain-extenders promotes hard-segment aggregation over that of the triol chainextender only.

Decomposition of the crystalline hard-segments in the form of a melting endotherm is observed in each of the adhesives excluding MDI-TMP-PPG. When TMP is the only chain-extender (MDI-TMP-PPG) a single exotherm is observed at 203°C with the enthalpy of the thermal process 4.9 J g^{-1}. This process is believed to be cure of any residual reactive groups and the small enthalpy obtained displays that the residual isocyanate content is low. It is also possible that this higher temperature exothermic transition is the reorganisation of the hard-segment as has been suggested within the literature.[4] Reorganisation to maximise hydrogen-bonds and π-π stacking interactions may result in the exotherm observed.

Of the diol chain-extenders used, DEPD has had the greatest influence on the hardsegment melting. Depreciation of the melting enthalpy of both the first (171°C 0.3 J g^{-1}) and second (219°C 0.6 J g^{-1}) melting enthalpies observed resulting in a reduced net melting enthalpy of 0.9 J g^{-1}. These typically small enthalpy values are

expected as 15% of the chain-extender content is TMP.[4]   Disruption of the hard-segment packing due to the influence of side groups on the diol chain-extenders is consistent with the observations of Gisselfält et al.[23] This observation is supported by the recovery and improvement observed for the hard-segment melting in BD. In the formulation consisting of MDI_2-BD hard blocks, the first melt at 175°C has a enthalpy of 2.6 J g^{-1} and the second melt at 224°C has a melting enthalpy of 0.5 J g^{-1}. BD has resulted in a net increase in the crystallisable component of the hardsegment. Chain-extender BD has two hydroxyl groups separated by three carbons which is the same as DEPD however, only a single methyl pendent group is present and this will have a lesser steric influence on the hard-segment packing than the two ethyl groups of DEPD. When PD is used the first melting endotherm occurs at 170°C for an enthalpy of 1.9 J g^{-1}. The second melting endotherm is observed at a higher temperature of 247°C for an enthalpy of 3.0 J g^{-1}. PD has the largest net melting enthalpy and is consistent with the literature as it is the shortest chainextender. A short chain length and low steric hindrance promotes packing and crystallinity within the hard-segment which helps deliver reinforcement to the microphase structure.[22,23]

Returning to the argument made by Ryan et al. who states that precipitation of the chain-extender within the hard-segment directly affects the packing arrangement and the ability to crystallise is consistent with the current data set.[21] Also contributing towards the disruption of hard-segment packing is the triol chain-extender TMP which was kept constant at 15 mole% of the total chain-extender content. Work by Petrović et al. reported that incorporation of TMP into the hard-segment resulted in a decrease in crystallinity due to the introduction of inhomogeneity within the packing arrangement.[20] It was reported that when a TMP mole% of 15% or greater is used, the hard-segment crystallinity was compromised. From the DSC data collected on the current adhesive set (MDI and PPG) it is clear that TMP has influenced the hardsegment packing (prepolymers of MDI with TMP observed in MALDI-MS spectra and as a result these will contained within the hard-segment of both urethane/urea).
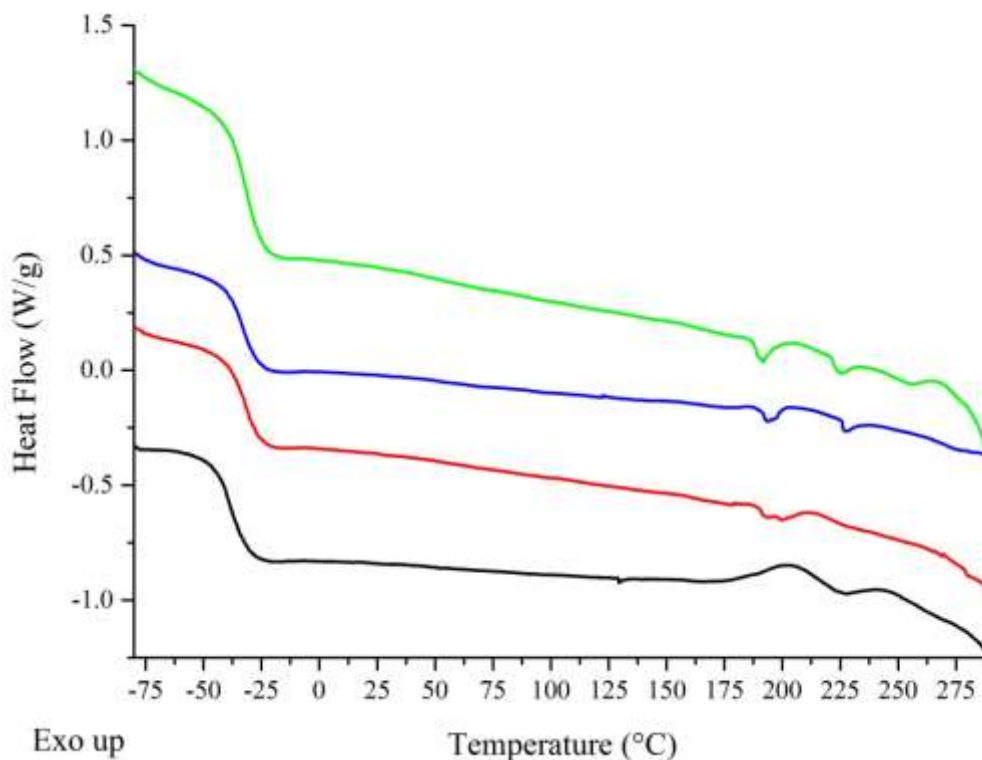
Figure 8.02: Stacked DSC thermograms for PU-U adhesives based on MDI and PCD. [MDI-TMP-PCD in black, MDI-TMP-PCD-DEPD in red, MDI-TMPPCD-BD in blue and MDI-TMP-PCD-PD in green].

As mentioned hard-segment length will contribute towards the packing arrangement within segmented polyurethanes. Based on the stoichiometry used during synthesis which was set a NCO:OH ratio of 2.2:1.0, small hard-segments would be expected. The hard-segment length will be composed of two/three MDI units coupled to the diol/triol chain-extender giving an average segment weight of 667 for the adhesive chain-extended with DEPD (631 for BD and 619 for PD). Packing of these small hard-segments will be poorer than that of long hard-segments; this combined with the disruption in the hard domains by TMP will contribute to the reduced hardsegment packing and crystallinity compared to TMP free formulations.[26] Mixing of the hard and soft-segment will be enhanced by the short block length as there will be less steric constrains on the penetration of short hard blocks into the soft-segment compared with long hard blocks. As the hard-segment content is effectively the same in each of the four formulations (mass of the diol chain-extender accounts for differences) any

475

differences in the morphology will originate from the diol chainextenders influence on the hard-segment packing arrangement.

Presented within figure 8.02 are the DSC thermograms of the fully cured PU adhesives based on MDI and PCD. These thermograms are of the second heating cycle for each cured adhesive. 2000 molecular weight PCD is used which reduces the hard-segment content compared to PPG based adhesives (decreases from 40 wt% to 25 wt%). PCD is a semi-crystalline soft-segment that has a $T_g$ss of -64°C covering a range of 9°C from -67°C to -58°C. Also present within the PCD thermogram is a melting endotherm at 50°C with a melting enthalpy of 57 J g^{-1}.

Adhesive formulation MDI-TMP-PCD which contains only the triol chain-extender TMP displays a shift in the $T_g$ss of +24°C to -40°C compared to PCD. The recorded glass transition covers a greater range than PCD (13°C from -44°C to -31°C) which is inherent of hard block aggregation formed in the microphase structure and the addition constraints they apply. Within the microphase structure will be isolated hard-segments which will act as physical anchoring points and thus reducing the motion of the soft-segment chains. This anchoring effect occurs at the hard-soft domain boundary and will raise the $T_g$ss. Also contained within the microphase structure will be regions of mixed hard and soft-segments which introduce addition conformational constraints which will broaden the range of the $T_g$ss.

Following diol chain-extension further elevation of the $T_g$ss is observed, with -31°C reached for DEPD, -33°C for BD and -32°C for PD. Similar to PPG based formulations, chain-extension has elevated the $T_g$ss as the microphase structure has become more phase mixed. Also evident is that each chain-extender results in a considerable shift in the $T_g$ss of around 10°C. This shift displays that urethane based hard-segments introduced by diol chain-extension mix better than urea based hardsegments formed during moisture cure (see TMP only formulation). This conclusion is drawn as formulations that contain diol chain-extenders will contain less free isocyanate (compared to TMP only formulation) and during moisture cure less urea groups will be formed. Each diol chain-extender possesses either a pendent methyl or ethyl group which will have a disruptive within the hard-segment. As each

diol chain-extended formulation will have a higher ratio of urethane-to-urea and each has a higher $T_g$ss it supports the hypothesis of disruption within the hard-segment resulting in greater phase mixing.

In the first heating cycle of MDI-TMP-PCD a melting endotherm of the soft-segment at 47°C is present which accounts for a melting enthalpy of 8.6 J g^{-1}. The depression of the melting point of the soft-segment within the PU-U network follows the classic theory of melting point depression of copolymer systems.[27,28] Dissolution of hardsegment impurities within the soft-segment will lower the melting temperature and reduce the enthalpy of melting as inhomogeneity now exists in the soft-segment crystalline packing arrangement. These imperfections in the crystalline order will affect the hydrogen-bonding involving ester carbonyl groups leading to a less tightly packed network and a reduction in crystallinity.

The formation of hard-segments by urethane or urea groups will contain stronger attractive forces (hydrogen-bonding and π-π stacking) compared to that of the esters in the soft-segment.[28] In a paper by Yilgor et al they determined by means of DFT calculations that hydrogen bond strength was of the order urea-urea (58.5 kJ mol^{-1}) > urethane-urethane (46.5 kJ mol^{-1}) > urea-ether (29.4 kJ mol^{-1}) > urethane-ester (23.6 kJ mol^{-1}).[29] This data supports the hypothesis present that urea will form stronger hydrogen bonds within the hard-segment compared to urethane but also display that both urethane/urea will form stronger hydrogen bonds with the polyether/ester softsegment.[16] Melting endotherms of the soft-segment were not observed for any of the chain-extended formulations which further supports the hypothesis that chainextension encourages phase mixing. It also further strengthens the argument that urethane hard-segments formed by diol chain-extenders mix better with the softsegment than the urea hard-segments.

For the current application the removal of soft-segment crystallisation is beneficial. The mixing of small blocks of hard-segment into the soft-segment is what is termed good phase mixing. Good phase mixing is the ability to have miscibility phases which disrupt large domain formation and therefore stop light scattering (domains either really small e.g. < 100 nm or very large e.g. mm in size). The net result is that all

features are either too small or large to scatter visible light giving an optically clear material.

Within the DSC thermograms of all formulations no glass transition of the hardsegment is visible (based on the literature would be expect between 70°C – 100°C). Failure to observe the glass transition within this set of formulations will be due to the weak nature of this transition and as a result of the low hard-segment content. Observation of the glass transition from hard-segments will become more difficult with increased phase mixing as the transition will become broader and weaker. This will be influenced by the short hard-segment length distribution and the size distribution of the hard-segment domains.[19] The absence of the hard-segment glass transition further displays the complexity of such PU-U systems.
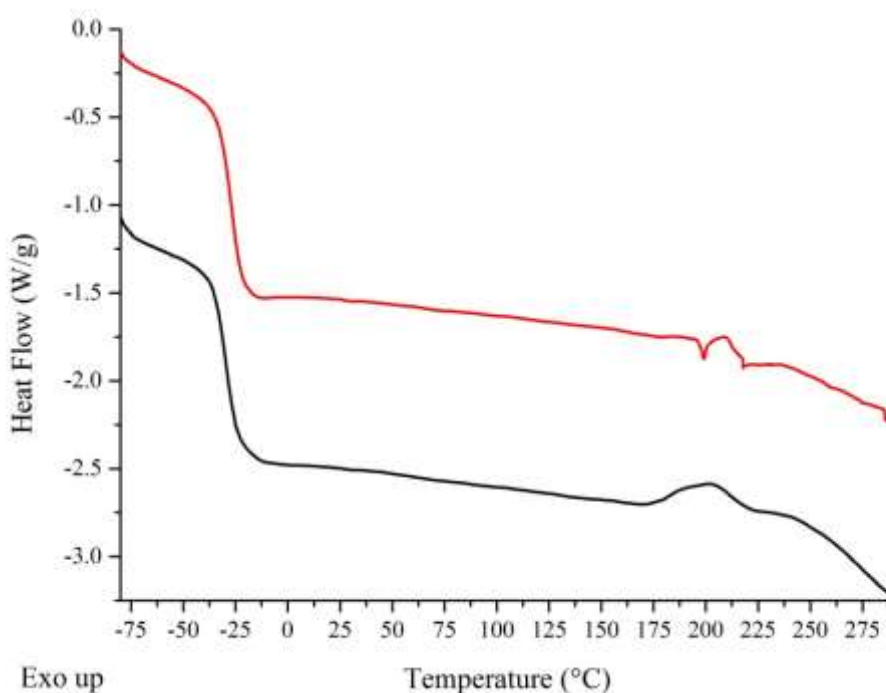
Figure 8.03: Stacked DSC thermograms for PU-U adhesives based on MDI and PDEGA. [MDI-TMP-PDEGA in black and MDI-TMP-PDEGA-DEPD in red]. Hard-segment melting endotherms within PCD based formulation was observed in all three diol chain-extended formulations but not in MDI-TMP-PCD. Each has comparably sized melting endotherms which was attributed to the degree of phase

mixing being similar. Within the TMP only formulation (MDI-TMP-PCD) a single exothermic curing peak is observed at 205°C for an enthalpy of cure 2.8 J g^{-1}. This residual curing peak is smaller than was previously observed for MDI-TMP-PPG and was attributed to the lower hard-segment content.

Following the introduction of diol chain-extenders, the hard-segment melting pattern was observed. In the formulation that contained DEPD which thus far has displayed the greatest influence on hard-segment morphology two melting endotherms are observed at 177°C and 193°C. The first melt occurs at 177°C and has a melting enthalpy of 0.2 J g^{-1}. Further indication that the presence of DEPD within the hardsegment influences the morphology is presented by the temperature of the second melt (193°C) and its small enthalpy (0.7 J g^{-1}). This result is consistent with previous data (MDI-TMP-PPG-DEPD) which displayed a depreciation in the melting character when DEPD is used as the diol chain-extender.

Chain-extension using diol BD results in an increase to the melting temperature of both melts which now occur at 193°C and 227°C respectively. As higher melting temperatures for the hard-segments in this formulation were obtained it displays that the domains are more intimately packed with respect to DEPD. However this is coupled with smaller melting enthalpies (0.6 J g^{-1} and 0.4 J g^{-1}) of the two melting peaks, indicating that the total hard-segment crystalline component has reduced compared to the TMP only formulation. For the final formulation within this PCD set, the hard-segment melting character is further complicated by the addition of a third peak. Both the first and second hard-segment melting endotherms in the PD chain-extended formulation display similar melt temperatures and enthalpies compared to BD ($T_{mh}1$ 192°C/0.6 J g^{-1} and $T_{mh}2$ 223°C/0.4 J g^{-1}). The third melting process which occurs at a higher temperature of 255°C will represent hard domains that consist of a highly packed well-ordered network.[7] As PD is the smallest and least hindered of the chain-extenders this is consistent with previous observation within this report and the literature.[19,20]

Presented within figure 8.03 are the DSC thermograms from the second heating scan of formulations based on MDI and PDEGA. Polyester PDEGA is fully amorphous as

it only displays a glass transition at -49°C (range of 3°C from -51°C to -48°C) with no melting peak. This polyester was implemented to determine the polyurethane morphology when the soft-segment has both ester and ether character.

The molecular weight of the soft-segment is 2500 which further reduces the hardsegment content to around 20 wt% (PPG based 40 wt% and PCD 25 wt%).

An elevation of the $T_g$ss by +19°C to -30°C was observed for the TMP only formulation (MDI-TMP-PDEGA). As the glass transition following polymerisation (and cure) covers a narrow range of 9°C it shows that the degree of phase separation is greater than in previous MDI based formulation. Reducing the hard-segment content will have had an influence on the microphase morphology being more phased separated.[4] Following chain-extension with DEPD the $T_g$ss increased by +4°C to -26°C. This was accompanied by a broadening of the glass transition range which displays that the morphology is now more mixed. Increased phase mixing is consistent with previous result within this chapter as the diol chain-extension improves the miscibility of the phases. This result displays that phase mixing occurs irrespective of the soft-segment functionality (although notably to varying extents) and therefore originates from the hard-to-soft-segment compatibility. Soft-segment molecular weight will influences the hard-segment content and will therefore have an influence on the final morphology of the polyurethane copolymer network.[30] This makes the observed phase separation/mixing a gauge of the compatibility of the two segments. Also consistent is that having more urethane or less urea enhances phase mixing in MDI based formulations.

Investigation of the hard-segment morphology based on the melting endotherms for both PDEGA adhesives displayed varying results (see heat flow/derivative versus temperature plots in appendix A). When TMP is the sole chain-extender a single curing exotherm is observed at 202°C. This curing event has a lowest enthalpy of cure at 2.4 J g^{-1} and this is consistent with this formulation having the lowest hardsegment content. Following the introduction of the diol chain-extender DEPD, the hard-segment melting character is observed in the form of three peaks at 174°C, 199°C and 218°C. The data collected on these formulations based on PDEGA with MDI follow

the same trends observed in PCD and PPG. The main trend established for MDI based formulations based on DSC analysis is that when both diol and triol chain-extenders are used the morphology of the PU-U becomes more mixed. Also established is that MDI hard blocks formed by diol chain-extension mix better with the soft-segment than hard blocks of urea. This greater miscibility of small hardsegments into the soft-segment will reduce the potential of forming ordered feature which will scatter visible light and therefore increase the likelihood of forming a clear final material.

8.12 Discussion of the Morphology in Aliphatic Polyurethane Adhesives

Formulations within this section were prepared in a similar synthetic procedure (see section 2.03 for procedure) to MDI based formulation. Again three soft-segments were used with TMP only and TMP plus diol chain-extended formulations giving 10 different adhesive for application. Introduction of IPDI into each formulation was the parameter of interest. Moreover the effect that this new hard-segment has on the morphology and adhesion properties were especially of interest. IPDI was used over another aromatic isocyanate as it possesses better UV stability and will give each formulation lower inherent viscosity which will assist application.

Presented within figure 8.04 are the DSC thermograms obtained during the second heating scan for all four formulations based on IPDI and PPG. The accompanying thermal data for these thermograms is presented within table 8.02. The $T_g$ss of PPG occurs at -70°C and covers a narrow range of 2°C. In formulation IPDI-TMP-PPG a low temperature glass transition for the soft-segment is visible at -33°C. The position of the glass transition has shifted by +37°C with respect to PPG and has also become broader as the range now spans 21°C from -41°C to -20°C. This considerable shift and broadening of the glass transition is a characteristic sign of phase mixing within the microstructure. Based on the hard-segment content and the polyether polyol used within this formulation it is consistent with similar polymers within the literature.[10]

Following the introduction of diol chain-extenders no considerable shift in the glass transition was observed with -32°C obtained for DEPD, -32°C obtained for BD and 33°C obtained for PD. However, the range of each has become broadened (see table

8.02). This result is an initial indication that the compatibility of the aliphatic hardsegment with the soft-segment is poorer than in previous MDI based formulations.

Table 8.02: Table of DSC data for IPDI based PU-U adhesives.

Formulation	HS wt%	$T_g$ss /°C	Range /°C	$T_g$hs /°C	$T_m$ss* /°C	Enthalpy /J g^{-1}	$T_m$hs1 /°C	Enthalpy /J g^{-1}	$T_m$hs2 /°C	Enthalpy /J g^{-1}
PPG	-	-70	-71 to -69	-	-	-	-	-	-	-
IPDI-TMP-PPG	33.8	-33	-41 to -20	93	-	-	169	0.4	233	2.1
IPDI-TMP-PPG-DEPD	39.3	-32	-41 to -15	-	-	-	-	-	202	0.1
IPDI-TMP-PPG-BD	37.7	-32	-42 to -21	-	-	-	177	0.2	210	0.3
IPDI-TMP-PPG-PD	37.1	-33	-42 to -23	-	-	-	-	-	253^x	4.2
PCD	-	-64	-67 to -58	-	50	57	-	-	-	-
IPDI-TMP-PCD	20.4	-52	-55 to -45	81	50	28	197	0.2	238	0.2
IPDI-TMP-PCD-DEPD	24.5	-47	-51 to -38	79	44	9	206	1.0	227	0.2
IPDI-TMP-PCD-BD	23.2	-48	-52 to -40	89	46	23	193	1.4	208	0.1
IPDI-TMP-PCD-PD	22.8	-48	-52 to -41	-	45	18	196	1.0	211	0.1
PDEGA	-	-49	-51 to -48	-	-	-	-	-	-	-
IPDI-TMP-PDEGA	17.0	-38	-42 to -36	-	-	-	199	2.0	235	0.1
IPDI-TMP-PDEGA-DEPD	20.6	-38	-41 to -36	-	-	-	207	1.2	229	0.1

*obtained on first heating cycle, $T_g$ss = soft-segment glass transition temperature, $T_g$hs = hard-segment glass transition temperature,

$T_m$ss = melting endotherm soft-segment, $T_m$hs = melting endotherm hard-segment, ^{x} = curing exotherm

This result was somewhat surprising based on previous results of MDI formulations where urethane hard-segments mixed better with the polyether soft-segment than urea hard-segments. Possibly the reduction in mixing and smaller shift of the glass transition with the incorporation of diol chain-extenders is due to the less polar hardsegment formed. A reduction in the polarity will reduce the compatibility with the polar polyether soft-segment and reduce the degree of mixing. It would be expected based on the structure of the isocyanate that the hard blocks will be less ordered compared to MDI due to the steric configuration of the non-planar isophorone ring which would be anticipated to pack less tightly. This is accompanied by the forfeit of π-π stacking by going to an aliphatic system.

If the hard blocks are indeed more asymmetric it could possibly mean that the volume that the hard block occupies is larger reducing their ability to penetrate the soft-segment. Considering the above arguments that the hard blocks are less ordered due to the removal of π-π stacking interactions and the non-planar geometry of the isocyanate hard blocks reducing their packing, hard blocks within these formulations could be described as having greater "flexibility" (less constrained). This greater "flexibility" will in turn reduce the stiffening effect that the cross-linked hardsegments have on the soft-segment. Soft-segment chains will therefore have greater mobility as the conformational constraints will be less resulting in the elevation of the $T_g$ss being reduced.

Observed in the triol only chain-extended formulation was the $T_g$ss and two further weaker thermal transitions. The first of these weak thermal transitions occurs at 27°C, this transition can be observed more clearly in the first derivative plot of the DSC thermogram (see appendix A) and appears to be some form of hard-segment dissociation/relaxation. Hard-segments which are highly disordered are considered to be the origin of this transition and may possibly be the result from hard blocks which contain the TMP chain-extender or it may be the thermal transition of the hard-to-soft domain interface. The next weak glass transition at 93°C is ascribed to ordered hard-segments which in this formulation will most probably contain urea groups formed during moisture cure. This value is within the range occupied for the glass transition of a pure hard-segment and further shows the complexity of polyurethanes.

Observation of the hard-segment glass transition is the result of the longer curing time in aliphatic systems allowing aggregation. Coupled with this greater curing time is a reduced viscosity which allows greater mobility to the system during cure. This will aid microphase separation as hard and soft-segments will have more time and mobility to aggregate or separate.

Within the three diol chain-extender formulations the aforementioned weak thermal transitions were not observed.[10,23] As these transitions are absent within these formulations, it further complements the argument that having a diol chain-extender of the type presented within this report as part of the hard-segment has a direct influence on the hard-segment morphology and overall PU-U microstructure.

Figure 8.04: Stacked DSC thermograms for PU-U adhesives based on IPDI and PPG. [IPDI-TMP-PPG in black, IPDI-TMP-PPG-DEPD in red, IPDI-TMPPPG-BD in blue and IPDI-TMP-PPG-PD in green].

Further information on the hard-segment morphology can be gained from the position and magnitude of hard-segment melting endotherms. For the TMP only formulation two melting endotherms were observed at 169°C and 233°C. The first and smaller melting endotherm (0.4 J g^{-1}) corresponds to the decomposition of hardsegments which

are highly unordered either through the presence of TMP or as they occur and the hard-to-soft interface. As the second melting peaks is both larger (2.1 J g^{-1}) and occurs at a higher melting temperature will corresponds to the decomposition of hard-segments which possess greater order. Hard-segments that decompose within this process will be a combination of urethane (formed during synthesis) and urea (formed during cure) that are intimately packed forming more cohesive domains. This TMP only chain-extended formulation has a more phase separated morphology than the diol chain-extended formulations.

The above statement is confirmed by viewing not only the reduced hard-segment melting endotherms but also reconsidering the $T_g$ss. Within the DEPD chainextended formulation only a single melting endotherm is observed at 202°C, this transition also has a reduced enthalpy of melting (0.1 J g^{-1}). This formulation also has the greatest $T_g$ss range (26°C) and is absent of any hard-segment glass transition character.

When BD is used as the chain-extender two hard-segment melting endotherms are observed at 177°C and 210°C. Both melting endotherms have small enthalpies of melting at 0.2 J g^{-1} and 0.3 J g^{-1} respectively. The position and magnitude of these melting endotherms coupled with the absence of any hard-segment glass transition displays that the microphase structure is considerably mixed. When PD is used the hard-segment is different as a single exotherm is observed at 252°C. At 4.2 J g^{-1} this exotherm is small and is believed to be sure of residual free isocyanate groups within the material. As this formulation possesses a lower $T_g$ss it identifies greater phase separation compared to DEPD or BD based formulations. Overall based on the hardsegment content and the polyol, the overall morphology will contain both separated and mixed domain structures.

To further probe the behaviour of IPDI based hard-segments and their influence on the overall PU-U morphology, the soft-segment PCD will next be discussed. As the molecular weight used is 2000 it will reduce the overall hard-segment content to 25 wt% and also reduce the amount of TMP and diol chain-extender added (see section 2.03). All second heat DSC thermograms for formulations containing IPDI and PCD are contained within figure 8.05 with the accompanying thermal data in table

8.02. As PCD is a semi-crystalline polymer the position of melting peak and size of the endotherm can also be used a means to investigating the morphology.

Firstly considering the $T_g$ss which is a known way of investigating the morphology, PCD has a $T_g$ss of -64°C which covers a range of 9°C (from -67°C to -58°C). A shift in the position of the $T_g$ss to -52°C is observed for IPDI-TMP-PCD and the glass transition occupies a similar range of 10°C. Following the introduction of diol chainextenders into the formulation, a shift of around +5°C is observed for each $T_g$ss with -47°C reached for DEPD, -48°C for BD and -48°C for PD. Introducing more urethane groups into the formulation through diol chain-extension encourages mixing of the phases (also observed for MDI based materials). This observation is further supported by the broadening of the glass transition range in each case. As the hardsegment content is lower in PCD based formulations the conformational constraints from hard-segment will be reduced compared to PPG. This in turn will be coupled with a reduced overall effect on the $T_g$ss value.
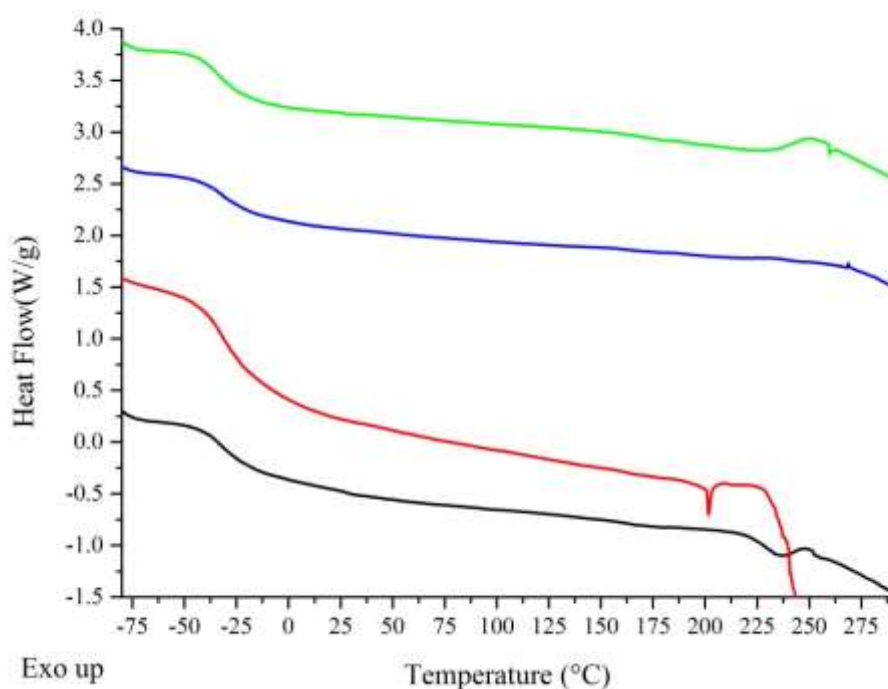

Figure 8.05: Stacked DSC thermograms for PU-U adhesives based on IPDI and PCD. [IPDI-TMP-PCD in black, IPDI-TMP-PCD-DEPD in red, IPDI-TMPPCD-BD in blue and IPDI-TMP-PCD-PD in green].

Observed on the first heating scan only of each formulation is a soft-segment melting endotherm. PCD has a melt which occurs at 50°C with an enthalpy of 57 J g^{-1}. In the first adhesive IPDI-TMP-PCD, the position of the melting endotherm does not shift and remains at 50°C, however, the enthalpy is reduced to 28 J g^{-1}. As the melt position is unchanged and with reference to the classical depression of melting point for copolymers systems the morphology within this system is phase separated.[27,28] Considering that the enthalpy has almost halved it displays a reduction in the overall crystalline order within PCD, however, this would be expected due the addition constraints on the soft-segment chains from the anchoring of the hard-segments. This point is clarified previously by the observation of the elevated $T_g$ss.

Identified from the position of $T_g$ss is that urethane hard-segments mix better with PCD than urea hard-segments. This observation is further supported by the position and enthalpy of the soft-segment melt which both decrease. In DEPD which has been identified as the diol chain-extender which has the greatest influence on the morphology, the observed melt occurs at 44°C for a reduced melting enthalpy of 9 J g^{-1}. Depreciation of the melting point by 6°C confirms migration of the hardsegment into the soft-segment, reducing the purity. A more phase mixed morphology is consistent with what is observed in the $T_g$ss of IPDI-TMP-PCDDEPD. A similar scenario is observed for BD and PD chain-extended formulations. Both display a lower melt temperature and a reduced enthalpy compared to pure PCD however, to a lesser extent than DEPD. Observation of the depressed melting point is further evidence that urethane based hard-segments mix better with the softsegment than urea hard-segment.

Based on the proposed phase separated structure both a hard-segment glass transition and melting should be present. A hard-segment glass transition was observed in all formulations with the exception of PD. The observed hard-segment glass transitions covered a range of 79°C to 89°C and were very weak. Plotting the first derivative of the heat flow versus temperature was required for successful identification (see appendix A). Glass transitions within this range were of "pure" hard-segment domain. Also observed on the thermogram is a lower temperature glass transition in all formulations except that of BD (TMP only 33°C, DEPD 25°C and PD 27°C) which

will display either highly unordered hard-segments or possibly the glass transition of the soft-to-hard interface (based on position). Glass transition behaviour of hard-segments within PU-Us is rather complex, which will be further complicated by the presence of urethane, urea and urethane-urea hard domains within these samples.

Hard-segment melts were observed for all four formulations. In the TMP only formulations two melting peaks are observed at 197°C and 238°C which are both broad plus weak broad (0.2 J g^{-1} and 0.2 J g^{-1} respectively). As the first melting peak occurs at a lower temperature, the hard-segment packing will be more disordered than of the hard-segments which melt at a higher temperature. The lower temperature melting peak will contain hard-segments which are constructed of urethane blocks from the prepolymer plus chain-extension with TMP and as a consequence of the triol chain-extenders presence will be highly unordered. The higher temperature melt will be constructed mostly of urea and will have a higher degree of order however; ATR evidence will be required to support this hypothesis and determine the order of the urea (see section 8.22).

Following diol chain-extension, the hard-segment melting character appears different. For each formulation two peaks were again observed however, they were both of different peak shape. A lower temperature small broad peak is now replaced with a small sharp peak which occurs at 206°C for DEPD, 193°C for BD and 196°C for PD. Introducing more urethane groups via diol chain extension has resulted in an increase in the lower melting peak and confirms that this peak represents urethane based hard blocks. As the peak shape is sharp it displays that chain-extension has promoted packing within these formulations. Greater packing within these systems may result from the lower compatibility of the hard and soft-segment. This coupled with the longer cure time and lower viscosity will potentially promote order as greater time and mobility for structural organisation will be available. At higher temperature the melting endotherm remains unchanged following diol chainextension and is consistent with being responsible for urea based hard-segment. Assignment of the high temperature melts based on the microstructure within the hard-segment will be further discussed in the following section where ATR analysis will be considered.

The final variation within this section is adhesives based on IPDI and PDEGA. PDEGA is a non-crystalline soft-segment with a $T_g$ss of -49°C which covers a range of 3°C. The molecular weight of the soft-segment is the greatest of all the softsegments tested at 2500. This increase in molecular weight reduces the hardsegment content to 20 wt% and it is anticipated that this will drive the microphase structure towards being phase separated. This is due to the hard-segment having a lower contribution to the overall segmented structure by weight and previous analysis which displays the lower miscibility of IPDI based hard-segments. Phase separation will be determined by the compatibility of the two segments and will be determined by DSC.
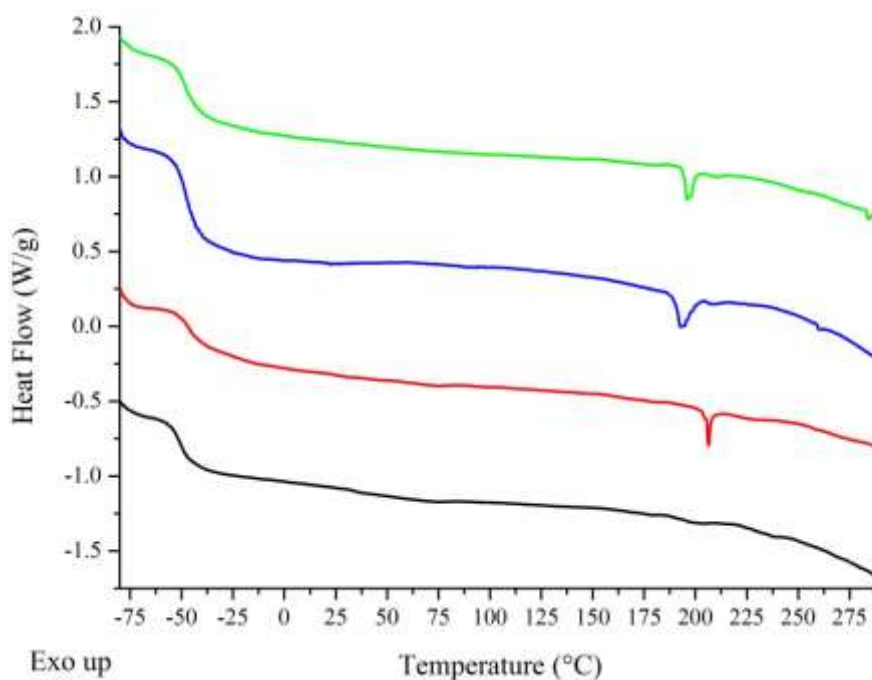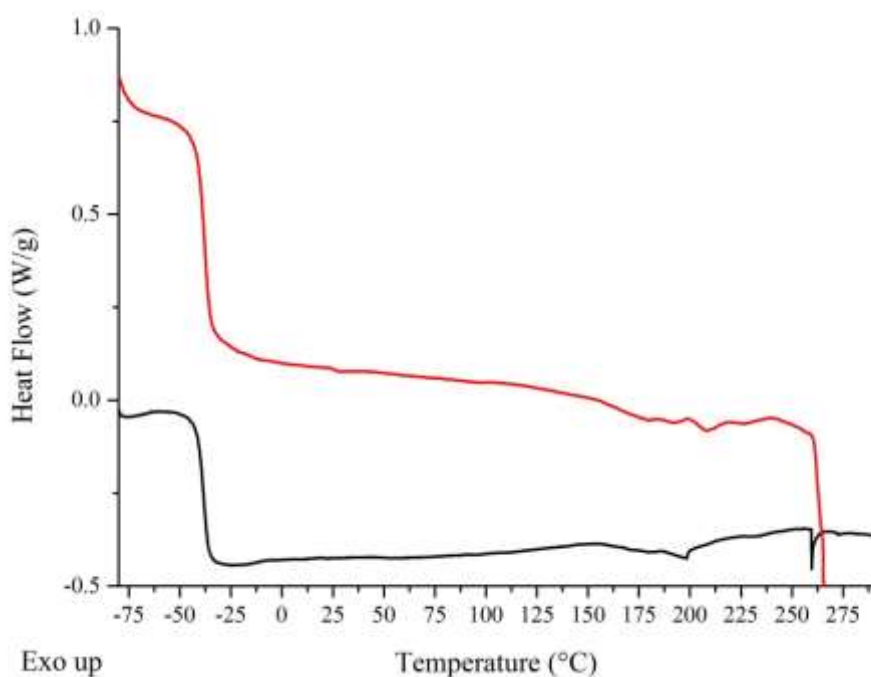

Figure 8.06: Stacked DSC thermograms for PU-U adhesives based on IPDI and PDEGA. [IPDI-TMP-PDEGA in black and IPDI-TMP-PDEGA-DEPD in red].
From inspection of figure 8.06 which contains the DSC thermograms of both PDEGA formulations, it is clear that the glass transition of the soft-segment is not markedly changed following diol chain-extension with both occurring at -38°C.

PDEGA has a $T_g$ss of -49°C which only shifts +11°C following polymerisation and in both cases a relatively narrow range of 6°C was obtained. Both small differences point towards a phase-separated morphology. This data displays an incompatibility between

the hard and soft-segments regardless of the composition (urethane or urea) which results in a phase separated structure.

Observation of the glass transition from the hard-segment was not possible in both formulations. Absence of this thermal transition will result from the reduced hardsegment content which will make the thermal event very weak and difficult to observe. A weak thermal transition at 25°C was observed in IPDI-TMP-PDEGADEPD (see appendix A) which may be the glass transition of the hard-to-soft interface.

In each formulation two broad endotherms are observed from the hard-segment. In IPDI-TMP-PDEGA these two peaks are visible at 199°C and 235°C with enthalpies of melting 2.0 J g^{-1} and 0.1 J g^{-1} respectively. Of the two peaks the first is especially broad (onset 162°C) and will possibly be composed of more than one type of hardsegment decomposition. For the diol chain-extended formulation two peaks were also observed at 207°C and 229°C for melting enthalpies of 1.2 J g^{-1} and 0.1 J g^{-1} respectively. The first melting peak was also very broad (onset 160°C) and will also contain more than one hard-segment decomposition. As the hard-segment content is much reduced (versus PPG and PCD) the presence of the chain-extender in the hardsegment is having a reduced effect resulting in a similar melting character in each. Due to the observed complexity in the melting endotherms inherent of the hardsegment assignment was difficult. This aside it would be expected that the lower temperature endotherms will be inherent hydrogen bond decompositions of more disordered domains possibly containing TMP and urethane with the higher temperature melt correspond to hydrogen bond decomposition of more ordered domains possibly containing urea.

8.13 Comparison of the Morphology in Aromatic and Aliphatic Polyurethane
Adhesive Based on Thermal Analysis

It is apparent from the DSC analysis performed on each PU-U adhesive that the final morphology is highly depended on the hard and soft-segment composition. Other parameters such as the synthetic procedure, thermal history and curing conditions will also affect the final morphology. As these parameters were similar in both sets, any

difference in the morphology should reflect the chemical compatibility of the segments.

Identified from DSC analysis of all twenty formulations is that a hard-segment consisting of IPDI leads to a more phase separated morphology than hard-segments consisting of MDI regardless of chain-extender. Possible factors that may influence this observation are viscosity, cure time, segment compatibility and domain size/adhesion. Within MDI based formulations the viscosity was higher in all cases and a result required higher application temperatures. Upon cooling the mobility within MDI-TMP-PPG would be lower than with IPDI-TMP-PPG for example as a result of the higher viscosity. Even though both formulations are operating above the $T_g$ss, the mobility of the MDI based system will be more limited. This higher viscosity may also reduce the moisture diffusion into the adhesive and to the reactive end groups; however, this would require further experimentation to prove.

Curing time will also affect the morphology of the final adhesive. MDI based formulations have a shorter curing time compared to IPDI based formulation and as a result will reach their gel point quicker. Once above the gel point the viscosity of the matrix will be much higher and will reduce the mobility of the system. This increased viscosity will perturb the migration and aggregation of hard-segments resulting in the morphology of the system being more mixed with MDI formulations.
From the DSC analysis obtained this would appear a possible explanation.

What drives this domain aggregation or phase separation will be governed by the compatibility of the two segments. Based on the DSC analysis obtained on the above systems, urethane containing hard-segment formed during the diol chain-extension step have a greater compatibility with the soft-segment in all cases compared to urea (and this is best observed in polyether based formulations). MDI based hardsegments have a higher polarity (also have greater scope for intermolecular interactions through π-π stacking) than the aliphatic IPDI based hard blocks and this will enhance the likelihood of these blocks mixing with the polar soft phase. The fact that urea based groups phase separate more than urethane (see $T_g$ss in table 8.01 and 8.02) displays that the adhesion between urea groups is greater than in urethane groups. This means that urea groups will tend to aggregate with one another over mixing.

Hard-segment domain size and adhesion will also be influenced by the three above parameters. When the viscosity is low, the cure time is long and the compatibility/difference in polarity is high, the resultant microphase morphology should be phase separated. If domain adhesion is high due to hydrogen bonds and $\pi\pi$ stacking interactions as in MDI the size of the domain should be smaller due to more intimate packing. Conversely these well packed domains are larger as the addition attractive forces (both hydrogen bonding and π-π stacking) pull more molecules into the cluster. Smaller hard-segments will be able to penetrate the softsegment more readily that the larger more hindered domains that IPDI will form. The amount of penetration or mixing will again be limited by the mobility within the system and the compatibility of the two segments. For the formulations within this report it would appear that MDI based segments will be both smaller (size not length) and have a greater compatibility with the soft-segment compared to IPDI.
Combined with the other factors mentioned this will result in the greater mixing.

When phase separation is high, the reinforcement of the adhesive matrix will be higher compared to phase mixed and the conformational constraints introduced on the soft-segment are less. Material of this type will be both strong and flexible. From DSC analysis it can be observed that IPDI based hard-segments lead to a more phase separated morphology than hard-segments containing MDI. Explaining this phase morphology in PU-Us is difficult as it will be influenced by a variety of different factors however, it appears to originate from the more polar MDI blocks mixing better than the less polar IPDI blocks. Investigation of the morphology of PU-U using DSC is a common technique with thermal transitions such as the $T_g ss$, $T_g hs$, $T_m ss$ and $T_m hs$ presenting information on the morphology. Obtaining information such as this has highlighted that the microphase structure in such systems is complex and DSC analysis alone is not sufficient to solve the morphology. Considering this argument it is not possible at this point to form a robust relationship based on the morphology and adhesion. That said it would appear from this initial analysis that the more phase separated the morphology, the greater the adhesion with the interface. This will be discussed further following subsequent ATR analysis which will help to further clarify the microphase morphology.

8.20 Morphology of Polyurethane Adhesives Based on Attenuated Total Reflectance Fourier Transform Infra-Red Spectroscopy
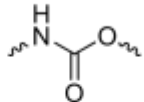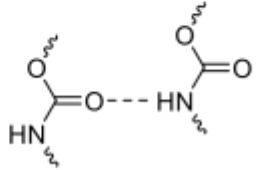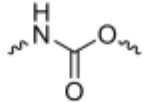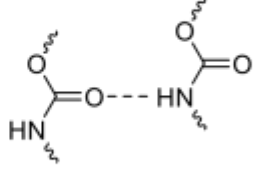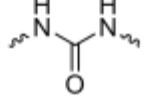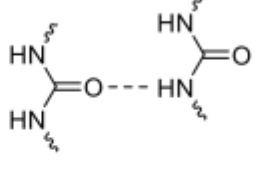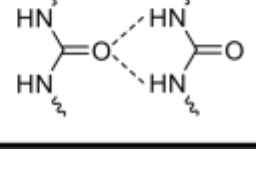
The use of FTIR in conjunction with DSC as a means of investigating the morphology of PU-U systems is a common method.[13,15] Furthermore investigation of both the N-H and C=O bands as a means of determining the microstructure are also extensively used.[31] Investigation of both these bands will be presented within this section with the peaks position and shape of most interest as it these will give an indication of the order within the hard-segment of the adhesive.

8.21 Discussion of the Morphology in Aromatic Polyurethane Adhesives

Within PU-U block copolymer systems hydrogen bonding plays an important role in determining the microphase morphology of the system. Hydrogen bonding is not the sole influencing factor in determining the morphology but can have a significant contribution. A combination of factors will have an influence on the PU-Us morphology e.g. compatibility, thermal history, stoichiometry etc. What is useful about hydrogen bonding is that it shifts both the N-H and C=O peaks and when combined together they can detail the microstructure within the PU-U. It is then possible from the position of the N-H and C=O to determine the degree of order or disorder within the PU-U. Hydrogen bonding between N-H and C=O functional groups along with π-π stacking interactions are the driving force behind the formation of hard-segments within both urethane and urea domains.

Within table 8.03 assignment of the possible N-H with C=O interactions are presented and the wavenumber range in which they can occur. Within this table are interactions of either free or hydrogen bonded configurations which display the varying degree of order/disorder. Omitted from the table are the hydrogen bonding interactions which can occur with the soft-segment (ether or ester) via the N-H group (it is these interactions that are responsible for phase mixing). These groups have been omitted from the table as they are often difficult to observe accurately. The NH peak which will be a combination of both urethane and urea will be considered as either free or hydrogen bonded. This peak with also contain an carbonyl overtone which will occur within the range of 3450 cm^{-1} – 3460 cm^{-1}.[29]

Table 8.03: Typical Infrared wavenumber ranges for N-H and C=O groups involved in hard domain formation. [14,21,32,33]

Functional Group	Wavenumber Range (cm^{-1})	Band Structure and Assignment	
Urethane/Urea N-H	3600-3500		Free
Urethane/Urea N-H	3360-3300		Hydrogen Bonded
Urethane C=O	1740-1730		Free Urethane
Urethane C=O	1730-1710		Hydrogen Bonded Urethane
Urea C=O	1710-1690		Free Urea
Urea C=O	1690-1655		Monodentate Hydrogen Bonded Urea
Urea C=O	1655-1620		Bidentate Hydrogen Bonded Urea

Also appearing at lower wavenumbers will be hydrogen bonding interactions between the hard and soft-segments. These interactions will involve the ether oxygen in PPG or PDEGA and the ester group in PCD or PDEGA. Hard-to-softsegment interactions occur at lower wavenumbers and appear in the typical range of between 3290 – 3260 cm^{-1}.[29]

Table 8.04: Deconvolution data of the N-H and C=O peak for each MDI adhesive type obtain using Gaussian fitting function.

Formulation	N-H						C=O					
	Free		C=O Overtone		H-Bonded		Free Ur		H-bonded Ur		Free U	
	cm^{-1}	%	cm^{-1}	%	cm^{-1}	%	cm^{-1}	%	cm^{-1}	%	cm^{-1}	%
MDI-TMP-PPG	3523	8.8	3367	2.5	3312	88.8	1731	15.0	1716	61.3	1681	23.7
MDI-TMP-PPG-DEPD	3515	13.4	3373	11.4	3305	75.2	1732	16.1	1714	72.9	1678	11.0
MDI-TMP-PPG-BD	3530	9.6	3393	3.5	3308	86.9	1732	18.8	1711	76.1	1673	5.1
MDI-TMP-PPG-PD	3532	14.9	3374	9.2	3303	75.9	1732	15.5	1715	74.1	1680	10.4
MDI-TMP-PCD	3540	7.9	3351	36.1	3324	56.0	1728	36.8	1712	56.7	1669	6.4
MDI-TMP-PCD-DEPD	3544	8.9	3346	38.7	3331	52.4	1733	15.2	1721	65.3	1692	19.5
MDI-TMP-PCD-BD	3546	10.5	3346	33.0	3333	56.5	1732	16.2	1721	60.2	1695	23.6
MDI-TMP-PCD-PD	3547	10.0	3345	36.3	3336	53.7	1733	15.2	1721	66.5	1692	18.3
MDI-TMP-PDEGA	3534	21.1	3462	1.4	3337	77.5	1728	49.5	1709	48.0	1655	2.4
MDI-TMP-PDEGA-DEPD	3534	22.0	3455	2.6	3338	75.4	1729	54.8	1711	43.5	1672	1.7

Ur = urethane, U = Urea

The above ranges (table 8.04) assigned to each mode of hydrogen bonding are only estimations and in experimentation the interaction will overlap with one another. Using these set ranges it is possible to interpret the degree of order/disorder within the N-H and C=O peaks. Deconvolution is performed by fitting Gaussian peaks to the experimental data and from the fitted data input from each chemical moiety can be evaluated. Peak fitting or deconvolution was performed on both the N-H and C=O peaks of each formulation and the results are presented within table 8.04.
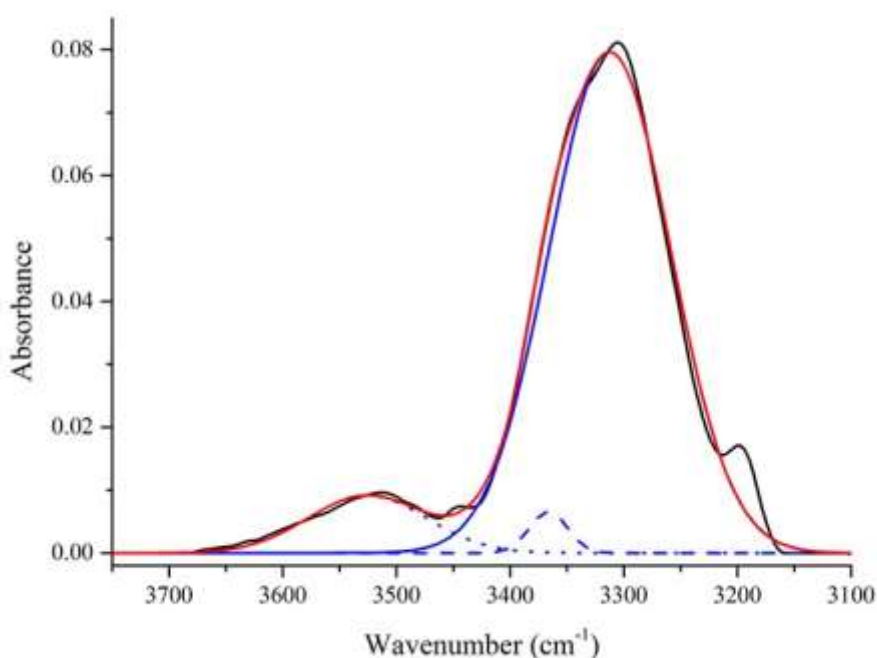
Figure 8.07: Deconvolution data for MDI-TMP-PPG of N-H region (appendix B figure B02). Data calculated using Gaussian fitting function. [Raw data in black, fit data in red, HS-HS fitted peak solid blue, carbonyl overtone dash blue, free N-H Dot and dot dash blue].

An example of the data obtained from deconvolution is shown within figure 8.07 for formulation MDI-TMP-PPG. The fit line obtained (red line) is the summation of the three fitted peaks used to detemine the free N-H, carbonayl overtone and hydrogen bonded N-H.

Deconvolution was performed using OriginPro version 9.0 with Gaussian, Lorentzian and Gaussan-Lorentzian cross functions fitted to identify the best peak fit (see appendix B).

Determined from the analysis was that the Guassian function resulted in the best fit in all cases. This was based on the confidence of fit (or R^2 value) obtained along with the standard errors calculated for both the peak position and peak area. During peak fitting of the N-H region only three peaks were fitted, one for hydrogen bonded groups, one for the carbonyl overtone and one for free groups. In fitting the carbonyl peak a similar procedure was used with three peaks fitted to account for free urethane, hydrogen bonded urethane and free urea.

Figure 8.08: Stacked spectra from N-H region of fully cured PU-U adhesives based on MDI and PPG. [MDI-TMP-PPG in black, MDI-TMP-PPG-DEPD in red, MDI-TMP-PPG-BD in blue and MDI-TMP-PPG-PD in green].

Presented within figure 8.08 are the isolated N-H peaks from each of the four PU-U systems based on MDI and PPG. Observation of both the peak shape and position for each N-H group it is clear that the hard-segment organisation is similar in all formulations. This similarity is consistent with previous DSC analysis which identified that each adhesive displayed phase mixing (diol chain-extension increased the amount of phase mixing) in all cases.

Figure 8.09: Stacked spectra from N-H region of fully cured PU-U adhesives based on MDI and PCD. [MDI-TMP-PCD in black, MDI-TMP-PCD-DEPD in red, MDI-TMP-PCD-BD in blue and MDI-TMP-PCD-PD in green].

The position of the peak ascribed to hydrogen bonded N-H groups is similar in each case ranging between 3307 cm^{-1} – 3300 cm^{-1} (values obtained for fitted data see table 8.04). The hydrogen bonding interactions represented here are those of N-H groups within the hard-segments of the microstructure. Peak fitting was based around obtaining the peak position of hard-to-hard interactions however; it is noted that within the peak area obtained there will be a contribution from hard-to-soft interactions. These interactions must be occurring to support previous data obtain by DSC that displays both a broadened and elevated temperature soft-segment glass transition (see section 8.11). Consumption of most N-H groups via hard-to-hard and hard-to-soft interactions is also displayed by the small amount of free groups available. The ratio of hydrogen bonded to free groups is 7:1 which would be expected within a phase mixed material. Any remaining free N-H groups will assist with the adhesive application of these PU-U systems however; this will be discussed further in a later section (see section 8.31).

Following the introduction of PCD the shape of the hydrogen bonded N-H peak is altered as shown in figure 8.09. This change in shape is the results of the greater contribution from the carbonyl overtone following the introduction of the ester softsegment. Estimation of the contribution from the carbonyl overtone by deconvolution displays values ranging from 44.6% to 47.3%. This would appear to be an over-estimation, however; it is consistently large in each case. Also evident is a shift of the N-H peak position to higher wavenumbers (3327 cm^{-1} – 3319 cm^{-1}) indicating that the contribution from phase mixed N-H groups is smaller. Reduced mixing is also consistent with previous DSC analysis for PCD based formulations and will increase the wavenumber value obtained as it will be more representative of hard-to-hard hydrogen bonding interactions (contribution from hard-to-soft-segment interactions will be reduced).

The ratio of hydrogen bonded to free N-H groups for these formulations is lower than PPG based materials and is around 4:1. The lower ratio obtained displays that the compatibility between the two segments is reduced which in turn lowers the possibility for hard-to-soft interactions. As hard-to-soft interactions become less frequent within the microstructure they will become more limited to the hard-soft domain boundaries. This observation is consistent with the emerging trend that PCD-based PU-Us are more phase-separated than PPG based PU-Us.

When PDEGA is used (figure 8.10), the ratio of hydrogen bonded to free N-H groups is further reduced to 2.5:1. Accompanying this reduced ratio is a peak shift to higher wavenumbers for the hydrogen bonded N-H signal. Peaks values obtained from deconvolution give values of 3339 cm^{-1} for the TMP only formulation and 3338 cm^{-1} for the DEPD chain-extended formulation. These higher values show that the contribution from hard-to-soft-segment interactions is further reduced and that hardsegment interactions now dominate the hydrogen bonded signal. Accompanying this clearer hydrogen bonded signal is an increase in the amount of free N-H as these groups form less hydrogen bonds with the soft-segment. These more incompatible hard domains will experience greater repulsion from the soft-segment than PPG and this will drive the system towards phase separation. DSC analysis identified that PDEGA based formulations experienced the smallest elevation of their $T_g$ss which is

consistent with the phase morphology observed by ATR. Both ATR and DSC analysis display that the morphology of PDEGA based PU-Us is phase separated however, to gain further information on the order of the hard-segment domains the carbonyl region will now be investigated.
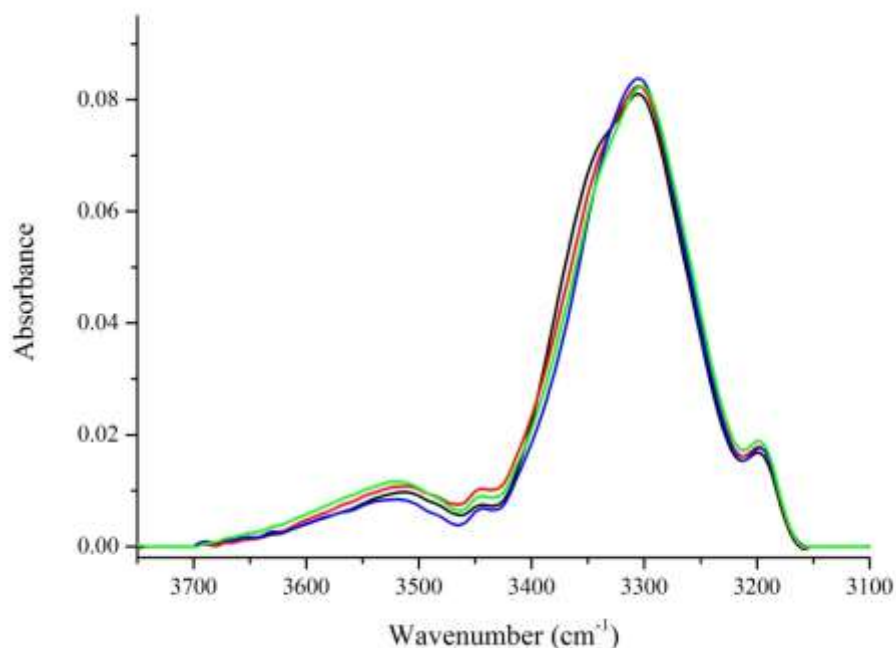

Figure 8.10: Stacked spectra from N-H region of fully cured PU-U adhesives based on MDI and PDEGA. [MDI-TMP-PDEGA in black and MDI-TMPPDEGA-DEPD in red].

Two trends have emerged from the peak fitting data collected from the N-H region in MDI based materials (a) the ratio of hydrogen bonded to free N-H groups decreases and (b) the contribution of hard-to-soft-segments interaction also decreases. An explanation for the first trend is that as phase mixing is reduced, the number of free N-H groups is increased. This is because the compatibility of the hard and softsegments decreases in the order PPG > PCD > PDEGA and results in any groups not consumed within hard-segment formation remaining free. An explanation of the second trend is that as each phase becomes more separated, the obtained value for the hydrogen bonded peak is more representative of hard-to-hard interactions. The presence of hard-to-soft interactions will shift this peak to lower wavenumbers as was shown by Yilgör et al.[16,29]
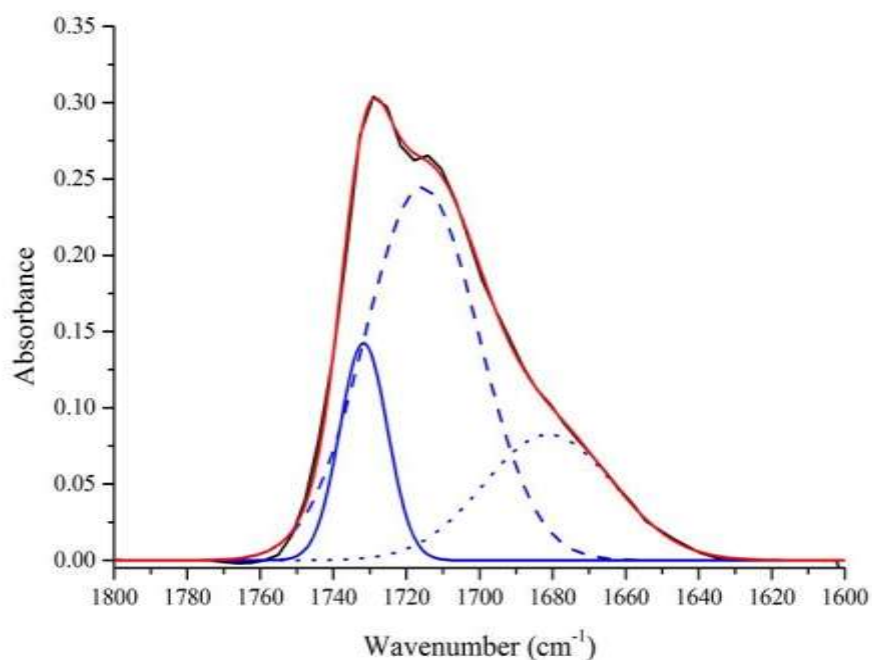
Figure 8.11: Deconvolution data for MDI-TMP-PPG of C=O region (appendix B figure B05). Data calculated using Gaussian fitting function. [Raw data in black, fit data in red, free carbonyl peaks solid blue, hydrogen bonded C=O dash blue and free urea Dot blue].

From inspection of the carbonyl peak it is possible to probe the order within the hard domains e.g. free/hydrogen bonded carbonyl groups from urethane or urea linkages.

Deconvolution was again used to interpret the data due to overlapping signals e.g. peaks from hydrogen bonded urethane overlaps with peak from free urea groups. Shown within figure 8.11 is the data obtained from deconvolution of the C=O for MDI-TMP-PPG. Obtained from deconvolution is the contribution of free urethane, hydrogen bonded urethane and free urea.

The convolution of these peaks is visible within figure 8.12 which shows carbonyl peaks of both urethane and urea moieties. The peak shape of the carbonyl region is similar in all four cases however; the TMP only chain-extended formulation has a greater tail at the lower wavenumber end in comparison to the diol chain-extended formulations. This urea tail in the TMP only formulation is formed by the greater amount of residual isocyanate which upon moisture cure will produce more urea based

groups. As urea carbonyls occur within the range of 1700 cm^{-1} – 1630 cm^{-1} the above carbonyl signals are consistent with what would be expected based on a moisture cured system.[16,29]
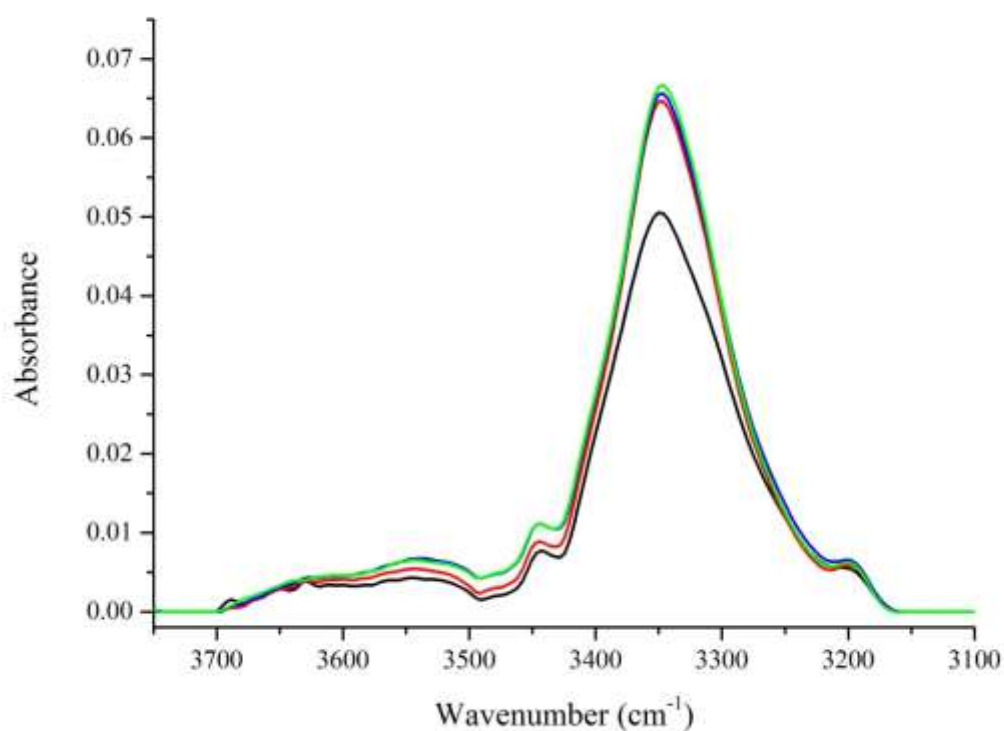

Figure 8.12: Stacked spectra from C=O region of fully cured PU-U adhesives based on MDI and PPG. [MDI-TMP-PPG in black, MDI-TMP-PPG-DEPD in red, MDI-TMP-PPG-BD in blue and MDI-TMP-PPG-PD in green].

Deconvolution of these peaks has identified differences in the kind of carbonyl groups within the microphase structure. For the TMP only formulations the amount of free urethane is essentially the same as that of each diol chain-extended formulations with the peak positions occur within tight range of 1733 cm^{-1} – 1728 cm^{-1}. The first difference is observed in the hydrogen bonded urethane range of the carbonyl peak. For the diol chain-extended formulations the assigned peak area for hydrogen bonded urethane ranges between 72.9% – 76.1%. The amount of hydrogen bonded urethane reduces to 61.3% in the TMP only formulation. This difference in hydrogen bonded urethane will result from: (a) the diol chain-extended formulations having an inherent greater concentration of urethane groups and (b) the shift to lower wavenumbers of carbonyl peak from the greater amount of urea in the TMP only formulation. This is

confirmed by the contribution of free urea within the TMP only formulation being double the contribution of each diol chain-extended formulation. These observations are consistent with what would be expected for diol chainextended systems in the literature.[14,21,32] This will account for the 10 percent increase in hydrogen bonded groups observed.
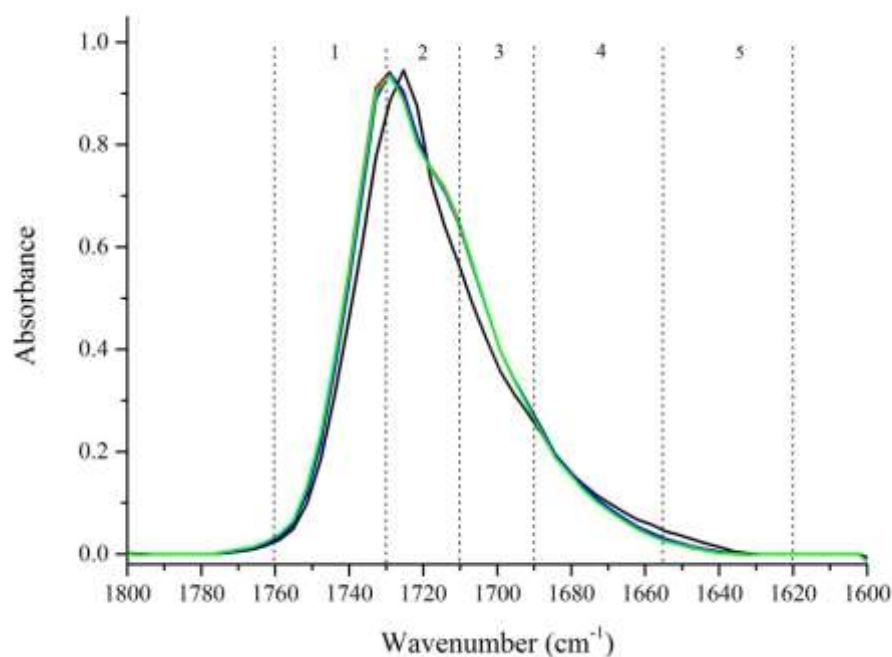
Figure 8.13: Stacked spectra from C=O region of fully cured PU-U adhesives based on MDI and PCD. [MDI-TMP-PCD in black, MDI-TMP-PCD-DEPD in red, MDI-TMP-PCD-BD in blue and MDI-TMP-PCD-PD in green].

Following the introduction of PCD, observing carbonyl signals inherent of the hardsegment is more difficult due to the large intensity of the soft-segment ester carbonyl peak (figure 8.13). However, from inspection of the peak shape it is apparent that there is a small difference between the TMP only and diol chain-extended formulations. Deconvolution data identified that the percentage of free urethane/ester in the TMP only formulation is double that of the diol chain-extended formulations (TMP only 36.8%, DEPD 15.2%, BD 16.2 and PD 15.2%). This is consistent with the emerging trend that diol chain-extension promotes structure of urethane based groups through the formation of hard blocks. As the carbonyl region is dominated by the ester carbonyl groups, this peak can be used to interpret the degree of order within the

crystalline soft-segment (will have a contribution of the free urethane peak). The position of the hydrogen bonded ester peak of the crystalline PCD soft-segment occurs at 1722 cm^{-1}.

In the TMP only formulation the peak only shifts 6 cm^{-1} to 1728 cm^{-1} due to reduction in the hydrogen bonding however, the adhesive layer remains crystalline and white. Following chain-extension the peak shifts a further 4 cm^{-1} – 5 cm^{-1} and the adhesive layer becomes clear. From previous DSC analysis (see section 8.11) it was identified that the urethane linkages formed during chain-extension mix more with the soft-segment and retard crystallisation. ATR has shown that the hydrogen bonding between ester groups has become weaker and shifted to higher wavenumbers due to phase mixing. This displays that phase mixing can be advantageous in the disruption of soft-segment crystallisation and that it can be followed by ATR analysis.

The previously mentioned difference between the formulations becomes more apparent when analysing the hydrogen bonded and free urea parts of the deconvolution data. In the TMP only formulation, the peak position of both the hydrogen bonded urethane and free urea occur at lower wavenumber of 1712 cm^{-1} and 1669 cm^{-1} respectively. The observed shift is the result of this formulation containing more urea based groups as a result of the greater residual free isocyanate which results in the peak occupying a broader range. The fitted area assigned to hydrogen bonded urethane will also contain free urea (see appendix B), this makes the peak at 1669 cm^{-1} monodentate hydrogen bonded urea and not free urea as headed in table 8.04. In the diol chain-extended formulations, the hydrogen bonded peaks occurs at 1721 cm^{-1} in all cases and displays the greater urethane content within these formulations. The positon of the final peak (occurs in the range 1695 cm^{-1} – 1692 cm^{-1}) displays that the urea based groups within the adhesive are mostly free and disordered.

Application of each diol chain-extended formulations required a greater temperature than for the TMP only chain-extended formulation. The higher temperature required to apply the diol chain-extended formulations will lead to a higher viscosity within the system during room temperature moisture. ATR data displays that the higher viscosity limits the ability of the urea groups to form ordered hard-segments. As the adhesive gels, the viscosity will become even greater and end group's mobility will become

further reduced. Based on the higher inherent viscosity of the diol chainextended formulations (based on application temperature), the lower order observed in urea based groups is consistent.
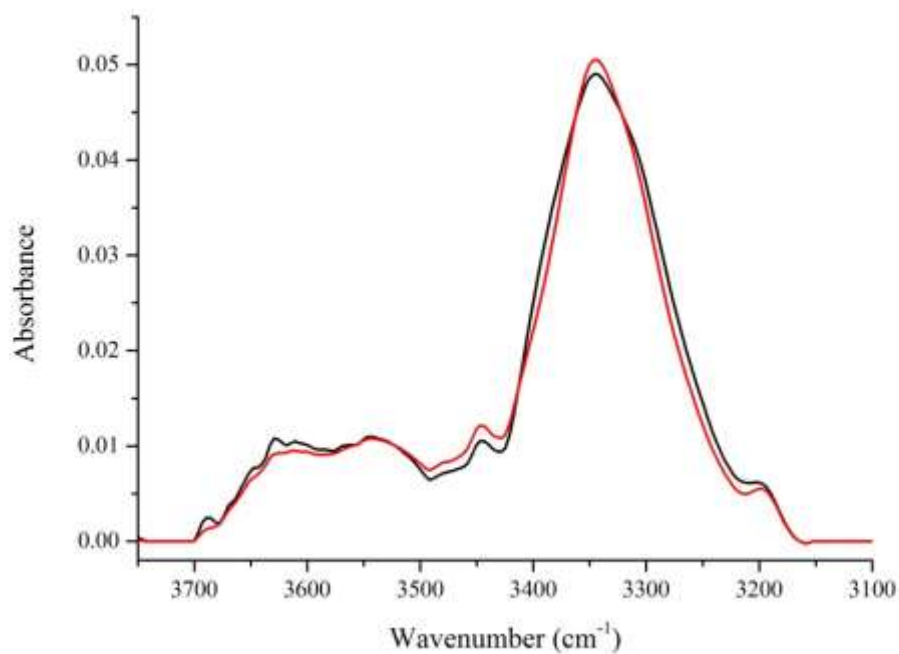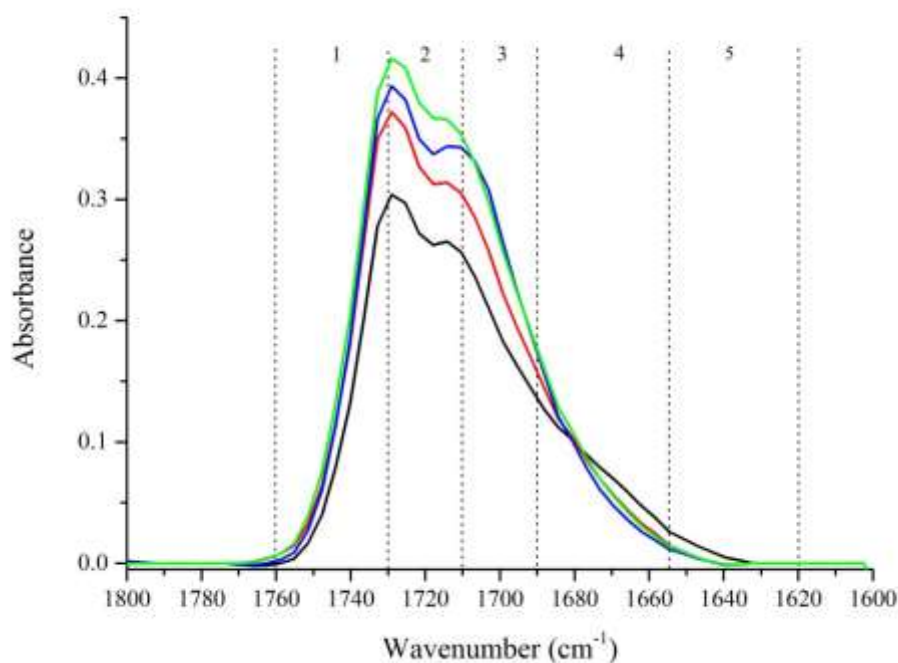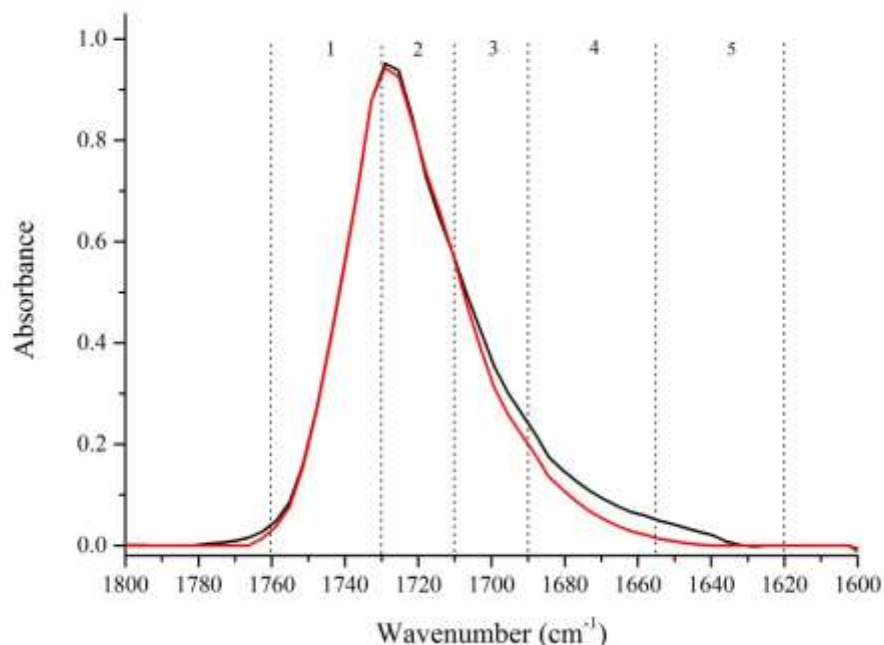

Figure 8.14: Stacked spectra from C=O region of fully cured PU-U adhesives based on MDI and PDEGA. [MDI-TMP-PDEGA in black and MDI-TMPPDEGA-DEPD in red].

For the final formulations based on PDEGA with MDI a very similar peak shape is obtained for both adhesives (figure 8.14). For the TMP only formulation a greater contribution from urea carbonyl groups is visible. The data collected from deconvolution in each case is similar with the main difference being the position of the peak assigned to free urea in MDI-TMP-PDEGA. This peak will in fact arise from monodentate hydrogen bonded urea groups and these are absent in the diol chain-extended formulation. The position of the free ester peak in unreacted PDEGA occurs at 1728 cm^{-1} and following reaction the position of the peak does not shift. This indicates that the soft-segment will be mostly phase separated which is consistent with analysis by DSC. The position of hydrogen bonded urethanes linkages is also similar in both adhesive formulation with 1709 cm^{-1} obtained for MDI-TMP-PDEGA and

1711 cm^{-1} for MDI-TMP-PDEGA-DEPD. This again is consistent with the argument of phase separation of the microphase structure in each case.

Based on MDI based formulations, the degree of phase separation goes by the order PDEGA > PCD > PPG. This is also the order of decreasing hard-segment content and follows classic diblock copolymer phase morphology behaviour. Deconvolution of the N-H and C=O peaks confirm the trend observed in DSC analysis that increasing phase separation occurs with decreasing hard-segment content.

8.22 Discussion of the Morphology in Aliphatic Polyurethane Adhesives

Already identified from DSC analysis is that microphase morphology of IPDI based adhesives is different from MDI based adhesives. Investigation of the microphase structure within IPDI based adhesives will now be performed with ATR. Again deconvolution was performed by fitting Gaussian peaks to both the N-H and C=O regions to determine the degree of order or disorder within the hard-segments of each aliphatic polyurethane adhesive. This analysis was carried out on all ten aliphatic adhesives with the deconvolution data presented within table 8.04.

Presented with figure 8.16 are the N-H regions for polyurethane adhesives based on IPDI with PPG. The peak shape of all four adhesives is very similar in each case and chain-extension does not appear to effect on the degree of order or disorder. Three components were fitted to each region: hydrogen bonded N-H which will include hard-to-hard plus hard-to-soft hydrogen bonding interactions, carbonyl overtone and free N-H. For the TMP only formulations the hydrogen bonded N-H occurs at 3342 cm^{-1} with the free N-H occurring at 3525 cm^{-1} with the ratio of these two peaks 7.3:1. The position of hydrogen bonded N-H peak displays phase mixing and this is confirmed by DSC data which display phase mixing based on the position of the $T_g$ss. Combined within the hydrogen bonded peak will be contribution from both hard-to-hard and hard-to-soft hydrogen bonding interactions involving the N-H groups. These interactions move the hydrogen bonded N-H peak to lower wavenumbers. In these formulations it is noted that these hard-to-soft interactions are reduced compared to MDI but will still contribute to the hydrogen bonded N-H peak.

Following diol chain-extension no considerable shift or change in peak shape is observed. The resulting ratio of hydrogen bonded to free N-H varies in each case with values of 6:1 obtained for DEPD, 3.4:1 obtained for BD and 9.1:1 obtained for PD. From the obtained ratios of hydrogen bonded to free it would indicate that chain-extension with DEPD and BD reduced hard-segment formation whereas PD promotes hard-segment formation. These observations are consistent with previous DSC analysis where it was identified that PD results in the greatest hard-segment formation (shown by greatest enthalpy of melt). Based on this initial analysis by ATR it displays the same trend as DSC that IPDI based formulations have better phase separation.

Figure 8.15: **Deconvolution data for IPDI-TMP-PPG of N-H region (appendix B figure B62). Data calculated using Gaussian fitting function. [Raw data in black, fit data in red, HS-HS fitted peak solid blue, carbonyl overtone dash blue and free N-H dot blue].**

Table 8.05: Deconvolution data of the N-H and C=O peak for each IPDI adhesive type obtain using a Gaussian fitting function.

	N-H						C=O							
Formulation	Free		C=O Overtone		H-Bonded		H-Bonded Ur		Free U		Monodentate U		Bidentate U	
	cm^{-1}	%	cm^{-1}	%	cm^{-1}	%	cm^{-1}	%	cm^{-1}	%	cm^{-1}	%	cm^{-1}	%
IPDI-TMP-PPG	3525	11.4	3421	2.7	3342	83.1	1719	38.9	1697	28.6	1672	16.3	1646	16.1
IPDI-TMP-PPG-DEPD	3516	14.1	3409	0.1	3337	84.8	1720	34.8	1698	33.9	1671	16.6	1646	14.7
IPDI-TMP-PPG-BD	3503	22.8	3407	0.5	3340	76.7	1721	31.6	1699	34.2	1669	18.7	1641	15.5
IPDI-TMP-PPG-PD	3536	9.7	3481	2.0	3345	88.3	1720	37.5	1698	18.5	1668	28.5	1637	15.5

	Free		C=O Overtone		H-Bonded		H-Bonded Ur Free Ester/Ur		Free U + Free U		Monodentate U		Bidentate	
	cm^{-1}	%	cm^{-1}	%	cm^{-1}	%	cm^{-1}	%	cm^{-1}	%	cm^{-1}	%	cm^{-1}	%
IPDI-TMP-PCD	3537	10.8	3379	16.1	3345	73.1	1729	35.5	1711	50.9	1664	5.8	1639	7.8
IPDI-TMP-PCD-DEPD	3537	18.3	3380	15.9	3350	65.8	1729	28.2	1712	58.7	1670	5.9	1644	7.2
IPDI-TMP-PCD-BD	3537	9.7	3381	15.6	3351	74.7	1727	30.0	1710	62.0	1668	1.1	1649	6.9
IPDI-TMP-PCD-PD	3525	8.9	3377	17.1	3346	74.0	1727	28.5	1710	62.2	1668	1.4	1647	7.9

	Free		C=O Overtone Free Ester/Ur		H-Bonded H-Bonded Ur		Free U + Bidentate U		Free C=O Overtone Monodentate U					
	cm^{-1}	%	cm^{-1}	%	cm^{-1}	%	cm^{-1}	%	cm^{-1}	%	cm^{-1}	%	cm^{-1}	%
IPDI-TMP-PDEGA	3541	13.6	3374	9.0	3363	77.5	1731	27.1	1723	54.0	1764	13.4	1638	5.5

| IPDI-TMP-PDEGA-DEPD | 3542 | 18.2 | 3374 | 6.9 | 3369 | 74.9 | 1731 | 21.1 | 1718 | 65.6 | 1675 | 6.4 | 1647 | 6.9 |

Ur = urethane, U = Urea

An example of the data obtained from deconvolution is shown within figure 8.15 for formulation IPDI-TMP-PPG. The fit line obtained (red line) is the summation of the three fitted peaks used to detemine the free N-H, carbonayl overtone and hydrogen bonded N-H.
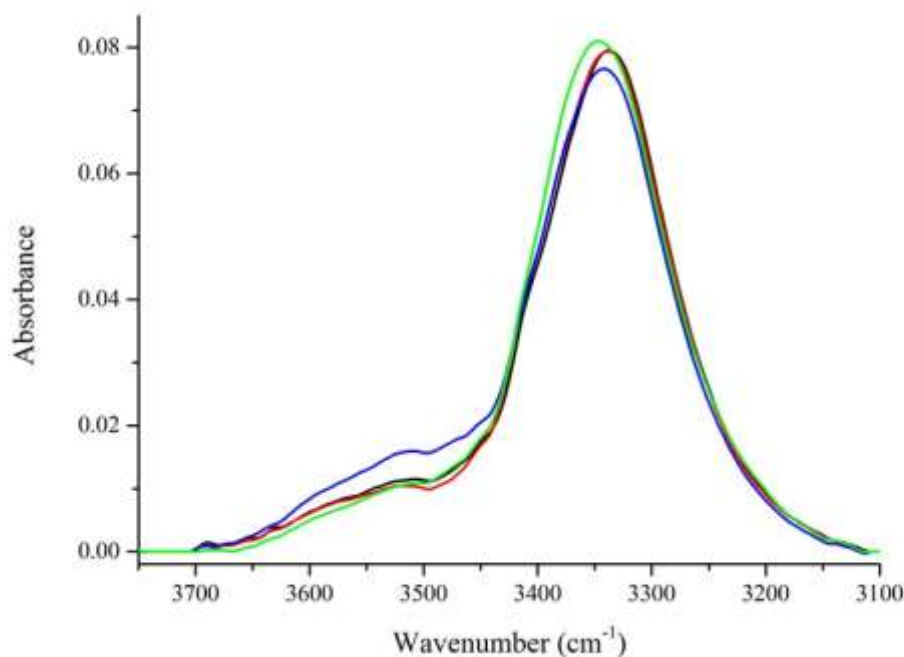
Figure 8.16: Stacked spectra from N-H region of fully cured PU-U adhesives based on IPDI and PPG. [IPDI-TMP-PPG in black, IPDI-TMP-PPG-DEPD in red, IPDI-TMP-PPG-BD in blue and IPDI-TMP-PPG-PD in green].

In the next set of adhesives with PCD as the soft-segment the peak shape is changed compared to PPG as shown in figure 8.17. This shift is the result of the increased contribution from the carbonyl overtone and a reduced contribution from hard-to-soft interactions. The peak position does indeed shift to a small degree with values in the range of 3345 cm^{-1} to 3351 cm^{-1} obtained. These values represent increased phase separation of the hard-segments which was also observed in DSC analysis. Confirmation that a small degree of phase mixing does occur is shown by DSC analysis which displayed depreciation of the soft-segment melting temperature and a reduced overall enthalpy of melt.

The ratio of hydrogen bonded to free N-H varies for each adhesive with 6.8:1 obtained for TMP only, 3.6:1 obtained for DEPD, 7.7:1 obtained for BD and 8.3:1 obtained for PD. Based on these ratios it would suggest that the formulation IPDI-TMP-PCD-DEPD has the highest degree of mixing. Considering previous DSC analysis this observation is consistent as this formulation has the broadest $T_g$ss range, the lowest depressed soft-segment melting endotherm and lowest enthalpy of melt for the soft-segment. It would be expected that these formulations would obtain higher bond strengths with TAc or PC than PPG based adhesives as there are more potential hydrogen bonding donors/acceptors along the soft-segment backbone however, this will be discussed in more detail within sections 8.31-8.33.

Figure 8.17: Stacked spectra from N-H region of fully cured PU-U adhesives based on IPDI and PCD. [IPDI-TMP-PCD in black, IPDI-TMP-PCD-DEPD in red, IPDI-TMP-PCD-BD in blue and IPDI-TMP-PCD-PD in green].

Adhesives which contain PDEGA as the soft-segment present a very similar peak shape to those of PCD based adhesives as shown in figure 8.18. DSC analysis confirms phase separation is increased moving to this soft-segment when compared to PPG or PCD. ATR also confirms that phase separation is increased as shown by the shift of

the N-H peak to higher wavenumbers with 3363 cm^{-1} reached for the TMP only adhesive and 3369 cm^{-1} for the DEPD adhesive. The greater shift for adhesive IPDI-TMP-PDEGA-DEPD displays that the hydrogen bonding is not as intimate and will occur due to the steric effects of the chain-extender. This is reflected in the ratio of hydrogen bonded to free N-H which decreases from 5.7:1 to 4.1:1 following chain-extension. This observation further confirms that the presence of DEPD within the hard-segment does affect the hydrogen bonding order however; this will become clearer following analysis of the carbonyl region.[21]

Figure 8.18: Stacked spectra from N-H region of fully cured PU-U adhesives based on IPDI and PDEGA. [IPDI-TMP-PDEGA in black and IPDI-TMPPDEGA-DEPD in red].

Out of all the soft-segment materials, PPG presents the best opportunity for viewing the environment of hard-segment carbonyl groups as it is not masked by a softsegment carbonyl peak. The carbonyl regions of IPDI based adhesives (as shown in figure 8.20) shown that the hard-segment has a high degree of order. For each adhesive there are four types of carbonyl: hydrogen bonded urethane, free urea, monodentate hydrogen bonded urea and bidentate hydrogen bonded urea. Other than free urea all other

interactions will be present in hard domains which are phase separated from the soft-segment and will act as physical reinforcement points for the polymer matrix.
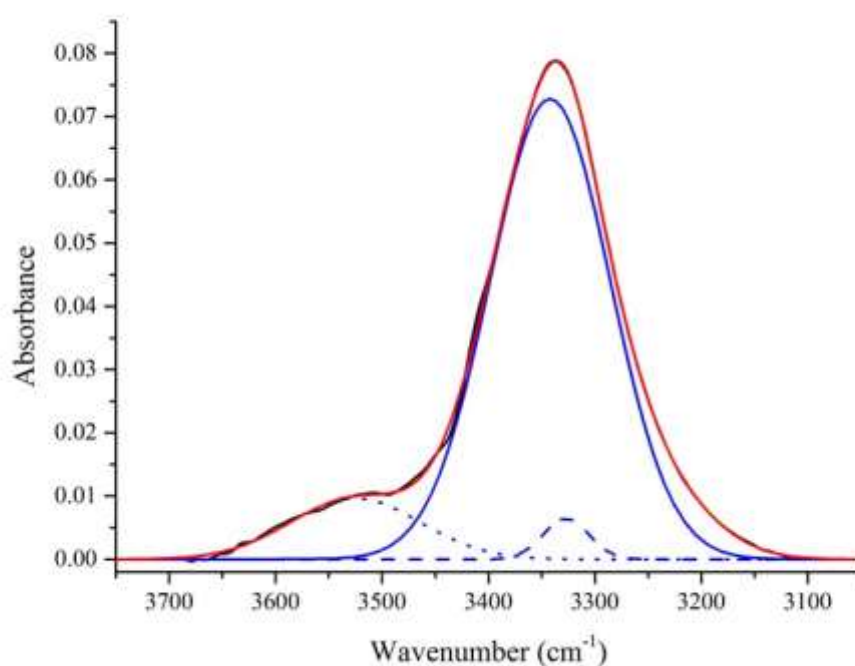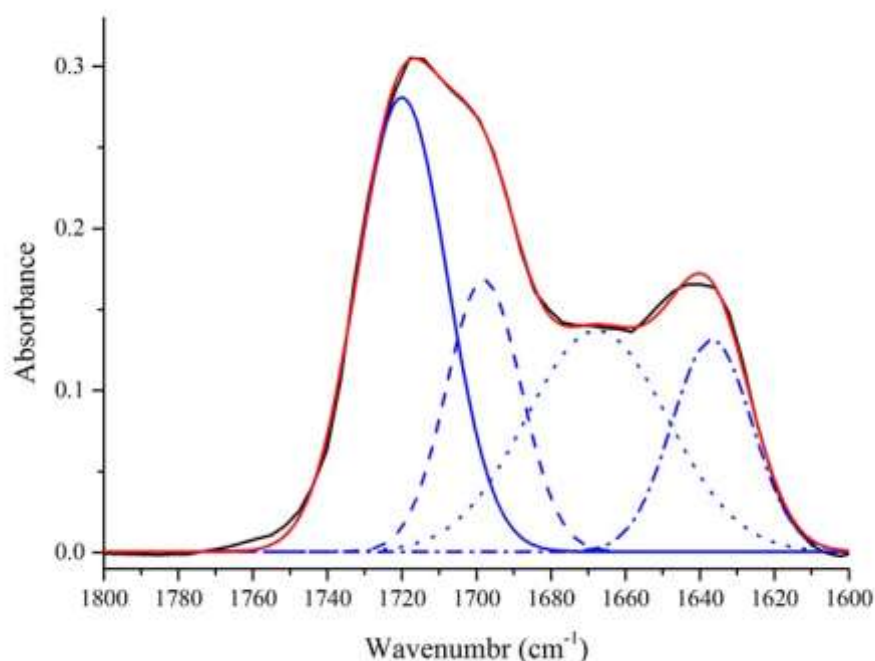

Figure 8.19: Deconvolution data for IPDI-TMP-PPG of C=O region (appendix B figure B65). Data calculated using Gaussian fitting function. [Raw data in black, fit data in red, free urethane carbonyl peaks solid blue, hydrogen bonded urethane dash blue, free/monodentate hydrogen bonded urea dot blue and bidentate hydrogen bonded urea dot dash blue].

Deconvolution was performed by fitting four peaks to the carbonyl region to identify the contribution from hydrogen bonded urethane, free urea, monodentate hydrogen bonded urea and bidentate hydrogen bonded urea. In the TMP only adhesive a large contribution of bidentate urea is observed compared to the each diol chain-extended formulations. As this adhesive contains more free isocyanate than the diol chainextended adhesives, this will result in the fully cured system having more urea containing groups. Formation of bidentate urea groups show high order within the hard-segment and the formation of these highly ordered interactions display phase separation. These bidentate urea groups are formed within all PPG based adhesives and the lower viscosity within IPDI based systems coupled with the slower cure time

will promote there formation. The identification of these groups also shows that within the mixed microstructure there are areas of phase separation which will toughen the cured adhesive.[15] Shown within figure 8.19 is the data obtained from deconvolution of the C=O for MDI-TMP-PPG. Obtained from deconvolution is the contribution of free urethane, hydrogen bonded urethane, monodentate urea and bidentate urea.
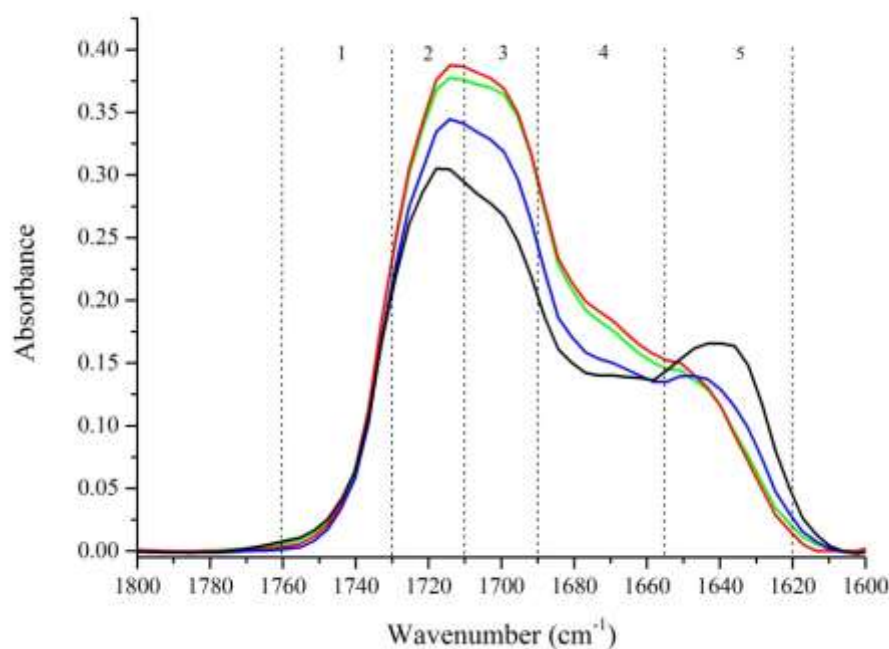
Figure 8.20: Stacked spectra from C=O region of fully cured PU-U adhesives based on IPDI and PPG. [IPDI-TMP-PPG in black, IPDI-TMP-PPG-DEPD in red, IPDI-TMP-PPG-BD in blue and IPDI-TMP-PPG-PD in green].

Following the introduction of the PCD as the soft-segment the interpretation of the hard-segment organisation is not as simple due to the presence of the large ester peaks (figure 8.21). This ester peak (unreacted ester carbonyl occurs at 1722 cm^{-1}) can be used as a means of determining the morphology of the system as phase mixing will move the peak to higher wavenumbers as hydrogen bonding between ester groups is disrupted. Following polymerisation irrespective of the chainextender composition the ester peak shifts by at least 5 cm^{-1} which displays that there is a contribution of the hard-segment within the soft-segment. This observation is supported by DSC analysis where a depression of the soft-segment melting point is observed coupled with a reduction in the melting enthalpy. The mixing of the hardsegment within the soft-

segment is not sufficient to disrupt crystallinity of the softsegment and a white adhesive layer is obtained.
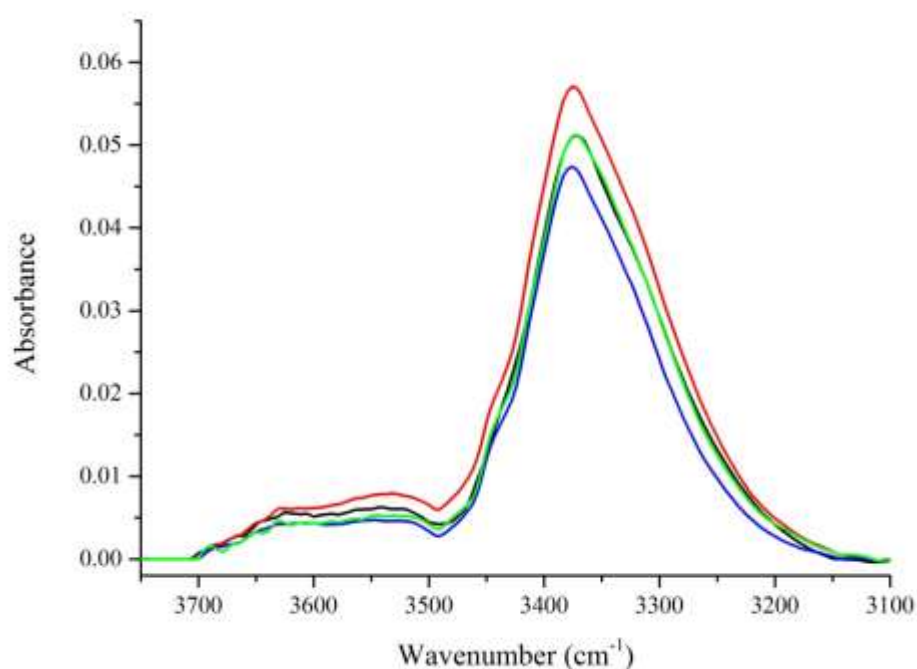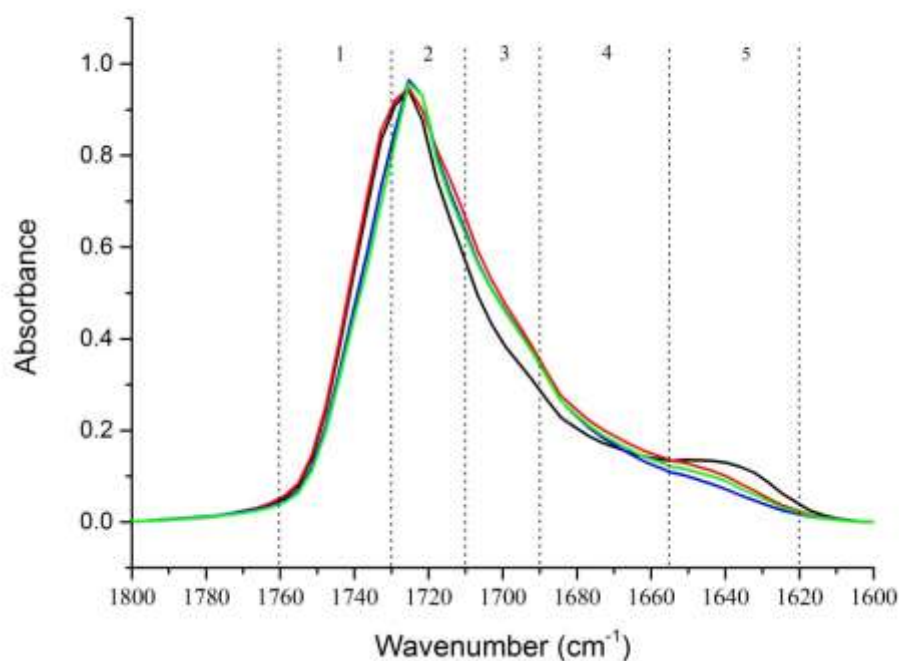

Figure 8.21: Stacked spectra from C=O region of fully cured PU-U adhesives based on IPDI and PCD. [IPDI-TMP-PCD in black, IPDI-TMP-PCD-DEPD in red, IPDI-TMP-PCD-BD in blue and IPDI-TMP-PCD-PD in green].

As the hard-segments are unable to sufficiently penetrate the soft-segment, a crystalline adhesive layer is observed. Combined with the fully ordered bidentate urea groups it displays that IPDI based hard-segment are less compatible with the soft-segment compared to MDI. As a consequence greater phase separation within the microstructure is obtained.
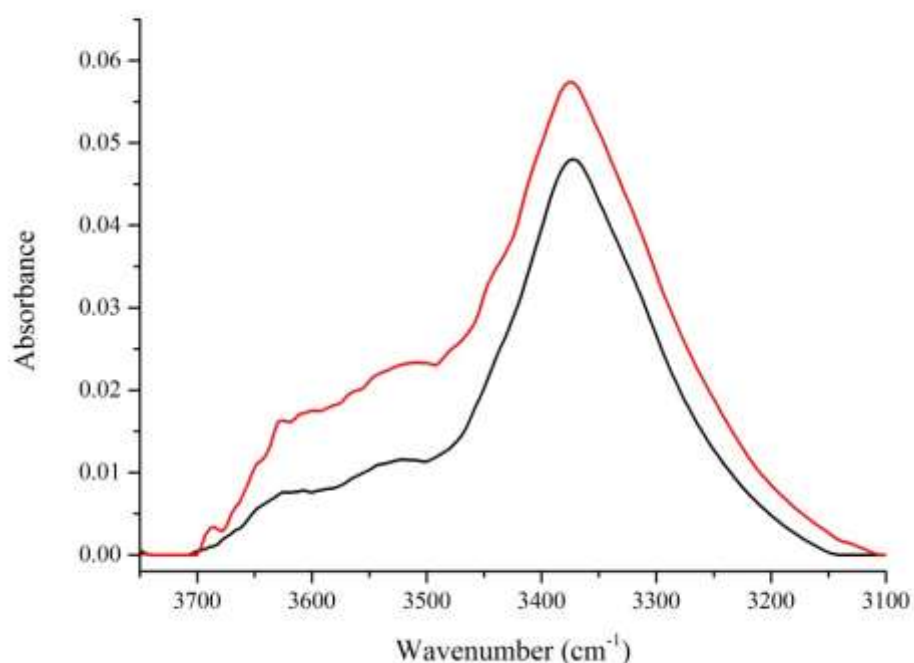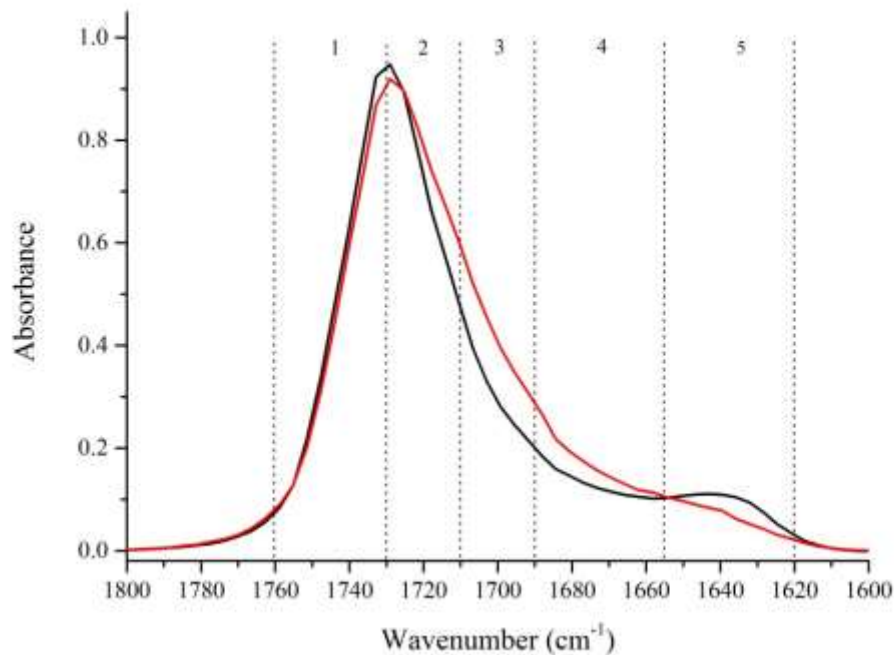
Figure 8.22: Stacked spectra from C=O region of fully cured PU-U adhesives based on IPDI and PDEGA. [IPDI-TMP-PDEGA in black and IPDI-TMPPDEGA-DEPD in red].

Based on previous analysis within this chapter it would be expected that PDEGA soft-segment will result in the greatest phase separation. This statement is based on DSC data which displayed only a small elevation in the $T_g$ss by 11°C. This small shift displays that there are minimal conformational constraints induced on the softsegment. These constraints will be limited to the hard-to-soft domain interface which limits the rise in the $T_g$ss. Phase separation is further displayed in the carbonyl region of both PDEGA based adhesives. The peak position occurs at 1731 cm^{-1} which is a small shift of 3 cm^{-1} compared to PDEGA in its unreacted state (unreacted peak position 1728 cm^{-1}). This small shift displays that there will only be a small degree of mixing with the greatest proportion of this accounted for by the hard-to-soft domain interface.

Within the TMP only chain-extended adhesive there is a higher proportion of bidentate hydrogen bonded urea compared to the DEPD chain-extended adhesive as shown within figure 8.22. This greater bidentate urea content arises from the greater free isocyanate content inherent of this formulation translating into a greater amount of urea in the carbonyl region. The ability for these urea groups to aggregate will result from

the extended curing time of the IPDI based adhesives allowing for motion of the end groups as the system is well above the soft-segment $T_g$ss. These groups will form strong anchoring blocks within the PU-U adhesive and serve as reinforcement points.

It is evident from observation of the peak shape within figure 8.18 that chainextension has an effect on the carbonyl. The observed broadening of the DEPD chain-extender peak compared to the TMP only formulation is inherent of the addition hydrogen bonded urethane carbonyl groups introduced. This again supports the argument of a greater phase separated structure. Also within this broadening will be a proportion of free urea and bidentate urea however, their contribution to the broadening of the peak will be lower than hydrogen bonded urethane. The reduced contribution from bidentate urea is inherent of the synthetic process in which free isocyanate groups are consumed during synthesis by the diol chain-extender. Thus upon application, the residual free isocyanate content is lower making the final urea content lower compared to the TMP only adhesive. More hydrogen bonding via urethane groups will also drive the microphase structure towards phase separation which brings the previously mentioned benefits.

ATR analysis of PU-U adhesives has further confirmed the data collected using DSC analysis. ATR analysis of the N-H region displays that the degree of mixing within N-H environments is reduced as you lower the hard-segment content and this is also shown in DSC through reduced elevation of the $T_g$ss. This also displays that the degree of phase separation increases with decreasing hard-segment content, as evident by the greater order within the C=O region for adhesive. The C=O region was also used to probe the degree of order within the soft-segment. It is especially useful for PCD as the position of the ester peak indicates the degree of order/disorder within the crystalline soft-segment. Analysis of this region displayed that even following chain-extension, the penetration of the hard-segment into the soft-segment was not sufficient enough to disrupt hydrogen bonding between ester groups and a white adhesive layer was obtained as a consequence. For the intended adhesive application PDEGA and IPDI based PU-U adhesives present the best system based on the phase separated morphology obtained however, this will be discussed further in section 8.32 and 8.33.

8.23 Comparison of the Morphology in Aromatic and Aliphatic Polyurethane Adhesive Based on Attenuated Total Reflectance Fourier Transform Infra-Red Spectroscopy

Following analysis of both the N-H and C=O regions of all twenty adhesive systems it is clear that MDI and IPDI give similar yet contrasting results. This remains true even when the same soft-segment and chain-extenders are used. Formulations based on IPDI display greater incompatibility or favour phase separation over MDI based adhesives. This main difference between the two different hard-segments will now be briefly compared based on soft-segment.

It is known that PPG based soft-segments have a tendency to mix with the hardsegment due to the affinity between the proton donor N-H group with the proton acceptor ether oxygen group. Phase mixing via these interactions is evident in the NH region of the ATR spectrum where the hydrogen bonded peak is shifted to lower wavenumber because of these hard-to-soft interactions. In MDI based formulations the hydrogen bonded N-H peak lies within the range 3302 cm^{-1} – 3312 cm^{-1} however; when IPDI is used this range is shifted to higher wavenumbers and occurs within the range 3337 cm^{-1} – 3345 cm^{-1}. As has been identified, IPDI based hard blocks possess a lower affinity for PPG than MDI and this results in the contribution from hard-to-soft hydrogen bonding interactions being reduced (results in a shift of 30 cm^{-1}).

This shift toward a more phase separated morphology is also shown in the C=O regions of PPG based PU-U adhesives. This is shown by the position of C=O peaks from IPDI occurring at lower wavenumbers compared to MDI based adhesives. Within MDI based formulations the major type of order within the hard-segment is via hydrogen bonded urethane. Within the urea region of MDI based C=O spectra there is mostly free urea with a small contribution from monodentate hydrogen bonded urea. For IPDI based adhesives the carbonyl region displays greater order as more carbonyl groups reside within hard-segment as shown by the peak position which ranges from 1719 cm^{-1} – 1721 cm^{-1}. Further evidence of greater order within the morphology is shown by the contribution from bidentate urea. These highly ordered groups only occur within hard-segments and further display the greater phase separation of IPDI based adhesives.

This trend is further observed in PCD based adhesives as the IPDI hard-segments are less compatible with the soft-segment. Within the N-H region for MDI based formulations the peak position shifts to higher wavenumbers (3324 cm^{-1} – 3336cm^{-1}). This is the result of a greater contribution from the carbonyl overtone which is a consequence of using the ester soft-segment and a reduction in the contribution from hard-to-soft interactions. This shift is even greater within IPDI based formulations with the peak now within the range 3331 cm^{-1} – 3345 cm^{-1}. Greater phase separation or a reduced contribution from hard-to-soft interactions is the reason behind the shift to higher wavenumbers.

These differences are also observed within the carbonyl regions. Within MDI based formulations no bidentate ordered urea was observed displaying that urea groups are not within highly ordered domains. This is in contrast to IPDI based formulations in which all formulations contain bidentate urea, with the TMP only formulation having the greatest contribution. This greater structure within the hard-segment was attributed to the slower curing time allowing for aggregation and ordering of urea hard-segments. The observed shift in the hydrogen bonded N-H peak to higher wavenumbers in PCD compared to PPG based formulations will also result from the reduction in the hard-segment content following the increase in soft-segment molecular weight.

The position of the ester peak was also a good indication of the degree of phase separation. PCD has a hydrogen bonded ester peak which resides at 1722 cm^{-1} when unreacted. When IPDI is used, the position of ester peak shifts to 1728 cm^{-1} – 1729 cm^{-1} and this is accompanied by a reduction in the crystalline order of the softsegment (evident from the reduction in the enthalpy of melt see section 8.12). Unlike was observed for the MDI based formulations, this reduction in crystalline order does not result in a clear adhesive layer. This agrees with DSC data collected for these samples and supports the argument that greater phase separation is present within these adhesives. Interestingly when MDI is used as the hard-segment, crystallisation of the soft-segment is no longer present following the introduction of the diol chain-extenders. Greater mixing of urethane based hard-segments result in a 5 cm^{-1} shift in the position of the ester carbonyl peak and the removal of crystallisation.

The formulations which display the greatest degree of phase separation are those which contain IPDI and PDEGA. The position of the hydrogen bonded N-H peak occurs around 25 cm^{-1} higher in IPDI based formulations compared to MDI (3363 cm^{-1} – 3369 cm^{-1} for both IPDI based formulations and 3337 cm^{-1} – 3338 cm^{-1} for MDI based formulations). This greater phase separation observed for PDEGA based adhesives will be influenced by the lower hard-segment content. The carbonyl region further confirms greater IPDI hard block phase separation by the presence of bidentate urea which is absent in all MDI based formulations.

8.30 The Relationship between Adhesive Strength and Morphology in Polyurethane Adhesives

IPDI based hard-segments result in greater phase separation within the microstructure compared to MDI based hard-segments. Evidence of this observation is present in both DSC and ATR analysis of morphology for each PU-U adhesive. As the hard-segment content is decreased, the degree of phase separation is increased (soft-segment phase separation goes in the order of PDEGA > PCD > PPG). Within this section a relationship between the adhesives phase morphology and the adhesion properties with TAc/PC will be constructed based on the peel strength obtained and the observed mode of failure in each case.

8.31 Discussion of the Peel strength Obtained using Aromatic Polyurethane Adhesives and the Relationship to Morphology

Thermal and spectroscopic analysis has determined that each set of PU-U adhesive becomes more phase separated with decreasing hard-segment content. PPG based adhesives have the most phase mixed morphology with respect to PCD and PDEGA. Within the literature it is stated that hard-segment contents of 50 wt% or greater result in microphase structure that is lamellar in nature with interweaving layers of both hard and soft-segments.[4] Within this system the hard-segment content is lower than this 50 wt% value ranging from 36.4% – 41.5 wt%, thus the expected microphase morphology will be more globular in nature.

Figure 8.23: Model of the microphase morphology in PPG based PU-Us. [Red rectangle = isocyanate, black line = PPG soft-segment and blue T-shape = TMP chain-extender].

This phase mixed morphology as shown in figure 8.23 will consists of hard-segment domains which are isolated from one another by soft-segment domains. These domains will be very close to one another and as a result the conformational constraints

induced on the soft-segment will be greater resulting in a significant increase in the $T_g$ss.

When the morphology is phase mixed poor adhesion within hard-segments and at the interface substrate is expected. As inter-domain adhesion is reduced reinforcement from hard-segments will be reduced as they are consumed in the formation of hardto-soft interactions. Also involvement of hydrogen bonding groups from the softsegment in hard-to-soft interactions will remove the potential for these groups to adhere to the substrate interface. From the data collected during 180° T-peel tensile testing the above hypothesis is consistent as the most common mode of failure obtained is adhesive at the interface. As the adhesive is applied in a reactive state there are two possible adhesion mechanisms: covalent bonding with reactive surface groups of the substrate with the free isocyanate and hydrogen bonding interactions at the adhesive-substrate interface.

Covalent bonds formed at the adhesive-substrate interface are only possible when there are reactive groups available to the free isocyanate groups of the reactive adhesive. Considering the peel strengths of TAc vs TAc(t) and using formulations MDI-TMP-PPG-DEPD as an example the values obtained after 30 days were 0.0 N mm^{-1} and 3.0 N mm^{-1} respectively. Presented at the interface of TAc are nonreactive acetate groups and the only available mechanism for adhesion is via hydrogen bonding. As the soft-segment hydrogen acceptor groups are either consumed in hard-to-soft interaction or are sterically hindered by the adjacent methyl group the resulting hydrogen bonding contribution will be low which is reflected in the low peel strength obtained. Following saponification, the peel strength increased to 3.0 N mm^{-1} as the TAc(t) interface now contains reactive hydroxyl groups however, the same adhesive mode of failure is obtained. The jump in peel strength obtained from the formation of covalent bonds between the reactive isocyanate and the surface hydroxyl groups has taken the peel strength above bench mark.

As the degree of phase mixing increases so do the physical constraints induced on the soft-segment polymer chains. This phenomenon can be clearly observed by monitoring the position of the soft-segment glass transition using DSC (temperature increases with phase mixing). Increasing the constraints on the soft-segment will also

influence the soft-segment ability to come into intimate contact with the substrate interface. This coupled with the reduced motion as the adhesive nears it soft-segment glass transition will limit the mobility of the system and reduce the hydrogen bonding potential with the substrate. In PPG a methyl group is positioned adjacent to every ether oxygen atom. These methyl groups will inhibit the hydrogen bonding ability of these hydrogen acceptor groups. It is believed that a combination phase mixing and soft-segment incompatibility result in the poor adhesion with TAc. Achieving the above bench mark peel strength in TAc(t) based laminates is therefore only possible due to the covalent bonding interactions formed. As an adhesive mode of failure is obtained it displays that the covalently bonded layer between the adhesive and substrate is weaker than the adhesion within the PU-U matrix.

The importance of having sufficient hydrogen bonding groups or reactive functional groups at the interface is further displayed in PC based laminates. Above bench mark peel strengths were obtained for all PPG based adhesives excluding MDI-TMPPPG-BD where an application issue was encountered. A greater affinity for the PC interface is shown by the greater peel strength measured and this improvement in adhesion was attributed to an improved compatibility.

This improved compatibility is clearer when the molecular structure is considered. Along the polymer backbone of PC many accessible carbonyl groups are present compared to TAc. These carbonyl groups can potentially form hydrogen bonds with the methyl groups of PPG or with the mixed hard-segment consisting of MDI. There is also the opportunity for π-π ring stacking between the MDI molecules of the adhesive and the bisphenol-A moiety of PC which will also improve the compatibility. From the peel strengths obtained an increase in peel strength with time is observed as the adhesive approaches full cure. The target reaction upon cure is urea formation via water ingress however; the introduction of cross links from isocyanurate, allophonate and biuret formation will also occur during cure.[34]
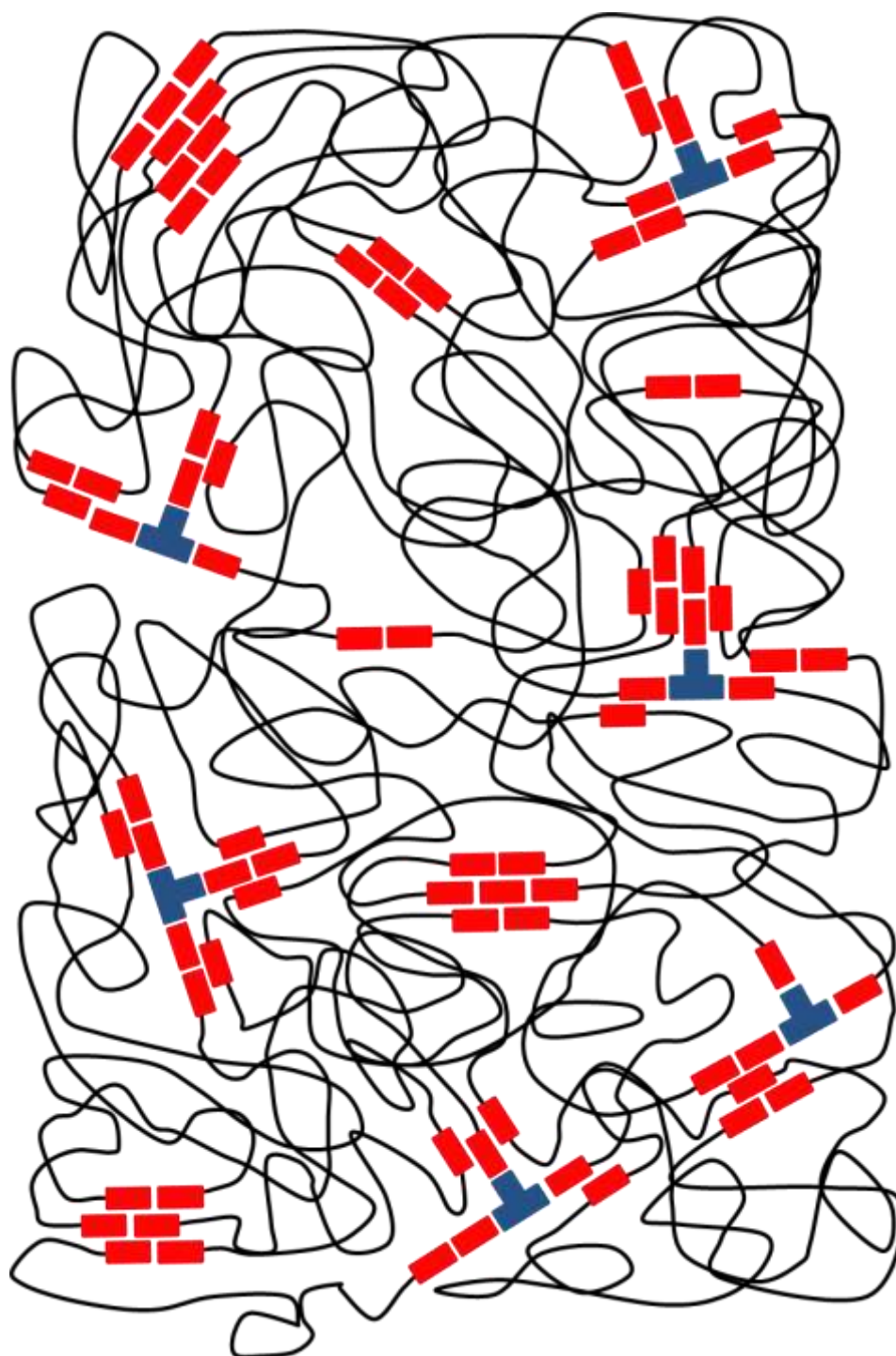
Figure 8.24: Model of the microphase morphology in PCD based PU-Us. [Red rectangle = isocyanate, black line = PCD soft-segment and blue T-shape = TMP chain-extender].

Following 30 days of curing all PC laminates failed adhesively at the interface. This adhesive failure displays that the interface is less stable than the adhesive matrix. In

each case the adhesive failure was coupled with significant deformation of the PC ply materials.

Moving to PCD based adhesives a change to the morphological model is introduced as shown in figure 8.24. Compared with PPG based adhesives an improvement is observed for all laminates excluding TAc. PC is the most compatible interface with negligible difference between treated and untreated substrates. The highest peel strengths is obtained following 30 days of curing with adhesive MDI-TMP-PCD where the final strength obtained was 8.3 N mm^{-1} (PC(t) laminate). A noticeable drop in the peel strength is observed following chain-extension regardless of formulation. DSC/ATR analysis displays that the degree of phase mixing increases following diol chain-extension. The migration of hard-segments into the softsegment retards crystallisation. The ester chains will be more constrained with reduced conformational mobility due to hard-to-soft interactions. The consequence of reducing the soft-segment mobility is that the soft-segment and substrate will no longer come into intimate contact. The reduced peel strength obtained supports this argument that an increasing in phase mixing correlates to a reduction in adhesion at the interface. The same explanation can be used to explain the absence of softsegment crystallisation. With the introduction of hard-to-soft interactions, the conformational mobility of the chains is reduced and as a result the ester groups no longer come into hydrogen bonding range removing the ability of the soft-segment to crystallise.

Interestingly for TAc the peel strength is still low even following the introduction of the ester soft-segment. Commonly in hot melt wood adhesives polyester softsegment are used to introduce matrix stability within the adhesive and promote adhesion to the surface via hydrogen bonding interaction.[35,36] Within this set of polyester based formulations above bench mark peel strengths are only obtained following saponification. This infers that physical covalent bonding is the main mechanism behind gaining bench mark peel strengths and that the ester groups within the current formulations are not sufficiently compatible with the TAc interface.
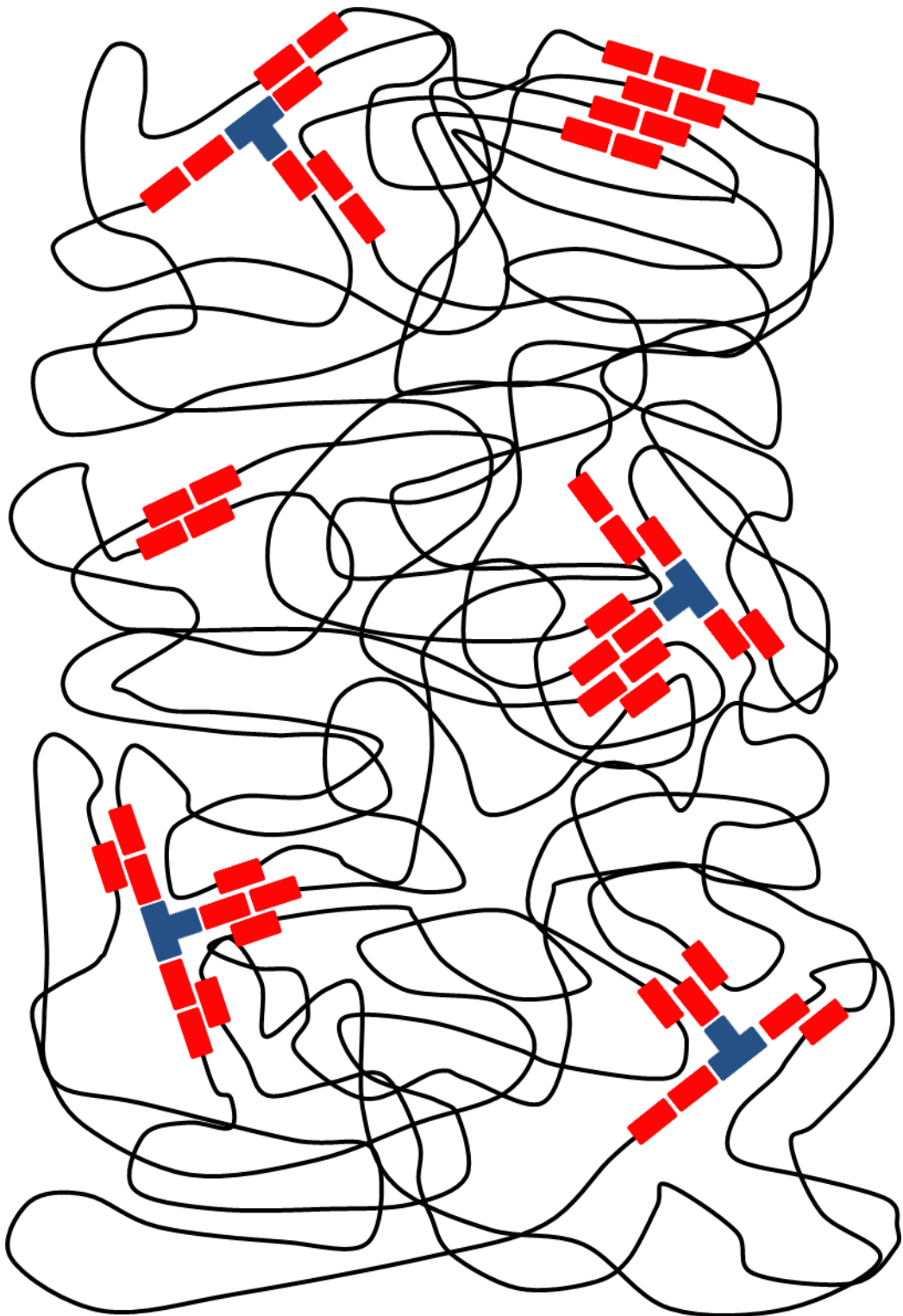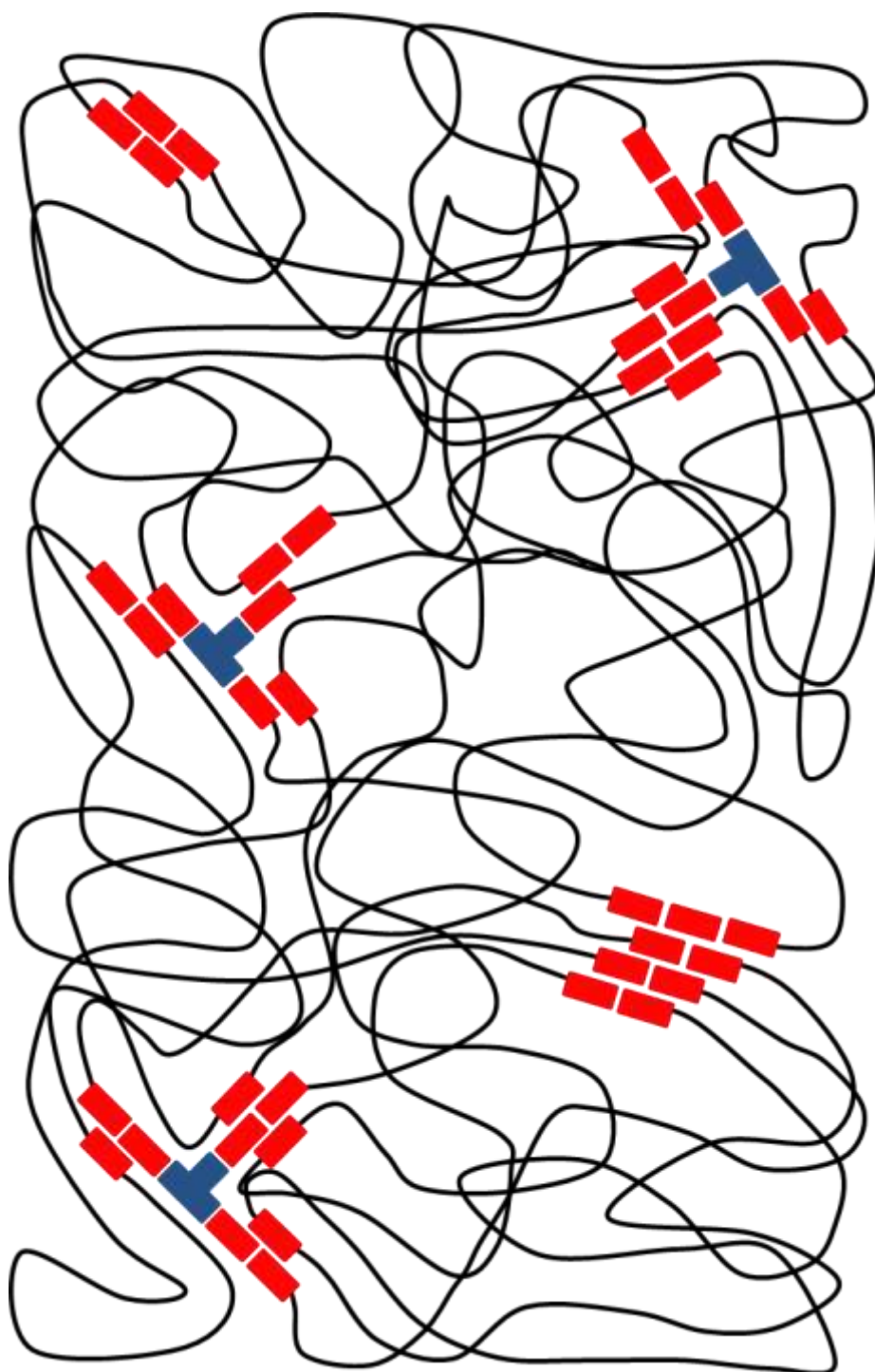
Figure 8.25: Model of the microphase morphology in PDEGA based PU-Us. [Red rectangle = isocyanate, black line = PDEGA soft-segment and blue T-shape = TMP chain-extender].

Following the introduction of PDEGA the morphological model is further altered to account for the reduction in hard-segment content (see figure 8.25) which is now between 18.7 - 22.1 wt%. Of the MDI based formulation prepared these have the greatest degree of phase separation. From the peel strength data collected, the same trend is observed with PC obtaining higher peel strengths than TAc. A reduction in peel strength following diol chain-extension was again observed supporting the relationship that as the degree of phase mixing increases the adhesion properties decrease. From the PDEGA adhesives, the only differing result compared with PPG and PCD was the increase in the peel strength of TAc which in both cases was > 1 N mm^{-1}. As PDEGA is an amorphous soft-segment containing both ester and ether groups, the degree of hydrogen bonding between chains will be less than PCD but greater than PPG. The data shows that the compatibility of PDEGA with TAc is greater than PCD or PPG.

Based on the peel strengths obtained from MDI PU-U adhesives the relationship between adhesive morphology and adhesion properties are as follows. When phase separation is increased within the microstructure of the PU-U adhesive, the adhesion properties also increase. As the molecular weight of the soft-segment increases, the degree of phase mixing is reduced. Diol chain-extension introduces addition phase mixing compared to the TMP only formulation in each set.

8.32 Discussion of the Peel Strength Obtained using Aliphatic Polyurethane Adhesives and the Relationship to Morphology

With the introduction of an aliphatic hard-segment the phase morphology obtained followed a similar trend as previous observed in MDI based formulations. The models used to compare the differences in phase morphology between the three adhesives sets will be the same (see figures 8.20, 8.24 and 8.25). Analysis of the morphology in previous sections within this chapter (see sections 8.12 and 8.22) identified that PPG displayed the highest degree of phase mixing. This is shown by the elevation of the $T_g$ss in all formulations coupled with the shift to lower wavenumbers of the N-H peak. The most phase separated adhesive system contained PDGEA as the soft-segment. What effect the morphology has on the adhesion properties with TAc and PC will now be investigated using 180° T-peel tensile testing.

The highest performing laminate with all IPDI and PPG based adhesives was TAc(t)TAc(t). Peel strengths ranged from 9.6 N mm^{-1} to 3.3 N mm^{-1} depending on formulation. The high peel strengths obtained where due to covalent bonds at the interface following the saponification process. This was confirmed by the low peel strengths obtained for TAc-TAc (ranging between 0.7 N mm^{-1} to 1.0 N mm^{-1}) as only hydrogen bonding interactions are available. Also observed was the reduction in the peel strength obtained for TAc(t)-TAc(t) laminates following diol chain-extension. High peel strength is obtained by having sufficient free isocyanate to react with the reactive hydroxyl groups at the TAc interface. Following chain-extension, the free isocyanate content is reduced which in turn reduces the probability of forming covalent bonds with the substrate. An adhesive mode of failure at the interface was obtained in all cases which displays that the adhesive matrix is stronger than the adhesive-substrate interface. In each case following 30 days of cure, the peel strength obtained was greater than 3 N mm^{-1} taking them above bench mark (excluding all TAc laminates and some laminates with IPDI-TMP-PPG-BD).

The mode of failure within hybrid laminates was at the PC interface which displays that the compatibility with the TAc(t) interface is greater than PC. This shift in the adhesive mode in failure displays that the covalent bond strength between the adhesive and the TAc(t) interface is greater than the hydrogen bonding strength between the adhesive with PC. As the adhesive is now fully aliphatic the ability to make an intimate contact with the TAc(t) interface will be improved as the glucopyranose rings will have greater compatibility with the isophorone ring moiety of the hard blocks. As these hard blocks forfeit π-π ring stacking they will be less ridged and impose less conformational constraints on the soft-segment (shown by reduced shift in $T_g$ss). ATR analysis displays that the hard-segments within the adhesive are highly ordered with hydrogen bonded urethane and bidentate hydrogen bonded urea carbonyl groups observed. Observation of these groups displays that the hard-segment are well ordered and will act as reinforcements to the adhesive.

Confirmation that the cross-linked matrix formed is of greater strength than the adhesive – substrate interface is shown by the adhesive mode of failure at the interface. However, in some cases the adhesive strength at the interface is greater than the

cohesive strength of the TAc ply as shown by the cohesive ply failure for IPDI-TMP-PPG-PD. Considering this point it is acknowledged that the adhesion strength is greater when there are sufficient chemical groups for covalent bond formation. The compatibility of each PPG based formulation with the interface is still low due to phase mixing which imposes additional conformational constraints on the soft-segment chains removing their ability to successfully hydrogen bond with the substrate. This coupled with PPG containing a methyl group adjacent to every ether heteroatom will limit the ability of the soft-segment chains to form hydrogen bonds with the substrate.

Introduction of a more phase separated morphology by using PCD as the softsegment gives comparable peel strengths to PPG. Excluding TAc and a few other exceptions the peel strength obtained surpass the bench mark of 3 N mm^{-1}. As the phase morphology has greater separation compared to PPG (shown by DSC and ATR analysis) and the soft-segment has greater functionality, the adhesion to the interface should be greater when covalent bonding interactions are removed. From the peel strengths collected TAc laminates range from 0.6 N mm^{-1} to 1.0 N mm^{-1} following 30 days of cure and from this data it is clear that adhesion has not improved. The reason for this unexpected result can be explained by investigation of the morphology of the adhesive.

In all cases the hard-segment is highly ordered as evident by the positons of the N-H and C=O peaks. As mentioned previously it is the compatibility of the soft-segment with the interface that dictates the peel strength when hydrogen bonding is the target method of adhesion. From inspection of the adhesive layer which is white in colour it displays that the soft-segment has crystallised. Upon the first heating scan of DSC analysis a melting endotherm is clearly observed which has shifted by ~5°C compared to unreacted PCD (IPDI-TMP-PCD). Crystallisation will consume a high proportion of the potential hydrogen accepting groups reducing the number of groups available to the interface. This crystallisation by soft-to-soft interactions will constrain the soft-segment chains and reduce the mobility. This will have the same effect as hard-to-soft interaction and perturb the adhesives ability to efficiently hydrogen bond with the interface as shown by the low peel strengths obtained for TAc-TAc.

The final set of PU-U adhesives based on a PDEGA soft-segment possesses the greatest degree of phase separation. Confirmation of this morphology was shown by both DSC and ATR analysis. The most significant result obtained for PDEGA formulations was the major increase in the peel strength obtained for TAc. For formulation IPDI-TMP-PDEGA, the peel strength at 7 days was low only registering 0.9 N mm^{-1} with a cohesive mode of failure observed within the adhesive. Following 30 days of cure, the mode of failure changed to a cohesive failure of the ply and a strength measurement was unobtainable. This result displays that the adhesive strength is greater than the cohesive strength of the TAc with ply failure occur preferentially over delamination. Following chain-extension, the mode of failure obtained was different with an adhesive failure at the interface obtained however, as the peel strength was 6.4 N mm^{-1} following 30 days of cure which is twice the bench mark value this result is still very positive.

Interestingly with this set of adhesive formulations, the need for saponification appears to be removed. In all previous formulations, saponification was essential if ≥ 3 N mm^{-1} peel strengths are to be obtained with TAc based laminates. The redundancy of saponification is shown by the similar peel strengths obtained for TAc-TAc and TAc(t)TAc(t). The two factors that are believed to deliver this result are: (a) greater phase separation of the morphology gives a less constrained softsegment which can effectively hydrogen bond with the interface and (b) the reduction in the free isocyanate content due to the higher soft-segment molecular weight reduces the probability of forming covalent bonds with the interface. The ability to hydrogen bond with the interface is also promoted by PDEGA being amorphous which removes the possibility that hydrogen donor groups become consumed by crystallisation as in PCD.

As the compatibility of the two segments is low, the drive toward phase separation is high forming isolated domains of hard-segment within a mass of soft-segment. It is believed due to the highly order hard-segments obtained (see ATR data in section 8.22) that self-organisation occurs preferentially over reaction with the reactive groups at interface. This point is shown by the same mode of failure and peel strength obtained for TAc/TAc and TAc(t)/TAc(t). These highly order hardsegments will reinforce the adhesive giving the material high strength once fully cured. This is evident in the other

laminates for both formulations which also form high peel strength laminates with all obtaining above bench mark values.

8.33 Comparison of the Peel Strength Obtained for Aromatic and Aliphatic Polyurethane Adhesives

Considering all the above discussed factors, the proposed relationship between phase morphology and adhesive properties is, as phase separation is increased the adhesive properties are also increased. This is shown in three ways: (a) the improved adhesive performance of IPDI compared to MDI formulations, (b) as the molecular weight is increased the hard-segment content is decreased giving a more phase separated morphology and (c) have accessible hydrogen bonding groups in the soft-segment is essential to obtain high peel strengths with TAc/PC.

The first point is confirmed by the greater elevation of the $T_g$ss in MDI based formulations. Elevated soft-segment glass transition is consequence of increased phase mixing which in turn reduces the conformational mobility of the soft-segment. This reduced motion results in less organised hard-segments which will limit the reinforcement of the adhesive but more crucially lowers the hydrogen bonding ability of the soft-segment. These effects are more pronounced in MDI formulations as the hard-segment has greater compatibility with the ether soft-segment which is in keeping with the literature.[37,38] This increased phase mixing of MDI based formulations is visible in the N-H peak of each adhesive which is shifted to lower wavenumbers. The compatibility of hard and soft-segment is further increase in MDI following chain-extension. This improved compatibility is believed to result from the greater polar nature of the hard-segment following the introduction of each diol chain-extender. IPDI based hard-segments show no improvement in segment compatibility following chain-extension and this will result in the greater strength obtained as the phase morphology has greater separation.

The second argument that confirms the proposed relationship is a consequence of the stoichiometry used which is kept constant throughout. The isocyanate/hydroxyl ratio is kept constant at 2.2:1.0 however; as the mass of soft-segment is increased, the required amount of isocyanate to serve this stoichiometric ratio is reduced. Calculation of the hard-segment content (see section 1.37) displays that it is reduced in the order

PPG > PCD > PDEGA, this is also the order of increasing soft-segment molecular weight (see sections 8.11 and 8.12 for hard-segment content data). Reducing the hard-segment content helps to drive the morphology toward phase separation and this phase separation effect is more pronounced in IPDI compared to MDI as shown in previous analysis.

The third point is evident from the peel strengths obtained for TAc/TAc which are extensively poor except for the exception of PDEGA based formulations with IPDI. This is displayed by the redundancy of saponification as it no longer has a significant effect on the peel strength obtained. This makes the target mode of adhesion different as it has now shifted from covalent bond to hydrogen bond formation. As shown IPDI based formulations have greater phase separation within the microphase structure which leads to greater adhesion compared to MDI based formulations.

8.40 The Relationship between Haze and Morphology in Polyurethane Adhesives

8.41 Discussion of the Haze in Aromatic Based Polyurethanes Adhesives and the Relationship to Morphology

The haze within the adhesive layer will be influenced by the adhesives morphology, application and cure (see section 2.17 for haze measurement procedure). The morphology obtained is strongly influenced by the soft-segment and hard-segment. MDI adhesives derived from PPG were very clear e.g. formulations MDI-TMP-PPG and MDI-TMP-PPG-DEPD have haze values of <1.1% and <0.4% respectively. In these cases the phase mixed morphology obtained inhibits large hard domain formation which could add haze through crystallisation. These low haze values display that within the phase mixed structure of the PU-U, the features formed are either small enough or large enough that they do scatter visible light. The importance of application in obtaining low haze is shown by MDI-TMP-PPG-BD and MDI-TMP-PPG-PD where issues were encountered during application. In the BD chain-extended version a large amount of bubbles are visible within the bond line resulting in an elevated haze value (feature of the correct magnitude to scatter light). These bubbles were believed to be the liberation of entrapped gas at the material solidifies during cure. When PD is used as the chain-extender, the material was very streaky due to the application via Meyer

bar. This results in a very uneven adhesive layer which also correlated to a > 1.5% haze value.

Following the introduction of the crystalline soft-segment the morphology changed by becoming more phased separated. For the TMP only chain-extended formulation this dramatically affected the haze as the adhesive layer was milky white. This greater phase separated morphology allowed crystallisation of the soft-segment leading to a >1.5% haze value. The increased haze due to soft-segment crystallisation occurs due to the ordered domains formed being of the correct magnitude to scatter visible light. Following diol chain-extension, crystallisation of the soft-segment is removed and does not reoccur even after an extended period of time (> 6 month). This change in adhesive layer occurs as the morphology becomes more phased mixed due to the migration of urethane based hard-segments obtained during chain-extension into the soft-segment. Therefore, phase mixing removes the ability of the soft-segment to form feature that scatter visible light and gives clear adhesive layers.

The high haze values obtained for both PDEGA based adhesives (>1.5% in each case) results from the very high viscosity making application difficult. Even with sufficient degassing of the adhesive before application bubbles remain within the adhesive which directly affects the haze. As the adhesive is very viscous, application was not homogeneous which resulted in the addition of defects in the form of streaks. The combination of bubbles and streaking account for the poor haze obtained (features of the correct magnitude to scatter light). It would be expected if application could be optimised that these adhesive would have lower haze due to the greater phase separation within the morphology and the amorphous soft-segment.

8.42 Discussion of the Haze in Aliphatic based Polyurethane Adhesives and the Relationship to Morphology

Following the previous discussion on the relationship between haze and morphology of PU-U adhesives for aromatic systems, the discussion will now be extended to aliphatic systems. Again the key parameters which determine the haze within the adhesive layer are the morphology, application and cure. In PPG based polyurethane low haze values are obtain and ranged from 0.3% to 0.8%. Such low values are inherent of the amorphous soft-segment PPG which is a low viscosity clear liquid.

This gives low viscosity clear adhesive formulations which can be readily applied as an adhesive. The phase mixed morphology yields very clear adhesives which is an advantage for low haze but is a disadvantage for peel strength.

Moving to the more phase-separated morphology found in PCD based adhesives the haze is > 1.5% in each case. As these adhesives have a high degree of phase separation, the penetration of the hard-segment into the ester soft-segment is low due to the incompatibility of the segments. The consequence is that soft-segment crystallisation is only reduced (shown by reduction is melting enthalpy see section 8.12 table 8.02) and is not fully inhibited giving a milky white adhesive layer. Therefore, within the soft-segment the crystallites formed are of the magnitude which interacts and scatters visible light. This high haze makes these adhesives no fit for the proposed purpose as they are out with the maximum haze value of 1.5%.

In the final set of adhesives which are based on the amorphous adipate PDEGA the haze value obtained was 0.7% for both formulations. The high degree of phase separation does not affect the clarity due to the soft-segment being amorphous. Both PDEGA adipate adhesives following formulation remain low in viscosity and aids application.

8.43 Comparison of the Haze Obtained for Aromatic and Aliphatic Polyurethane Adhesives

Identified from the haze measurements obtained from MDI and IPDI based adhesives is that the relationship between haze and morphology is not a simple relationship and is dependent on the system used. It is possible to design and optically clear adhesive by following some simplified rules:

1. Use of a non-crystalline soft-segment promotes low haze as is evident in PPG and PDEGA based adhesive with IPDI
2. Aliphatic based adhesives are lower in viscosity which aids application and reduces the number of defects in the adhesive layer e.g. trapped bubbles, streaks etc. thus aiding low haze
3. Having a low hard-segment content will help reduce hazing from hardsegment crystallisation and reinforce the material through phase separation

4. Using non-linear or branched chain-extenders reduces the crystalline order within the hard-segment reducing haze.

It is also worth noting that for PCD, the introduction of diol chain-extenders removes crystallisation from the adhesive layer when a hard-segment of MDI is used. In the same IPDI based formulations each adhesive layer was highly crystalline and again reinforces that haze cannot be simply linked to morphology by a simple relationship. This statement is true as factors such as application can influence the haze and subsequent cure which will affect the final morphology.

Considering the above rules and other evidence design of a low haze adhesive layer capable of bonding TAc or PC will require a low viscosity aliphatic formulation with a non-crystallisable soft-segment which is sufficiently phase separated. Successful implementation of this relationship is only possible if the soft-segment has sufficiently functionality which facilitates hydrogen bonding with the interface as in PDEGA.

References

(1) Yen, M. S.; Cheng, K. L. *Journal of Applied Polymer Science* **1994**, *52*, 1707.
(2) Thapliyal, B. P.; Chandra, R. *Polymer International* **1991**, *24*, 7.
(3) Rek, V.; Bravar, M. *Journal of Elastomers and Plastics* **1983**, *15*, 33.
(4) Petrović, Z. S.; Javni, I.; Divjaković, V. *Journal of Polymer Science Part B: Polymer Physics* **1998**, *36*, 221.
(5) Ren, D.; Frazier, C. E. *International Journal of Adhesion and Adhesives* **2013**, *45*, 118.
(6) Wang, L.-F.; Wei, Y.-H. *Colloids and Surfaces B: Biointerfaces* **2005**, *41*, 249.
(7) Martin, D. J.; Meijs, G. F.; Gunatillake, P. A.; McCarthy, S. J.; Renwick, G.

M. *Journal of Applied Polymer Science* **1997**, *64*, 803.

(8)   Li, F.; Hou, J.; Zhu, W.; Zhang, X.; Xu, M.; Luo, X.; Ma, D.; Kim, B. K. *Journal of Applied Polymer Science* **1996**, *62*, 631.

(9)   Chen, T. K.; Chui, J. Y.; Shieh, T. S. *Macromolecules* **1997**, *30*, 5068.

(10)   Velankar, S.; Cooper, S. L. *Macromolecules* **2000**, *33*, 382.

(11)   Velankar, S.; Cooper, S. L. *Macromolecules* **2000**, *33*, 395.

(12)   Korley, L. T. J.; Pate, B. D.; Thomas, E. L.; Hammond, P. T. *Polymer* **2006**, *47*, 3073.

(13)   Tereshatov, V.; Makarova, M.; Senichev, V.; Slobodinyuk, A. *Colloid Polym Sci* **2012**, *290*, 641.

(14)   Daniel-da-Silva, A. L.; Bordado, J. C. M.; Martín-Martínez, J. M. *Journal of Applied Polymer Science* **2008**, *107*, 700.

(15)   Tereshatov, V. V.; Makarova, M. A.; Senichev, V. Y.; Volkova, E. R.; Vnutskikh, Z. A.; Slobodinyuk, A. I. *Colloid Polym Sci* **2015**, *293*, 153.

(16)   Yilgör, E.; Yurtsever, E.; Yilgör, I. *Polymer* **2002**, *43*, 6561.

(17)   Jena, K. K.; Chattopadhyay, D. K.; Raju, K. V. S. N. *European Polymer Journal* **2007**, *43*, 1825.

(18)   Seymour, R. W.; Cooper, S. L. *Macromolecules* **1973**, *6*, 48.

(19)   Li, Y.; Gao, T.; Liu, J.; Linliu, K.; Desper, C. R.; Chu, B. *Macromolecules* **1992**, *25*, 7365.

(20)   Šebenik, U.; Krajnc, M. *International Journal of Adhesion and Adhesives* **2007**, *27*, 527.

(21)   Li, W.; Ryan, A. J.; Meier, I. K. *Macromolecules* **2002**, *35*, 6306.

(22)   Sanchez-Adsuar, M. S.; Martín-Martínez, J. M. *Journal of Adhesion Science and Technology* **1997**, *11*, 1077.

(23)   Gisselfält, K.; Helgee, B. *Macromolecular Materials and Engineering* **2003**, *288*, 265.

(24)   Koberstein, J. T.; Leung, L. M. *Macromolecules* **1992**, *25*, 6205.

(25)   Clauβ, S.; Dijkstra, D. J.; Gabriel, J.; Kläusler, O.; Matner, M.; Meckel, W.; Niemz, P. *International Journal of Adhesion and Adhesives* **2011**, *31*, 513.

(26)   Neff, R.; Adedeji, A.; Macosko, C. W.; Ryan, A. J. *Journal of Polymer Science Part B: Polymer Physics* **1998**, *36*, 573.

(27)   Nishi, T.; Wang, T. T. *Macromolecules* **1975**, *8*, 909.

(28)   Painter, P. C.; Shenoy, S. L.; Bhagwagar, D. E.; Fishburn, J.; Coleman, M. M. *Macromolecules* **1991**, *24*, 5623.

(29)   Yılgör, E.; Yılgör, İ.; Yurtsever, E. *Polymer* **2002**, *43*, 6551.

(30)   Leibler, L. *Macromolecules* **1980**, *13*, 1602.

(31)   Wen, T.-C.; Fang, J.-C.; Gopalan, A. *Journal of Applied Polymer Science* **2001**, *82*, 1462.

(32)   Elwell, M. J.; Ryan, A. J.; Grünbauer, H. J. M.; Van Lieshout, H. C. *Polymer* **1996**, *37*, 1353.

(33)   Elwell, M. J.; Ryan, A. J.; Grünbauer, H. J. M.; Van Lieshout, H. C. *Macromolecules* **1996**, *29*, 2960.

(34)   da Silva, A. L. D.; Martín-Martínez, J. M.; Carlos Moura Bordado, J. *International Journal of Adhesion and Adhesives* **2008**, *28*, 29.

(35)   Petrie, E. M. *Metal Finishing* **2008**, *106*, 39.

(36)   Tout, R. *International Journal of Adhesion and Adhesives* **2000**, *20*, 269.

(37)   Chattopadhyay, D. K.; Prasad, P. S. R.; Sreedhar, B.; Raju, K. V. S. N. *Progress in Organic Coatings* **2005**, *54*, 296.

(38)   Chattopadhyay, D. K.; Sreedhar, B.; Raju, K. V. S. N. *Polymer* **2006**, *47*, 3814.

Chapter 9 Final Conclusions and Further Work

9.10 Recap of the Project Aims

The aims set at the beginning of this thesis were:

- Development of an optically clear adhesive which must have a haze of < 1.5% when laminated between two layers of plastic (cellulose triacetate or bisphenol-A polycarbonate or hybrid containing one of each layer)

- Development of an adhesive which is capable of bonding cellulose triacetate, bisphenol-A polycarbonate and any other laminates combinations containing these plastics

- Production of a fully cured laminate with a peel strength of $\geq$ 3 N mm^{-1} as determined by 180° T-peel testing

- Production of a fully cured adhesive free of thermal transitions within the window of -20°C to 100°C which would otherwise affect the in-use performance.

This section will present the conclusions on each set of formulations and their ability to fulfil these aims and further work required. A final conclusion on what is required to obtain an optically clear adhesive capable of bonding TAc and PC will also be established.

9.20 Conclusions

Within the previous chapter, it was identified that both the hard and soft-segments have an influence on the final morphology of the adhesive. This morphology will then influence the final adhesion properties of the fully cured PU-U. The most significant conclusions drawn from the work shown in previously chapters within this thesis will now be presented.

9.21 Adhesive based on MDI and PPG

Beginning with formulations based on MDI and PPG, obtaining an optically clear adhesive presented mixed results. Two formulations recorded a haze value below the 1.5% set value, namely MDI-TMP-PPG and MDI-TMP-PPG-DEPD, with the later displaying a low value of < 0.4%. Conversely, the other diol chain-extended

formulations displayed haze values of greater than 1.5% due to excessive bubbling and applications issues which presented feature of the correct magnitude to scatter visible light. Therefore it can be concluded that the PPG soft-segment promotes optically clear adhesive when application is performed successfully.

Across this set of adhesives, both PC/PC and PC(t)/PC(T) performed above the benchmark 3 N mm^{-1} with the exception of MDI-TMP-PPG-PD where an application issue was encountered. For TAc/TAc, however, all peel strengths obtained were below benchmark and the strengths obtained ranged between 0.0 N mm^{-1} – 0.6 N mm^{-1}. In order to obtain benchmark values saponification of the interface was required. Using this surface treatment, hydroxyl groups are reintroduced at the interface. These groups are then available to the reactive prepolymer adhesive and covalent bond formation is possible. This method allowed for peel strength of ≥ 3 N mm^{-1} to be obtained. It can be concluded that these adhesive have an affinity with PC based laminates but display an incompatibility toward TAc based laminates. This incompatibility however, is overcome by the saponification surface treatment.

Thermally, these formulations were stable above the maximum processing temperature and it would be anticipated that no degradation would be encountered as a result. This thermal stability was measured using TGA, with the onset of degradation occurring between 294°C to 312°C. It is therefore possible to draw the conclusion that these adhesives will be stable at the maximum processing temperature of 100°C.

Unfortunately theses adhesives do not fulfil all the set aims, and the areas which are not satisfied will now be highlighted. Firstly the requirement for surface treatment of TAc in order to gain benchmark peel strengths is not ideal. The surface treatment requires a caustic 2.5 M solution of sodium hydroxide, which is a health hazard and may also result in weakening of the TAc substrate. This solution is difficult to remove and its caustic nature requires chemically resistant parts, which will make scale-up to production more costly.

Another area in which these formulations do not meet the set aims is the position of the soft-segment glass transition temperature ($T_g$ss). Each formulation once fully cured has a $T_g$ss which exceeds -20°C. The $T_g$ss ranges from -8°C to 7°C and each diol

chain-extended formulations displayed a shift in the $T_g$ss compared to the TMP only formulation. This greater shift following diol chain-extension displays that the compatibility of urethane based hard-segments with PPG is greater than urea based hard-segments. This conclusion is drawn from the DSC data collected, and is shown by MDI-TMP-PPG presenting the lowest $T_g$ss. DSC has allowed, through observing the shift in the $T_g$ss to determine that the morphology within MDI and PPG based adhesives is phase mixed. It can be concluded that a phased mixed morphology will yield low haze but at the expense of good adhesion to both substrate types (TAc requires saponification).

9.22 Adhesives based on MDI and PCD

The next adhesive set formulated, still MDI-based but now contain the polyester softsegment PCD. For the first formulation which was absent of a diol chain-extender, the haze value recorded was > 1.5% due to crystallite formation of the correct magnitude to scatter visible light. In all cases where a diol-chain extender is added to the formulation, the haze value was < 1.5%. It has already been observed that urethane groups mix better than urea groups with the soft-segment. In this instance, it can be concluded that by introducing phase mixing through diol chain-extension it is possible to retard soft-segment crystallisation. The migration of these hard blocks into the soft-segment will result in hard-to-soft interactions occurring. These interactions will introduce addition confirmation constraints to the soft-segment which will reduce the order of soft-to-soft interactions. The consequence of these interactions is the inability to crystallise.

From peel testing it was displayed that formulations based on MDI and PCD, have an affinity for the PC interface. This is shown by the high peel strengths obtained for PC/PC which ranged from 4.8 N mm^{-1} to 8.2 N mm^{-1} and PC(t)/PC(t) which ranged from 4.0 N mm^{-1} to 8.3 N mm^{-1}. This observation is further supported by evidence obtained using hybrid laminates. For both hybrid laminate the mode of failure was adhesive at the TAc(t) interface, thus confirming the affinity of this adhesive set for PC over TAc.

It can also be concluded that formulations based on MDI and PCD are incapable of forming a laminate of peel strength ≥ 3 N mm^{-1} on TAc. Saponification of the TAc interface is essential to gain a ≥ 3 N mm^{-1} peel strength. However, this was only achieved using MDI-TMP-PCD. This suggests that upon reducing the free isocyanate content via diol chain-extension has a knock on effect which is a reduction in the peel strength obtained. This reduction in peel strength was consistent for all diol chain-extended formulations and is due to a reduced probability of forming covalent bonds at the interface. The main conclusion drawn from this set of formulations is that high peel strength can be obtained at the expense of haze or vice versa, but it is not possible to obtain both. This is the main drawback identified for this set of formulations along with the inability to bond TAc.

The thermal stability of these formulations was also well above specification. Onsets of degradation ranged from 297°C to 316°C, with diol chain-extension responsible for around a 20°C reduction in the onset temperature. This small reduction however, did not affect the potential for these adhesives to be used within the intended application as they are all stable well above the maximum processing temperature of 100°C.

Already established thus far, is that these formulations cannot be used for the intended application as they either do not meet the 1.5% haze value or the 3 N mm^{-1} benchmark peel strength. Further data that supports these conclusions can also be observed form the DSC analysis carried out on this set of formulations. Within the DSC thermogram of the TMP only chain-extended formulation, a soft-segment melting endotherm is present. This melting peak confirms that crystallisation of the soft-segment is responsible for the high haze value obtained. Diol chain-extension results in a shift of the $T_g$ss to higher temperatures with values obtained ranging from -32°C to -30°C. It can be concluded that increasing the molecular weight has resulted in the $T_g$ss remaining lower than -20°C. The positive temperature shift of the $T_g$ss following diol chain-extension is evidence that the degree of phase mixing has increased. These two pieces of data support the conclusion that increasing the degree of phase mixing is responsible for the removal of the soft-segment crystallisation. Therefore by introducing more urethane groups via diol chainextension it is possible to increase the degree of phase mixing within the microstructure.

9.23 Adhesives based on MDI and PDEGA

The morphological behaviour of the MDI-based hard segments was then tested using PDEGA which has both ester and ether function groups along the backbone structure. Formulations based on MDI and PDEGA prepared by the bulk prepolymer method were of high viscosity and difficult to apply. This high viscosity results in bubbles becoming easily trapped within the adhesive layer and accounts for the high haze obtained. These formulations are in keeping with previous MDI-based formulations as they possess an affinity for PC over TAc. This conclusion is further supported by the mode of failure in all hybrid laminated being adhesive at the TAc(t) interface.

Following observation of all MDI-based formulations it can be concluded that the aromatic groups within the hard-segments of the adhesive boost the compatibility with the aromatic bisphenol-A PC substrate. As the peel strength of TAc/TAc was greater than 1 N mm^{-1} in both formulations it can be concluded that PDEGA must be interacting with the interface. It is believed that the aromatic hard-segments within these formulations inhibit movement of the soft-segment which removes the mobility required to form an intimate bond with the TAc interface, which consequently removes the potential for a peel strength ≥ 3 N mm^{-1} to be obtained.

Thermally these formulations were stable well above the maximum processing temperature with 313°C recorded for the TMP only formulation and 316°C for the DEPD chain-extended formulation. This displays that at the maximum processing temperature of 100°C no degradation should occur. It can be concluded that formulations containing an aromatic hard-segment based on MDI, will be stable above the maximum processing temperature.

DSC analysis displayed a smaller shift in the $T_g$ss compared to PPG and PCD based formulations. This confirmed greater phase separation within the adhesive and displays the greater adhesion to TAc compared to PPG or PCD. Phase separation indicates that the compatibility of the phases is lower but it will also be a consequence of the reduced hard-segment content. Consistent within these formulations was the shift of the $T_g$ss following diol chain-extension. For the TMP only formulations the recorded $T_g$ss was -30°C which shifted to -26°C following chain-extension with

DEPD. Thus supporting the conclusion that diol chainextension promotes phase mixing.

9.24 Adhesives based on IPDI and PPG

Returning to the initial soft-segment of PPG some noticeable changes to the properties of the final PU-U were apparent compared to the MDI series. Following implementation of an aliphatic hard-segment a shift in the peel strength is noticeable. Interestingly for these formulations, the laminate which boasts the best performance is TAc(t)/TAc(t), with peel strengths of 3.3 N mm^{-1} to 9.6 N mm^{-1} obtained. This high performance does not correlate to improved performance on TAc/TAc which displayed poor results. It can be concluded from this result that it is indeed the softsegment that is responsible for adhesion to the interface when covalent bond formation is not possible.

The compatibility of this set of adhesive has changed with respect to the MDI-based series. Laminates based on PC performed above benchmark in all cases with PC/PC, with the only exception being IPDI-TMP-PPG-BD. This result is in keeping with MDI-based formulations however, the compatibility towards PC is not retained within hybrid laminates. For all hybrid laminates an adhesive mode of failure at the PC or PC(t) interface was obtained. In conclusion, upon moving to an all aliphatic polyurethane adhesive, the compatibility with PC has been reduced. This shift in the compatibility towards TAc(t) may be the result of the greater cure time allowing for more covalent bonds to be formed. This covalently bonded interface will be of higher strength than the PC interface which will primarily be based on H-bonding.

Haze values collected for each of the formulations based on IPDI and PPG were < 0.8%. This high clarity is inherent of both the starting materials which are low viscosity liquids. It can therefore be concluded that the final haze value of the adhesive is dependent on both the hard-segment and soft-segment.

Thermally, these materials were stable well above the maximum processing temperature of 100°C. The onset of degradation ranged from 250°C to 278°C which is a reduction compared to MDI-based formulations. Drawn from this result is that aliphatic isocyanates will still yield materials which possess a high enough thermal

resistance required for the intended application. Introduction of the aliphatic hardsegment does have a distinct impact on the observed shift of the $T_g$ss. Data supporting this statement is obtained from the position of the $T_g$ss obtained by DSC analysis, with the $T_g$ss ranging between -33°C to -28°C. It can be concluded that the compatibility of IPDI and PPG is lower than the compatibility of MDI and PPG. This is shown by a reduced shift in the $T_g$ss of around 30°C and this displays greater phase separation in IPDI-based formulations compared to MDI-based formulations. Within this set of formulations, the only aim not satisfied was obtaining a laminate of peel strength ≥ 3 N mm^{-1} with TAc.

9.25 Adhesives based on IPDI and PCD

Further changes to the morphology were observed using IPDI with PCD. Peel strength data obtained was the highest of the four sets presented thus far. This is especially true for PC/PC which recorded the peel strength of 10.5 N mm^{-1}. Thus it can be concluded that having a soft-segment with greater functionality will boost the peel strength obtained. These high peel strengths obtained however, did not translate to improved adhesion with TAc which still recorded below benchmark. It can be concluded from this result that both the soft-segment and the final morphology will impact the adhesion properties. This conclusion will become more apparent in the remainder of this section.

Obtaining high peel strength has come at the expense of haze as all four formulations recorded a value of $> 1.5\%$. The high haze value obtained is a consequence of the crystalline soft-segment used. This is confirmed by the soft-segment melting endotherm observed in the first heating scan of each DSC thermogram. It can be concluded that use of a crystallisable soft-segment will enhance peel strength but will increase the haze as a result. Utilisation of crystallisation in this way is common in hot-melt and reactive hot-melt adhesives but is not suitable for the current application. Crystallisation of the soft-segment also indicates the phase-separated morphology of this adhesive set. Previously in MDI-based formulations it was possible to inhibit this crystallisation behaviour using diol chain-extenders which increased phase mixing. This increase in phase mixing does occur with IPDI-based formulations, although, the migration of the hard blocks into the soft-segment is not sufficient enough to stop

crystallisation. Evidence of this increase in phase mixing is shown by the depression of the melt temperature and enthalpy of melting. This result both confirms chain-extension improves phase mixing and that IPDI is less compatible with PCD than MDI.

The conclusion drawn from this set of adhesives is that a phase separated morphology will give better adhesion properties but at the expense of haze. Also ester functional groups within the soft-segment increase intermolecular adhesion of the matrix.

9.26 Adhesives based on IPDI and PDEGA

Formulations synthesised from IPDI and PDEGA are the only adhesives that satisfy all the aims outlined at the beginning of this thesis (see section 1.39). This statement will now be justified by firstly considering the peel strength data collected. The most significant result obtained using these formulations were the high peel strengths obtained with TAc/TAc. As previously stated, out of all the formulations tested only adhesives based on IPDI and PDEGA were able to deliver this aim. For the TMP only formulation, a cohesive failure of the TAc substrate was recorded for each test. When the DEPD chain-extended formulation was used the peel strengths obtained was > 6 N mm^{-1} which is twice the set benchmark. Laminates which were surface treated by saponification, gave results of the same magnitude for both adhesives. It can therefore be concluded that adhesion is not occurring via covalent bond formation. As the hard-segment content is between 17% – 20.6%, the potential for covalent bond formation is reduced compared with PPG and PCD, meaning most isocyanate groups will be consumed during the formation of hard blocks.

Most likely the dominant modes of adhesion will be a mixture of chemical and mechanical. H-bonding is believed to be the main form of adhesion occurring and will account for the strength observed with the PDEGA soft-segment. Also possible is mechanical adhesion via the adhesive penetrating the substrate and following cure it will give the lock and key type mechanism. This mode is possible due to the lower viscosity and slower curing rate of these formulations. It can be concluded that using a polyurethane adhesive based on IPDI and PDEGA, it is possible to obtain peel strengths of ≥ 3 N mm^{-1} with both TAc and PC without the requirement for any surface treatments.

Both formulations delivered haze values which were below the 1.5% maximum haze value. The average value obtained in both cases was < 0.7% haze which is around half the maximum value. From this result it is concluded that to obtain a polyurethane adhesive with a final haze value of < 1.5% haze, the soft-segment must be non-crystalline. This was achievable using PDEGA as the combination of both ether and ester groups preventing crystallisation, resulting in an amorphous softsegment.

Thermally these formulations satisfy the aims set out at the beginning of this thesis. The onset of degradation recorded for the TMP only chain-extended formulation was 293°C, with a similar value of 297°C recorded for the adhesive containing the diol chain-extender DEPD. It can therefore be concluded that any of the PU-U adhesive used within this thesis would be thermally stable for the intended application. This conclusion is drawn from the thermal stability being governed by the resistance of both urethane and urea bonds to thermal cleavage, it has been shown that this occurs well above the maximum processing temperature of 100°C.

The next piece of thermal information is the $T_g$ss of each cured PU-U, with both occurring at a temperature lower than -20°C. In the TMP only chain-extended formulation, the observed $T_g$ss was -38°C and this same value was also obtained for the DEPD chain-extended formulation. Both the $T_g$ss and the range in which is occurs is well out with the -20°C set temperature and this satisfies the aim set out initially. It can therefore be concluded that to obtain a PU-U adhesive with a $T_g$ss of less than -20°C a soft-segment of molecular weight $\geq$ 2000 is required with an aliphatic hard-segment such as IPDI.

The final conclusion from the presented work is as follows. Obtaining an optically clear adhesive which has a haze of < 1.5%, is void of thermal transition between 20°C to 100°C which will interfere with the adhesive in use performance, can bond both untreated TAc and PC with a peel strength of $\geq$ 3 N mm^{-1} is only possible using a polyurethane adhesive based on IPDI and PDEGA.

9.30 Further work

Now that a successful formulation has been identified in IPDI-TMP-PDEGA-DEPD, optimisation of the application and cure are required. Currently the full cure time is in

the region of 30 days which for a lamination is too slow. In order for this adhesive to be used within production it must fully cure within hours rather than days. A faster cure is required because there is the potential for slippage if the adhesive is liquid when the laminate is collected on the storage roll. This will introduce both a slight curve to the material and more importantly, optical defects.

The first optimisation step that would be required would be a detailed rheology study to determine the actual viscosity of IPDI-TMP-PDEGA-DEPD at both the temperature of synthesis and applications. This study would be combined with dynamic mechanical thermal analysis (DMTA) which would allow for characterisation of the fully cured adhesive. The data collected by DMTA would be complementary to DSC and further the understanding of the cured PU-U. DMTA would also help with the location of weak transitions such as the hard-segment glass transition which are difficult to observe using DSC. Further characterisation of the microphase structure using both SAXS (small angle X-ray scatter) and WAXS (wide angle X-ray scatter) would be of interest as this would allow for characterisation of the crystallite size of each PU-U material.

It would also be of interest if more time was available to vary the stoichiometry during synthesis. During the prepolymer synthetic procedure used there are two potential places to vary the stoichiometry, either at the initial prepolymer stage or at the chain-extension stage. In the first instance the size of the prepolymer will increase as the ratio approaches 1:1 and this will reduce the free NCO content. It would be expected that this process would result in an increase in viscosity but it has the potential to reduce the cure time. At the chain-extension step, the stoichiometry can be changed to increase the size of the hard blocks. This would be carried out by adding additional diisocyanate as the chain-extender is added. It would also be of interest to attempt some one-pot synthesis to determine if the synthetic procedure can be simplified but yield the same adhesion performance.

It would also be of interest to determine the optimum TMP content which currently is set at 15 mole% of the total chain-extender content. Trialling a blended polyol system using siloxanes to reduce the hydrophilicity and reduced the potential for

depolymerisation of the adipate through hydrolysis would also be of interest. If more time was available hexamethylene diisocyanate (HMDI) based polyurethanes would have been investigated. It would not be expected that using HMDI would have an adverse effect on the properties of the polyurethane adhesives. If successful the implementation of HMDI would reduce the cost of the adhesive as the hexamethylene diamine starting material used in the synthesis of HMDI is readily produced as it is starting material in polyamide synthesis.

Another area of interest is the cure time of the adhesive which currently takes around 30 days to reach full cure. The current curing catalysts are DBDTL and triethylamine which are common polyurethanes catalysts. These catalysts are used in the formation of urethane and urea. Urea formation is advantages for strengths as it promotes adhesion within the hard block but the CO_2 side product is unwanted in lamination. Therefore if more time was available other curing strategies such as trimerisation, silane moisture cure, oxazolidines or blue light acrylic cure would be attempted. These methods of cure would reduce the cure time and allow for reduced lamination times.

If more time was allowed it would have been of interest to further characterise the interface left following peel testing. Previously this was carried out by visual inspection or ATR. It would be of more interest to try more surface sensitive techniques such as XPS (X-ray photoelectron spectroscopy) or SIMS (secondary ion mass spectroscopy) to determine if adhesive failures. These techniques would be able to identify very then adhesive layers which are undetectable by ATR (penetration depth ~ 2 μm). Further characterisation using SEM (scanning electron microscopy) to picture the fracture surface and use of AFM (atomic force microscopy) to map the fracture surface would also have been attempted to further understand each failure.

Finally large scale laminations would have been attempted if the previously outlined work had been complete. These large scale laminations would be used to characterise the quality of the adhesive following lamination. The quality would be gauged on the cure time, haze value, peel strength and number of optical defects. Only when successful large scale laminations have been performed and passes would the adhesive be used in production.

Appendix B - Deconvolution of N-H and C=O peaks to gain an insight in to the microstructure of PU-Us

Deconvolution of MDI and PPG based formulations

1 - MDI-TMP-PPG

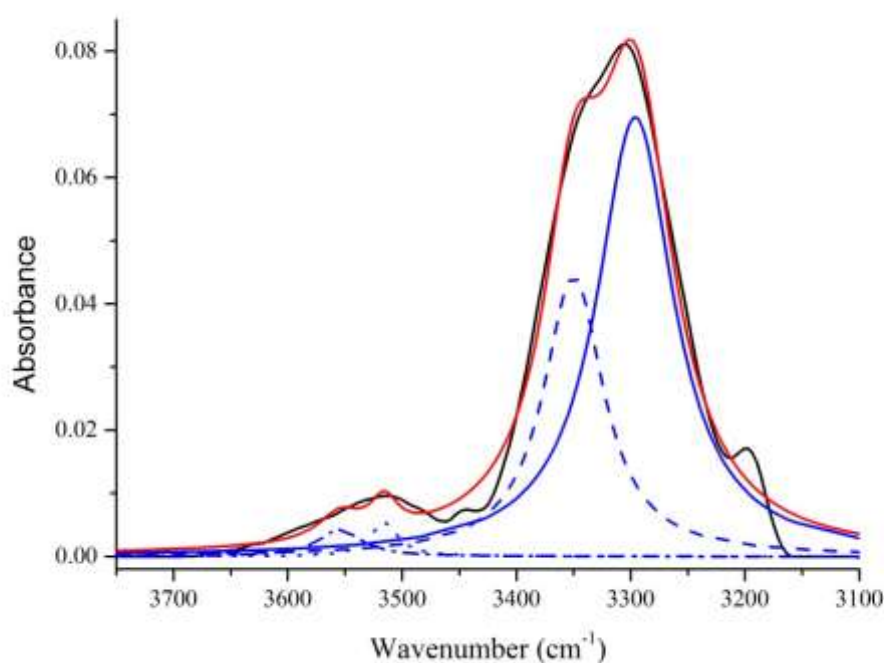**N-H Region Deconvolution**

Lorentzian Fit of N-H

Figure B01: Deconvolution data for MDI-TMP-PPG of N-H region. Data calculated using Lorentzian fitting function. [Raw data in black, fit data in red, HS-HS fitted peak solid blue, carbonyl overtone dash blue, free N-H Dot and dot dash blue].

      1: Deconvolution data of N-H region collected using Lorentzian function of MDI-TMP-PPG.

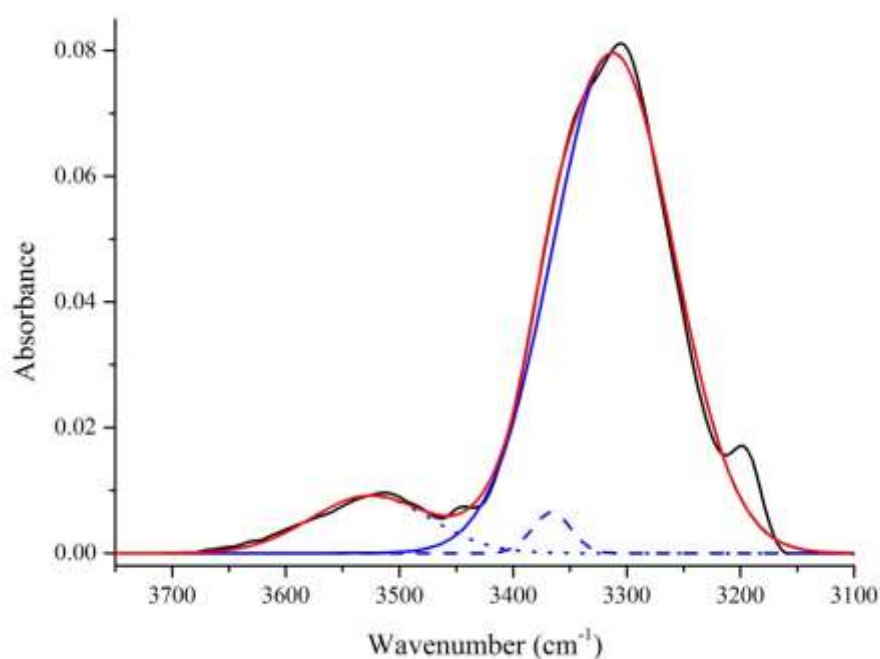| MDI-TMP-PPG					
Peak Position/cm^{-1}	Standard Error/cm^{-1}	Area	Standard Error	Area/%	Fit R^2 value
3554	11.10	0.311	0.22	2.2	
3516	5.6	0.250	0.19	1.8	0.988
3350	1.60	4.46	0.51	32.1	
3296	1.44	8.87	0.54	63.9	

Gaussian Fit of N-H

Figure B02: Deconvolution data for MDI-TMP-PPG of N-H region. Data calculated using Gaussian fitting function. [Raw data in black, fit data in red, HS-HS fitted peak solid blue, carbonyl overtone dash blue, free N-H Dot and dot dash blue].

Table B02: Deconvolution data of N-H region collected using Gaussian function of MDI-TMP-PPG.

MDI-TMP-PPG					
Peak Position/cm^{-1}	Standard Error/cm^{-1}	Area	Standard Error	Area/%	Fit R^2 value
3525	3.80	1.201	7.6×10^{-2}	8.8	
3366	2.86	0.277	0.12	2.5	0.993
3312	2.20	10.68	0.17	88.7	

Gaussian-Lorentzian Fit of N-H

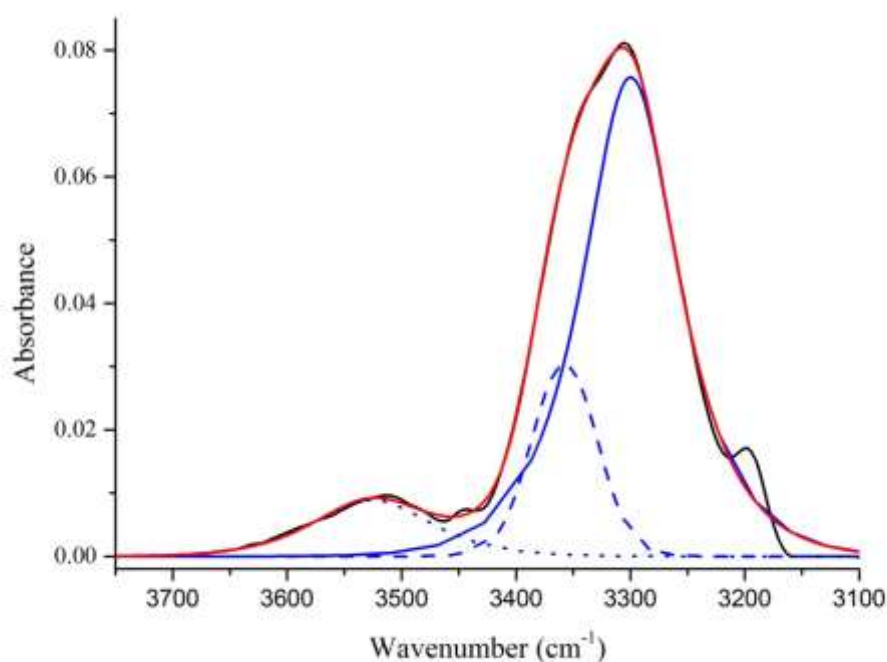**Figure B03: Deconvolution data for MDI-TMP-PPG of N-H region. Data calculated using Gaussian-Lorentzian cross fitting function. [Raw data in black, fit data in** red**, HS-HS fitted peak** solid blue**, carbonyl overtone** dash blue**, free N-H** Dot **and** dot dash blue**].**

3: Deconvolution data of N-H region collected using GaussianLorentzian cross function of MDI-TMP-PPG.

MDI-TMP-PPG

Table B0

Peak Position/cm^{-1}	Standard Error/cm^{-1}	Area	Standard Error	Area/%	Fit R^2 value
3525	4.20	0.009	4.7x10^{-4}	4.0	
3357	7.40	0.030	8.6x10^{-3}	32.2	0.996
3300	7.00	0.076	9.7x10^{-4}	63.8	

C=O Region Deconvolution
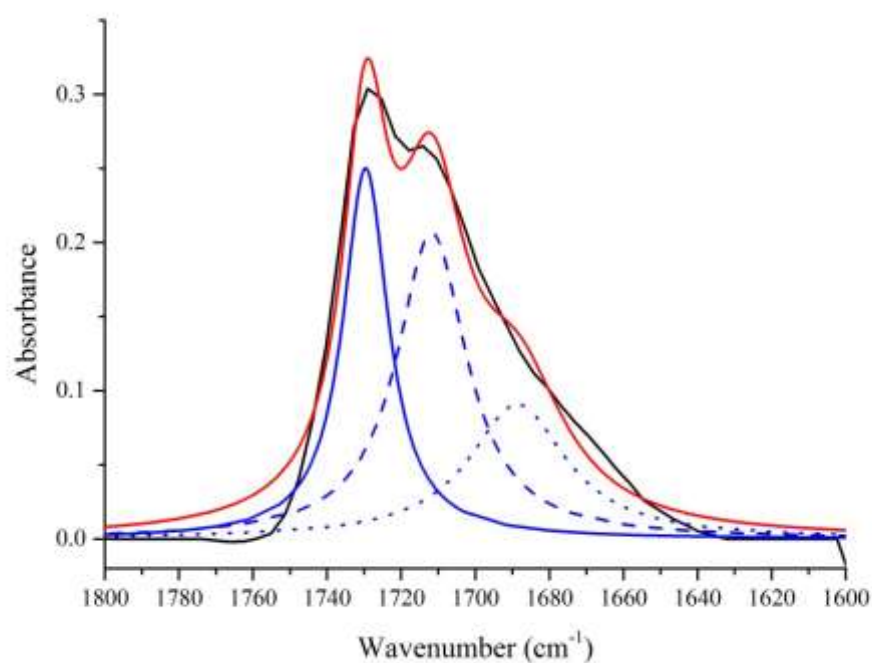
Lorentzian Fit of C=O

Figure B04: Deconvolution data for MDI-TMP-PPG of C=O region. Data calculated using Lorentzian fitting function. [Raw data in black, fit data in red, free carbonyl peaks solid blue, hydrogen bonded C=O dash blue and free urea Dot blue].

Table B0

4: Deconvolution data of C=O region collected using Lorentzian function of MDI-TMP-PPG.

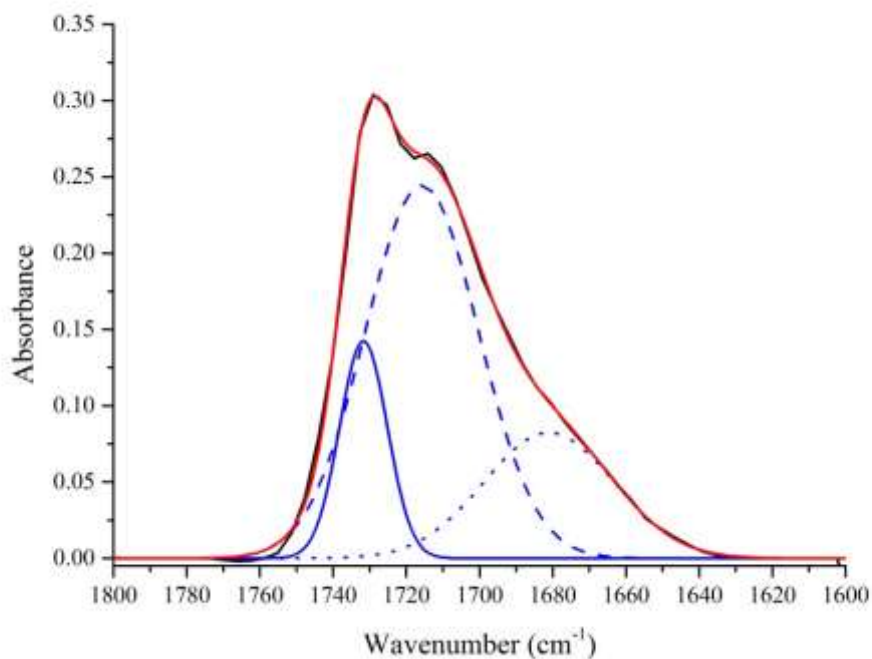|		MDI-TMP-PPG			
Peak Position/cm^{-1}	Standard Error/cm^{-1}	Area	Standard Error	Area/%	Fit R^2 value
1729	0.63	5.862	1.33	32.8	
1712	1.13	7.448	3.07	41.6	0.975
1688	4.04	4.573	2.09	25.6	

Gaussian Fit of C=O

Figure B05: Deconvolution data for MDI-TMP-PPG of C=O region. Data calculated using Gaussian fitting function. [Raw data in black, fit data in red, free carbonyl peaks solid blue, hydrogen bonded C=O dash blue and free urea Dot blue].

Table B0

5: **Deconvolution data of C=O region collected using Gaussian function of MDI-TMP-PPG.**

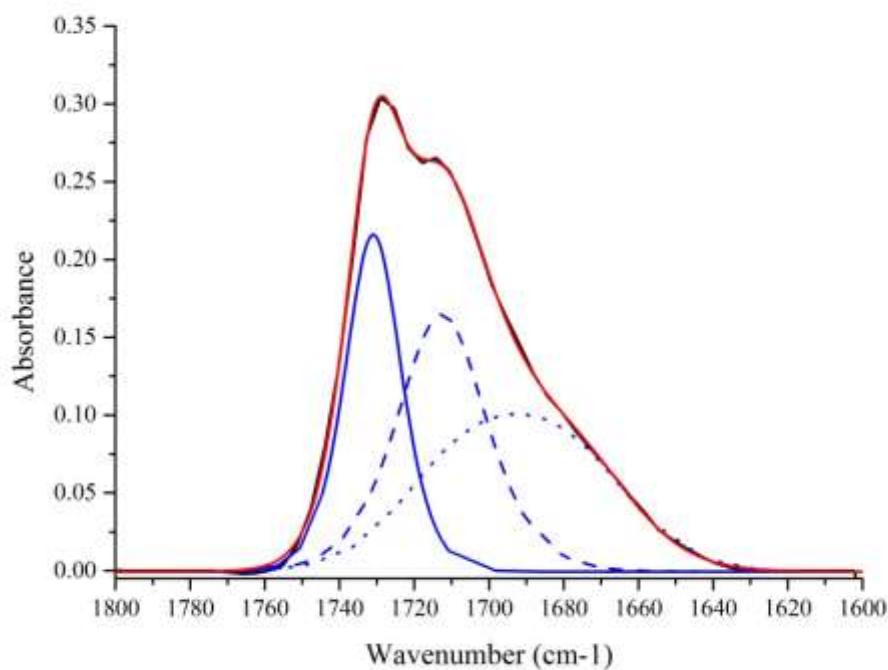|	MDI-TMP-PPG				
Peak Position/cm^{-1}	Standard Error/cm^{-1}	Area	Standard Error	Area/%	Fit R^2 value
1731	0.28	2.327	0.29	15.0	
1716	1.42	9.502	0.75	61.3	0.997
1681	4.02	3.673	0.80	23.7	

Gaussian-Lorentzian Fit of C=O

Figure B06: Deconvolution data for MDI-TMP-PPG of C=O region. Data calculated using Gaussian-Lorentzian cross fitting function. [Raw data in black, fit data in red, free carbonyl peaks solid blue, hydrogen bonded C=O dash blue and free urea Dot blue].

Table B0

6:     Deconvolution   data   of   C=O   region   collected   using GaussianLorentzian cross function of MDI-TMP-PPG.

MDI-TMP-PPG					
Peak Position/cm^{-1}	Standard Error/cm^{-1}	Area	Standard Error	Area/%	Fit R^2 value
1731	3.91	0.216	0.08	44.8	
1713	8.64	0.165	0.21	34.2	0.998
1692	4.28	0.102	0.01	21.0	

2 - MDI-TMP-PPG-DEPD

N-H Region Deconvolution
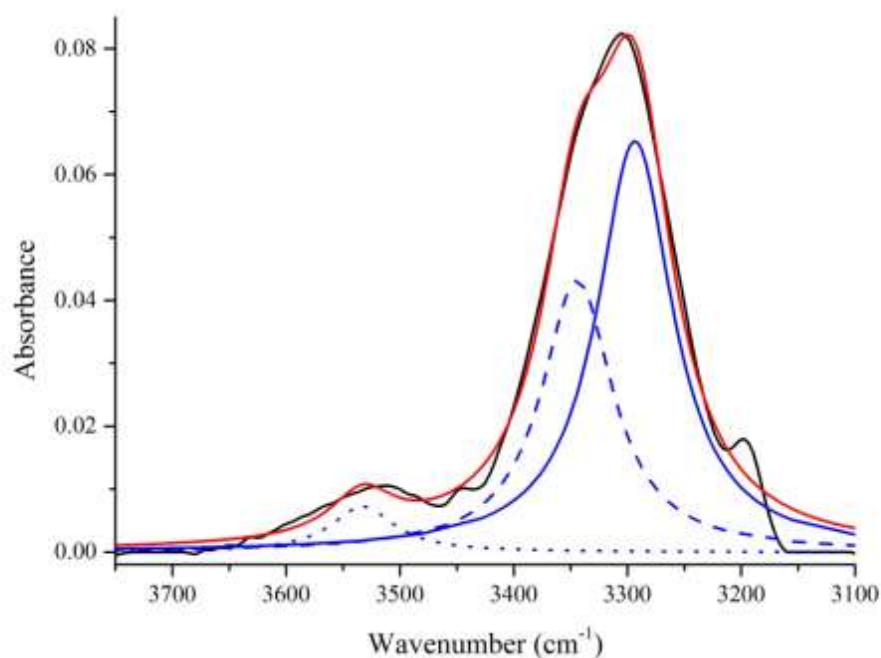
Lorentzian Fit of N-H

Figure B07: Deconvolution data for MDI-TMP-PPG-DEPD of N-H region. Data calculated using Lorentzian fitting function. [Raw data in black, fit data in red, HS-HS fitted peak solid blue, carbonyl overtone dash blue and free N-H Dot blue].

Table B07: Deconvolution data of N-H region collected using Lorentzian function of MDI-TMP-PPG-DEPD.

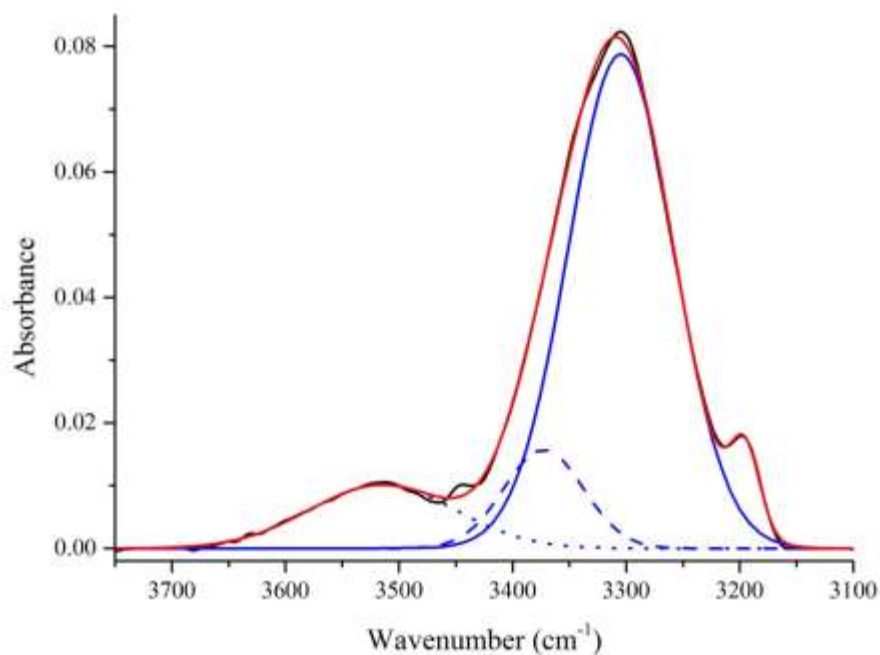| MDI-TMP-PPG-DEPD					
Peak Position/cm^{-1}	Standard Error/cm^{-1}	Area	Standard Error	Area/%	Fit R^2 value
3533	4.50	0.778	0.12	5.5	
3344	2.45	5.193	0.74	36.5	0.989
3293	1.75	8.374	0.73	58.1	

Gaussian Fit of N-H

Figure B08: Deconvolution data for MDI-TMP-PPG-DEPD of N-H region. Data calculated using Gaussian fitting function. [Raw data in black, fit data in red, HS-HS fitted peak solid blue, carbonyl overtone dash blue and free N-H Dot blue].

Table B08: Deconvolution data of N-H region collected using Gaussian function of MDI-TMP-PPG-DEPD.

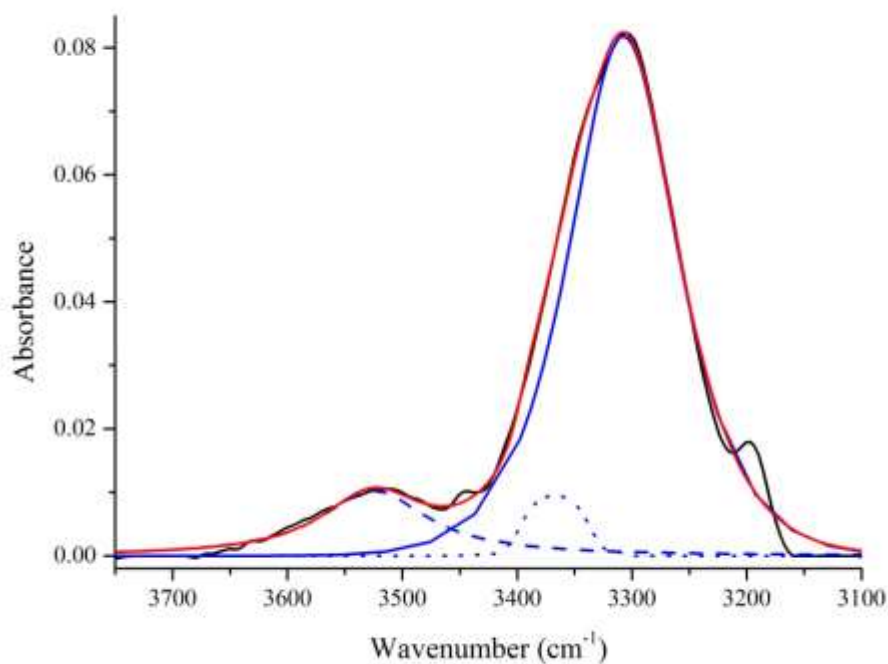| MDI-TMP-PPG-DEPD					
Peak Position/cm^{-1}	Standard Error/cm^{-1}	Area	Standard Error	Area/%	Fit R^2 value
3514	1.64	1.633	0.037	13.4	
3372	4.33	1.386	0.39	11.4	0.999
3305	1.95	9.168	0.39	75.2	

Gaussian-Lorentzian Fit of N-H

Figure B09: **Deconvolution data for MDI-TMP-PPG-DEPD of N-H region. Data calculated using Gaussian-Lorentzian cross fitting function. [Raw data in black, fit data in red, HS-HS fitted peak solid blue, carbonyl overtone dash blue and free N-H Dot blue].**

Table B09: **Deconvolution data of N-H region collected using GaussianLorentzian cross function of MDI-TMP-PPG-DEPD.**

MDI-TMP-PPG-DEPD					
Peak Position/cm^{-1}	Standard Error/cm^{-1}	Area	Standard Error	Area/%	Fit R^2 value
3525	3.31	0.010	-	10.1	
3367	3.09	0.009	0.002	9.3	0.995
3307	1.56	0.082	0.001	80.6	

C=O Region Deconvolution
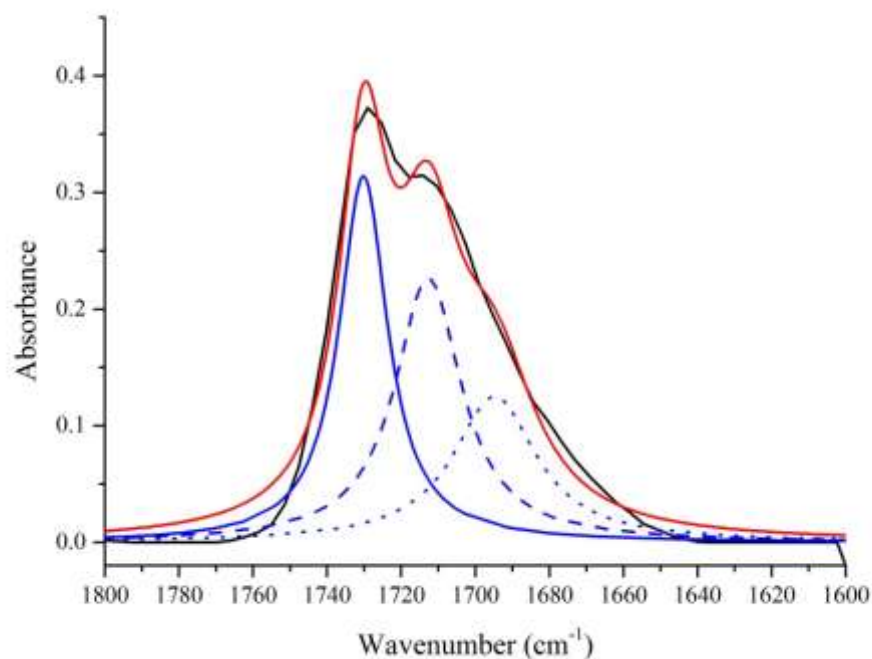
Lorentzian Fit of C=O

Figure B10: Deconvolution data for MDI-TMP-PPG-DEPD of C=O region. Data calculated using Lorentzian fitting function. [Raw data in black, fit data in red, free carbonyl peaks solid blue, hydrogen bonded carbonyl dash blue and free urea Dot blue].

Table B10: Deconvolution data of C=O region collected using Lorentzian function of MDI-TMP-PPG-DEPD.

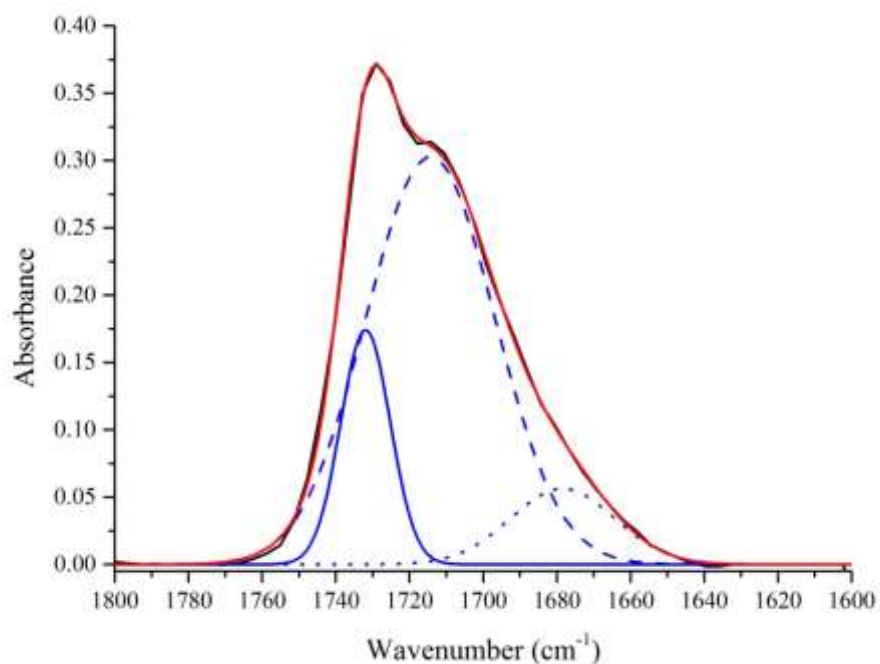| MDI-TMP-PPG-DEPD					
Peak Position/cm^{-1}	Standard Error/cm^{-1}	Area	Standard Error	Area/%	Fit R^2 value
1730	0.63	7.824	1.70	37.3	
1713	1.26	7.749	4.48	37.0	0.980
1695	3.84	5.389	3.11	25.7	

Gaussian Fit of C=O

Figure B11: Deconvolution data for MDI-TMP-PPG-DEPD of C=O region. Data calculated using Gaussian fitting function. [Raw data in black, fit data in red, free carbonyl peaks solid blue, hydrogen bonded carbonyl dash blue and free urea Dot blue].

Table B11: Deconvolution data of C=O region collected using Gaussian function of MDI-TMP-PPG-DEPD.

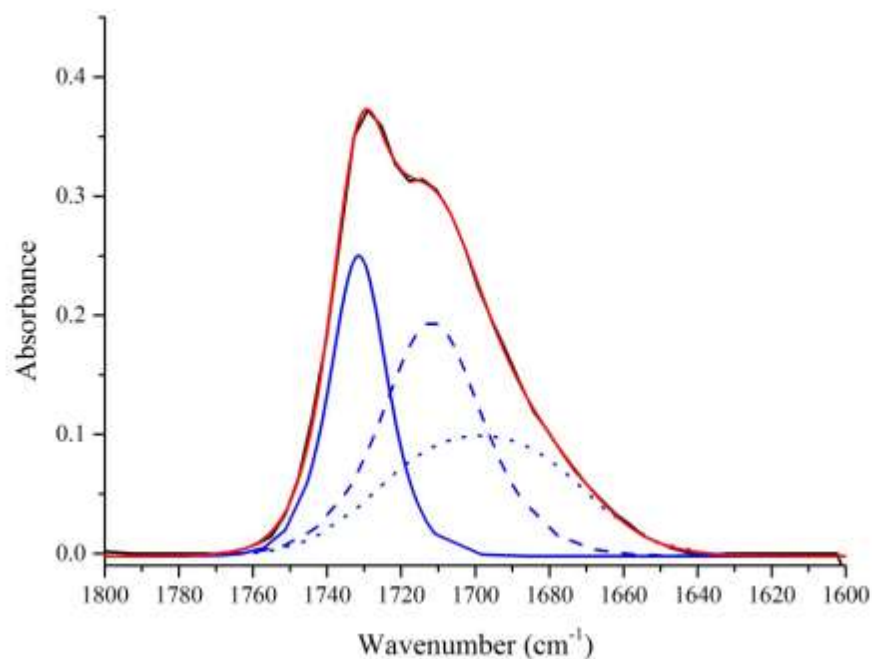| MDI-TMP-PPG-DEPD					
Peak Position/cm^{-1}	Standard Error/cm^{-1}	Area	Standard Error	Area/%	Fit R^2 value
1732	0.26	2.937	0.30	16.1	
1714	1.31	13.24	0.56	72.9	0.997
1678	3.97	2.00	0.66	11.0	

Gaussian-Lorentzian Fit of C=O

Figure B12: Deconvolution data for MDI-TMP-PPG-DEPD of C=O region. Data calculated using Gaussian-Lorentzian cross fitting function. [Raw data in black, fit data in red, free carbonyl peaks solid blue, hydrogen bonded carbonyl dash blue and free urea Dot blue].

Table B12: Deconvolution data of C=O region collected using GaussianLorentzian cross function of MDI-TMP-PPG-DEPD.

MDI-TMP-PPG-DEPD					
Peak Position/cm^{-1}	Standard Error/cm^{-1}	Area	Standard Error	Area/%	Fit R^2 value
1731	1.79	0.252	0.02	45.9	
1712	7.28	0.196	0.07	35.7	0.998
1698	1.49	0.101	0.06	18.4	

3 - MDI-TMP-PPG-BD

N-H Region Deconvolution
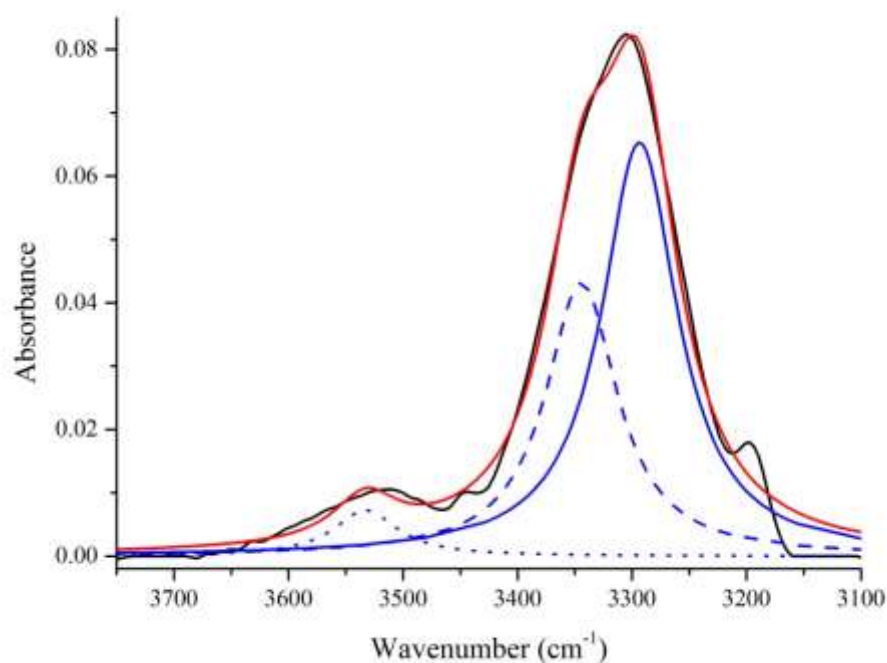
Lorentzian Fit of N-H

Figure B13: Deconvolution data for MDI-TMP-PPG-BD of N-H region. Data calculated using Lorentzian fitting function. [Raw data in black, fit data in red, HS-HS fitted peak solid blue, carbonyl overtone dash blue and free N-H Dot blue].

Table B13: Deconvolution data of N-H region collected using Lorentzian function of MDI-TMP-PPG-BD.

MDI-TMP-PPG-BD					
Peak Position/cm^{-1}	Standard Error/cm^{-1}	Area	Standard Error	Area/%	Fit R^2 value
3569	11.12	0.280	.19	2.1	
3525	5.82	0.269	0.17	2.0	0.989
3337	2.40	4.875	0.78	36.8	
3291	1.93	7.929	0.79	59.1	

Gaussian Fit of N-H

Figure B14: Deconvolution data for MDI-TMP-PPG-BD of N-H region. Data calculated using Gaussian fitting function. [Raw data in black, fit data in red, HS-HS fitted peak solid blue, carbonyl overtone dash blue and free N-H Dot blue].

Table B14: Deconvolution data of N-H region collected using Gaussian function of MDI-TMP-PPG-BD.

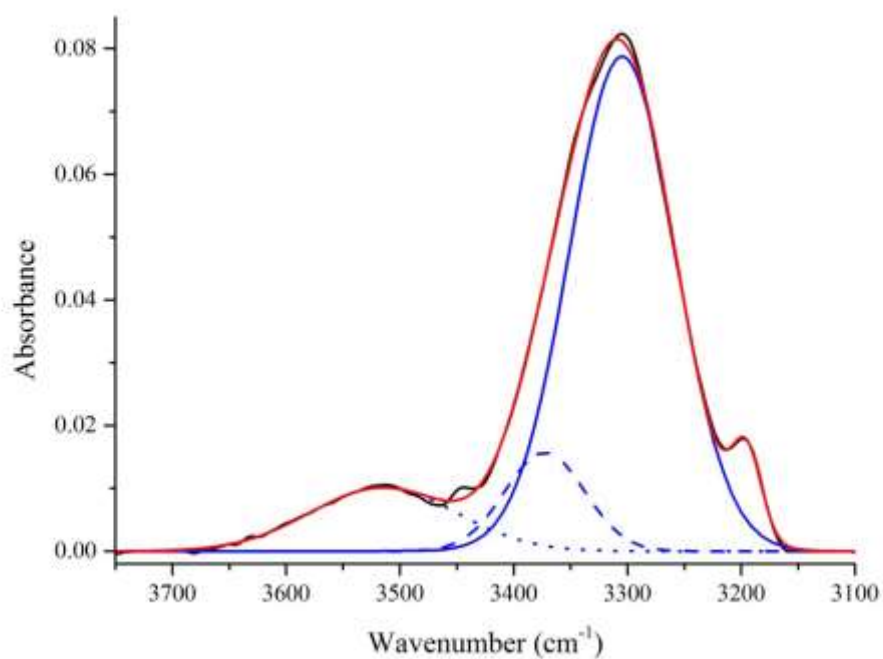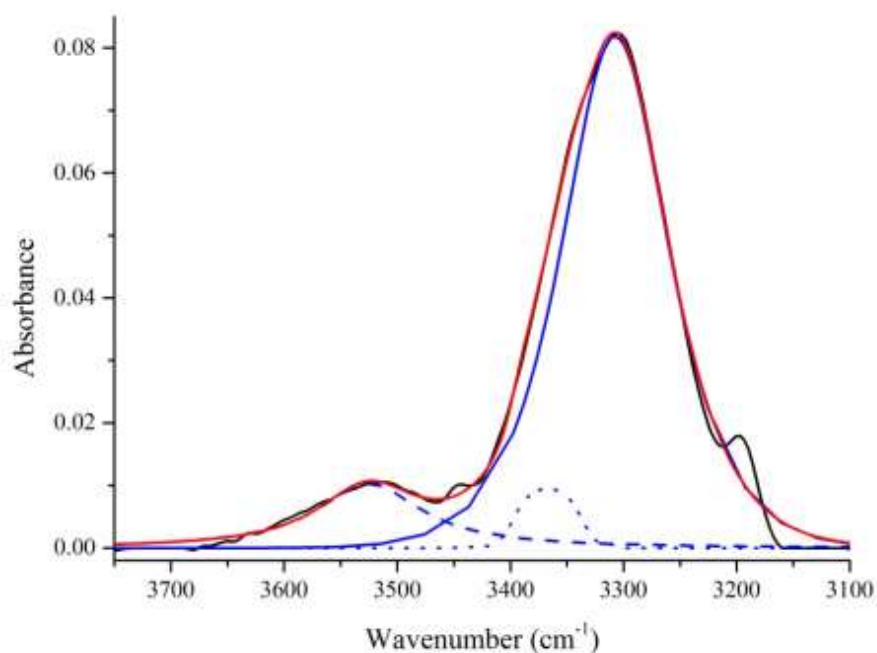| MDI-TMP-PPG-BD					
Peak Position/cm^{-1}	Standard Error/cm^{-1}	Area	Standard Error	Area/%	Fit R^2 value
3530	1.37	1.080	0.02	9.6	
3392	3.44	0.398	0.08	3.5	0.999
3308	0.42	9.770	0.08	86.9	

Gaussian-Lorentzian Fit of N-H

Figure B15: Deconvolution data for MDI-TMP-PPG-BD of N-H region. Data calculated using Gaussian-Lorentzian cross fitting function. [Raw data in black, fit data in red, HS-HS fitted peak solid blue, carbonyl overtone dash blue and free N-H Dot blue].

Table B15: Deconvolution data of N-H region collected using GaussianLorentzian cross function of MDI-TMP-PPG-BD.

MDI-TMP-PPG-BD					
Peak Position/cm^{-1}	Standard Error/cm^{-1}	Area	Standard Error	Area/%	Fit R^2 value
3539	3.36	0.008	5.2×10^{-4}	7.8	
3356	17.21	0.005	2.8×10^{-4}	5.6	0.999
3307	0.38	0.082	5.7×10^{-4}	86.6	

C=O Region Deconvolution

Lorentzian Fit of C=O

Figure B16: **Deconvolution data for MDI-TMP-PPG-BD of C=O region. Data calculated using Lorentzian fitting function. [Raw data in black, fit data in red, free carbonyl peaks solid blue, hydrogen bonded carbonyl dash blue and free urea dot blue].**

Table B16: **Deconvolution data of C=O region collected using Lorentzian function of MDI-TMP-PPG-BD.**

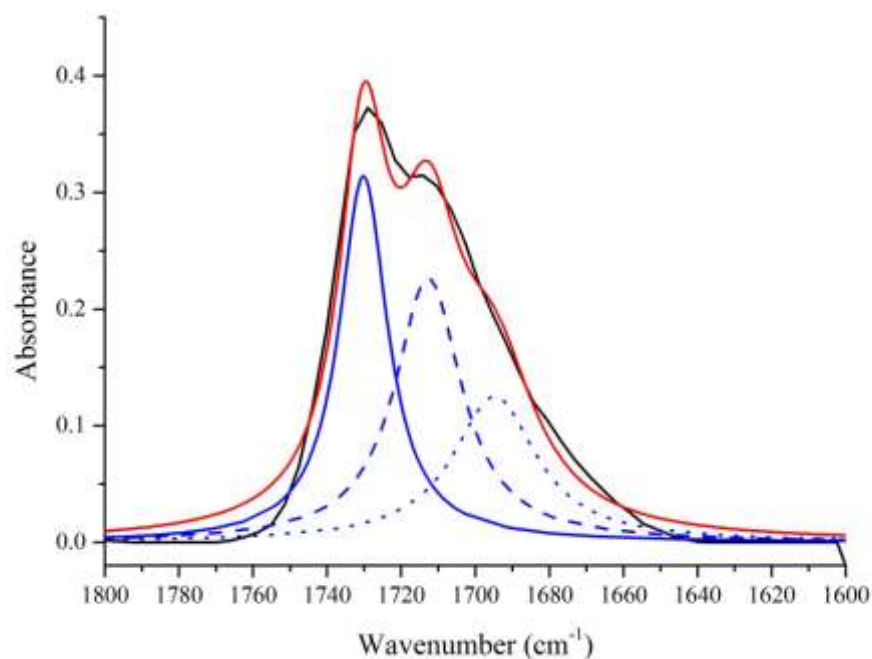| MDI-TMP-PPG-BD					
Peak Position/cm^{-1}	Standard Error/cm^{-1}	Area	Standard Error	Area/%	Fit R^2 value
1730	0.69	7.769	1.98	34.8	
1714	1.66	6.716	5.87	30.0	0.981
1700	3.24	7.868	4.31	35.2	

Gaussian Fit of C=O

Figure B17: Deconvolution data for MDI-TMP-PPG-BD of C=O region. Data calculated using Gaussian fitting function. [Raw data in black, fit data in red, free carbonyl peaks solid blue, hydrogen bonded carbonyl dash blue and free urea dot blue].

Table B17: Deconvolution data of C=O region collected using Gaussian function of MDI-TMP-PPG-BD.

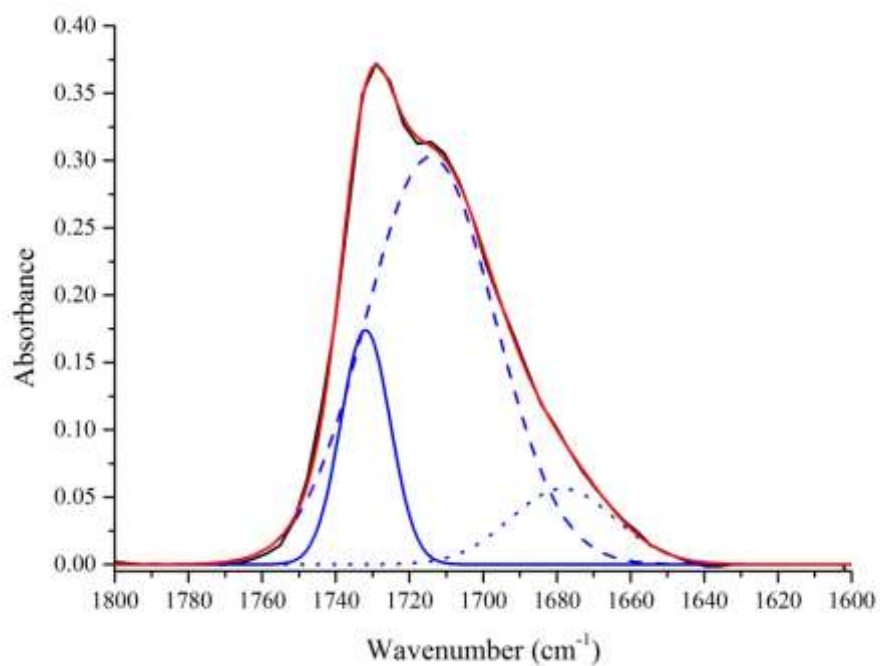| MDI-TMP-PPG-BD					
Peak Position/cm^{-1}	Standard Error/cm^{-1}	Area	Standard Error	Area/%	Fit R^2 value
1732	0.22	3.647	0.34	18.8	
1711	0.68	14.73	0.50	76.1	0.998
1673	3.33	0.978	0.31	5.1	

Gaussian-Lorentzian Fit of C=O

Figure B18: Deconvolution data for MDI-TMP-PPG-BD of C=O region. Data calculated using Gaussian-Lorentzian cross fitting function. [Raw data in black, fit data in red, free carbonyl peaks solid blue, hydrogen bonded carbonyl dash blue and free urea dot blue].

Table B18: Deconvolution data of C=O region collected using GaussianLorentzian cross function of MDI-TMP-PPG-BD.

MDI-TMP-PPG-BD					
Peak Position/cm^{-1}	Standard Error/cm^{-1}	Area	Standard Error	Area/%	Fit R^2 value
1731	2.56	0.293	0.26	45.2	
1710	10.39	0.274	0.18	42.2	0.998
1691	3.14	0.082	0.01	12.6	

4 - MDI-TMP-PPG-PD
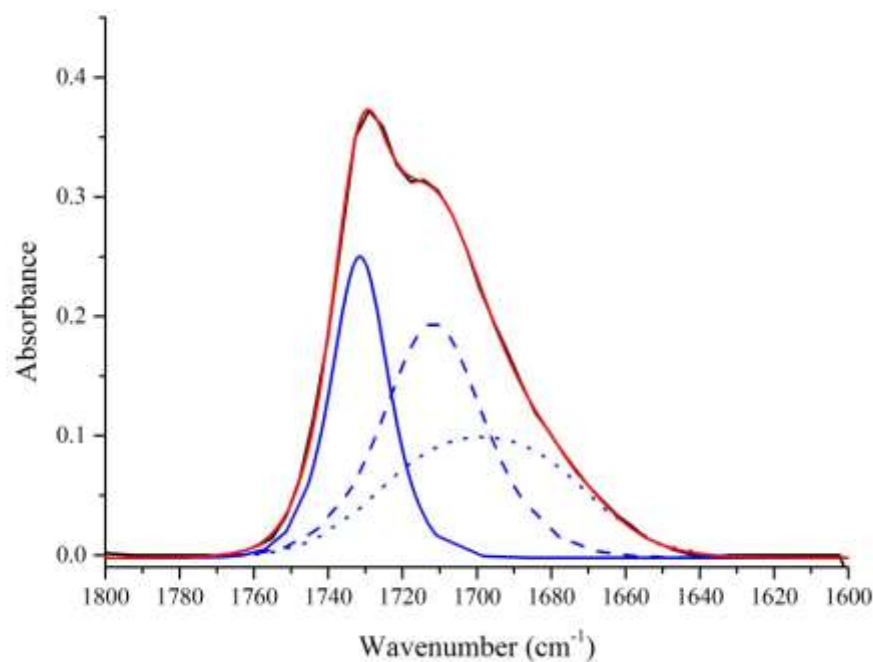
N-H Region Deconvolution

Lorentzian Fit of N-H

Figure B19: **Deconvolution data for MDI-TMP-PPG-PD of N-H region. Data calculated using Lorentzian fitting function. [Raw data in black, fit data in red, HS-HS fitted peak solid blue, carbonyl overtone dash blue, free N-H dot and dot dash blue].**

Table B19: Deconvolution data of N-H region collected using Lorentzian function of MDI-TMP-PPG-PD.

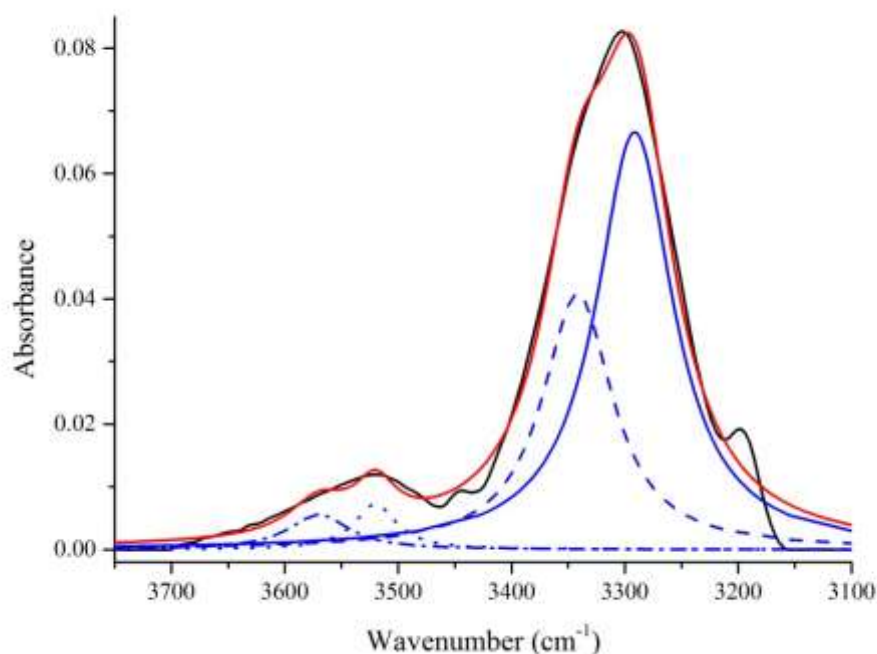| MDI-TMP-PPG-PD					
Peak Position/cm^{-1}	Standard Error/cm^{-1}	Area	Standard Error	Area/%	Fit R^2 value
3570	11.14	0.568	0.30	3.9	
3520	5.67	0.514	0.27	3.5	0.988
3342	2.62	4.844	0.77	33.3	
3291	1.82	8.601	0.77	59.2	

Gaussian Fit of N-H

Figure B20: Deconvolution data for MDI-TMP-PPG-PD of N-H region. Data calculated using Gaussian fitting function. [Raw data in black, fit data in red, HS-HS fitted peak solid blue, carbonyl overtone dash blue, free N-H dot and dot dash blue].

Table B20: Deconvolution data of N-H region collected using Gaussian function of MDI-TMP-PPG-PD.

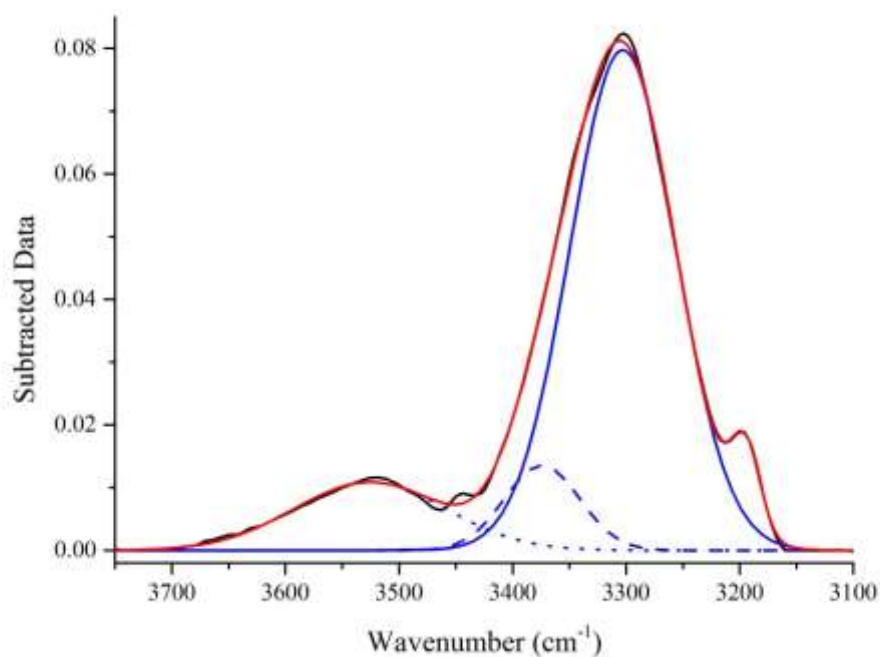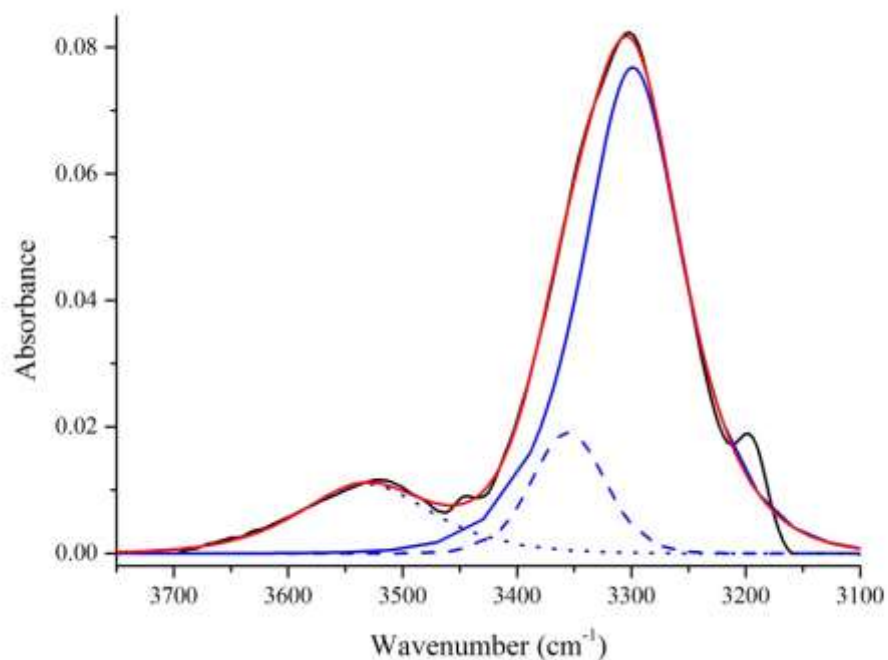| MDI-TMP-PPG-PD					
Peak Position/cm^{-1}	Standard Error/cm^{-1}	Area	Standard Error	Area/%	Fit R^2 value
3525	1.28	1.832	0.03	14.9	
3374	3.33	1.129	0.26	9.2	0.999
3303	1.31	9.311	0.26	75.9	

Gaussian-Lorentzian Fit of N-H

Figure B21: Deconvolution data for MDI-TMP-PPG-PD of N-H region. Data calculated using Gaussian-Lorentzian cross fitting function. [Raw data in black, fit data in red, HS-HS fitted peak solid blue, carbonyl overtone dash blue and free N-H dot and dot dash blue].

Table B21: Deconvolution data of N-H region collected using GaussianLorentzian cross function of MDI-TMP-PPG-PD.

MDI-TMP-PPG-PD					
Peak Position/cm^{-1}	Standard Error/cm^{-1}	Area	Standard Error	Area/%	Fit R^2 value
3532	4.21	0.011	4.9x10^{-4}	11.1	
3355	19.7	0.019	0.01	11.1	0.995
3299	10.73	0.077	0.02	77.8	

C=O Region Deconvolution

Lorentzian Fit of C=O

Figure B22: Deconvolution data for MDI-TMP-PPG-PD of C=O region. Data calculated using Lorentzian fitting function. [Raw data in black, fit data in red, free carbonyl peaks solid blue, hydrogen bonded carbonyl dash blue and free urea dot blue].

Table B22: Deconvolution data of C=O region collected using Lorentzian function of MDI-TMP-PPG-PD.

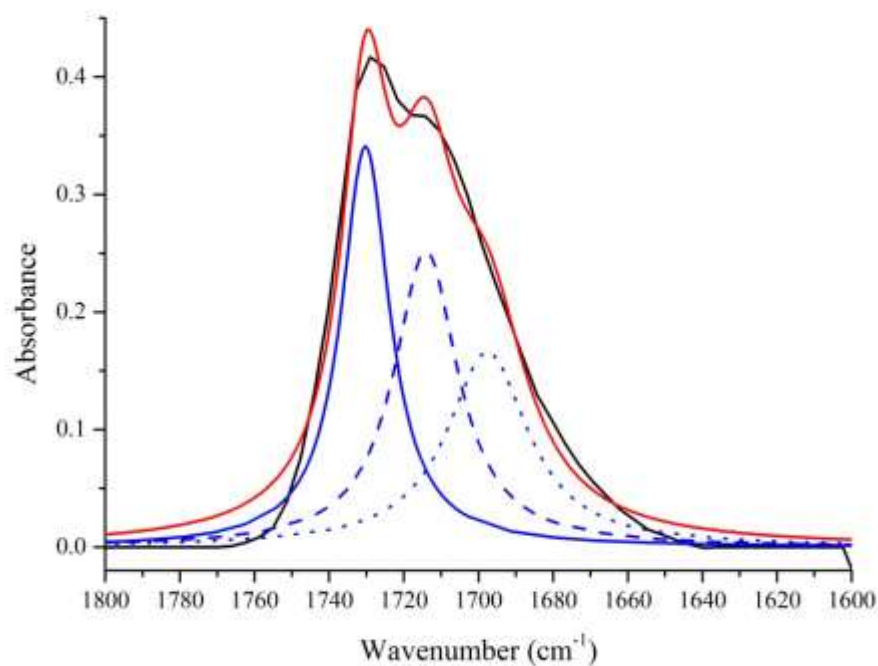| MDI-TMP-PPG-PD					
Peak Position/cm^{-1}	Standard Error/cm^{-1}	Area	Standard Error	Area/%	Fit R^2 value
1730	0.71	8.452	2.14	35.9	
1714	1.30	8.212	5.55	34.8	0.982
1698	3.47	6.906	3.81	29.3	

Gaussian Fit of C=O

Figure B23: **Deconvolution data for MDI-TMP-PPG-PD of C=O region. Data calculated using Gaussian fitting function. [Raw data in black, fit data in red, free carbonyl peaks solid blue, hydrogen bonded carbonyl dash blue and free urea dot blue].**

Table B23: Deconvolution data of C=O region collected using Gaussian function of MDI-TMP-PPG-PD.

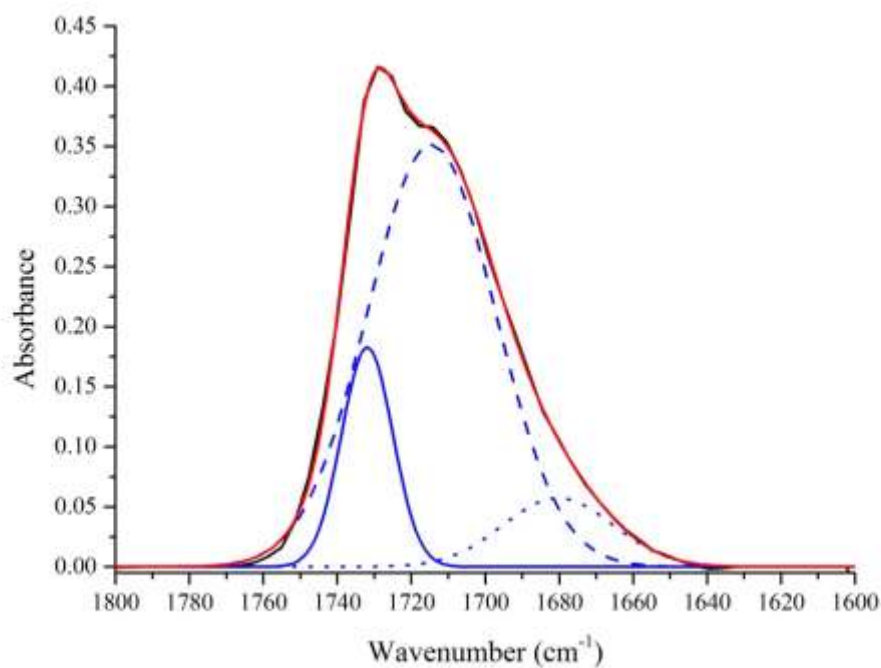| MDI-TMP-PPG-PD					
Peak Position/cm^{-1}	Standard Error/cm^{-1}	Area	Standard Error	Area/%	Fit R^2 value
1732	0.26	3.173	0.35	15.5	
1715	1.50	15.19	0.79	74.1	0.998
1680	5.60	2.138	0.95	10.4	

Gaussian-Lorentzian Fit of C=O

Figure B24: Deconvolution data for MDI-TMP-PPG-PD of C=O region. Data calculated using Gaussian-Lorentzian cross fitting function. [Raw data in black, fit data in red, free carbonyl peaks solid blue, hydrogen bonded carbonyl dash blue and free urea dot blue].

Table B24: Deconvolution data of C=O region collected using GaussianLorentzian cross function of MDI-TMP-PPG-PD.

	MDI-TMP-PPG-PD				
Peak Position/cm^{-1}	Standard Error/cm^{-1}	Area	Standard Error	Area/%	Fit R^2 value
1732	2.00	0.250	0.10	41.7	
1713	10.95	0.260	0.26	43.6	0.999
1697	55.13	0.088	0.13	14.7	

Deconvolution of MDI and PPG based formulations

5 - MDI-TMP-PCD

N-H Region Deconvolution

Lorentzian Fit of N-H

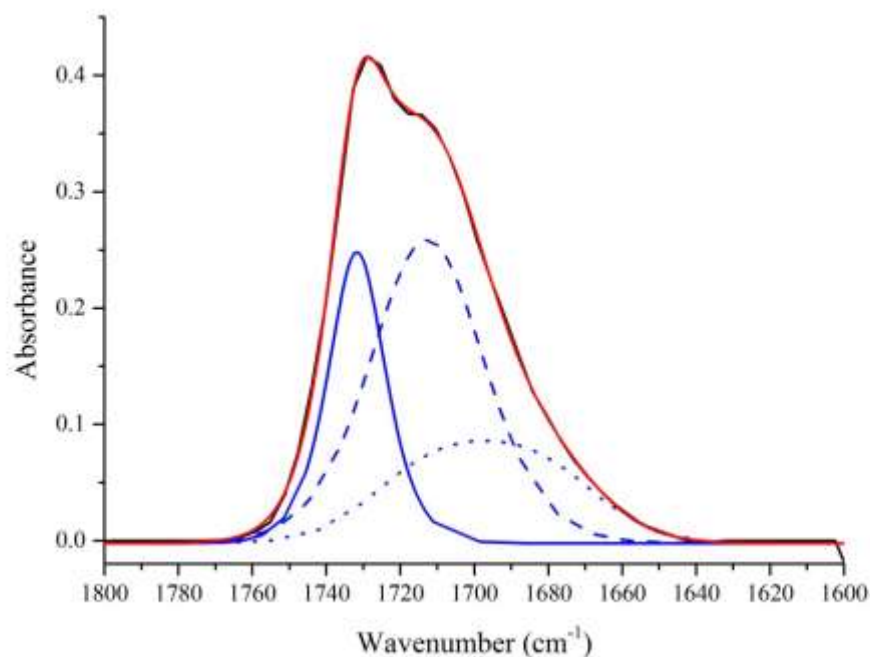**Figure B25:** **Deconvolution data for MDI-TMP-PCD of N-H region. Data calculated using Lorentzian fitting function. [Raw data in black, fit data in red, HS-HS fitted peak solid blue, carbonyl overtone dash blue, free N-H dot and dot dash blue].**

Table B25: Deconvolution data of N-H region collected using Lorentzian function of MDI-TMP-PCD.

MDI-TMP-PCD

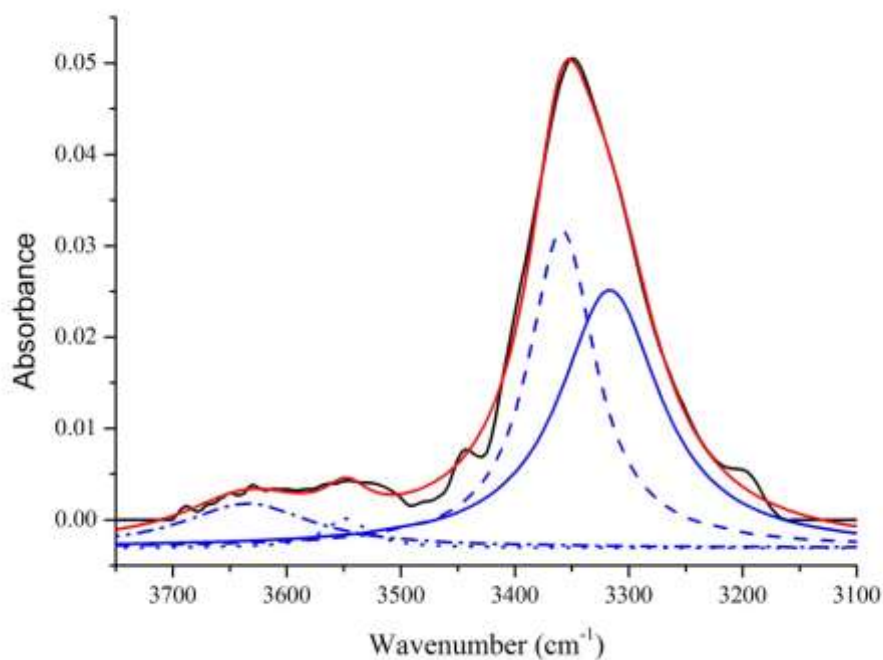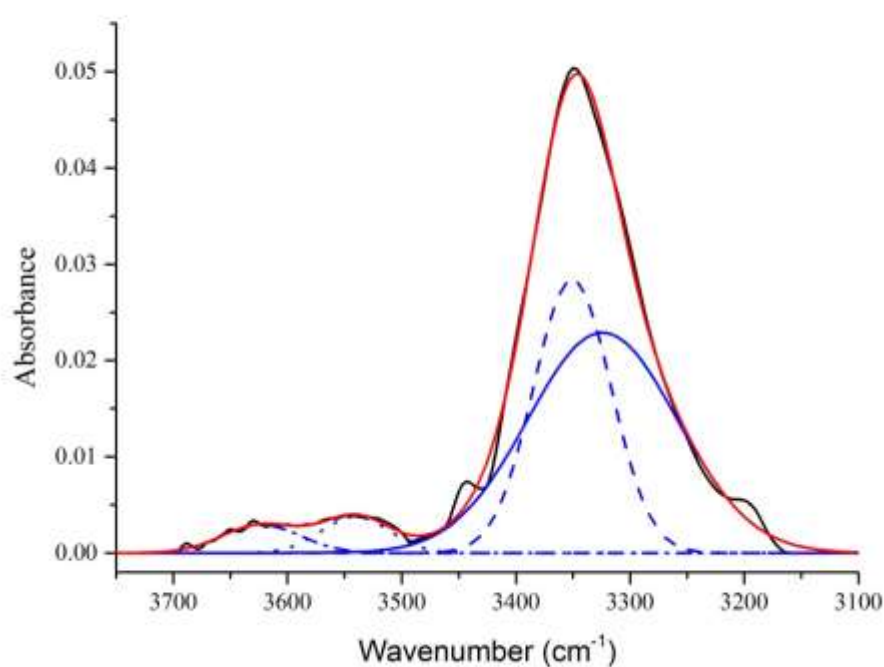| Peak Position/cm^{-1}	Standard Error/cm^{-1}	Area	Standard Error	Area/%	Fit R^2 value
3634	6.89	1.043	0.22	10.5	
3548	3.71	0.236	0.09	2.4	0.995
3357	1.56	3.887	0.69	39.2	
3317	4.62	4.739	0.85	47.8	

Gaussian Fit of N-H

Figure B26: Deconvolution data for MDI-TMP-PCD of N-H region. Data calculated using Gaussian fitting function. [Raw data in black, fit data in red, HS-HS fitted peak solid blue, carbonyl overtone dash blue, free N-H dot and dot dash blue].

Table B26: Deconvolution data of N-H region collected using Gaussian function of MDI-TMP-PCD.

| MDI-TMP-PCD | | | | | |
Peak Position/cm^{-1}	Standard Error/cm^{-1}	Area	Standard Error	Area/%	Fit R^2 value
3623	8.34	0.253	0.05	7.9	
3540	5.78	0.283	0.06		0.997
3351	0.60	2.420	0.16	36.1	
3324	1.68	3.755	0.16	56.0	

Gaussian-Lorentzian Fit of N-H

Figure B27: Deconvolution data for MDI-TMP-PCD of N-H region. Data calculated using Gaussian-Lorentzian cross fitting function. [Raw data in black, fit data in red, HS-HS fitted peak solid blue, carbonyl overtone dash blue, free N-H dot and dot dash blue].

Table B27: Deconvolution data of N-H region collected using GaussianLorentzian cross function of MDI-TMP-PCD.

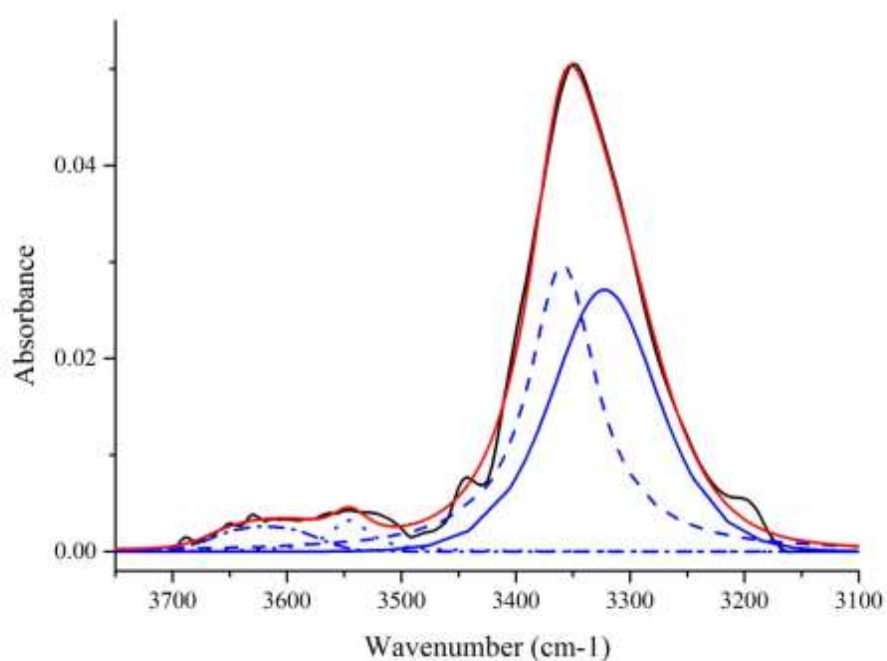|	MDI-TMP-PCD				
Peak Position/cm^{-1}	Standard Error/cm^{-1}	Area	Standard Error	Area/%	Fit R^2 value
3619	14.71	0.003	3.4×10^{-4}		
3545	10.45	0.003	7.8×10^{-4}	9.3	0.995
3359	1.50	0.029	-	47.3	
3322	5.26	0.027	4.2×10^{-3}	43.4	

C=O Region Deconvolution

Lorentzian Fit of C=O

Figure B28: **Deconvolution data for MDI-TMP-PCD of C=O region. Data calculated using Lorentzian fitting function. [Raw data in black, fit data in** **red****, free ester carbonyl peaks** **solid blue****, free urethane carbonyl** **dash blue****, hydrogen bonded urethane** **dot blue** **and free urea** **dot dash blue****].**

Table B28: **Deconvolution data of C=O region collected using Lorentzian function of MDI-TMP-PCD.**

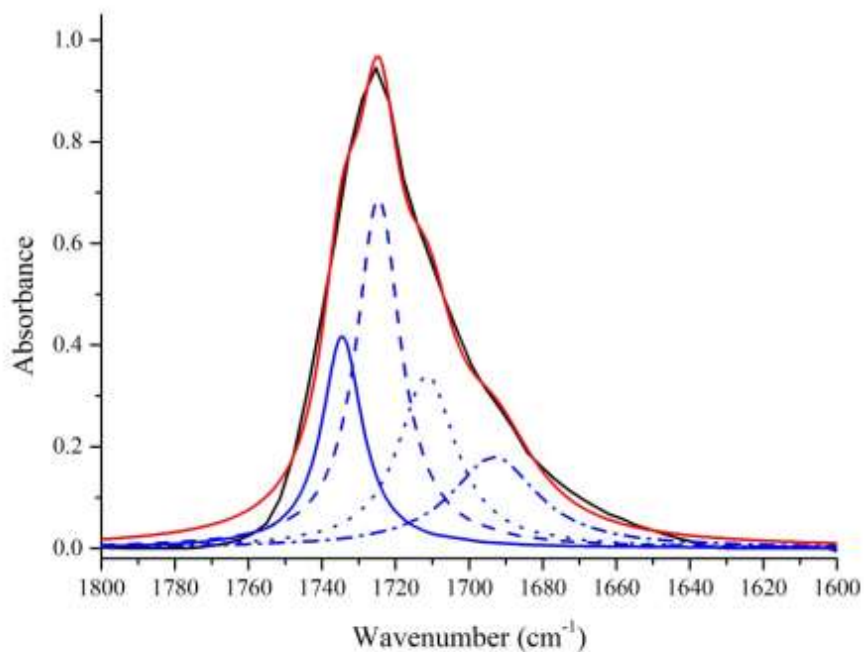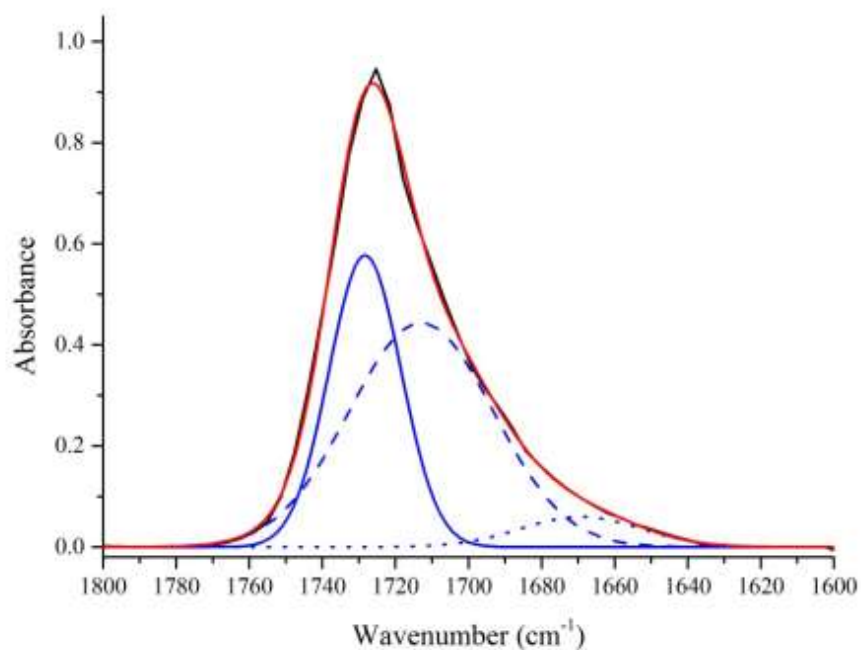| MDI-TMP-PCD					
Peak Position/cm^{-1}	Standard Error/cm^{-1}	Area	Standard Error	Area/%	Fit R^2 value
1735	1.26	8.762	4.58	20.4	
1725	0.77	15.84	9.09	36.9	0.990
1711	1.92	10.187	8.75	23.7	
1693	4.21	8.131	4.44	18.9	

Gaussian Fit of C=O

Figure B29: Deconvolution data for MDI-TMP-PCD of C=O region. Data calculated using Gaussian fitting function. [Raw data in black, fit data in red, free ester carbonyl peaks solid blue, hydrogen bonded urethane carbonyl dash blue and free urea dot blue].

Table B29: Deconvolution data of C=O region collected using Gaussian function of MDI-TMP-PCD.

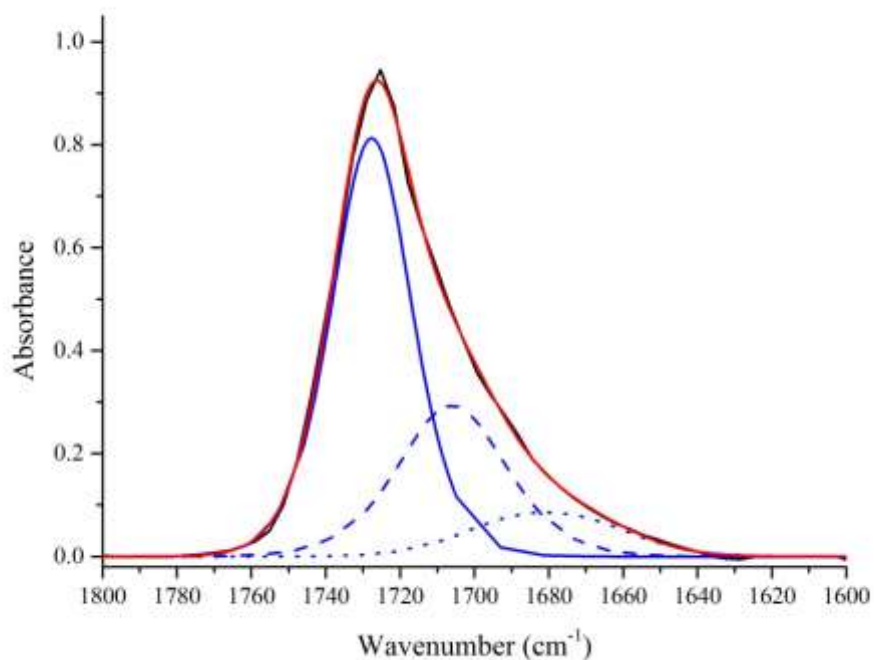| Peak Position/cm⁻¹	Standard Error/cm⁻¹	Area	Standard Error	Area/%	Fit R² value
1728	0.27	14.245	1.56	36.8	
1713	2.62	21.877	0.96	56.7	0.999
1669	8.59	2.473	1.43	6.4	

Gaussian-Lorentzian Fit of C=O

Figure B30: Deconvolution data for MDI-TMP-PCD of C=O region. Data calculated using Gaussian-Lorentzian cross fitting function. [Raw data in black, fit data in red, free ester carbonyl peaks solid blue, hydrogen bonded urethane carbonyl dash blue and free urea dot blue].

Table B30: Deconvolution data of C=O region collected using GaussianLorentzian cross function of MDI-TMP-PCD.

MDI-TMP-PCD					
Peak Position/cm^{-1}	Standard Error/cm^{-1}	Area	Standard Error	Area/%	Fit R^2 value
1728	2.11	0.812	0.21	68.2	
1706	11.56	0.293	0.61	24.6	0.999
1681	10.1	0.085	0.40	7.2	

6 - MDI-TMP-PCD-DEPD

N-H Region Deconvolution
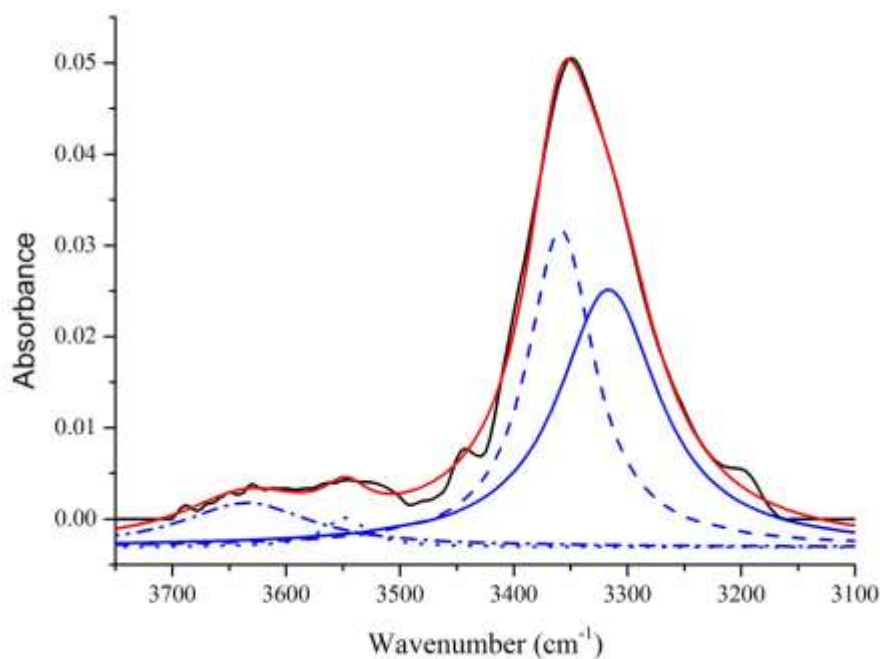
Lorentzian Fit of N-H

Figure B31: Deconvolution data for MDI-TMP-PCD-DEPD of N-H region. Data calculated using Lorentzian fitting function. [Raw data in black, fit data in red, HS-HS fitted peak solid blue, carbonyl overtone dash blue, free N-H dot and dot dash blue].

Table B31: Deconvolution data of N-H region collected using Lorentzian function of MDI-TMP-PCD-DEPD.

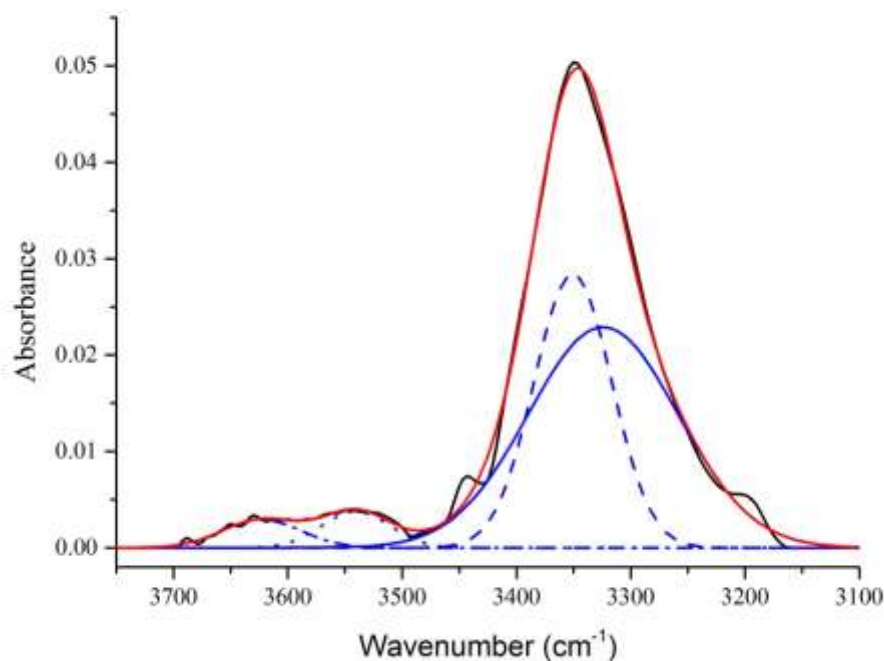| MDI-TMP-PCD-DEPD					
Peak Position/cm^{-1}	Standard Error/cm^{-1}	Area	Standard Error	Area/%	Fit R^2 value
3617	6.40	0.230	.08	2.5	
3552	4.50	0.204	0.07	2.3	0.994
3355	1.28	5.401	0.48	59.6	
3316	2.48	3.223	0.48	35.6	

Gaussian Fit of N-H

Figure B32: Deconvolution data for MDI-TMP-PCD-DEPD of N-H region. Data calculated using Gaussian fitting function. [Raw data in black, dit data in red, HS-HS fitted peak solid blue, carbonyl overtone dash blue, free N-H dot and dot dash blue].

Table B32: Deconvolution data of N-H region collected using Gaussian function of MDI-TMP-PCD-DEPD.

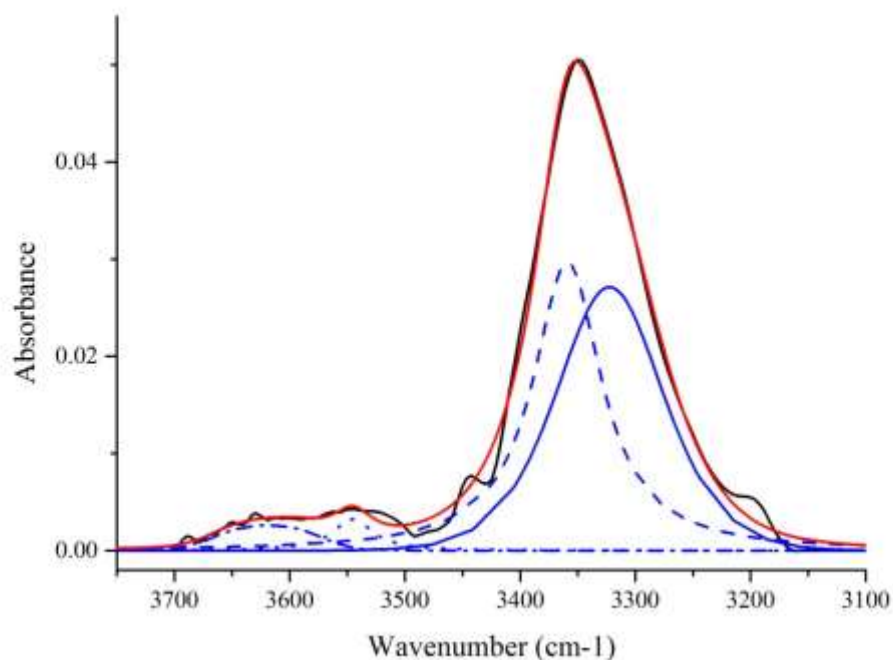| MDI-TMP-PCD-DEPD					
Peak Position/cm^{-1}	Standard Error/cm^{-1}	Area	Standard Error	Area/%	Fit R^2 value
3627	8.11	0.275	0.07	8.9	
3544	6.04	0.456	0.08		0.998
3345	0.41	3.195	0.17	38.7	
3331	1.15	4.231	0.17	56.0	

Gaussian-Lorentzian Fit of N-H

Figure B33: Deconvolution data for MDI-TMP-PCD-DEPD of N-H region. Data calculated using Gaussian-Lorentzian cross fitting function. [Raw data in black, fit data in red, HS-HS fitted peak solid blue, carbonyl overtone dash blue, free N-H dot and dot dash blue].

Table B33: Deconvolution data of N-H region collected using GaussianLorentzian cross function of MDI-TMP-PCD-DEPD.

MDI-TMP-PCD-DEPD					
Peak Position/cm^{-1}	Standard Error/cm^{-1}	Area	Standard Error	Area/%	Fit R^2 value
3628	12.2	0.005	4.3×10^{-4}	9.9	
3546	6.59	0.003	0.001		0.997
3358	5.29	0.038	-	44.8	
3324	13.70	0.039	0.019	45.3	

C=O Region Deconvolution
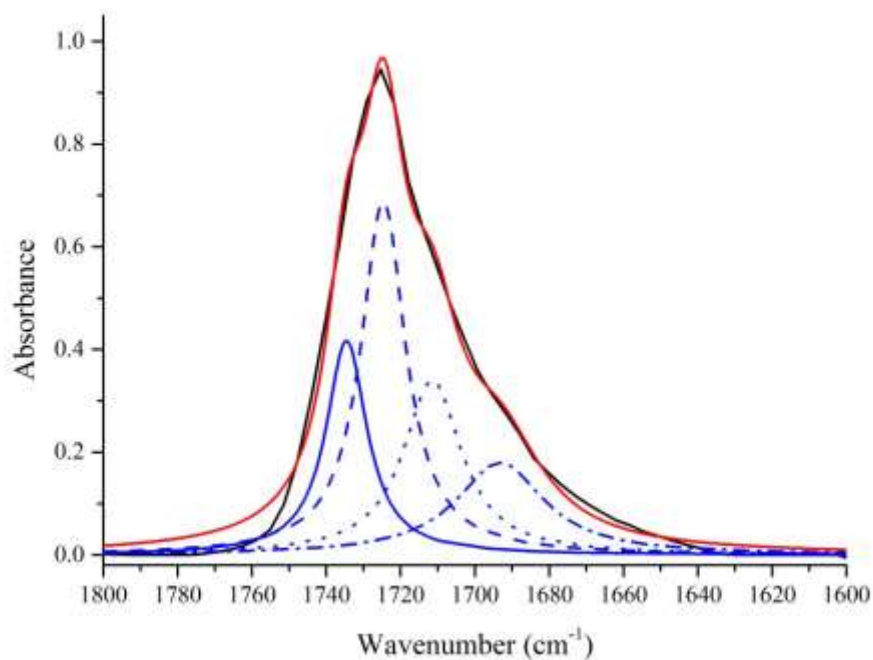
Lorentzian Fit of C=O

Figure B34: Deconvolution data for MDI-TMP-PCD-DEPD of C=O region. Data calculated using Lorentzian fitting function. [Raw data in black, fit data in red, free ester carbonyl peaks solid blue, free urethane carbonyl dash blue, hydrogen bonded urethane dot blue and free urea dot dash blue].

Table B34:   Deconvolution data of C=O region collected using Lorentzian function of MDI-TMP-PCD-DEPD.

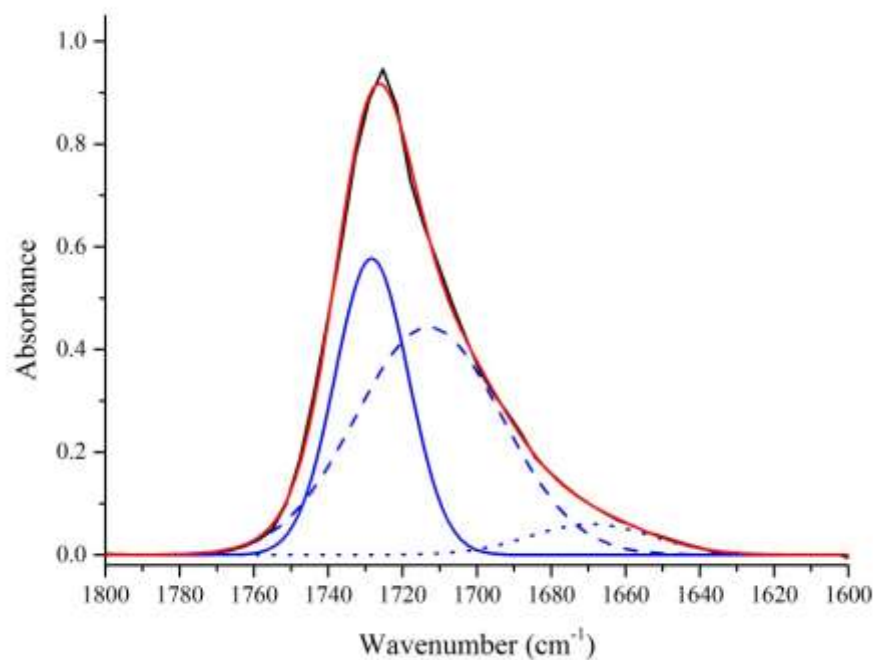| MDI-TMP-PCD-DEPD					
Peak Position/cm^{-1}	Standard Error/cm^{-1}	Area	Standard Error	Area/%	Fit R^2 value
1735	1.35	10.91	6.47	20.4	
1727	1.24	12.21	12.39	36.9	
1713	1.60	14.93	11.77	23.7	0.990
1696	4.07	8.12	5.65	18.9	

Gaussian Fit of C=O

Figure B35: Deconvolution data for MDI-TMP-PCD-DEPD of C=O region. Data calculated using Gaussian fitting function. [Raw data in black, dit data in red, dree ester carbonyl peaks solid blue, hydrogen bonded urethane carbonyl dash blue and free urea dot blue].

Table B35: Deconvolution data of C=O region collected using Gaussian function of MDI-TMP-PCD-DEPD.

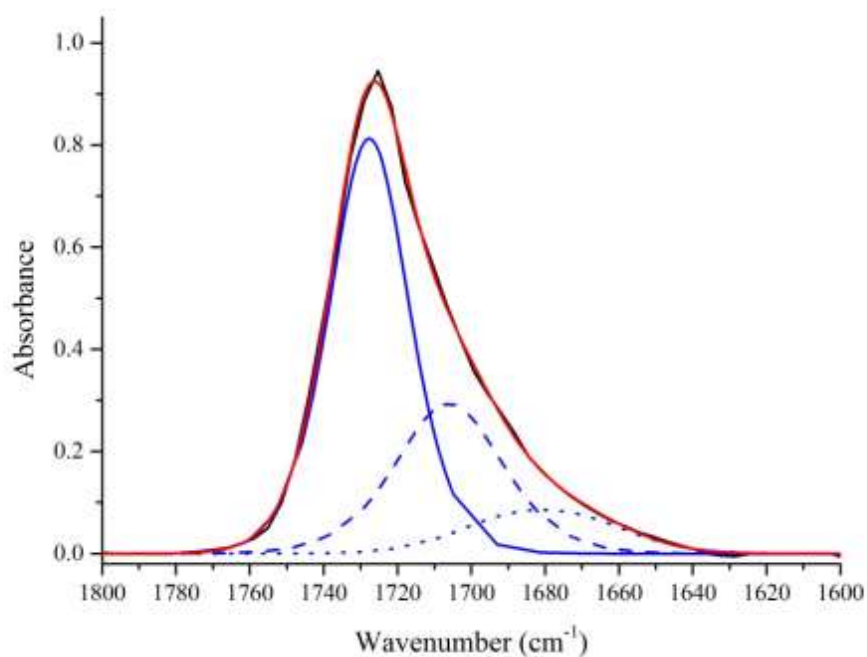| MDI-TMP-PCD-DEPD					
Peak Position/cm^{-1}	Standard Error/cm^{-1}	Area	Standard Error	Area/%	Fit R^2 value
1733	0.22	6.272	0.80	15.2	
1721	2.25	26.949	4.98	65.3	0.999
1693	12.68	8.06	5.587	19.5	

Gaussian-Lorentzian Fit of C=O

Figure B36: **Deconvolution data for MDI-TMP-PCD-DEPD of C=O region. Data calculated using Gaussian-Lorentzian cross fitting function. [Raw data in black, Ffit data in** red**, free ester carbonyl peaks** solid blue**, hydrogen bonded urethane carbonyl** dash blue **and free urea** dot blue**].**

Table B36: **Deconvolution data of C=O region collected using GaussianLorentzian cross function of MDI-TMP-PCD-DEPD.**

MDI-TMP-PCD-DEPD					
Peak Position/cm⁻¹	Standard Error/cm⁻¹	Area	Standard Error	Area/%	Fit R² value
1734	1.63	0.640	0.20	45.3	
1718	6.48	0.502	0.14	35.5	0.999
1695	9.79	0.271	0.13	19.2	

7 - MDI-TMP-PCD-BD

N-H Region Deconvolution
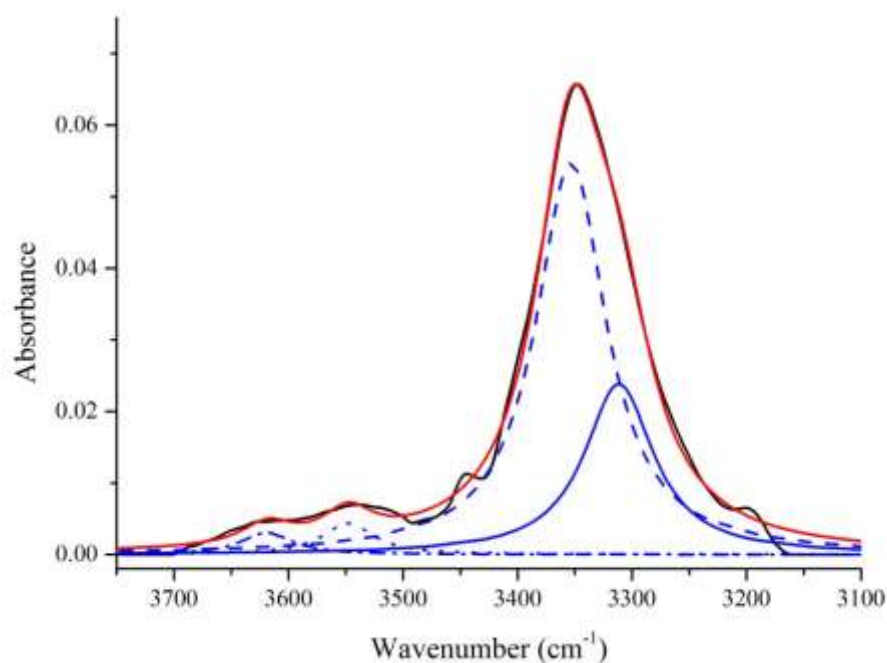
Lorentzian Fit of N-H

Figure B37: Deconvolution data for MDI-TMP-PCD-BD of N-H region. Data calculated using Lorentzian fitting function. [Raw data in black, fit data in red, HS-HS fitted peak solid blue, carbonyl overtone dash blue, free N-H dot and dot dash blue].

Table B37: Deconvolution data of N-H region collected using Lorentzian function of MDI-TMP-PCD-BD.

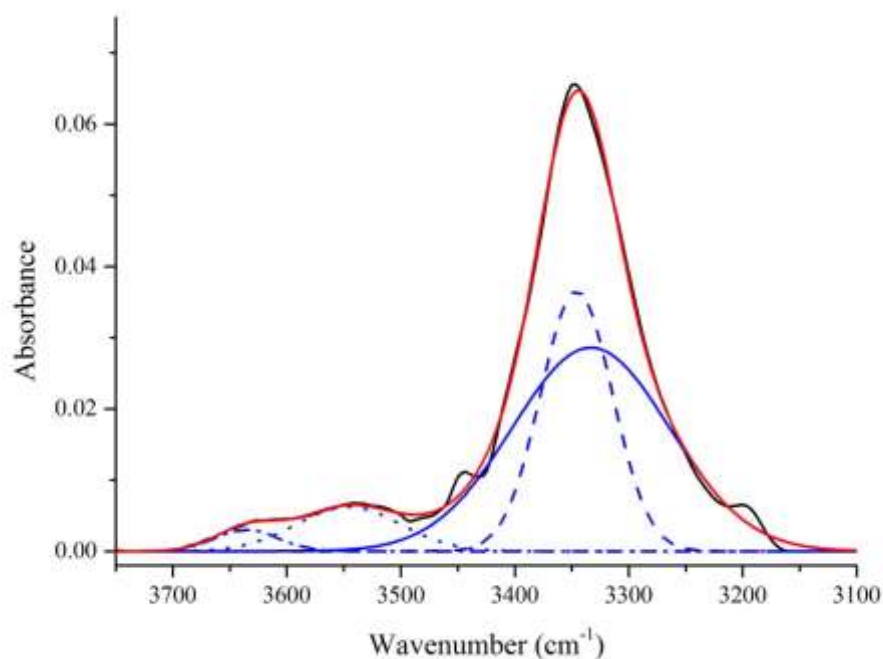| MDI-TMP-PCD-BD					
Peak Position/cm^{-1}	Standard Error/cm^{-1}	Area	Standard Error	Area/%	Fit R^2 value
3619	5.86	0.262	8.6×10^{-2}	2.7	
3545	4.10	0.374	9.1×10^{-2}	2.8	0.994
3353	1.34	6.438	0.52	65.6	
3311	2.93	2.747	0.51	28.0	

Gaussian Fit of N-H

Figure B38: **Deconvolution data for MDI-TMP-PCD-BD of N-H region. Data calculated using Gaussian fitting function. [Raw data in black, fit data in red, HS-HS fitted peak solid blue, carbonyl overtone dash blue, free N-H dot and dot dash blue].**

Table B38: **Deconvolution data of N-H region collected using Gaussian function of MDI-TMP-PCD-BD.**

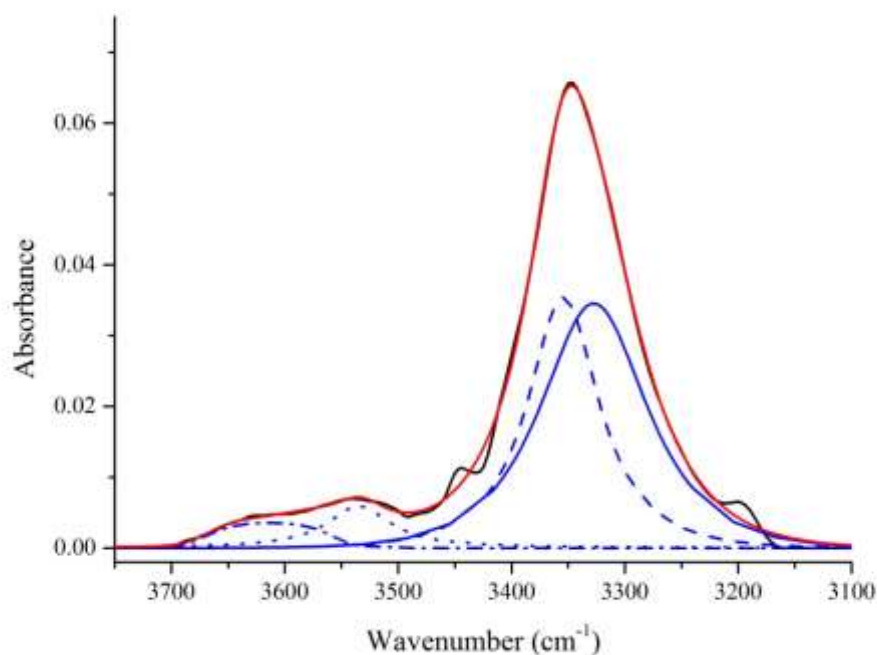| MDI-TMP-PCD-BD					
Peak Position/cm⁻¹	Standard Error/cm⁻¹	Area	Standard Error	Area/%	Fit R² value
3635	6.42	0.210	7.2×10^{-2}		
3546	5.01	0.717	8.7×10^{-2}	10.5	0.998
3346	0.44	2.888	0.16	33.3	
3333	1.07	4.947	0.16	53.7	

Gaussian-Lorentzian Fit of N-H

Figure B39: **Deconvolution data for MDI-TMP-PCD-BD of N-H region. Data calculated using Gaussian-Lorentzian cross fitting function. [Raw data in black, fit data in red, HS-HS fitted peak solid blue, carbonyl overtone dash blue, free N-H dot and dot dash blue].**

Table B39: **Deconvolution data of N-H region collected using GaussianLorentzian cross function of MDI-TMP-PCD-BD.**

MDI-TMP-PCD-BD					
Peak Position/cm^{-1}	Standard Error/cm^{-1}	Area	Standard Error	Area/%	Fit R^2 value
3613	31.2	3.53x10^{-3}	9.56x10^{-4}		
		5.9x10^{-3}	9.6x10^{-4}	11.9	
3534	22.1	3.54x10^{-2}	3.00x10^{-2}		
3354	3.70			44.6	0.998
3327	20.4	3.45x10^{-2}	3.1x10^{-2}	43.5	

C=O Region Deconvolution
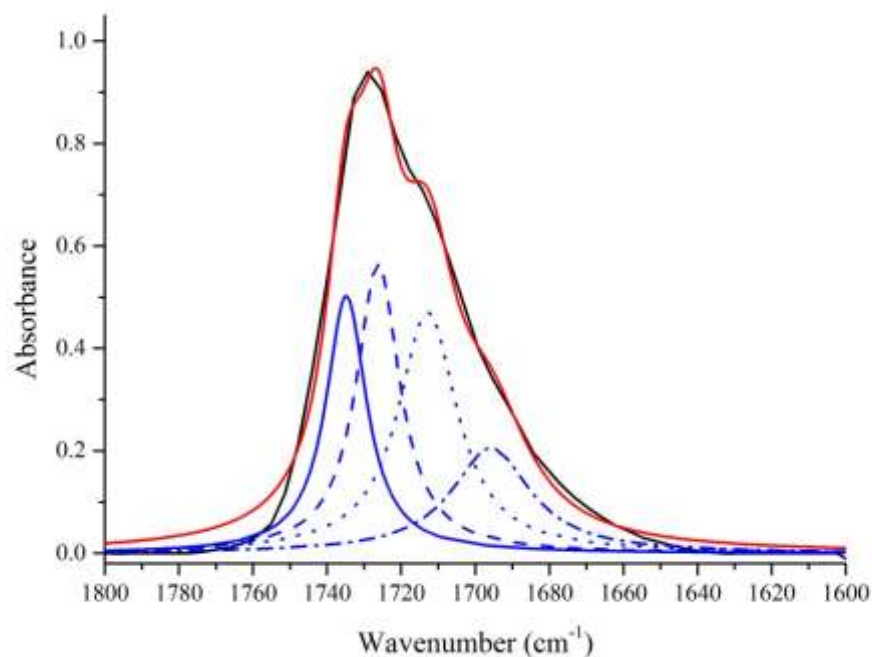
Lorentzian Fit of C=O

Figure B40: **Deconvolution data for MDI-TMP-PCD-BD of C=O region. Data calculated using Lorentzian fitting function. [Raw data in black, fit data in red, free ester carbonyl peaks solid blue, free urethane carbonyl dash blue, hydrogen bonded urethane dot blue and free urea dot dash blue].**

Table B40: **Deconvolution data of C=O region collected using Lorentzian function of MDI-TMP-PCD-BD.**

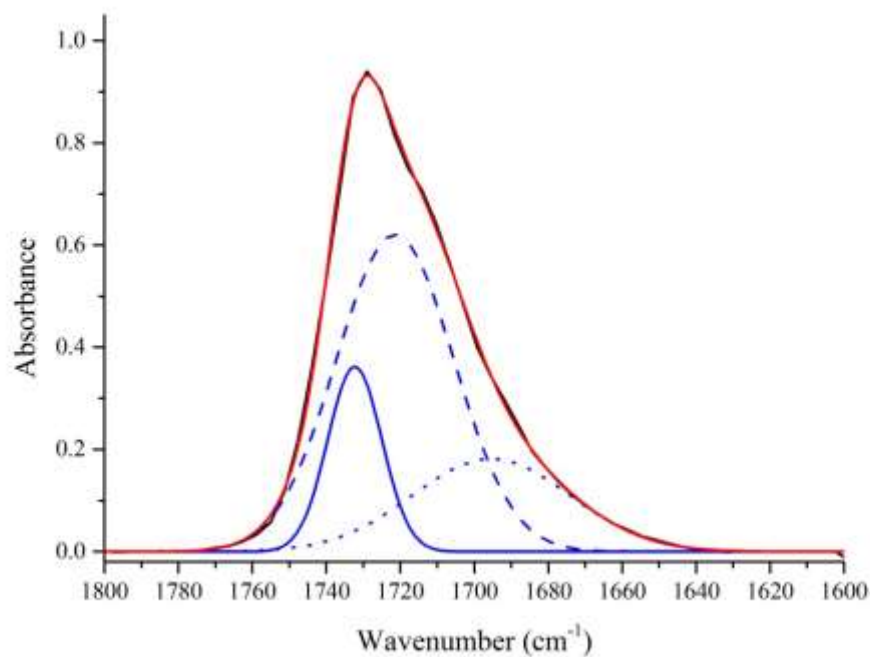| MDI-TMP-PCD-BD					
Peak Position/cm^{-1}	Standard Error/cm^{-1}	Area	Standard Error	Area/%	Fit R^2 value
1735	1.26	10.484	5.84	23.0	
1726	1.18	12.629	11.17	27.7	0.989
1713	1.58	14.302	11.13	30.9	
1696	4.08	8.364	5.52	18.4	

Gaussian Fit of C=O

Figure B41: Deconvolution data for MDI-TMP-PCD-BD of C=O region. Data calculated using Gaussian fitting function. [Raw data in black, fit data in red, free ester carbonyl peaks solid blue, hydrogen bonded urethane carbonyl dash blue and free urea dot blue].

Table B41: Deconvolution data of C=O region collected using Gaussian function of MDI-TMP-PCD-BD.

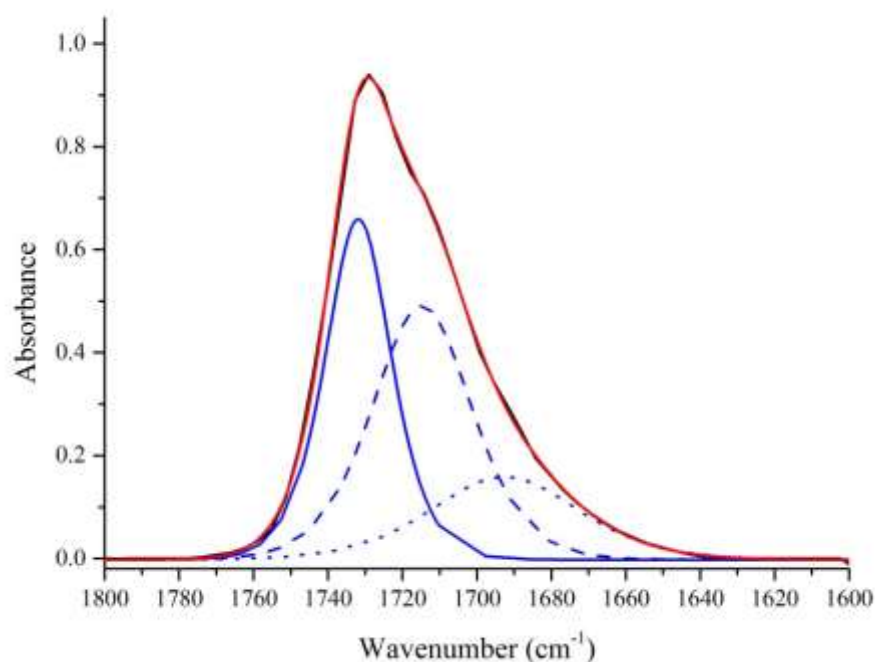| MDI-TMP-PCD-BD					
Peak Position/cm^{-1}	Standard Error/cm^{-1}	Area	Standard Error	Area/%	Fit R^2 value
1732	0.23	6.637	0.78	16.2	
1721	1.93	24.646	6.56	60.2	0.999
1695	14.46	9.67	7.10	23.6	

Gaussian-Lorentzian Fit of C=O

Figure B42: **Deconvolution data for MDI-TMP-PCD-BD of C=O region. Data calculated using Gaussian-Lorentzian cross fitting function. [Raw data in black, fit data in red, free ester carbonyl peaks solid blue, hydrogen bonded urethane carbonyl dash blue and free urea dot blue].**

Table B42: **Deconvolution data of C=O region collected using GaussianLorentzian cross function of MDI-TMP-PCD-BD.**

MDI-TMP-PCD-BD					
Peak Position/cm^{-1}	Standard Error/cm^{-1}	Area	Standard Error	Area/%	Fit R^2 value
1732	2.72	0.661	0.61	50.3	
1715	7.33	0.493	1.63	37.5	0.999
1693	13.2	0.160	1.22	12.2	

8 - MDI-TMP-PCD-PD

N-H Region Deconvolution
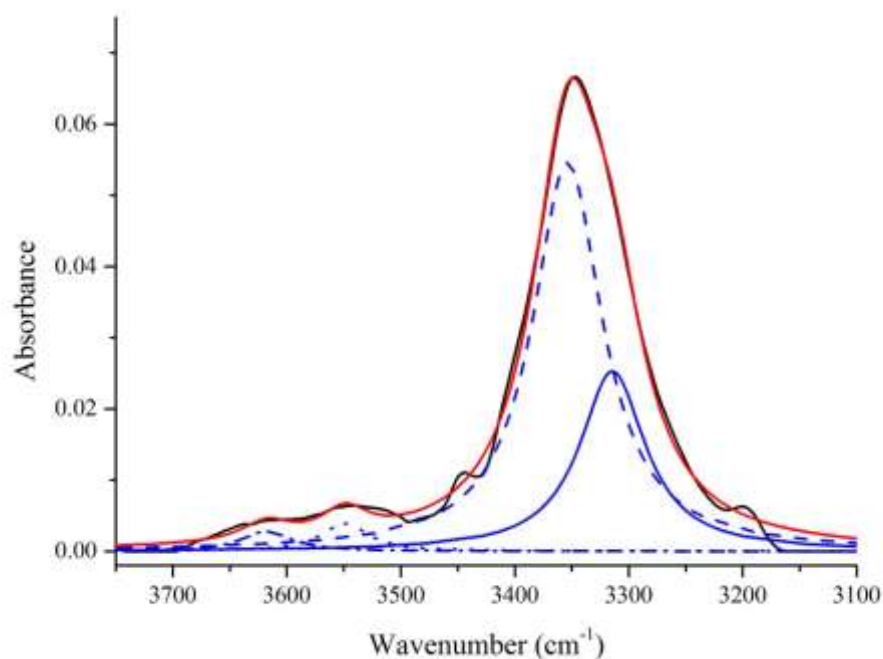
Lorentzian Fit of N-H

Figure B43: Deconvolution data for MDI-TMP-PCD-PD of N-H region. Data calculated using Lorentzian fitting function. [Raw data in black, fit data in red, HS-HS fitted peak solid blue, carbonyl overtone dash blue, free N-H dot and dot dash blue].

Table B43: Deconvolution data of N-H region collected using Lorentzian function of MDI-TMP-PCD-PD.

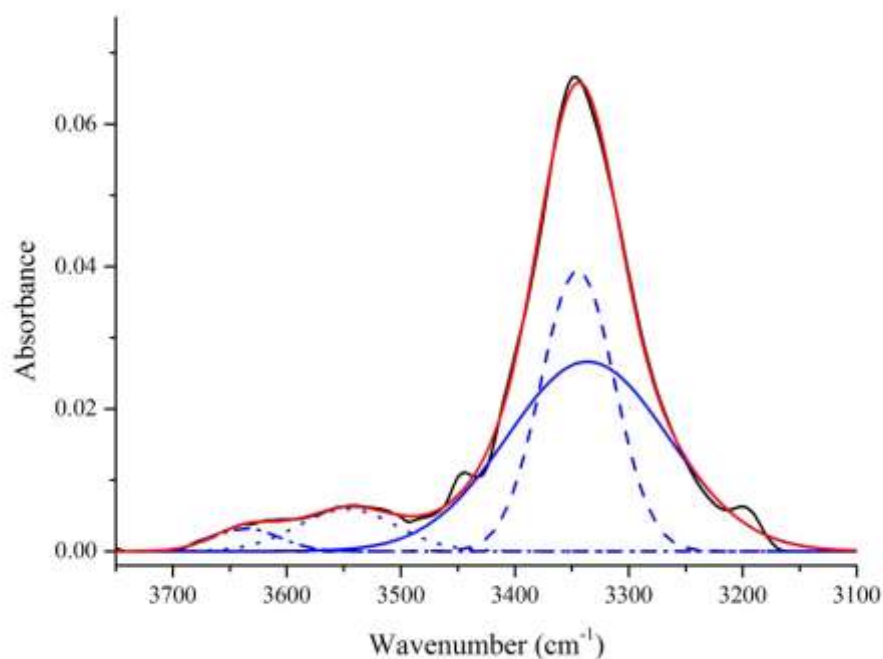| MDI-TMP-PCD-PD					
Peak Position/cm^{-1}	Standard Error/cm^{-1}	Area	Standard Error	Area/%	Fit R^2 value
3618	6.49	0.238	8.4x10^{-2}	2.5	
3549	4.32	0.308	8.6x10^{-2}	3.2	
3354	1.44	6.396	0.55	65.8	0.995
3314	2.75	2.772	0.54	28.5	

Gaussian Fit of N-H

Figure B44: **Deconvolution data for MDI-TMP-PCD-PD of N-H region. Data calculated using Gaussian fitting function. [Raw data in black, fit data in red, HS-HS fitted peak solid blue, carbonyl overtone dash blue, free N-H dot and dot dash blue].**

Table B44: Deconvolution data of N-H region collected using Gaussian function of MDI-TMP-PCD-PD.

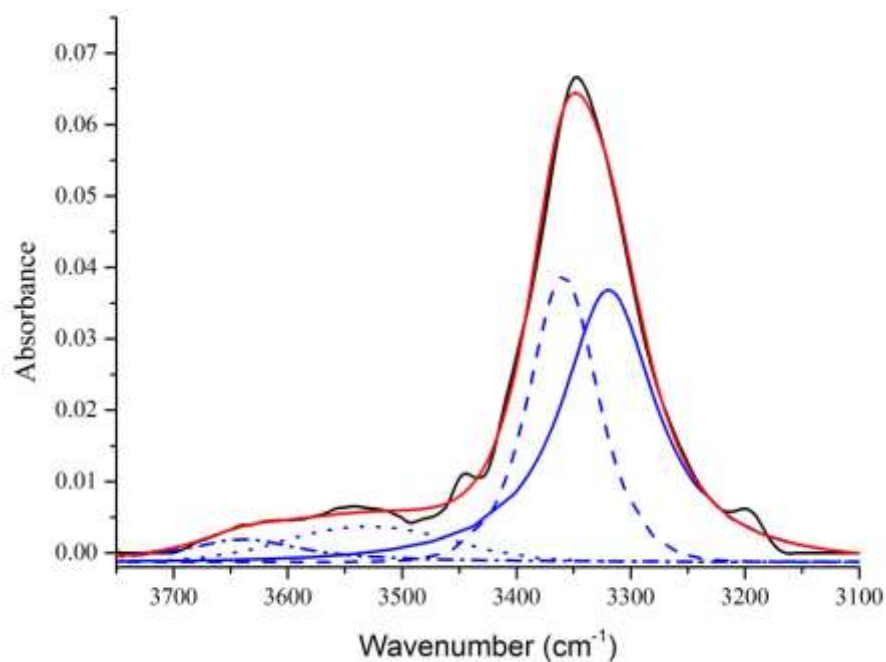| MDI-TMP-PCD-PD					
Peak Position/cm^{-1}	Standard Error/cm^{-1}	Area	Standard Error	Area/%	Fit R^2 value
3636	7.01	0.234	7.2×10^{-2}		
3547	5.32	0.641	8.5×10^{-2}	10.0	0.998
3345	0.39	3.177	0.17	36.3	
3336	0.97	4.701	0.16	53.7	

Gaussian-Lorentzian Fit of N-H

Figure B45: Deconvolution data for MDI-TMP-PCD-PD of N-H region. Data calculated using Gaussian-Lorentzian cross fitting function. [Raw data in black, fit data in red, HS-HS fitted peak solid blue, carbonyl overtone dash blue, free N-H dot and dot dash blue].

Table B45: Deconvolution data of N-H region collected using GaussianLorentzian cross function of MDI-TMP-PCD-PD.

MDI-TMP-PCD-PD					
Peak Position/cm^{-1}	Standard Error/cm^{-1}	Area	Standard Error	Area/%	Fit R^2 value
3639	-	3.18×10^{-3}	-		
		4.95×10^{-3}	1.4×10^{-4}	10.1	
3529	3.77	4.0×10^{-2}	5.0×10^{-4}		
3359	0.32			46.4	0.994
3319	1.84	3.8×10^{-2}	4.3×10^{-4}	44.2	

C=O Region Deconvolution
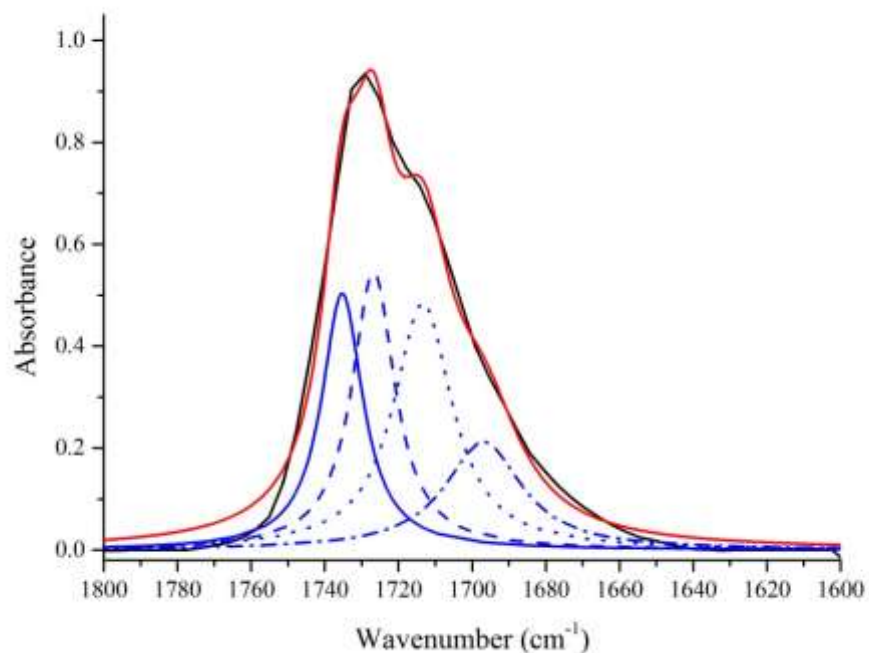
Lorentzian Fit of C=O

Figure B46: Deconvolution data for MDI-TMP-PCD-BD of C=O region. Data calculated using Lorentzian fitting function. [Raw data in black, fit data in red, free ester carbonyl peaks solid blue, free urethane carbonyl dash blue, hydrogen bonded urethane dot blue and free urea dot dash blue].

Table B46: Deconvolution data of C=O region collected using Lorentzian function of MDI-TMP-PCD-BD.

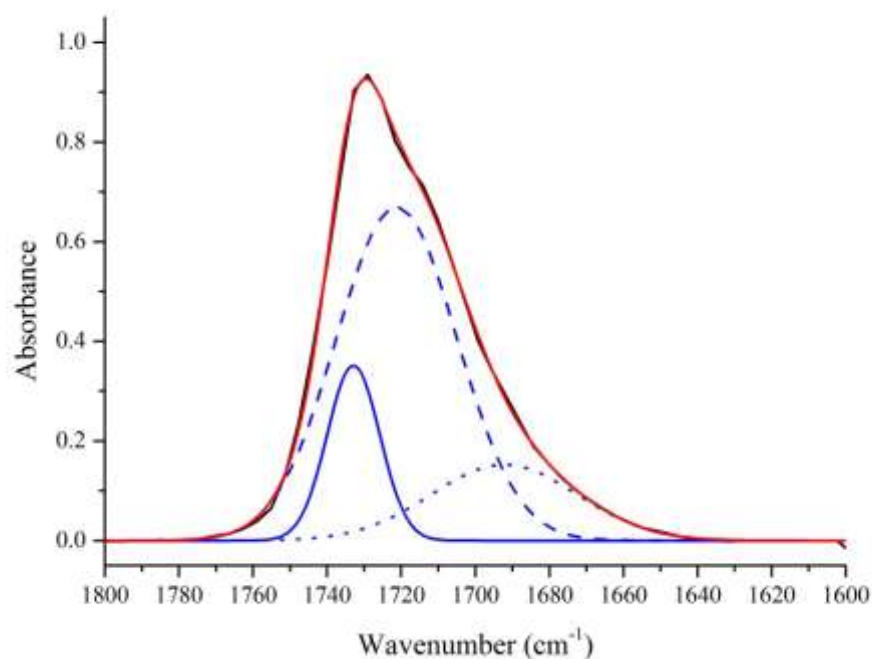|		MDI-TMP-PCD-PD			
Peak Position/cm^{-1}	Standard Error/cm^{-1}	Area	Standard Error	Area/%	Fit R^2 value
1735	1.43	10.725	6.76	23.4	
1727	1.25	12.146	12.96	26.4	0.990
1713	1.63	14.61	12.37	31.8	
1697	4.17	8.454	6.02	18.4	

Gaussian Fit of C=O

Figure B47: Deconvolution data for MDI-TMP-PCD-PD of C=O region. Data calculated using Gaussian fitting function. [Raw data in black, fit data in red, free ester carbonyl peaks solid blue, hydrogen bonded urethane carbonyl dash blue and free urea dot blue].

Table B47: Deconvolution data of C=O region collected using Gaussian function of MDI-TMP-PCD-PD.

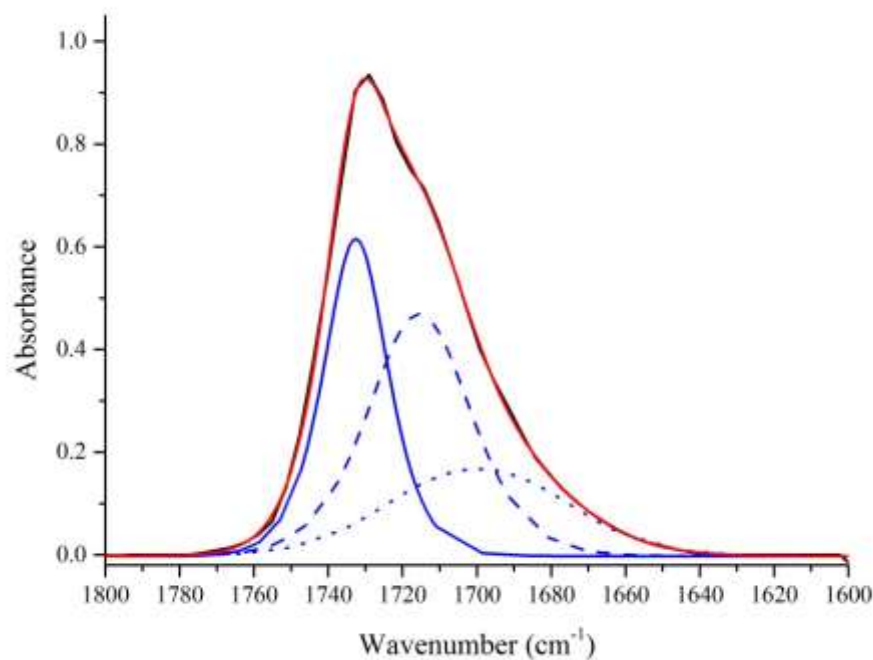| MDI-TMP-PCD-PD					
Peak Position/cm^{-1}	Standard Error/cm^{-1}	Area	Standard Error	Area/%	Fit R^2 value
1733	0.23	6.246	0.80	15.2	
1721	2.33	27.317	4.94	66.5	0.999
1692	13.4	7.52	5.55	18.3	

Gaussian-Lorentzian Fit of C=O

Figure B48: Deconvolution data for MDI-TMP-PCD-PD of C=O region. Data calculated using Gaussian-Lorentzian cross fitting function. [Raw data in black, fit data in red, free ester carbonyl peaks solid blue, hydrogen bonded urethane carbonyl dash blue and free urea dot blue].

Table B48: Deconvolution data of C=O region collected using GaussianLorentzian cross function of MDI-TMP-PCD-PD.

MDI-TMP-PCD-PD					
Peak Position/cm^{-1}	Standard Error/cm^{-1}	Area	Standard Error	Area/%	Fit R^2 value
1733	2.24	0.617	0.24	49.0	
1715	7.87	0.472	0.60	37.5	0.999
1700	5.03	0.169	0.53	13.4	

9 - MDI-TMP-PDEGA

N-H Region Deconvolution
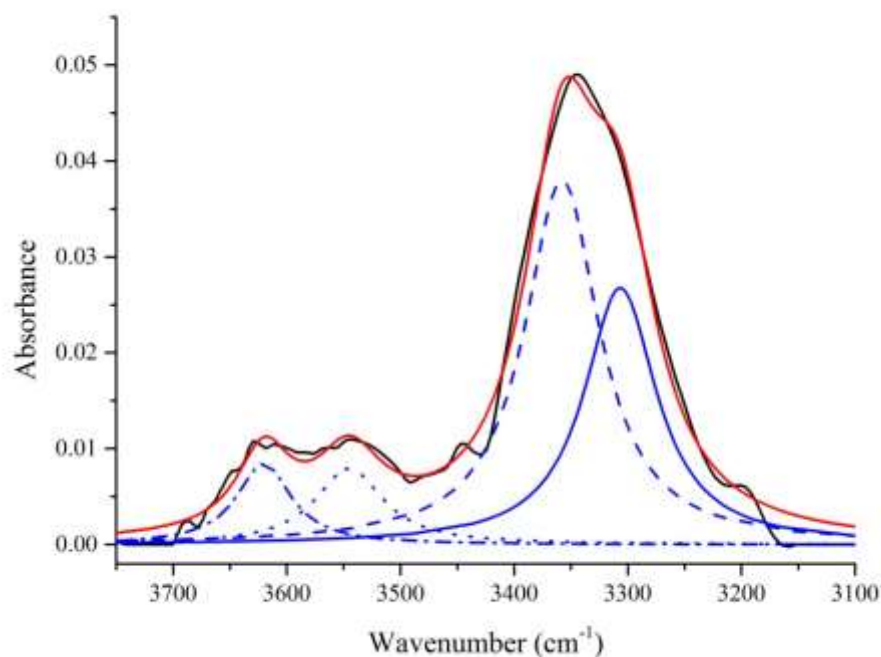
Lorentzian Fit of N-H

Figure B49: Deconvolution data for MDI-TMP-PDEGA of N-H region. Data calculated using Lorentzian fitting function. [Raw data in black, fit data in red, HS-HS fitted peak solid blue, carbonyl overtone dash blue, free N-H dot and dot dash blue].

Table B49: Deconvolution data of N-H region collected using Lorentzian function of MDI-TMP-PDEGA.

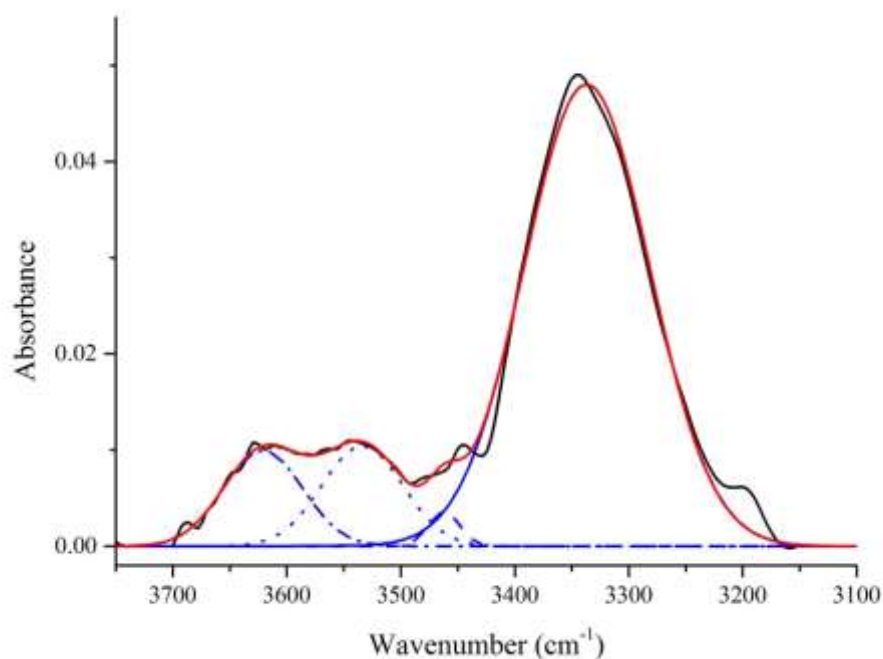| MDI-TMP-PDEGA					
Peak Position/cm^{-1}	Standard Error/cm^{-1}	Area	Standard Error	Area/%	Fit R^2 value
3620	2.71	0.775	0.12	8.0	
3545	3.48	0.909	0.15	9.3	0.989
3358	1.79	4.783	0.46	49.2	
3307	2.37	3.257	0.44	33.5	

Gaussian Fit of N-H

Figure B50: **Deconvolution data for MDI-TMP-PDEGA of N-H region. Data calculated using Gaussian fitting function. [Raw data in black, fit data in red, HS-HS fitted peak solid blue, carbonyl overtone dash blue, free N-H dot and dot dash blue].**

Table B50: Deconvolution data of N-H region collected using Gaussian function of MDI-TMP-PDEGA.

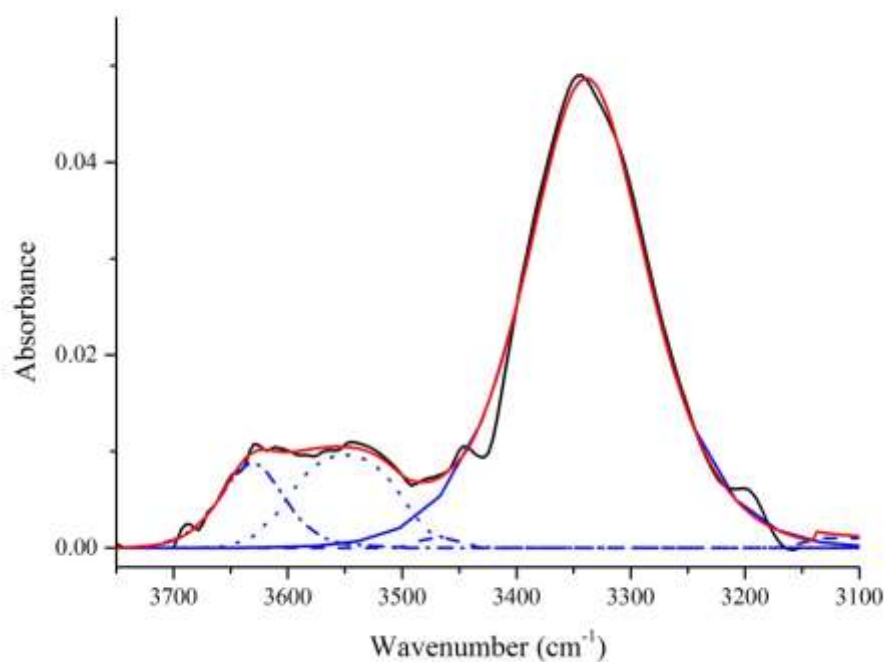| MDI-TMP-PDEGA					
Peak Position/cm^{-1}	Standard Error/cm^{-1}	Area	Standard Error	Area/%	Fit R^2 value
3621	6.48	0.866	0.16	21.1	
3534	5.31	0.930	0.19		0.992
3462	3.41	0.123	5.1×10^{-2}	1.4	
3337	0.41	6.630	4.4×10^{-2}	77.5	

Gaussian-Lorentzian Fit of N-H

Figure B51: Deconvolution data for MDI-TMP-PDEGA of N-H region. Data calculated using Gaussian-Lorentzian cross fitting function. [Raw data in black, fit data in red, HS-HS fitted peak solid blue, carbonyl overtone dash blue, free N-H dot and dot dash blue].

Table B51:   Deconvolution   data   of   N-H   region   collected   using GaussianLorentzian cross function of MDI-TMP-PDEGA.

MDI-TMP-PDEGA					
Peak Position/cm^{-1}	Standard Error/cm^{-1}	Area	Standard Error	Area/%	Fit R^2 value
3631	18.43	8.79x10^{-3}	1.3x10^{-3}		
		9.62x10^{-3}	1.6x10^{-3}	27.7	
3550	19.00	1.02x10^{-3}	3.7x10^{-4}		
3468	8.06			1.5	0.993
3339	0.43	4.87x10^{-2}	3.7x10^{-3}	71.5	

C=O Region Deconvolution
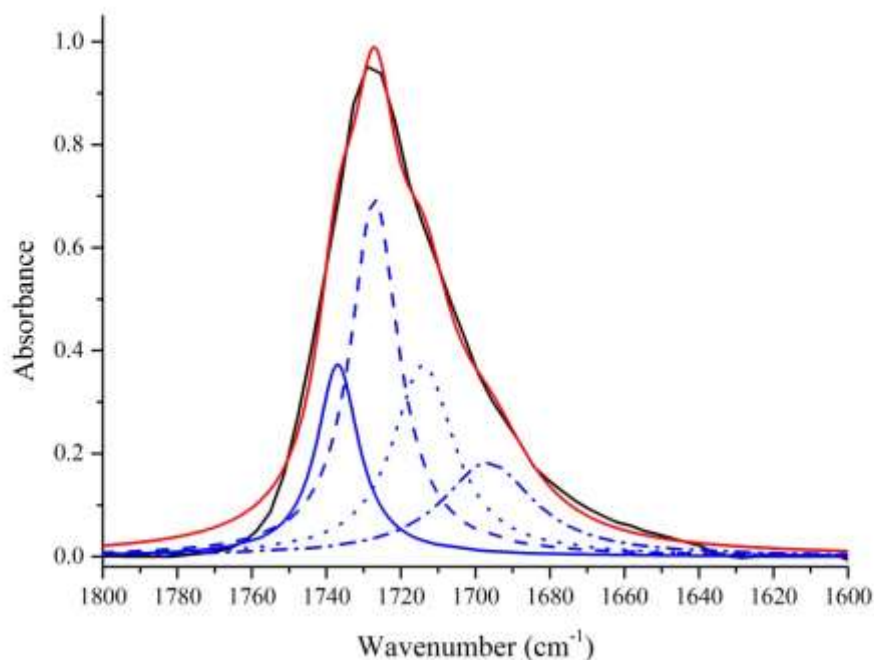
Lorentzian Fit of C=O

Figure B52: Deconvolution data for MDI-TMP-PDEGA of C=O region. Data calculated using Lorentzian fitting function. [Raw data in black, fit data in red, free ester carbonyl peaks solid blue, free urethane carbonyl dash blue, hydrogen bonded urethane dot blue and free urea dot dash blue].

Table B52: Deconvolution data of C=O region collected using Lorentzian function of MDI-TMP-PDEGA.

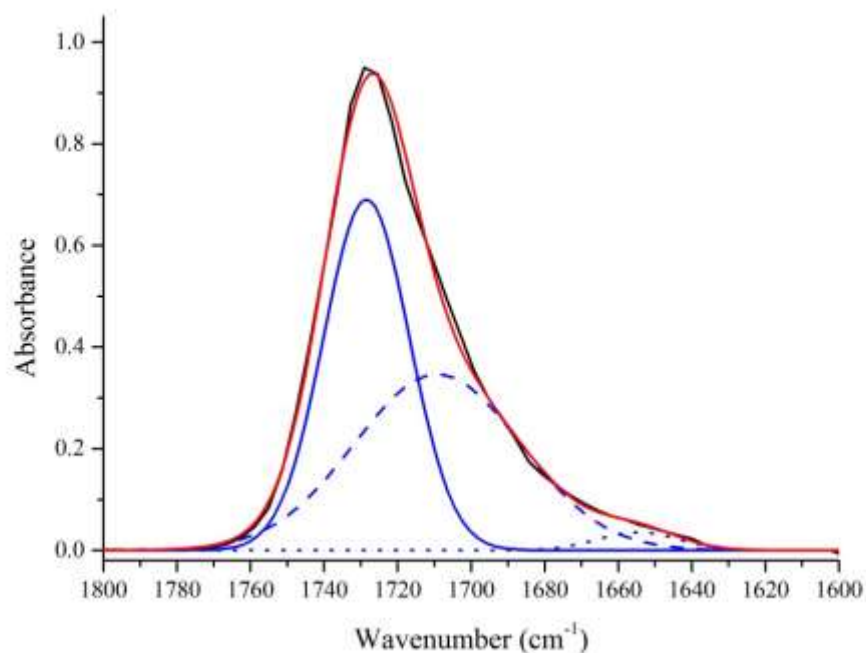| MDI-TMP-PDEGA					
Peak Position/cm^{-1}	Standard Error/cm^{-1}	Area	Standard Error	Area/%	Fit R^2 value
1737	2.03	8.052	7.52	17.7	
1727	1.02	17.095	16.4	37.6	0.990
1714	2.80	11.750	15.25	25.8	
1697	5.98	8.621	6.93	18.9	

Gaussian Fit of C=O

Figure B53: Deconvolution data for MDI-TMP-PDEGA of C=O region. Data calculated using Gaussian fitting function. [Raw data in black, fit data in red, free ester carbonyl peaks solid blue, hydrogen bonded urethane carbonyl dash blue and free urea dot blue].

Table B53: Deconvolution data of C=O region collected using Gaussian function of MDI-TMP-PDEGA.

MDI-TMP-PDEGA					
Peak Position/cm^{-1}	Standard Error/cm^{-1}	Area	Standard Error	Area/%	Fit R^2 value
1728	0.0	20.22	0.40	49.5	
1709	0.0	19.611	0.62	48.0	0.998
1655	3.06	0.993	0.27	2.4	

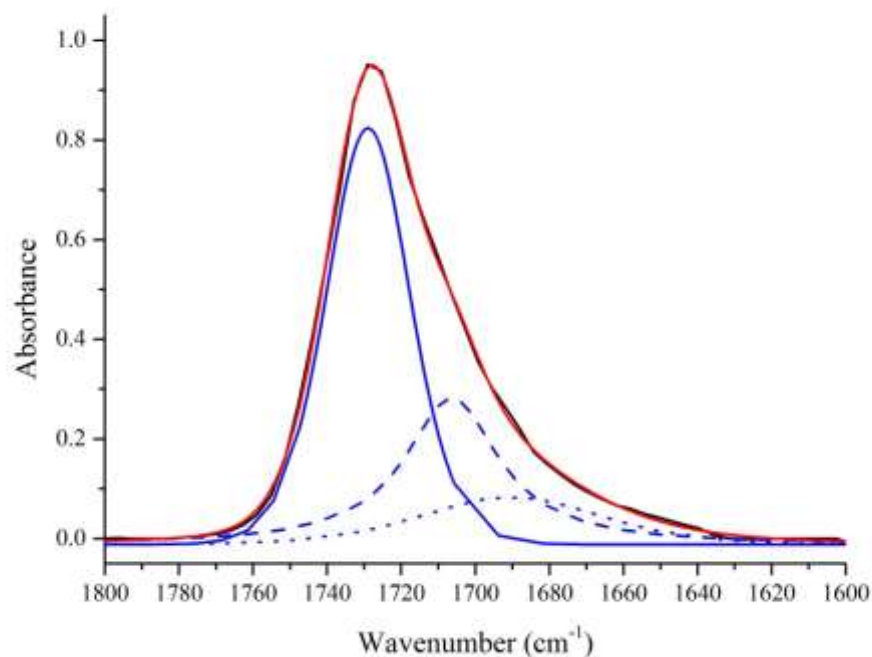*Gaussian-Lorentzian Fit of C=O*

Figure B54: Deconvolution data for MDI-TMP-PDEGA of C=O region. Data calculated using Gaussian-Lorentzian cross fitting function. [Raw data in black, fit data in red, free ester carbonyl peaks solid blue, hydrogen bonded urethane carbonyl dash blue and free urea dot blue].

Table B54: Deconvolution data of C=O region collected using GaussianLorentzian cross function of MDI-TMP-PDEGA.

MDI-TMP-PDEGA					
Peak Position/cm^{-1}	Standard Error/cm^{-1}	Area	Standard Error	Area/%	Fit R^2 value
1729	0.82	0.835	0.11	68.3	
1706	2.86	0.293	0.15	24.0	0.999
1690	7.14	9.42x10^{-2}	0.26	7.7	

10 - MDI-TMP-PDEGA-DEPD

N-H Region Deconvolution
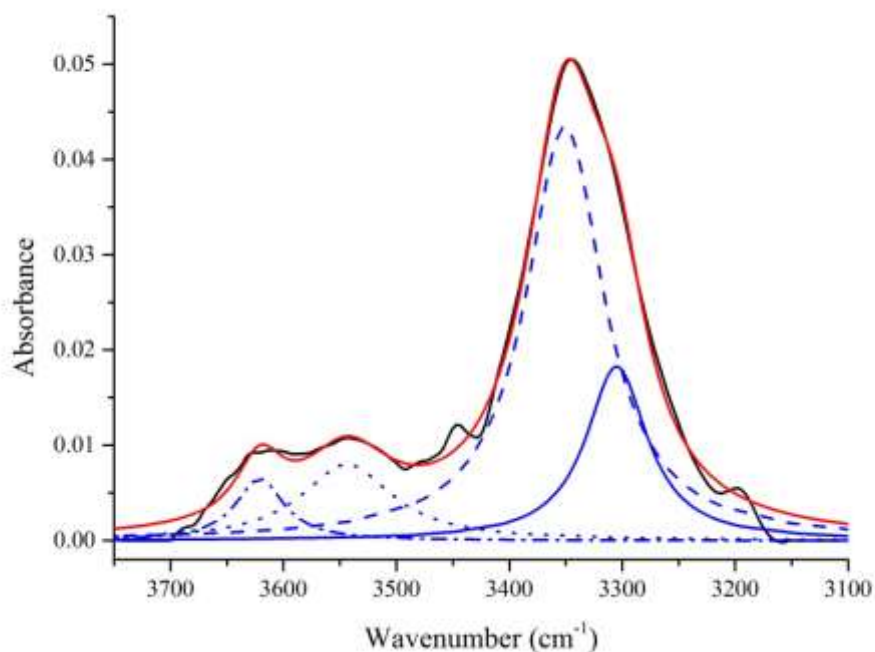
Lorentzian Fit of N-H

Figure B55: Deconvolution data for MDI-TMP-PDEGA-DEPD of N-H region. Data calculated using Lorentzian fitting function. [Raw data in black, fit data in red, HS-HS fitted peak solid blue, carbonyl overtone dash blue, free N-H dot and dot dash blue].

Table B55: Deconvolution data of N-H region collected using Lorentzian function of MDI-TMP-PDEGA-DEPD.

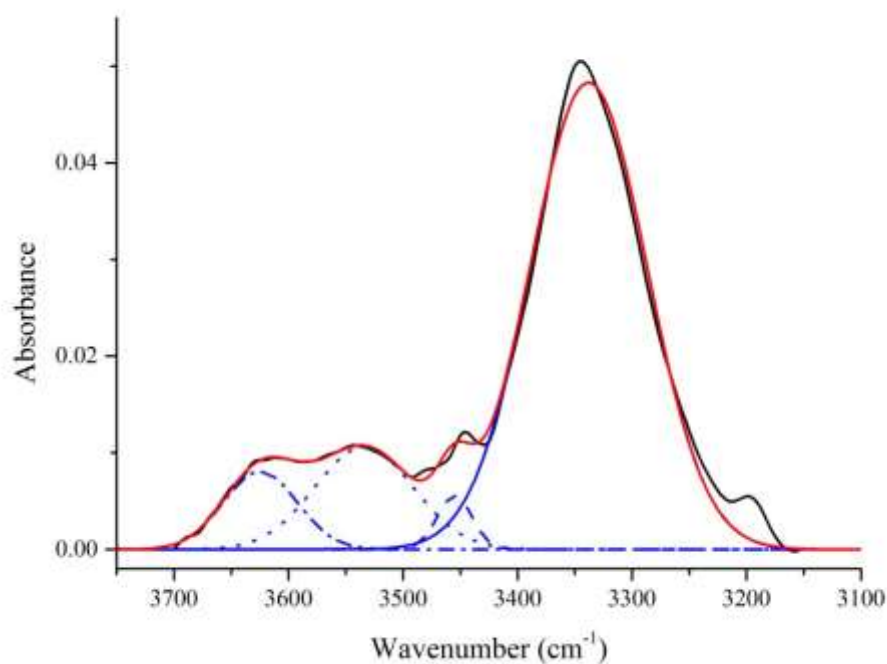| MDI-TMP-PDEGA-DEPD					
Peak Position/cm^{-1}	Standard Error/cm^{-1}	Area	Standard Error	Area/%	Fit R^2 value
3621	2.68	0.528	0.12	5.6	
3544	4.03	1.230	0.19	13.1	0.992
3351	1.75	5.719	0.48	61.0	
3305	2.71	1.895	0.43	20.2	

Gaussian Fit of N-H

Figure B56: **Deconvolution data for MDI-TMP-PDEGA-DEPD of N-H region. Data calculated using Gaussian fitting function. [Raw data in black, fit data in red, HS-HS fitted peak solid blue, carbonyl overtone dash blue, free N-H dot and dot dash blue].**

Table B56: **Deconvolution data of N-H region collected using Gaussian function of MDI-TMP-PDEGA-DEPD.**

MDI-TMP-PDEGA-DEPD					
Peak Position/cm^{-1}	Standard Error/cm^{-1}	Area	Standard Error	Area/%	Fit R^2 value
3625	2.344	0.213	0.20	22.0	
3534	6.39	1.147	0.26		0.992
3455	2.34	0.213	7.3x10^{-2}	2.6	
3338	0.42	6.167	4.5x10^{-2}	75.4	

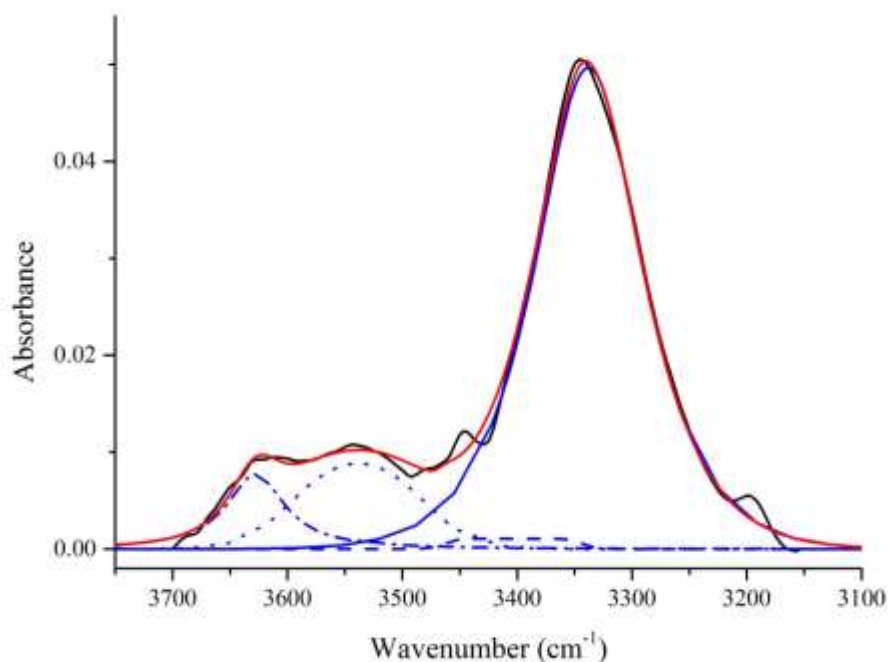*Gaussian-Lorentzian Fit of N-H*

Figure B57: Deconvolution data for MDI-TMP-PDEGA-DEPD of N-H region. Data calculated using Gaussian-Lorentzian cross fitting function. [Raw data in black, fit data in red, HS-HS fitted peak solid blue, carbonyl overtone dash blue, free N-H dot and dot dash blue].

Table B57: Deconvolution data of N-H region collected using GaussianLorentzian cross function of MDI-TMP-PDEGA-DEPD.

MDI-TMP-PDEGA-DEPD					
Peak Position/cm^{-1}	Standard Error/cm^{-1}	Area	Standard Error	Area/%	Fit R^2 value
3628	17.44	7.71×10^{-3}	-		
		8.82×10^{-3}	5.1×10^{-4}	24.6	
3539	4.79				
		1.09×10^{-3}	2.1×10^{-3}		
3403	17.44			1.6	0.996
3338	1.864	4.97×10^{-2}	1.1×10^{-3}	73.8	

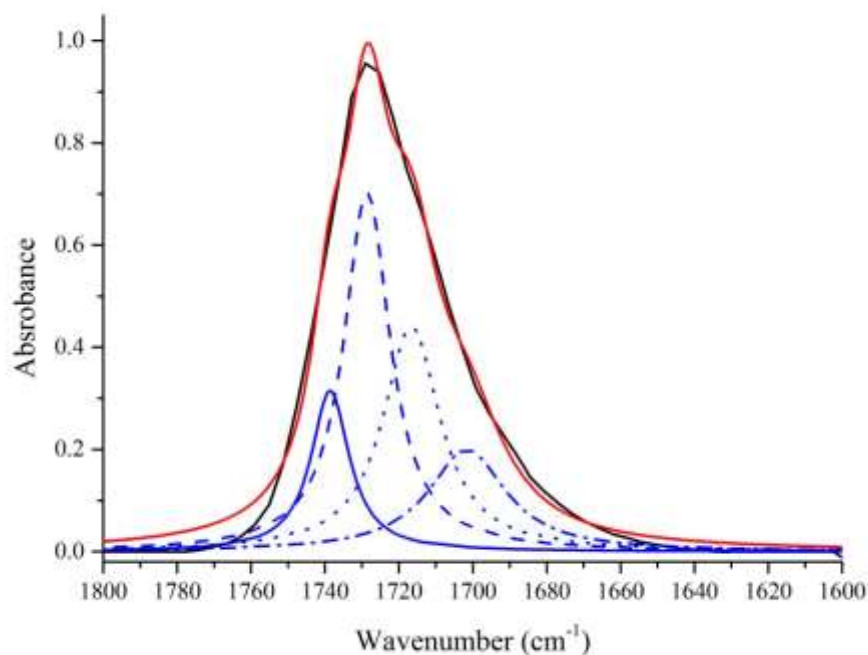## C=O Region Deconvolution

Lorentzian Fit of C=O

Figure B58: **Deconvolution data for MDI-TMP-PDEGA-DEPD of C=O region. Data calculated using Lorentzian fitting function. [Raw data in black, fit data in red, free ester carbonyl peaks solid blue, free urethane carbonyl dash blue, hydrogen bonded urethane dot blue and free urea dot dash blue].**

Table B58: **Deconvolution data of C=O region collected using Lorentzian function of MDI-TMP-PDEGA-DEPD.**

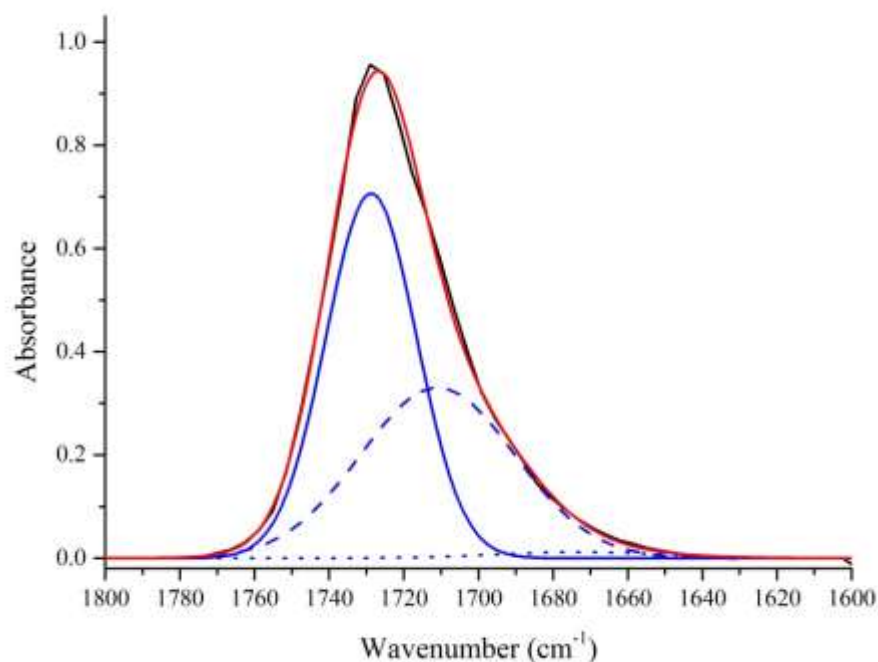| MDI-TMP-PDEGA-DEPD					
Peak Position/cm^{-1}	Standard Error/cm^{-1}	Area	Standard Error	Area/%	Fit R^2 value
1739	1.53	6.230	4.86	14.2	
1729	0.92	16.772	12.40	38.2	0.991
1717	1.95	12.96	14.49	29.5	
1702	5.08	8.001	7.05	18.2	

Gaussian Fit of C=O

Figure B59: Deconvolution data for MDI-TMP-PDEGA-DEPD of C=O region. Data calculated using Gaussian fitting function. [Raw data in black, fFit data in red, free ester carbonyl peaks solid blue, hydrogen bonded urethane carbonyl dash blue and free urea dot blue].

Table B59: Deconvolution data of C=O region collected using Gaussian function of MDI-TMP-PDEGA-DEPD.

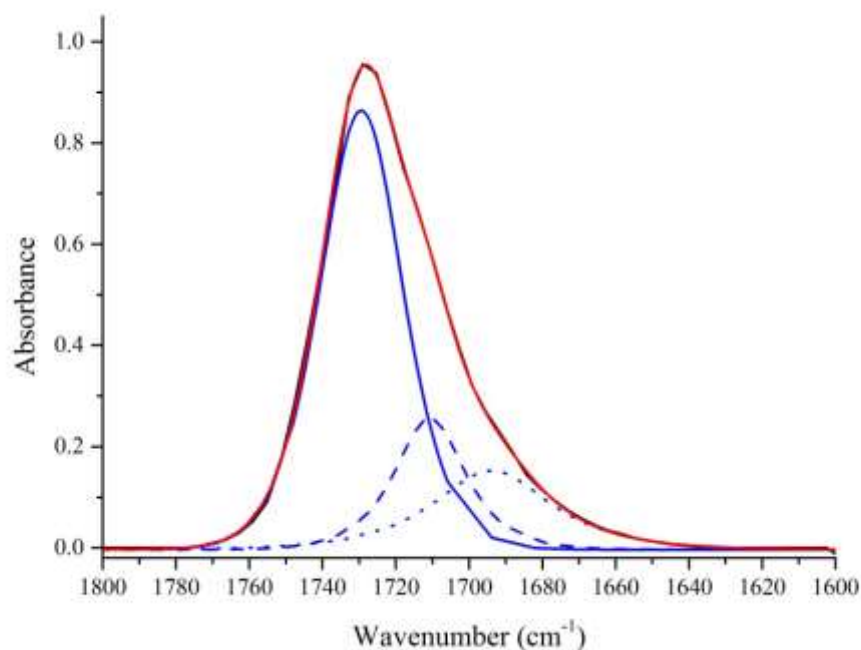| MDI-TMP-PDEGA-DEPD					
Peak Position/cm^{-1}	Standard Error/cm^{-1}	Area	Standard Error	Area/%	Fit R^2 value
1729	0.0	21.516	0.48	54.8	
1711	0.0	17.105	0.76	43.5	0.998
1672	0.0	0.667	0.41	1.7	

Gaussian-Lorentzian Fit of C=O

Figure B60: Deconvolution data for MDI-TMP-PDEGA-DEPD of C=O region. Data calculated using Gaussian-Lorentzian cross fitting function. [Raw data in black, fit data in red, free ester carbonyl peaks solid blue, hydrogen bonded urethane carbonyl dash blue and free urea dot blue].

Table B60: Deconvolution data of C=O region collected using GaussianLorentzian cross function of MDI-TMP-PDEGA-DEPD.

MDI-TMP-PDEGA-DEPD					
Peak Position/cm^{-1}	Standard Error/cm^{-1}	Area	Standard Error	Area/%	Fit R^2 value
1729	4.27	0.867	0.26	68.3	
1711	12.10	0.259	0.50	20.2	0.999
1694	15.02	0.156	0.28	12.2	

11 - IPDI-TMP-PPG

N-H Region Deconvolution
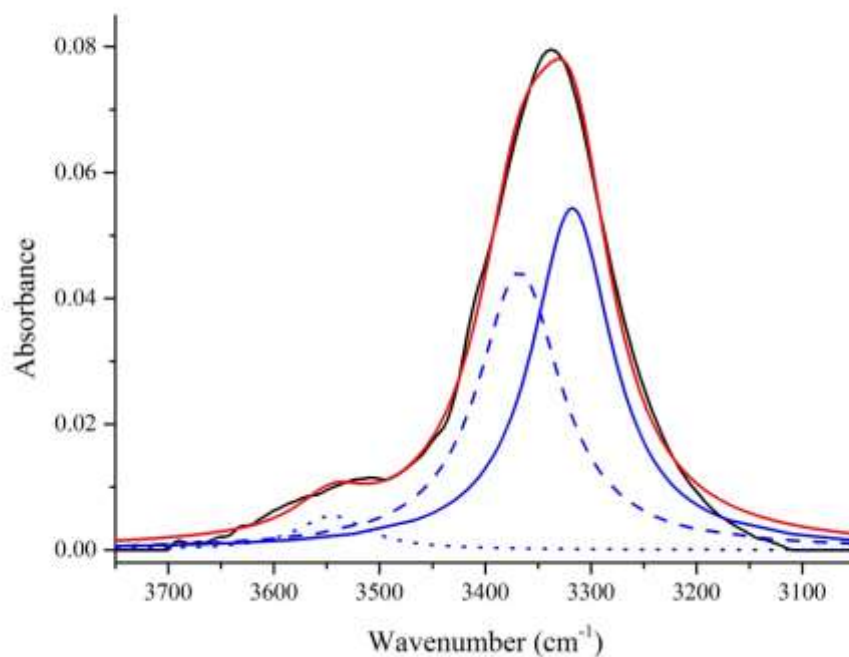
Lorentzian Fit of N-H

Figure B61: Deconvolution data for IPDI-TMP-PPG of N-H region. Data calculated using Lorentzian fitting function. [Raw data in black, fit data in red, HS-HS fitted peak solid blue, carbonyl overtone dash blue and free N-H dot blue].

Table B61: Deconvolution data of N-H region collected using Lorentzian function of IPDI-TMP-PPG.

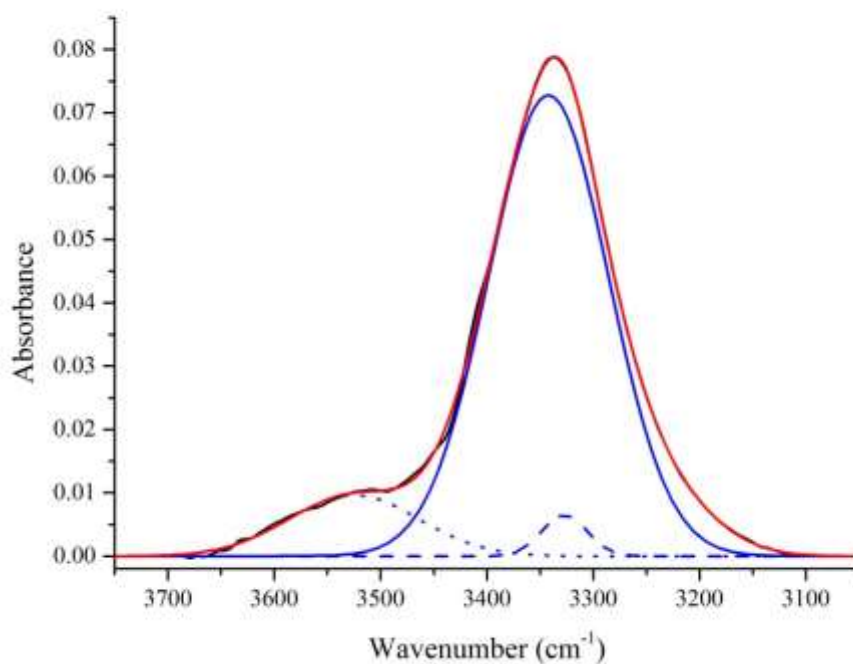| IPDI-TMP-PPG					
Peak Position/cm^{-1}	Standard Error/cm^{-1}	Area	Standard Error	Area/%	Fit R^2 value
3545	5.23	0.689	0.12	4.5	
3368	3.38	6.653	1.11	43.7	0.993
3318	2.46	7.856	1.06	51.7	

Gaussian Fit of N-H

Figure B62: Deconvolution data for IPDI-TMP-PPG of N-H region. Data calculated using Gaussian fitting function. [Raw data in black, fit data in red, HS-HS fitted peak solid blue, carbonyl overtone dash blue and free N-H dot blue].

Table B62: Deconvolution data of N-H region collected using Gaussian function of IPDI-TMP-PPG.

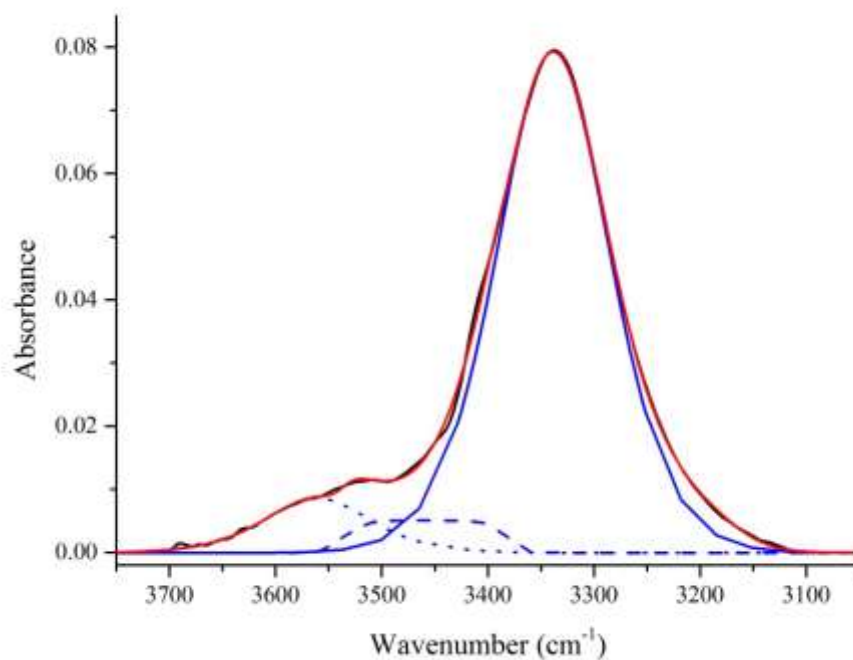| IPDI-TMP-PPG					
Peak Position/cm^{-1}	Standard Error/cm^{-1}	Area	Standard Error	Area/%	Fit R^2 value
3525	1.85	1.481	4.0×10^{-2}	11.4	
3342	1.44	10.298	0.28	2.7	0.999
3327	1.28	0.349	8.0×10^{-2}	83.1	

Gaussian-Lorentzian Fit of N-H

Figure B63: **Deconvolution data for IPDI-TMP-PPG of N-H region. Data calculated using Gaussian-Lorentzian cross fitting function. [Raw data in black, fit data in red, HS-HS fitted peak solid blue, carbonyl overtone dash blue and free N-H dot blue].**

Table B63: **Deconvolution data of N-H region collected using GaussianLorentzian cross function of IPDI-TMP-PPG.**

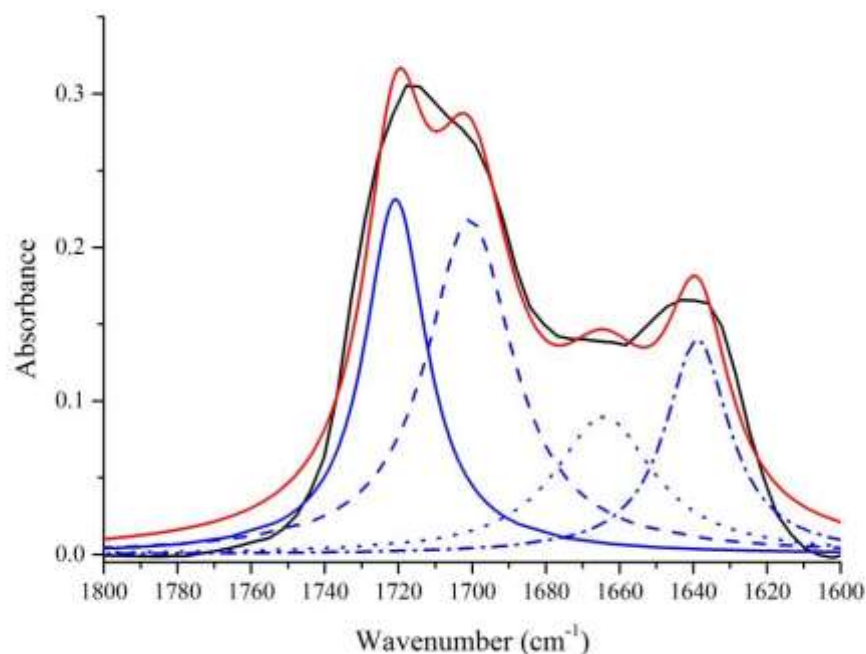| IPDI-TMP-PPG					
Peak Position/cm^{-1}	Standard Error/cm^{-1}	Area	Standard Error	Area/%	Fit R^2 value
3561	8.53	8.62×10^{-3}	2.5×10^{-4}	8.8	
3461	2.80	5.12×10^{-3}	2.80	5.2	0.999
3338	0.55	7.93×10^{-2}	1.91×10^{-4}	86.0	

C=O Region Deconvolution

Lorentzian Fit of C=O

Figure B64: Deconvolution data for IPDI-TMP-PPG of C=O region. Data calculated using Lorentzian fitting function. [Raw data in black, fit data in red, free urethane carbonyl peaks solid blue, hydrogen bonded urethane dash blue, free/monodentate hydrogen bonded urea dot blue and bidentate hydrogen bonded urea dot dash blue].

Table B64: Deconvolution data of C=O region collected using Lorentzian function of IPDI-TMP-PPG.

IPDI-TMP-PPG					
Peak Position/cm^{-1}	Standard Error/cm^{-1}	Area	Standard Error	Area/%	Fit R^2 value
1721	1.14	7.418	2.27	28.0	
1701	1.76	9.777	3.89	36.9	0.968
1664	3.68	4.650	3.61	17.5	
1639	1.53	4.654	1.83	17.6	

Gaussian Fit of C=O
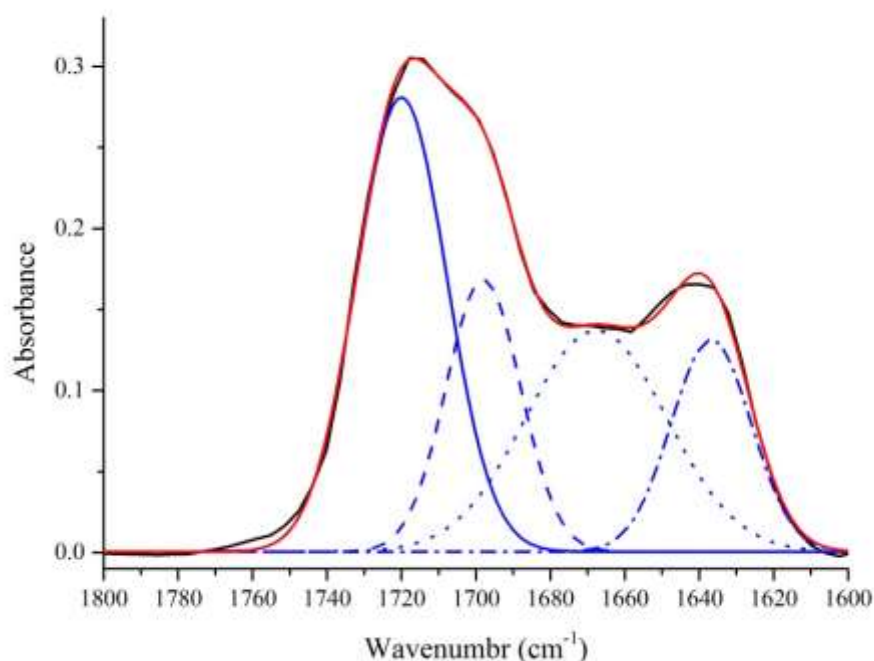

Figure B65: **Deconvolution data for IPDI-TMP-PPG of C=O region. Data calculated using Gaussian fitting function. [Raw data in black, fit data in red, free urethane carbonyl peaks solid blue, hydrogen bonded urethane dash blue, free/monodentate hydrogen bonded urea dot blue and bidentate hydrogen bonded urea dot dash blue].**

Table B65: Deconvolution data of C=O region collected using Gaussian function of IPDI-TMP-PPG.

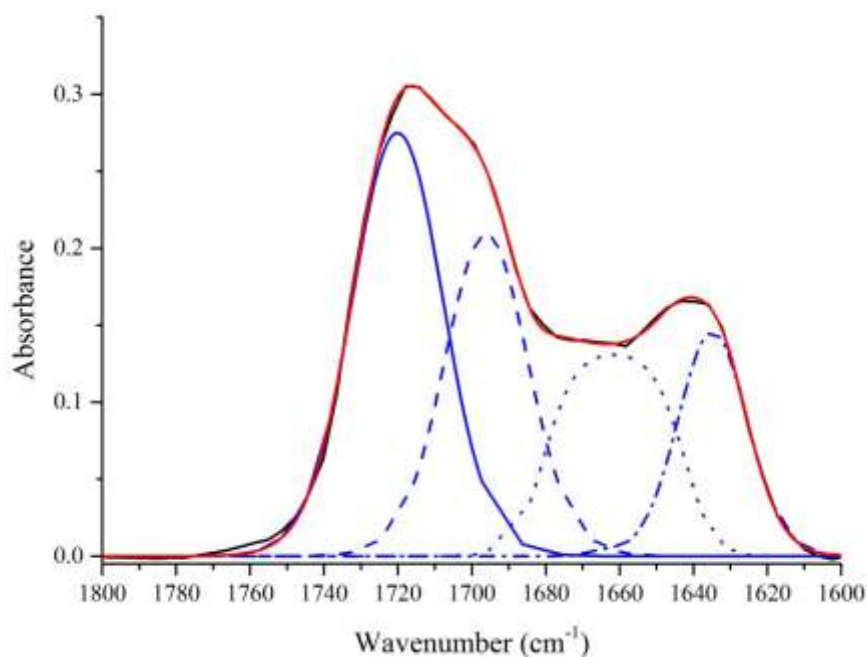| IPDI-TMP-PPG					
Peak Position/cm^{-1}	**Standard Error/cm^{-1}**	**Area**	**Standard Error**	**Area/%**	**Fit R^2 value**
1720	0.94	8.530	0.63	37.5	
1698	0.93	4.217	1.82	18.5	0.998
1668	1.76	6.478	3.10	28.5	
1637	1.19	3.529	1.59	15.5	

Gaussian-Lorentzian Fit of C=O

Figure B66: **Deconvolution data for IPDI-TMP-PPG of C=O region. Data calculated using Gaussian-Lorentzian cross fitting function. [Raw data in black, fit data in red, free urethane carbonyl peaks solid blue, hydrogen bonded urethane dash blue, free/monodentate hydrogen bonded urea dot blue and bidentate hydrogen bonded urea dot dash blue].**

Table B66: **Deconvolution data of C=O region collected using GaussianLorentzian cross function of IPDI-TMP-PPG.**

IPDI-TMP-PPG					
Peak Position/cm^{-1}	Standard Error/cm^{-1}	Area	Standard Error	Area/%	Fit R^2 value
1720	5.99	0.275	3.6×10^{-2}	36.2	
1696	6.92	0.209	0.12	27.5	
1661	6.95	0.131	9.0×10^{-3}	17.2	0.999
1635	3.81	0.145	4.4×10^{-2}	19.1	

12 - IPDI-TMP-PPG-DEPD

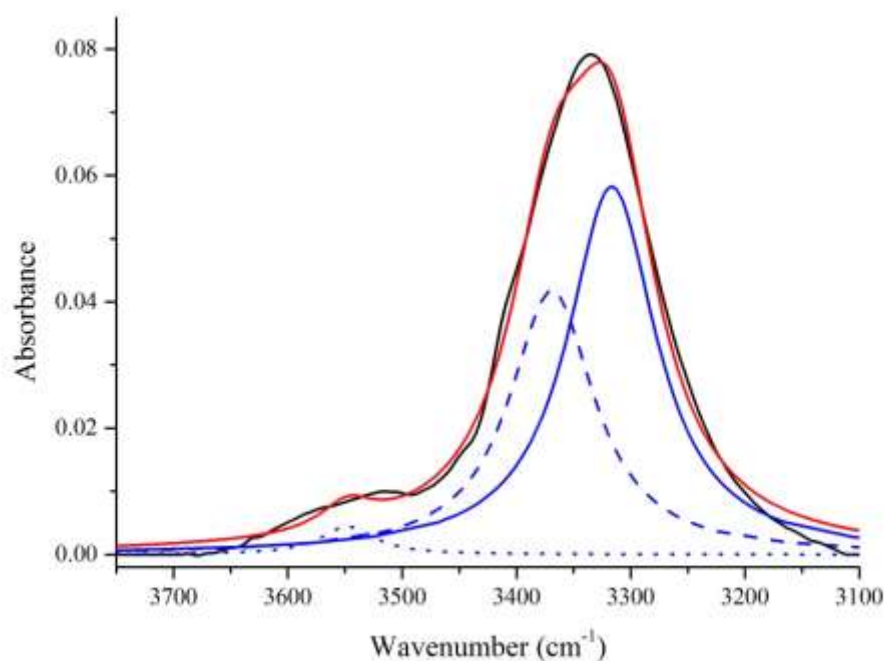## N-H Region Deconvolution

Lorentzian Fit of N-H

Figure B67: Deconvolution data for IPDI-TMP-PPG-DEPD of N-H region. Data calculated using Lorentzian fitting function. [Raw data in black, fit data in red, HS-HS fitted peak solid blue, carbonyl overtone dash blue and Free N-H dot blue].

Table B67: Deconvolution data of N-H region collected using Lorentzian function of IPDI-TMP-PPG-DEPD.

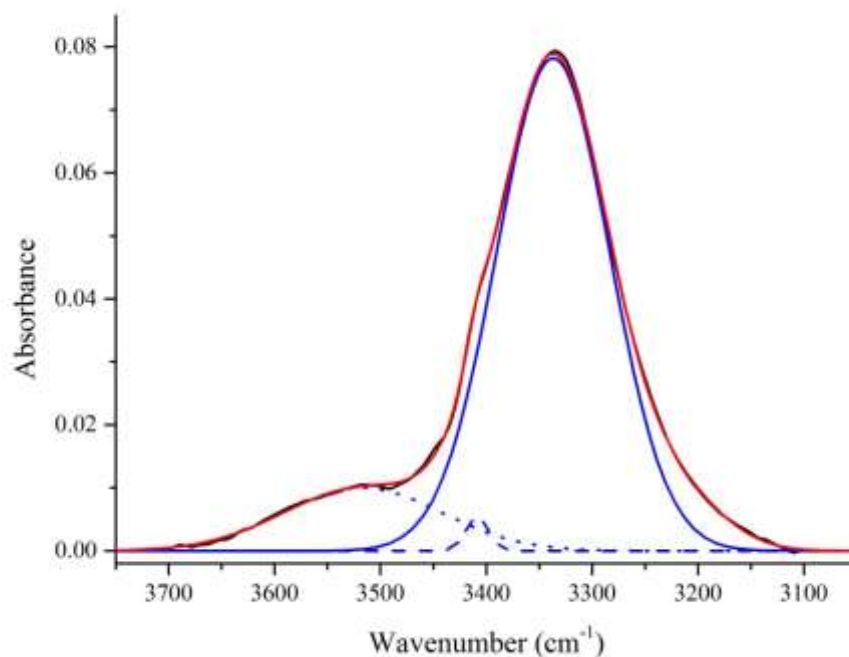| IPDI-TMP-PPG-DEPD					
Peak Position/cm^{-1}	Standard Error/cm^{-1}	Area	Standard Error	Area/%	Fit R^2 value
3548	5.60	0.400	9.5x10^{-2}	2.7	
3369	2.93	5.932	0.92	39.7	0.993
3317	2.22	8.628	0.90	57.6	

Gaussian Fit of N-H

Figure B68: Deconvolution data for IPDI-TMP-PPG-DEPD of N-H region. Data calculated using Gaussian fitting function. [Raw data in black, fit data in red, HS-HS fitted peak solid blue, carbonyl overtone dash blue and free N-H dot blue].

Table B68: Deconvolution data of N-H region collected using Gaussian function of IPDI-TMP-PPG-DEPD.

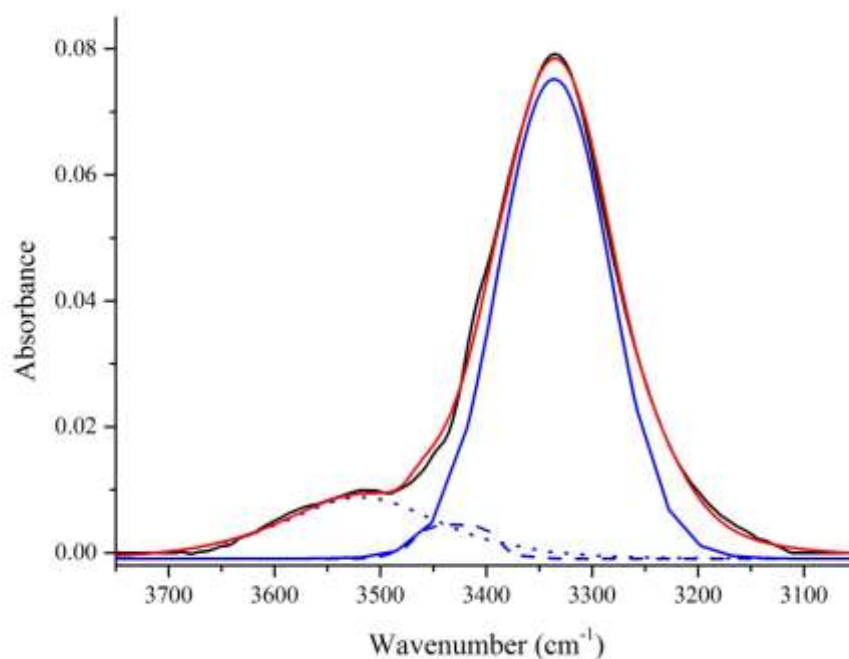| IPDI-TMP-PPG-DEPD					
Peak Position/cm^{-1}	Standard Error/cm^{-1}	Area	Standard Error	Area/%	Fit R^2 value
3517	1.93	1.877	4.2×10^{-2}	14.1	
3409	0.53	0.145	1.4×10^{-2}	0.1	0.999
3337	0.27	10.463	0.11	84.8	

Gaussian-Lorentzian Fit of N-H

Figure B69: **Deconvolution data for IPDI-TMP-PPG-DEPD of N-H region. Data calculated using Gaussian-Lorentzian cross fitting function. [Raw data in black, fit data in red, HS-HS fitted peak solid blue, carbonyl overtone dash blue and free N-H dot blue].**

Table B69: Deconvolution data of N-H region collected using GaussianLorentzian cross function of IPDI-TMP-PPG-DEPD.

IPDI-TMP-PPG-DEPD					
Peak Position/cm^{-1}	Standard Error/cm^{-1}	Area	Standard Error	Area/%	Fit R^2 value
3518	8.00	9.74×10^{-3}	19.2	8.8	
3429	3.56	5.38×10^{-3}	4.41	5.2	0.998
3336	4.38	7.61×10^{-2}	4.66	86.0	

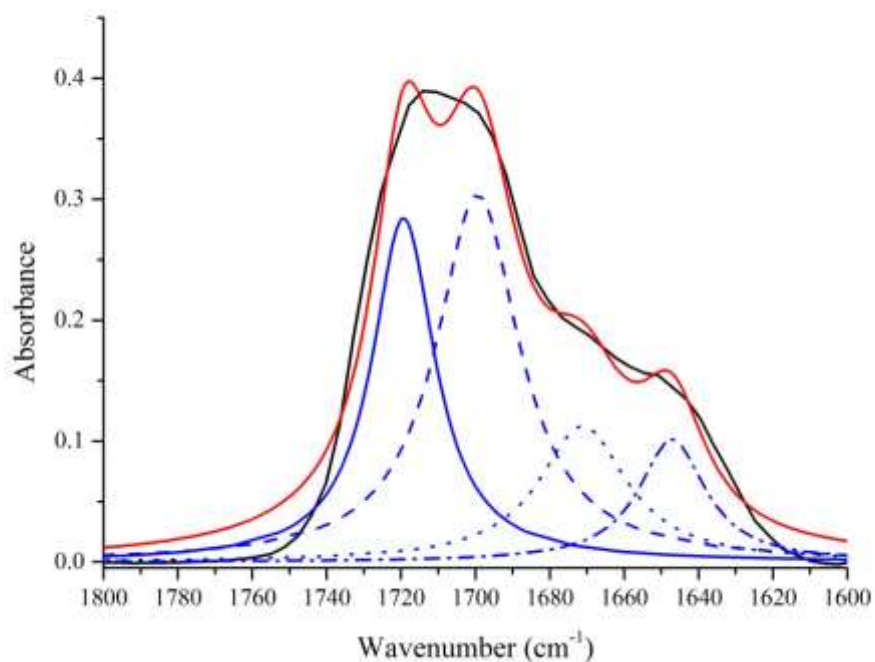## C=O Region Deconvolution

Lorentzian Fit of C=O

Figure B70: Deconvolution data for IPDI-TMP-PPG-DEPD of C=O region. Data calculated using Lorentzian fitting function. [Raw data in black, fit data in red, free urethane carbonyl peaks solid blue, hydrogen bonded urethane dash blue, free/monodentate hydrogen bonded urea dot blue and bidentate hydrogen bonded urea dot dash blue].

Table B70: Deconvolution data of C=O region collected using Lorentzian function of IPDI-TMP-PPG-DEPD.

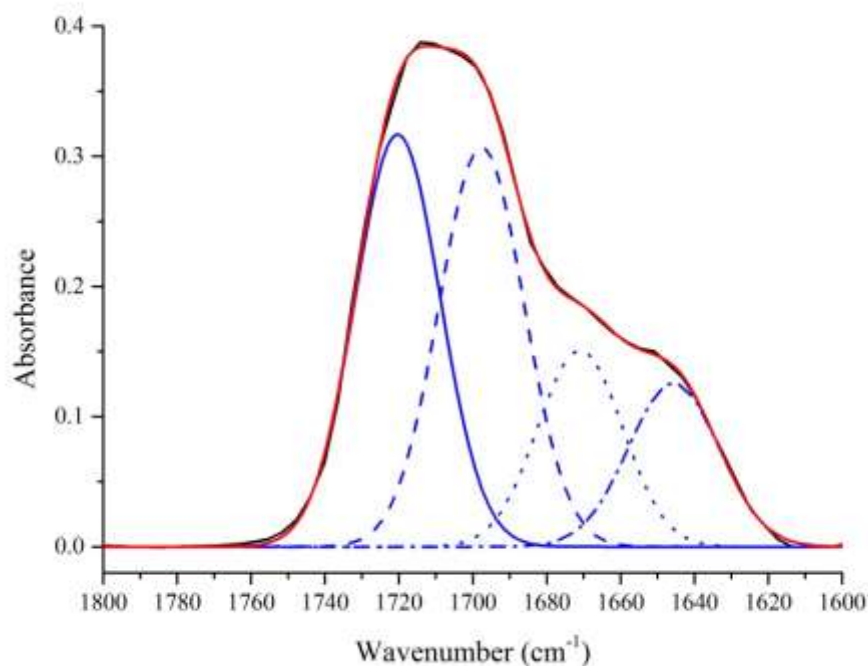| IPDI-TMP-PPG-DEPD					
Peak Position/cm^{-1}	Standard Error/cm^{-1}	Area	Standard Error	Area/%	Fit R^2 value
1719	1.18	9.164	2.94	29.8	
1699	1.43	12.981	5.70	42.3	0.974
1671	3.42	5.094	5.07	16.6	
1647	2.83	3.471	2.29	11.3	

Gaussian Fit of C=O

Figure B71: Deconvolution data for IPDI-TMP-PPG-DEPD of C=O region. Data calculated using Gaussian fitting function. [Raw data in black, fit data in red, free urethane carbonyl peaks solid blue, hydrogen bonded urethane dash blue, free/monodentate hydrogen bonded urea dot blue and bidentate hydrogen bonded urea dot dash blue].

Table B71: Deconvolution data of C=O region collected using Gaussian function of IPDI-TMP-PPG-DEPD.

IPDI-TMP-PPG-DEPD					
Peak Position/cm^{-1}	Standard Error/cm^{-1}	Area	Standard Error	Area/%	Fit R^2 value
1720	1.26	9.104	1.20	34.8	
1698	0.77	8.868	2.12	33.9	0.999
1671	1.55	4.354	1.68	16.6	
1646	2.25	3.853	0.75	14.7	

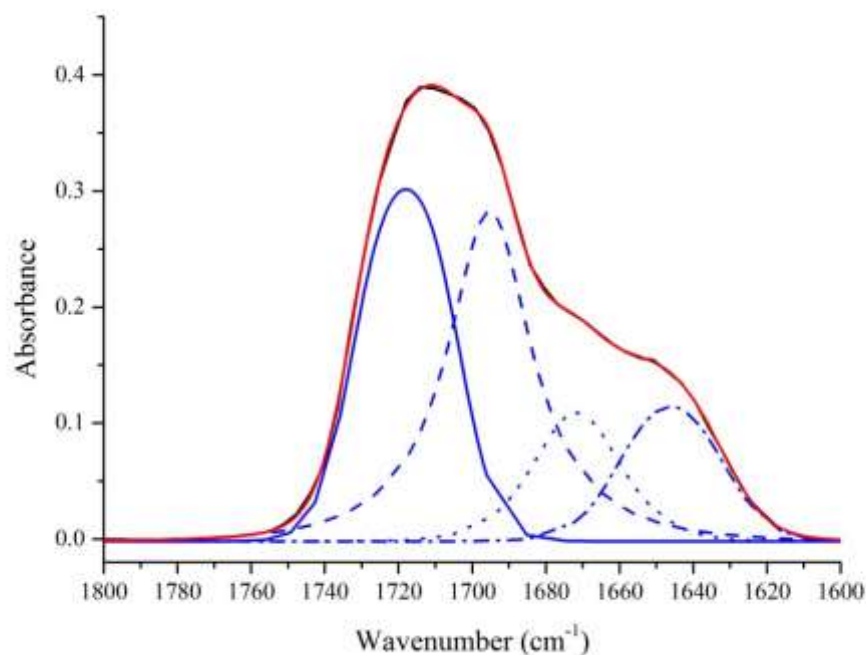*Gaussian-Lorentzian Fit of C=O*

Figure B72: **Deconvolution data for IPDI-TMP-PPG-DEPD of C=O region. Data calculated using Gaussian-Lorentzian cross fitting function. [Raw data in black, fit data in red, free urethane carbonyl peaks solid blue, hydrogen bonded urethane dash blue, free/monodentate hydrogen bonded urea dot blue and bidentate hydrogen bonded urea dot dash blue].**

Table B72: **Deconvolution data of C=O region collected using GaussianLorentzian cross function of IPDI-TMP-PPG-DEPD.**

IPDI-TMP-PPG-DEPD					
Peak Position/cm^{-1}	Standard Error/cm^{-1}	Area	Standard Error	Area/%	Fit R^2 value
1718	0.97	0.303	8.3×10^{-3}	37.3	
1695	1.83	0.284	5.3×10^{-2}	34.9	
1672	8.10	0.111	6.8×10^{-2}	13.6	0.999
1646	10.78	0.116	0.11	14.2	

13 - IPDI-TMP-PPG-BD

N-H Region Deconvolution

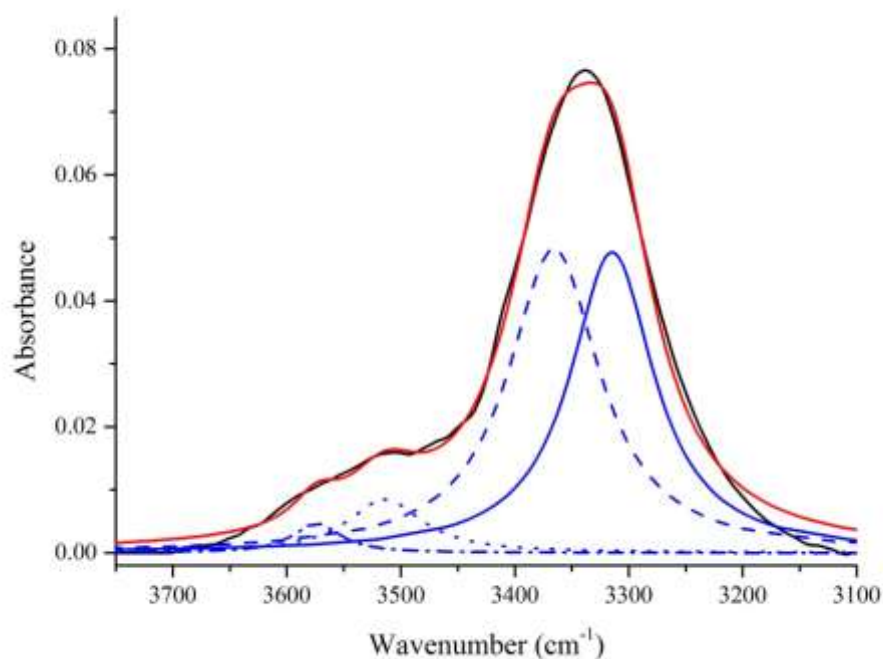*Lorentzian Fit of N-H*

Figure B73: Deconvolution data for IPDI-TMP-PPG-BD of N-H region. Data calculated using Lorentzian fitting function. [Raw data in black, fit data in red, HS-HS fitted peak solid blue, carbonyl overtone dash blue and free N-H dot blue].

Table B73: Deconvolution data of N-H region collected using Lorentzian function of IPDI-TMP-PPG-BD.

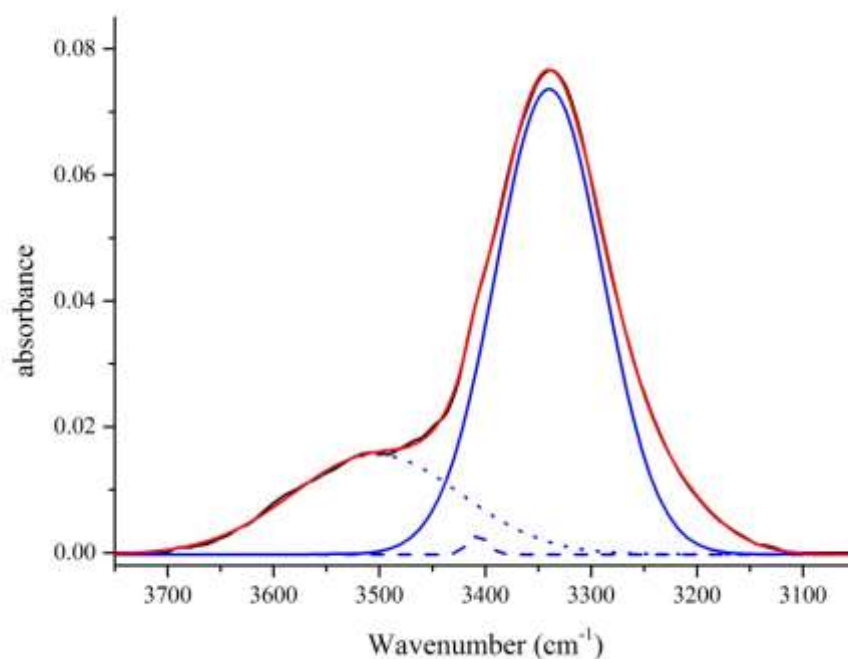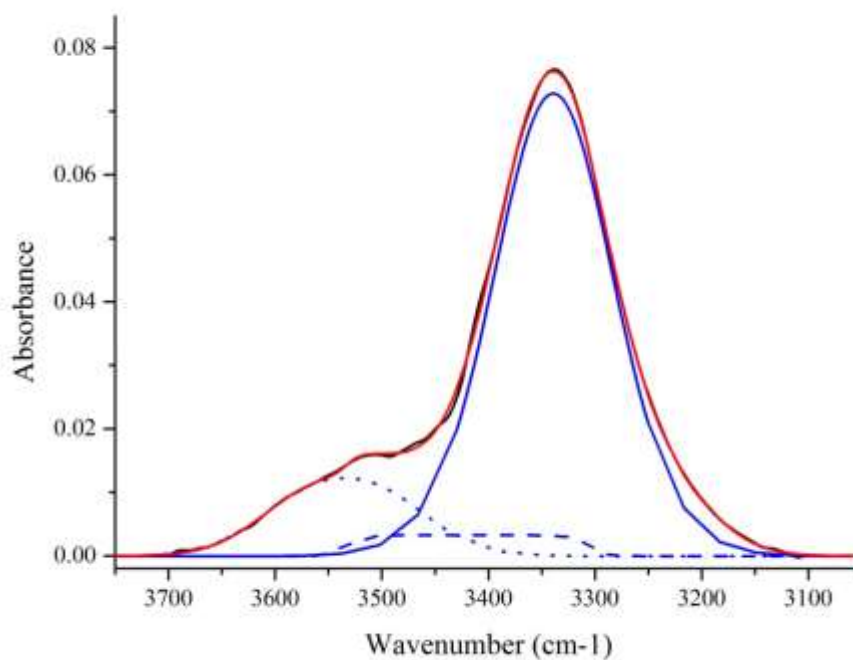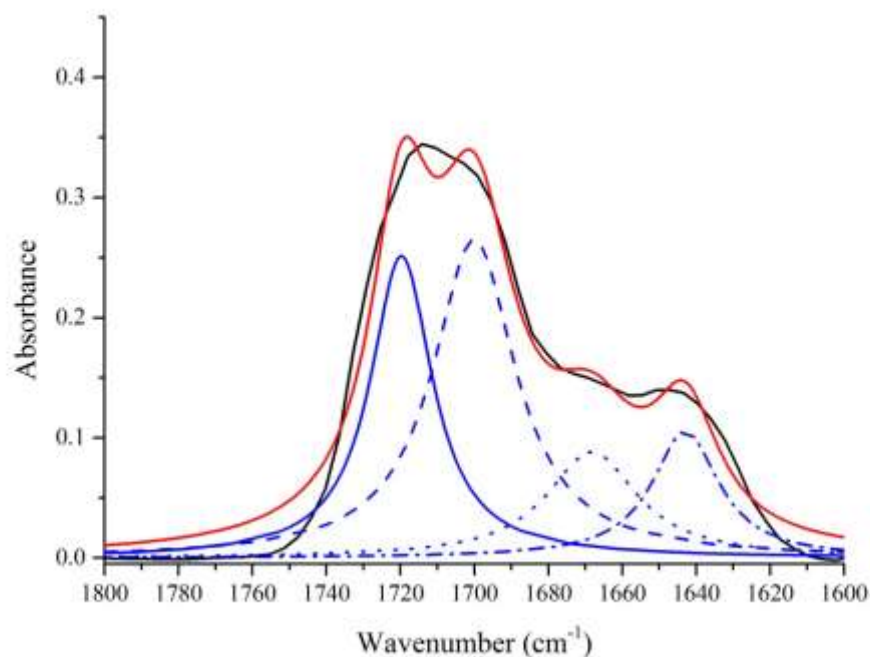| IPDI-TMP-PPG-BD					
Peak Position/cm⁻¹	Standard Error/cm⁻¹	Area	Standard Error	Area/%	Fit R^2 value
3574	7.16	0.369	0.25	2.4	
3514	6.57	1.067	0.41	6.9	
3366	3.52	7.416	1.33	49.0	0.992
3315	2.85	6.709	1.18	48.4	

Gaussian Fit of N-H

Figure B74: Deconvolution data for IPDI-TMP-PPG-BD of N-H region. Data calculated using Gaussian fitting function. [Raw data in black, fit data in red, HS-HS fitted peak solid blue, carbonyl overtone dash blue and free N-H dot blue].

Table B74: Deconvolution data of N-H region collected using Gaussian function of IPDI-TMP-PPG-BD.

IPDI-TMP-PPG-BD					
Peak Position/cm^{-1}	Standard Error/cm^{-1}	Area	Standard Error	Area/%	Fit R^2 value
3503	1.65	3.162	7.3×10^{-2}	22.8	
3407	0.74	7.05×10^{-2}	9.9×10^{-3}	0.5	0.999
3340	0.59	9.381	0.19	76.7	

Gaussian-Lorentzian Fit of N-H

Figure B75: **Deconvolution data for IPDI-TMP-PPG-BD of N-H region. Data calculated using Gaussian-Lorentzian cross fitting function. [Raw data in black, fit data in red, HS-HS fitted peak solid blue, carbonyl overtone dash blue and free N-H dot blue].**

Table B75: **Deconvolution data of N-H region collected using GaussianLorentzian cross function of IPDI-TMP-PPG-BD.**

IPDI-TMP-PPG-BD					
Peak Position/cm^{-1}	Standard Error/cm^{-1}	Area	Standard Error	Area/%	Fit R^2 value
3535	3.31	1.23×10^{-2}	3.3×10^{-4}	13.1	
3419	3.21	3.31×10^{-3}	5.0×10^{-4}	3.5	0.999
3339	0.60	7.29×10^{-2}	5.4×10^{-4}	83.4	

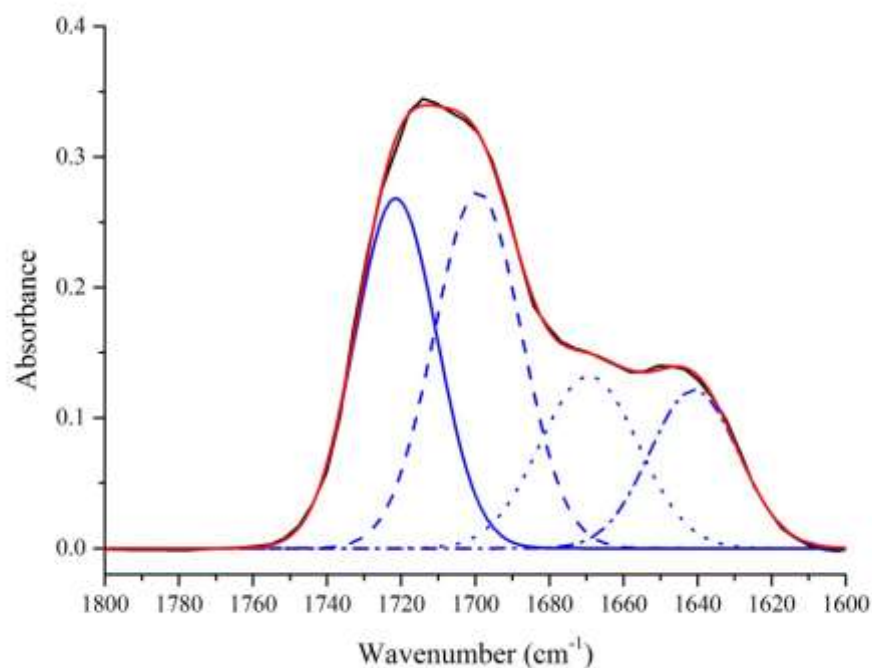## C=O Region Deconvolution

Lorentzian Fit of C=O

Figure B76: Deconvolution data for IPDI-TMP-PPG-BD of C=O region. Data calculated using Lorentzian fitting function. [Raw data in black, fit data in red, free urethane carbonyl peaks solid blue, hydrogen bonded urethane dash blue, free/monodentate hydrogen bonded urea dot blue and bidentate hydrogen bonded urea dot dash blue].

Table B76: Deconvolution data of C=O region collected using Lorentzian function of IPDI-TMP-PPG-BD.

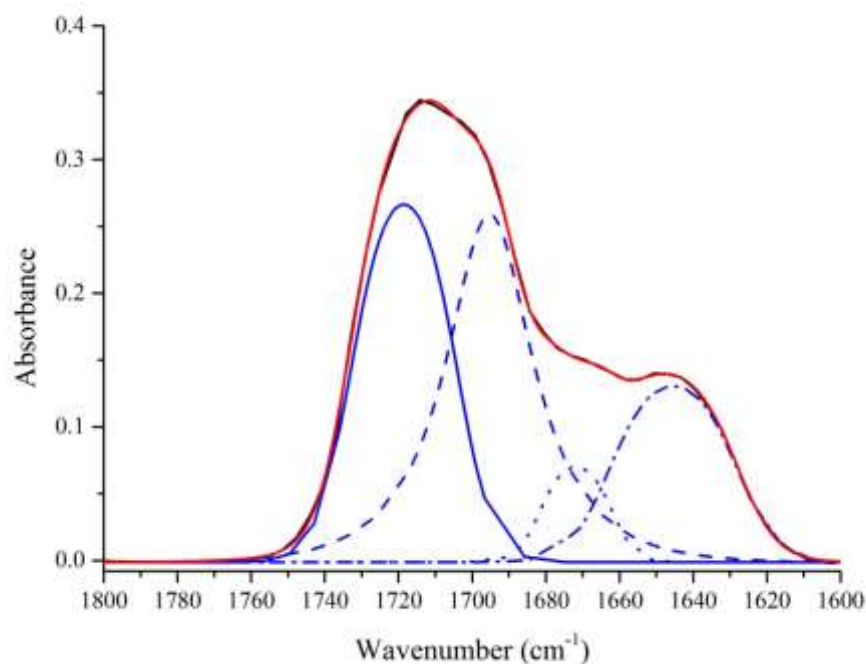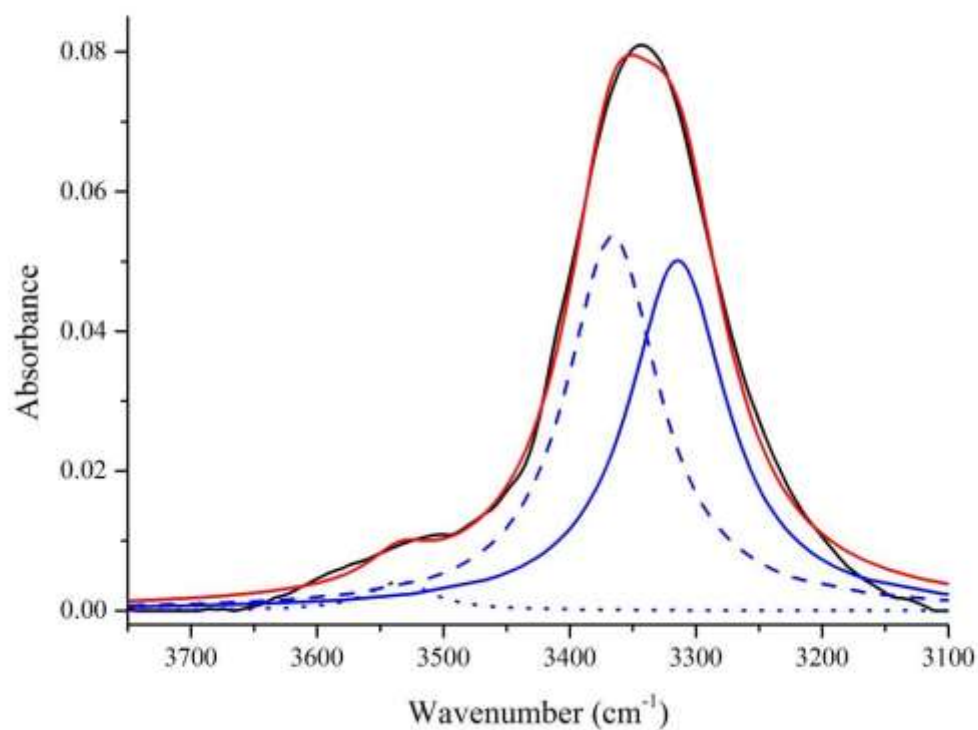| IPDI-TMP-PPG-BD					
Peak Position/cm^{-1}	Standard Error/cm^{-1}	Area	Standard Error	Area/%	Fit R^2 value
1720	1.20	8.019	2.57	29.6	
1700	1.53	11.323	4.49	41.8	0.969
1668	3.72	4.132	3.85	15.2	
1643	2.35	3.637	1.89	13.4	

Gaussian Fit of C=O

Figure B77: Deconvolution data for IPDI-TMP-PPG-BD of C=O region. Data calculated using Gaussian fitting function. [Raw data in black, fit data in red, free urethane carbonyl peaks solid blue, hydrogen bonded urethane dash blue, free/monodentate hydrogen bonded urea dot blue and bidentate hydrogen bonded urea dot dash blue].

Table B77: Deconvolution data of C=O region collected using Gaussian function of IPDI-TMP-PPG-BD.

IPDI-TMP-PPG-BD					
Peak Position/cm^{-1}	Standard Error/cm^{-1}	Area	Standard Error	Area/%	Fit R^2 value
1721	1.40	7.415	1.22	31.6	
1699	0.94	8.033	2.11	34.2	0.999
1669	1.63	4.385	1.67	18.7	
1641	2.04	3.633	0.74	15.5	

Gaussian-Lorentzian Fit of C=O

Figure B78: Deconvolution data for IPDI-TMP-PPG-BD of C=O region. Data calculated using Gaussian-Lorentzian cross fitting function. [Raw data in black, fit data in red, free urethane carbonyl peaks solid blue, hydrogen bonded urethane dash blue, free/monodentate hydrogen bonded urea dot blue and bidentate hydrogen bonded urea dot dash blue].

Table B78: Deconvolution data of C=O region collected using GaussianLorentzian cross function of IPDI-TMP-PPG-BD.

IPDI-TMP-PPG-BD					
Peak Position/cm^{-1}	Standard Error/cm^{-1}	Area	Standard Error	Area/%	Fit R^2 value
1718	1.09	0.268	6.9x10^{-3}	36.6	
1695	1.52	0.261	2.8x10^{-2}	35.7	
1672	1.49	7.11x10^{-2}	9.9x10^{-3}	9.7	0.999
1645	0.78	0.132	3.8x10^{-3}	18.0	

14 - IPDI-TMP-PPG-PD

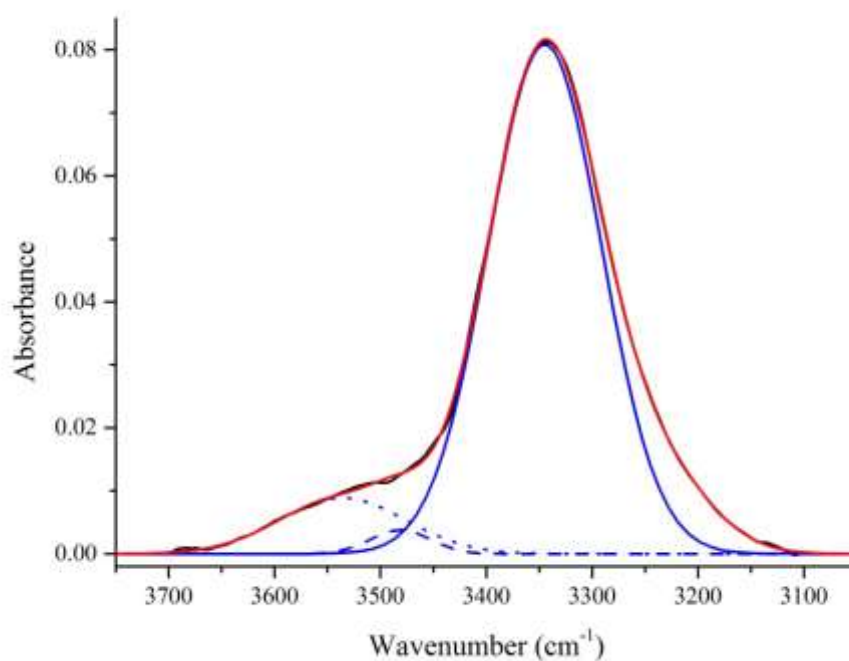**N-H Region Deconvolution**

Lorentzian Fit of N-H

Figure B79: **Deconvolution data for IPDI-TMP-PPG-PD of N-H region. Data calculated using Lorentzian fitting function. [Raw data in black, fit data in red, HS-HS fitted peak solid blue, carbonyl overtone dash blue and free N-H dot blue].**

Table B79: Deconvolution data of N-H region collected using Lorentzian function of IPDI-TMP-PPG-BD.

IPDI-TMP-PPG-PD

Peak Position/cm^{-1}	Standard Error/cm^{-1}	Area	Standard Error	Area/%	Fit R^2 value
3534	5.77	0.401	9.8×10^{-2}	2.6	
3366	2.21	7.546	0.91	49.0	0.994
3314	2.53	7.448	0.89	48.4	

Gaussian Fit of N-H

Figure B80: Deconvolution data for IPDI-TMP-PPG-PD of N-H region. Data calculated using Gaussian fitting function. [Raw data in black, fit data in red, HS-HS fitted peak solid blue, carbonyl overtone dash blue and free N-H dot blue].

Table B80: Deconvolution data of N-H region collected using Gaussian function of IPDI-TMP-PPG-BD.

IPDI-TMP-PPG-PD

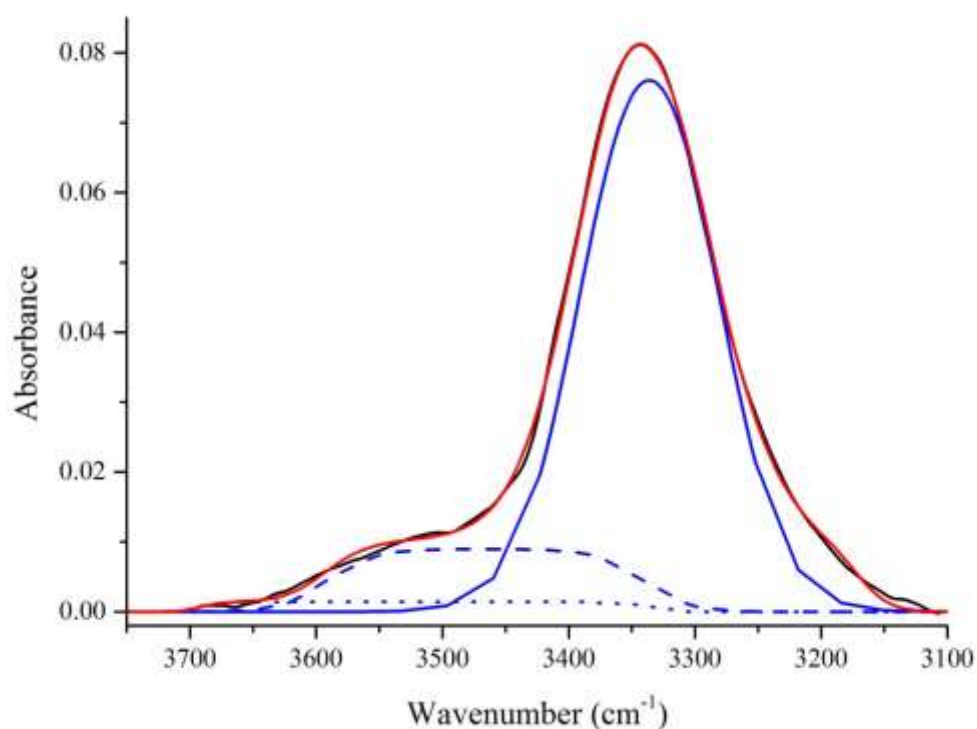| Peak Position/cm⁻¹	Standard Error/cm⁻¹	Area	Standard Error	Area/%	Fit R² value
3536	8.08	1.329	0.16	9.7	
3481	1.68	0.270	0.12	2.0	0.999
3345	0.44	10.821	0.13	88.3	

Gaussian-Lorentzian Fit of N-H

Figure B81: Deconvolution data for IPDI-TMP-PPG-PD of N-H region. Data calculated using Gaussian-Lorentzian cross fitting function. [Raw data in black, fit data in red, HS-HS fitted peak solid blue, carbonyl overtone dash blue and free N-H dot blue].

Table B81: Deconvolution data of N-H region collected using GaussianLorentzian cross function of IPDI-TMP-PPG-PD.

IPDI-TMP-PPG-PD

Peak Position/cm⁻¹	Standard Error/cm⁻¹	Area	Standard Error	Area/%	Fit R^2 value
3515	0.0	8.92×10^{-3}	3.1×10^{-4}	4.6	
3466	0.0	8.97×10^{-3}	3.9×10^{-4}	4.7	0.999
3336	0.0	7.61×10^{-2}	4.4×10^{-4}	90.7	

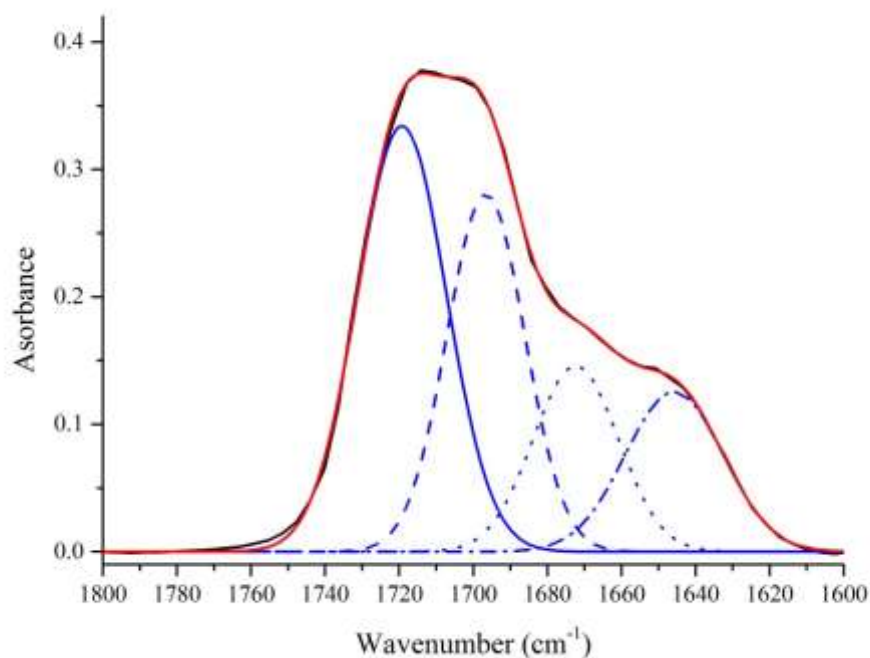## C=O Region Deconvolution

Lorentzian Fit of C=O
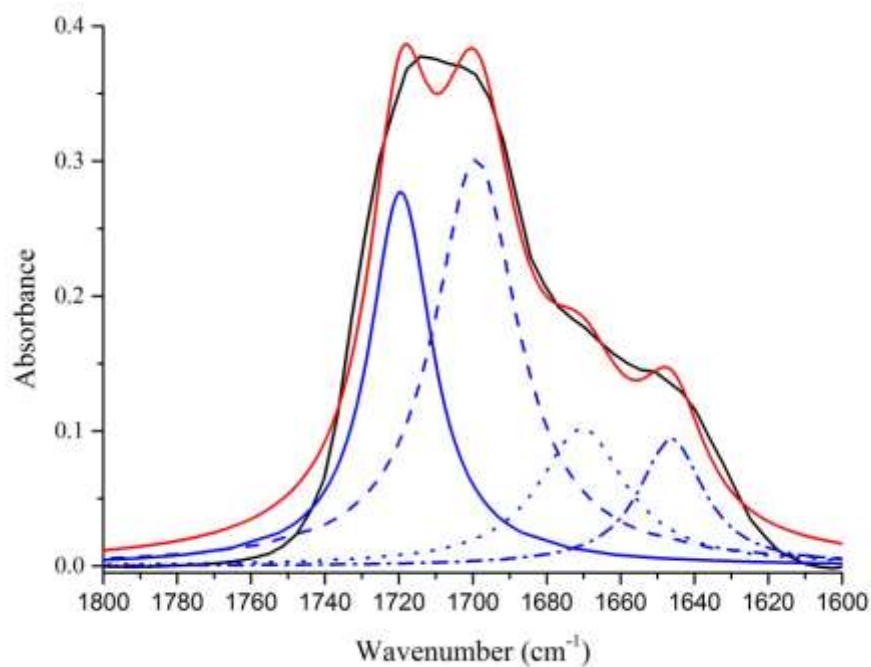
Figure B82: Deconvolution data for IPDI-TMP-PPG-PD of C=O region. Data calculated using Lorentzian fitting function. [Raw data in black, fit data in red, free urethane carbonyl peaks solid blue, hydrogen bonded urethane dash blue, free/monodentate hydrogen bonded urea dot blue and bidentate hydrogen bonded urea dot dash blue].

Table B82: Deconvolution data of C=O region collected using Lorentzian function of IPDI-TMP-PPG-PD.

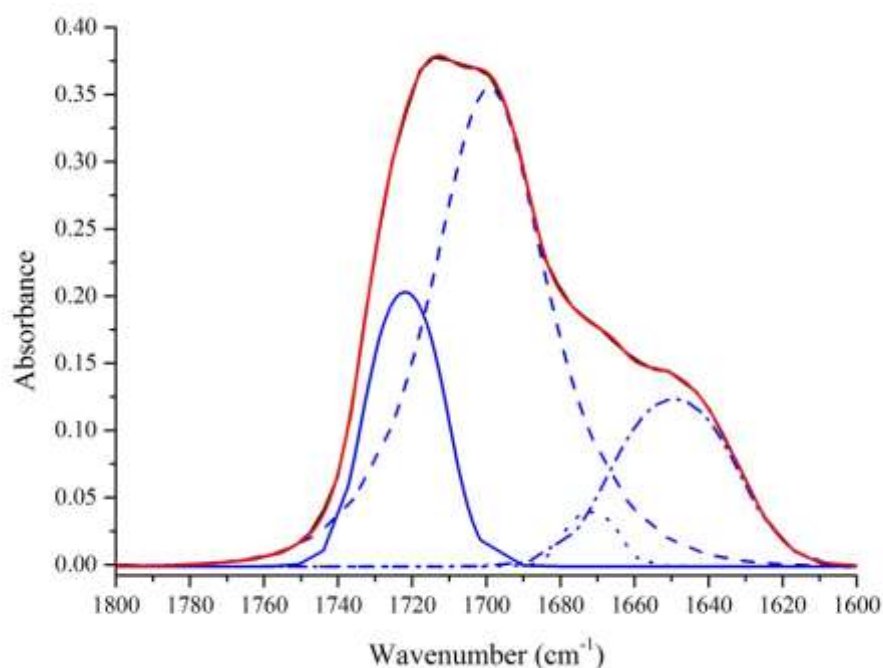|		**IPDI-TMP-PPG-PD**			
Peak Position/cm^{-1}	**Standard Error/cm^{-1}**	**Area**	**Standard Error**	**Area/%**	**Fit R^2 value**
1719	1.11	8.975	2.67	30.0	
1699	1.33	13.041	5.18	43.6	0.975
1670	3.46	4.618	4.57	15.8	
1646	2.77	3.185	2.06	10.6	

Gaussian Fit of C=O

Figure B83: Deconvolution data for IPDI-TMP-PPG-PD of C=O region. Data calculated using Gaussian fitting function. [Raw data in black, fit data in red, free urethane carbonyl peaks solid blue, hydrogen bonded urethane dash blue, free/monodentate hydrogen bonded urea dot blue and bidentate hydrogen bonded urea dot dash blue].

Table B83: Deconvolution data of C=O region collected using Gaussian function of IPDI-TMP-PPG-PD.

IPDI-TMP-PPG-PD					
Peak Position/cm^{-1}	Standard Error/cm^{-1}	Area	Standard Error	Area/%	Fit R^2 value
1719	0.91	28.281	0.92	38.9	
1697	0.75	7.394	1.62	28.6	0.999
1672	1.64	4.211	1.55	16.3	
1646	2.21	4.158	0.69	16.1	

Gaussian-Lorentzian Fit of C=O

Figure B84: Deconvolution data for IPDI-TMP-PPG-PD of C=O region. Data calculated using Gaussian-Lorentzian cross fitting function. [Raw data in black, fit data in red, free urethane carbonyl peaks solid blue, hydrogen bonded urethane dash blue, free/monodentate hydrogen bonded urea dot blue and bidentate hydrogen bonded urea dot dash blue].

Table B84: Deconvolution data of C=O region collected using GaussianLorentzian cross function of IPDI-TMP-PPG-PD.

IPDI-TMP-PPG-PD					
Peak Position/cm^{-1}	Standard Error/cm^{-1}	Area	Standard Error	Area/%	Fit R^2 value
1722	0.50	0.204	7.7×10^{-3}	28.2	
1699	0.67	0.356	8.7×10^{-3}	49.1	
1672	0.96	0.040	4.5×10^{-3}	5.5	0.999
1649	0.65	0.124	3.0×10^{-3}	17.2	

15 - IPDI-TMP-PCD

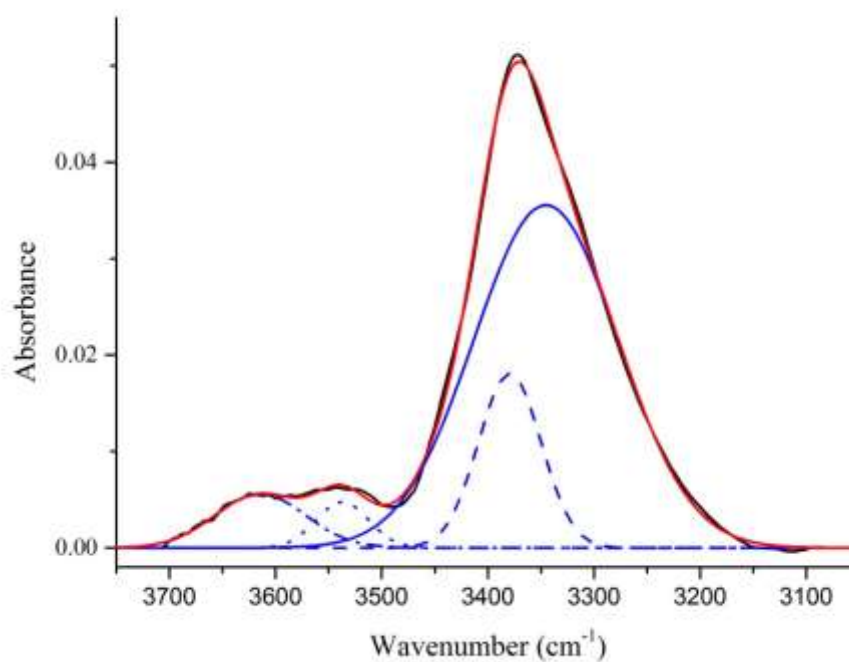## N-H Region Deconvolution

Lorentzian Fit of N-H
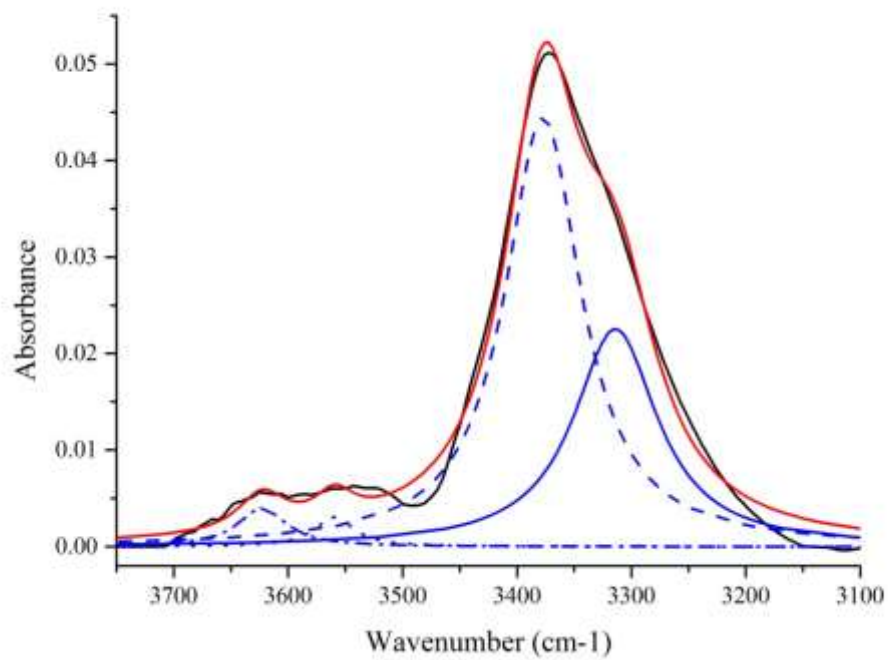
Figure B85: Deconvolution data for IPDI-TMP-PCD of N-H region. Data calculated using Lorentzian fitting function. [Raw data in black, fit data in red, HS-HS fitted peak solid blue, carbonyl overtone dash blue and free N-H dot blue].

Table B85

: Deconvolution data of N-H region collected using Lorentzian function of IPDI-TMP-PCD.

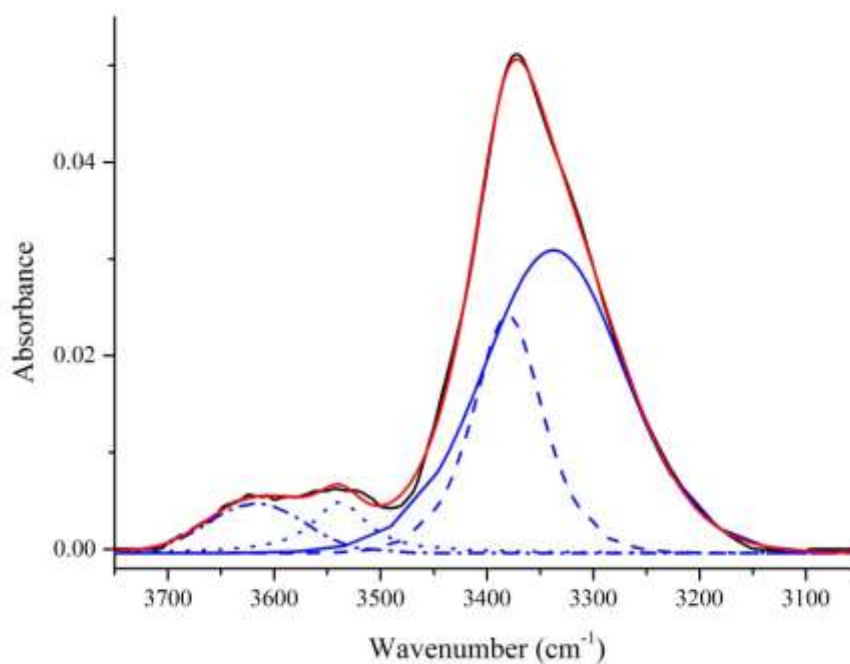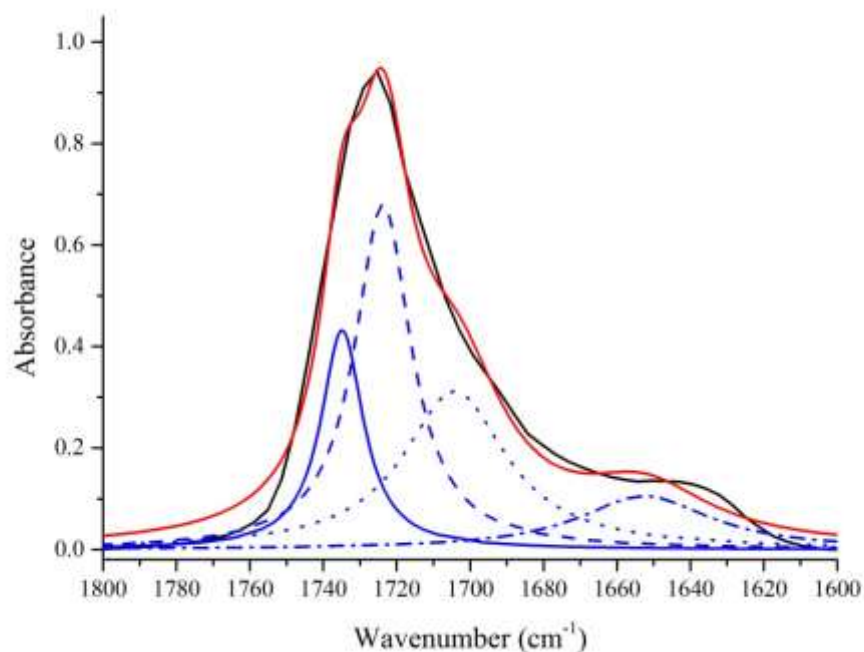| IPDI-TMP-PCD					
Peak Position/cm^{-1}	Standard Error/cm^{-1}	Area	Standard Error	Area/%	Fit R^2 value
3623	4.99	0.324	9.0×10^{-2}	3.5	
3559	5.60	0.201	8.6×10^{-2}	2.2	0.990
3377	1.10	5.666	0.33	60.6	
3314	2.48	3.161	0.33	33.8	

Gaussian Fit of N-H

Figure B86: Deconvolution data for IPDI-TMP-PCD of N-H region. Data calculated using Gaussian fitting function. [Raw data in black, fit data in red, HS-HS fitted peak solid blue, carbonyl overtone dash blue and free N-H dot blue].

Table B86

: Deconvolution data of N-H region collected using Gaussian function of IPDI-TMP-PCD.

Peak Position/cm^{-1}	Standard Error/cm^{-1}	Area	Standard Error	Area/%	Fit R^2 value
3614	3.54	0.598	4.3×10^{-2}		
			4.2×10^{-2}	10.8	
3537	2.08	0.297	5.7×10^{-2}		
3379	0.45	1.339		16.1	0.999
3345	0.59	6.075	6.2×10^{-2}	73.1	

Gaussian-Lorentzian Fit of N-H

Figure B87:   Deconvolution data for IPDI-TMP-PCD of N-H region.   Data calculated using Gaussian-Lorentzian cross fitting function. [Raw data in black,

Table B87
fit data in red, HS-HS fitted peak solid blue, carbonyl overtone dash blue and free N-H dot blue].

: **Deconvolution data of N-H region collected using GaussianLorentzian cross function of IPDI-TMP-PCD.**

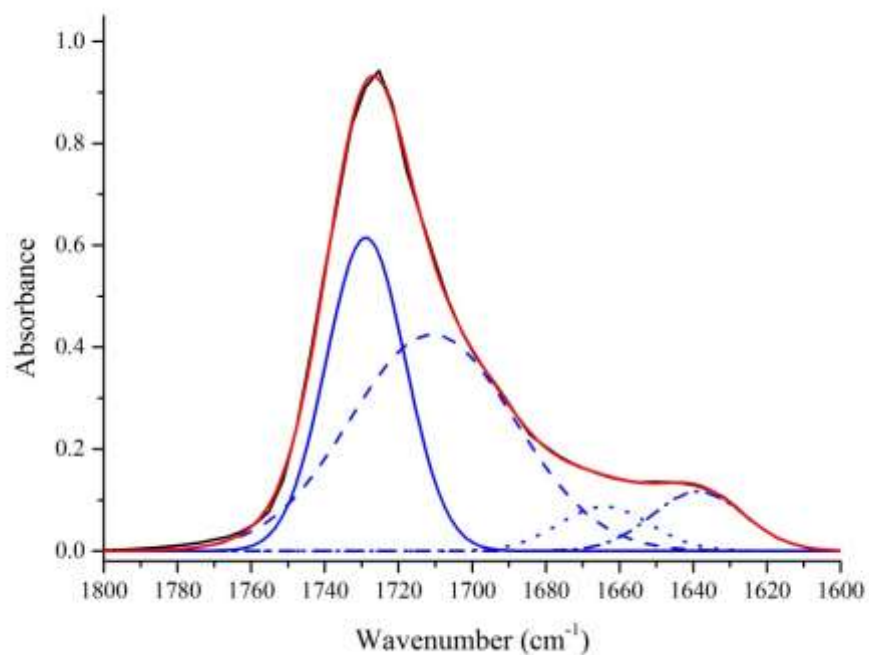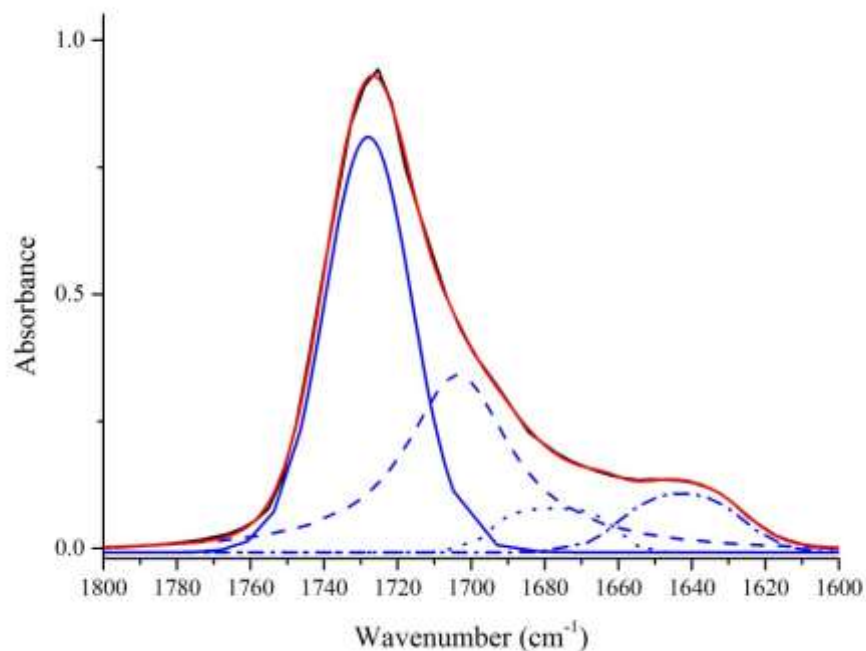|	IPDI-TMP-PCD				
Peak Position/cm^{-1}	**Standard Error/cm^{-1}**	**Area**	**Standard Error**	**Area/%**	**Fit R^2 value**
3617	5.25	5.1×10^{-3}	2.4×10^{-4}		
		5.25×01^{-3}	3.3×10^{-4}	15.6	
3538	3.50	2.46×10^{-2}	2.0×10^{-2}		
3380	0.82			37.1	0.999
3337	27.011	3.13×10^{-2}	1.7×10^{-2}	47.3	

C=O Region Deconvolution

Lorentzian Fit of C=O

Figure B88: Deconvolution data for IPDI-TMP-PCD of C=O region. Data calculated using Lorentzian fitting function. [Raw data in black, fit data in red, free urethane carbonyl peaks solid blue, hydrogen bonded urethane dash blue, free/monodentate hydrogen bonded urea dot blue and bidentate hydrogen bonded urea dot dash blue].

Table B88: Deconvolution data of C=O region collected using Lorentzian function of IPDI-TMP-PCD.

IPDI-TMP-PCD					
Peak Position/cm^{-1}	Standard Error/cm^{-1}	Area	Standard Error	Area/%	Fit R^2 value
1735	1.35	9.543	5.86	17.9	
1724	1.24	19.915	11.55	37.3	0.985
1704	4.10	16.703	8.61	31.3	

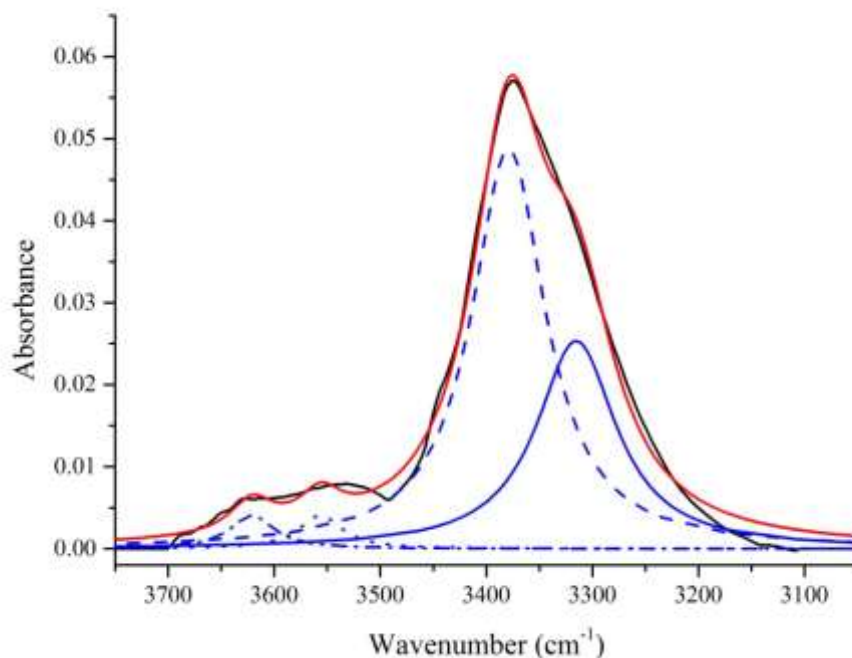| 1652 | 4.45 | 7.264 | 2.61 | 13.6 |

Gaussian Fit of C=O

Figure B89: **Deconvolution data for IPDI-TMP-PCD of C=O region. Data calculated using Gaussian fitting function. [Raw data in black, fit data in red, free urethane carbonyl peaks solid blue, hydrogen bonded urethane dash blue, free/monodentate hydrogen bonded urea dot blue and bidentate hydrogen bonded urea dot dash blue].**

Table B89: Deconvolution data of C=O region collected using Gaussian function of IPDI-TMP-PCD.

IPDI-TMP-PCD					
Peak Position/cm^{-1}	Standard Error/cm^{-1}	Area	Standard Error	Area/%	Fit R^2 value
1729	0.20	16.594	1.10	33.5	
1711	1.69	23.775	0.70	50.9	0.999
1664	4.54	2.708	1.84	5.8	
1639	4.17	3.642	1.32	7.8	

Gaussian-Lorentzian Fit of C=O

Figure B90: **Deconvolution data for IPDI-TMP-PCD of C=O region. Data calculated using Gaussian-Lorentzian cross fitting function. [Raw data in black, fit data in red, free urethane carbonyl peaks solid blue, hydrogen bonded urethane dash blue, free/monodentate hydrogen bonded urea dot blue and bidentate hydrogen bonded urea dot dash blue].**

Table B90: **Deconvolution data of C=O region collected using GaussianLorentzian cross function of IPDI-TMP-PCD.**

IPDI-TMP-PCD					
Peak Position/cm^{-1}	Standard Error/cm^{-1}	Area	Standard Error	Area/%	Fit R^2 value
1728	0.69	0.817	2.3×10^{-2}	59.7	
1704	3.93	0.349	-	25.5	
1678	6.47	8.64×10^{-2}	3.2×10^{-2}	6.3	0.999
1643	2.43	0.116	9.6×10^{-3}	8.5	

16 - IPDI-TMP-PCD-DEPD

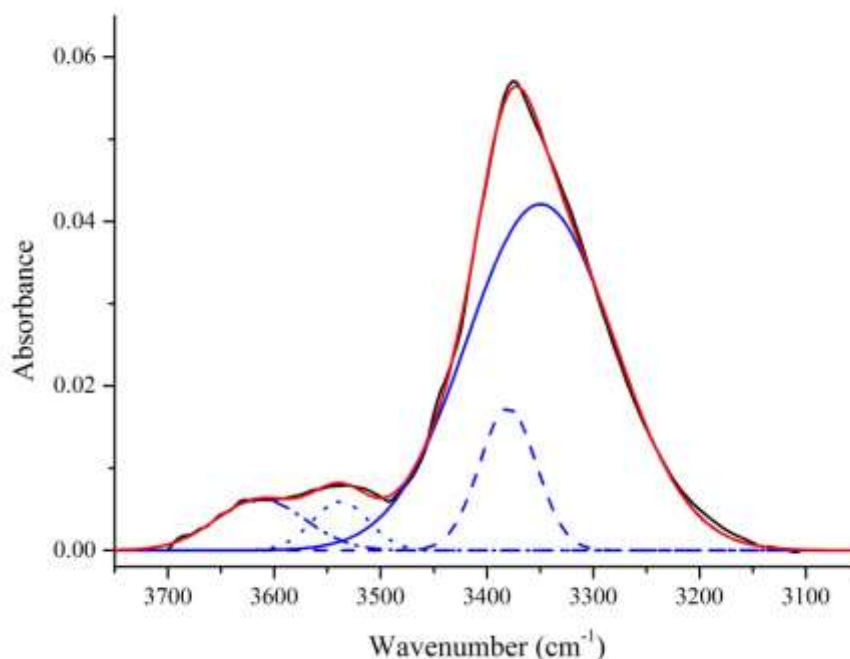## N-H Region Deconvolution

Lorentzian Fit of N-H

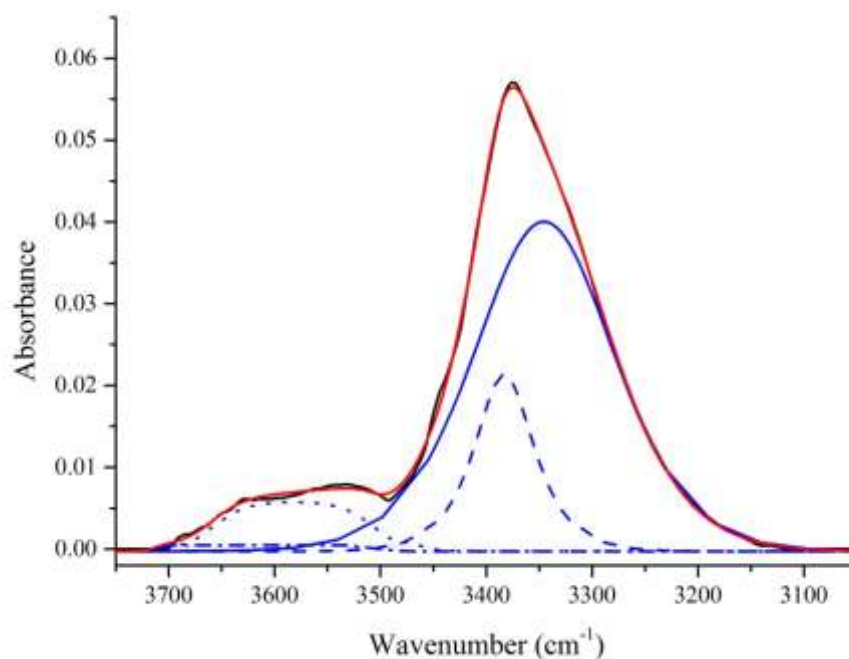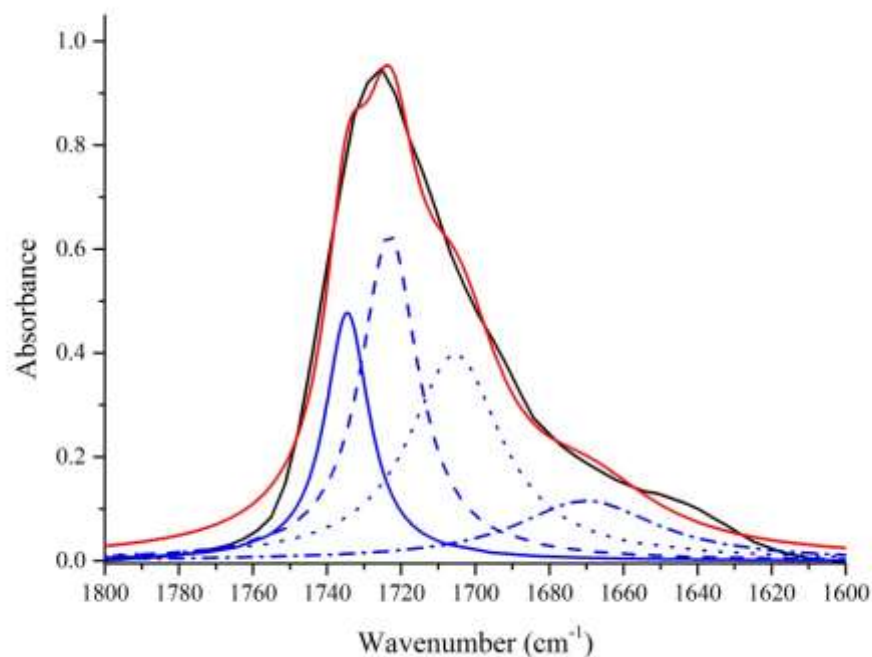**Figure B91: Deconvolution data for IPDI-TMP-PCD-DEPD of N-H region. Data calculated using Lorentzian fitting function. [Raw data in black, fit data in red, HS-HS fitted peak solid blue, carbonyl overtone dash blue and free N-H dot blue].**

Table B91: Deconvolution data of N-H region collected using Lorentzian function of IPDI-TMP-PCD-DEPD.

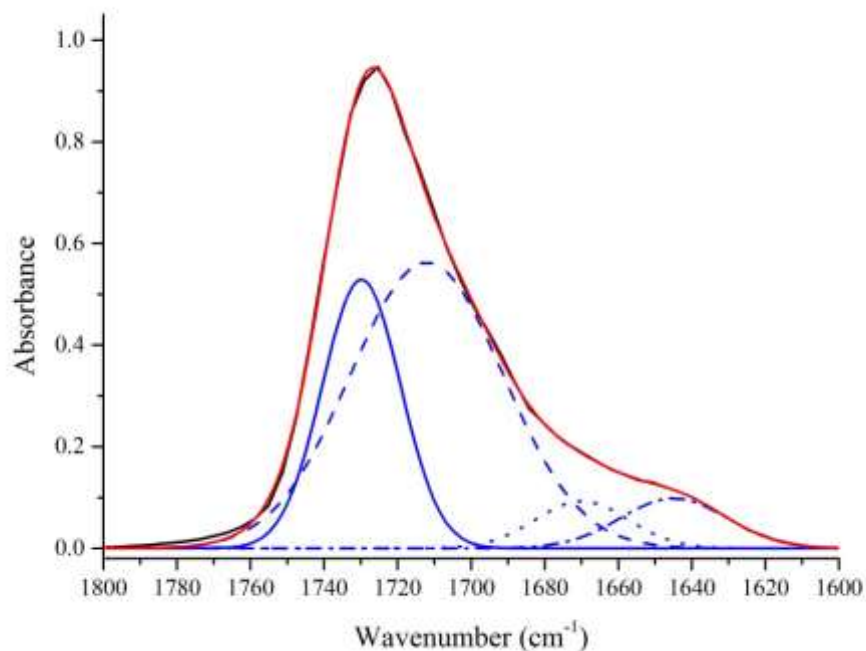| IPDI-TMP-PCD-DEPD					
Peak Position/cm^{-1}	Standard Error/cm^{-1}	Area	Standard Error	Area/%	Fit R^2 value
3621	4.66	0.322	9.1×10^{-2}	3.0	
3556	4.63	0.318	9.7×10^{-2}	3.0	0.993
3379	1.03	6.469	0.34	60.2	
3315	2.22	3.636	0.34	33.8	

Gaussian Fit of N-H

Figure B92: Deconvolution data for IPDI-TMP-PCD-DEPD of N-H region. Data calculated using Gaussian fitting function. [Raw data in black, fit data in red, HS-HS fitted peak solid blue, carbonyl overtone dash blue and free N-H dot blue].

Table B92: Deconvolution data of N-H region collected using Gaussian function of IPDI-TMP-PCD-DEPD.

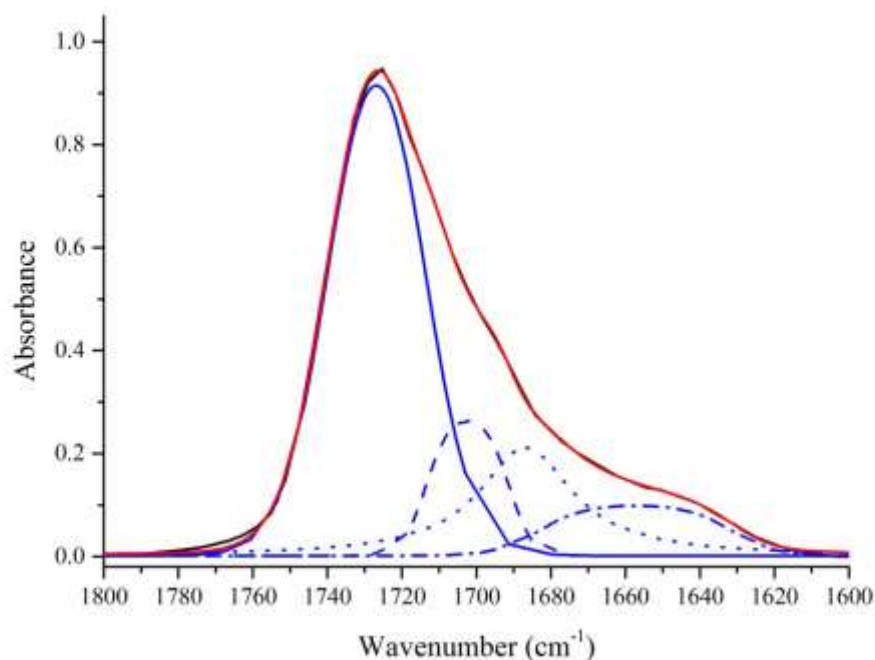| IPDI-TMP-PCD-DEPD					
Peak Position/cm^{-1}	Standard Error/cm^{-1}	Area	Standard Error	Area/%	Fit R^2 value
3613	4.16	0.652	5.7x10^{-2}		
			5.7x10^{-2}	18.3	
3537	2.29	0.393	4.7x10^{-2}		
3380	0.44	1.158		15.9	0.999
3350	0.44	7.324	5.3x10^{-2}	65.8	

Gaussian-Lorentzian Fit of N-H

Figure B93: Deconvolution data for IPDI-TMP-PCD-DEPD of N-H region. Data calculated using Gaussian-Lorentzian cross fitting function. [Raw data in black, fit data in red, HS-HS fitted peak solid blue, carbonyl overtone dash blue and free N-H dot blue].

Table B93: Deconvolution data of N-H region collected using GaussianLorentzian cross function of IPDI-TMP-PCD-DEPD.

IPDI-TMP-PCD-DEPD					
Peak Position/cm^{-1}	Standard Error/cm^{-1}	Area	Standard Error	Area/%	Fit R^2 value
3609	$1.1x01^{-4}$	$7.62x10^{-4}$	$3.4x10^{-4}$		
		$6.02x10^{-3}$	$3.7x10^{-4}$	9.9	
3582	4.44	$2.16x10^{-2}$	$1.7x10^{-2}$		
3383	0.87			31.4	0.999
3345	15.92	$4.03x10^{-2}$	$1.5x10^{-2}$	58.7	

C=O Region Deconvolution

Lorentzian Fit of C=O

Figure B94: Deconvolution data for IPDI-TMP-PCD-DEPD of C=O region. Data calculated using Lorentzian fitting function. [Raw data in black, fit data in red, free urethane carbonyl peaks solid blue, hydrogen bonded urethane dash blue, free/monodentate hydrogen bonded urea dot blue and bidentate hydrogen bonded urea dot dash blue].

Table B94: Deconvolution data of C=O region collected using Lorentzian function of IPDI-TMP-PCD-DEPD.

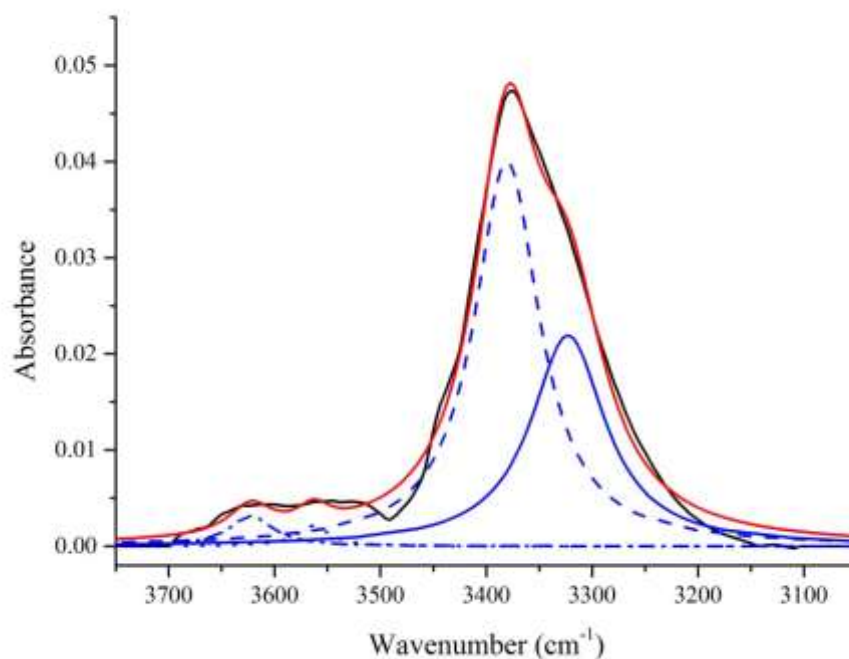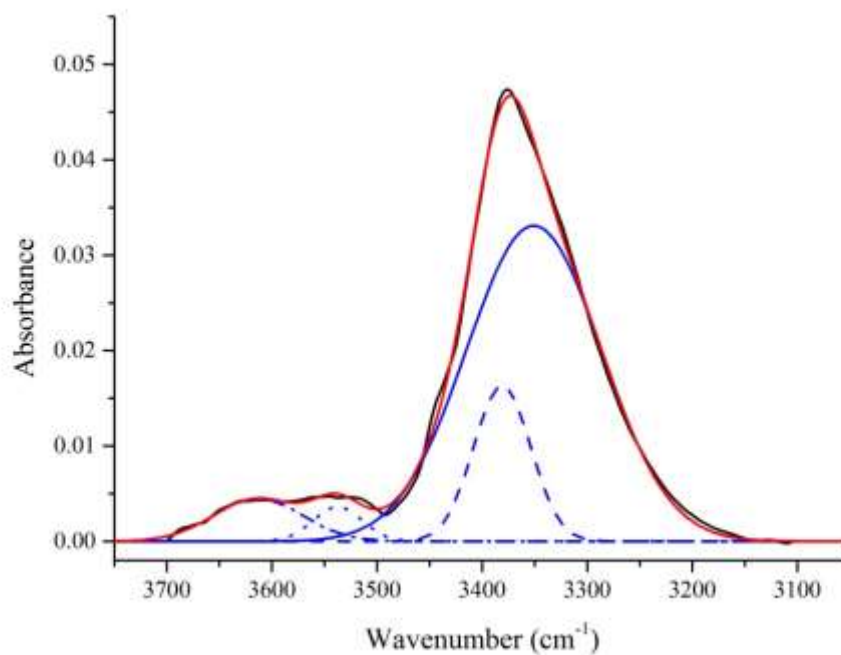| IPDI-TMP-PCD-DEPD					
Peak Position/cm^{-1}	Standard Error/cm^{-1}	Area	Standard Error	Area/%	Fit R^2 value
1734	1.36	10.874	6.56	19.1	
1723	1.35	18.474	8.13	32.5	0.987
1705	3.60	19.034	13.18	33.5	
1670	7.82	8.508	5.27	15.0	

Gaussian Fit of C=O

Figure B95: Deconvolution data for IPDI-TMP-PCD-DEPD of C=O region. Data calculated using Gaussian fitting function. [Raw data in black, fit data in red, free urethane carbonyl peaks solid blue, hydrogen bonded urethane dash blue, free/monodentate hydrogen bonded urea dot blue and bidentate hydrogen bonded urea dot dash blue].

Table B95: Deconvolution data of C=O region collected using Gaussian function of IPDI-TMP-PCD-DEPD.

IPDI-TMP-PCD-DEPD					
Peak Position/cm^{-1}	Standard Error/cm^{-1}	Area	Standard Error	Area/%	Fit R^2 value
1730	0.30	14.085	1.45	28.2	
1712	1.85	29.316	0.80	58.7	0.999
1670	5.31	2.951	3.01	5.9	
1645	8.33	3.578	2.19	7.2	

Gaussian-Lorentzian Fit of C=O

Figure B96: Deconvolution data for IPDI-TMP-PCD-DEPD of C=O region. Data calculated using Gaussian-Lorentzian cross fitting function. [Raw data in black, fit data in red, free urethane carbonyl peaks solid blue, hydrogen bonded urethane dash blue, free/monodentate hydrogen bonded urea dot blue and bidentate hydrogen bonded urea dot dash blue].

Table B96: Deconvolution data of C=O region collected using GaussianLorentzian cross function of IPDI-TMP-PCD-DEPD.

IPDI-TMP-PCD-DEPD					
Peak Position/cm^{-1}	Standard Error/cm^{-1}	Area	Standard Error	Area/%	Fit R^2 value
1727	1.49	0.913	1.1×10^{-2}	61.6	
1702	4.36	0.262	7.0×10^{-2}	17.7	0.999
1687	4.35	0.210	-	14.1	
1657	9.22	9.71×10^{-2}	2.2×10^{-2}	6.6	

17 - IPDI-TMP-PCD-BD

N-H Region Deconvolution

Lorentzian Fit of N-H

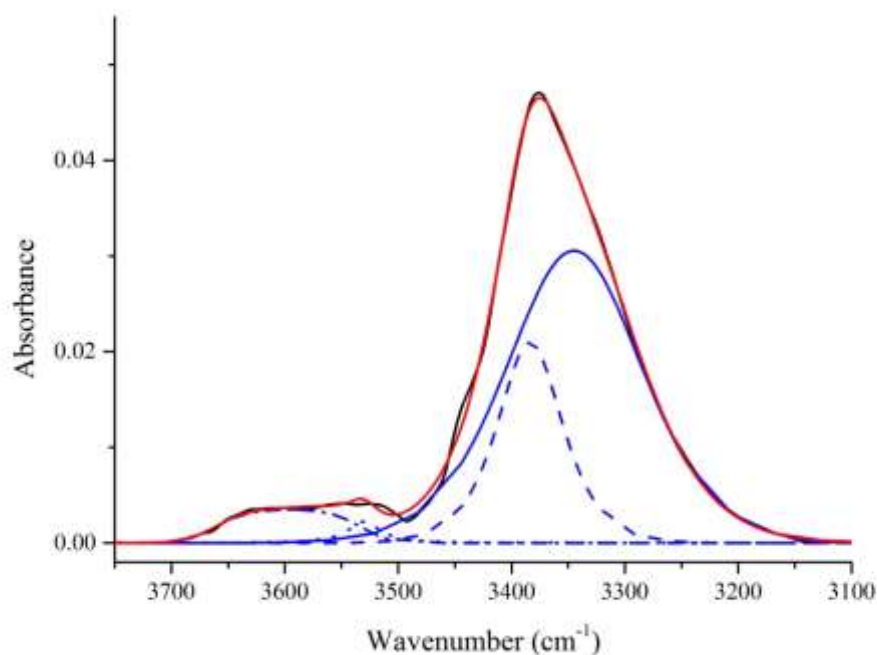**Figure B97: Deconvolution data for IPDI-TMP-PCD-BD of N-H region. Data calculated using Lorentzian fitting function. [Raw data in black, fit data in red, HS-HS fitted peak solid blue, carbonyl overtone dash blue and free N-H dot blue].**

Table B97: Deconvolution data of N-H region collected using Lorentzian function of IPDI-TMP-PCD-BD.

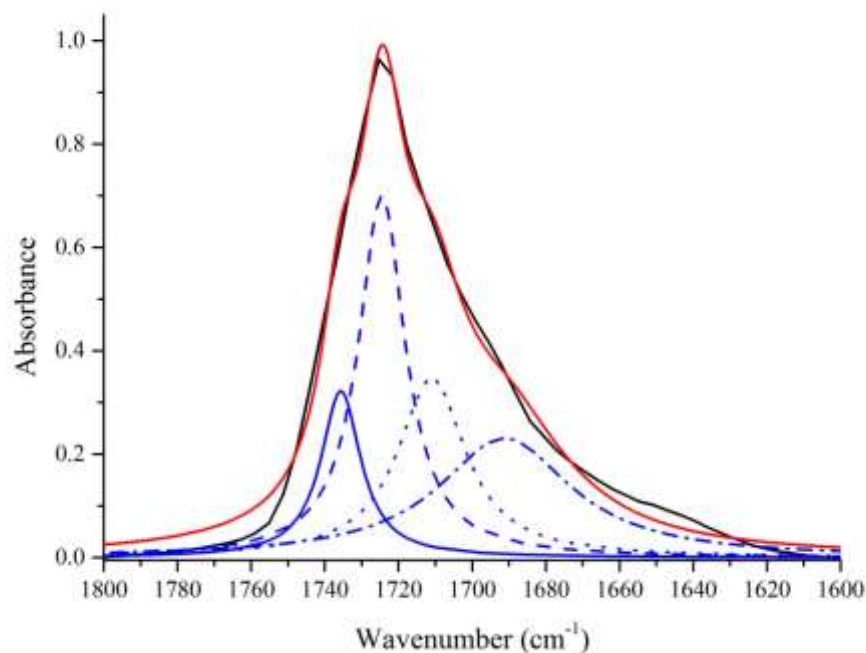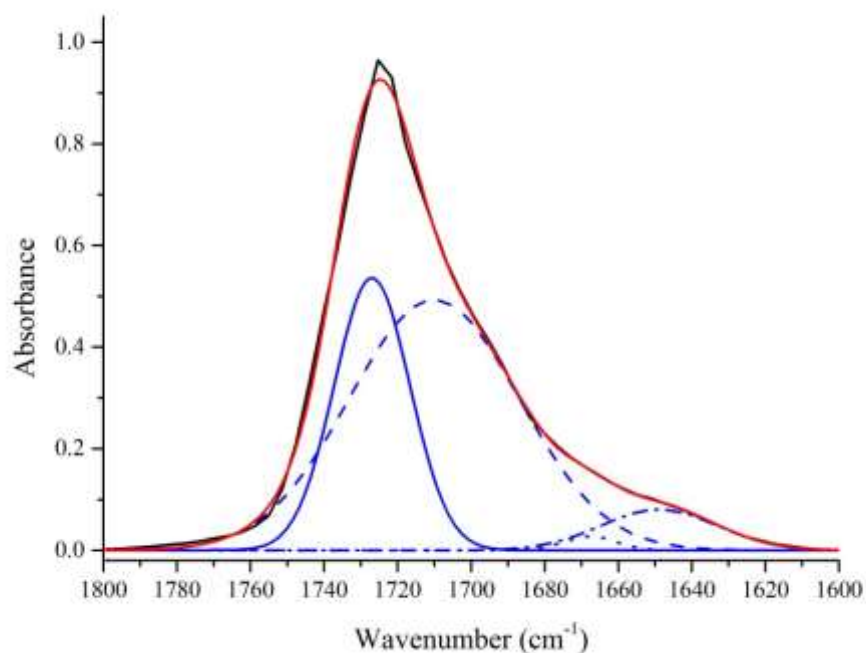| IPDI-TMP-PCD-BD					
Peak Position/cm^{-1}	Standard Error/cm^{-1}	Area	Standard Error	Area/%	Fit R^2 value
3622	5.25	0.248	7.3×10^{-2}	3.1	
3563	6.23	0.125	6.6×10^{-2}	1.6	0.991
3381	1.00	4.703	0.28	58.6	
3323	2.24	2.949	1.2×10^{-3}	36.7	

Gaussian Fit of N-H

Figure B98: Deconvolution data for IPDI-TMP-PCD-BD of N-H region. Data calculated using Gaussian fitting function. [Raw data in black, fit data in red, HS-HS fitted peak solid blue, carbonyl overtone dash blue and free N-H dot blue].

Table B98: Deconvolution data of N-H region collected using Gaussian function of IPDI-TMP-PCD-BD.

		IPDI-TMP-PCD-BD			
Peak Position/cm^{-1}	Standard Error/cm^{-1}	Area	Standard Error	Area/%	Fit R^2 value
3613	4.48	0.478	4.4×10^{-2}		
3537	2.69	0.212	4.1×10^{-2}	9.7	
3381	0.51	1.113	5.7×10^{-2}	15.6	0.998
3351	0.60	5.330	6.1×10^{-2}	74.7	

Gaussian-Lorentzian Fit of N-H

Figure B99: Deconvolution data for IPDI-TMP-PCD-BD of N-H region. Data calculated using Gaussian-Lorentzian cross fitting function. [Raw data in black, fit data in red, HS-HS fitted peak solid blue, carbonyl overtone dash blue and free N-H dot blue].

Table B99: Deconvolution data of N-H region collected using GaussianLorentzian cross function of IPDI-TMP-PCD-BD.

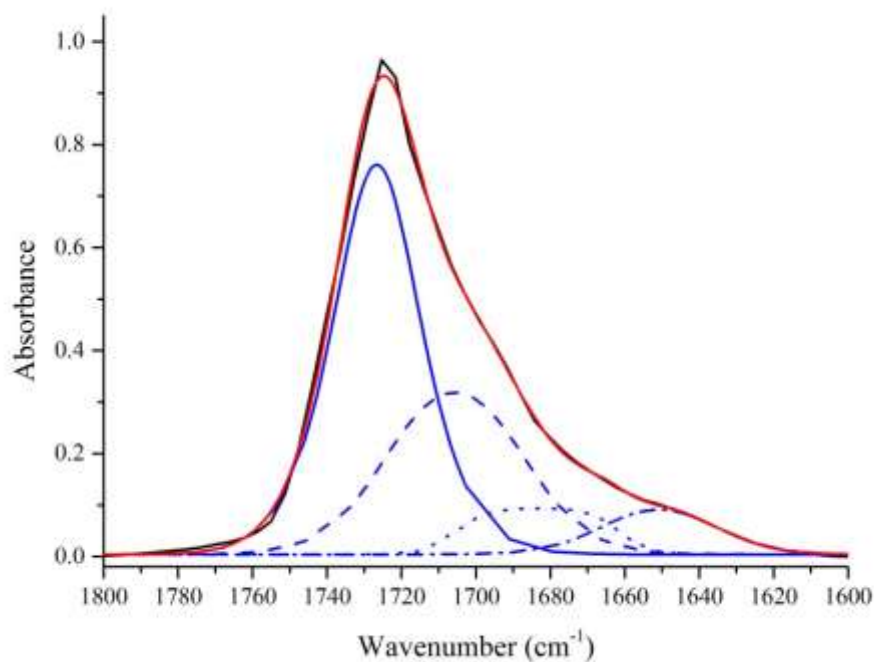| IPDI-TMP-PCD-BD					
Peak Position/cm^{-1}	Standard Error/cm^{-1}	Area	Standard Error	Area/%	Fit R^2 value
3597	18.69	3.49×10^{-3}	2.4×10^{-4}		
		2.24×10^{-3}	-	10.1	
3530	5.67	2.1×10^{-2}	9.4×10^{-3}		
3384	1.04			36.6	0.999
3345	11.68	3.06×10^{-2}	8.4×10^{-3}	53.3	

C=O Region Deconvolution
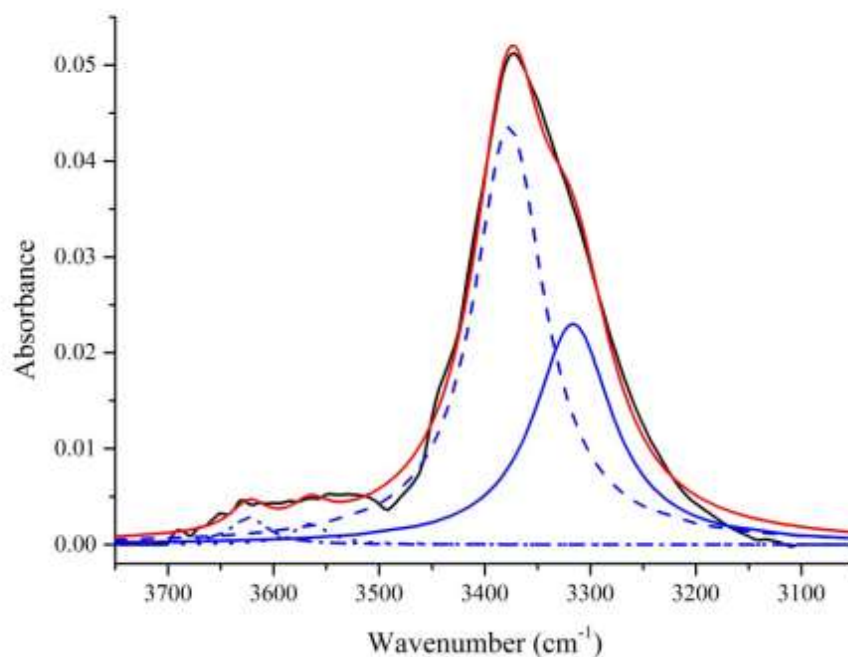
Lorentzian Fit of C=O

Figure B100: Deconvolution data for IPDI-TMP-PCD-BD of C=O region. Data calculated using Lorentzian fitting function. [Raw data in black, fit data in red, free urethane carbonyl peaks solid blue, hydrogen bonded urethane dash blue, free/monodentate hydrogen bonded urea dot blue and bidentate hydrogen bonded urea dot dash blue].

Table B100: Deconvolution data of C=O region collected using Lorentzian function of IPDI-TMP-PCD-BD.

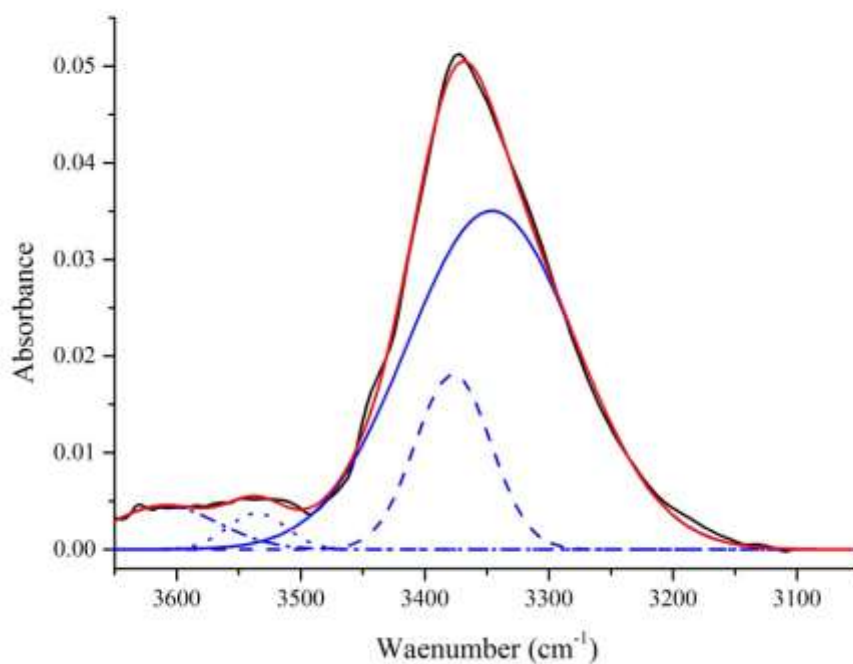| IPDI-TMP-PCD-BD					
Peak Position/cm^{-1}	Standard Error/cm^{-1}	Area	Standard Error	Area/%	Fit R^2 value
1736	1.33	6.667	3.66	12.9	
1724	0.73	16.984	9.62	32.8	0.990
1711	2.68	12.200	13.23	23.6	
1691	6.48	15.844	8.09	30.7	

Gaussian Fit of C=O

Figure B101: Deconvolution data for IPDI-TMP-PCD-BD of C=O region. Data calculated using Gaussian fitting function. [Raw data in black, fit data in red, free urethane carbonyl peaks solid blue, hydrogen bonded urethane dash blue, free/monodentate hydrogen bonded urea dot blue and bidentate hydrogen bonded urea dot dash blue].

Table B101: Deconvolution data of C=O region collected using Gaussian function of IPDI-TMP-PCD-BD.

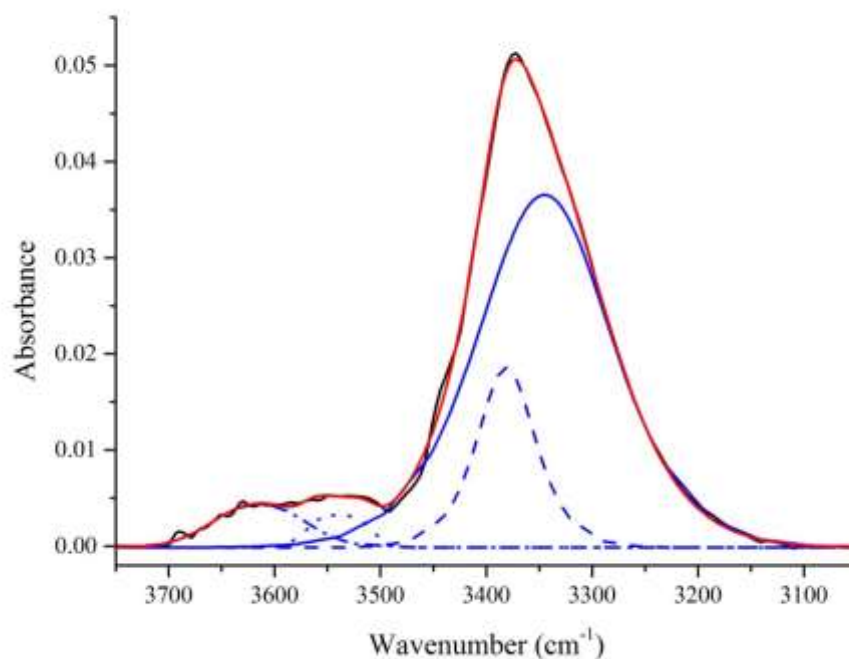| IPDI-TMP-PCD-BD					
Peak Position/cm^{-1}	Standard Error/cm^{-1}	Area	Standard Error	Area/%	Fit R^2 value
1727	0.288	13.833	1.22	30.0	
1710	1.40	28.555	1.00	62.0	0.998
1668	4.13	0.486	1.10	1.4	
1649	9.38	3.177	1.51	6.9	

Gaussian-Lorentzian Fit of C=O

Figure B102: Deconvolution data for IPDI-TMP-PCD-BD of C=O region. Data calculated using Gaussian-Lorentzian cross fitting function. [Raw data in black, fit data in red, free urethane carbonyl peaks solid blue, hydrogen bonded urethane dash blue, free/monodentate hydrogen bonded urea dot blue and bidentate hydrogen bonded urea dot dash blue].

Table B102: Deconvolution data of C=O region collected using GaussianLorentzian cross function of IPDI-TMP-PCD-BD.

IPDI-TMP-PCD-BD					
Peak Position/cm^{-1}	Standard Error/cm^{-1}	Area	Standard Error	Area/%	Fit R^2 value
1727	4.72	0.757	1.422	60.7	
1706	7.49	0.314	1.04	25.2	
1683	4.35	8.92×10^{-2}	0.49	7.1	0.998
1651	4.66	8.73×10^{-2}	0.14	7.0	

18 - IPDI-TMP-PCD-PD

N-H Region Deconvolution
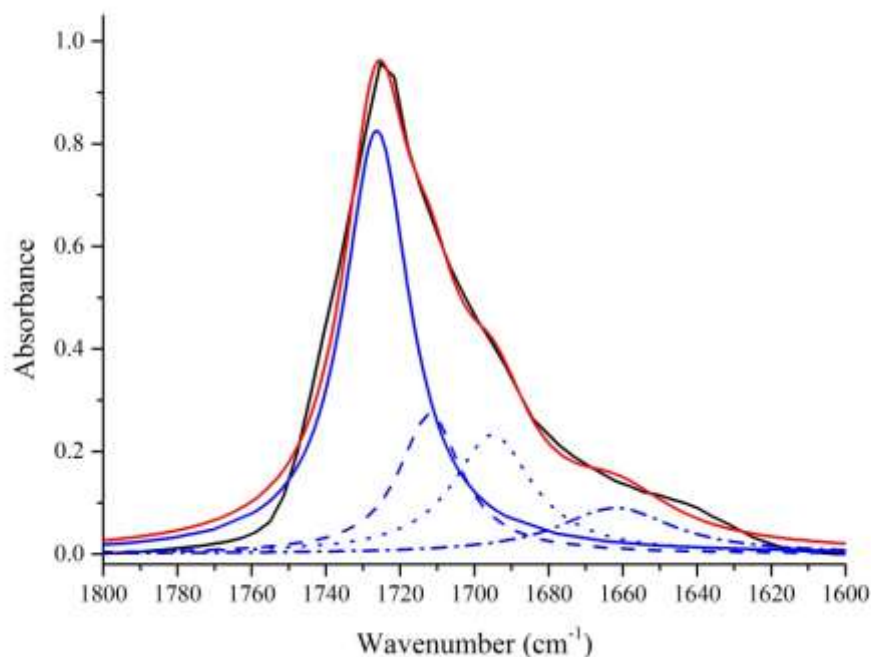
Lorentzian Fit of N-H

Figure B103: Deconvolution data for IPDI-TMP-PCD-PD of N-H region. Data calculated using Lorentzian fitting function. [Raw data in black, fit data in red, HS-HS fitted peak solid blue, carbonyl overtone dash blue and free N-H dot blue].

Table B103: Deconvolution data of N-H region collected using Lorentzian function of IPDI-TMP-PCD-PD.

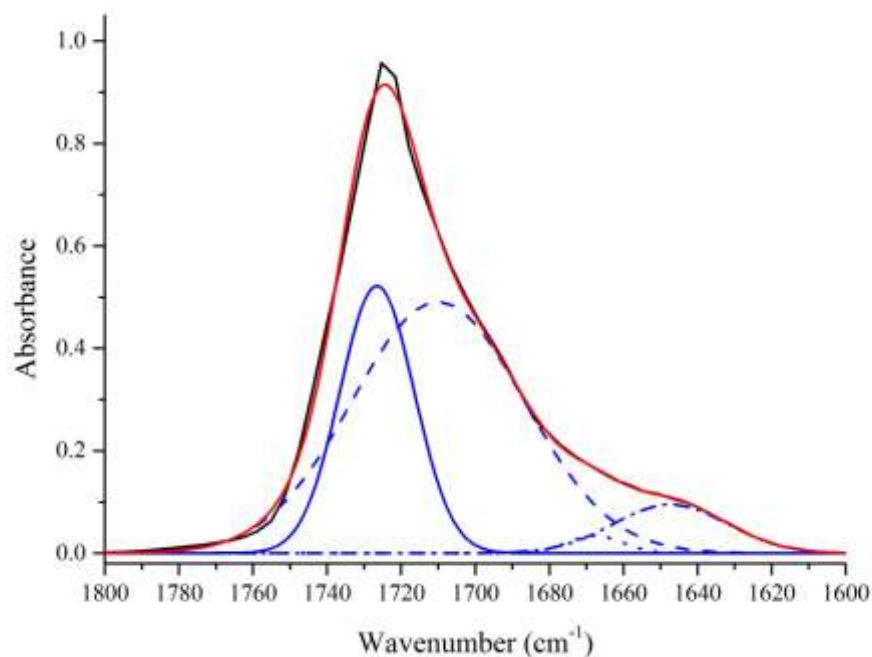| IPDI-TMP-PCD-PD					
Peak Position/cm^{-1}	Standard Error/cm^{-1}	Area	Standard Error	Area/%	Fit R^2 value
3623	5.44	0.193	7.1×10^{-2}	2.1	
3565	6.82	0.140	7.2×10^{-2}	1.5	0.992
3377	1.05	5.560	0.31	60.8	
3316	2.31	3.243	0.32	35.6	

Gaussian Fit of N-H

Figure B104: Deconvolution data for IPDI-TMP-PCD-PD of N-H region. Data calculated using Gaussian fitting function. [Raw data in black, fit data in red, HS-HS fitted peak solid blue, carbonyl overtone dash blue and free N-H dot blue].

Table B104: Deconvolution data of N-H region collected using Gaussian function of IPDI-TMP-PCD-PD.

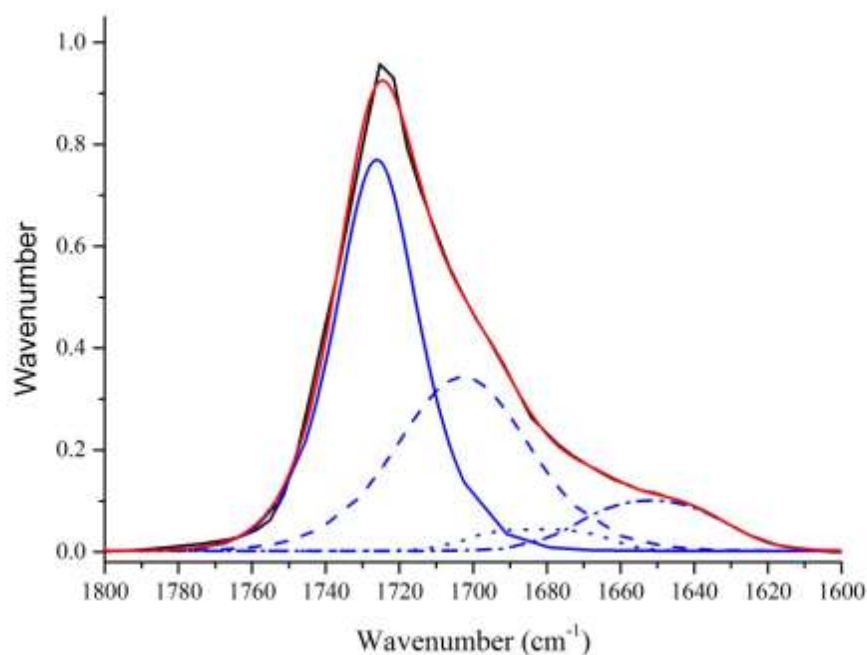| IPDI-TMP-PCD-PD					
Peak Position/cm^{-1}	Standard Error/cm^{-1}	Area	Standard Error	Area/%	Fit R^2 value
3610	5.46	0.495	5.4×10^{-2}		
			5.1×10^{-2}	8.9	
3535	2.85	0.224			
			7.7×10^{-2}		
3377	0.56	1.382		17.1	0.998
3346	0.72	5.982	8.1×10^{-2}	74.0	

Gaussian-Lorentzian Fit of N-H

Figure B105: Deconvolution data for IPDI-TMP-PCD-PD of N-H region. Data calculated using Gaussian-Lorentzian cross fitting function. [Raw data in black, fit data in red, HS-HS fitted peak solid blue, carbonyl overtone dash blue and free N-H dot blue].

Table B105: Deconvolution data of N-H region collected using GaussianLorentzian cross function of IPDI-TMP-PCD-PD.

IPDI-TMP-PCD-PD					
Peak Position/cm^{-1}	Standard Error/cm^{-1}	Area	Standard Error	Area/%	Fit R^2 value
3615	2.82	4.48×10^{-3}	1.9×10^{-4}		
		3.36×10^{-3}	4.0×10^{-4}	12.4	
3539	1.13	1.87×10^{-2}	2.8×10^{-3}		
3381	0.99			29.6	0.999
3345	2.81	3.67×10^{-2}	2.7×10^{-3}	58.0	

C=O Region Deconvolution
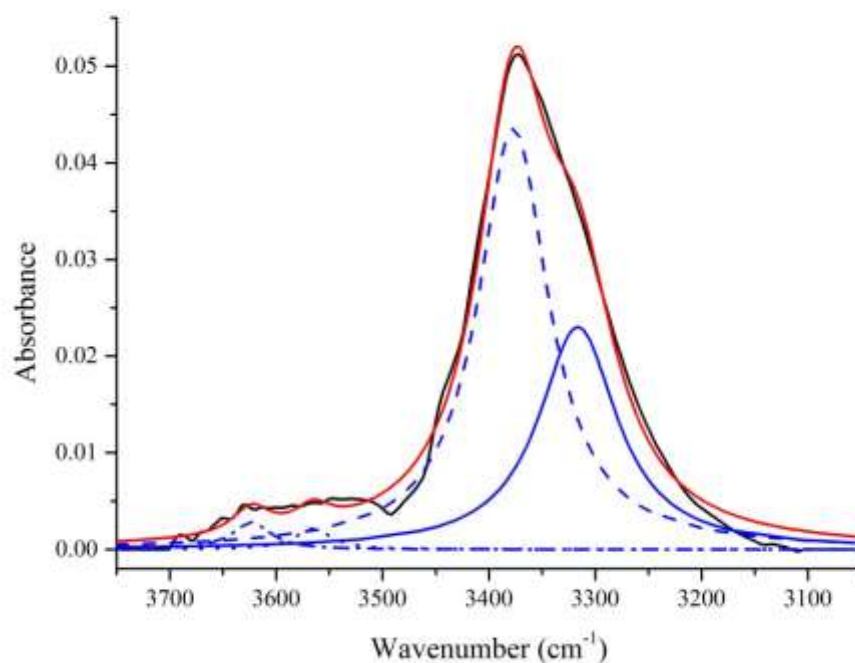
Lorentzian Fit of C=O

Figure B106: Deconvolution data for IPDI-TMP-PCD-PD of C=O region. Data calculated using Lorentzian fitting function. [Raw data in black, fit data in red, free urethane carbonyl peaks solid blue, hydrogen bonded urethane dash blue, free/monodentate hydrogen bonded urea dot blue and bidentate hydrogen bonded urea dot dash blue].

Table B106: Deconvolution data of C=O region collected using Lorentzian function of IPDI-TMP-PCD-PD.

| IPDI-TMP-PCD-PD					
Peak Position/cm^{-1}	Standard Error/cm^{-1}	Area	Standard Error	Area/%	Fit R^2 value
1726	1.20	28.323	7.68	54.4	
1712	2.82	8.769	14.97	16.8	0.985
1695	5.21	9.56	11.14	18.4	
1662	7.27	5.399	3.66	10.4	

Gaussian Fit of C=O

Figure B107: Deconvolution data for IPDI-TMP-PCD-PD of C=O region. Data calculated using Gaussian fitting function. [Raw data in black, fit data in red, free urethane carbonyl peaks solid blue, hydrogen bonded urethane dash blue, free/monodentate hydrogen bonded urea dot blue and bidentate hydrogen bonded urea dot dash blue].

Table B107: Deconvolution data of C=O region collected using Gaussian function of IPDI-TMP-PCD-PD.

IPDI-TMP-PCD-PD					
Peak Position/cm^{-1}	Standard Error/cm^{-1}	Area	Standard Error	Area/%	Fit R^2 value
1726	0.33	13.112	1.32	28.5	
1710	1.48	28.573	1.09	62.2	
1668	4.60	0.642	1.32	1.4	0.997
1647	7.05	3.641	1.48	7.9	

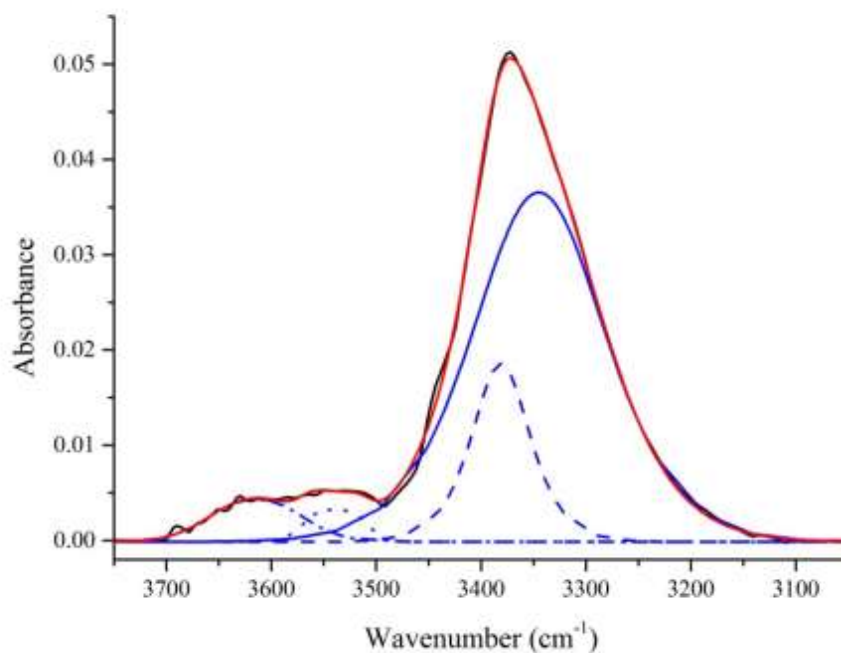*Gaussian-Lorentzian Fit of C=O*

Figure B108: Deconvolution data for IPDI-TMP-PCD-PD of C=O region. Data calculated using Gaussian-Lorentzian cross fitting function. [Raw data in black, fit data in red, free urethane carbonyl peaks solid blue, hydrogen bonded urethane dash blue, free/monodentate hydrogen bonded urea dot blue and bidentate hydrogen bonded urea dot dash blue].

Table B108: Deconvolution data of C=O region collected using GaussianLorentzian cross function of IPDI-TMP-PCD-PD.

IPDI-TMP-PCD-PD					
Peak Position/cm^{-1}	Standard Error/cm^{-1}	Area	Standard Error	Area/%	Fit R^2 value
1726	3.73	0.767	0.83	61.4	
1703	30.57	0.341	0.67	27.3	
1682	29.94	4.21×10^{-2}	0.48	6.1	0.997
1651	53.81	9.86×10^{-2}	0.24	4.1	

19 - IPDI-TMP-PDEGA

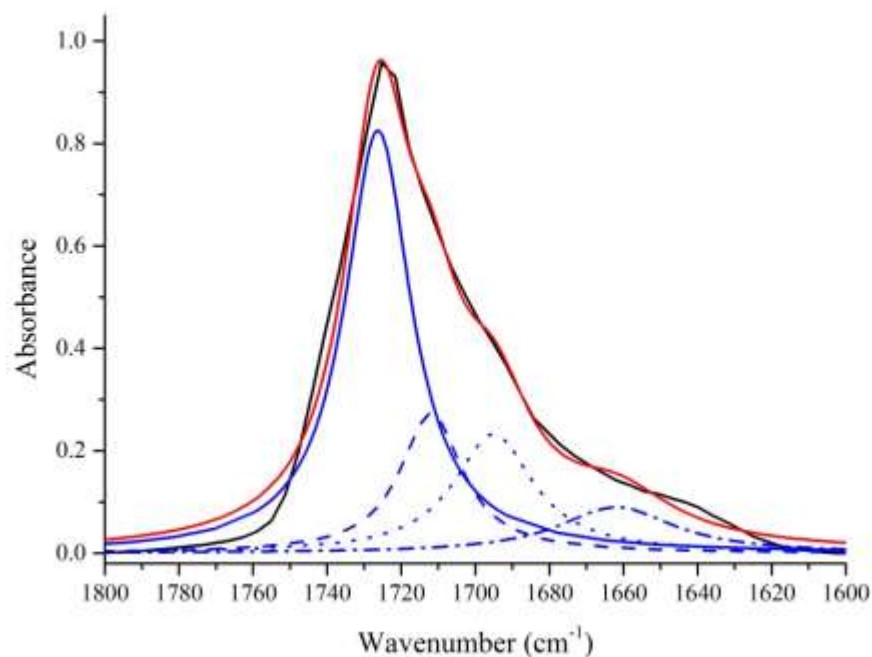## N-H Region Deconvolution

Lorentzian Fit of N-H

Figure B109: Deconvolution data for IPDI-TMP-PDEGA of N-H region. Data calculated using Lorentzian fitting function. [Raw data in black, fit data in red, HS-HS fitted peak solid blue, carbonyl overtone dash blue and free N-H dot blue].

Table B109:   Deconvolution data of N-H region collected using Lorentzian function of IPDI-TMP-PDEGA.

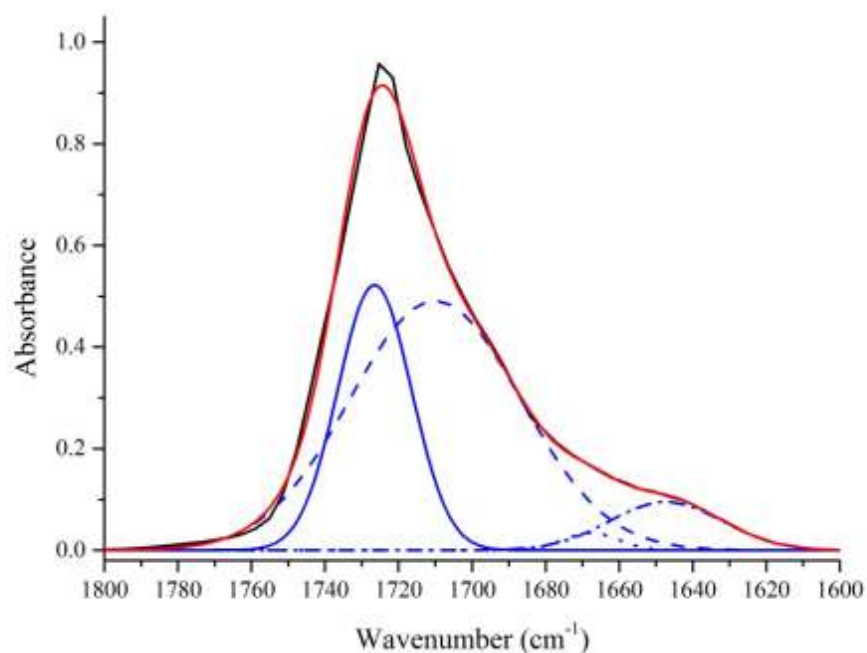| IPDI-TMP-PDEGA					
Peak Position/cm^{-1}	Standard Error/cm^{-1}	Area	Standard Error	Area/%	Fit R^2 value
3621	3.58	0.284	9.4×10^{-2}	2.7	
3541	4.67	0.822	0.19	7.8	
3377	1.89	7.833	0.57	73.9	0.991
3310	3.97	1.635	0.45	15.6	

Gaussian Fit of N-H
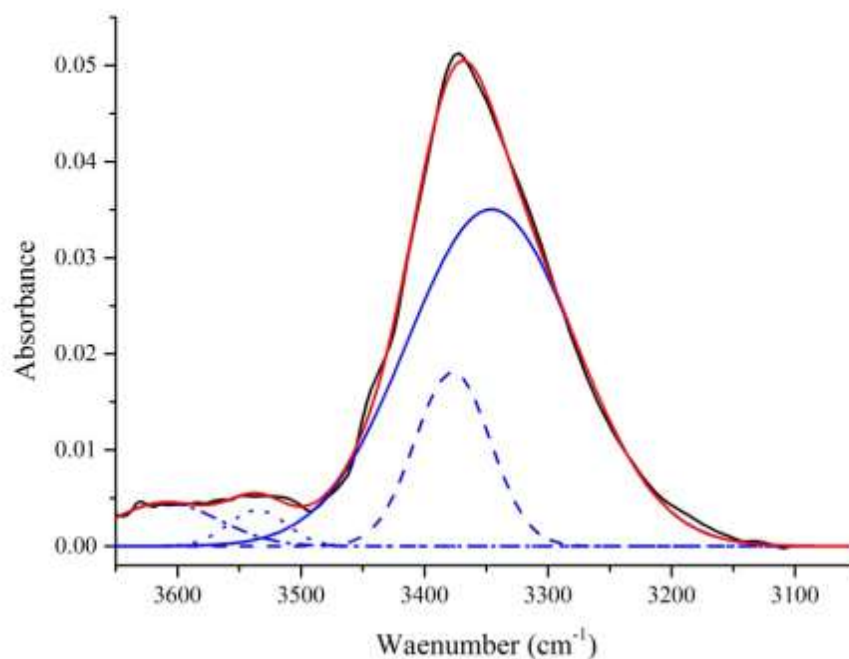
Figure B110: Deconvolution data for IPDI-TMP-PDEGA of N-H region. Data calculated using Gaussian fitting function. [Raw data in black, fit data in red, HS-HS fitted peak solid blue, carbonyl overtone dash blue and free N-H dot blue].

Table B110: Deconvolution data of N-H region collected using Gaussian function of IPDI-TMP-PDEGA.

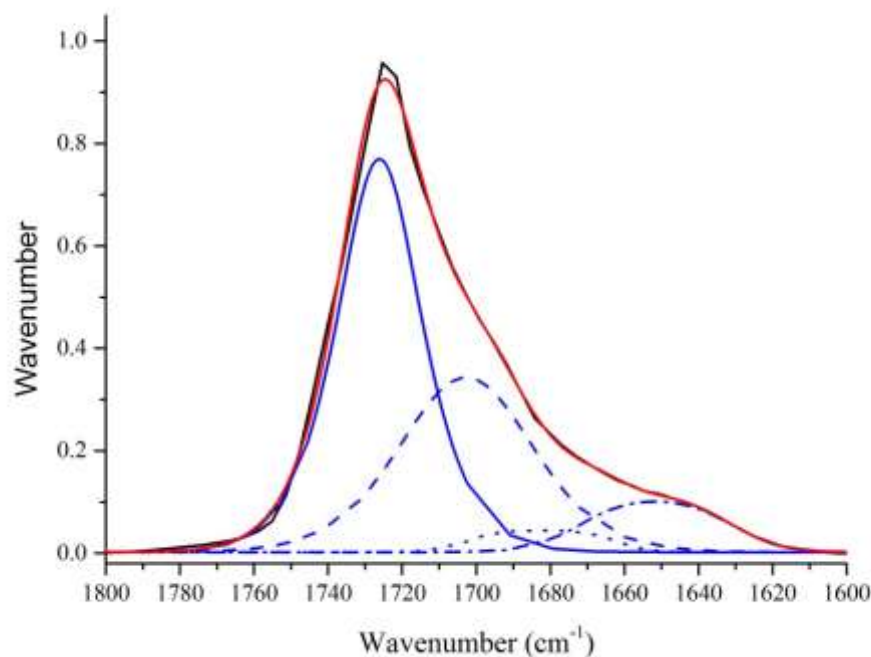| IPDI-TMP-PDEGA					
Peak Position/cm⁻¹	Standard Error/cm⁻¹	Area	Standard Error	Area/%	Fit R^2 value
3621	2.30	0.619	3.9×10^{-2}		
3541	1.84	0.622	4.4×10^{-2}	13.6	
3374	0.45	0.826	4.0×10^{-2}	9.0	0.999
3363	0.31	7.122	3.9×10^{-2}	77.5	

Gaussian-Lorentzian Fit of N-H

Figure B111: Deconvolution data for IPDI-TMP-PDEGA of N-H region. Data calculated using Gaussian-Lorentzian cross fitting function. [Raw data in black, fit data in red, HS-HS fitted peak solid blue, carbonyl overtone dash blue and free N-H dot blue].

Table B111: Deconvolution data of N-H region collected using GaussianLorentzian cross function of IPDI-TMP-PDEGA.

IPDI-TMP-PDEGA					
Peak Position/cm^{-1}	Standard Error/cm^{-1}	Area	Standard Error	Area/%	Fit R^2 value
3625	2.17	5.58x10^{-3}	2.5x10^{-4}		
		8.56x10^{-3}	-	14.9	
3544	2.21	1.51x10^{-2}	5.3x10^{-2}		
3377	0.79			26.3	0.999
3358	32.97	3.38x10^{-2}	5.3x10^{-2}	47.3	

C=O Region Deconvolution

Lorentzian Fit of C=O

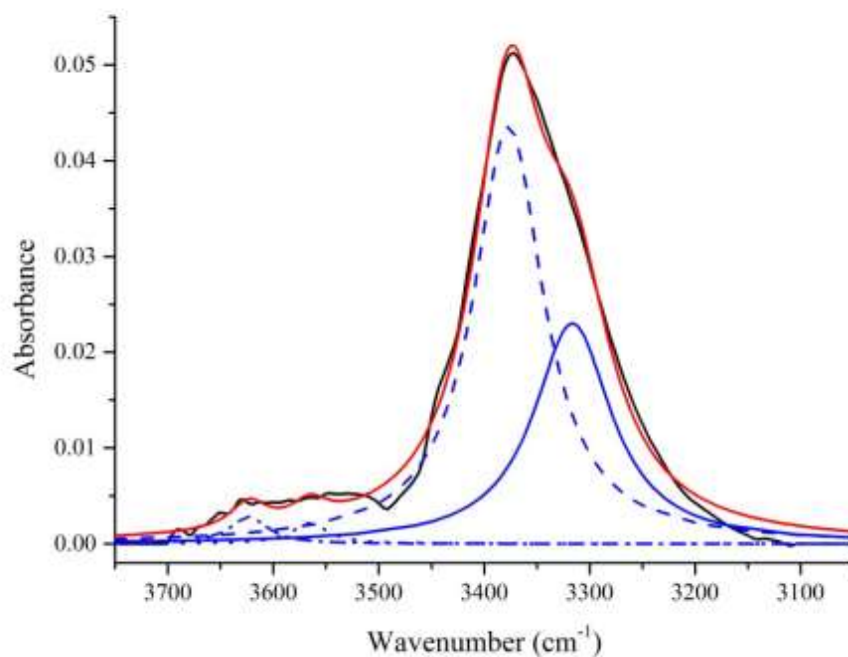**Figure B112: Deconvolution data for IPDI-TMP-PDEGA of C=O region. Data calculated using Lorentzian fitting function. [Raw data in black, fit data in red, free urethane carbonyl peaks solid blue, hydrogen bonded urethane dash blue, free/monodentate hydrogen bonded urea dot blue and bidentate hydrogen bonded urea dot dash blue].**

Table B112: Deconvolution data of C=O region collected using Lorentzian function of IPDI-TMP-PDEGA.

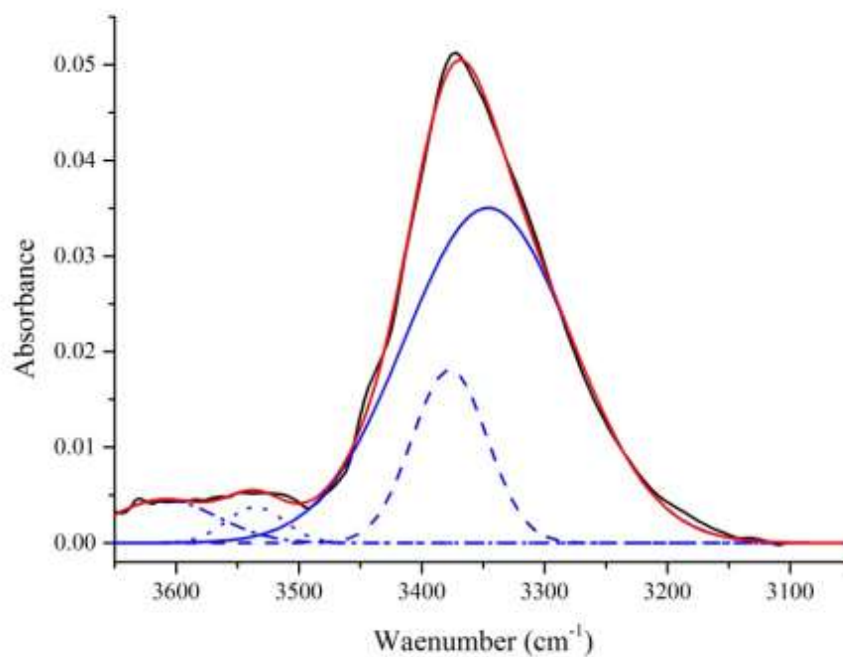| IPDI-TMP-PDEGA					
Peak Position/cm^{-1}	Standard Error/cm^{-1}	Area	Standard Error	Area/%	Fit R^2 value
1738	1.86	7.126	6.48	14.5	
1728	1.19	19.12	13.77	38.8	0.988
1713	4.40	16.75	9.48	34.0	
1651	4.37	6.31	1.89	12.8	

Gaussian Fit of C=O

Figure B113: Deconvolution data for IPDI-TMP-PDEGA of C=O region. Data calculated using Gaussian fitting function. [Raw data in black, fit data in red, free urethane carbonyl peaks solid blue, hydrogen bonded urethane dash blue, free/monodentate hydrogen bonded urea dot blue and bidentate hydrogen bonded urea dot dash blue].

Table B113: Deconvolution data of C=O region collected using Gaussian function of IPDI-TMP-PDEGA.

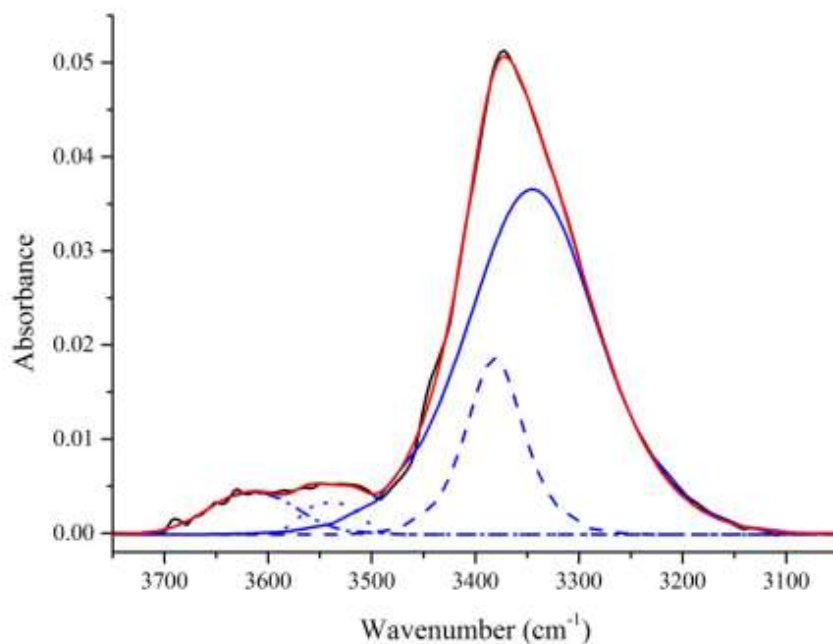| IPDI-TMP-PDEGA					
Peak Position/cm^{-1}	Standard Error/cm^{-1}	Area	Standard Error	Area/%	Fit R^2 value
1731	0.21	11.750	2.22	27.1	
1723	3.82	23.450	2.26	54.0	0.999
1674	9.10	5.833	5.357	13.4	
1638	2.03	2.390	1.81	5.5	

Gaussian-Lorentzian Fit of C=O

Figure B114: **Deconvolution data for IPDI-TMP-PDEGA of C=O region. Data calculated using Gaussian-Lorentzian cross fitting function. [Raw data in black, fit data in** red**, free urethane carbonyl peaks** solid blue**, hydrogen bonded urethane** dash blue**, free/monodentate hydrogen bonded urea** dot blue **and bidentate hydrogen bonded urea** dot dash blue**].**

Table B114: **Deconvolution data of C=O region collected using GaussianLorentzian cross function of IPDI-TMP-PDEGA.**

IPDI-TMP-PDEGA					
Peak Position/cm^{-1}	Standard Error/cm^{-1}	Area	Standard Error	Area/%	Fit R^2 value
1732	0.93	0.768	0.38	59.3	
1714	15.90	0.305	0.21	23.6	
1680	7.72	0.113	3.0×10^{-2}	8.8	0.999
1643	2.75	0.107	5.43×10^{-3}	8.3	

20 - IPDI-TMP-PDEGA-DEPD

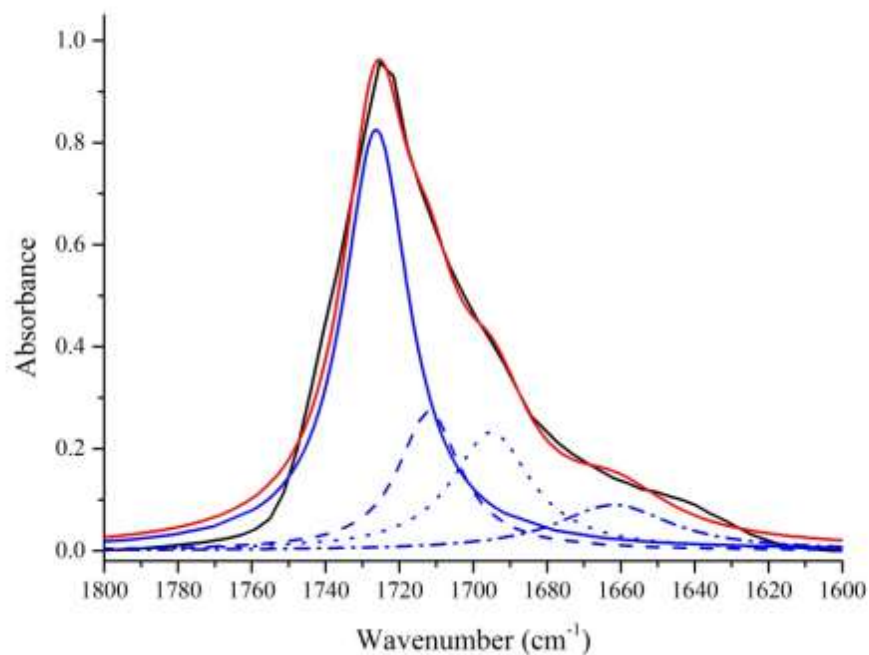# N-H Region Deconvolution

Lorentzian Fit of N-H

Figure B115: Deconvolution data for IPDI-TMP-PDEGA-DEPD of N-H region. Data calculated using Lorentzian fitting function. [Raw data in black, fit data in red, HS-HS fitted peak solid blue, carbonyl overtone dash blue and free N-H dot blue].

Table B115: Deconvolution data of N-H region collected using Lorentzian function of IPDI-TMP-PDEGA-DEPD.

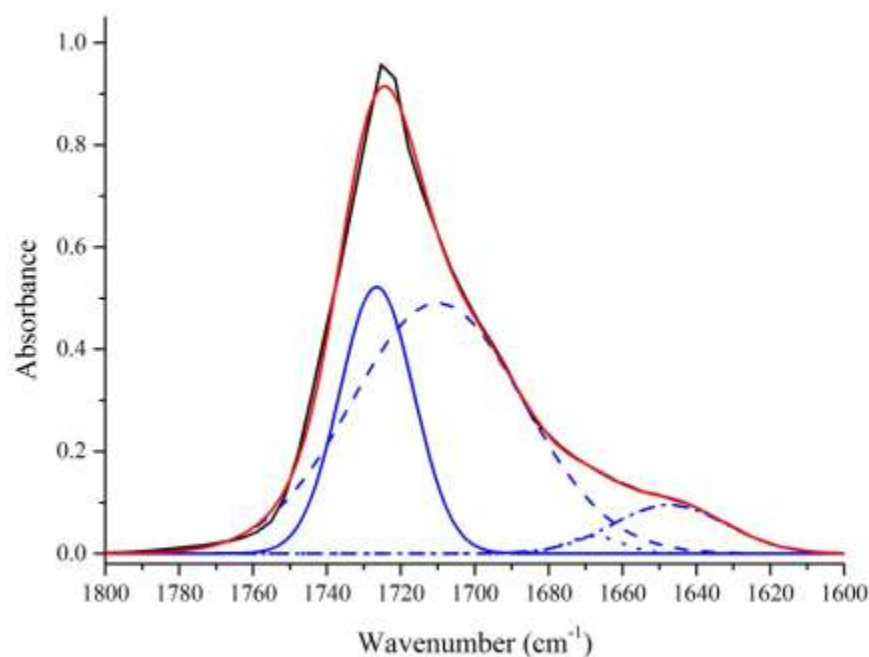| IPDI-TMP-PDEGA-DEPD					
Peak Position/cm^{-1}	Standard Error/cm^{-1}	Area	Standard Error	Area/%	Fit R^2 value
3613	2.78	0.799	0.23	5.1	
3529	3.97	2.660	0.58	17.0	0.987
3379	2.55	9.899	1.16	63.2	
3303	5.73	2.314	0.82	14.8	

Gaussian Fit of N-H

Figure B116: Deconvolution data for IPDI-TMP-PDEGA-DEPD of N-H region. Data calculated using Gaussian fitting function. [Raw data in black, fit data in red, HS-HS fitted peak solid blue, carbonyl overtone dash blue and free N-H dot blue].

Table B116: Deconvolution data of N-H region collected using Gaussian function of IPDI-TMP-PDEGA-DEPD.

IPDI-TMP-PDEGA-DEPD					
Peak Position/cm^{-1}	Standard Error/cm^{-1}	Area	Standard Error	Area/%	Fit R^2 value
3621	2.40	1.208	9.6x10^{-2}	18.2	
3542	2.51	1.274	0.12		0.999
3374	0.60	0.935	4.8x10^{-2}	6.9	
3368	0.58	10.204	8.1x10^{-2}	74.9	

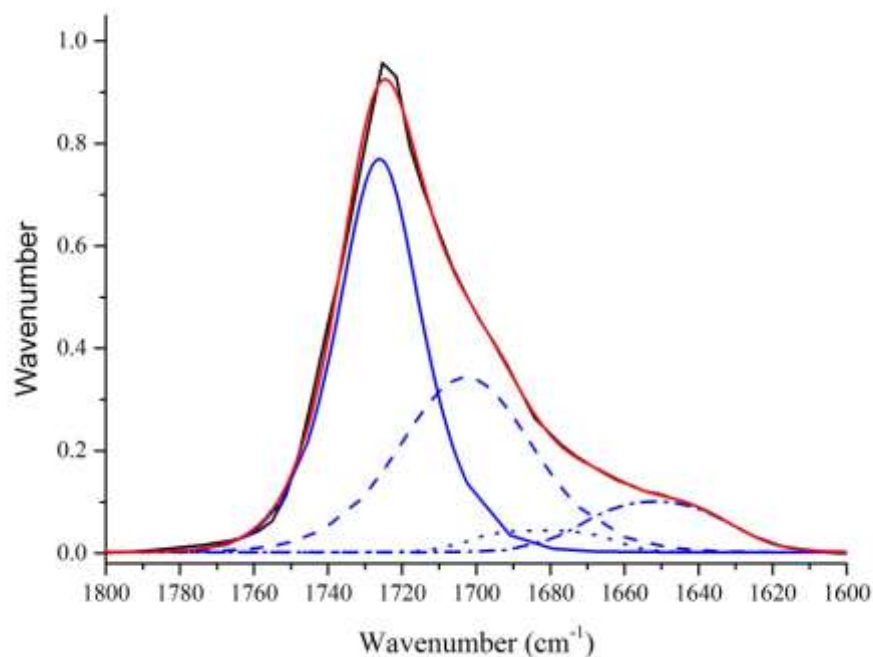*Gaussian-Lorentzian Fit of N-H*

Figure B117: **Deconvolution data for IPDI-TMP-PDEGA-DEPD of N-H region. Data calculated using Gaussian-Lorentzian cross fitting function. [Raw data in black, fit data in red, HS-HS fitted peak solid blue, carbonyl overtone dash blue and free N-H dot blue].**

Table B117: Deconvolution data of N-H region collected using GaussianLorentzian cross function of IPDI-TMP-PDEGA-DEPD.

IPDI-TMP-PDEGA-DEPD					
Peak Position/cm^{-1}	Standard Error/cm^{-1}	Area	Standard Error	Area/%	Fit R^2 value
3624	3.92	1.27×10^{-2}	1.3×10^{-3}		
3545	4.17	1.45×10^{-2}	1.7×10^{-3}	32.2	
		1.84×10^{-2}			
3375	1.04		0.103	21.8	0.999
3366	18.34	3.88×10^{-2}	0.103	45.9	

C=O Region Deconvolution

Lorentzian Fit of C=O

Figure B118: Deconvolution data for IPDI-TMP-PDEGA-DEPD of C=O region. Data calculated using Lorentzian fitting function. [Raw data in black, fit data in red, free urethane carbonyl peaks solid blue, hydrogen bonded urethane dash blue, free/monodentate hydrogen bonded urea dot blue and bidentate hydrogen bonded urea dot dash blue].

Table B118: Deconvolution data of C=O region collected using Lorentzian function of IPDI-TMP-PDEGA-DEPD.

IPDI-TMP-PDEGA-DEPD					
Peak Position/cm^{-1}	Standard Error/cm^{-1}	Area	Standard Error	Area/%	Fit R^2 value
1738	1.69	13.336	4.66	12.3	
1728	1.03	16.703	13.27	32.0	0.990
1714	2.88	16.377	14.63	31.4	
1690	8.89	12.625	7.74	24.2	

Gaussian Fit of C=O

Figure B119: Deconvolution data for IPDI-TMP-PDEGA-DEPD of C=O region. Data calculated using Gaussian fitting function. [Raw data in black, fit data in red, free urethane carbonyl peaks solid blue, hydrogen bonded urethane dash blue, free/monodentate hydrogen bonded urea dot blue and bidentate hydrogen bonded urea dot dash blue].

Table B119: Deconvolution data of C=O region collected using Gaussian function of IPDI-TMP-PDEGA-DEPD.

IPDI-TMP-PDEGA-DEPD					
Peak Position/cm^{-1}	Standard Error/cm^{-1}	Area	Standard Error	Area/%	Fit R^2 value
1731	0.26	9.766	1.75	12.3	
1718	2.43	30.413	0.67	32.0	
1675	6.25	2.988	4.01	31.4	0.999
1647	11.68	3.186	2.49	24.2	

Gaussian-Lorentzian Fit of C=O

Figure B120: Deconvolution data for IPDI-TMP-PDEGA-DEPD of C=O region. Data calculated using Gaussian-Lorentzian cross fitting function. [Raw data in black, fit data in red, free urethane carbonyl peaks solid blue, hydrogen bonded urethane dash blue, free/monodentate hydrogen bonded urea dot blue and bidentate hydrogen bonded urea dot dash blue].

Table B120: Deconvolution data of C=O region collected using GaussianLorentzian cross function of IPDI-TMP-PDEGA-DEPD.

IPDI-TMP-PDEGA-DEPD					
Peak Position/cm^{-1}	Standard Error/cm^{-1}	Area	Standard Error	Area/%	Fit R^2 value
1731	3.82	0.657	0.29	52.9	
1712	14.85	0.458	0.36	36.9	
1672	5.31	7.56×10^{-2}	4.6×10^{-2}	6.1	0.999
1636	8.35	5.10×10^{-2}	3.0×10^{-2}	4.1	

Appendix A - Using first derivative plots of DSC thermograms to identify weak thermal transitions such as hard segment glass transitions

OriginPro version 9.0 was used for data manipulation of DSC data and plotting of the first derivative of temperature versus heat flow scans. Differentiation of the DSC thermogram was performed using a first derivative coupled with a Savitzky-Golay smoothing function.

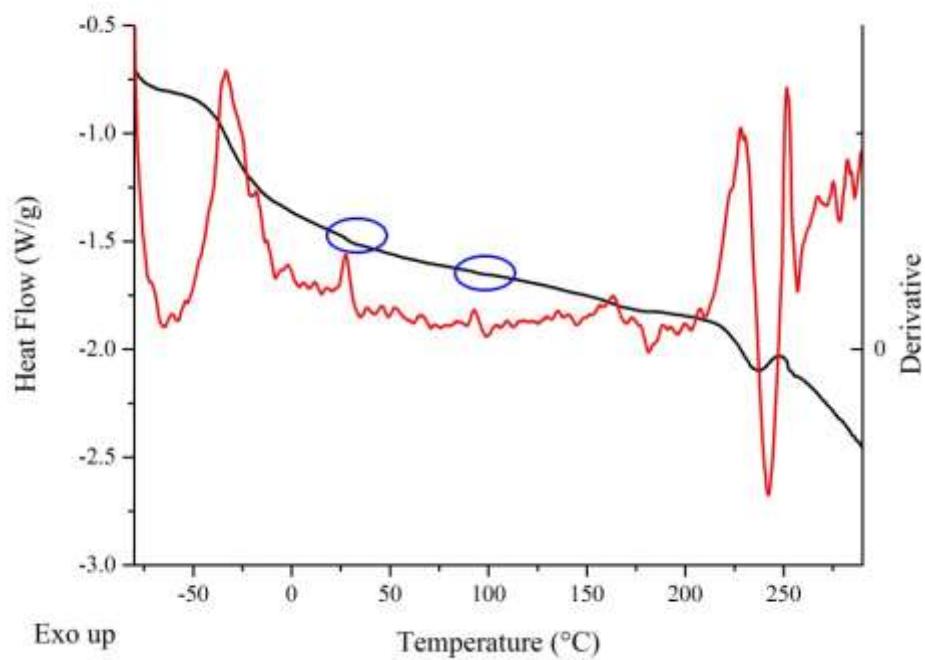## MDI and PPG based adhesives
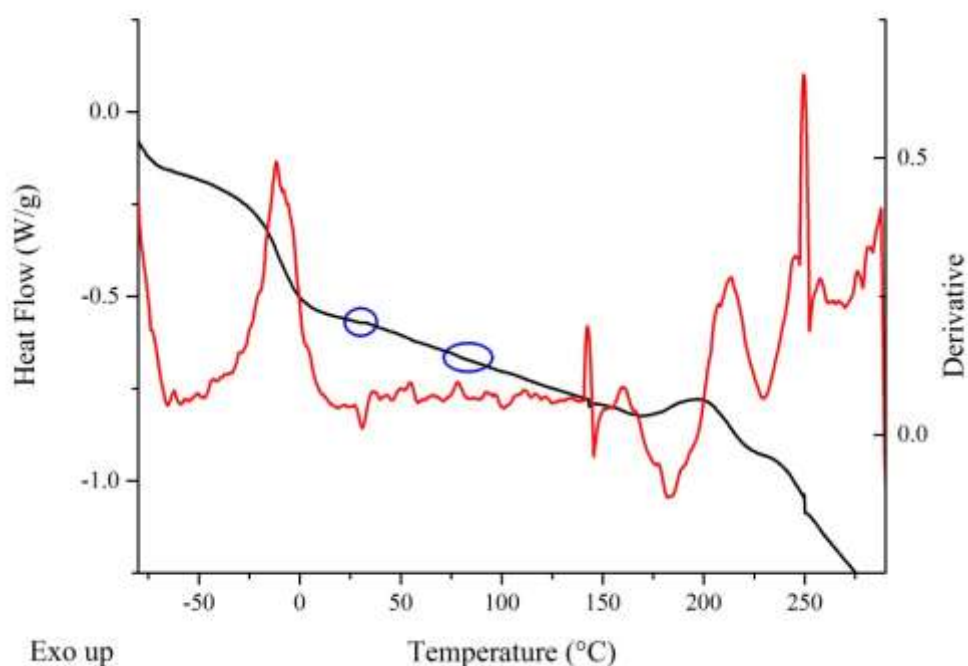
Figure A01: MDI-TMP-PPG DSC thermogram in black and first derivative plot in red. Weak thermal transitions circled in blue.
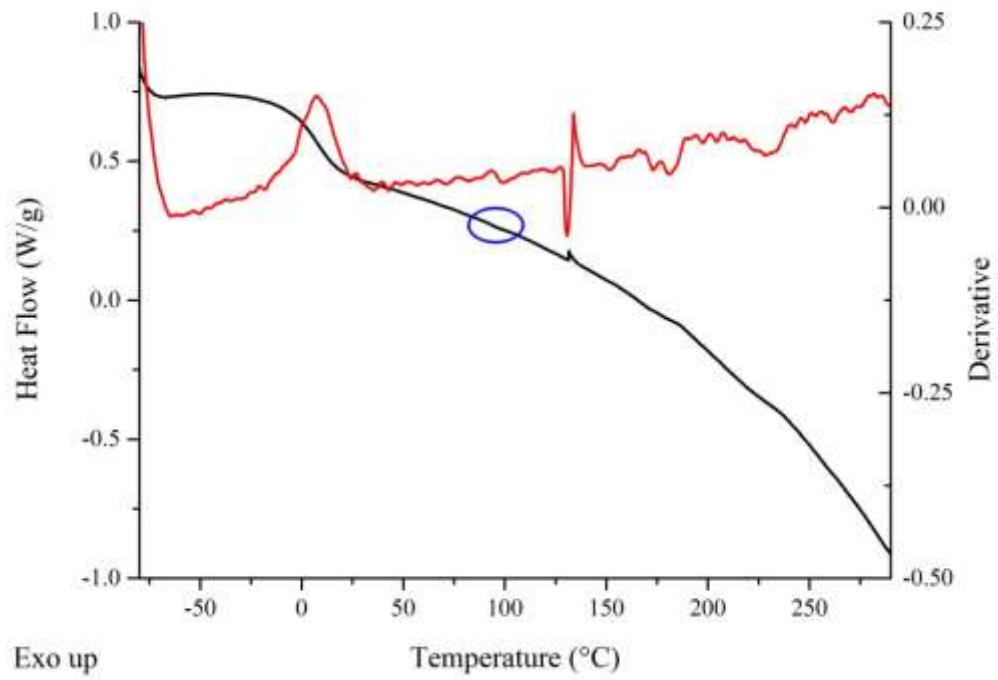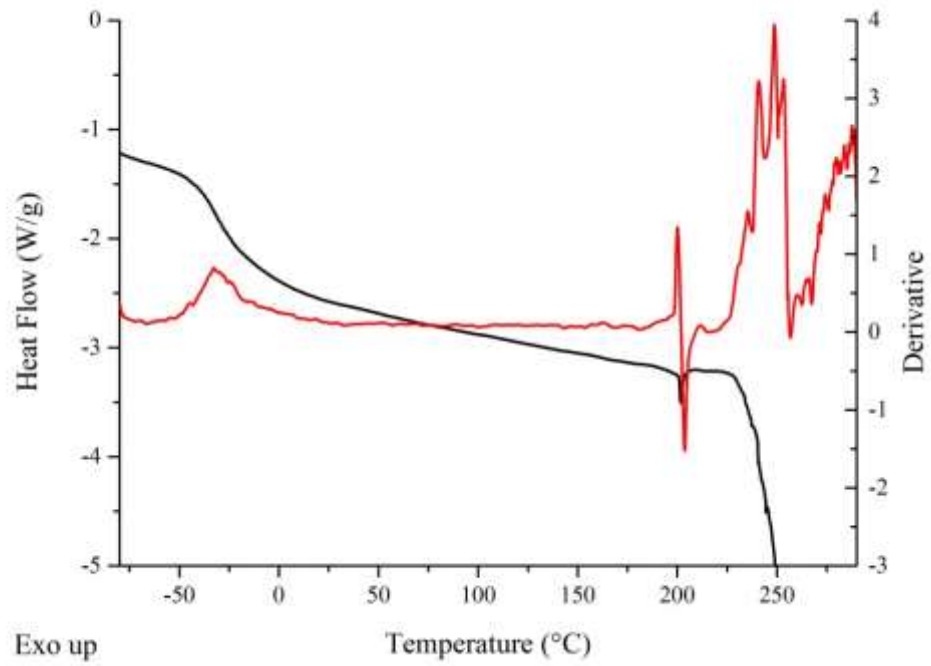
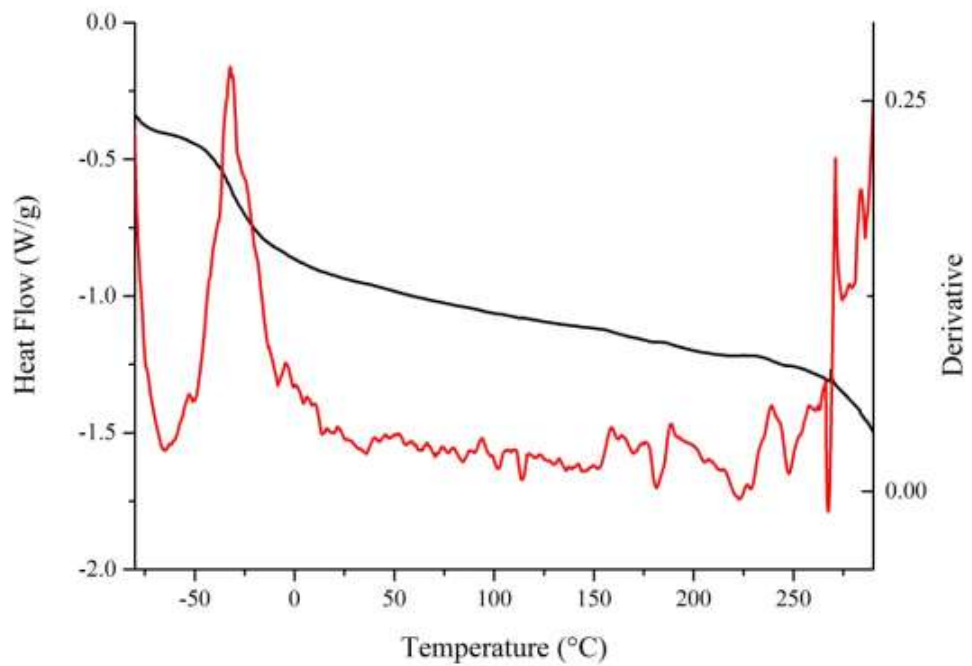**Figure A02: MDI-TMP-PPG-DEPD DSC thermogram in black and first derivative plot in red. Weak thermal transition circled in blue.**
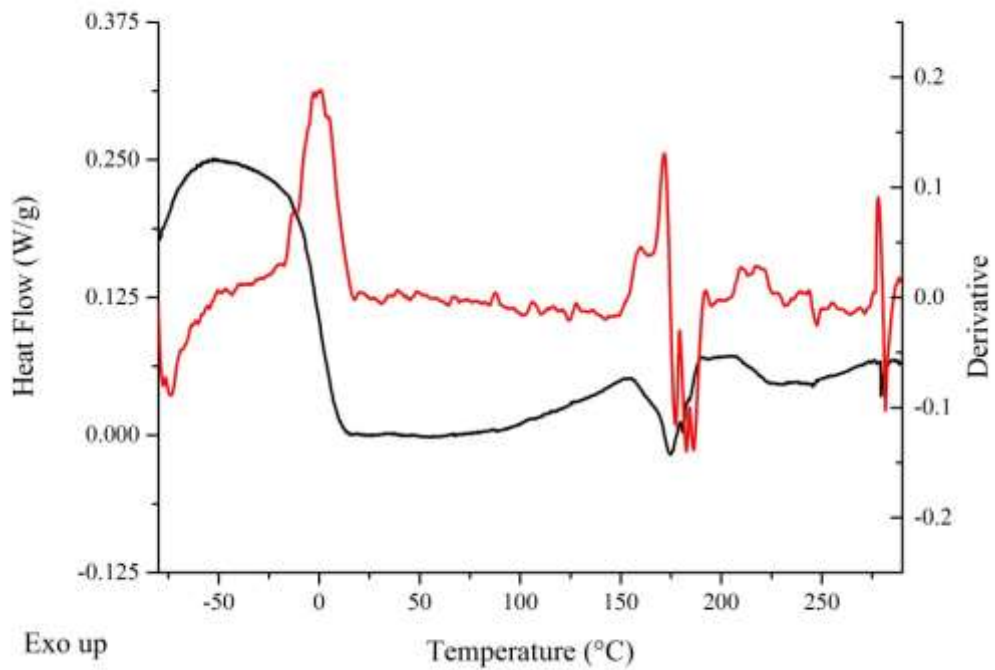
Figure A03: MDI-TMP-PPG-BD DSC thermogram in black and first derivative plot in red.
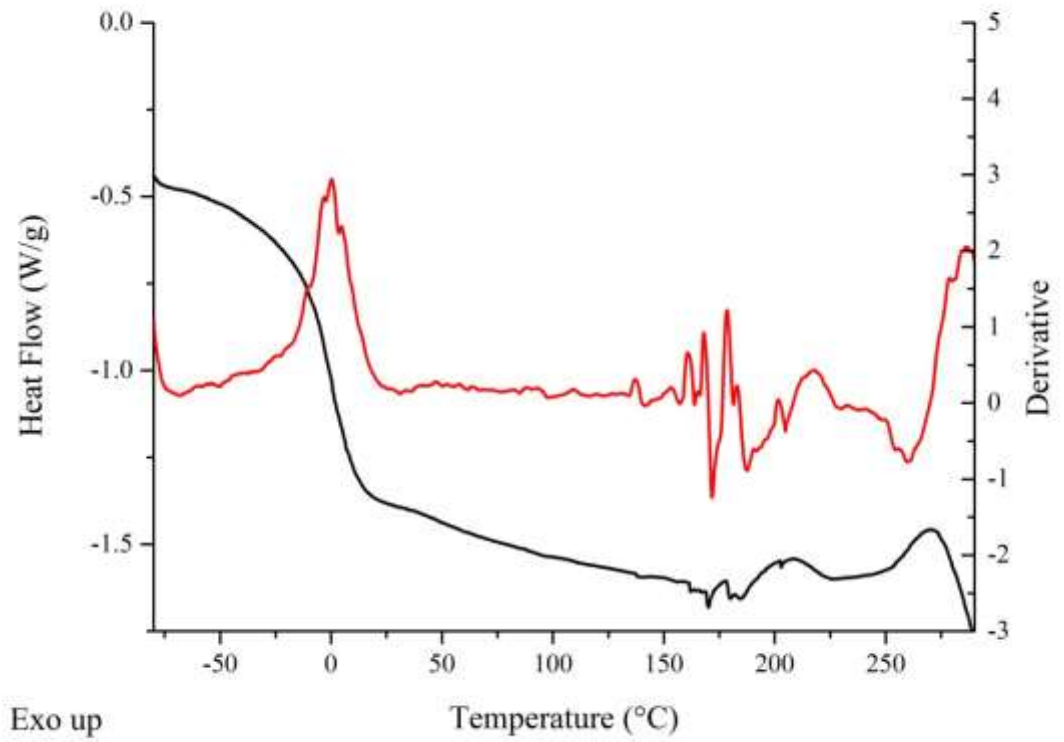
Figure A04: MDI-TMP-PPG-PD DSC thermogram in black and first derivative plot in red.

MDI and PCD based adhesives
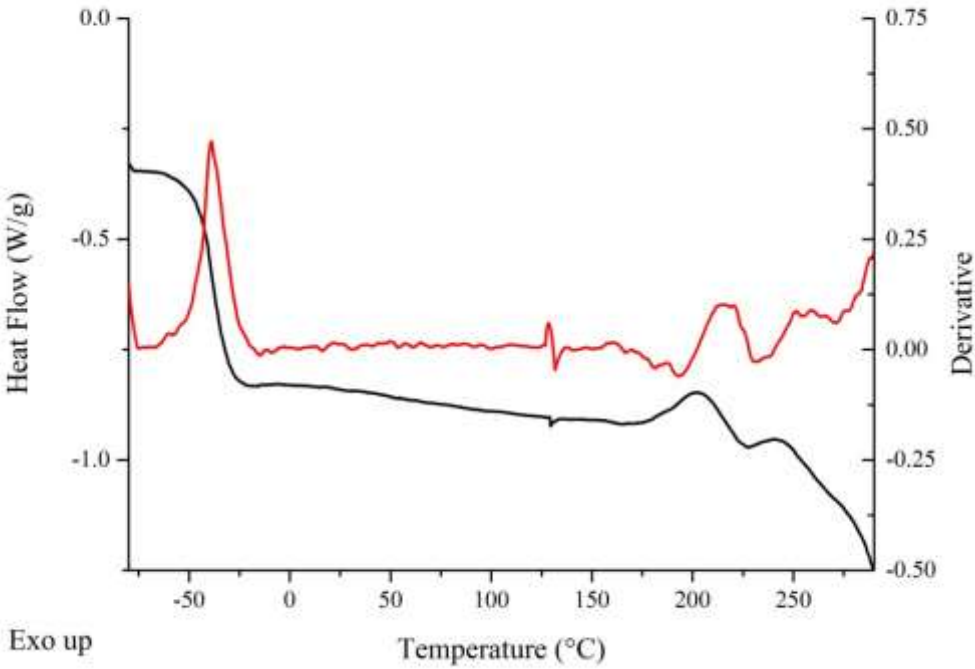
Figure A05: MDI-TMP-PCD DSC thermogram in black and first derivative plot in red.
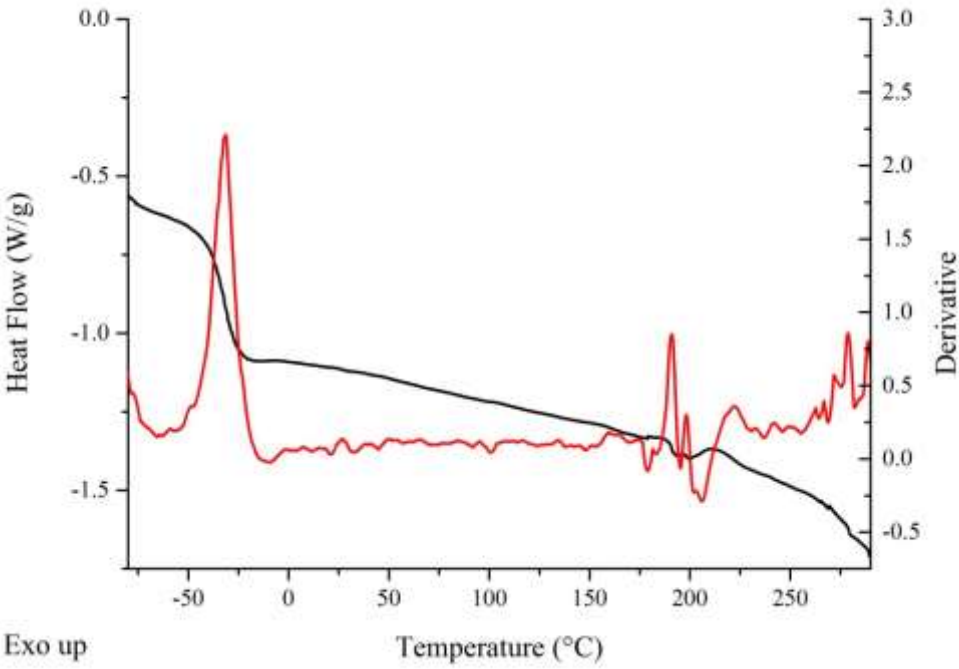
Figure A06: MDI-TMP-PCD-DEPD DSC thermogram in black and first derivative plot in red.
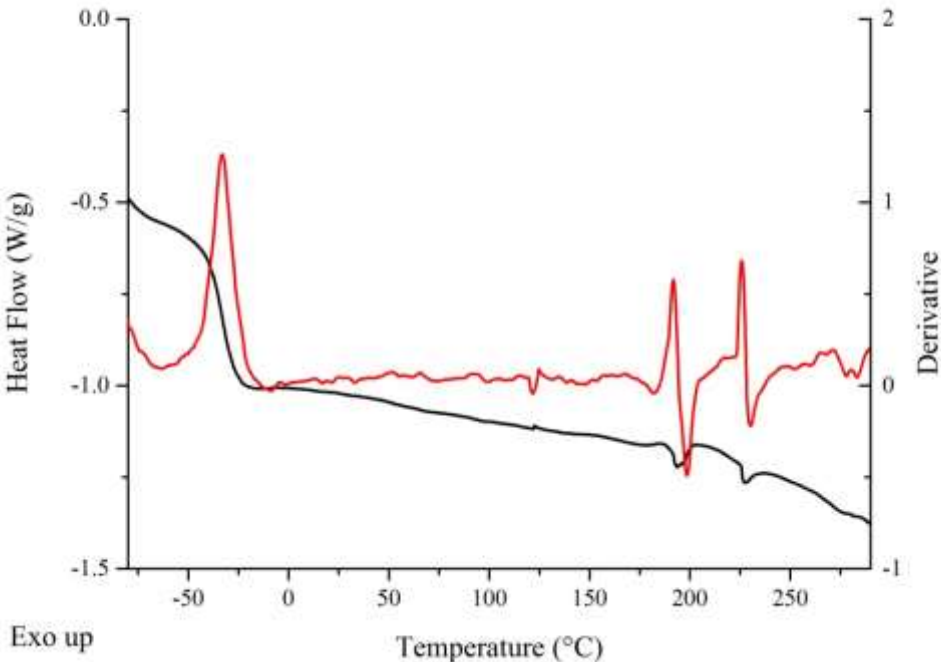
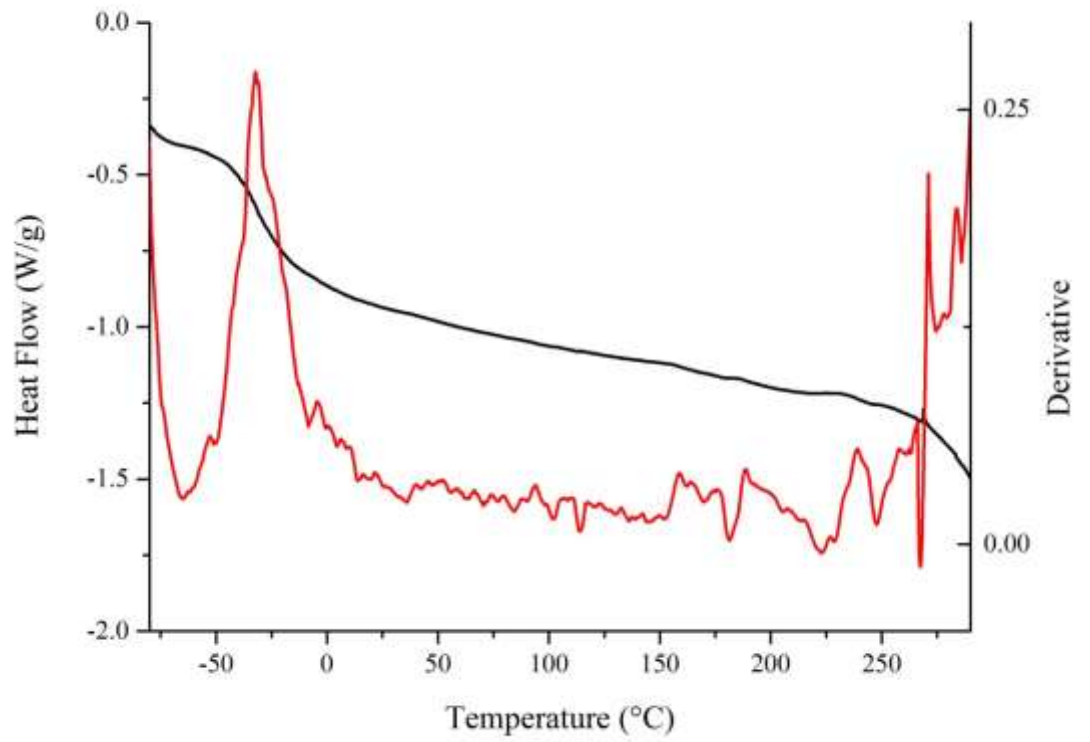**Figure A07: MDI-TMP-PCD-BD DSC thermogram in black and first derivative plot in red.**
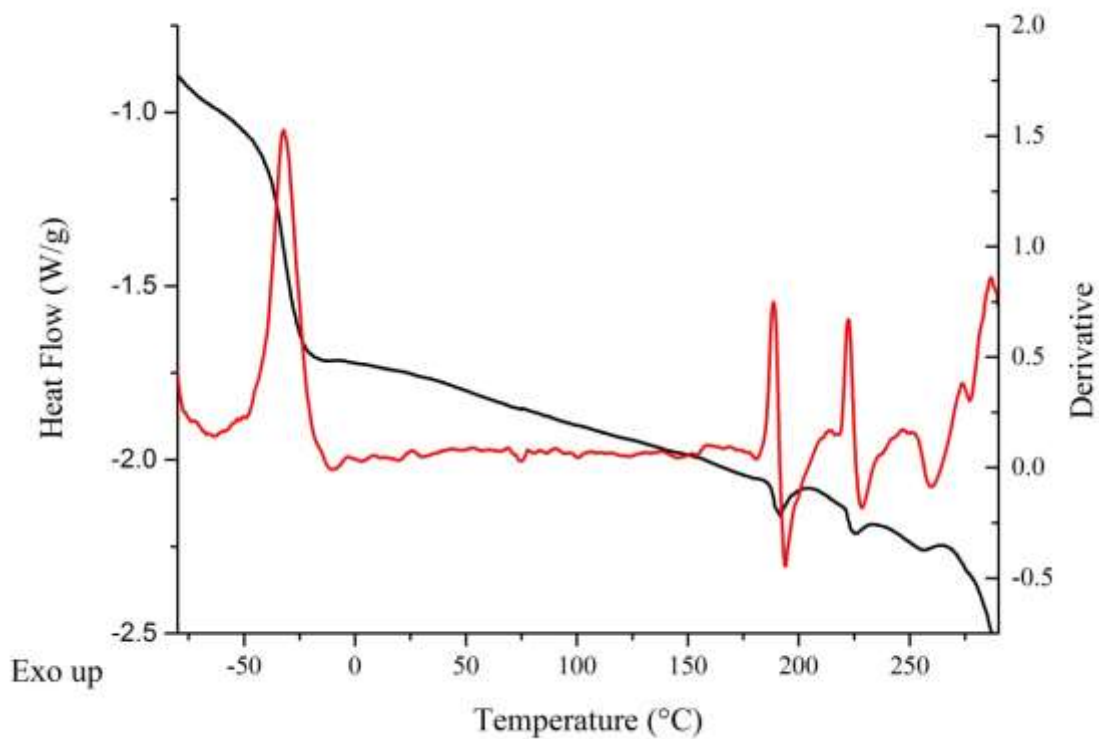
Figure A08: MDI-TMP-PCD-PD DSC thermogram in black and first derivative plot in red.

MDI and PDEGA based adhesives
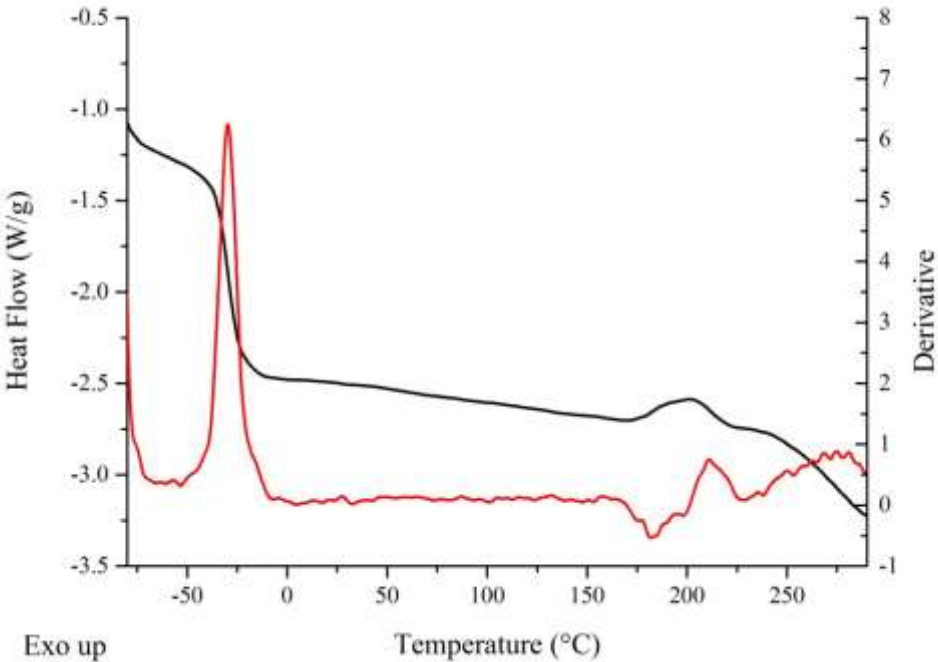
Figure A09: MDI-TMP-PDEGA DSC thermogram in black and first derivative plot in red.
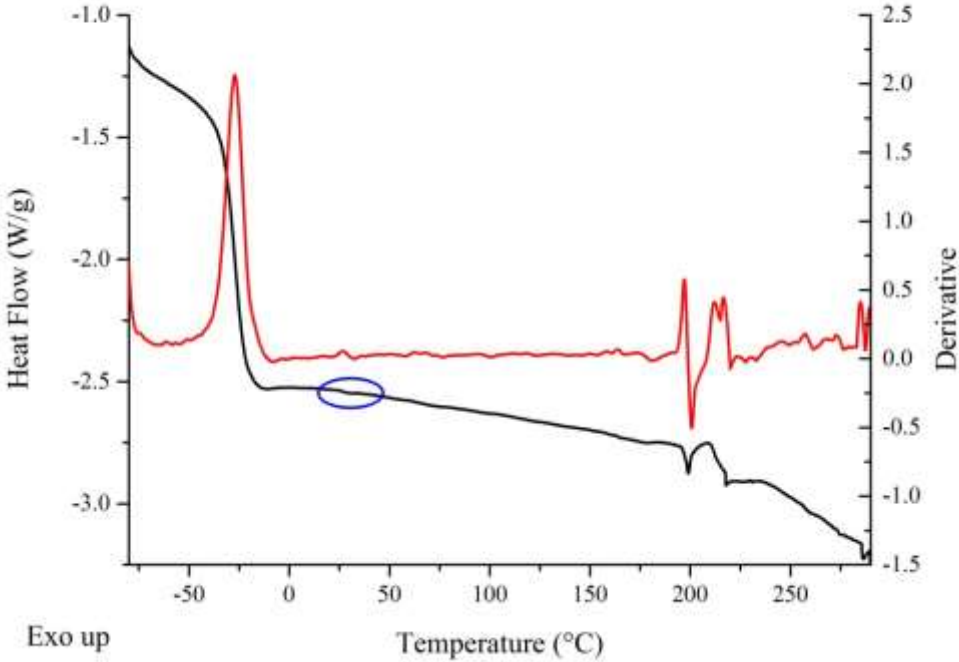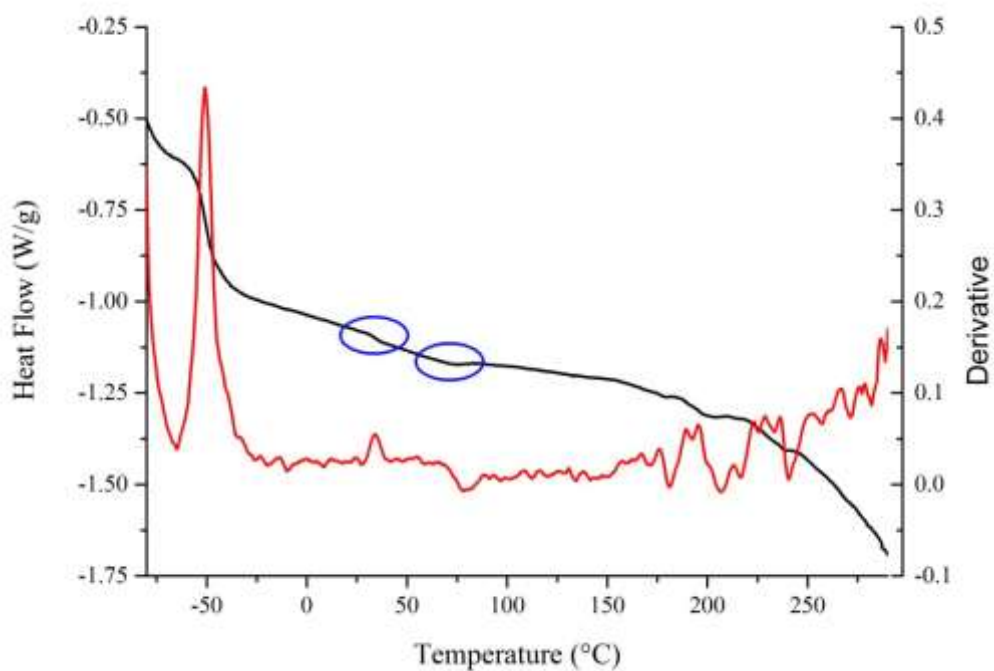
Figure A10: MDI-TMP-PDEGA-DEPD DSC thermogram in black and first derivative plot in red. Weak thermal transition circled in blue.
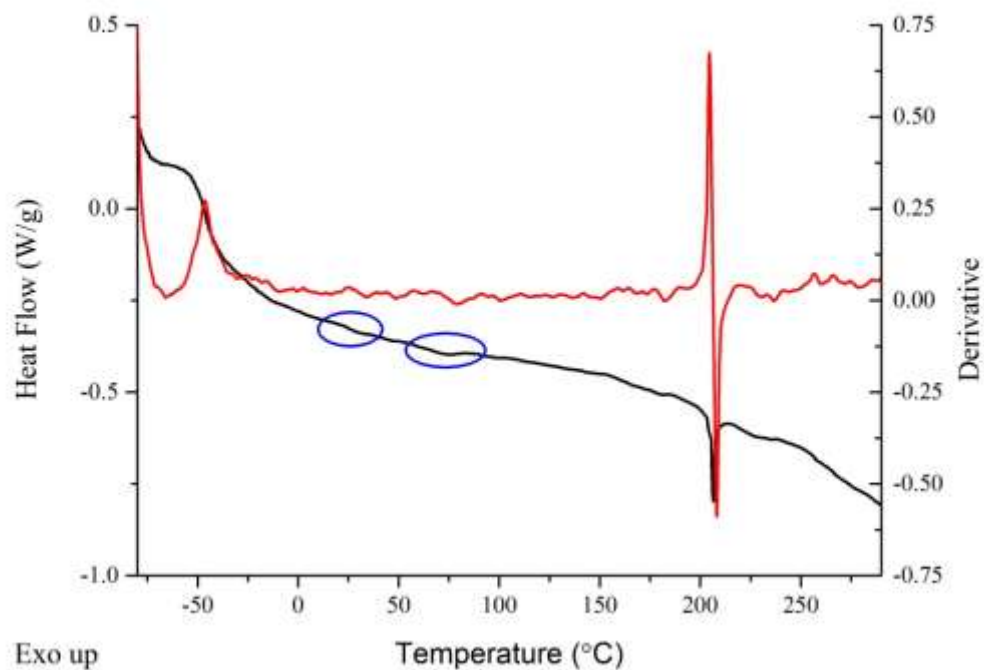
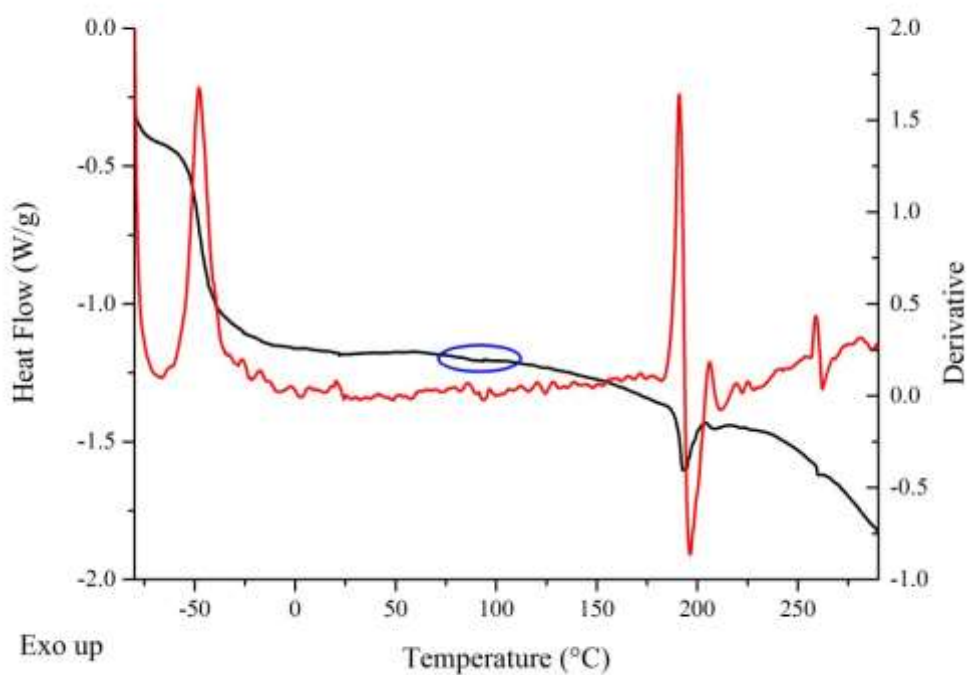**IPDI and PPG based adhesives**

Figure A11: IPDI-TMP-PPG DSC thermogram in black and first derivative plot in red. Weak thermal transitions circled in blue.

Figure A12: IPDI-TMP-PPG-DEPD DSC thermogram in black and first derivative plot in red.

Figure A13: IPDI-TMP-PPG-BD DSC thermogram in black and first derivative plot in red.

Figure A14: IPDI-TMP-PPG-PD DSC thermogram in black and first derivative plot in red.

IPDI and PCD based adhesives

Figure A15: IPDI-TMP-PCD DSC thermogram in black and first derivative plot in red. Weak thermal transitions circled in blue.

Figure A16: IPDI-TMP-PCD-DEPD DSC thermogram in black and first derivative plot in red. Weak thermal transitions circled in blue.

Figure A17: IPDI-TMP-PCD-BD DSC thermogram in black and first derivative plot in red. Weak thermal transition circled in blue.
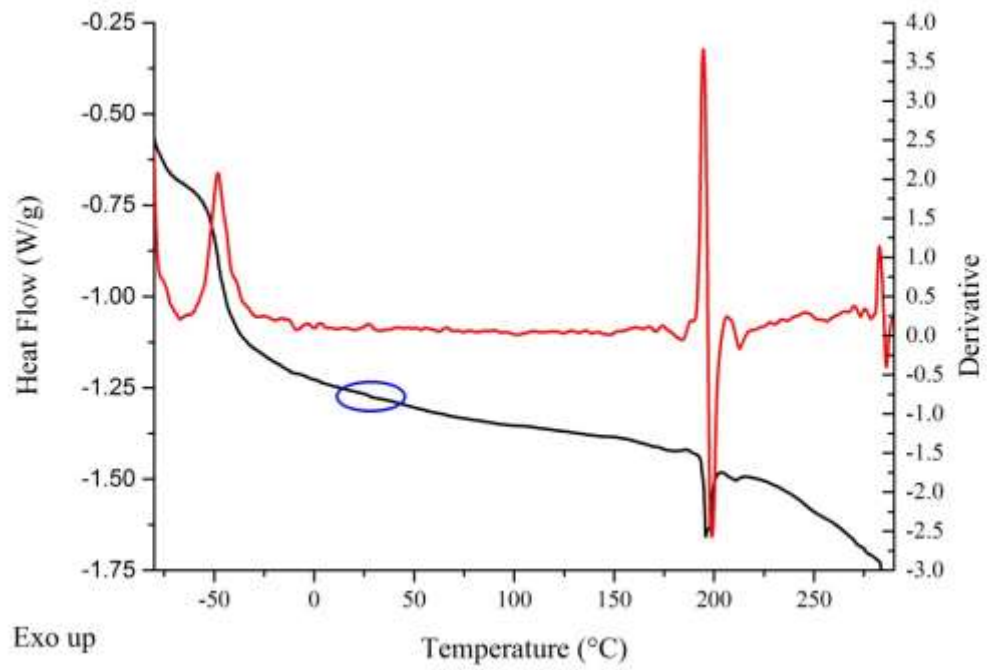
Figure A18: IPDI-TMP-PCD-PD DSC thermogram in black and first derivative plot in red. Weak thermal transition circled in blue.

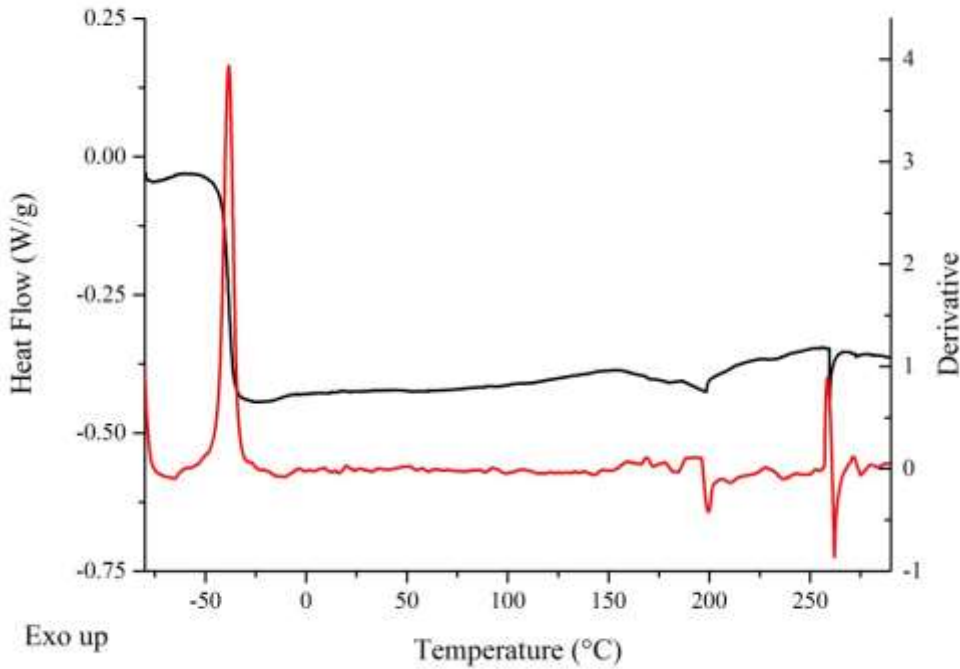**IPDI and PDEGA based adhesives**

Figure A19: IPDI-TMP-PDEGA DSC thermogram in black and first derivative plot in red.
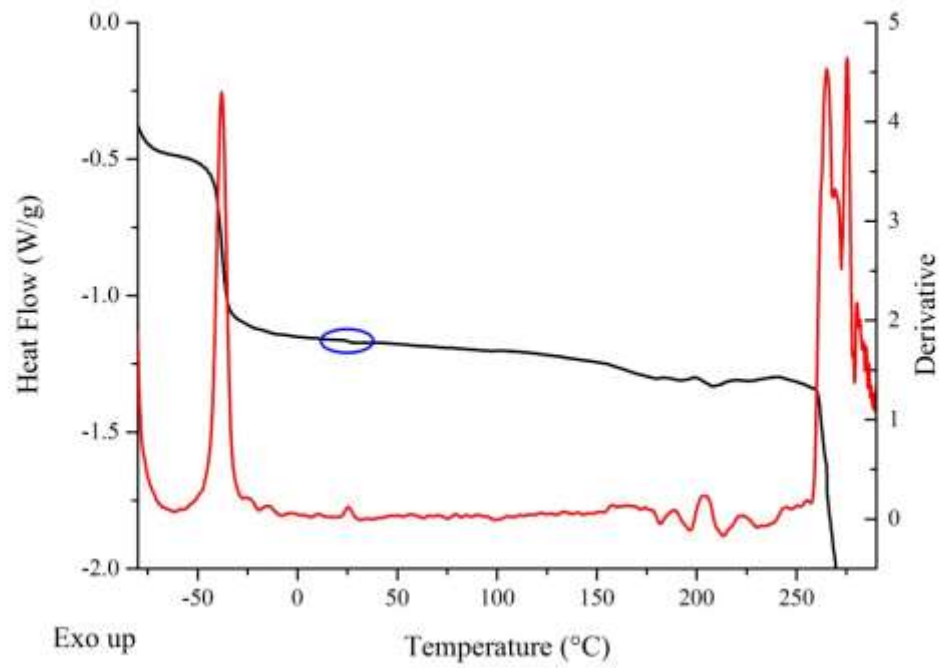
Figure A20: IPDI-TMP-PDEGA-DEPD DSC thermogram in black and first derivative plot in red. Weak thermal transition circled in blue.